

Arthritis & Rheumatology

An Official Journal of the American College of Rheumatology
www.arthritisrheum.org and wileyonlinelibrary.com

Editor

Richard J. Bucala, MD, PhD
Yale University School of Medicine, New Haven

Deputy Editor

Daniel H. Solomon, MD, MPH, Boston

Co-Editors

Joseph E. Craft, MD, New Haven
David T. Felson, MD, MPH, Boston
Richard F. Loeser Jr., MD, Chapel Hill
Peter A. Nigrovic, MD, Boston
Christopher T. Ritchlin, MD, MPH, Rochester
John Varga, MD, Chicago

Co-Editor and Review Article Editor

Robert Terkeltaub, MD, San Diego

Clinical Trials Advisor

Michael E. Weinblatt, MD, Boston

Journal Publications Committee

Nora G. Singer, MD, Chair, Cleveland
Kelli D. Allen, PhD, Chapel Hill
Shervin Assassi, MD, MS, Houston
Cecilia P. Chung, MD, MPH, Nashville
Eric J. Gapud, MD, PhD, Baltimore
Kim D. Jones, RN, PhD, FNP, Portland
Brian L. Kotzin, MD, Los Angeles
Linda C. Li, PT, MSc, PhD, Vancouver

Editorial Staff

Jane S. Diamond, MPH, Managing Editor, Atlanta
Patricia K. Reichert, Assistant Managing Editor, Atlanta
Lesley W. Allen, Senior Manuscript Editor, Atlanta
Patricia L. Mabley, Manuscript Editor, Atlanta
Kristin W. Mitchell, Manuscript Editor, Atlanta
Emily W. Wehby, MA, Manuscript Editor, Atlanta
Michael Weinberg, MA, Manuscript Editor, Atlanta
Kelly Barraza, Editorial Coordinator, Atlanta
Brittany Swett, Editorial Assistant, New Haven
Carolyn Roth, Senior Production Editor, Boston

Associate Editors

Daniel Aletaha, MD, MS, Vienna
Heather G. Allore, PhD, New Haven
Lenore M. Buckley, MD, MPH, New Haven
Daniel J. Clauw, MD, Ann Arbor
Robert A. Colbert, MD, PhD, Bethesda
Karen H. Costenbader, MD, MPH, Boston
Nicola Dalbeth, MD, FRACP, Auckland
Kevin D. Deane, MD, Denver
Patrick M. Gaffney, MD, Oklahoma City

Mark C. Genovese, MD, Palo Alto
Andrew H. Haims, MD, New Haven
Insoo Kang, MD, New Haven
Arthur Kavanaugh, MD, La Jolla
Wan-Uk Kim, MD, PhD, Seoul
S. Sam Lim, MD, MPH, Atlanta
Anne-Marie Malfait, MD, PhD, Chicago
Paul A. Monach, MD, PhD, Boston
Chester V. Oddis, MD, Pittsburgh
Andras Perl, MD, PhD, Syracuse

Janet E. Pope, MD, MPH, FRCPC,
London, Ontario
Timothy R. D. J. Radstake, MD, PhD, Utrecht
William Robinson, MD, PhD, Palo Alto
Georg Schett, MD, Erlangen
Nan Shen, MD, Shanghai
Betty P. Tsao, PhD, Charleston
Ronald van Vollenhoven, MD, PhD, Amsterdam
Fredrick M. Wigley, MD, Baltimore

Advisory Editors

Tatsuya Atsumi, MD, PhD, Sapporo
Charles Auffray, PhD, Lyon
Dominique Baeten, MD, PhD, Amsterdam
André Ballesteros-Tato, PhD, Birmingham
Lorenzo Beretta, MD, Milan
Bryce A. Binstadt, MD, PhD, Minneapolis
Jaime Calvo-Alen, MD, Vitoria
Scott Canna, MD, Pittsburgh

Andrew P. Cope, MD, PhD, London
Niek de Vries, MD, PhD, Amsterdam
Jörg H. W. Distler, MD, Erlangen
Liana Fraenkel, MD, MPH, New Haven
Erica Herzog, MD, PhD, New Haven
Hui-Chen Hsu, PhD, Birmingham
Mariana J. Kaplan, MD, Bethesda
Jonathan Kay, MD, Worcester
Dwight H. Kono, MD, La Jolla

Martin A. Kriegel, MD, PhD, New Haven
Francis Lee, MD, PhD, New Haven
Sang-Il Lee, MD, PhD, Jinju
Bing Lu, PhD, Boston
Tony R. Merriman, PhD, Otago
Yukinori Okada, MD, PhD, Osaka
Raghunatha Yammani, PhD, Winston-Salem
Kazuki Yoshida, MD, MPH, MS, Boston

AMERICAN COLLEGE OF RHEUMATOLOGY

David I. Daikh, MD, PhD, San Francisco, **President**
Paula Marchetta, MD, MBA, New York, **President-Elect**

Charles M. King, MD, Tupelo, **Treasurer**
Ellen M. Gravallese, MD, Worcester, **Secretary**
Mark Andrejeski, Atlanta, **Executive Vice-President**

© 2018 American College of Rheumatology. All rights reserved. No part of this publication may be reproduced, stored or transmitted in any form or by any means without the prior permission in writing from the copyright holder. Authorization to copy items for internal and personal use is granted by the copyright holder for libraries and other users registered with their local Reproduction Rights Organization (RRO), e.g. Copyright Clearance Center (CCC), 222 Rosewood Drive, Danvers, MA 01923, USA (www.copyright.com), provided the appropriate fee is paid directly to the RRO. This consent does not extend to other kinds of copying such as copying for general distribution, for advertising or promotional purposes, for creating new collective works or for resale. Special requests should be addressed to: permissions@wiley.com

Access Policy: Subject to restrictions on certain backfiles, access to the online version of this issue is available to all registered Wiley Online Library users 12 months after publication. Subscribers and eligible users at subscribing institutions have immediate access in accordance with the relevant subscription type. Please go to onlinelibrary.wiley.com for details.

The views and recommendations expressed in articles, letters, and other communications published in Arthritis & Rheumatology are those of the authors and do not necessarily reflect the opinions of the editors, publisher, or American College of Rheumatology. The publisher and the American College of Rheumatology do not investigate the information contained in the classified advertisements in this journal and assume no responsibility concerning them. Further, the publisher and the American College of Rheumatology do not guarantee, warrant, or endorse any product or service advertised in this journal.

Cover design: Todd Machen

♻️ This journal is printed on acid-free paper.

Arthritis & Rheumatology

An Official Journal of the American College of Rheumatology
www.arthritisrheum.org and wileyonlinelibrary.com

VOLUME 70

JUNE 2018

NO. 6

In This Issue	A15
Clinical Connections	A17
Special Articles	
Editorial: Ensuring the Future of Rheumatology: A Multi-Dimensional Challenge and Call to Action <i>William F. Harvey, Afton L. Hassett, and Sharad Lakhanpal</i>	797
Editorial: STATus of STAT3 in Psoriatic Arthritis <i>John D. Mountz</i>	801
Review: Cell Death, Nucleic Acids, and Immunity: Inflammation Beyond the Grave <i>Keith B. Elkon</i>	805
2015 American College of Rheumatology Workforce Study: The Role of Graduate Medical Education in Adult Rheumatology <i>Marcy B. Bolster, Anne R. Bass, Jonathan S. Hausmann, Chad Deal, Marcia Ditmyer, Kamilah L. Greene, Seetha U. Monrad, and Daniel F. Battafarano</i>	817
Common Language Description of the Term Rheumatic and Musculoskeletal Diseases (RMDs) for Use in Communication With the Lay Public, Healthcare Providers, and Other Stakeholders Endorsed by the European League Against Rheumatism (EULAR) and the American College of Rheumatology (ACR) <i>Désirée van der Heijde, David I. Daikh, Neil Betteridge, Gerd R. Burmester, Afton L. Hassett, Eric L. Matteson, Ronald van Vollenhoven, and Sharad Lakhanpal</i>	826
Rheumatoid Arthritis	
Switching From Reference Adalimumab to SB5 (Adalimumab Biosimilar) in Patients With Rheumatoid Arthritis: Fifty-Two-Week Phase III Randomized Study Results <i>Michael E. Weinblatt, Asta Baranauskaite, Eva Dokoupilova, Agnieszka Zielinska, Janusz Jaworski, Artur Racewicz, Margarita Pileckyte, Krystyna Jedrychowicz-Rosiak, Inyoung Baek, and Jeehoon Ghil</i>	832
Transcriptional Profiling of Synovial Macrophages Using Minimally Invasive Ultrasound-Guided Synovial Biopsies in Rheumatoid Arthritis <i>Arthur M. Mandelin II, Philip J. Homan, Alexander M. Shaffer, Carla M. Cuda, Salina T. Dominguez, Emily Bacalao, Mary Carns, Monique Hinchcliff, Jungwha Lee, Kathleen Aren, Anjali Thakrar, Anna B. Montgomery, S. Louis Bridges Jr., Joan M. Bathon, John P. Atkinson, David A. Fox, Eric L. Matteson, Christopher D. Buckley, Costantino Pitzalis, Deborah Parks, Laura B. Hughes, Laura Geraldino-Pardilla, Robert Ike, Kristine Phillips, Kerry Wright, Andrew Filer, Stephen Kelly, Eric M. Ruderman, Vince Morgan, Hiam Abdala-Valencia, Alexander V. Misharin, G. Scott Budinger, Elizabeth T. Bartom, Richard M. Pope, Harris Perlman, and Deborah R. Winter</i>	841
Psoriatic Arthritis	
Augmented Th17 Differentiation Leads to Cutaneous and Synovio-Enthesal Inflammation in a Novel Model of Psoriatic Arthritis <i>Lu Yang, Melania H. Fanok, Aranzazu Mediero-Munoz, Laura K. Fogli, Carmen Corciulo, Shahla Abdollahi, Bruce N. Cronstein, Jose U. Scher, and Sergei B. Koralov</i>	855
Systemic Lupus Erythematosus	
Long-Term Safety and Efficacy of Belimumab in Patients With Systemic Lupus Erythematosus: A Continuation of a Seventy-Six-Week Phase III Parent Study in the United States <i>Richard A. Furie, Daniel J. Wallace, Cynthia Aranow, James Fettiplace, Barbara Wilson, Prafull Mistry, David A. Roth, and David Gordon</i>	868
Twin DNA Methylation Profiling Reveals Flare-Dependent Interferon Signature and B Cell Promoter Hypermethylation in Systemic Lupus Erythematosus <i>Constance J. Ulf-Møller, Fazila Asmar, Yi Liu, Anders J. Svendsen, Florence Busato, Kirsten Grønbaek, Jörg Tost, and Søren Jacobsen</i>	878
Antiphospholipid Syndrome	
Antiphospholipid Antibodies Inhibit Trophoblast Toll-Like Receptor and Inflammasome Negative Regulators <i>Melissa J. Mulla, Ingrid C. Weel, Julie A. Potter, Stefan M. Gysler, Jane E. Salmon, Maria T. S. Peraçoli, Carla V. Rothlin, Lawrence W. Chamley, and Vikki M. Abrahams</i>	891
The American College of Rheumatology is Launching an Open Access Journal and Seeking an Editor-in-Chief	902

Systemic Sclerosis

- A Multicenter Study of the Validity and Reliability of Responses to Hand Cold Challenge as Measured by Laser Speckle Contrast Imaging and Thermography: Outcome Measures for Systemic Sclerosis–Related Raynaud’s Phenomenon
Jack D. Wilkinson, Sarah A. Leggett, Elizabeth J. Marjanovic, Tonia L. Moore, John Allen, Marina E. Anderson, Jason Britton, Maya H. Buch, Francesco Del Galdo, Christopher P. Denton, Graham Dinsdale, Bridgett Griffiths, Frances Hall, Kevin Howell, Audrey MacDonald, Neil J. McHugh, Joanne B. Manning, John D. Pauling, Christopher Roberts, Jacqueline A. Shipley, Ariane L. Herrick, and Andrea K. Murray..... 903
- Skin Gene Expression Is Prognostic for the Trajectory of Skin Disease in Patients With Diffuse Cutaneous Systemic Sclerosis
Giuseppina Stifano, Thierry Sornasse, Lisa M. Rice, Leo Na, Haiyin Chen-Harris, Dinesh Khanna, Angelika Jahreis, Yuqing Zhang, Jeff Siegel, and Robert Lafyatis..... 912
- Molecular Basis for Dysregulated Activation of NKX2-5 in the Vascular Remodeling of Systemic Sclerosis
Athina Dritsoula, Ioannis Papaioannou, Sandra G. Guerra, Carmen Fonseca, Javier Martin, Ariane L. Herrick, David J. Abraham, Christopher P. Denton, and Markella Ponticos..... 920
- Transforming Growth Factor β Activation Primes Canonical Wnt Signaling Through Down-Regulation of Axin-2
Justin Gillespie, Rebecca L. Ross, Clarissa Corinaldesi, Filomena Esteves, Emma Derrett-Smith, Michael F. McDermott, Gina M. Doody, Christopher P. Denton, Paul Emery, and Francesco Del Galdo..... 932

Clinical Images

- Paraparesis Revealing Tophaceous Gout
Pierre Pottecher, Pierre Martz, and Paul Ornetti..... 942

Pediatric Rheumatology

- Reversal of Sepsis-Like Features of Neutrophils by Interleukin-1 Blockade in Patients With Systemic-Onset Juvenile Idiopathic Arthritis
Nienke M. ter Haar, Tamar Tak, Michal Mokry, Rianne C. Scholman, Jenny M. Meerding, Wilco de Jager, Anouk Verwoerd, Dirk Foell, Thomas Vogl, Johannes Roth, Pieter H. C. Leliefeld, Jorg van Loosdregt, Leo Koenderman, Sebastiaan J. Vastert, and Sytze de Roock..... 943
- Brief Report: The Genetic Profile of Rheumatoid Factor–Positive Polyarticular Juvenile Idiopathic Arthritis Resembles That of Adult Rheumatoid Arthritis
Anne Hinks, Miranda C. Marion, Joanna Cobb, Mary E. Comeau, Marc Sudman, Hannah C. Ainsworth, John Bowes, Juvenile Idiopathic Arthritis Consortium for Immunochip, Mara L. Becker, John F. Bohnsack, Johannes-Peter Haas, Daniel J. Lovell, Elizabeth D. Mellins, J. Lee Nelson, Ellen Nordal, Marilyn Punaro, Ann M. Reed, Carlos D. Rose, Alan M. Rosenberg, Marite Rygg, Samantha L. Smith, Anne M. Stevens, Vibeke Videm, Carol A. Wallace, Lucy R. Wedderburn, Annie Yarwood, Rae S. M. Yeung, Carl D. Langefeld, Susan D. Thompson, Wendy Thomson, and Sampath Prahalad..... 957
- Brief Report: Novel *UNC13D* Intronic Variant Disrupting an NF- κ B Enhancer in a Patient With Recurrent Macrophage Activation Syndrome and Systemic Juvenile Idiopathic Arthritis
Grant S. Schulert, Mingce Zhang, Ammar Husami, Ndate Fall, Hermine Brunner, Kejian Zhang, Randy Q. Cron, and Alexei A. Grom..... 963

Concise Communication

- Screening High-Resolution Computed Tomography of the Chest to Detect Interstitial Lung Disease in Systemic Sclerosis: A Global Survey of Rheumatologists
Elana J. Bernstein, Dinesh Khanna, and David J. Lederer..... 971

Letters

- Patient Perceptions of the Raynaud’s Condition Score Diary Provide Insight Into Its Performance in Clinical Trials of Raynaud’s Phenomenon: Comment on the Article by Denton et al
John D. Pauling, Lesley A. Saketkoo, and Robyn T. Domsic..... 973
- Reply
Christopher P. Denton and Ariane L. Herrick..... 974
- Consideration of Antisynthetase Syndrome Features in Classifying Patients as Having Idiopathic Inflammatory Myopathy: Comment on the Article by Lundberg et al
Santos Castañeda, Lorenzo Cavagna, and Miguel A. González-Gay, on behalf of the American and European Network of Antisynthetase Syndrome Collaborative Group..... 975
- Reply
Anna Tjärnlund, Matteo Bottai, and Ingrid E. Lundberg..... 976

ACR Announcements..... A19

Cover image: The figure on the cover (from Pottecher et al, page 942) shows a dual-energy computed tomographic image of the foot of a patient with paraparesis and severe gait impairment. DECT revealed bulky tophus formations in the feet (green), as well as the presence of urate in an extradural mass at T10.

In this Issue

Highlights from this issue of *A&R* | By Lara C. Pullen, PhD

Neutrophils Play Important Role in Systemic-Onset Juvenile Idiopathic Arthritis

Although systemic-onset juvenile idiopathic arthritis (JIA) has a clear autoinflammatory signature, very little is known about the role of neutrophils in the disease. **p. 943** In this issue, ter Haar et al (p. 943) report results from the first study to describe the phenotype, function, and transcriptome of neutrophils during the systemic inflammatory response of systemic-onset JIA. The investigators found that neutrophil counts were not only markedly increased at the onset of disease but their presence correlated with levels of inflammatory mediators. RNA-sequencing analysis demonstrated a substantial up-regulation of inflammatory processes in neutrophils from patients with active systemic-onset JIA. The pattern significantly

overlapped with the transcriptome of sepsis, suggesting that neutrophils play an important role in the early inflammatory phase of the disease.

Upon isolating neutrophils from patients with active systemic-onset JIA, the investigators found that the neutrophils displayed a primed phenotype characterized by increased reactive oxygen species production, CD62L shedding, and secretory vesicle degranulation. When they examined patients treated with recombinant interleukin-1 receptor antagonist (rIL-1Ra) therapy, however, they found that those patients had normalized neutrophil counts that occurred within days of initiating treatment. Moreover, the primed neutrophil phenotype was reversed as the patients achieved clinical remission.

The differences in neutrophils were also obvious when the researchers compared neutrophils from patients with short disease duration to those from patients who had experienced symptoms for >1 month. Specifically, patients with a short disease duration had high neutrophil counts, more immature neutrophils, and a complete response to rIL-1Ra compared to patients with more established disease. In addition, *in vitro* studies revealed that rIL-1Ra antagonized the priming effect of IL-1 β on neutrophils from healthy individuals. Taken together, the data support the hypothesis that neutrophils play an important role in systemic-onset JIA. Moreover, it appears that IL-1 blockade is an effective strategy to both reduce neutrophil numbers and decrease the inflammatory activity of systemic-onset JIA.

Ultrasound-Guided Synovial Biopsies Pave the Way for Precision Medicine for RA

Rheumatologists do not yet have reliable biomarkers that they can use to predict therapeutic response in patients with rheumatoid arthritis (RA). Since the most reproducible biomarker for RA to date is the reduction in the numbers of sublining synovial macrophages, researchers have come to believe that a precision medicine advancement in the treatment of RA will likely hinge on the ability to obtain quality samples from the joint. If this is true, rheumatologists will need a clinically actionable method to collect synovial tissue of a high enough quality that it can be analyzed using high-throughput strategies. New advances in ultrasound technology may make this possible by facilitating minimally invasive ultrasound-guided synovial tissue biopsy.

In this issue, Mandelin et al (p. 841) report the results of their study that was designed to evaluate the use of ultrasound-guided synovial biopsy in RA. Their findings suggest that rheumatologists could feasibly obtain synovial tissue biopsy specimens that are of



Figure 1. Ultrasound-guided synovial biopsy of an inflamed wrist using an 18-gauge \times 1.5-inch needle.

high enough quality that they can be analyzed using cutting-edge technologies. Moreover, they found that ultrasound-guided synovial biopsy was well tolerated, with patients reporting minimal adverse effects. When the investigators compared synovial tissue and isolated macrophages from patients with RA and patients with osteoarthritis, they found that the RNA was of comparable quality between the 2 groups.

Whole tissue samples from patients with RA exhibited a high degree of transcriptional heterogeneity. However, in a more detailed sample analysis, the transcriptional profile of isolated RA synovial macrophages indicated that there was a subpopulation of patients who expressed 6 novel transcriptional modules that were associated with disease activity and therapy. The investigators concluded that such samples could theoretically be combined with corresponding clinical information to create a precision medicine-based approach to the treatment and management of RA.

Rheumatoid Arthritis: Switching From Adalimumab to Biosimilar Is OK

In this issue, Weinblatt et al (p. 832) report their analysis of transition data from a 52-week randomized trial of adalimumab (ADA) and the biosimilar SB5. They analyzed data from 542 patients (273 in the ADA overall group, 269 in the SB5 group; 129 in the ADA/ADA group, and 125 in the ADA/SB5 group). The percentage of patients meeting the American College of Rheumatology 20% improvement criteria (ACR20) at week 24 was the primary

p. 832

efficacy assessment in an earlier phase of the study. In the current phase the researchers found that the percentage of patients who met this end point, as well as the percentages meeting the ACR50 and ACR70, after the transition from ADA to SB5 were maintained through 52 weeks. Moreover, the response rates were comparable across treatment groups throughout the study. For example, the ACR20 response rate at week 52 ranged from 73.4% to 78.8% across all treatment groups. The ACR20, ACR50, and

ACR70 response rates were similar to those previously described for ADA.

When the investigators measured radiographic progression, they found that it also was minimal and comparable across treatment groups. SB5 was also well tolerated in patients with RA such that when the investigators switched patients from ADA to SB5, they did not see any treatment-emergent issues such as increased adverse events, increased immunogenicity, or loss of efficacy.

Genetic Profile of Rheumatoid Factor–Positive Polyarticular Juvenile Idiopathic Arthritis

Juvenile idiopathic arthritis (JIA) is a diagnosis that encompasses 7 heterogeneous categories of chronic childhood arthritides.

Approximately 5% of children with JIA have rheumatoid factor (RF)–positive arthritis, and these children phenotypically resemble patients with adult rheumatoid arthritis (RA). In this issue, Hinks et al (p. 957) describe the results of the largest genetic study of RF-positive polyarticular JIA to date. They focused their efforts on determining whether any of the previously associated RA loci or oligoarticular/RF-negative polyarticular JIA loci were associated with RF-positive polyarticular JIA. Their intention was to more fully understand the pathophysiologic relationships of inflammatory arthropathies.

The investigators noted that the HLA region was strongly associated with RF-positive polyarticular JIA. When they looked more closely, they found that 19 of 44 RA risk loci and 6 of 27 oligoarticular/RF-negative polyarticular JIA risk loci were associated with RF-positive polyarticular JIA. When they calculated a weighted genetic risk score (wGRS) of RA, they found that it was better at predicting RF-positive polyarticular JIA than was the wGRS of oligoarticular/RF-negative polyarticular JIA. Moreover, the genetic profile of patients with RF-positive polyarticular JIA was more like that of patients with RA with an onset age of 16–29 years than that of patients with RA with an onset age of ≥ 70 years. Thus, the researchers found that RF-positive

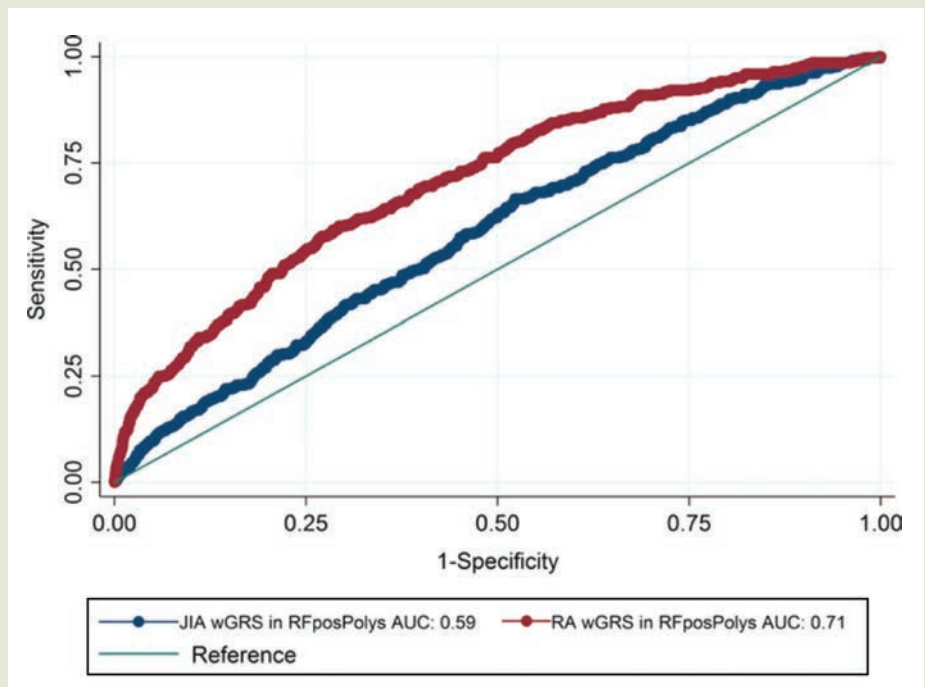


Figure 1. Comparison of the wGRS generated using loci associated with the highest risk of RA with the wGRS generated using loci associated with the highest risk of oligoarticular/RF-negative polyarticular JIA for the purpose of predicting cases of RF-positive polyarticular JIA (RFposPolys). AUC = area under the curve.

polyarticular JIA is genetically more similar to adult RA than to the most common JIA categories. The authors concluded from this that RF-positive polyarticular JIA appears to be a childhood-onset presentation of autoantibody-positive RA. If true, this would suggest that there is a common disease mechanism that could point toward novel therapeutic targets and shared treatment strategies.

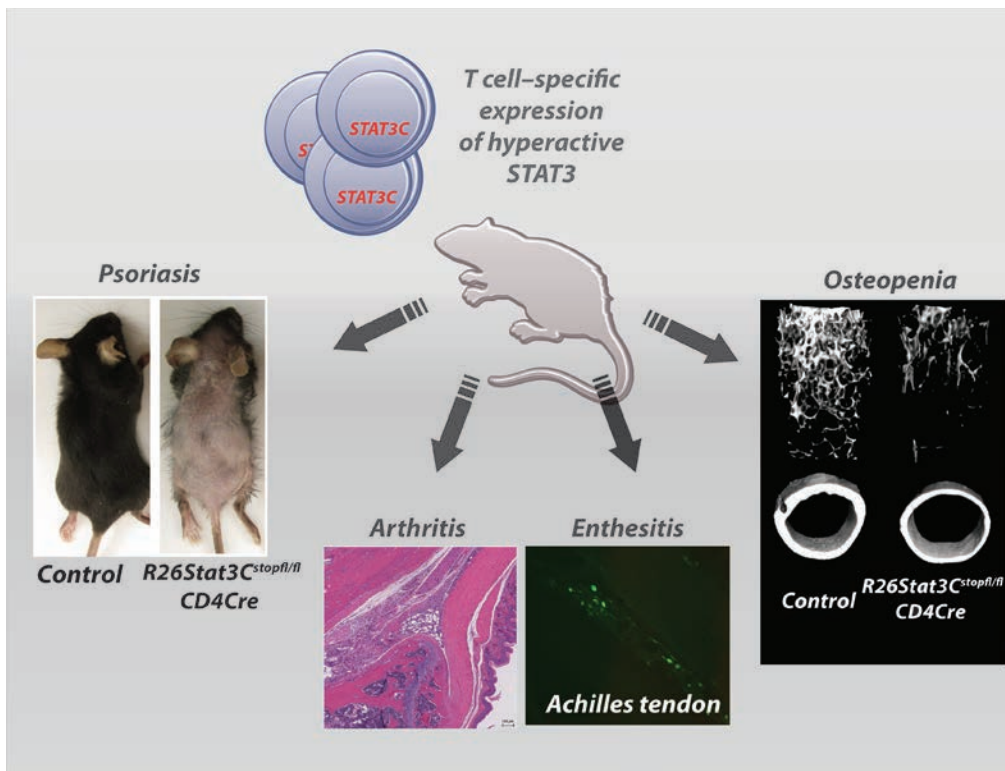
Clinical Connections

Augmented Th17 Differentiation Leading to Cutaneous and Synovio-Enthesal Inflammation in a Novel Model of Psoriatic Arthritis

Yang et al, *Arthritis Rheumatol* 2018;70:855–867.

CORRESPONDENCE

Sergei B. Koralov, PhD: sergei.koralov@med.nyu.edu



KEY POINTS

- Mice with T cell-specific overexpression of a hyperactive STAT3 allele faithfully recapitulate many of the characteristic clinical features of PsA, including entesitis.
- An increase in osteoclast progenitor cells and RANKL-producing cells promotes osteopenia in these mice.
- Inhibiting Th17 effector cytokines IL-17 and IL-22 ameliorates the disease of R26Stat3C^{stopfl/fl} CD4Cre mice.

SUMMARY

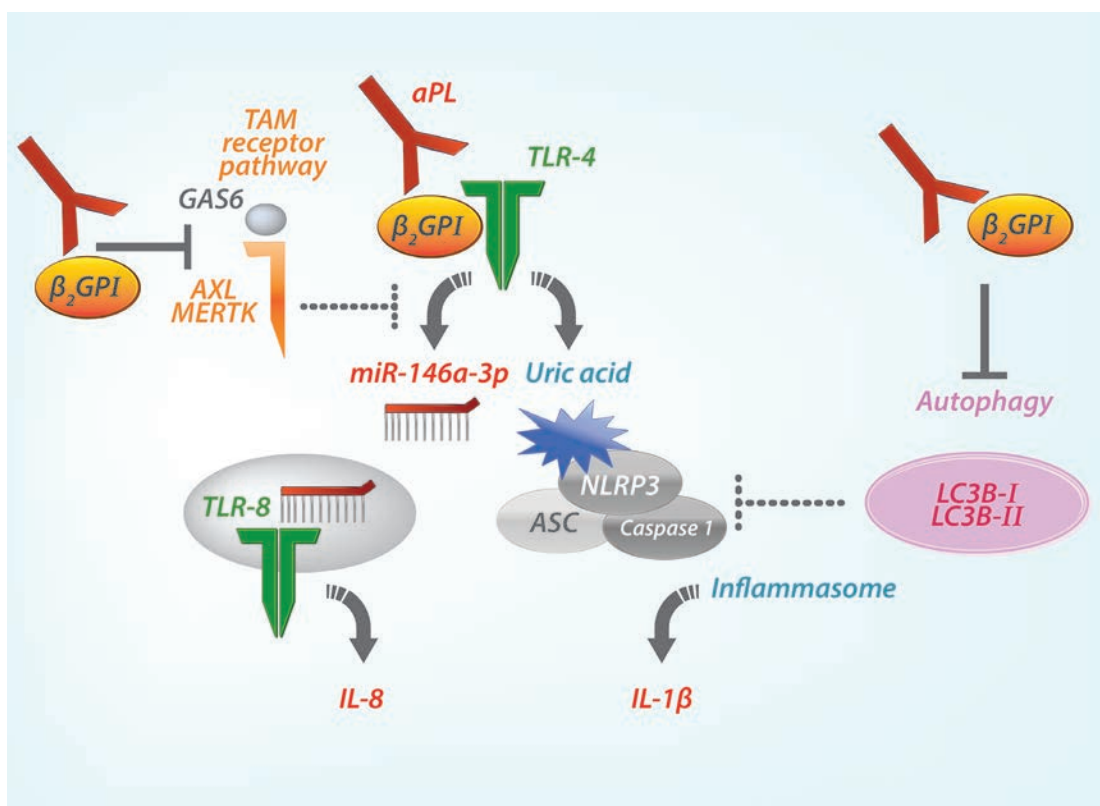
Psoriatic arthritis (PsA) is a debilitating disease characterized by chronic inflammation of the skin and joints. T helper subset 17 (Th17) cells, which produce interleukin-17 (IL-17), have been previously implicated in chronic inflammatory diseases, including psoriasis and PsA. Yang and colleagues have generated and characterized a novel PsA mouse model, R26Stat3C^{stopfl/fl} CD4Cre, in which T cell-specific expression of a hyperactive STAT3 allele drives augmented Th17 responses. STAT3 is a critical mediator of cytokine signaling and is important in the regulation of T cell differentiation. Chronic Th17-mediated inflammation leads to the development of psoriasis, entesitis, arthritis, and osteopenia in these animals, recapitulating many of the salient features of PsA. Upon closer examination, the authors observed an increase in the percentage of osteoclast progenitors and RANKL-producing cells in the bone marrow of these mice, promoting the differentiation of bone-resorbing osteoclasts. Blocking Th17 effector cytokines IL-17 and IL-22 ameliorated the disease phenotypes observed in this novel mouse model of PsA.

Antiphospholipid Antibodies Inhibit Trophoblast Toll-Like Receptor and Inflammasome Negative Regulators

Mulla et al, *Arthritis Rheumatol* 2018;70:891–902.

CORRESPONDENCE

Vikki M. Abrahams, PhD: vikki.abrahams@yale.edu



KEY POINTS

- aPL inhibit basal trophoblast TAM receptor signaling and autophagy.
- Disabling of the TAM receptor pathway by aPL results in TLR-4 activation, leading to subsequent TLR-8-mediated IL-8 release.
- Impaired basal autophagy by aPL allows inflammasome activity, leading to IL-1 β production

SUMMARY

Women with antiphospholipid antibodies (aPL) are at risk for pregnancy complications associated with poor placentation and placental inflammation, but our understanding of the mechanisms involved is incomplete. aPL recognizing β_2 -glycoprotein I (β_2 GPI) activate placental trophoblast Toll-like receptor 4 (TLR-4), leading to microRNA-146a-3p/TLR-8-mediated interleukin-8 (IL-8) secretion and uric acid/NLRP3-mediated IL-1 β production. Despite these triggers, the trophoblast does not generate a classic inflammatory response to the TLR-4 activator, lipopolysaccharide. It appears that trophoblast TLR-4 function and subsequent inflammasome activation is tightly controlled, and aPL override this braking mechanism. Mulla and colleagues show that human trophoblast TLR and inflammasome function are tightly regulated by immunomodulatory pathways—TAM receptor activity and autophagy. Disabling of the TAM receptor signaling pathway by aPL results in TLR-4 activation, leading to TLR-8-mediated IL-8 release, while impaired autophagy by aPL allows inflammasome activity, leading to IL-1 β production. These advances in the understanding of the mechanisms by which aPL drive placental inflammation may guide predictive markers and therapeutic targets for preventing obstetric antiphospholipid syndrome.

Arthritis & Rheumatology

An Official Journal of the American College of Rheumatology
www.arthritisrheum.org and wileyonlinelibrary.com

EDITORIAL

Ensuring the Future of Rheumatology: A Multi-Dimensional Challenge and Call to Action

William F. Harvey,¹ Afton L. Hassett,² and Sharad Lakhanpal³

The article by Bolster et al in this issue of *Arthritis & Rheumatology* (1) and an article by Battafarano et al recently published in *Arthritis Care & Research* (2) project a startling picture of the future of the rheumatology workforce in the US. The 2015 Rheumatology Workforce study describes how, based on a variety of contributing factors, there will be inadequate numbers of practicing rheumatologists and rheumatology health professionals to care for patients with rheumatic and musculoskeletal diseases in the coming years. It further describes how limitations in our training pipeline may exacerbate this situation. These two important articles serve as a call to action to understand and address the wide range of factors that contribute to these issues. This will require important strategic initiatives by professional societies, government, practice groups, and training programs in order to assure a healthy and vibrant rheumatology workforce. Indeed, the new strategic plan for the American College of Rheumatology (ACR) represents an important starting point for this process. In this editorial, we will summarize some key workforce study findings presented in the articles by Bolster et al (1) and Battafarano et al (2) and highlight some of the key strategies to consider as we rise to meet these challenges.

Key factors affecting the rheumatology workforce

The 2015 Rheumatology Workforce Study highlighted several factors that underlie the challenges

ahead, which can best be summarized as monumental problems with both supply and demand. The demand for rheumatologists will be driven by the changing demographics of the US. As described by Battafarano et al (2), predictably, as our population ages and the prevalence of some rheumatic diseases increases, we will need more providers to care for these patients. More intriguing, however, are some heretofore undescribed supply factors that will have a dramatic impact. The same aging demographic that will result in increasing the prevalence of rheumatic disease will also lead to the impending retirement of a significant portion of our workforce. The generations of baby boomers and their children are proportionately larger than the generations that follow, resulting in a shrinking workforce.

Perhaps one of the most important contributions of this workforce study are the novel findings based on two other important demographic shifts. Our specialty is privileged to be an attractive one for women; this is to the betterment of our society and to the population of women who are often disproportionately affected by autoimmune diseases. Women in medicine tend to feel the responsibilities of maintaining a work-life balance more acutely than men do. As such, many women in medicine choose to work part time. Factoring this reality into the data is a major methodologic advance represented in the 2015 Rheumatology Workforce Study. There are also newly anticipated generational differences, with millennials of both sexes expected to place even greater value on work-life balance in a way that will also result in more providers choosing not to work full time. The answer to this is not to question their work ethic or dedication, but rather to embrace strategies that will welcome more millennials into the workforce. Necessarily, a wide array of actions will be needed and every rheumatologist and rheumatology health professional has a role to play in our future, as

¹William F. Harvey, MD, MSc: Tufts Medical Center, Boston, Massachusetts; ²Afton L. Hassett, PsyD: University of Michigan, Ann Arbor; ³Sharad Lakhanpal, MD: Rheumatology Associates and UT Southwestern Medical Center, Dallas, Texas.

Address correspondence to Sharad Lakhanpal, MD, Rheumatology Associates, 8144 Walnut Hill Lane, Suite 800, Dallas, TX 75231. E-mail: lakhanpal@arthdocs.com.

Submitted for publication January 23, 2018; accepted January 24, 2018.

do our professional societies, our government, and our patients. We will highlight some of the most important actions we can take to help avert the predictions given in the two workforce study articles.

Improve recruitment and training

When we reflect on how we chose rheumatology, often we can point to an experience during our training. It was frequently a caring mentor, a challenging case, an inspirational attending physician, or early exposure to the intriguing nature of rheumatology that was most influential. Medical training necessarily focuses on the breadth of the field, but we must ensure that exposure to rheumatology happens in a meaningful way throughout the long journey of training. All medical school graduates should attain a basic level of knowledge and skills about rheumatic and musculoskeletal diseases during undergraduate medical education. Further, fundamental musculoskeletal and rheumatology curricula should be included in primary care residency training programs.

We need to elevate rheumatologists to positions of prominence in communities, hospitals, universities, and departments of medicine. As medical school curricula shift to earlier exposure to clinical experience, we need rheumatologists volunteering as small group preceptors, physical examination instructors, and career mentors. We need rheumatology practitioners to reach out to local schools and communities and engage in the unique and invaluable mentorship and teaching that they can provide. We need curricula that highlight the depth and complexity of medicine embodied in our specialty. We need our women and men to support all students, trainees, and faculty, but especially women and underrepresented minorities at each stage of their career so that they see our specialty as their natural home within medicine. There is a need for rheumatology mentoring of medical students and residents.

We challenge every rheumatologist, in academic settings or private practice, to find a way to inspire a new trainee in our field. Further, when we are successful in our endeavors to inspire the next generation of rheumatology professionals, we need adequate numbers of and funding for training programs. While the number of students entering medical school has risen substantially, the number of residency and fellow training slots has not. There is a need for increased graduate medical education funding to add more rheumatology fellowship training programs. That likely will require both new and larger programs and a renewed commitment from governments, universities, and professional organizations such as the

ACR, Rheumatology Research Foundation (RRF), and Arthritis Foundation, to step up and provide funding.

Address retention and distribution

Less often discussed is the distribution of rheumatologists within the country, and this is particularly evident in pediatrics. There are a significant number of states without a single pediatric rheumatologist, and most pediatric rheumatologists work in academic and urban settings. Even in states like Massachusetts with robust numbers of rheumatologists, there are localities across the state and in neighboring ones where “rheumatology deserts” exist. Encouraging qualified candidates from underserved areas to enter rheumatology training may help mitigate shortages in those areas, since these new trainees will be more likely to go back to their native regions. Therefore, we must strive to create new rheumatology training programs in regions that do not have one while also creating more training positions nationally. In many specialties, including family medicine, data suggest that trainees are most likely to practice within 50–100 miles of their training program (3), and so more training positions in Boston, New York, and San Francisco cannot be the only approach. We also need to focus on creating incentives, government and otherwise, for rheumatology providers to choose to practice where they are most needed. There is a need to enable international rheumatology trainees to stay in the US and not have to return to their home countries after training. Visa programs should be developed that will allow international trainees to stay here and encourage them to work in underserved areas. Finally, student loan forgiveness programs, especially for pediatric rheumatology, will help to attract bright young physicians into rheumatology.

Promote scientific discovery

Rheumatology saw a boom in interest following the advent of biologic therapies. The impact of these therapies on our patients and our specialty cannot be overstated; however, it is likely that some of the decreased interest in our specialty in recent years is due to two related factors (4). The first factor is the lack of new therapies in many disease areas. There were only one or two novel drugs approved in rheumatology in each of the last three years. Second, there is a marked slow-down in investment in research. The breakthrough therapies that will entice the next generation to enter our field are threatened by inadequate funding for biomedical research that fails to keep pace with general economic indices of growth. Decline in funding also threatens the pipeline of

the next generation of rheumatology researchers who will make the discoveries and treat the patients who will desperately need our services. There seems to be a trend among academic rheumatologists to move into private practice for financial reasons and better job security. This is a challenge when we need to add to and develop new training programs. Thus, there is a critical need for increased funding for rheumatology research in order to realize the cures our patients envision and increase faculty retention to train future rheumatology professionals.

Tackle reimbursement and payment redesign

Rheumatologists earn less than many other specialists in medicine (5), and with the rising cost of medical training (6) many potential candidates choose more lucrative specialties. Therefore, our efforts to improve reimbursement for services not only affect the health of existing practices but incentivize future generations. The ACR and many other organizations spend a great deal of time advocating for changes to provider reimbursement with this fact in mind. As the payment paradigm shifts from fee for service to value-based payment, we see both threats and opportunities. Current programs designed to create value-based incentives, such as the Physician Quality Reporting System, the Merit-based Incentive Payment System, and Accountable Care Organizations, are wholly inadequate with respect to appropriate recognition of and reimbursement for the scope of services we provide. Because we believe unquestionably that rheumatologists provide the best value to patients with rheumatic diseases, the ACR seeks to develop payment models designed by, and intended for, practicing rheumatologists. By shifting partially away from office-based encounters to supporting important activities such as care coordination, consultation expertise, telephone and telemedicine encounters, and multidisciplinary care teams, physician-focused payment models could help us do more with less.

Leaders in government do not understand how best to care for patients with rheumatic disease, and so we must continue efforts in advocacy to educate them and provide solutions and a path forward. We should advocate to reduce administrative and practice hassles by reducing insurance barriers and health care regulations. A fair amount of time is spent every day in these unproductive activities by providers and their staff. If these could be eliminated, more time could be spent by rheumatologists and rheumatology health care providers in patient care. It may also encourage physicians considering retirement for these reasons to continue in the workforce. Elimination of these barriers to patient care may incentivize retired

rheumatologists and care providers to consider returning to work in part-time or locum positions.

Enhance workforce diversity

The stark numbers presented by both Bolster et al (1) and Battafarano et al (2) require innovative solutions. Even doubling the number of trainees completing fellowship programs will be insufficient. Creating a new payment model that helps us keep patients who don't need it out of the hospital and, to some extent, out of our offices will likewise be insufficient. To meet the looming workforce shortage we will need to find new ways to work with other physicians and other health professionals to supplement the care we provide. The current state of education for nurse practitioners (NPs) and physician assistants (PAs) largely misses rheumatology, and this will have to change. Practices wishing to hire these individuals must often train them on the job with few resources. To promote the preparation of NPs and PAs for the care of our patients, the Association of Rheumatology Health Professionals (ARHP) recently developed the NP/PA Rheumatology Curriculum Outline. To help support the costs of training, the RRF will support Mentored NP/PA Education Awards to help bring these high-value providers on board. Yet, too few NPs and PAs are drawn to rheumatology—this is due in part to a lack of outreach and exposure to educational programs. Effective outreach and promotion of the benefits of the field are required. Revisiting practice models will be required to maximize the workforce. For example, physical and occupational therapists, nurses, behavioral scientists, and practice managers trained in maximizing reimbursement and efficiency are poised to have an important impact as well. Many of these efforts are well underway, but more must be done.

Conclusions

The ACR and the ARHP have several key missions, among them education, research, advocacy, and patient care. It is easy to see that meeting the projected workforce shortage requires activity from the full breadth of our efforts. The latest ACR strategic plan (7) challenges the entire College to understand how the work they do will benefit our workforce and increase the numbers of rheumatologists and rheumatology health professionals available to meet this need. We will likewise need training programs and their academic affiliates to work at local levels to bolster our numbers. And because the practice community represents the linchpin of our connection to patients and communities, we will need to find more ways to ensure their survival and create opportunities for

growth. The ACR and ARHP remain focused on ensuring a vibrant future for our providers and for the growing number of patients who will surely need us.

AUTHOR CONTRIBUTIONS

All authors drafted the article, revised it critically for important intellectual content, and approved the final version to be published.

REFERENCES

1. Bolster MB, Bass AR, Hausmann JS, Deal C, Ditmyer M, Greene KL, et al. 2015 American College of Rheumatology workforce study: the role of graduate medical education in adult rheumatology. *Arthritis Rheumatol* 2018;70:817–25.
2. Battafarano DF, Ditmyer M, Bolster MB, Fitzgerald JD, Deal C, Bass AR, et al. 2015 American College of Rheumatology workforce study: supply and demand projections of adult rheumatology workforce, 2015–2030. *Arthritis Care Res (Hoboken)* 2018;70:617–26.
3. Fagan EB, Gibbons C, Finnegan SC, Petterson S, Peterson LE, Phillips RL Jr, et al. Family medicine graduate proximity to their site of training: policy options for improving the distribution of primary care access. *Fam Med* 2015;47:124–30.
4. Al-Ansari SS, Khafagy MA. Factors affecting the choice of health specialty by medical graduates. *J Family Community Med* 2006;13:119–23.
5. Grisham S. Medscape Rheumatologist Compensation Report 2017. URL: <https://www.medscape.com/slideshow/compensation-2017-rheumatology-6008588>.
6. Grischkan J, George BP, Chaiyachati K, Friedman AB, Dorsey ER, Asch DA. Distribution of medical education debt by specialty, 2010–2016. *JAMA Intern Med* 2017;177:1532–5.
7. American College of Rheumatology. ACR 2017–2022 strategic plan. URL: <https://www.rheumatology.org/Portals/0/Files/ACR-Strategic-Plan.pdf>.

EDITORIAL

STATus of STAT3 in Psoriatic Arthritis

John D. Mountz

Joint disease and enthesopathy are seen in about one-third of patients with psoriasis and are usually preceded by the cutaneous manifestations of psoriasis. However, the relationships between the pathogenesis of psoriatic skin disease and pathogenesis of psoriatic arthritis have not been defined, and the central question as to whether psoriatic skin disease initiates development of joint disease remains unresolved. It has been shown that constitutive hyperexpression of STAT3 using a STAT3C construct targeted to keratinocytes is sufficient to induce cutaneous psoriasis-like lesions. When combined with global expression of a mutant form of the gp130 allele, a cytokine receptor signal transducer, the STAT3C construct leads to arthritis in mice (1,2). In this issue of *Arthritis & Rheumatology*, Yang and colleagues introduce a new mouse model that is unique in that it embodies all of the major features of cutaneous psoriasis and psoriatic arthritis, including skin disease, joint disease, and an enthesopathy, as well as osteopenia (3). This experimental disease model also is based on constitutive hyperexpression of STAT3 using the STAT3C construct, but in this case, the targeting of the construct to CD4⁺ T cells has been found to be sufficient to induce all of the manifestations.

STAT3 signaling plays a key role in normal cell functions, including cell growth, survival and proliferation, apoptosis, and inflammation. It is activated by numerous cytokines and growth factors through JAK-mediated phosphorylation of tyrosine-705 or phosphorylation of serine-727 through a variety of serine/threonine protein kinases (MAP kinase, mechanistic target of rapamycin, and protein kinase C δ), which is required for maximal STAT3 transcriptional activity. The STAT-3 proteins occur as inactive monomers in the cytoplasm until their phosphorylation,

which prompts their dimerization. The dimers are translocated to the nucleus, where they bind to specific DNA elements that regulate transcription of an array of genes. Almost 2 decades ago, Darnell and coworkers engineered the constitutively dimerizable STAT3 molecule, STAT3C, by substituting cysteine residues for tyrosine within the C-terminal loop of the SH2 domain of the STAT3 molecule (4). STAT3C was shown to drive transcription, not only stimulating cell growth and proliferation but also promoting transformation. Subsequently, naturally occurring constitutive activation of STAT3 has been identified in several human malignancies.

STAT3C should not be confused with the naturally occurring isoforms of STAT3 function that result from an alternative splicing event of STAT3 at exon 23. This results in the expression of a truncated form of STAT3 (STAT3 β) (5) that lacks serine-727. Although initially thought to act in a dominant-negative manner, it is a biologically active molecule capable of modulating the tumorigenic functions of STAT3. The differential expression of these 2 isoforms represents just one aspect of the complex network of mechanisms that regulate the magnitude of STAT3 signaling and that modify its effects on transcription in a manner that depends on physiologic conditions and cellular context. Thus, a limitation of the use of the constitutively active STAT3C construct is that it not only exaggerates STAT3 activity but also functions independently of many of these biologically relevant regulatory constraints. Nevertheless, the use of STAT3C in mouse models of diseases has proven useful in providing novel insights into potential pathogenic pathways.

As described above, the constitutive hyperexpression of STAT3 in keratinocytes alters the proliferation and development of the keratinocytes, resulting in the hyperkeratosis characteristic of skin psoriasis as well as psoriasis-like inflammation of the skin. In this keratinocyte mouse model, the dysregulated growth of the keratinocytes induces an influx of macrophages that produce interleukin-6 (IL-6) and IL-1, which, in the context of the dysregulated cytokine milieu, promotes the development of the characteristic inflammatory skin response, including development of Th17 and Th22 cells. In

Supported by the NIH (grant R01-AI-071110) and the US Department of Veterans Affairs (grant 1I01BX000600-01).

John D. Mountz, PhD, MD: University of Alabama at Birmingham.

Address correspondence to John D. Mountz, PhD, MD, Division of Clinical Immunology and Rheumatology, Department of Medicine, Shelby Interdisciplinary Biomed Research Building, Room SHEL 307, 1825 University Boulevard, Birmingham, AL 35294. E-mail: jdmountz@uab.edu.

Submitted for publication January 11, 2018; accepted in revised form February 6, 2018.

conjunction with the gp130 mutation, this inflammatory response is sufficient to elicit joint disease. The newly introduced model of STAT3C expression in CD4⁺ T cells provides an alternative paradigm in which STAT-associated dysregulation of CD4⁺ T cells can act as a primary initiating event that drives inflammatory skin disease and hyperkeratosis, as well as joint involvement (Figure 1).

Yang and colleagues provide a detailed description of the disease manifestations in their current report. In terms of the potential pathogenic mechanism, they focus primarily on the examination of the role of STAT3-driven augmentation of the activity of the Th17 cell subset of CD4⁺ T cells. The role of IL-22 is examined through use of IL-22-knockout mice. While Th17 cells produce IL-22 as well as IL-17, IL-22 is produced predominantly by a distinct lineage of CD4⁺ T cells (Th22 cells). Increased

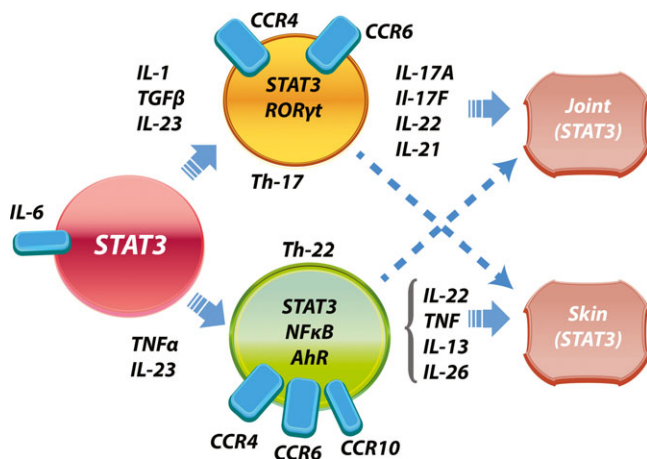


Figure 1. Promotion of psoriasis and psoriatic arthritis by STAT3 in CD4⁺ T cells. In the current study by Yang and colleagues (3), the authors demonstrated that constitutive hyperexpression of the STAT3 gene in mouse CD4⁺ T cells was sufficient to promote psoriasis-like skin disease, psoriasis-like arthritis, and enthesopathy. Taken together with other data, the results suggest a model in which constitutive expression of STAT3, with or without interleukin-6 (IL-6) signaling, promotes an inflammatory environment, including the production of IL-1, transforming growth factor β (TGF β), and IL-23, which promote the development and differentiation of Th17 cells (upper pathway). The same conditions in the presence of tumor necrosis factor (TNF) and IL-23 lead to the sustained development of Th22 T cells (lower pathway). Th17 cells express the characteristic transcription factors STAT3 and retinoic acid receptor-related orphan nuclear receptor γ t (ROR γ t), the chemokine receptors CCR4 and CCR6, and the cytokines IL-17A, IL-17F, IL-22, and IL-21. Collectively, these promote development of a psoriasis-like arthritis, and individuals with higher STAT3 transcriptional activity are more susceptible to joint disease (upper pathway). Th22 cells express the canonical transcription factors STAT3, NF- κ B, and aryl hydrocarbon receptor (AhR), the chemokine receptors CCR4, CCR6, and CCR10, and the cytokines IL-22, TNF, IL-13, and IL-26. Collectively, these promote development of skin psoriasis, and individuals with high STAT3 transcriptional activity are more likely to develop skin disease (lower pathway).

frequencies of IL-22-producing cells with characteristics of Th22 cells are a feature of psoriasis and psoriatic arthritis, in addition to the increased frequencies of Th17 cells (6). Cytokine-induced STAT3 signaling has been shown to play a role in the development, differentiation, and expansion of both Th17 and Th22 cells. It is increasingly clear that although Th17 and Th22 cells share many commonalities, their differences extend well beyond their cytokine expression profile. Commonalities include the fact that both cell subsets are induced by IL-6-mediated up-regulation of STAT3. Furthermore, both Th17 and Th22 cells rely on IL-23 for sustained activity and differentiation, which is of great interest since genetic susceptibilities associated with IL-23 and the IL-23 receptor have been reported both in psoriasis and in psoriatic arthritis. Moreover, both cell subsets express the chemokine receptors CCR6 and CCR4.

Differences between Th17 and Th22 cells include the fact that development of Th17 cells is induced/promoted by IL-6 in combination with transforming growth factor β and IL-1 signaling (7), whereas Th22 T cell development is induced/promoted by IL-6 in combination with tumor necrosis factor (TNF) signaling. IL-23 induction leads to the production of IL-17A, IL-17F, and IL-22, as well as TNF, IL-6, IL-21, and IL-26, by Th17 cells, whereas it leads to the production of IL-22 and TNF, as well as IL-13 and IL-26, by Th22 cells. Furthermore, Th22 cells, but not Th17 cells, express CCR10 in addition to CCR6 and CCR4, and also express the aryl hydrocarbon receptor (AhR).

Analysis of samples from patients with psoriasis has indicated increased levels of IL-22 and Th22 cells in the involved skin or peripheral blood (7). Somewhat surprisingly, the numbers of Th22 cells are very low in the involved joints of patients with psoriatic arthritis (7), although they are high in the involved joints of ~60% of patients with rheumatoid arthritis (RA) (8). These differences could potentially reflect the relative ability of the microenvironment at the different sites to promote or sustain Th22 cells when compared to Th17 cells. It also has been suggested that preferential homing of subpopulations of T cells, including Th17 and Th22 cells, to specific sites may affect the manifestation of skin symptoms in psoriasis, and also may affect the differences in the arthritis phenotype associated with psoriatic arthritis when compared to RA. Although Th17 and Th22 cells share some chemokine receptors, Th22 cells also express CCR10 and skin-specific homing receptors that have been described in psoriasis (9). Further analysis of the new model may provide insights into this critical question.

An unexpected finding in the study by Yang et al (3) was that when the mice with constitutive hyperexpression of Stat3 in CD4⁺ T cells were backcrossed to IL-22-knockout

mice, a significant reduction in the psoriatic arthritis manifestations, as well as a reduction in the skin phenotype, was observed. Whereas the observed reduction in the skin phenotype in these mice is consistent with prior evidence showing that IL-22 has a more prominent effect on psoriatic skin disease, joint disease has been more closely associated with IL-17. An association between IL-17, RANK ligand expression, and osteoclastogenesis is well established. Based on the observed reduction in RANK ligand levels in the IL-22–knockout mice, the authors speculated that this previously undescribed role for IL-22 in psoriatic joint disease could be attributed to the ability of IL-22 to stimulate RANK ligand expression. This was based on findings from a previous study demonstrating that IL-22 stimulated RANK ligand expression in synoviocytes from patients with RA, and IL-22–treated fibroblasts stimulated osteoclast differentiation from monocytes in the absence of RANK ligand (8). As mentioned above, the increase in the number of Th22 cells was more prominent in the joints of patients with psoriatic arthritis compared to those with RA. Thus, the intriguing finding of a potential role for IL-22 in psoriatic joint disease will need to be further evaluated to determine the extent to which the mouse model corresponds to psoriatic joint disease in humans.

A key feature of the newly introduced model is the description of the development of an enthesopathy. Enthesopathy is one of the initial features that can be used to clearly distinguish psoriatic arthritis from RA (10). The understanding of the interrelationship between the enthesis and synovium and its significance is evolving. A close anatomic integration between the enthesis and synovium, resulting in a synovio-enthesal complex, has been described (11). It has been proposed that the enthesis fibrocartilage that is located adjacent to synovium, such as in the joints, bursa, or tendons, is dependent on the synovium for lubrication and nutrition. The enthesis functions to stiffen the tendon or ligament and helps to create a more gradual change in mechanical properties between soft and hard tissues. The enthesis insert itself is a vascularized fibrocartilaginous structure, although it is unclear if the close association with the joint can lead to inflammation in the adjacent vascular synovium. Which of the novel features of this mouse model leads to the enthesopathy is unclear and is a subject for future investigation.

Limitations of the current analysis by Yang and colleagues (3) examining the pathogenesis of psoriatic arthritis in a mouse model mirror those in analyses of human psoriasis and psoriatic arthritis; however, ultimately, the model may provide resolution of some of the outstanding questions. Questions remaining include the need to fully understand the functional consequences of the localized production of multiple cytokines by Th17 and Th22 cells,

which have not been explored fully to date. Of importance, this mouse model of psoriatic arthritis also may enable informative analysis of the heterogeneity and plasticity of CD4⁺ T cells within the specific pathogenic settings. The Th17 cell population is heterogeneous in terms of the levels of production of the signature cytokines. In psoriasis, there are at least 3 subpopulations of Th17 cells that are characterized by their production of both IL-22 and IL-17, or production of only IL-17 or only IL-22 (7). This is consistent with the finding that in the BXD2 mouse model of arthritis, CD4⁺ spleen T cells produce either IL-17 or IL-21, but not both (12). The basis for the propensity of individual Th17 and Th22 cells to produce one cytokine is unknown, but may reflect prior signaling interactions that modulate the activity of STAT3 or other transcription factors, such as AhR (13) or retinoic acid receptor–related orphan nuclear receptor γ t. Although the mouse model would enable informative single-cell analyses by excluding the levels of “noise” intrinsic in patient samples, it is possible that the STAT3C construct bypasses these modulating effects and favors the development of specific subpopulations. Testing of the role of single-nucleotide polymorphisms in modifying the downstream effects of STAT transcription should be possible, however.

As in human psoriasis and psoriatic arthritis, the collection of features manifested in the mice described in the Yang article raises the question as to which features are primary events and which are secondary. Resolution of this issue is central to the development of effective therapeutic strategies. This extends beyond the potential cascade of events that could be initiated by dysregulated cytokines and circulating immune cells. One example is the potential release of endogenous proinflammatory mediators from a primary site that then induces responses at secondary sites. This possibility has been invoked in terms of the postulated initiation of psoriatic arthritis by the compromised synovio-enthesal complex (11).

A second example is the question of the role of the altered microbiota that has been observed in psoriasis and patients with psoriatic arthritis (14). AhR, which is highly expressed by Th22 cells and regulates their expansion, recognizes numerous naturally occurring molecules, including dietary flavonoids and common bacteria, as well as xenobiotics, including dioxin. IL-22–producing cells have been shown to be central to maintenance of the intestinal barrier, and STAT3/T helper cell down-regulation of IL-22 compromises the gut barrier (15). It would be important to develop a method of testing in which the primary effects of the altered microbiome in disease could be differentiated from the secondary effects. This concept was recently highlighted by findings that negated those in previous reports of an altered microbiome in mice with inflammasome deregulation (16).

In summary, the new mouse model characterized by Yang et al (3) highlights the importance of STAT3 signaling in psoriasis and psoriatic arthritis. As in cancer, this should provide a framework for analysis of pathogenesis and disease susceptibility, although therapeutic targeting of STAT3 has proven difficult to date, due to its central importance in so many critical biologic processes.

AUTHOR CONTRIBUTIONS

Dr. Mountz drafted the article, revised it critically for important intellectual content, and approved the final version to be published.

REFERENCES

1. Sano S, Chan KS, Carbajal S, Clifford J, Peavey M, Kiguchi K, et al. Stat3 links activated keratinocytes and immunocytes required for development of psoriasis in a novel transgenic mouse model. *Nat Med* 2005;11:43–9.
2. Yamamoto M, Nakajima K, Takaishi M, Kitaba S, Magata Y, Kataoka S, et al. Psoriatic inflammation facilitates the onset of arthritis in a mouse model. *J Invest Dermatol* 2015;135:445–53.
3. Yang L, Fanok MH, Mediero-Munoz A, Fogli LK, Corciulo C, Abdollahi S, et al. Augmented Th17 differentiation leads to cutaneous and synovio-entheseal inflammation in a novel model of psoriatic arthritis. *Arthritis Rheumatol* 2018;70:855–67.
4. Bromberg JF, Wrzeszczynska MH, Devgan G, Zhao Y, Pestell RG, Albanese C, et al. Stat3 as an oncogene. *Cell* 1999;98:295–303.
5. Maritano D, Sugrue ML, Tininini S, Dewilde S, Strobl B, Fu X, et al. The STAT3 isoforms α and β have unique and specific functions. *Nat Immunol* 2004;5:401–9.
6. Mitra A, Raychaudhuri SK, Raychaudhuri SP. Functional role of IL-22 in psoriatic arthritis. *Arthritis Res Ther* 2012;14:R65.
7. Benham H, Norris P, Goodall J, Wechalekar MD, FitzGerald O, Szentpetery A, et al. Th17 and Th22 cells in psoriatic arthritis and psoriasis. *Arthritis Res Ther* 2013;15:R136.
8. Kim KW, Kim HR, Park JY, Park JS, Oh HJ, Woo YJ, et al. Interleukin-22 promotes osteoclastogenesis in rheumatoid arthritis through induction of RANKL in human synovial fibroblasts. *Arthritis Rheum* 2012;64:1015–23.
9. Jones SM, Dixey J, Hall ND, McHugh NJ. Expression of the cutaneous lymphocyte antigen and its counter-receptor E-selectin in the skin and joints of patients with psoriatic arthritis. *Br J Rheumatol* 1997;36:748–57.
10. Moll JM, Wright V. Psoriatic arthritis. *Semin Arthritis Rheum* 1973;3:55–78.
11. McGonagle D, Lories RJ, Tan AL, Benjamin M. The concept of a “synovio-entheseal complex” and its implications for understanding joint inflammation and damage in psoriatic arthritis and beyond. *Arthritis Rheum* 2007;56:2482–91.
12. Ding Y, Li J, Wu Q, Yang P, Luo B, Xie S, et al. IL-17RA is essential for optimal localization of follicular Th cells in the germinal center light zone to promote autoantibody-producing B cells. *J Immunol* 2013;191:1614–24.
13. Azizi G, Yazdani R, Mirshafiey A. Th22 cells in autoimmunity: a review of current knowledge. *Eur Ann Allergy Clin Immunol* 2015;47:108–17.
14. Scher JU, Littman DR, Abramson SB. Microbiome in inflammatory arthritis and human rheumatic diseases [review]. *Arthritis Rheumatol* 2016;68:35–45.
15. Backert I, Koralov SB, Wirtz S, Kitowski V, Billmeier U, Martini E, et al. STAT3 activation in Th17 and Th22 cells controls IL-22-mediated epithelial host defense during infectious colitis. *J Immunol* 2014;193:3779–91.
16. Mamantopoulos M, Ronchi F, Van Hauwermeiren F, Vieira-Silva S, Yilmaz B, Martens L, et al. Nlrp6- and ASC-dependent inflammasomes do not shape the commensal gut microbiota composition. *Immunity* 2017;47:339–48e4.

REVIEW

Cell Death, Nucleic Acids, and Immunity

Inflammation Beyond the Grave

Keith B. Elkon

Cells of the innate immune system are rigged with sensors that detect nucleic acids derived from microbes, especially viruses. It has become clear that these same sensors that respond to nucleic acids derived from damaged cells or defective intracellular processing are implicated in triggering diseases such as lupus and arthritis. The ways in which cells die and the concomitant presence of proteins and peptides that allow nucleic acids to re-enter cells profoundly influence innate immune responses. In this review, we briefly discuss different types of programmed necrosis, such as pyroptosis, necroptosis, and NETosis, and explains how nucleic acids can engage intracellular receptors and stimulate inflammation. Host protective mechanisms that include compartmentalization of receptors and nucleases as well as the consequences of nuclease deficiencies are explored. In addition, proximal and distal targets in the nucleic acid stimulation of inflammation are discussed in terms of their potential amenability to therapy for the attenuation of innate immune activation and disease pathogenesis.

Introduction

Rheumato-immunologists began paying attention to cell death after the discovery in 1992 that a mutation in the *fas* gene caused acceleration of autoimmunity in the MRL/lpr lupus mouse strain (1). *Fas* encodes a cell surface death receptor, CD95, that promotes apoptosis of activated immune cells. Loss of *fas* function leads to accumulation of lymphocytes, including those with autoreactivity. Further interest in cell death was prompted by the observation that many autoantigens redistribute to the cell surface following induction of apoptosis (2). During the last 25 years, the importance of cell death pathways and the way in which immune cells respond to dead and dying cells have been studied intensively and shown to be important across diseases.

Early studies of cell death made a fundamental distinction between apoptosis and necrosis, with apoptosis being controlled by a biochemical program and immunologically silent, whereas necrosis is immediate, uncontrolled, and inflammatory. While it remains true that rapid uncontrolled cell death—for example, as induced by infarction, trauma, or burns—leads to damage of the cell membrane and spillage of cell contents (necrosis), it has become apparent that necrosis can also occur by programmed biochemical pathways (as discussed in detail below). Involvement of executioner caspases (which are cysteine proteases that help degrade intracellular proteins) can also serve to distinguish apoptosis from necrosis (3). If they are involved, then death is more likely to be apoptotic, whereas failure to engage executioner caspases leads to necrosis and inflammatory cell death. It has also become apparent that, following necrotic forms of cell death, nucleic acids are prominent, if not dominant, activators of innate immunity. Even during apoptotic cell death, it is the presence of nucleic acids on apoptotic cells or nucleic acids coating the blebs released from dying cells that have the potential to engage B cell receptors and partially activate B lymphocytes.

Dr. Elkon's work is supported by the NIH (grant R21-AR-072377) and the Lupus Research Alliance.

Keith B. Elkon, MD: University of Washington, Seattle.

Dr. Elkon is co-founder of Resolve Therapeutics and AMDAX Therapeutics and holds patents (intellectual property and license owned by the University of Washington) for an RNase-Ig fusion protein, RSLV132 (a product of Resolve Therapeutics currently in phase II clinical trials in SLE) and a small-molecule inhibitor of cGAS (a product of AMDAX Therapeutics still in the preclinical stage of development). He has received consulting fees, speaking fees, and/or honoraria from Celgene, AstraZeneca, Merck Research Laboratories, MedImmune, and Bellbrook Laboratories (less than \$10,000 each).

Address correspondence to Keith B. Elkon, MD, Division of Rheumatology, University of Washington, Room E541, 750 Republican Street, Seattle, WA 98109. E-mail: elkon@uw.edu.

Submitted for publication November 15, 2017; accepted in revised form February 8, 2018.

What are PAMPs and DAMPs?

The discoveries of antigen receptors on cells of the adaptive immune system, including T and B lymphocytes, as well as the fundamental principles that determine self and non-self recognition through “education” in the thymus and in the bone marrow, respectively, were elucidated in the 1980s. What are the receptors and fundamental principles of self/non-self recognition in cells of the innate immune system (herein focusing particularly on macrophages and dendritic cells)? In 1989, Charles Janeway hypothesized that cells of the innate immune system also have germline-encoded receptors that could recognize foreign antigens (4). These receptors were named pattern recognition receptors (PRRs).

The primary consequences of PRR engagement in innate immune cells are expression of costimulatory proteins, and release of chemokines and cytokines (Figure 1). The microbial ligands that trigger PRRs, designated pathogen-associated molecular patterns (PAMPs), include the bacterial cell wall component lipid polysaccharide, the bacterial protein flagellin, and viral nucleic acids. Challenged by evidence that inflammation can arise during tissue damage with the release of dead and dying cells in the absence of infection (i.e., sterile inflammation and the “danger model” [5]), concepts were expanded to include host-derived ligands (designated damage-associated molecular patterns [DAMPs]), such as nucleic acids, monosodium urate monohydrate (MSU) crystals, and high mobility group box chromosomal protein 1 (HMGB-1).

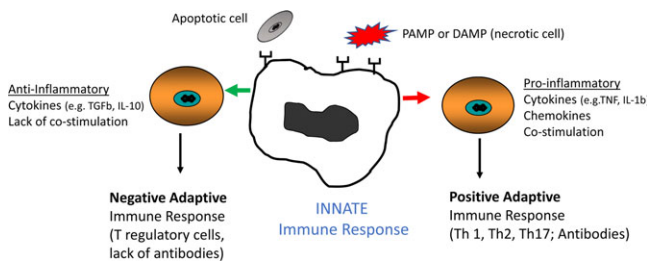


Figure 1. Basic concepts of innate cell stimulation by damage-associated molecular patterns (DAMPs) or pathogen-associated molecular patterns (PAMPs). Either DAMPs or PAMPs are capable of activating cells of the innate immune system, such as macrophages and dendritic cells. Depending on the nature of the molecular pattern, either anti- or proinflammatory responses can be elicited. These responses impact both the inflammatory environment and communication with T cells. Whereas intact apoptotic cells are immunologically silent or stimulate antiinflammatory responses as well as negative adaptive responses (left panel), release of cellular content from necrotic cells is almost always inflammatory (right panel). Note that DAMPs and PAMPs also impact B cells both by serving as antigens activating the B cell receptor and, following internalization, by activation of sensors such as Toll-like receptor 7 (TLR-7) and TLR-9 (see also Figure 3). TGF β = transforming growth factor β ; IL-10 = interleukin-10; TNF = tumor necrosis factor.

Since the initial inflammatory response by the innate immune system can be identical when activated by PAMPs or DAMPs, the fundamental questions raised are whether and how the innate immune system distinguishes self from foreign? The answer, similar to the lessons learned from adaptive immunity, is that the innate immune system employs a variety of overlapping strategies that vary in time with the outcome, depending on both the nature of the stimulus and the quantity and quality of the host response. With regard to self antigens released as DAMPs, how cells die plays a critical role in alerting the innate immune system to “friend or foe.”

How cells die determines noninflammatory versus inflammatory consequences

Beyond the simple apoptosis/necrosis dichotomy, at least 13 different biochemical forms of cell death have been recognized (6). Different names have been given to these forms of death, depending on the inductive stimulus (e.g., starvation, end-stage maturation, or gene damage), cell type (e.g., cornification in skin cells, pyroptosis in macrophages, or neutrophil extracellular trap [NET] formation in neutrophils), and involvement of caspases. In the current review, the following different types of cell death are discussed: apoptosis, necrosis, necroptosis, pyroptosis, and NET formation. Each of these types of cell death can have either a negative impact or a positive impact on inflammation and autoimmunity (Figure 1). Host cell mechanisms that function to reduce inflammation from cell-derived material are also considered herein. It should be emphasized that an immune response, even when involving inflammatory cytokines, is not necessarily deleterious, as many of these responses are part of a wound repair process or tend to trigger healing pathways (for review, see ref. 7).

Although the outcomes in each form of cell death (as discussed below) differ, what most have in common is the generation of a macromolecular structure or platform comprising the key effector molecules required for execution of the program (e.g., apoptosome in apoptosis, necrosome in necroptosis, and inflammasome in pyroptosis). A detailed description of the components and biochemical function of these structures would be too lengthy for the current review (for more detail, see specific references included in the descriptions of each form of cell death).

Apoptosis and postapoptotic necrosis

Apoptosis can be triggered by extracellular signals via activation of a “death receptor” or by intracellular

events such as DNA damage, endoplasmic reticulum stress, or lack of nutrient support. Elimination of cells by apoptosis plays obligate roles in normal immune system development, tissue homeostasis, and immune regulation. Apoptosis initiated by death receptor signaling is termed extrinsic apoptosis, while that induced by intracellular stresses is termed intrinsic apoptosis. Both apoptotic pathways converge on activation of the caspases—caspase 8 for the extrinsic pathway, and caspase 9 for the intrinsic pathway. The ensuing proteolytic cascade leads apoptotic cells to undergo distinct morphologic changes, including dismantling of the cytoskeleton and alterations in the lipid composition of the cell membrane. The latter event, especially the appearance of phosphatidylserine on the cell surface, serves as a signal to phagocytes, which readily engulf apoptotic cells (a process also called “efferocytosis”) prior to the loss of membrane integrity by the dying cells. Apoptotic cells are thereby “packaged” for phagocytosis, and their contents are not released into the intracellular space. For this reason, apoptosis is generally considered a non-inflammatory and immunologically silent form of cell death. Efferocytosis may induce the stimulation of transforming growth factor β and interleukin-10 (IL-10), both of which are immunosuppressive cytokines, thereby further diminishing the chance for autoimmunity (Figure 1).

With regard to the relevance of apoptosis in disease, delay in the engulfment of apoptotic cells results in 2 events that impact immune responses. Blebbing with the production of microparticles (MPs) may occur. MPs are a special class of extracellular vesicles that also include exosomes and microvesicles. The MPs contain nucleic acids as well as surface-exposed DNA, and are implicated in cell–cell communication and either functional suppression or stimulation of immune cells depending on the cellular origin of the MPs and patient context (8,9). A second and very significant consequence of delayed clearance for immune homeostasis is that the cell membranes of apoptotic cells break down and release their intracellular contents in the process of postapoptotic necrosis (Figure 2). The released nucleic acids appear to be the main source of DAMPs. However, extra- and intracellular nucleases, as well as limited re-entry into the cells, help to prevent persistent inflammation, as discussed below.

There is considerable evidence in mouse models that failure to clear apoptotic cells leads to inflammation and/or autoimmunity (10). Genetic deletion of receptors or ligands that facilitate apoptotic cell clearance, such as the early complement components, milk fat globule–epidermal growth factor 8, c-Mer, Axl, and Tyro, and T cell immunoglobulin and mucin domain–containing protein 4, predisposes individuals to the

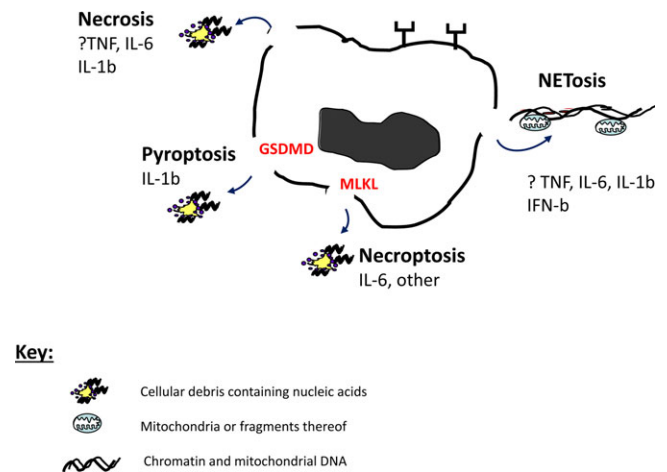


Figure 2. Immediate or programmed forms of necrosis stimulate inflammation. Programmed forms of necrosis include pyroptosis, necroptosis, and neutrophil extracellular trap (NET) formation. Common features are damage to the cell membrane and release of cytokines, although this is less well established for NET formation. Gasdermin D (GSDMD) and mixed-lineage kinase domain–like (MLKL) protein are proteins involved in pore formation in pyroptosis and necroptosis, respectively. How chromatin escapes from neutrophils during NET formation is unknown. TNF = tumor necrosis factor; IL-6 = interleukin-6; IFN- β = interferon- β .

development of lupus, although the disease is usually mild unless other susceptibility factors are present. Some patients with systemic lupus erythematosus (SLE) have reduced clearance of apoptotic cells, as evidenced by an increased number of apoptotic cells in their germinal centers (11). However, which molecular pathways are defective remains unclear. Both in vitro and in vivo experiments strongly support the idea that the early complement components are required for the clearance of apoptotic cells (12,13). The high frequency of SLE in patients with C1q, C4, and C2 deficiency (for review, see ref. 14) may be explained, in part, by impaired clearance of dying cells. Inappropriately low levels of C-reactive protein in patients with SLE may further reduce apoptotic cell clearance (15).

Pyroptosis

Pyroptosis is a form of cell death most commonly induced by bacterial PAMPs (16). These PAMPs are recognized by the PRR cytosolic sensors, leading to the assembly of multiprotein complexes called inflammasomes (17). Inflammasome platforms can be assembled not only by PAMPs—for example, gram-negative bacteria can activate nonclassic NLRP3 inflammasomes, and bacterial Rho-inactivating toxins can activate the pyrin inflammasomes—but also by DAMPs that are released by

stressed and dead cells—for example, MSU crystals, as well as DNA, can activate the classic NLRP3 inflammasome. Assembly of the inflammasome leads, in turn, to activation of specific members of the caspase family, termed the inflammatory caspases (human caspases 1, 4, and 5); human caspases 4 and 5 are functionally homologous to murine caspase 11 (for review, see ref. 18).

Activation of the inflammatory caspases leads to 2 events that render pyroptosis distinct from apoptosis. First, the catalytic activity of caspase 1 is required for the maturation and bioactivity of 2 key cytokines, IL-1 β and IL-18 (19). These cytokines are synthesized as inactive precursors, and their cleavage by caspase 1 renders them active. Once activated and released from the cell, these cytokines are able to initiate complex and pleiotropic inflammatory events. How do these cytokines, which lack the leader sequences that allow secretion of most cytokines via the Golgi apparatus, exit the cell? Recent observations indicate that the inflammatory caspases cleave, and thereby activate, the pore-forming molecule gasdermin D (GSDMD), an executioner of pyroptosis (20,21). Activation of GSDMD leads to disruption of the cell membrane, cellular swelling, and rupture, thereby inducing the release of intracellular contents (Figure 2). The lytic nature of pyroptosis stands in obvious contrast to the tidy packaging and phagocytosis associated with apoptosis.

With regard to the relevance of pyroptosis in disease, there is no definite association between gram-negative bacteria, activation of the inflammasome, and pyroptosis in rheumatic disorders. Nevertheless, uric acid released by stressed or dying cells (22), MSU crystals, and also intracytoplasmic DNA stimulate inflammasome platforms to generate IL-1 β . Although it is recognized that hyperuricemia is largely a consequence of increased production or reduced excretion of uric acid, the extent to which uric acid derived from dying cells contributes to gout is not known. However, blockade of IL-1 β with IL-1 receptor antagonist (IL-1Ra) is an effective, albeit expensive, therapy for this disease. The pyrin inflammasome is stimulated by bacterial toxins that inactivate the GTP binding protein RhoA (23). Missense mutations in the MEFV gene, which encodes pyrin, autoactivate the pyrin inflammasome, and human subjects with these gene mutations develop familial Mediterranean fever (FMF), a process that, in significant part, can be attributed to the release of IL-1 β . Once again, proof of principle is provided by studies showing that IL-1 β production can be blocked with IL-1Ra or by antibodies to IL-1 β , each of which has been shown to be an effective form of treatment for colchicine-resistant FMF (24).

Necroptosis

Necroptosis is a caspase-independent form of programmed cell death that is morphologically similar to necrosis. Necroptotic cells swell and rupture, releasing their intracellular contents in a manner analogous to necrotic and pyroptotic cells. However, the mechanisms by which necroptosis occur are distinct. Necroptosis is mediated by the activation of receptor-interacting protein kinase 1 (RIPK-1) and RIPK-3. The RIP kinases are activated by ligation of many of the same “death receptors,” such as tumor necrosis factor (TNF) receptor or Fas (CD95), that induce the extrinsic pathway of apoptosis. Strikingly, however, the molecules that induce extrinsic apoptosis suppress necroptosis. The outcome of death receptor signaling is therefore pleiotropic, and is determined by the relative abundance and activity of the signaling components that bind to the cytoplasmic tails of these receptors (25). Specifically, the relative lack of bioactive caspase 8 or increased levels of cellular FLICE-like inhibitory protein promote necroptosis rather than apoptosis.

Once activated, the RIP kinases phosphorylate an effector molecule, mixed-lineage kinase domain-like protein, which disrupts the cell membrane (26) (Figure 2). This mechanism of programmed membrane disruption is analogous to the execution of pyroptosis by GSDMD. As a lytic form of cell death, it has been hypothesized that necroptosis may promote inflammation through the release of DAMPs, although the precise mechanisms by which this occurs remain to be determined.

With regard to its relevance in disease, necroptotic death is seen in virus infections (e.g., cytomegalovirus) that produce caspase inhibitors, and has also been implicated in neurodegeneration and inflammatory bowel disease (27). Expression levels of RIPK and RIPK-3 are reported to be reduced in patients with SLE (28). In contrast, in murine collagen-induced arthritis, the levels of these kinases are increased and could be shown to play a role in inflammation, especially in the absence of interferon- γ (IFN γ) (29).

Neutrophils and NET formation

Neutrophils are short-lived cells that may die by apoptosis, necrosis, or NET formation. Since they are the most abundant white blood cell in the circulation and are first responders to infection and injury, their mode of death is particularly important. NET formation is a programmed form of neutrophil necrosis (30), although a similar process has been described in eosinophils and basophils. This form of rapid cell death is characterized by the extrusion of

chromatin in a NET-like structure, accompanied by the release of neutrophil-derived enzymes and mitochondria or their fragments. NET formation is stimulated by exposure of neutrophils to certain bacteria and immune complexes containing RNA, which, in turn, stimulates the intracellular Toll-like receptor 8 (TLR-8), the dominant TLR in neutrophils. Depending on the stimulus, the NET formation program requires activation of the enzyme peptidylarginine deiminase type 4 (PAD4), leading to citrullination of histone H3 and unpacking of chromatin, as well as activation of NADPH oxidase (NOX) or mitochondrial reactive oxygen species (ROS)-generating systems.

With regard to its relevance in disease, increased generation of NETs and/or impaired NET clearance have been implicated in the pathogenesis of autoimmune disorders, including SLE, vasculitis, and rheumatoid arthritis (RA) (31). In SLE, low-density granulocytes undergo spontaneous NET formation *ex vivo*, strongly suggesting that this process is initiated *in vivo*. Patients with SLE have increased circulating levels of NETs, and evidence of NET formation can also be found in tissue (32). Some studies have shown that patients with SLE or vasculitis have an impaired ability to degrade NETs (33), which leads to increased inflammation and type I IFN production. These observations have been supported by mouse studies in which pharmacologic inhibition of NET formation in lupus-prone mice, either by inhibition of PAD4 activity or by inhibition of mitochondrial ROS, ameliorates disease (34,35). However, an argument refuting the notion that NET formation is required for disease development has been made in genetic studies of MRL/lpr mice in which deficiency of either PAD4 or NOX-2 did not protect against disease (36,37).

Generation of ROS is necessary for NET formation in most contexts, and we and other investigators recently demonstrated that generation of ROS, rather than NOX-2, by mitochondria is key to the oxidation of DNA and, in particular, the oxidation of mitochondrial DNA (mtDNA) (34,38). Furthermore, oxidized mtDNA was proven to be highly inflammatory through activation of the stimulator of IFN genes (STING) pathway, inducing IFN β and other inflammatory cytokines (34). In gout, neutrophils that ingest MSU crystals stimulate inflammatory cytokines and can induce NET formation. Interestingly, gouty tophi are composed, in part, of aggregated NETs, which degrade cytokines and help in the resolution of inflammation (39). Recent studies in mice revealed that a combined deficiency of DNase1 and DNase1L3 led to clotting of the vessels by NETs in a disease resembling thrombotic microangiopathies (40).

Extra- and intracellular nucleases protect against inflammation and autoimmunity

If excessive nucleic acids are released by necrosis or via the programmed pathways of necrosis (as discussed above), how do they re-enter the cell? One of the earliest re-entry mechanisms identified in SLE was a mechanism in which IgG autoantibodies form immune complexes with nucleoprotein particles and engage the activating Fc γ receptor type IIA (Fc γ RIIA) on plasmacytoid dendritic cells (PDCs) and other cells. This, in turn, leads to phagocytosis and downstream activation of intracellular TLRs to stimulate the production of type I IFNs and inflammatory cytokines (41). Other re-entry pathways include internalization facilitated by HMGB-1 or the related mitochondrial protein Tfam, through the receptor for advanced glycation end products (RAGE). There are fewer well-defined mechanisms associated with endocytosis of MPs, which possibly involves scavenger receptor 1

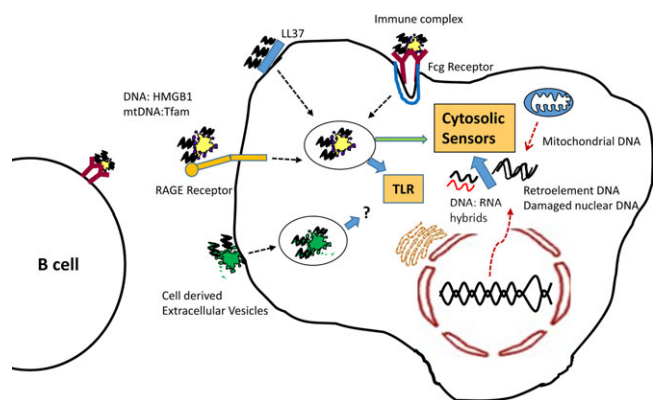


Figure 3. Nucleic acids gain access to intracellular sensors through multiple routes. Extracellular nucleic acids (DNA or RNA) can be captured by autoantibodies, bind to highly cationic peptides such as LL37, or interact with nucleic acid binding proteins such as high mobility group box chromosomal protein 1 (HMGB-1) to gain re-entry into cells. A professional phagocytic cell, such as the macrophage depicted on the right, may uptake molecules by all of these pathways, whereas in other cell types, uptake may be more restricted. Endocytosis of nucleic acid complexes may be receptor mediated (the Fc γ receptor and receptor for advanced glycation end products [RAGE] are shown), but in other cases, mechanisms are less clear (see discussions in the text). In many situations, nucleic acid complexes that enter endosomes generally trigger Toll-like receptors (TLRs) but can escape into the cytosol (green arrow). Intracellular nucleic acids gain access to sensors through different mechanisms—mitochondrial DNA (mtDNA) may be released directly from the damaged organelle or re-enter the cell after binding to the protein called Tfam. The cytosolic sensors can be activated by DNA:RNA hybrids as well as nuclear DNA arising from retroelements or nuclear damage. Note that cell debris, especially highly charged DNA and RNA, may also engage and be internalized by the B cell receptor, thereby delivering to the B cell signals through the B cell receptor as well as through TLRs.

and DNA in complex with the neutrophil peptide LL37, binding to cell surface glycoproteins (42) (Figure 3). It is relevant to note that the function of HMGB-1 is influenced by its redox state: depending on the cysteine(s) oxidized, HMGB-1 can activate TLR-4 or CXCL12, or be completely inactive (for review, see ref. 43). Since nucleic acids that have gained re-entry are now “ectopic,” they are seen as foreign invaders and activate nucleic acid sensors (Figure 3).

As emphasized above, inflammatory forms of cell death are associated with release of cellular contents, including the release of DNA and RNA into the tissue and bloodstream. Nucleic acids, whether derived from host or microbes, are powerful DAMPs and PAMPs that elicit inflammation through multiple PRRs, as detailed below. Extracellular nucleases such as DNase I, DNase I L3, and RNase H1 provide the first line of protection by degrading the DNA and RNA that may be either free or, more commonly, associated with proteins to form complexes (Table 1 and Figure 3). Cell surface-associated chromatin on MPs is degraded by a secreted DNase called DNASE1L3 that contains a positively charged C-terminal peptide facilitating DNA digestion, even when protein bound (44). There are many specialized nucleases within the cell, some of which are free in the cytosol, such as DNase III (TREX1), whereas others are compartmentalized in endosomes (DNase II) (Table 1). TREX1 is an abundant 3-5'-exonuclease with a preference for single-stranded DNA (ssDNA) and has been implicated in the degradation of DNA arising from retroelements and mitochondria, although digestion is less efficient if the DNA is oxidized (i.e., contains 8-OH deoxyguanine) (45). DNA:RNA hybrids that may be produced by an infection with retroviruses or that may occur in the life cycle of endogenous retroelements are degraded by RNase H2

enzymes (Table 1). Mitochondrial DNA has recently received much attention as an agonist capable of stimulating type I IFNs and other cytokines (34,38). Since it is readily oxidized, mtDNA is less efficiently degraded by DNases such as TREX1, leading to activation of TLR-9 and a DNA sensor, cyclic GMP-AMP (cGAMP) synthase (cGAS) (34) (see further details below).

With regard to the relevance of nucleases in disease, in normal individuals, cell debris is cleared with no long-term consequences, despite the fact that nucleic acids are partly shielded from nucleases by the proteins to which they are bound. “Interferonopathies” are a group of monogenic orphan diseases that affect children and are characterized by a type I IFN gene expression signature in the circulating blood (46). The best-studied interferonopathy is Aicardi-Goutières syndrome (AGS) (47), a disease characterized by abnormalities in the skin and brain resulting in severe neurologic defects, with ~75% of patients being profoundly disabled in the first few years of life (48). The expression of lupus-like features, including the characteristic serologic findings (49), in many of these patients is consistent with the idea that elevated levels of type I IFNs other than IFN α can also contribute to the pathogenesis of SLE. It is also relevant to point out that type I IFN signatures are seen not only in SLE, but also in patients with Sjögren’s syndrome, dermatomyositis, or scleroderma.

Molecular genetic studies have revealed that interferonopathies are produced by a number of mutations in genes that are involved in nucleic acid metabolism. Most relevant, in patients with AGS, mutations in TREX1, RNASEH1, ADAR, and IFIH1 activate pathways that stimulate the production of IFN β (50,51) (Table 1). Therefore, in diseases such as SLE and the interferonopathies, the burden of nucleic acids exceeds the

Table 1. Nucleases associated with autoimmune and autoinflammatory diseases*

Nuclease, location	Substrate	Disease association (type)	References
DNase I			
Blood	ssDNA, dsDNA	SLE (human)	85
Intestine	ssDNA, dsDNA	Thrombotic microangiopathies (mouse)	40
DNase II			
Endosome	DNA, nuclear fragments	SLE-like disease, arthritis (mouse)	86, 87
DNase III (TREX1)			
Cytosol	ssDNA, dsDNA	AGS, RVCL, SLE (human)	50, 88
DNase I L3			
Blood	DNA in chromatin	SLE, HUVS (human)	89
RNase H2			
Cytosol	RNA:DNA hybrid, DNA with misincorporated ribonucleotides	AGS (human)	50

* Note that neutrophil extracellular trap-associated thrombotic microangiopathies occur only with combined deficiency of DNase1 and DNase1L3 in mice. ssDNA = single-stranded DNA; dsDNA = double-stranded DNA; SLE = systemic lupus erythematosus; AGS = Aicardi Goutières’s syndrome; RVCL = retinal vasculopathy with cerebral leukoencephalopathy; HUVS = hypocomplementemic urticarial vasculitis.

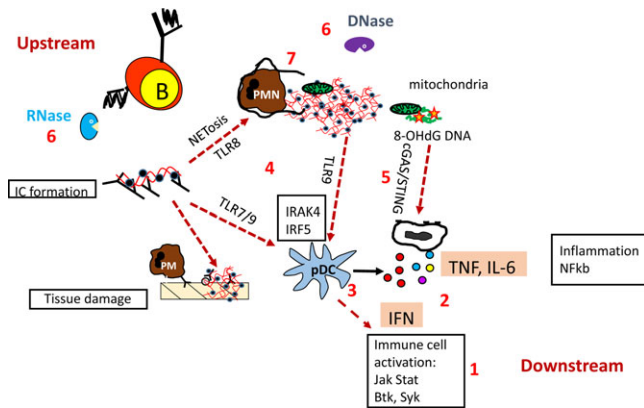


Figure 5. Potential points of therapeutic intervention in response to nucleic acid stimulation of sensors. Biologic or small-molecule drugs have been used in patients or in preclinical models to block cytokines (approach no. 2) or downstream signaling events (approach no. 1). Antibodies targeting plasmacytoid dendritic cells (pDC) are in early clinical trials (approach no. 3). The intracellular Toll-like receptor (TLR) sensors can be inhibited directly by oligonucleotides, or TLR signaling can be modulated by chemical inhibitors of interleukin-1 receptor-associated kinase 4 (IRAK-4) or interferon regulatory factor 5 (IRF-5) (approach no. 4). Similarly, cyclic GMP-AMP synthase/stimulator of interferon genes (cGAS/STING) activation or signaling can be attenuated by antimetabolic drugs or TANK-binding kinase 1 inhibitors (approach no. 5). Nucleases such as DNase and RNase can degrade nucleic acid antigens (approach no. 6) that are free, in immune complexes (ICs), or released by neutrophil extracellular trap (NET) formation. Inhibitors of peptidylarginine deiminase type 4 or mitochondrial reactive oxygen species inhibit the process of NET formation (approach no. 7). See text for further details. B = B lymphocyte; PMN = polymorphonuclear (cell); 8-OHdG = 8-OH deoxyguanine; TNF = tumor necrosis factor; IL-6 = interleukin-6; IFN = interferon.

RNA receptors, referred to as retinoic acid-inducible gene I (RIG-I)-like receptors (RLRs), comprise 3 DExD/H-box RNA helicases, RIG-I, melanoma differentiation-associated protein 5 (MDA-5), and laboratory of genomics and physiology 2 (LGP-2). These receptors are widely expressed across tissues and cell types. The RLR proteins sense virus RNA in the cytoplasm of infected cells, but differ in their specificities. RIG-I recognizes 5'-triphosphorylated, uncapped RNA as well as RNA bearing 5'-diphosphates. MDA-5 recognizes long dsRNA and branched, high-molecular RNA forms. Following activation, RIG-I and MDA-5 bind to the mitochondrial antiviral signaling (MAVS) adapter protein (also known as IFN β promoter stimulator 1) that forms a scaffold for stimulation of IFN β and other inflammatory cytokines via various pathways (as shown in Figure 4). LGP-2 may be a negative regulator of these processes.

At least 13 cytosolic DNA sensors have been identified (for review, see ref. 62). All of these DNA sensors stimulate the production of type I IFNs or promote the

assembly of an inflammasome complex, leading to the activation of caspase 1 and subsequent secretion of IL-1 β and IL-18 (Figure 4). The absent in melanoma 2 (AIM-2)-like receptors, of which there are 4 in humans and 13 in mice, have in common a DNA-binding domain known as HIN (hematopoietic expression, IFN-inducible nature, and nuclear localization) and a pyrin signaling domain (63). The biologic role of all of these DNA sensors in vivo, aside from cGAS, has been questioned (64), and a recent study suggests that cGAS-STING, rather than AIM-2, is responsible for inflammasome activation in myeloid cells (65). With regard to the sensor cGAS, binding of dsDNA to cGAS causes a conformational change in the active site of cGAS, which utilizes ATP and GTP to synthesize the cyclic dinucleotide 2'-5'-cGAMP (66). Subsequently, cGAMP functions as an endogenous second messenger binding directly to the adapter protein STING. Dimerization of STING results in the translocation of STING from the endoplasmic reticulum to the Golgi, with recruitment and activation of TANK-binding kinase 1 (TBK-1) and the transcription factor IFN regulatory factor 3 (IRF-3), culminating in the synthesis of IFN β (67) (Figure 4).

With regard to the relevance of cytosolic receptors in disease, key questions regarding their role in immune stimulation in autoimmune and autoinflammatory diseases include the following. 1) Are the stimulatory nucleic acids derived from outside of the cell or inside the cell? 2) Which main sensors are stimulated? 3) What is the connection between nucleic acid immune activation and antinuclear antibody (ANA) production?

In the interferonopathies, stimulatory nucleic acids almost certainly originate from within the cell, due to defective nucleic acid metabolism and accumulation of nucleic acids, resulting in stimulation of the cytosolic sensors. In SLE and related disorders, extracellular origins, such as immune complexes, MPs, and extruded nuclei, can activate both TLRs and cytosolic sensors once internalized. Intriguingly, recent studies have implicated retroelement-derived nucleic acids in immune activation in SLE and Sjögren's syndrome. The short interspersed nuclear element Alu was detected in immune complexes in SLE (68), and the type 1 long interspersed nuclear element was detected in the kidneys and salivary glands of patients with Sjögren's syndrome and patients with SLE, respectively (69). Could cell-intrinsic activation stimulate and prime for extrinsic (particularly immune complex) stimulation? Could both endosomal and cytosolic sensors be involved at different phases of disease?

Given the pivotal role of cGAS-STING in the generation of type I IFNs and the central role played by type I IFNs in the pathogenesis of SLE, cGAS expression and cGAMP production were investigated in SLE

patients (70). There was an increase in cGAS transcript expression in ~one-third of SLE patients, and ~15% of patients had detectable cGAMP dinucleotide in their peripheral blood mononuclear cells. Interestingly, the patients with detectable cGAMP had a higher SLE Disease Activity Index score than did patients without activation of the pathway (70).

With regard to RNA sensors, aggregation of MAVS has been demonstrated in patients with SLE, which may be associated with oxidation of mtDNA (71,72). Hasan et al (73) reported that expression of messenger RNA for TBK-1 (a protein downstream of cGAS as well as RLRs) was significantly increased in SLE patients, especially in monocytes. Finally, several patients with gain-of-function mutations in the adapter protein STING developed the autoinflammatory/autoimmune diseases STING-associated vasculopathy with onset in infancy and chilblain lupus (74,75). Very likely, the phenotypic expression of disease is influenced by a multitude of other gene variants and environmental factors.

The hallmark of systemic autoimmune diseases is the presence of ANAs. Considering the importance of nucleic acids (as discussed in this review), it would be helpful to ascertain whether excessive exposure to, or defective removal/degradation of, nucleic acids is sufficient to stimulate the production of ANAs. Studies of patients with the interferonopathy AGS revealed highly statistically significant increases in the levels of autoantibodies to Sm/RNP and to SSA/SSB (49). Considering that nucleic acid stimulation of cytokines is a feature intrinsic to cells in patients with AGS (Figure 3), this suggests that cytokines, especially type I IFNs, can be sufficient to stimulate the generation of ANAs, but these findings do not exclude the possibility that other stimuli, such as B cell receptor engagement by cell debris or, in the case of DNase1L3 deficiency, stimulation by MPs, may also have a role (44). Presumably, IFN acts through its adjuvant effect, leading to activation of all types of immune cells (76). Since most patients with monogenic interferonopathies generate autoantibodies but do not develop full-blown SLE, other genetic variants, for example, mutations in PTPN22, BLK, and BANK1, that may influence B cell function are likely required for the expression of high-affinity antibodies that lead to the development of such systemic diseases as glomerulonephritis.

How are self and non-self DNA/RNA distinguished?

The special case of mitochondria—is 1.5 billion years not enough? Mitochondria are self-contained organelles that evolved from a protokaryote that was co-opted into eukaryotic cells ~1.5 billion years ago. They perform

vital functions within the cell. They produce high-efficiency energy by generating ATP through oxidative phosphorylation, and mitochondrial proteins such as Bcl-2 and Bax/Bak control cell survival and death by regulating mitochondrial membrane potential. Mitochondria are readily damaged through hyper- or hypopolarization of their membranes, as well as by generation of ROS. Damaged mitochondria are usually removed by the process of mitophagy, but neutrophils appear to be poor at mitophagy and, therefore, extrude damaged mitochondria as a way to prevent untoward damage within the cell (34,38). Mitochondria thus have an impact on immunity, because 1) their DNA is rich in CpG DNA (potential TLR-9 ligand) and can gain entry into cells through binding to Tfam (77), 2) ROS oxidizes mtDNA (potential cGAS ligand) that cannot be efficiently repaired within the organelle, 3) in mammalian cells, they are the only source of cardiolipin (antigenic target of some autoantibodies), and 4) the damaged organelle can be extruded (making it accessible to the immune system). Furthermore, like their ancient bacterial forebears, mitochondrial peptides have an N-terminal-formylated methionine that stimulates the production of chemokines. Taken together, these findings suggest that, while a necessity for the eukaryotic lifestyle, mitochondria pose an outside danger to innate immunity (78).

Modified nucleic acids. It took decades to determine how cells of the adaptive immune system are able to distinguish self from foreign antigens, and research is still ongoing. Although some of the mechanisms are ancient (for example, cGAS-STING is estimated to have evolved 600 million years ago), our understanding of the rules for distinguishing self from foreign by innate immune sensors is at an early stage. As discussed above, distinguishing self from non-self in innate immunity relies on nondiscriminatory strategies that include degradation of extracellular nucleic acids (mostly from self), limited cell-type expression of some sensors, and intracellular location of all known nucleic acid sensors. Discriminatory strategies that identify differences between self and foreign nucleic acids by sequence, chemical modifications, or structure are being discovered. For RNA, 5'-capping of the terminus is an excellent example, as this feature is present in many viruses but not in host RNA (79). RNA-reactive TLRs can detect both virus and mammalian RNA, but here again, sequence and structure are most likely key determinants of ligand avidity, as TLR-7 and TLR-8 preferentially bind unmodified uridine-rich ssRNAs (80,81). Many of the small RNAs associated with their protein antigens (e.g., Sm/RNP, Ro/La) in SLE fit this category (polyuridine-rich RNAs).

With regard to DNA, oxidation of DNA and CpG methylation demonstrate selectivity of processing and recognition, as discussed above. Whereas DNase I can

degrade oxidized DNA, oxidation impairs activity of the intracellular DNase TREX1, resulting in the increased likelihood of stimulation of cGAS (45). TLR-9 is the main sensor of DNA and was originally thought to distinguish microbial DNA from mammalian DNA, on the basis of reactivity with hypomethylated CpG motifs, which are less commonly found in mammalian DNA but are common in bacterial and viral DNA. TLR-9 can also detect mammalian DNA. Nevertheless, DNA sequence is still relevant, because mammalian DNA sequences enriched for CpG dinucleotides are more potent activators of TLR-9 than DNA sequences devoid of CpG dinucleotides (82). Potential sources of immunostimulatory mammalian DNA include CpG islands, mitochondrial DNA, and retroelements (Figure 3).

Therapeutic opportunities and concluding remarks

A deeper understanding of the origin of immunostimulatory nucleic acids and their consequences will enable a broad approach to the treatment of diseases associated with release of cell debris. As shown in Figure 5, specific targets can be used, and in some cases have already been used, to mitigate the inflammatory effects of nucleic acids or nucleoprotein complexes.

Currently, biologic therapies that block cytokines are in widespread use (approach no. 2 in Figure 5), and newer small-molecule drugs such as Janus kinase inhibitors (approach no. 1 in Figure 5) are being introduced to attenuate their downstream effects. Studies of cell depletion (e.g., depletion of T or B lymphocytes) have largely failed, but depletion of PDCs (approach no. 3 in Figure 5) represents an attractive target in type I IFN-related diseases. Drug strategies that target the intracellular sensors themselves are a logical approach, but inhibitory oligonucleotides that block TLRs (approach no. 4 in Figure 5), although effective *in vitro*, have not emerged as a viable therapy for patients. Two potentially relevant targets downstream of the TLRs are IL-1 receptor-associated kinase 4 and IRF-5, and efforts are under way to block the function of these proteins (83). Interestingly, antimalarial drugs were shown to inhibit cGAS *in vitro* (approach no. 5 in Figure 5), and modified forms are now being tested in preclinical models of disease, such as in a model of AGS (84). Finally, degradation of the extracellular nucleic acids could prevent nucleic acid accumulation during inflammation or immune complex production (approach no. 6 in Figure 5).

In general, strategies to inhibit the most upstream pathways are desirable, since they are the least likely to limit inflammatory responses to microbes in host defense. Chemical inhibitors are more likely to have off-target

effects as compared to biologics. A deeper understanding of cell death and intracellular nucleic acid metabolism will undoubtedly help refine our therapeutic approach in patients with a wide range of autoinflammatory and autoimmune disorders.

ACKNOWLEDGMENT

I would like to thank Sladjana Skopelja-Gardner and other colleagues at the University of Washington for providing comments and discussion.

AUTHOR CONTRIBUTIONS

Dr. Elkon was involved in drafting the article, revising it critically for important intellectual content, and approving the final version to be published.

REFERENCES

1. Watanabe-Fukunaga R, Brannan CI, Copeland NG, Jenkins NA, Nagata S. Lymphoproliferation disorder in mice explained by defects in Fas antigen that mediates apoptosis. *Nature* 1992;356:314–7.
2. Casciola-Rosen LA, Anhalt G, Rosen A. Autoantigens targeted in systemic lupus erythematosus are clustered in two populations of surface structures on apoptotic keratinocytes. *J Exp Med* 1994; 179:1317–30.
3. Martin SJ, Henry CM, Cullen SP. A perspective on mammalian caspases as positive and negative regulators of inflammation. *Mol Cell* 2012;46:387–97.
4. Janeway CA Jr. Approaching the asymptote? Evolution and revolution in immunology. *Cold Spring Harb Symp Quant Biol* 1989; 54:1–13.
5. Matzinger P. The danger model: a renewed sense of self. *Science* 2002;296:301–5.
6. Vandenabeele P, Galluzzi L, Vanden Berghe T, Kroemer G. Molecular mechanisms of necroptosis: an ordered cellular explosion. *Nat Rev Mol Cell Biol* 2010;11:700–14.
7. Shaw TJ, Martin P. Wound repair: a showcase for cell plasticity and migration. *Curr Opin Cell Biol* 2016;42:29–37.
8. Pisetsky DS, Gauley J, Ullal AJ. Microparticles as a source of extracellular DNA. *Immunol Res* 2011;49:227–34.
9. Robbins PD, Dorronsoro A, Booker CN. Regulation of chronic inflammatory and immune processes by extracellular vesicles. *J Clin Invest* 2016;126:1173–80.
10. Nagata S, Hanayama R, Kawane K. Autoimmunity and the clearance of dead cells. *Cell* 2010;140:619–30.
11. Baumann I, Kolowos W, Voll RE, Manger B, Gaipf U, Neuhuber WL, et al. Impaired uptake of apoptotic cells into tingible body macrophages in germinal centers of patients with systemic lupus erythematosus. *Arthritis Rheum* 2002;46:191–201.
12. Mevorach D, Mascarenhas J, Gershov DA, Elkon KB. Complement-dependent clearance of apoptotic cells by human macrophages. *J Exp Med* 1998;188:2313–20.
13. Botto M, Dell'Agnola C, Bygrave AE, Thompson EM, Cook HT, Petry F, et al. Homozygous C1q deficiency causes glomerulonephritis associated with multiple apoptotic bodies. *Nat Genet* 1998;19:56–9.
14. Manderson AP, Botto M, Walport MJ. The role of complement in the development of systemic lupus erythematosus. *Annu Rev Immunol* 2004;22:431–56.
15. Gershov D, Kim S, Brot N, Elkon KB. C-reactive protein binds to apoptotic cells, protects the cells from assembly of the terminal complement components, and sustains an antiinflammatory

- innate immune response: implications for systemic autoimmunity. *J Exp Med* 2000;192:1353–64.
16. Cookson BT, Brennan MA. Pro-inflammatory programmed cell death. *Trends Microbiol* 2001;9:113–4.
 17. Martinon F, Burns K, Tschopp J. The inflammasome: a molecular platform triggering activation of inflammatory caspases and processing of proIL- β . *Mol Cell* 2002;10:417–26.
 18. Franchi L, Munoz-Planillo R, Nunez G. Sensing and reacting to microbes through the inflammasomes. *Nat Immunol* 2012;13:325–32.
 19. Sansonetti PJ, Phalipon A, Arondel J, Thirumalai K, Banerjee S, Akira S, et al. Caspase-1 activation of IL-1 β and IL-18 are essential for *Shigella flexneri*-induced inflammation. *Immunity* 2000;12:581–90.
 20. Kayagaki N, Stowe IB, Lee BL, O'Rourke K, Anderson K, Warming S, et al. Caspase-11 cleaves gasdermin D for non-canonical inflammasome signalling. *Nature* 2015;526:666–71.
 21. Shi J, Zhao Y, Wang K, Shi X, Wang Y, Huang H, et al. Cleavage of GSDMD by inflammatory caspases determines pyroptotic cell death. *Nature* 2015;526:660–5.
 22. Rock KL, Latz E, Ontiveros F, Kono H. The sterile inflammatory response. *Annu Rev Immunol* 2010;28:321–42.
 23. Dorfleutner A, Stehlik C. A dRAStic RHOA block of pyrin inflammasome activation. *Nat Immunol* 2016;17:900–2.
 24. Pascart T, Richette P. Current and future therapies for gout. *Expert Opin Pharmacother* 2017;18:1201–11.
 25. Linkermann A, Green DR. Necroptosis. *N Engl J Med* 2014;370:455–65.
 26. Sun L, Wang H, Wang Z, He S, Chen S, Liao D, et al. Mixed lineage kinase domain-like protein mediates necrosis signaling downstream of RIP3 kinase. *Cell* 2012;148:213–27.
 27. Weinlich R, Oberst A, Beere HM, Green DR. Necroptosis in development, inflammation and disease. *Nat Rev Mol Cell Biol* 2017;18:127–36.
 28. Zhu L, Yang X, Chen W, Li X, Ji Y, Mao H, et al. Decreased expressions of the TNF-alpha signaling adapters in peripheral blood mononuclear cells (PBMCs) are correlated with disease activity in patients with systemic lupus erythematosus. *Clin Rheumatol* 2007;26:1481–9.
 29. Lee SH, Kwon JY, Kim SY, Jung K, Cho ML. Interferon- γ regulates inflammatory cell death by targeting necroptosis in experimental autoimmune arthritis. *Sci Rep* 2017;7:10133.
 30. Brinkmann V, Reichard U, Goosmann C, Fauler B, Uhlemann Y, Weiss DS, et al. Neutrophil extracellular traps kill bacteria. *Science* 2004;303:1532–5.
 31. Lee KH, Kronbichler A, Park DD, Park Y, Moon H, Kim H, et al. Neutrophil extracellular traps (NETs) in autoimmune diseases: a comprehensive review. *Autoimmun Rev* 2017;16:1160–73.
 32. Gupta S, Kaplan MJ. The role of neutrophils and NETosis in autoimmune and renal diseases. *Nat Rev Nephrol* 2016;12:402–13.
 33. Hakkim A, Furnrohr BG, Amann K, Laube B, Abed UA, Brinkmann V, et al. Impairment of neutrophil extracellular trap degradation is associated with lupus nephritis. *Proc Natl Acad Sci U S A* 2010;107:9813–8.
 34. Lood C, Blanco LP, Purmalek MM, Carmona-Rivera C, de Ravin SS, Smith CK, et al. Neutrophil extracellular traps enriched in oxidized mitochondrial DNA are interferogenic and contribute to lupus-like disease. *Nat Med* 2016;22:146–53.
 35. Knight JS, Zhao W, Luo W, Subramanian V, O'Dell AA, Yalavarthi S, et al. Peptidylarginine deiminase inhibition is immunomodulatory and vasculoprotective in murine lupus. *J Clin Invest* 2013;123:2981–93.
 36. Campbell AM, Kashgarian M, Shlomchik MJ. NADPH oxidase inhibits the pathogenesis of systemic lupus erythematosus. *Sci Transl Med* 2012;4:157ra41.
 37. Gordon RA, Herter JM, Rosetti F, Campbell AM, Nishi H, Kashgarian M, et al. Lupus and proliferative nephritis are PAD4 independent in murine models. *JCI Insight* 2017;2:92926.
 38. Caielli S, Athale S, Domic B, Murat E, Chandra M, Bancheureau R, et al. Oxidized mitochondrial nucleoids released by neutrophils drive type I interferon production in human lupus. *J Exp Med* 2016;213:697–713.
 39. Schauer C, Janko C, Munoz LE, Zhao Y, Kienhofer D, Frey B, et al. Aggregated neutrophil extracellular traps limit inflammation by degrading cytokines and chemokines. *Nat Med* 2014;20:511–7.
 40. Jimenez-Alcazar M, Rangaswamy C, Panda R, Bitterling J, Simsek YJ, Long AT, et al. Host DNases prevent vascular occlusion by neutrophil extracellular traps. *Science* 2017;358:1202–6.
 41. Bave U, Vallin H, Alm GV, Ronnblom L. Activation of natural interferon- α producing cells by apoptotic U937 cells combined with lupus IgG and its regulation by cytokines. *J Autoimmun* 2001;17:71–80.
 42. Chamilos G, Gregorio J, Meller S, Lande R, Kontoyiannis DP, Modlin RL, et al. Cytosolic sensing of extracellular self-DNA transported into monocytes by the antimicrobial peptide LL37. *Blood* 2012;120:3699–707.
 43. Pisetsky DS. The translocation of nuclear molecules during inflammation and cell death. *Antioxid Redox Signal* 2014;20:1117–25.
 44. Sisirak V, Sally B, D'Agati V, Martinez-Ortiz W, Ozcazar ZB, David J, et al. Digestion of chromatin in apoptotic cell microparticles prevents autoimmunity. *Cell* 2016;166:88–101.
 45. Gehrke N, Mertens C, Zillinger T, Wenzel J, Bald T, Zahn S, et al. Oxidative damage of DNA confers resistance to cytosolic nuclease TREX1 degradation and potentiates STING-dependent immune sensing. *Immunity* 2013;39:482–95.
 46. Crow YJ, Manel N. Aicardi-Goutières syndrome and the type I interferonopathies. *Nat Rev Immunol* 2015;15:429–40.
 47. Aicardi J, Goutières F. A progressive familial encephalopathy in infancy with calcifications of the basal ganglia and chronic cerebrospinal fluid lymphocytosis. *Ann Neurol* 1984;15:49–54.
 48. Crow YJ, Chase DS, Lowenstein Schmidt J, Szykiewicz M, Forte GM, Gornall HL, et al. Characterization of human disease phenotypes associated with mutations in TREX1, RNASEH2A, RNASEH2B, RNASEH2C, SAMHD1, ADAR, and IFIH1. *Am J Med Genet A* 2015;167A:296–312.
 49. Cuadrado E, Vanderver A, Brown KJ, Sandza A, Takanohashi A, Jansen MH, et al. Aicardi-Goutières syndrome harbours abundant systemic and brain-reactive autoantibodies. *Ann Rheum Dis* 2015;74:1931–9.
 50. Crow YJ. Type I interferonopathies: mendelian type I interferon up-regulation. *Curr Opin Immunol* 2015;32:7–12.
 51. Rice GI, del Toro Duany Y, Jenkinson EM, Forte GM, Anderson BH, Ariaudo G, et al. Gain-of-function mutations in IFIH1 cause a spectrum of human disease phenotypes associated with upregulated type I interferon signaling. *Nat Genet* 2014;46:503–9.
 52. Lee-Kirsch MA, Gong M, Chowdhury D, Senenko L, Engel K, Lee YA, et al. Mutations in the gene encoding the 3'-5' DNA exonuclease TREX1 are associated with systemic lupus erythematosus. *Nat Genet* 2007;39:1065–7.
 53. Namjou B, Kothari PH, Kelly JA, Glenn SB, Ojwang JO, Adler A, et al. Evaluation of the TREX1 gene in a large multi-ancestral lupus cohort. *Genes Immun* 2011;12:270–9.
 54. Lood C, Arve S, Ledbetter J, Elkon KB. TLR7/8 activation in neutrophils impairs immune complex phagocytosis through shedding of Fc γ RIIA. *J Exp Med* 2017;214:2103–19.
 55. Monteith AJ, Kang S, Scott E, Hillman K, Rajfur Z, Jacobson K, et al. Defects in lysosomal maturation facilitate the activation of innate sensors in systemic lupus erythematosus. *Proc Natl Acad Sci U S A* 2016;113:E2142–51.
 56. Ahn J, Gutman D, Saijo S, Barber GN. STING manifests self DNA-dependent inflammatory disease. *Proc Natl Acad Sci U S A* 2012;109:19386–91.
 57. Doedens JR, Jones WD, Hill K, Mason MJ, Gersuk VH, Mease PJ, et al. Blood-borne RNA correlates with disease activity and IFN-stimulated gene expression in systemic lupus erythematosus. *J Immunol* 2016;197:2854–63.
 58. Bave U, Magnusson M, Eloranta ML, Perers A, Alm GV, Ronnblom L. Fc γ RIIa is expressed on natural IFN- α -producing

- cells (plasmacytoid dendritic cells) and is required for the IFN- α production induced by apoptotic cells combined with lupus IgG. *J Immunol* 2003;171:3296–302.
59. Furie R, Khamashta M, Merrill JT, Werth VP, Kalunian K, Brohawn P, et al. Anifrolumab, an anti-interferon- α receptor monoclonal antibody, in moderate-to-severe systemic lupus erythematosus. *Arthritis Rheumatol* 2017;69:376–86.
 60. Bhattacharyya S, Varga J. Endogenous ligands of TLR4 promote unresolving tissue fibrosis: implications for systemic sclerosis and its targeted therapy. *Immunol Lett* 2017;S0165–2478:30321–8.
 61. Elshabrawy HA, Essani AE, Szekanecz Z, Fox DA, Shahrara S. TLRs, future potential therapeutic targets for RA. *Autoimmun Rev* 2017;16:103–13.
 62. Dempsey A, Bowie AG. Innate immune recognition of DNA: a recent history. *Virology* 2015;479–480:146–52.
 63. Brunette RL, Young JM, Whitley DG, Brodsky IE, Malik HS, Stetson DB. Extensive evolutionary and functional diversity among mammalian AIM2-like receptors. *J Exp Med* 2012;209:1969–83.
 64. Vance RE. Cytosolic DNA sensing: the field narrows. *Immunity* 2016;45:227–8.
 65. Gaidt MM, Ebert TS, Chauhan D, Ramshorn K, Pinci F, Zuber S, et al. The DNA inflammasome in human myeloid cells is initiated by a STING-cell death program upstream of NLRP3. *Cell* 2017;171:1110–24e18.
 66. Gao D, Wu J, Wu YT, Du F, Aroh C, Yan N, et al. Cyclic GMP-AMP synthase is an innate immune sensor of HIV and other retroviruses. *Science* 2013;341:903–6.
 67. Cai X, Chiu YH, Chen ZJ. The cGAS-cGAMP-STING pathway of cytosolic DNA sensing and signaling. *Mol Cell* 2014;54:289–96.
 68. Hung T, Pratt GA, Sundararaman B, Townsend MJ, Chaivorapol C, Bhangale T, et al. The Ro60 autoantigen binds endogenous retroelements and regulates inflammatory gene expression. *Science* 2015;350:455–9.
 69. Mavragani CP, Sagalovskiy I, Guo Q, Nezos A, Kapsogeorgou EK, Lu P, et al. Expression of long interspersed nuclear element 1 retroelements and induction of type I interferon in patients with systemic autoimmune disease. *Arthritis Rheumatol* 2016;68:2686–96.
 70. An J, Durcan L, Karr RM, Briggs TA, Rice GI, Teal TH, et al. Expression of cyclic GMP-AMP synthase in patients with systemic lupus erythematosus. *Arthritis Rheumatol* 2017;69:800–7.
 71. Shao WH, Shu DH, Zhen Y, Hilliard B, Priest SO, Cesaroni M, et al. Prion-like aggregation of mitochondrial antiviral signaling protein in lupus patients is associated with increased levels of type I interferon. *Arthritis Rheumatol* 2016;68:2697–707.
 72. Buskiewicz IA, Montgomery T, Yasewicz EC, Huber SA, Murphy MP, Hartley RC, et al. Reactive oxygen species induce virus-independent MAVS oligomerization in systemic lupus erythematosus. *Sci Signal* 2016;9:ra115.
 73. Hasan M, Dobbs N, Khan S, White MA, Wakeland EK, Li QZ, et al. Cutting edge: inhibiting TBK1 by compound II ameliorates autoimmune disease in mice. *J Immunol* 2015;195:4573–7.
 74. König N, Fiehn C, Wolf C, Schuster M, Cura Costa E, Tungler V, et al. Familial chilblain lupus due to a gain-of-function mutation in STING. *Ann Rheum Dis* 2017;76:468–72.
 75. Liu Y, Jesus AA, Marrero B, Yang D, Ramsey SE, Montealegre Sanchez GA, et al. Activated STING in a vascular and pulmonary syndrome. *N Engl J Med* 2014;371:507–18.
 76. Ronnblom L, Elkon KB. Cytokines as therapeutic targets in SLE. *Nat Rev Rheumatol* 2010;6:339–47.
 77. Julian MW, Shao G, Bao S, Knoell DL, Papenfuss TL, VanGundy ZC, et al. Mitochondrial transcription factor A serves as a danger signal by augmenting plasmacytoid dendritic cell responses to DNA. *J Immunol* 2012;189:433–43.
 78. Rongvaux A. Innate immunity and tolerance toward mitochondria. *Mitochondrion* 2017. E-pub ahead of print.
 79. Goubau D, Schlee M, Deddouche S, Puijssers AJ, Zillinger T, Goldeck M, et al. Antiviral immunity via RIG-I-mediated recognition of RNA bearing 5'-diphosphates. *Nature* 2014;514:372–5.
 80. Lau CM, Broughton C, Tabor AS, Akira S, Flavel RA, Mamula MJ, et al. RNA-associated autoantigens activate B cells by combined B cell receptor/Toll-like receptor 7 engagement. *J Exp Med* 2005;202:1171–7.
 81. Vollmer J, Tluk S, Schmitz C, Hamm S, Jurk M, Forsbach A, et al. Immune stimulation mediated by autoantigen binding sites within small nuclear RNAs involves Toll-like receptors 7 and 8. *J Exp Med* 2005;202:1575–85.
 82. Uccellini MB, Busconi L, Green NM, Busto P, Christensen SR, Shlomchik MJ, et al. Autoreactive B cells discriminate CpG-rich and CpG-poor DNA and this response is modulated by IFN- α . *J Immunol* 2008;181:5875–84.
 83. Genung NE, Guckian KM. Small molecule inhibition of interleukin-1 receptor-associated kinase 4 (IRAK4). *Prog Med Chem* 2017;56:117–63.
 84. An J, Woodward J, Minie M, Sun X, Tanaka L, Peng Y, et al. Novel anti-malarial drug derivative inhibited type I interferon production and autoimmune inflammation through inhibition of cGAS-STING pathway in *trex1*^{-/-} mouse [abstract]. *Arthritis Rheumatol* 2016;68 Suppl 10. URL: <http://acrabstracts.org/abstract/novel-anti-malarial-drug-derivative-inhibited-type-i-interferon-production-and-autoimmune-inflammation-through-inhibition-of-cgas-sting-pathway-in-trex1-mouse/>.
 85. Yasutomo K, Horiuchi T, Kagami S, Tsukamoto H, Hashimura C, Urushihara M, et al. Mutation of DNASE1 in people with systemic lupus erythematosus. *Nat Genet* 2001;28:313–4.
 86. Rodero MP, Tesser A, Bartok E, Rice GI, Della Mina E, Depp M, et al. Type I interferon-mediated autoinflammation due to DNase II deficiency. *Nat Commun* 2017;8:2176.
 87. Kawane K, Ohtani M, Miwa K, Kizawa T, Kanbara Y, Yoshioka Y, et al. Chronic polyarthritis caused by mammalian DNA that escapes from degradation in macrophages. *Nature* 2006;443:998–1002.
 88. Stam AH, Kothari PH, Shaikh A, Gschwendter A, Jen JC, Hodgkinson S, et al. Retinal vasculopathy with cerebral leukoencephalopathy and systemic manifestations. *Brain* 2016;139:2909–22.
 89. Al-Mayouf SM, Sunker A, Abdwani R, Arawi SA, Almurshedi F, Alhashmi N, et al. Loss-of-function variant in DNASE1L3 causes a familial form of systemic lupus erythematosus. *Nat Genet* 2011;43:1186–8.

SPECIAL ARTICLE

2015 American College of Rheumatology Workforce Study

The Role of Graduate Medical Education in Adult Rheumatology

Marcy B. Bolster,¹ Anne R. Bass,² Jonathan S. Hausmann,³ Chad Deal,⁴ Marcia Ditmyer,⁵
Kamilah L. Greene,⁶ Seetha U. Monrad,⁷ and Daniel F. Battafarano⁸

Objective. Graduate medical education (GME), through fellowship training, plays a critical role in preparing new rheumatologists for our workforce and is an essential component when addressing the gap of excess demand for adult rheumatology care. This study was undertaken to assess the demographic characteristics and employment trends of new entrants entering the rheumatology workforce and the impact this will have on the supply of rheumatologists over the next 15 years.

Methods. Primary and secondary data sources were used to develop an integrated workforce model. Factors specific to new graduates entering the workforce included available and filled fellowship positions, gender shifts, planned work schedules (part-time or full-time), practice settings (academic or non-academic, private practice), and number of international medical graduates (IMGs) anticipating US practice.

Results. In 2015, there were 113 adult rheumatology programs, with 431 of 468 available positions filled. Using the 215 actual positions available annually in

fellowship programs as a starting point, after all factors were applied, the projected clinical full-time equivalent number entering the workforce each year was 107; this number was affected significantly by gender and generational trends. In addition, 17% of IMGs self-identified their plan to practice outside the US. Confounding predictions included a large proportion of current rheumatologists planning retirement with substantially reduced patient loads by 2030.

Conclusion. The current US adult rheumatology workforce is in jeopardy of accelerated decline at a time when demands on the workforce face tremendous growth. The current GME training structure cannot support the increased demand. Potential strategies to address this gap include innovative mechanisms for GME funding to increase fellowship training positions, incentives for pursuing rheumatology training (e.g., loan repayment programs), and novel means for recruitment of care to underserved areas of the US.

The views expressed herein are those of the authors and do not reflect the official policy or position of Brooke Army Medical Center, the US Army Medical Department, the US Army Office of the Surgeon General, the Department of the Army, the Department of Defense, or the US Government.

Supported by the American College of Rheumatology.

¹Marcy B. Bolster, MD: Massachusetts General Hospital, Boston; ²Anne R. Bass, MD: Weill Cornell Medical College, New York, New York; ³Jonathan S. Hausmann, MD: Boston Children's Hospital and Beth Israel Deaconess Medical Center, Boston, Massachusetts; ⁴Chad Deal, MD: Cleveland Clinic, Cleveland, Ohio; ⁵Marcia Ditmyer, PhD: University of California, Los Angeles, and University of Nevada, Las Vegas; ⁶Kamilah L. Greene, BBA: American College of Rheumatology, Atlanta, Georgia; ⁷Seetha U. Monrad, MD: University of Michigan, Ann Arbor; ⁸Daniel F. Battafarano, DO, MACP: San Antonio Military Medical Center, Fort Sam Houston, Texas.

Address correspondence to Marcy B. Bolster, MD, Rheumatology Fellowship Training Program, Massachusetts General Hospital, 55 Fruit Street, Boston, MA 02114. E-mail: mbolster@mgh.harvard.edu.

Submitted for publication July 31, 2017; accepted in revised form January 24, 2018.

A decade has passed since the previous assessment of the rheumatology workforce (1,2). The 2005 US Rheumatology Workforce Study was conducted to better understand factors affecting the supply of and demand for rheumatologists, to quantify these factors where possible, to project likely paths for the evolution of workforce supply and demand, and to assess the implications (1,2). Since 2005, projections of a workforce shortage have increased significantly. The Council on Graduate Medical Education has projected a deficiency of 85,000 physicians in 2020, a shortfall equaling ~10% of the current physician workforce (3). The Association of American Medical Colleges has similarly made projections and predicted a shortage of 124,000 full-time physicians by 2025 (4).

In 2005, an American College of Rheumatology (ACR) Workforce Study estimated the adult rheumatology

workforce to be 4,946 providers and projected growth of only 1.2% by 2025, resulting in a projected deficit of 2,576 rheumatologists (1,2). A significant gender shift in the workforce from 30.2% women to 43.6% women by 2025 was also predicted. In response to the projected gap in supply, the ACR supported initiatives to expand the number of rheumatology fellowship positions, improve practice efficiency, and increase the recruitment of nurse practitioners (NPs) and physician assistants (PAs) into rheumatology practice. As a result, available rheumatology fellowship positions increased nearly 19%, from 396 to 470 between 2005 and 2015. The ACR Committee on Training and Workforce convened a Workforce Study Group (WSG) to conduct the 2015 Rheumatology Workforce Study in consultation with the Academy of Academic Leadership. Among the WSG leadership were rheumatologists with expertise in graduate medical education (GME). The WSG was charged with updating rheumatology workforce projections, capturing a realistic view of clinical full-time equivalents (FTEs), and producing a comprehensive picture of access to care. The 2015 Workforce Study used a comprehensive, patient-centered, integrative framework approach to assess the current workforce and to project the supply of and demand for adult rheumatology services through 2030.

This article summarizes results pertaining to adult rheumatology training programs, demographic characteristics, and employment trends of graduates entering the adult rheumatology workforce. Additionally, the impact of GME on the supply of and demand for adult rheumatology care through 2030 is described.

METHODS

Workforce Study Group. The WSG, comprising volunteers with diverse backgrounds, broad perspectives, and a wide range of expertise relative to rheumatology workforce issues, included 3 fellowship program directors and 2 division directors. The WSG worked collaboratively to develop data collection procedures, design the workforce survey of ACR/Association of Rheumatology Health Professionals (ARHP) members, catalog critical supply and demand factors for adult rheumatology services, select the workforce study modeling process, and approve the final workforce study findings (5).

Data collection. A mixed methods approach was employed using both primary and secondary data to evaluate workforce issues and inform the development of the workforce model. Primary data, collected through electronic surveys of ACR/ARHP members and 2014–2015 rheumatology fellows-in-training (FITs), were supplemented by focus group data. Data were collected from many secondary sources such as the ACR membership database, American Medical Association (AMA), American Board of Internal Medicine, Rheumatology Nurses Society, and National Commission on Certification of Physician Assistants, as well as other published data for the purpose of

assessing the current base workforce and potential factors that would have a direct impact on the future workforce.

Workforce study modeling. The workforce study model incorporated an integrated workforce framework that combined socioeconomic and epidemiologic factors that drive demand with utilization rates that incorporate the current use of health care services. Supply factors included demographic breakdown of new graduate entrants, geographic distribution of programs, practice settings, productivity metrics (e.g., relative value units [RVUs]), retirement trends/succession planning, and workload trends. Demand factors included practice trends for providers, disease prevalence, population demographics, per capita income, cost of rheumatology care, and physician distribution per population, encompassing geographic trends.

Clinical FTE. The WSG recognized the importance of including both actual numbers of and clinical FTE for adult rheumatology practitioners entering the workforce. Clinical FTE describes the percentage of work effort devoted to clinical care to reflect a more realistic picture of patient access to care (e.g., 2 providers each caring for patients 50% of the time would together equate to 1.0 total clinical FTE). There are many factors that contribute to patient access to care, such as the number of female physicians (who tend to work fewer hours and see fewer patients [4]), part-time versus full-time workers, and retirement trends (4,5). Information from the literature and the guidance of the WSG, which included members from both the academic and the non-academic, private practice workforce, led to the assumption that 80% of the adult rheumatology workforce worked in non-academic private practice settings, with the remaining 20% in academic settings. Additionally, based on available data (both primary and secondary) regarding the distribution of workload in academic settings, the WSG reached consensus on the definition of a clinical FTE for purposes of the workforce study: 1.0 clinical FTE for adult rheumatology physicians working in non-academic private practice settings and 0.5 clinical FTE for adult rheumatologists working in academic settings.

Sensitivity testing. Sensitivity testing is a technique used to determine how different values of an independent variable impact a particular dependent variable under a given set of assumptions. Once the base-case model (starting point of 2015) was completed and the results were validated by the WSG, sensitivity testing was used to ascertain a best-case and worst-case scenario as it affects access to care, making it possible to estimate a range for supply of and demand for services through 2030. The base-case model incorporated best-estimated values of all selected parameters as determined through data collected from primary and secondary sources, as well as guidance from the WSG. This model represented status quo or unchanged assumptions across the workforce. The factors identified included changes in demographic parameters, anticipated retirements, part-time versus full-time employment, percentage working in academic versus non-academic settings, available adult fellowship positions, and non-physician providers (NPs and PAs) working in rheumatology (Table 1).

RESULTS

Systematic process outcomes. The following outcomes are a product of the systematic process used to

Table 1. Supply and demand model assumptions (base-case, best-case, and worst-case models)*

	Base-case model assumptions	Best-case model assumptions	Worst-case model assumptions
Supply factors			
Geographic	No changes in the geographic distribution through 2030 Physicians practicing in MSAs worked on average 15% fewer hours per week Mean 53 hours	No geographic changes in the model	No geographic changes in the model
Productivity (RVUs)	No factor applied for adults, due to low growth rate	No factor applied for adults, due to low growth rate	No factor applied for adults, due to low growth rate
Succession planning	~50% will retire through 2030 25% patient load reduction for those planning to retire (0.75 FTE)	Reduced retirement percentage to 40% for 2020, 2025, 2030	Increased retirement percentage to 60% for 2020, 2025, 2030
Sex	In 2015, 59.2% men and 40.8% women Expected 14% increase in the number of women by 2030 Women work 7 fewer hours/week and treat 30% fewer patients	Percentage of women decreased by 10% for 2020, 2025, 2030	Percentage of women increased by 10% for 2020, 2025, 2030
Full-time versus PT employment	~18% of the workforce work PT (0.5 FTE)	Percentage working PT decreased to 10% for 2020, 2025, 2030	Percentage working PT increased to 25% for 2020, 2025, 2030
Practice setting	90% working PT are women 80% non-academic private practice settings (1.0 FTE) 20% academic settings (0.5 FTE)	Percentage working in non-academic, private practice settings increased to 90% for 2020, 2025, 2030	Percentage working in non-academic, private practice settings decreased to 75% for 2020, 2025, 2030
New graduate entrants	215 graduates annually; ~1.4% will not graduate ~83% of IMGs stay in US ~18.3% work PT (0.5 FTE)	100% fill-rate, 25% increase in new graduates	50% fill-rate, stable number of new graduates
Non-physician providers (NPs/PAs)	~2% to 5% increase into rheumatology	Increase to 30% into rheumatology	Increase to 10% into rheumatology
Demand factors			
Patients with OA and other nonrheumatic diseases	~25% patient load	Decreased patient load to 0%	Increased patient load to 50%
Aging population	~18% patients ≥65 years of age ~25% patients ≥65 years of age	No change in the aging population rates	No change in the aging population rates
Prevalence of disease	~23% adult females ~18.6% adult males ~25% of all adult doctor-diagnosed arthritis by 2030	No change in the aging population rates	No change in the aging population rates

* Data are from the American College of Rheumatology 2015 Workforce Study (5). Sensitivity analysis was completed to see how changes in key parameters of the assumptions influenced supply and demand projections. All assumption factors have a synergistic effect that varies due to unexpected changes in estimated economic, geographic, and demographic variables. Best-case and worst-case scenarios were used to see how these changes may affect the rheumatology workforce. MSAs = metropolitan statistical areas; RVUs = relative value units; FTE = full-time equivalent; PT = part-time; IMGs = international medical graduates; NPs = nurse practitioners; PAs = physician assistants; OA = osteoarthritis.

determine the workforce model assumptions about the future rheumatology workforce needs and projected supply. It should be noted that these were not results of the workforce model but rather the preliminary product of the process in which the factors were determined to develop each model: base-case, best-case, and worst-case for access to care.

Supply factors. Data were collected from 94% of the 2014–2015 FITs, including demographic profiles and anticipated practice patterns. Based on the primary information gathered, in conjunction with secondary data, 3 major demographic changes emerged: 1) an increase in the number of retiring rheumatology physicians

and non-physician providers (e.g., NPs and PAs); 2) an anticipated increase in the percentage of women entering the adult rheumatology physician workforce; and 3) an anticipated increase in the number of new entrants seeking part-time employment. Of note, due to the small number of NPs and PAs in the rheumatology workforce, gender shift trends were not significant in the model, and therefore were not included.

Demand factors. Regression modeling with backward stepwise analysis was used to determine which factors significantly contributed to the demand for rheumatology services ($F = 39.06$, $P < 0.001$; $R^2 = 0.37$). Pearson's chi-square test was used to determine model fit

($P = 0.81$). There was no presence of multicollinearity. Major demand factors included health care utilization patterns, disease prevalence, and changes in patient demographics. Based on the regression results, ~50% of demand was due to the growth of the aging US population.

Sensitivity testing. Base-case supply projections assumed no increases in the number of training programs or changes in practice settings (non-academic private practice versus academic). In the best-case scenario for access to care, the supply of the adult rheumatology workforce increased to 5,989 and demand decreased to 6,692 clinical FTE by 2030. This reduced the excess demand from over 100% to 11.7%. In contrast, the worst-case scenario decreased the supply to 3,592 and increased demand to 8,666. This increased the excess demand to ~140%. The assumptions used in the base-case workforce model reflected the best estimates given the economic, social, and political climates in 2015. Table 1 provides the assumptions used in the base-case model, best-case model, and worst-case model for access to care.

Fellowship training programs. The number of adult rheumatology fellowship training programs increased from 108 (in 2005–2006) to 113 (in 2015–2016), with an associated increase in the number of available positions (396 in 2006–2007 to 470 in 2015–2016) (6–8) (Figure 1), reflecting both an increase in the number of programs as well as available positions within the

programs. It should be noted that not all positions are filled each year (e.g., 431 of 468 positions were filled in 2014–2015). At the same time, ~50 applicants to adult rheumatology fellowships fail to match each year.

There is a disproportionate number of adult rheumatology training programs across the US, with a much larger number of training programs in the Northeast and Mid-Atlantic regions (Figure 2). Except for California, regions west of the Mississippi have very few programs. Many states in the Northwest, Southwest, and North Central US have no programs or 1 rheumatology fellowship training program. In contrast, 13 states have 3 or more programs, and 8 states have 5 or more training programs.

New graduates. In 2014–2015, there were a total of 431 Accreditation Council for Graduate Medical Education (ACGME) adult fellows (211 first-year and 220 second-year fellows), 50 third-year fellows, and 8 fourth-year fellows (6). Of the ACGME fellows (first- and second-year fellows), 53% were IMGs and 57% were women (6). Of those who matriculate, ~1.4% do not graduate, and a projected 17% of international medical graduates (IMGs) plan to practice outside the US, resulting in ~18% fewer total graduates entering the workforce upon graduation. Therefore, it was projected that 176 of the potential 215 new graduates will enter the US adult rheumatology workforce each year (6,7). This provided an actual base-case number of total new graduates for further projections.

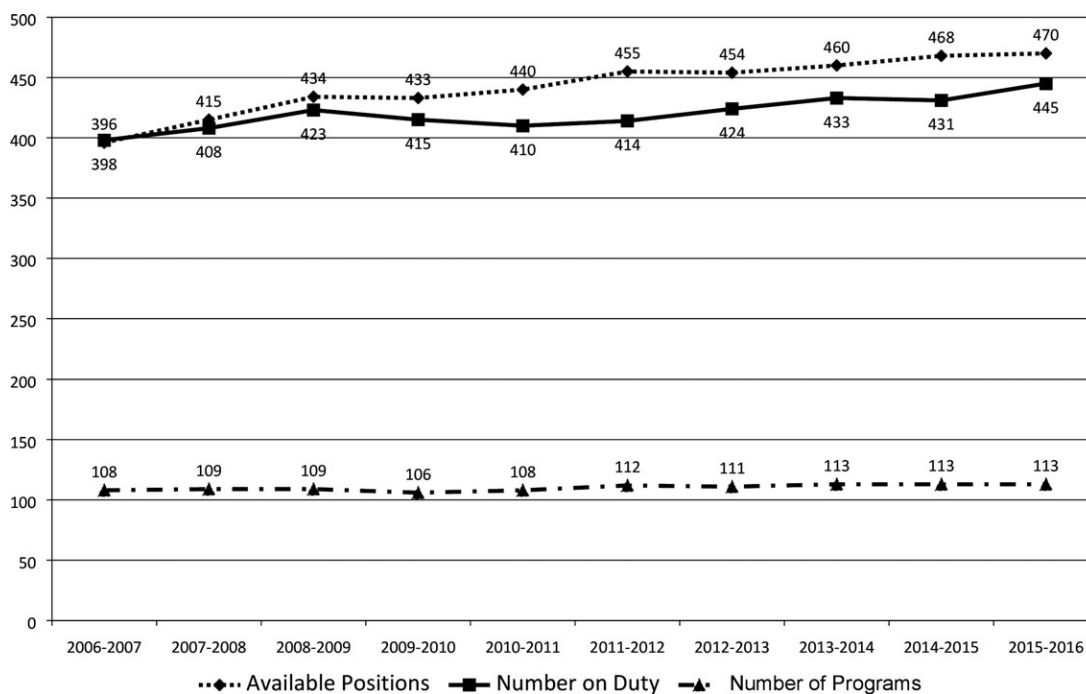


Figure 1. Adult rheumatology programs and positions in 2006–2007 through 2015–2016. The number of adult rheumatology training programs, available positions, and filled positions in the US in each academic year are shown. Data are from the Accreditation Council for Graduate Medical Education Data Resource Book, 2015–2016.

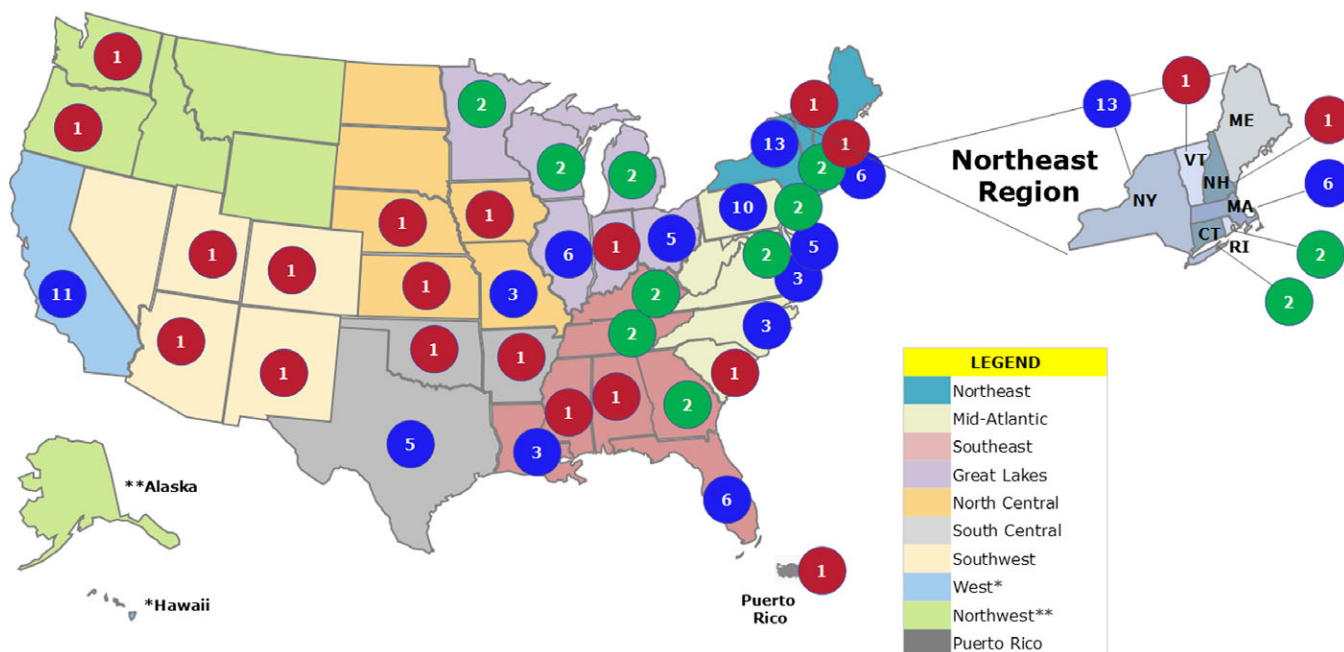


Figure 2. Number of adult rheumatology training programs in each US state in 2015. The numbers contained within the circles denote the number of fellowship programs in each state. Red indicates 1 program, green indicates 2 programs, and blue indicates 3 or more programs. * = includes Hawaii; ** = includes Alaska.

FIT survey data. While primary data were only a small portion of the development of the workforce study, information gathered from the FITs was used to help further develop factors used in the workforce study model associated with new graduates (5). A total of 351 adult rheumatology fellows, both first and second year (82%), completed the survey (7) (Table 2). Of those who responded to each item, ~63% (n = 214) were female, ~50% (n = 171) were IMGs, and most reported being white (49%; n = 164) of non-Hispanic origin (94%; n = 311). Most adult rheumatology FITs (83.2%; n = 292) were in a 2-year rheumatology fellowship program, the ACGME requirement for training. Of 113 fellows pursuing 3 or more years of fellowship training (23.3% of all FITs), 65.5% were US medical graduates and the remainder were IMGs. Student loan debt was carried by most US medical graduate FITs (70.6%). Among those with debt, 44.4% owe more than \$100,000 and 12.2% owe more than \$300,000 (7) (Figure 3).

More than 80% of adult rheumatology fellows reported they would work full-time (n = 283), with ~20% reporting that they planned to work part-time or were not sure at the time of the survey. Approximately 40% of the adult rheumatology FIT respondents planned to seek employment in an academic health center (n = 138). Of these, ~71% (n = 98) were women. A small proportion of FITs (4.6%; n = 14) had plans to pursue rheumatology before medical school, and the majority of FITs made

their decision to pursue rheumatology during their second or third year of residency training. Intellectual interest, lifestyle, clinical exposure, and mentorship were impor-

Table 2. Self-reported demographic characteristics of adult rheumatology fellows-in-training 2014–2015*

Sex (n = 341)	
Male	127 (37.2)
Female	214 (62.8)
Where graduated (n = 343)	
US medical school	172 (50.1)
Non-US medical school	171 (49.9)
Ethnicity (n = 331)	
Hispanic	20 (6.0)
Non-Hispanic	311 (94.0)
Race (n = 336)	
American Indian or Alaskan Native	2 (0.6)
Asian	143 (42.5)
African American	11 (3.3)
Native Hawaiian or other Pacific Islander	3 (0.9)
White	164 (48.8)
>2 races	13 (3.9)
Age, years (n = 330)	
25–30	110 (33.3)
31–35	174 (52.7)
36–40	35 (10.6)
41–45	6 (1.8)
>45	5 (1.5)
Length of fellowship (n = 351)	
2 years	292 (83.2)
>2 years	59 (16.8)

* Values are the number (%). Data were obtained from a survey of 2014–2015 fellows (n = 351) (7). The number of responses varied for some demographic characteristics; thus, the total does not equal 351 for each category.

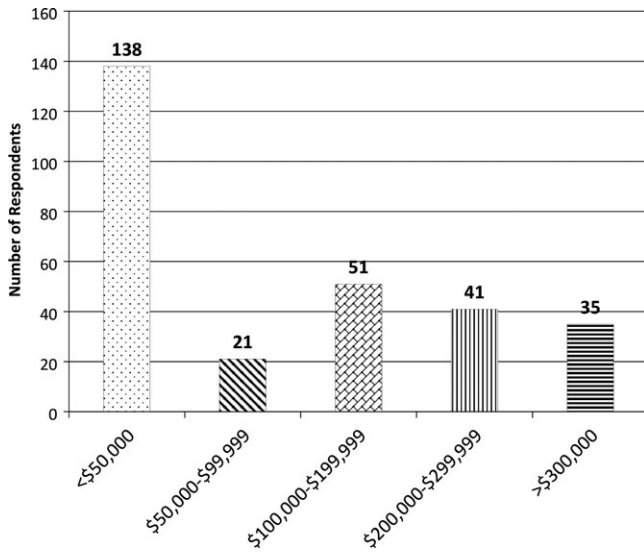


Figure 3. Reported student loan debt of adult rheumatology fellows-in-training in 2015 (7).

tant factors reported in making the decision to pursue rheumatology subspecialty training. Income potential was the least likely contributor to this decision-making process (6.1%; n = 21).

Workforce projections. Women constitute a growing proportion of the physician workforce. The AMA reported that female physicians worked 7 fewer hours per week than male physicians, and treated ~30% fewer patients than did their male counterparts per year (4,9,10). For the purposes of the workforce study, several

factors were considered, and the following were applied to new graduates entering the workforce. The number of fellowship programs and available positions would remain constant from 2015 through 2030 with all positions filled each year; 18% fewer total graduates due to both IMGs leaving to practice outside the US upon graduation and a small percent of natural attrition; 18% would seek part-time employment; and 59% of the new entrants would be women.

With these combined factors, the projected clinical FTE for adult rheumatology graduates was 107 per year, a significant decrease from the total of 215 possible new physician entrants per year. Importantly, it should be noted that the projected clinical FTE of 107 quantitates the clinical care providers available and/or the potential access to care number for patients rather than the total number of providers.

Retirement and succession planning projections. More than 50% of adult rheumatologists reported retirement plans over the next 10–15 years (Figure 4), 80% of whom anticipated decreasing their patient load by at least 25% before retirement. Therefore, a factor of 0.75 FTE was applied to reflect the proportion of those anticipating retirement.

Supply and demand projections. The projections for supply and demand for adult rheumatology services compared the total number of adult rheumatology providers to the projected clinical FTE of all providers from 2015 to 2030 (5). The base-case model indicated an excess demand for adult rheumatology providers of 1,118 FTE

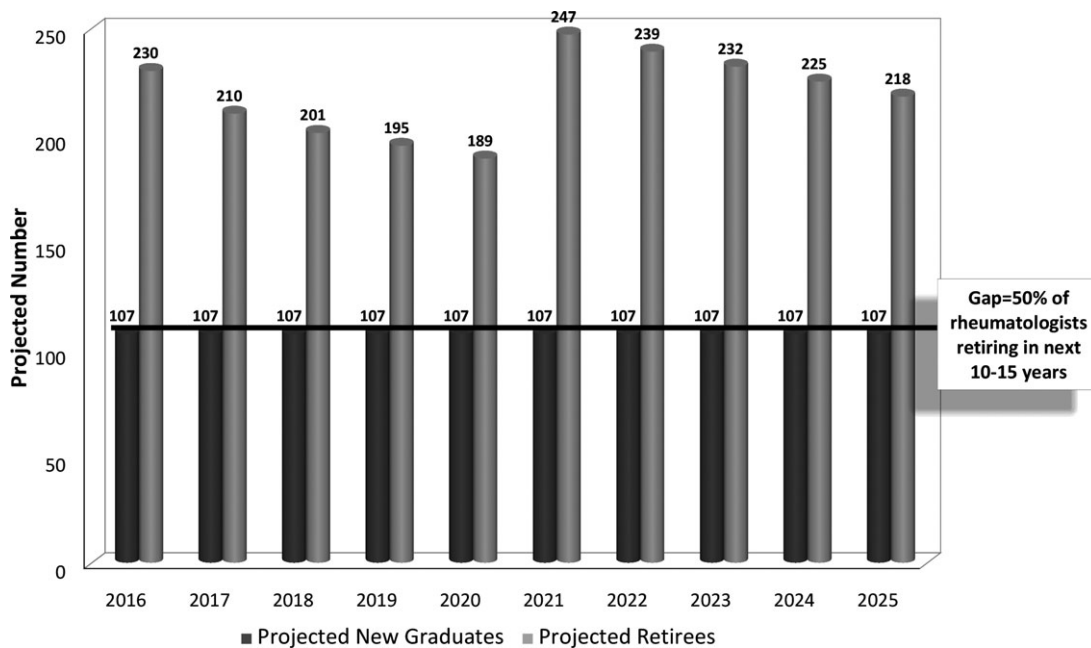


Figure 4. Adult rheumatologists 2016–2025. The projected numbers of retirees versus fellow graduates are shown in clinical full-time equivalents.

in 2015. By 2030, the excess demand would be 4,729 FTE, representing an increase of 137.8% (difference between the projected workforce FTE supply of 3,455 and the projected FTE need of 8,184) from the base-case model (5). Sensitivity testing produced the best-case and worst-case scenarios for access to care based on potential changes through 2030.

The excess demand would vary from 5,566 (+182% change) in the worst-case scenario to 1,388 (+26.6% change) in the best-case scenario for access to care, which is a range of >4,000 clinical FTE. While these best-case and worst-case scenarios identified extremes, they are helpful in distinguishing different ranges in the workforce as they compare to the base-case model that may occur in trends across the next 15 years.

DISCUSSION

This study analyzed the ACR workforce study from a GME perspective to evaluate the status of the current workforce, assess need, address retirement rates, facilitate planning for training of new entrants, and maximize access to care potential. While total numbers of providers (including non-physician providers) were projected, the WSG clearly defined clinical FTE to better project available clinical providers for patient access to care. This factor, clinical FTEs, was included with all other factors to provide the best projection for the future rheumatology workforce. Any projected deficit in supply should be used to inform GME innovations to train more rheumatologists available for patient care.

While men currently comprise 59% of the rheumatology workforce, there is an anticipated gender shift occurring due to the current adult rheumatology workforce beginning to retire and being replaced by new graduates. By 2030, it is anticipated that men will constitute only 43% of the workforce. In that regard, the literature has reported that female physicians work, on average, 7 fewer hours each week, and see 30% fewer patients than their male counterparts (4,9,10). Additionally, notably, 60% of FITs plan to enter private practice, a smaller proportion than the currently estimated 80% of rheumatologists in non-academic private practice. Each of these shifts contributes significantly to the reduced supply of rheumatologists over the next 15 years.

Moreover, millennials (born between 1982 and 2004) comprise 6% of the current workforce but by 2030 will comprise 44% of the rheumatology workforce (11), surpassing the baby boomers to become the largest proportion of the American workforce (12,13). Millennials see 5% fewer patients now than did their counterparts in 2005 (4,12). In comparing patient visits with male compared to

female providers, there was a drop in the average number of patient visits between 2005 and 2015; female millennials, on average, had ~35% fewer patient visits, whereas the decline in average patient visits for male millennial providers was 17% (5). The ability to work flexibly and find a job near other family members has been reported as a high priority by more millennials (12,14). Additionally, millennials were more likely to have made, or to be willing to make, sacrifices for family and personal responsibilities (9,10).

Approximately 53% of the US adult rheumatology FITs are IMGs and, importantly, nearly 20% of IMG FITs plan to practice outside the US, thus not necessarily contributing to reducing the US workforce supply gap. While IMGs do not have the same burden of loan repayment as most US medical school graduates have incurred (13), they may have immigration and work visa-related pressures affecting post-fellowship career choices. These factors, along with gender and millennial factors, significantly contribute to the lower estimate of only 107 new graduate clinical FTEs per year.

In light of the potential increases in demand for adult rheumatology services, succession planning patterns were critical to the workforce supply model. The accuracy of physician supply projections has been questioned because of uncertainty about physician retirement patterns. Data from the literature suggest that physicians tend to retire at a more advanced age than individuals in other occupations (4); therefore, primary data were used to assist in succession planning projections over the next 15 years. Of the 50% of rheumatologists who reported plans to retire over the next 15 years, a significant proportion plan to reduce their clinical patient load (5). These high projections will clearly impact access to care for patients with rheumatic diseases as the aging workforce retires and/or reduces patient workload and is replaced by new graduates. Innovative strategies to expand GME training positions must be established to address these potential deficits, while in parallel addressing practice design and efficiency.

The US adult rheumatology workforce is thus projected to experience multifaceted limitations in its growth potential over the next 15 years, amplifying the already increasing gap between supply and rising demand for rheumatology care. To target closure of this gap by increasing new graduate entrants into rheumatology would require the training of more than 4,000 providers over the next 15 years; this is unrealistic, requiring a more than doubling of the number of available fellowship positions. Nonetheless, increasing GME positions in rheumatology and targeting underserved locations are requisite to addressing the looming supply-demand chasm and regional maldistribution.

Between 2005 and 2015, the percentage of internal medicine residents entering rheumatology has remained stable at ~4% (6,8). During this period, the number of internal medicine residents has increased, thus resulting in a small increase in entrants into rheumatology. During this period, the number of rheumatology fellowship training programs has also increased from 108 to 113, and the number of available first-year rheumatology fellowship positions has increased by 35%, from 156 to 210. Approximately 50 applicants to rheumatology fellowships fail to match each year, and 100 failed to match in 2016. With <10 open or unmatched rheumatology fellowship positions each year, it is apparent that there are many potential applicants available for fellowship selection, suggesting that physicians will be available to fill fellowship positions if additional GME slots are made available.

The Centers for Medicare and Medicaid Services have been the single largest supporter of GME financing for residency and fellowship training since the 1980s, and each ACGME-accredited program receives direct GME funds proportionate to the share of the hospital's care provided to Medicare patients (15). In 2014, the Institute of Medicine delineated the importance of reassessing GME support, distribution, and governance to better address the changing health care landscape and the already occurring changes in workforce needs; it is imperative that modifications in GME financing occur to address the workforce shortage (15).

Following the 2005 US Workforce Study, the Rheumatology Research Foundation (RRF) initiated a grant program to provide partial salary support for rheumatology fellows. These grants were initially valued at \$25,000 per fellow and, since 2015, \$50,000 per fellow per year (current estimate of up to 50% salary and fringe benefits support per fellow). In total, support has ranged from \$500,000 to \$1,400,000 per year, and over the past 14 years the RRF has awarded a remarkable 392 grants, totaling just under \$11,000,000 in partial salary support for fellows. This grant funding mechanism has been crucial for providing rheumatology fellow salary support and growing the workforce, and we encourage its continuation.

Providing incentives for IMG FITs to remain in the US to practice is another way to bolster the workforce. Most IMGs do not have student debt, but many face immigration and visa-related obstacles that impact choice of practice location. Unless IMGs hold US citizenship or permanent residency status, they are often not eligible for grants to fund salary and/or research and are thus less likely to train in 3-year training programs. Therefore, they are more likely to provide direct patient care after completing 2 years of fellowship training. Strong advocacy may be needed to increase the number of J1

waiver slots in underserved areas (allowing many IMGs to remain in the US after graduation), and to reduce barriers to visa renewal for these important members of the field, especially given that more than half of rheumatology FITs are now graduates of medical schools outside the US.

The 2015 Workforce Study projected not only a deficit but also a growing maldistribution of rheumatologists. Metropolitan areas have a higher density of rheumatologists (5). These data have not changed substantially relative to the 2005 Workforce Study, and there have not been significant actions to resolve this imbalanced distribution. It has been demonstrated previously that most trainees enter practice in close geographic proximity to their training program (16). Important to this consideration is that there are 5 states with no rheumatology training programs. The RRF recently developed a fellowship training award targeting programs in underserved areas. More such targeted GME funding mechanisms are needed.

Strengths of this study included the incorporation of several robust databases from different sources (1–4,6,8,17). In addition, the secondary data were supplemented by primary data from rheumatology providers, FITs, and patients; primary data provided current and reliable information about new entrants into our field. Importantly, estimates and projections for workforce supply and demand were based upon FTEs rather than numbers of health care providers. This approach provides a more accurate estimate of supply from the vantage point of the patient than a simple enumeration of practitioners.

There were several limitations to this study, including determining the actual number of rheumatologists in the workforce treating patients as well as the number of currently board-certified physicians who are no longer treating patients. Defining an accurate breakdown between those working in non-academic, private practice and academic settings was also a limitation. The modeling was based on a stable number of new entrants into the workforce, with projections for part-time practice and practice setting derived from both primary and secondary data sources. The response rate to the ACR membership survey, while sufficient (38.5%) (5), may not have been representative of the entire population of rheumatology practitioners. Last, the use of cross-sectional data to project forward, reflecting changes across time, was also a limitation.

Planning for the future of the rheumatology workforce is vital. GME provides the necessary inflow of rheumatologists into our specialty and is thus of fundamental importance in filling the gap between rheumatology supply and demand. It is imperative that the rheumatology specialty adopt innovative approaches to augment the supply of rheumatologists, and while this was one of the strategic plans derived from the 2005

Workforce Study, the workforce landscape has since changed significantly due to shifts in demographics, practice setting, and part-time work. These new projections underlined a well-defined picture of adjusted provider clinical productivity that clearly portrays the need. These projections more accurately approximated the patient-centered approach to care access and demonstrated that merely increasing fellowship positions will not suffice. A multipronged approach is warranted and must include both increased recruitment of trainees into rheumatology and improved geographic distribution of rheumatologists. The 2015 Workforce Study not only informed us of the magnitude of the supply versus demand chasm, but added insight into the requirement for novel mechanisms as we move forward. To escalate recruitment, it is important to increase mentoring opportunities for medical students and internal medicine residents. Consideration may be given to incentives such as student loan repayment, geographic redistribution, and attracting IMG fellows to remain in the US for practice.

Additionally, it is imperative to address physician burnout and foster continued dedication to rheumatology practice for those entering the field, by advocating for policies that increase practice efficiency and reduce barriers to patient access. At the same time, innovative approaches to rheumatology care are needed since the number of FITs would have to more than double to meet our needs in the coming years. Increased recruitment of NPs and PAs to rheumatology, practice redesign, use of telemedicine to extend our reach, and further collaboration with primary care physicians in the co-management of patients with some rheumatic diseases are some approaches to consider. It is, however, evident that we must train more rheumatologists, and this will require innovative GME funding mechanisms.

In conclusion, the specialty of rheumatology is facing a crisis of diminishing supply in the face of growing demand. Demographic shifts related to generation, gender, productivity, and immigration status, along with the aging practitioner population, are creating a trajectory that is diverging from the increasing demand for rheumatology care. This study provides data and valuable insight into the role of GME and the challenges of sustaining an adequate supply of rheumatologists over the next 15 years.

AUTHOR CONTRIBUTIONS

All authors were involved in drafting the article or revising it critically for important intellectual content, and all authors approved the final version to be published. Dr. Bolster had full access to all of the data in the study and takes responsibility for the integrity of the data and the accuracy of the data analysis.

Study conception and design. Bolster, Hausmann, Deal, Ditmyer, Greene, Monrad, Battafarano.

Acquisition of data. Bolster, Hausmann, Deal, Ditmyer, Greene, Monrad, Battafarano.

Analysis and interpretation of data. Bolster, Bass, Hausmann, Deal, Ditmyer, Monrad, Battafarano.

REFERENCES

1. American College of Rheumatology. 2005 workforce study of rheumatologists: final report. Prepared by Lewin Group, May 2006. URL: <https://www.rheumatology.org/Portals/0/Files/LewinReport.pdf>.
2. Deal CL, Hooker R, Harrington T, Birnbaum N, Hogan P, Bouchery E, et al. The United States rheumatology workforce: supply and demand, 2005–2025. *Arthritis Rheum* 2007;56:722–9.
3. Council on Graduate Medical Education (COGME). Twentieth report: advancing primary care. 2010. URL: <https://www.hrsa.gov/advisorycommittees/bhpradvisory/cogme/Reports/twentiethreport.pdf>.
4. Association of American Medical Colleges. The complexities of physician supply and demand: projections from 2013 to 2015. URL: https://www.aamc.org/download/426242/data/ihsreportdownload.pdf?cm_mmc=AAMC_-_ScientificAffairs_-_PDF_-_ihsreport.
5. American College of Rheumatology Workforce Study Group. The 2015 workforce study of rheumatology specialists in the United States. 2016. URL: <https://www.rheumatology.org/learning-center/statistics/workforce-study>.
6. ACGME. Rheumatology programs academic year 2014–2015. United States. URL: <https://apps.acgme.org/ads/Public/Reports/ReportRun?ReportId=11&CurrentYear=2017&AcademicYearId=2014>.
7. Hausmann JS, Monrad S, Ditmyer M, Bolster MB, Imundo LF, Battafarano D. The future of rheumatology: pediatric and adult fellows-in-training results from the 2015 ACR/ARHP workforce study [abstract]. *Arthritis Rheumatol* 2016; 68 Suppl 10. URL: <http://acrabstracts.org/abstract/the-future-of-rheumatology-pediatric-and-adult-fellows-in-training-results-from-the-2015-acrarhp-workforce-study/>.
8. ACGME. Rheumatology programs academic year 2015–2016. United States. URL: <https://apps.acgme.org/ads/Public/Reports/ReportRun?ReportId=8&CurrentYear=2017&SpecialtyId=&AcademicYearId=2015>.
9. Staiger DO, Auerbach DI, Buerhara PI. Comparison of physician estimates and supply projections. *JAMA* 2009;302:1674–80.
10. Tsugawa Y, Jena AB, Figueroa JF, Orav EJ, Blumenthal DM, Jha AK. Comparison of hospital mortality and readmission rates for Medicare patients treated by male vs. female physicians. *JAMA Internal Medicine* 2017;177:206–13.
11. Bureau of Labor Statistics. Occupational outlook handbook. 2015. URL: <http://www.bls.gov/ooh/a-z-index.htm#P>.
12. Young J. Millennial providers and work-life balance: are they on to something? Perspective on the Acute Care Continuum. December 2016. URL: <https://www.vituity.com/blog/millennial-providers-and-work-life-balance-are-they-on-to-something>.
13. The Pew Research Center. Millennials overtake Baby Boomers as America's largest generation. 2016. URL: <http://www.pewresearch.org/fact-tank/2016/04/25/millennials-overtake-baby-boomers/>.
14. Global generations. A global study on work-life challenges across generations. 2015. URL: [http://www.ey.com/Publication/vwLUAssets/EY-global-generations-a-global-study-on-work-life-challenges-across-generations/\\$FILE/EY-global-generations-a-global-study-on-work-life-challenges-across-generations.pdf](http://www.ey.com/Publication/vwLUAssets/EY-global-generations-a-global-study-on-work-life-challenges-across-generations/$FILE/EY-global-generations-a-global-study-on-work-life-challenges-across-generations.pdf).
15. Institute of Medicine of the National Academies of Sciences. Graduate medical education that meets the nation's health needs. 2014. URL: <https://www.nap.edu/read/18754/chapter/1>.
16. American College of Rheumatology Committee on Rheumatology Training and Workforce Issues. Regional distribution of adult rheumatologists. *Arthritis Rheum* 2013;65:3017–25.
17. Association of American Medical Colleges. 2017 update: the complexities of physician supply and demand: projections from 2015 to 2030. URL: https://aamc-black.global.ssl.fastly.net/production/media/filer_public/a5/c3/a5c3d565-14ec-48fb-974b-99fafaeceb00/aamc_projections_update_2017.pdf.

SPECIAL ARTICLE

Common Language Description of the Term Rheumatic and Musculoskeletal Diseases (RMDs) for Use in Communication With the Lay Public, Healthcare Providers, and Other Stakeholders Endorsed by the European League Against Rheumatism (EULAR) and the American College of Rheumatology (ACR)

Désirée van der Heijde,¹ David I. Daikh,² Neil Betteridge,³ Gerd R. Burmester,⁴ Afton L. Hassett,⁵ Eric L. Matteson,⁶ Ronald van Vollenhoven,⁷ and Sharad Lakhanpal⁸

A European League Against Rheumatism–American College of Rheumatology working group consisting of practicing and academic rheumatologists, a rheumatology researcher, and a patient representative created a succinct general statement describing rheumatic and musculoskeletal diseases (RMDs) in adults and children in language that can be used in conversations with the lay public, media, healthcare providers, and other stakeholders. Based on the literature review, several elements were deemed important for inclusion in the description of RMDs. First, RMDs encompass many different diseases that can affect individuals at any age, including children. Second, there are various pathophysiological pathways underlying different RMDs. Third, the impact of RMDs on individuals and society should be emphasized. The working group agreed that the language

should be comprehensible to the lay public. Thus, the following description of RMDs has been developed: “Rheumatic and musculoskeletal diseases (RMDs) are a diverse group of diseases that commonly affect the joints, but can affect any organ of the body. There are more than 200 different RMDs, affecting both children and adults. They are usually caused by problems of the immune system, inflammation, infections, or gradual deterioration of joints, muscles, and bones. Many of these diseases are long term and worsen over time. They are typically painful and limit function. In severe cases, RMDs can result in significant disability, having a major impact on both quality of life and life expectancy.” This description can be used by rheumatology groups, researchers, and those who work in advocacy and education related to RMDs.

This article is published simultaneously in the June 2018 issue of *Annals of the Rheumatic Diseases*.

¹Désirée van der Heijde, MD, PhD: Leiden University Medical Center, Leiden, The Netherlands; ²David I. Daikh, MD, PhD: University of California San Francisco and San Francisco VA Medical Center, San Francisco, California; ³Neil Betteridge: Neil Betteridge Associates, London, UK; ⁴Gerd R. Burmester, MD: Charité—University Medicine Berlin, Free University, and Humboldt University Berlin, Berlin, Germany; ⁵Afton L. Hassett, PsyD: University of Michigan, Ann Arbor; ⁶Eric L. Matteson, MD: Mayo Clinic College of Medicine, Rochester, Minnesota; ⁷Ronald van Vollenhoven, MD, PhD: Amsterdam Rheumatology and Immunology Center, Amsterdam, The Netherlands; ⁸Sharad Lakhanpal, MBBS, MD: Rheumatology Associates and UT Southwestern Medical Center, Dallas, Texas.

Address correspondence to Désirée van der Heijde, MD, PhD, Leiden University Medical Center, Department of Rheumatology, PO Box 9600, 2300 RC Leiden, The Netherlands. E-mail: mail@dvan derheijde.nl.

Submitted for publication October 19, 2017; accepted in revised form January 15, 2018.

The field of rheumatology encompasses a wide range of medical conditions that affect many organ systems. These conditions reflect diverse pathogenic mechanisms and result in functional limitations, diminished quality of life, and increased patient mortality. In addition, although rheumatic conditions in total are among the most common of all medical problems, many of the individual diseases are uncommon or even rare. This situation results in an ever-present dilemma for the field. Most of the public and policymakers around the world do not know about many of the rheumatic and musculoskeletal diseases (RMDs) and even if they have heard of them, there is broad lack of awareness about the complexity and enormous importance of this area of medicine.

To further public awareness and support policies directed towards lessening the impact of these diseases on patients and society, a working group from the European

League Against Rheumatism (EULAR) and the American College of Rheumatology (ACR), consisting of practicing and academic rheumatologists, a patient representative, and a rheumatology health professional, has developed a formal description of these conditions. The goal of this effort was to create a succinct general statement describing RMDs in adults and children in language that can be used in conversations with the general population with and without RMDs; media; healthcare providers; policymakers at local, national and international levels; health insurance companies; charities; employers; and other stakeholders.

Several elements were deemed important for inclusion in the description of RMDs by the group. First, it should be emphasized that RMDs encompass many different diseases that can affect persons at any age, including children. Second, it should be clear that there are various pathophysiological causes of RMDs. Third, the impact of RMDs on individuals and society should be emphasized. Finally, the language should be easily understood by the lay public. Here we will discuss various aspects that provide relevant background information, which can be used during the discussion about the importance of RMDs with the relevant stakeholders.

Methodology

The participants of the working group were selected based on their position in the respective organizations. For EULAR this was the president, the chair of the EULAR standing committee of clinical affairs, the EULAR liaison to the ACR, and a patient representative. For the ACR, the president and president-elect of the ACR, the president of the Association of Rheumatology Health Professionals, and the president of the Rheumatology Research Foundation were included. The group met once in person, had one teleconference, and all other exchanges were conducted by e-mail. There was a scoping review of the literature with emphasis on “grey literature” such as reports from the European Union (EU).

RMDs encompass many different diseases that can affect persons at any age, including children

Data suggest that there are over 200 RMDs; some conditions are very common, while others are rare. Lists of RMDs have been compiled in a number of publications and survey results. For example, the ACR web site features a detailed list, as does the EULAR web site (1,2). The latter is considered the official list as applied by the European Union of Medical Specialists (EUMS) (see Supplementary Appendix, on the *Arthritis &*

Rheumatology web site at <http://onlinelibrary.wiley.com/doi/10.1002/art.40448/abstract>). In addition, the Arthritis Foundation, a patient organization in the USA, and the ACR maintain patient-oriented lists of RMDs (3,4).

Well-known and prevalent examples of RMDs are rheumatoid arthritis (RA), osteoarthritis (OA), and gout. According to a conservative estimate of the United Nations, symptomatic OA, or degenerative joint disease, affects 15% of people worldwide, and it is estimated that by 2050, over 130 million people will suffer from OA worldwide and 40 million will be severely disabled (5).

RA is the most common autoimmune inflammatory form of arthritis and affects approximately 1 in 100 persons worldwide, with women affected twice as commonly as men (6).

Gout is the most common cause of inflammatory arthritis in men and has a prevalence in the USA and Europe of about 4% (7,8).

Many other RMDs are less common, but cause significant morbidity and mortality. For example, systemic lupus erythematosus, which affects women approximately 9 times more frequently than men, is a systemic autoimmune disease that frequently causes arthritis and dysfunction of connective tissues among many other systemic manifestations (9,10). The overall lifetime risk for developing an inflammatory RMD including RA, gout, lupus, and others for an adult in the USA has been calculated as 1 in 12 for women and 1 in 20 for men (11). Many RMDs are uncommon or rare, which contributes to the lack of familiarity and/or experience with many RMDs on the part of general practitioners. RMDs frequently affect joints resulting in arthritis, and also frequently involve other internal organs and the skin. Although arthritis is commonly considered as a disease of aging, many RMDs—including many that cause disabling arthritis—occur in children. Lack of awareness of these conditions in both children and adults can lead to excessive and unnecessary damage and disability (12–15).

There are various pathophysiological pathways of RMDs

Review of these many diseases and conditions indicates that they develop through a diverse range of pathogenic pathways, most of which are not completely understood. Many result from dysregulation and activation of immune mechanisms that lead to inflammation and tissue damage. Some of these are classified as autoimmune diseases. Other RMDs result from acute or chronic damage to musculoskeletal structures including bone, cartilage, muscle, tendon, ligament, and blood vessels. Other primary metabolic, endocrine, neurologic, and infectious diseases can lead to secondary dysfunction and damage of

musculoskeletal tissue. For example, prolonged hyperglycemia in diabetes can result in changes in the structure of tendons and other soft tissues resulting in impaired mobility and joint function. The metabolic changes of the iron-storage disease hemochromatosis can result in degenerative arthritis in the hands. In addition, an increasing number of genetic variations and mutations are associated with the development of RMDs.

RMDs result in a major burden for both the individual and the society

Many of the diseases are chronic and as they can start as early as during childhood (e.g., juvenile idiopathic arthritis) or young adulthood (e.g., spondyloarthritis), patients suffer with their disease for decades. Moreover, most RMDs worsen over time with increasing impact on both the physical and psychological conditions of the patient. Some patients die prematurely as a result of the condition or comorbidities, although if appropriately treated, mortality is relatively low in most of these conditions.

Large population studies emphasize that RMDs are highly prevalent worldwide. The eumusc.net project is a collaboration of 22 organizations in 17 member states of the EU investigating musculoskeletal health in Europe (16). Their report summarizes the epidemiology of major RMDs, impact on the individual and society, and management and health services utilization. They concluded that musculoskeletal problems are the most common cause of severe long-term pain and disability in the EU and lead to significant healthcare and social support costs. Moreover, RMDs are a major cause of loss of work productivity resulting in significant economic costs and may have serious impact on quality of life, affecting those with the conditions and their relatives.

Musculoskeletal pain is prevalent in the EU with just over one-fifth (22%) of the population reporting current or long-term muscle, bone, and joint problems in a survey performed by the EU in 2007 (17). Exactly a quarter of all EU respondents say that at some point in their life they have experienced chronic (lasting for at least 3 months) restrictive pain affecting muscles, joints, neck, or back which affected their ability to carry out activities of daily living. Such pain is reported more by women than by men (28% versus 22%). Musculoskeletal pain is the second most common complaint underlying long-term treatment contributing to major healthcare costs (17). Twenty-four percent of the respondents to the survey received long-term treatment for RMDs (second after hypertension with 36% of respondents). It is likely that the overall burden of arthritis is underestimated in virtually every population. A recent study from the USA

using national data from a health interview survey and doctor-diagnosed arthritis and symptoms revealed that arthritis affected 91.2 million (36.8%) of the adult population, including about 29% of men and 55% of women between the ages of 18 and 65 (18).

RMDs were the most frequent reason among non-infectious diseases to consult the primary care physician in the UK in 2003, and this was increasing with age and higher in female patients in all age categories (16). In Germany, 11.2% of the total cost of illness in 2008 was spent on musculoskeletal and connective tissue diseases (16). These numbers appear to be rapidly increasing. For example, a recent report provides data on doctor-diagnosed OA in the USA between 2013 and 2015 (19). A total of 54.4 million Americans (22.7%) had doctor-diagnosed OA and this percentage was even higher among adults with heart disease (49.3%), diabetes (47.1%), and obesity (30.6%). In 2012, 54% of people in the USA over age 18 reported suffering a musculoskeletal problem, and the prevalence approached 75% for those aged 65 and older (*The Burden of Musculoskeletal Diseases in the United States*) (20). Several factors have an impact on the prevalence of RMDs, including sex, age, body mass index, and physical activity. As the population is aging this has a major impact on the prevalence of RMDs. For example, the EU will have 58 million more people aged 65 and over in 2050 in comparison to 2004 (16). Similarly, obesity is increasing, which again will lead to a higher prevalence of RMDs.

RMDs have led to significant reduction in function and quality of life as well as increased disability. Among those with OA, 43.5% of the adults experienced limitations in activity attributable to OA, and there was a significant increase of 20% in the proportion of adults reporting these limitations since 2002. The disability-adjusted life year (DALY) is a measure to compare impact of various diseases on disability and can be interpreted as the loss of 1 year of healthy life. The World Health Organization (WHO) listed OA as the eighth leading cause of impact measured by DALYs in their report on global burden of disease (21). Another way of assessing the impact on disability is the years lived with disability (YLD). The WHO listed musculoskeletal diseases as the third cause for disability among noncommunicable diseases assessed by YLDs. And among musculoskeletal diseases, OA was the most common disease, followed by RA, "other musculoskeletal diseases," and gout (22). As common and impactful as musculoskeletal diseases are, such surveys do not always include the entire range of RMDs. This further underscores the high prevalence and cost of these conditions and emphasizes the need for a unifying definition of RMD. An example of defining the global burden of "other musculoskeletal disorders" was presented in a large study in 2010 (23,24).

The International Quality of Life Assessment project examined the effect of multiple chronic conditions on populations in Denmark, France, Germany, Italy, Japan, The Netherlands, Norway, and the USA using the 36-item Short Form Health Survey (SF-36). This showed that arthritis, chronic lung disease, and congestive heart failure were the conditions with the highest impact on SF-36 physical component summary score. RA had a significant negative effect on the SF-36 mental component summary score. Arthritis had the highest impact on health-related quality of life (HRQoL) in the general population (25). A large survey study in The Netherlands which compared HRQoL (using SF-36 or SF-24) across a wide range of long-term conditions showed that people with musculoskeletal conditions (included are back impairments, RA, OA/other joint complaints) reported the lowest levels of physical functioning, role functioning, and pain (26).

A Spanish study showed that rheumatic diseases are among the diseases that produce the largest impairment in HRQoL and daily functioning (27). When the definition of the burden of disease includes a measure of function and of HRQoL that is weighted by the prevalence of disease, RMDs, as a group, may be considered on a par with other major diseases such as neurologic, cardiac, or pulmonary diseases (16).

For many of the RMDs, it is important to recognize the disease early to have the best option to start treatment early and prevent or limit long-term consequences. To achieve this, EULAR has started the awareness campaign “Don’t delay, connect today.” The best example is RA. Early diagnosis, improved treatment options, and applying treatment-to-target principles have improved the percentage of patients in (sustained) remission, and improved the quality of life and work productivity (28,29). Even overall excess mortality in patients with RA in comparison to the general population, which was apparent in previous decades, is lower and even no longer present when RA is diagnosed and treated early and intensively (30,31).

Cause-specific morbidities, such as cardiovascular disease, are greater in many of the RMDs, and may also be declining with improved disease management (32).

Workforce taking care of patients with RMDs

A range of practitioners manage musculoskeletal problems. These include medical specialists, general practitioners, community pharmacists, physical therapists (physiotherapists, chiropractors), occupational therapists, and behavioral therapists (counselors, psychologists, and social workers). Rheumatologists, including pediatric rheumatologists, are the specialists with the most broad

and specific training for diagnosing and treating RMDs. Rheumatology specialty training standardized by EUMS across the EU and the Accreditation Council for Graduate Medical Education in the USA requires proficiency in general internal medicine followed by detailed training in the pathogenesis, diagnosis, and management of the entire range of RMDs (1,2).

The number of practicing rheumatologists varies widely. The average number of rheumatologists in the EU is 1.7 per 100,000 inhabitants, ranging from 0.5 in Ireland to 4.2 in France (16). Similarly, in the USA, the number of rheumatologists ranges from greater than 2 per 100,000 in heavily populated regions to fewer than 1.5 per 1,000,000 in more rural regions (30). However, due to a variety of factors affecting physician workforce, including the increasing prevalence of RMDs, these numbers are changing rapidly. For example, recent workforce projections in the USA estimate that by 2025 the average number of rheumatologists in the large majority of the country will be 0.5–1.0 per 100,000 inhabitants (33). There is also a severe shortage of pediatric rheumatologists, as substantiated by a survey in the USA (34). Other specialists caring for patients with RMDs are orthopedic surgeons, internists, and rehabilitation specialists. There is also a wide variation in the workforce of allied health professionals. The number of physiotherapists varies enormously across EU countries from 34 per 100,000 inhabitants in Ireland to 234 per 100,000 in Finland (16). Similarly, the variation in occupational therapists ranges from 2 per 100,000 inhabitants in Italy to 100 per 100,000 in Sweden and Denmark (16). In contrast, in the USA, there were about 114,600 occupational therapy jobs listed in 2014 for a population of close to 318,500,000 (360 per 100,000) (35).

Based on the above data and considerations, the following common language description of RMDs was endorsed by both EULAR and ACR: RMDs are a diverse group of diseases that commonly affect the joints, but can affect any organ of the body. There are more than 200 different RMDs, affecting both children and adults. They are usually caused by problems of the immune system, inflammation, infections, or gradual deterioration of joints, muscles, and bones. Many of these diseases are long term and worsen over time. They are typically painful and limit function. In severe cases, RMDs can result in significant disability, having a major impact on both quality of life and life expectancy.

Summary

The description of RMDs is a succinct statement in common language detailing many of the important aspects of these conditions. Given the prevalence and impact of

RMDs as well as the availability of effective management options, it is important to be able to communicate clearly what RMDs are with the public and stakeholders. It is especially imperative to communicate the impact and importance of RMDs to healthcare policymakers.

The many unanswered questions about the causes of RMDs, the importance of improved diagnosis for RMDs, and clear need for effective and safe treatments that are unavailable for many of these diseases emphasize the importance of increased research on RMDs. At the same time, the fact that many recent advances have been made in developing new therapies for RMDs so that many people are now treated very effectively—with prevention of disability and comorbidity—emphasizes how critical it is that patients have ready access to diagnosis and care for these conditions. We hope that the description of RMDs provided in this report will enable improved communication about and advocacy for these conditions and the patients who suffer from them.

ACKNOWLEDGMENTS

We thank Tadej Avcin, Maurizio Cutolo, Heinz Marchesi, Antonia Ravelli, and Di Skingle for helping to draft the first version of the description, which served as the basis for the final endorsed description of RMDs.

AUTHOR CONTRIBUTIONS

All authors drafted the article, revised it critically for important intellectual content, and approved the final version to be published.

REFERENCES

- American College of Rheumatology. Core curriculum outline for rheumatology fellowship programs. URL: http://www.rheumatology.org/Portals/0/Files/Core%20Curriculum%20Outline_2015.pdf.
- European Union of Medical Specialists. Training requirements in rheumatology. URL: <https://uemsrheumatology.eu/news-and-events/news/news-more/training-requirements-in-rheumatology>.
- Arthritis Foundation. Types of arthritis. URL: <http://www.arthritis.org/about-arthritis/types/>.
- American College of Rheumatology. Diseases and conditions. URL: <http://www.rheumatology.org/I-Am-A/Patient-Caregiver/Diseases-Conditions>.
- World Health Organization. Osteoarthritis. URL: http://www.who.int/medicines/areas/priority_medicines/Ch6_12Osteo.pdf.
- Cross M, Smith E, Hoy D, Carmona L, Wolfe F, Vos T, et al. The global burden of rheumatoid arthritis: estimates from the global burden of disease 2010 study. *Ann Rheum Dis* 2014;73:1316–22.
- Zhu Y, Pandya BJ, Choi HK. Prevalence of gout and hyperuricemia in the US general population: the National Health and Nutrition Examination Survey 2007–2008. *Arthritis Rheum* 2011;63:3136–41.
- Kuo CF, Grainge MJ, Zhang W, Doherty M. Global epidemiology of gout: prevalence, incidence and risk factors. *Nat Rev Rheumatol* 2015;11:649–62.
- Danchenko N, Satia JA, Anthony MS. Epidemiology of systemic lupus erythematosus: a comparison of worldwide disease burden. *Lupus* 2006;15:308–18.
- Carter EE, Barr SG, Clarke AE. The global burden of SLE: prevalence, health disparities and socioeconomic impact. *Nat Rev Rheumatol* 2016;12:605–20.
- Crowson CS, Matteson EL, Myasoedova E, Michet CJ, Ernste FC, Warrington KJ, et al. The lifetime risk of adult-onset rheumatoid arthritis and other inflammatory autoimmune rheumatic diseases. *Arthritis Rheum* 2011;63:633–9.
- Bykerk V, Emery P. Delay in receiving rheumatology care leads to long-term harm [editorial]. *Arthritis Rheum* 2010;62:3519–21.
- Raza K, Stack R, Kumar K, Filer A, Detert J, Bastian H, et al. Delays in assessment of patients with rheumatoid arthritis: variations across Europe. *Ann Rheum Dis* 2011;70:1822–5.
- Gladman DD, Thavaneswaran A, Chandran V, Cook RJ. Do patients with psoriatic arthritis who present early fare better than those presenting later in the disease? *Ann Rheum Dis* 2011;70:2152–4.
- Foster HE, Eltringham MS, Kay LJ, Friswell M, Abinun M, Myers A. Delay in access to appropriate care for children presenting with musculoskeletal symptoms and ultimately diagnosed with juvenile idiopathic arthritis. *Arthritis Rheum* 2007;57:921–7.
- EUMUSC.net. Musculoskeletal health in Europe report v5.0. URL: <http://eumusc.net/publications.cfm>.
- European Commission. Special Eurobarometer. Health in the European Union. September 2007. URL: http://ec.europa.eu/commfrontoffice/publicopinion/archives/ebs/ebs_272e_en.pdf.
- Jafarzadeh SR, Felson DT. Updated estimates suggest a much higher prevalence of arthritis in United States adults than previous ones. *Arthritis Rheumatol* 2018;70:185–92.
- Barbour KE, Helmick CG, Boring M, Brady TJ. Vital Signs: prevalence of doctor-diagnosed arthritis and arthritis-attributable activity limitation: United States, 2013–2015. *MMWR Morb Mortal Wkly Rep* 2017;66:246–53.
- United States Bone and Joint Initiative. The burden of musculoskeletal diseases in the United States web site. URL: <http://www.boneandjointburden.org/>.
- Mathers C, Stevens G, Mascarenhas M. Global health risks: mortality and burden of disease attributable to selected major risks. Geneva: WHO Press; 2009.
- World Health Organization. WHO global burden of disease 2004. URL: http://www.who.int/healthinfo/global_burden_disease/YLD14_30_2004.xls.
- Smith E, Hoy DG, Cross M, Vos T, Naghavi M, Buchbinder R, et al. The global burden of other musculoskeletal disorders: estimates from the Global Burden of Disease 2010 study. *Ann Rheum Dis* 2014;73:1462–9.
- Hoy DG, Smith E, Cross M, Sanchez-Riera L, Blyth FM, Buchbinder R, et al. Reflecting on the global burden of musculoskeletal conditions: lessons learnt from the global burden of disease 2010 study and the next steps forward. *Ann Rheum Dis* 2015;74:4–7.
- Alonso J, Ferrer M, Gandek B, Ware JE Jr, Aaronson NK, Mosconi P, et al. Health-related quality of life associated with chronic conditions in eight countries: results from the International Quality of Life Assessment (IQOLA) Project. *Qual Life Res* 2004;13:283–98.
- Sprangers MA, de Regt EB, Andries F, van Agt HM, Bijl RV, de Boer JB, et al. Which chronic conditions are associated with better or poorer quality of life? *J Clin Epidemiol* 2000;53:895–907.
- Loza E, Abásolo L, Jover JA, Carmona L, EPISER Study Group. Burden of disease across chronic diseases: a health survey that measured prevalence, function, and quality of life. *J Rheumatol* 2008;35:159–65.
- Overman CL, Jurgens MS, Bossema ER, Jacobs JW, Bijlsma JW, Geenen R. Change of psychological distress and physical disability in patients with rheumatoid arthritis over the last two decades. *Arthritis Care Res (Hoboken)* 2014;66:671–8.
- Nikiphorou E, Guh D, Bansback N, Zhang W, Dixey J, Williams P, et al. Work disability rates in RA: results from an inception cohort with 24 years follow-up. *Rheumatology (Oxford)* 2012;51:385–92.
- Gwinnutt JM, Symmons DP, MacGregor AJ, Chipping JR, Marshall T, Lunt M, et al. Twenty-year outcome and association between early

- treatment and mortality and disability in an inception cohort of patients with rheumatoid arthritis: results from the Norfolk arthritis register. *Arthritis Rheumatol* 2017;69:1566–75.
31. Zhang Y, Lu N, Peloquin C, Dubreuil M, Neogi T, Aviña-Zubieta JA, et al. Improved survival in rheumatoid arthritis: a general population-based cohort study. *Ann Rheum Dis* 2017;76:408–13.
 32. Myasoedova E, Gabriel SE, Matteson EL, Davis JM III, Thorneau TM, Crowson CS. Decreased cardiovascular mortality in patients with incident Rheumatoid Arthritis (RA) in recent years: dawn of a new era in cardiovascular disease in RA? *J Rheumatol* 2017;44:732–9.
 33. Academy for Academic Leadership. 2015 ACR/ARHP workforce study in the United States: adult rheumatologist supply and demand projections for 2015–2030. URL: <https://www.rheumatology.org/portals/0/files/ACR-Workforce-Study-2015.pdf>.
 34. Battafarano D, Monrad S, Ditmyer M, Imundo L, Klein-Gitelman M. 2015 ACR/ARHP workforce study in the United States: pediatric rheumatologist supply and demand projections for 2015–2030 [abstract]. *Arthritis Rheumatol* 2016;68 Suppl 10. URL: <http://acrabstracts.org/abstract/2015-acrarhp-workforce-study-in-the-united-states-pediatric-rheumatologist-supply-and-demand-projections-for-2015-2030/>.
 35. Bureau of Labor Statistics, US Department of Labor. Occupational outlook handbook: occupational therapists. URL: <https://www.bls.gov/ooh/healthcare/occupational-therapists.htm>.

Switching From Reference Adalimumab to SB5 (Adalimumab Biosimilar) in Patients With Rheumatoid Arthritis

Fifty-Two–Week Phase III Randomized Study Results

Michael E. Weinblatt,¹ Asta Baranauskaite,² Eva Dokoupilova,³ Agnieszka Zielinska,⁴
Janusz Jaworski,⁵ Artur Racewicz,⁶ Margarita Pileckyte,² Krystyna Jedrychowicz-Rosiak,⁷
Inyoung Baek,⁸ and Jeehoon Ghil⁸

Objective. The 24-week equivalent efficacy and comparable safety results of the biosimilar SB5 and reference adalimumab (ADA) from the phase III randomized study in patients with moderate-to-severe rheumatoid arthritis (RA) have been reported previously. We undertook this transition study to evaluate patients who switched from ADA to SB5 or who continued to receive SB5 or ADA up to 52 weeks.

Methods. In this phase III study, patients were initially randomized 1:1 to receive SB5 or ADA (40 mg subcutaneously every other week). At 24 weeks, patients receiving ADA were rerandomized 1:1 to continue with ADA (ADA/ADA group) or to switch to SB5 (ADA/SB5 group) up to week 52; patients receiving SB5 continued with SB5 for 52 weeks (SB5 group). Efficacy, safety, and immunogenicity were evaluated up to 52 weeks.

Results. The full analysis set population consisted of 542 patients (269 in the SB5 group, 273 in the ADA overall group [patients who were randomized to receive ADA at week 0], 125 in the ADA/SB5 group, and 129 in the ADA/ADA group). The percentages of patients meeting the American College of Rheumatology 20%, 50%, or

70% improvement criteria (achieving an ACR20, ACR50, or ACR70 response) at week 24 were maintained after the transition from ADA to SB5, and these response rates were comparable across treatment groups throughout the study. ACR20 response rates ranged from 73.4% to 78.8% at week 52. Radiographic progression was minimal and comparable across treatment groups. The safety profile and the incidence of antidrug antibodies were comparable across treatment groups after transition.

Conclusion. SB5 was well tolerated over 1 year in patients with RA, with efficacy, safety, and immunogenicity comparable to those of ADA. Switching from ADA to SB5 had no treatment-emergent issues such as increased adverse events, increased immunogenicity, or loss of efficacy.

Biologic disease-modifying antirheumatic drugs (bDMARDs), including tumor necrosis factor (TNF) inhibitors such as adalimumab (ADA), have been used successfully to treat patients with rheumatoid arthritis (RA) (1). According to the updated 2016 European

ClinicalTrials.gov identifier: NCT02167139.

Supported by Samsung Bioepis.

¹Michael E. Weinblatt, MD: Brigham and Women's Hospital, Boston, Massachusetts; ²Asta Baranauskaite, MD, PhD, Margarita Pileckyte, MD, PhD: Lithuanian University of Health Sciences, Kaunas, Lithuania; ³Eva Dokoupilova, MD: Medical Plus, Uherske Hradiste, Czech Republic, and University of Veterinary and Pharmaceutical Sciences, Brno, Czech Republic; ⁴Agnieszka Zielinska, MD: Medica Pro Familia, Warsaw, Poland; ⁵Janusz Jaworski, MD, PhD: Reumatika-Centrum Reumatologii, Warsaw, Poland; ⁶Artur Racewicz, MD, PhD: Zdrowie Osteo-Medic, Białystok, Poland; ⁷Krystyna Jedrychowicz-Rosiak, MD: Mazowieckie Centrum Badań Klinicznych, Grodzisk Mazowiecki, Poland; ⁸Inyoung Baek, PhD, Jeehoon Ghil, MD: Samsung Bioepis, Incheon, Republic of Korea.

Dr. Weinblatt has received consulting fees and/or honoraria from AbbVie, Amgen, Novartis, Roche, GlaxoSmithKline, Merck,

Samsung Bioepis, Crescendo Bioscience, and AstraZeneca (less than \$10,000 each) and from Bristol-Myers Squibb, Eli Lilly and Company, Pfizer, and UCB (more than \$10,000 each) and research support from Amgen, Bristol-Myers Squibb, Crescendo Bioscience, Sanofi, and UCB. Dr. Baranauskaite has received consulting fees (less than \$10,000) and research support from Samsung Bioepis. Drs. Dokoupilova, Zielinska, Jaworski, Racewicz, Pileckyte, and Jedrychowicz-Rosiak have received research support from Samsung Bioepis. Drs. Baek and Ghil own stock or stock options in Samsung Bioepis.

Address correspondence to Michael E. Weinblatt, MD, Harvard Medical School, Division of Rheumatology, Immunology, and Allergy, Brigham and Women's Hospital, 75 Francis Street, Boston, MA 02115. E-mail: MWEINBLATT@PARTNERS.ORG.

Submitted for publication October 10, 2017; accepted in revised form February 6, 2018.

League Against Rheumatism (EULAR) recommendations, addition of a bDMARD should be considered in patients who do not achieve the treatment target and have poor prognostic factors (2). In the absence of poor prognostic factors, other conventional synthetic DMARDs (csDMARDs) may be tried. The American College of Rheumatology (ACR) similarly recommends the step-up therapy; however, either bDMARDs or csDMARDs may be used regardless of prognostic factors (3). Treatment with bDMARDs is often associated with high costs (4,5), and the advent of biosimilars provides the potential to reduce costs and increase patient access to such therapies (4,6). Several biosimilars targeting TNF have been approved recently for use in the US and Europe, and the use of these biosimilars is recommended by EULAR (2).

ADA is a recombinant human IgG1 specific for TNF that is approved for the treatment of RA as well as several other inflammatory conditions (7). SB5 (Imraldi; Samsung Bioepis) was developed as an ADA biosimilar and has an identical amino acid sequence and physicochemical and in vitro functional properties similar to those of reference ADA (8). The European Commission granted a marketing authorization for SB5 in August 2017. Pharmacokinetic (PK) equivalence and comparable safety for SB5 and ADA were demonstrated in a phase I study in healthy individuals (8). In a phase III randomized study in patients with moderate-to-severe RA, equivalent efficacy was demonstrated for SB5 and ADA, as seen in percentages of patients meeting the ACR 20% improvement criteria (achieving an ACR20 response) (9) (72.4% and 72.2%, respectively) and additional efficacy end points up to 24 weeks; SB5 was well tolerated, with PK, safety, and immunogenicity profiles comparable to those of ADA (10).

Growing numbers of biosimilars for various biologic agents have been approved or are in various stages of clinical development; however, there are limited clinical and real-world data regarding the effects of switching from reference biologic agents to biosimilars (11). An important clinical consideration for the use of biosimilars is whether switching from reference product might result in loss of efficacy or increased immunogenicity or other safety concerns. Data derived from appropriately designed switching clinical trials and real-world experience can help fill this information gap and provide useful evidence in clinical decision-making (11).

As mentioned above, the 24-week results of the phase III clinical study evaluating SB5 and ADA demonstrated comparable ACR20 response rates, PK, safety, and immunogenicity in patients with moderate-to-severe RA (10). The objective of the current 52-week transition study was to evaluate the safety,

immunogenicity, and efficacy of continuing SB5 treatment versus switching from ADA to SB5 (as will occur in clinical practice) versus continuing ADA treatment.

PATIENTS AND METHODS

Methods have been described previously in detail (10) and are briefly summarized herein.

Patient inclusion and exclusion criteria. The study included patients ages 18–75 years with moderate-to-severe RA treated with methotrexate (MTX) for ≥ 6 months and receiving a stable MTX dosage of 10–25 mg/week for ≥ 4 weeks before screening. Patients had active disease (≥ 6 swollen joints, ≥ 6 tender joints, and either an erythrocyte sedimentation rate [ESR] ≥ 28 mm/hour or a serum C-reactive protein [CRP] level ≥ 1.0 mg/dl). Pertinent exclusions included previous treatment with biologic agents and active or latent tuberculosis infection at screening (10).

Study design. This 52-week, phase III, randomized, double-blind, parallel-group study was conducted at 51 sites in 7 countries. Patients were initially randomized 1:1 to receive SB5 or ADA (40 mg subcutaneously every other week). Patients receiving ADA were randomized again 1:1 at week 24 to continue with ADA or to switch to SB5 up to week 52; patients receiving SB5 were also randomized for purposes of blinding and continued with SB5 for the 52 weeks of the study (see Supplementary Figure 1, available on the *Arthritis & Rheumatology* web site at <http://onlinelibrary.wiley.com/doi/10.1002/art.40444/abstract>).

The study was conducted in accordance with the ethical principles that have their origin in the Declaration of Helsinki and that are consistent with International Conference on Harmonisation Guidelines for Good Clinical Practice. Each study center's independent ethics committee or institutional review board reviewed and approved the protocol and study. All patients provided written informed consent before study entry.

Study assessments. The primary efficacy end point of the study, the ACR20 response rate at week 24, has been reported previously (10). Efficacy assessments up to week 52 included the ACR20, ACR50, and ACR70 response rates and the ACR index of improvement in RA response rate (12), the Disease Activity Score in 28 joints (13) using the ESR (DAS28-ESR), and the EULAR response (good, moderate, or no response) (14). Post hoc analyses were performed on the Simplified Disease Activity Index (SDAI) (15), the Clinical Disease Activity Index (CDAI) (16), the remission rate based on the DAS28-ESR (score of < 2.6), SDAI (score of ≤ 3.3), and CDAI (score of ≤ 2.8), and the proportion of patients with low disease activity based on the DAS28-ESR (score of ≤ 3.2), SDAI (score of 3.3–11.0), and CDAI (score of 2.8–10.0). A Boolean-based remission was determined based on a swollen joint count of ≤ 1 , a tender joint count of ≤ 1 , a CRP level of ≤ 10 mg/liter, and a visual analog scale score of ≤ 10 mm on the patient's global assessment of disease activity.

Radiographs of the hands and feet were obtained at baseline and at week 52 and were evaluated centrally by 2 independent qualified readers who were blinded with regard to patient identity, treatment, and assessment time point. When the score change was within the top 5% of cases with the highest score differences between readers, the radiographs required consensus review by the primary readers. The

mean joint erosion score and joint space narrowing score of the 2 readers were used to calculate the modified Sharp/van der Heijde score (SHS) (17).

Treatment-emergent adverse events (AEs) (graded as mild, moderate, or severe), serious AEs (SAEs), vital sign abnormalities, and clinical laboratory abnormalities were monitored as part of safety assessments. Immunogenicity assessments included monitoring for the development of anti-drug antibodies and neutralizing antibodies.

Immunogenicity was analyzed as emergent (positive for ≥ 1 antidrug antibody after transition among patients with negative 24-week overall antidrug antibody results), boosted (increased titer of antidrug antibodies at any time compared with the highest titer up to week 24), and total (seroconverted to positive for antidrug antibodies or boosted their preexisting antidrug antibody titer during the transition period). Antidrug antibodies were detected using electrochemiluminescence bridging (Meso Scale Discovery), employing an SB5 single-tagged immunoassay. Subgroup analyses based on the antidrug antibody status of the patients were performed in the treatment groups following transition at 24 weeks up to 52 weeks for the various efficacy parameters.

Statistical analysis. Sample size determination was described previously (10). Efficacy assessments were performed on the full analysis set, which comprised all randomized patients (intent-to-treat principle). The following treatment groups were compared: patients who were randomized to receive SB5 at week 0 (SB5 group), patients who were randomized to receive ADA at week 0 (ADA overall group), and patients in the ADA group who were rerandomized at week 24

to continue ADA (ADA/ADA group) or to switch to SB5 (ADA/SB5 group). Results are presented with no imputation for missing data. The safety population included all patients who received ≥ 1 dose of study drug after rerandomization at week 24. Safety results were compared for the SB5/SB5 group (patients in the SB5 group who were rerandomized to continue SB5), ADA/SB5 group, and ADA/ADA group. All efficacy and safety results were summarized descriptively by treatment group. Statistical analyses were performed using SAS software, version 9.2 or higher (SAS Institute).

RESULTS

Patients. The study was initiated on May 12, 2014 and completed on October 19, 2015. A total of 544 patients were randomized to the SB5 ($n = 271$) or ADA overall ($n = 273$) groups; 254 patients (93.7%) in the SB5 group and 254 (93.0%) in the ADA overall group completed the 24-week study (10). At week 24, the 254 patients in the SB5 group continued to receive SB5 (SB5/SB5 group); patients in the ADA overall group were randomized to transition to SB5 (ADA/SB5 group [$n = 125$]) or to continue ADA (ADA/ADA group [$n = 129$]). The full analysis set population consisted of 542 patients (269 in the SB5 group, 273 in the ADA overall group, 125 in the ADA/SB5 group, and 129 in

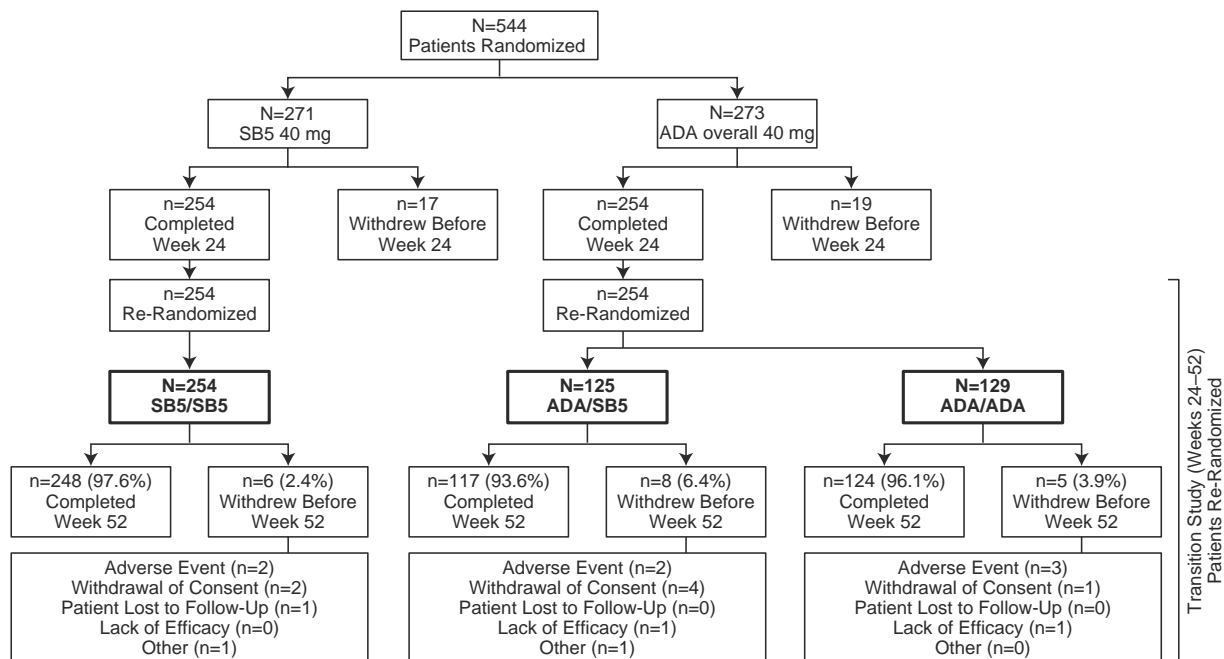


Figure 1. Patient disposition summary. The percentages of patients who completed or discontinued are based on the numbers of patients who were rerandomized at week 24. The SB5 group included patients who were randomized to receive the biosimilar SB5 at week 0. The adalimumab (ADA) overall group included patients who were randomized to receive reference ADA at week 0. The SB5/SB5 group included patients receiving SB5 who were randomized to continue SB5. The ADA/SB5 group included patients receiving ADA who were randomized to switch to SB5. The ADA/ADA group included patients receiving ADA who were randomized to continue ADA.

the ADA/ADA group). Patient disposition for the 52-week study is summarized in Figure 1.

Patient demographics and baseline characteristics at study start (week 0) and disease activity at weeks 0 and 24 (rerandomization time point) are shown in Table 1. Overall, baseline characteristics and disease activity were well balanced across treatment groups.

Efficacy assessments. The ACR response rates were not affected after transition from ADA to SB5 at week 24, and results for the ADA/SB5 and ADA/ADA groups were comparable up to week 52 (Figure 2). Efficacy was also comparable between the SB5 and ADA/ADA groups throughout the study. Efficacy was maintained from week 24 up to week 52 across treatment groups. Analysis of the DAS28, SDAI, and CDAI showed comparable trends across all treatment groups during the study; results

from 24 weeks to 52 weeks (full analysis set) are shown in Supplementary Figure 2, <http://onlinelibrary.wiley.com/doi/10.1002/art.40444/abstract>. Other efficacy end points (e.g., Boolean-based remission; low disease activity based on the DAS28, SDAI, and CDAI) were also comparable at week 52 among treatment groups (Table 2).

Radiographic results were comparable across all treatment groups, as seen in the change from baseline at week 52 in joint erosion score, joint space narrowing score, SHS, and the proportion of patients with change from baseline in the SHS >0 (Table 2). Mean \pm SD changes in SHS were 0.2 ± 2.5 in the SB5 group, 0.4 ± 2.6 in the ADA overall group, 0.3 ± 2.7 in the ADA/SB5 group, and 0.5 ± 2.4 in the ADA/ADA group. Radiographic progression was minimal, as seen in the cumulative probability plot of change from baseline in

Table 1. Patient demographics at baseline and disease activity at baseline and week 24*

	SB5 group (n = 271)	ADA overall group (n = 273)	ADA/SB5 group (n = 125)	ADA/ADA group (n = 129)
Demographics at baseline				
Age, years	49.8 \pm 12.7	52.5 \pm 11.9	51.7 \pm 11.3	52.8 \pm 12.3
Sex, no. (%)				
Female	217 (80.1)	224 (82.1)	105 (84.0)	103 (79.8)
Male	54 (19.9)	49 (17.9)	20 (16.0)	26 (20.2)
BMI, kg/m ²	26.2 \pm 4.8	27.0 \pm 5.1	27.2 \pm 5.3	26.9 \pm 5.0
Disease duration, years	5.4 \pm 4.4	5.5 \pm 4.3	5.3 \pm 4.1	5.6 \pm 4.5
MTX dose, mg/week	15.1 \pm 4.6	15.4 \pm 4.4	15.4 \pm 4.5	15.2 \pm 4.4
Duration of MTX use, months	39.5 \pm 38.4	37.8 \pm 34.9	38.3 \pm 33.8	39.5 \pm 37.2
RF positive, no. (%)	203 (74.9)	185 (67.8)	80 (64.0)	94 (72.9)
Disease activity at baseline				
Swollen joint count	15.8 \pm 8.0	15.5 \pm 7.5	14.5 \pm 6.4	16.3 \pm 8.3
Tender joint count	23.9 \pm 11.7	24.1 \pm 10.8	23.8 \pm 10.5	24.3 \pm 11.3
HAQ DI score	1.3 \pm 0.6	1.4 \pm 0.6	1.4 \pm 0.6	1.4 \pm 0.7
DAS28-ESR	6.5 \pm 0.7	6.5 \pm 0.71	6.5 \pm 0.6	6.4 \pm 0.8
CRP, mg/liter	11.5 \pm 19.0	12.6 \pm 19.0	13.0 \pm 20.8	11.9 \pm 15.7
ESR, mm/hour	39.6 \pm 13.3	39.6 \pm 13.9	40.5 \pm 14.3	39.3 \pm 14.0
Physician's global assessment, 0–100-mm VAS	59.8 \pm 16.9	60.6 \pm 15.4	60.6 \pm 14.7	61.0 \pm 16.1
Patient's global assessment, 0–100-mm VAS	58.5 \pm 20.3	59.4 \pm 18.7	59.1 \pm 18.0	59.9 \pm 19.6
Patient's assessment of pain, 0–100-mm VAS	59.2 \pm 20.7	60.8 \pm 19.7	61.0 \pm 19.6	60.6 \pm 20.0
ACR-N	NA	NA	NA	NA
Disease activity at week 24				
Swollen joint count	3.2 \pm 4.5	3.3 \pm 4.9	3.3 \pm 5.0	3.3 \pm 4.7
Tender joint count	7.4 \pm 7.4	8.4 \pm 9.6	8.1 \pm 9.1	8.4 \pm 10.0
HAQ DI score	0.8 \pm 0.6	0.9 \pm 0.6	0.9 \pm 0.6	0.9 \pm 0.6
DAS28-ESR	3.7 \pm 1.2	3.8 \pm 1.4	3.7 \pm 1.4	3.8 \pm 1.3
CRP, mg/liter	5.6 \pm 10.3	5.8 \pm 8.6	6.1 \pm 9.9	5.3 \pm 6.7
ESR, mm/hour	18.9 \pm 14.8	19.0 \pm 14.2	18.6 \pm 12.8	19.6 \pm 15.5
Physician's global assessment, 0–100-mm VAS	23.6 \pm 16.4	25.0 \pm 17.8	25.0 \pm 18.0	24.0 \pm 17.1
Patient's global assessment, 0–100-mm VAS	33.7 \pm 21.7	35.1 \pm 22.0	36.7 \pm 22.4	33.1 \pm 21.4
Patient's assessment of pain, 0–100-mm VAS	35.6 \pm 21.8	37.0 \pm 23.3	38.6 \pm 23.4	34.7 \pm 22.9
ACR-N	40.2 \pm 28.7	39.6 \pm 29.2	38.4 \pm 29.6	41.5 \pm 28.8

* Except where indicated otherwise, values are the mean \pm SD. SB5 group = patients randomized to receive the biosimilar SB5 at week 0; adalimumab (ADA) overall group = patients randomized to receive reference ADA at week 0; ADA/SB5 group = patients receiving ADA rerandomized to switch to SB5; ADA/ADA group = patients receiving ADA rerandomized to continue ADA; BMI = body mass index; MTX = methotrexate; RF = rheumatoid factor; HAQ DI = Health Assessment Questionnaire disability index; DAS28-ESR = Disease Activity Score in 28 joints using the erythrocyte sedimentation rate; CRP = C-reactive protein; VAS = visual analog scale; ACR-N = American College of Rheumatology index of improvement in rheumatoid arthritis; NA = not applicable.

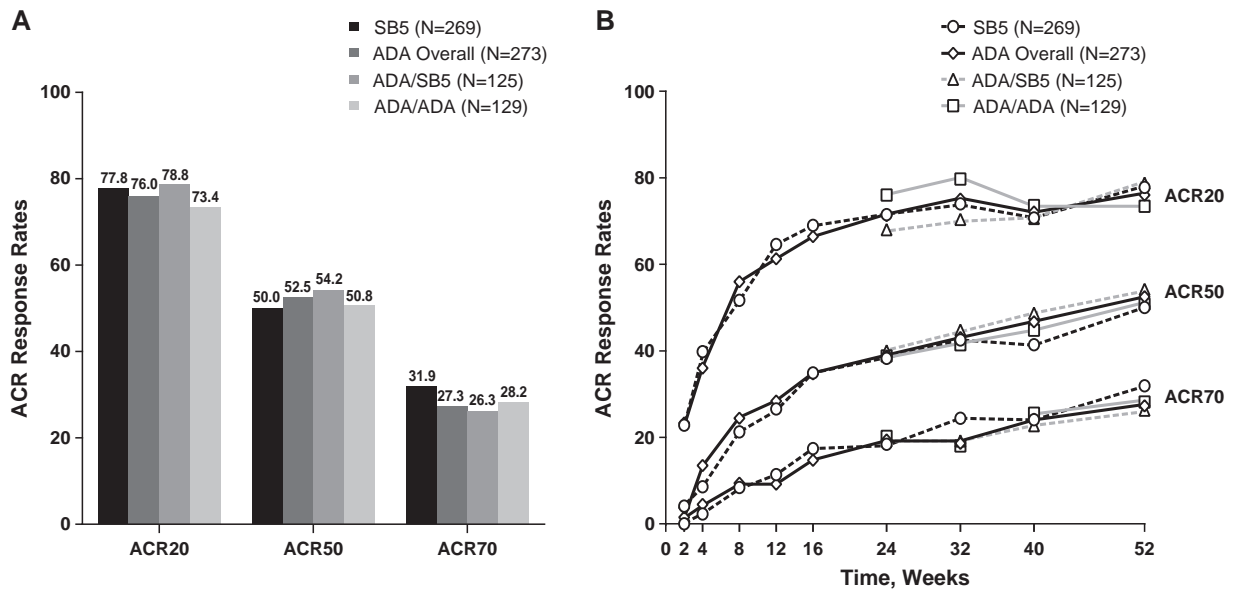


Figure 2. Percentages of patients meeting the American College of Rheumatology 20%, 50%, or 70% improvement criteria (achieving an ACR20, ACR50, or ACR70 response) in the full analysis set population. **A**, ACR response rates at 52 weeks in the different treatment groups. **B**, ACR response rates over the 52-week period in the different treatment groups. See Figure 1 for other definitions.

Table 2. Efficacy end points at week 52 in the full analysis set*

	SB5 group (n = 269)	ADA overall group (n = 273)	ADA/SB5 group (n = 125)	ADA/ADA group (n = 129)
ACR response rate, %				
ACR20	77.8	76.0	78.8	73.4
ACR50	50.0	52.5	54.2	50.8
ACR70	31.9	27.3	26.3	28.2
DAS28-ESR				
Mean change from baseline	-3.05	-2.97	-3.02	-2.92
LDA, no./total no. (%)†	118/247 (47.8)	112/242 (46.3)	55/118 (46.6)	57/124 (46.0)
Remission, no./total no. (%)†	75/247 (30.4)	70/242 (28.9)	34/118 (28.8)	36/124 (29.0)
SDAI				
Mean change from baseline	-29.0	-28.0	-28.2	-27.8
LDA, no./total no. (%)†	88/247 (35.6)	95/242 (39.3)	46/118 (39.0)	49/124 (39.5)
Remission, no./total no. (%)†	55/247 (22.3)	46/242 (19.0)	23/118 (19.5)	23/124 (18.5)
CDAI				
Mean change from baseline	-28.5	-27.4	-27.50	-27.3
LDA, no./total no. (%)†	84/248 (33.9)	91/242 (37.6)	45/118 (38.1)	46/124 (37.1)
Remission, no./total no. (%)†	52/248 (21.0)	47/242 (19.4)	23/118 (19.5)	24/124 (19.4)
Boolean-based remission, no./total no. (%)†‡	35/247 (14.2)	31/242 (12.8)	17/118 (14.4)	14/124 (11.3)
Radiographic results				
Change from baseline in joint erosion score, mean ± SD	0.1 ± 1.6	0.2 ± 1.3	0.2 ± 1.4	0.2 ± 1.2
Change from baseline in joint space narrowing score, mean ± SD	0.1 ± 1.3	0.2 ± 1.8	0.1 ± 1.5	0.3 ± 1.9
Change from baseline in SHS, mean ± SD	0.2 ± 2.5	0.4 ± 2.6	0.3 ± 2.7	0.5 ± 2.4
Proportion of patients with change from baseline in SHS >0, no./total no. (%)†	48/241 (19.9)	57/238 (23.9)	22/114 (19.3)	35/124 (28.2)

* ACR20 = American College of Rheumatology 20% improvement criteria; LDA = low disease activity; SDAI = Simplified Disease Activity Index; CDAI = Clinical Disease Activity Index; SHS = modified Sharp/van der Heijde score (see Table 1 for other definitions).

† Number of patients with available data at each time point.

‡ Determined based on 28-swollen joint count ≤1, 28-tender joint count ≤1, CRP level ≤10 mg/liter, and VAS score ≤10 mm on patient's global assessment.

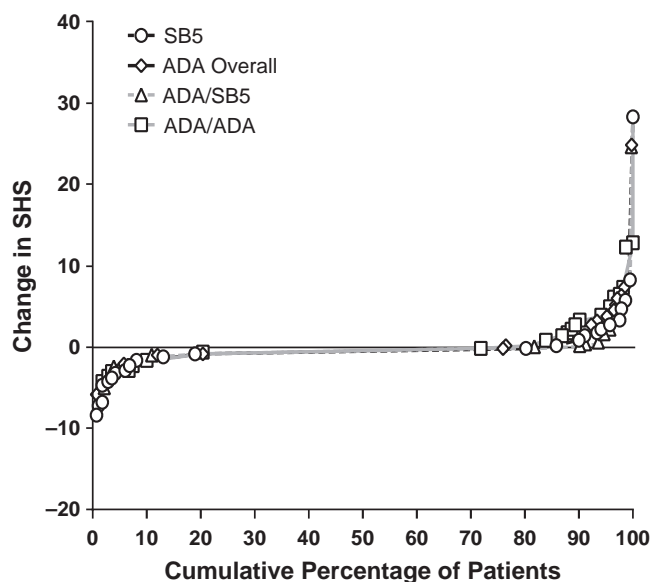


Figure 3. Cumulative probability change from baseline in modified Sharp/van der Heijde score (SHS) at week 52. Data are based on patients for whom radiographic assessment results were available at each visit. See Figure 1 for other definitions.

SHS at week 52, and was comparable for the different treatment groups (Figure 3).

Subgroup analyses of ACR response rate, EULAR response, and proportion of patients with low disease

activity and remission (according to the DAS28, SDAI, and CDAI) showed a trend toward decreased efficacy in antidrug antibody-positive patients ($n = 84$) compared with antidrug antibody-negative patients ($n = 423$) in all treatment groups (see Supplementary Table 1, <http://onlinelibrary.wiley.com/doi/10.1002/art.40444/abstract>). Mean DAS28, SDAI, and CDAI values tended to improve in antidrug antibody-negative patients and tended to worsen in antidrug antibody-positive patients across all treatment groups (24–52 weeks); the magnitude of the changes was comparable in all treatment groups (see Supplementary Figure 3, <http://onlinelibrary.wiley.com/doi/10.1002/art.40444/abstract>).

Safety. Safety was comparable across treatment groups after week 24. Treatment-emergent AEs that occurred after week 24 in the SB5/SB5, ADA/SB5, and ADA/ADA groups are summarized in Table 3. There were no cases of active tuberculosis in any treatment group and no deaths during the transition period. Malignancies were reported in 1 patient each in the SB5/SB5 group (small cell lung cancer), ADA/SB5 group (glioblastoma multiforme), and ADA/ADA group (seminoma). Injection-site reactions were reported in 2 patients in the ADA/ADA group only. The proportion of patients with any treatment-emergent AEs was comparable among the SB5/SB5 (32.3%), ADA/SB5 (37.6%), and ADA/ADA (33.1%) groups. Similar results were

Table 3. Summary of safety profile after transition*

	SB5/SB5 group ($n = 254$)	ADA/SB5 group ($n = 125$)	ADA/ADA group ($n = 127$)
Patients with ≥ 1 treatment-emergent AE	82 (32.3)	47 (37.6)	42 (33.1)
Treatment-emergent AEs reported in $\geq 2\%$ of patients			
Nasopharyngitis	11 (4.3)	4 (3.2)	3 (2.4)
Latent tuberculosis	8 (3.1)	1 (0.8)	7 (5.5)
Spinal pain	5 (2.0)	3 (2.4)	2 (1.6)
Bronchitis	5 (2.0)	2 (1.6)	2 (1.6)
Urinary tract infection	5 (2.0)	3 (2.4)	0 (0.0)
Rheumatoid arthritis	4 (1.6)	3 (2.4)	4 (3.1)
Upper respiratory tract infection	4 (1.6)	5 (4.0)	0 (0.0)
Increased ALT level [†]	3 (1.2)	1 (0.8)	3 (2.4)
Headache	2 (0.8)	3 (2.4)	4 (3.1)
Positive <i>Mycobacterium tuberculosis</i> complex test result [‡]	2 (0.8)	4 (3.2)	1 (0.8)
Any serious treatment-emergent AE	6 (2.4)	4 (3.2)	4 (3.1)
Treatment-emergent AEs leading to study drug discontinuation	1 (0.4)	2 (1.6)	3 (2.4)
Serious infection	0 (0.0)	2 (1.6)	0 (0.0)
Active tuberculosis	0 (0.0)	0 (0.0)	0 (0.0)
Injection-site reaction [§]	0 (0.0)	0 (0.0)	2 (1.6)
Malignancy [¶]	1 (0.4)	1 (0.8)	1 (0.8)
Death	0 (0.0)	0 (0.0)	0 (0.0)

* Values are the number (%) of patients. SB5/SB5 group = patients in the SB5 group rerandomized to continue the biosimilar SB5; AE = adverse event; ALT = alanine aminotransferase (see Table 1 for other definitions).

[†] Based on investigator's discretion.

[‡] Treatment-emergent AE led to study drug discontinuation in 1 patient in the ADA/SB5 group and 1 patient in the ADA/ADA group.

[§] Numbers based on the high-level group term of administration site reaction.

[¶] Small cell lung cancer in SB5/SB5 group; glioblastoma multiforme in ADA/SB5 group; seminoma in ADA/ADA group.

seen in the antidrug antibody–positive and antidrug antibody–negative subgroups within each treatment group (data not shown).

Immunogenicity. The incidence of overall antidrug antibodies (emergent and boosted) was comparable across treatment groups after transition at week 24 (40 of 254 patients [15.7%] in the SB5/SB5 group, 21 of 125 patients [16.8%] in the ADA/SB5 group, and 23 of 126 patients [18.3%] in the ADA/ADA group). Emergent antidrug antibodies occurred in 9 of 160 patients (5.6%) in the SB5/SB5 group, 5 of 80 patients (6.3%) in the ADA/SB5 group, and 11 of 87 patients (12.6%) in the ADA/ADA group. Boosted responses were reported in 31 of 94 patients (33.0%) in the SB5/SB5 group, 16 of 45 patients (35.6%) in the ADA/SB5 group, and 12 of 39 patients (30.8%) in the ADA/ADA group.

DISCUSSION

Previous results from this phase III randomized study showed equivalent efficacy for SB5 and ADA at week 24, and SB5 was well tolerated with PK, safety, and immunogenicity profiles comparable to those of ADA (10). In this 52-week transition study, patients in the ADA group were rerandomized at week 24 to either continue with ADA or switch to SB5 up to week 52, and patients receiving SB5 continued with SB5 up to week 52. This study design allowed for the comparison of efficacy and safety of SB5 in patients who switched from ADA to SB5 with efficacy and safety in those who continued to receive SB5 or ADA for the entire 52-week period.

The ACR response rates were similar across all treatment groups, both at week 52 and over the course of the study. Importantly, comparison of the ADA/SB5 and ADA/ADA treatment groups showed that efficacy was maintained after transition from ADA to SB5. In addition, there was minimal radiographic progression in all treatment groups over the course of 52 weeks. The ACR20, ACR50, and ACR70 response rates achieved in this study were similar to those described previously for ADA (18–21), and the radiographic results were also consistent with historical data for ADA (19).

Analysis of treatment-emergent AEs after transition showed that SB5 was well tolerated after switching from ADA, with comparable safety profiles across treatment groups after transition. This transition study was designed to assess ~100 patients per group so that an increase in the frequency of injection-site reactions to $\geq 1\%$ could be detected. No injection-site reactions occurred in the ADA/SB5 group, and 2 patients in the ADA/ADA group experienced injection-site reactions.

Rates of SAEs and treatment-emergent AEs leading to study drug discontinuation were low and similar across treatment groups, ranging from 2.4% to 3.2% of patients and from 0.4% to 2.4% of patients, respectively. No potential cases of anaphylaxis were identified based on retrospective analysis using related AEs (e.g., pruritus, flushing, dyspnea, hypotonia, syncope, incontinence, vomiting) and blood pressure (systolic blood pressure <90 mm Hg or $>30\%$ decrease from baseline) as defined by the National Institute of Allergy and Infectious Diseases/Food Allergy and Anaphylaxis Network criteria (22). There were no cases of active tuberculosis or deaths. Thus, based on the safety results from the 24-week study (10) and the safety results presented herein, SB5 is well tolerated up to 1 year of treatment with no significant safety issues.

The incidence of antidrug antibodies after transition was comparable across treatment groups, and the occurrence of newly emergent antidrug antibodies in patients who switched from ADA to SB5 (ADA/SB5 group) was not higher than that of patients in the ADA/ADA group. The formation of antibodies to ADA may reduce efficacy because of increased clearance (7,21,23). Therefore, similar to previous findings (21,23), it was not surprising that ACR response rates were decreased in patients who were antidrug antibody positive compared with those who were antidrug antibody negative. Consistent with historical results, there was no apparent correlation between the development of antidrug antibodies and AEs, including injection-site reactions (7,24).

Several biosimilars of ADA and other bDMARDs have either been marketed or are in clinical development (11,25). One of the key clinical considerations when prescribing biosimilars are the effects of switching patients from a reference product to a biosimilar (11). Importantly, biosimilars are expected to have the same clinical effects as the reference product, and efficacy and safety should not be compromised when switching from a reference product to a biosimilar (26). To test for potential changes in safety and efficacy following transition from reference biologic agents to biosimilars, some studies have incorporated a transition design (25). Several of these switch studies use an open-label extension design in which all patients receive the biosimilar product following a double-blind randomized trial (25). For example, the transition studies evaluating the infliximab biosimilar CT-P13 for RA (Program Evaluating the Autoimmune Disease Investigational Drug cT-p13 in RA Patients) or ankylosing spondylitis (Program Evaluating the Autoimmune Disease Investigational Drug cT-p13 in AS Patients) and those for the etanercept biosimilar SB4 were open-label, single-arm extension studies (11,27–29). The ADA

biosimilar ABP 501 has a similar ongoing single-arm, open-label extension study to evaluate efficacy and safety during transition from ADA to the biosimilar (11,30). In other studies, patients are rerandomized after a blinded treatment phase to transition to the biosimilar from the reference product, such as the study with the infliximab biosimilar SB2 and the switching study of CT-P13 in Norway (the NOR-SWITCH trial) (11,31). Such switching studies will provide valuable data that will be useful in clinical decision-making for transition from reference biologic agents to biosimilars.

One of the strengths of the transitional design of this 52-week study is that it allows for direct comparison between maintenance groups (the SB5/SB5 and ADA/ADA groups) and the transition group (the ADA/SB5 group) and shows that switching does not have negative effects in terms of reduced efficacy or increased AEs or immunogenicity. A limitation of this transition study was that it was not designed for statistical comparisons of equivalence; however, the results from this study provide valuable data on switching from a reference product to a biosimilar.

In conclusion, SB5 was well tolerated over 1 year in patients with RA, with efficacy, safety, and immunogenicity comparable to those of ADA. Switching from ADA to SB5 had no treatment-emergent issues such as increased AEs, increased immunogenicity, or loss of efficacy.

ACKNOWLEDGMENTS

The authors thank the patients who were involved in the study, the study personnel who made this work possible, and the study investigators in the following countries: Bosnia and Herzegovina (S. Sokolovic, M. Mekic, N. Prodanovic, B. Gajic, E. Karaselimovic-Dzambasovic, B. Pojskic); Bulgaria (A. Toncheva, P. Dimitar, L. Rodina, M. Geneva-Popova, I. Staykov, R. Stoilov); Czech Republic (L. Podrazilova, Z. Mosterova, G. Simkova, J. Kopackova, Z. Stejfova, J. Vencovsky, Z. Urbanova, L. Janska, D. Galatikova); Lithuania (S. Stropuviene, I. Sniuoliene); Poland (J. Niebrzydowski, K. Sitek-Ziolkowska, M. Rell-Bakalarska, R. Kolasa, S. Daniluk, B. Sliwowska, M. Bartosik-Twardowska, J. Brzezicki, M. Konieczny, S. Jeka); Republic of Korea (J. Choe, S. Bae, Y. Kang); Ukraine (L. Prystupa, Z. Vyacheslav, I. Gasanov, R. Yatsyshyn, D. Rekalov, O. Iaremenko, M. Stanislavchuk, V. Tseluyko). Medical writing assistance was provided by Beena John, PhD, from C4 MedSolutions (Yardley, PA), a CHC Group company, and was funded by Samsung Bioepis.

AUTHOR CONTRIBUTIONS

All authors were involved in drafting the article or revising it critically for important intellectual content, and all authors approved the final version to be published. Dr. Weinblatt had full access to all

of the data in the study and takes responsibility for the integrity of the data and the accuracy of the data analysis.

Study conception and design. Weinblatt, Baek, Ghil.

Acquisition of data. Baranauskaite, Dokoupilova, Zielinska, Jaworski, Racewicz, Pileckyte, Jedrychowicz-Rosiak.

Analysis and interpretation of data. Weinblatt, Baek, Ghil.

ROLE OF THE STUDY SPONSOR

Samsung Bioepis funded the study and facilitated the study design, provided writing assistance for the manuscript, and reviewed and approved the manuscript prior to submission. The authors independently collected the data, interpreted the results, and had the final decision to submit the manuscript for publication. Samsung Bioepis also funded medical writing assistance provided by Beena John, PhD (C4 MedSolutions, Yardley, PA; a CHC Group company). Publication of this article was not contingent upon approval by Samsung Bioepis.

REFERENCES

- McInnes IB, O'Dell JR. State-of-the-art: rheumatoid arthritis. *Ann Rheum Dis* 2010;69:1898–906.
- Smolen JS, Landewe R, Bijlsma J, Burmester G, Chatzidionysiou K, Dougados M, et al. EULAR recommendations for the management of rheumatoid arthritis with synthetic and biological disease-modifying antirheumatic drugs: 2016 update. *Ann Rheum Dis* 2017;76:960–77.
- Singh JA, Saag KG, Bridges SL Jr, Akl EA, Bannuru RR, Sullivan MC, et al. 2015 American College of Rheumatology guideline for the treatment of rheumatoid arthritis. *Arthritis Care Res (Hoboken)* 2016;68:1–25.
- Dorner T, Strand V, Castaneda-Hernandez G, Ferraccioli G, Isaacs JD, Kvien TK, et al. The role of biosimilars in the treatment of rheumatic diseases. *Ann Rheum Dis* 2013;72:322–8.
- Graudal N, Hubeck-Graudal T, Faurschou M, Baslund B, Jürgens G. Combination therapy with and without tumor necrosis factor inhibitors in rheumatoid arthritis: a meta-analysis of randomized trials. *Arthritis Care Res (Hoboken)* 2015;67:1487–95.
- Hirsch BR, Lyman GH. Biosimilars: a cure to the U.S. health care cost conundrum? *Blood Rev* 2014;28:263–8.
- Humira (adalimumab) medication guide. North Chicago: AbbVie; 2016.
- Shin D, Lee Y, Kim H, Kornicke T, Fuhr R. A randomized phase I comparative pharmacokinetic study comparing SB5 with reference adalimumab in healthy volunteers. *J Clin Pharm Ther* 2017;42:672–8.
- Felson DT, Anderson JJ, Boers M, Bombardier C, Furst D, Goldsmith C, et al. American College of Rheumatology preliminary definition of improvement in rheumatoid arthritis. *Arthritis Rheum* 1995;38:727–35.
- Weinblatt ME, Baranauskaite A, Niebrzydowski J, Dokoupilova E, Zielinska A, Jaworski J, et al. Phase III randomized study of SB5, an adalimumab biosimilar, versus reference adalimumab in patients with moderate-to-severe rheumatoid arthritis. *Arthritis Rheumatol* 2018;70:40–8.
- Moots R, Azevedo V, Coindreau JL, Dorner T, Mahgoub E, Mysler E, et al. Switching between reference biologics and biosimilars for the treatment of rheumatology, gastroenterology, and dermatology inflammatory conditions: considerations for the clinician. *Curr Rheumatol Rep* 2017;19:37.
- Schiff M, Weaver A, Keystone E, Moreland L, Spencer-Green G. Comparison of ACR response, numeric ACR, and ACR AUC as measures of clinical improvement in RA clinical trials [abstract]. *Arthritis Rheum* 1999;42 Suppl:S81.
- Prevoo ML, van 't Hof MA, Kuper HH, van Leeuwen MA, van de Putte LB, van Riel PL. Modified disease activity scores that include twenty-eight-joint counts: development and validation in

- a prospective longitudinal study of patients with rheumatoid arthritis. *Arthritis Rheum* 1995;38:44–8.
14. Van Gestel AM, Prevoo ML, van 't Hof MA, van Rijswijk MH, van de Putte LB, van Riel PL. Development and validation of the European League Against Rheumatism response criteria for rheumatoid arthritis: comparison with the preliminary American College of Rheumatology and the World Health Organization/International League Against Rheumatism criteria. *Arthritis Rheum* 1996;39:34–40.
 15. Smolen JS, Breedveld FC, Schiff MH, Kalden JR, Emery P, Eberl G, et al. A Simplified Disease Activity Index for rheumatoid arthritis for use in clinical practice. *Rheumatology (Oxford)* 2003;42:244–57.
 16. Aletaha D, Nell VP, Stamm T, Uffmann M, Pflugbeil S, Machold K, et al. Acute phase reactants add little to composite disease activity indices for rheumatoid arthritis: validation of a clinical activity score. *Arthritis Res Ther* 2005;7:R796–806.
 17. Van der Heijde DM, van Riel PL, Gribnau FW, Nuver-Zwart IH, van de Putte LB. Effects of hydroxychloroquine and sulphasalazine on progression of joint damage in rheumatoid arthritis. *Lancet* 1989;1:1036–8.
 18. Breedveld FC, Weisman MH, Kavanaugh AF, Cohen SB, Pavelka K, van Vollenhoven R, et al. The PREMIER study: a multicenter, randomized, double-blind clinical trial of combination therapy with adalimumab plus methotrexate versus methotrexate alone or adalimumab alone in patients with early, aggressive rheumatoid arthritis who had not had previous methotrexate treatment. *Arthritis Rheum* 2006;54:26–37.
 19. Keystone EC, Kavanaugh AF, Sharp JT, Tannenbaum H, Hua Y, Teoh LS, et al. Radiographic, clinical, and functional outcomes of treatment with adalimumab (a human anti-tumor necrosis factor monoclonal antibody) in patients with active rheumatoid arthritis receiving concomitant methotrexate therapy: a randomized, placebo-controlled, 52-week trial. *Arthritis Rheum* 2004;50:1400–11.
 20. Weinblatt ME, Keystone EC, Furst DE, Kavanaugh AF, Chartash EK, Segurado OG. Long term efficacy and safety of adalimumab plus methotrexate in patients with rheumatoid arthritis: ARMADA 4 year extended study. *Ann Rheum Dis* 2006;65:753–9.
 21. Weinblatt ME, Keystone EC, Furst DE, Moreland LW, Weisman MH, Birbara CA, et al. Adalimumab, a fully human anti-tumor necrosis factor α monoclonal antibody, for the treatment of rheumatoid arthritis in patients taking concomitant methotrexate: the ARMADA trial. *Arthritis Rheum* 2003;48:35–45.
 22. Sampson HA, Munoz-Furlong A, Campbell RL, Adkinson NF Jr, Bock SA, Branum A, et al. Second symposium on the definition and management of anaphylaxis: summary report—second National Institute of Allergy and Infectious Disease/Food Allergy and Anaphylaxis Network symposium. *Ann Emerg Med* 2006;47:373–80.
 23. Bartelds GM, Krieckaert CL, Nurmohamed MT, van Schouwenburg PA, Lems WF, Twisk JW, et al. Development of antidrug antibodies against adalimumab and association with disease activity and treatment failure during long-term follow-up. *JAMA* 2011;305:1460–8.
 24. Van de Putte LB, Atkins C, Malaise M, Sany J, Russell AS, van Riel PL, et al. Efficacy and safety of adalimumab as monotherapy in patients with rheumatoid arthritis for whom previous disease modifying antirheumatic drug treatment has failed. *Ann Rheum Dis* 2004;63:508–16.
 25. Lai Z, La Noce A. Key design considerations on comparative clinical efficacy studies for biosimilars: adalimumab as an example. *RMD Open* 2016;2:e000154.
 26. US Food and Drug Administration. Scientific considerations in demonstrating biosimilarity to a reference product: guidance for industry. 2015. URL: <http://www.fda.gov/downloads/drugs/guidancecomplianceregulatoryinformation/guidances/ucm291128.pdf>.
 27. Yoo DH, Prodanovic N, Jaworski J, Miranda P, Ramitterre E, Lanzon A, et al. Efficacy and safety of CT-P13 (biosimilar infliximab) in patients with rheumatoid arthritis: comparison between switching from reference infliximab to CT-P13 and continuing CT-P13 in the PLANETRA extension study. *Ann Rheum Dis* 2017;76:355–63.
 28. Park W, Yoo DH, Miranda P, Brzosko M, Wiland P, Gutierrez-Urena S, et al. Efficacy and safety of switching from reference infliximab to CT-P13 compared with maintenance of CT-P13 in ankylosing spondylitis: 102-week data from the PLANETAS extension study. *Ann Rheum Dis* 2017;76:346–54.
 29. Emery P, Vencovsky J, Sylwestrzak A, Leszczynski P, Porawska W, Stasiuk B, et al. Long-term efficacy and safety in patients with rheumatoid arthritis continuing on SB4 or switching from reference etanercept to SB4. *Ann Rheum Dis* 2017. E-pub ahead of print.
 30. Cohen S, Genovese MC, Choy E, Perez-Ruiz F, Matsumoto A, Pavelka K, et al. Efficacy and safety of the biosimilar ABP 501 compared with adalimumab in patients with moderate to severe rheumatoid arthritis: a randomised, double-blind, phase III equivalence study. *Ann Rheum Dis* 2017;76:1679–87.
 31. Jorgensen KK, Olsen IC, Goll GL, Lorentzen M, Bolstad N, Haavardsholm EA, et al. Switching from originator infliximab to biosimilar CT-P13 compared with maintained treatment with originator infliximab (NOR-SWITCH): a 52-week, randomised, double-blind, non-inferiority trial. *Lancet* 2017;389:2304–16.

Transcriptional Profiling of Synovial Macrophages Using Minimally Invasive Ultrasound-Guided Synovial Biopsies in Rheumatoid Arthritis

Arthur M. Mandelin II,¹ Philip J. Homan,¹ Alexander M. Shaffer,¹ Carla M. Cuda,¹ Salina T. Dominguez,¹ Emily Bacalao,¹ Mary Carns,¹ Monique Hinchcliff,¹ Jungwha Lee,¹ Kathleen Aren,¹ Anjali Thakrar,¹ Anna B. Montgomery,¹ S. Louis Bridges Jr.,² Joan M. Bathon,³ John P. Atkinson,⁴ David A. Fox,⁵ Eric L. Matteson,⁶ Christopher D. Buckley,⁷ Costantino Pitzalis,⁸ Deborah Parks,⁴ Laura B. Hughes,² Laura Geraldino-Pardilla,³ Robert Ike,⁵ Kristine Phillips,⁵ Kerry Wright,⁶ Andrew Filer,⁷ Stephen Kelly,⁸ Eric M. Ruderman,¹ Vince Morgan,¹ Hiam Abdala-Valencia,¹ Alexander V. Misharin,¹ G. Scott Budinger,¹ Elizabeth T. Bartom,¹ Richard M. Pope,¹ Harris Perlman,¹ and Deborah R. Winter¹

Objective. Currently, there are no reliable biomarkers for predicting therapeutic response in patients with rheumatoid arthritis (RA). The synovium may unlock critical information for determining efficacy, since a reduction in the numbers of sublining synovial macrophages remains the most reproducible biomarker. Thus, a clinically actionable method for the collection of synovial tissue, which can be analyzed using high-throughput strategies, must become a reality. This study was undertaken to assess the feasibility of utilizing synovial biopsies as a precision medicine-based approach for patients with RA.

Methods. Rheumatologists at 6 US academic sites were trained in minimally invasive ultrasound-guided synovial tissue biopsy. Biopsy specimens obtained from patients with RA and synovial tissue from patients with osteoarthritis (OA) were subjected to histologic analysis, fluorescence-activated cell sorting, and RNA sequencing (RNA-seq). An optimized protocol for digesting synovial tissue was developed to generate high-quality RNA-seq libraries from isolated macrophage populations. Associations were determined between macrophage transcriptional profiles and clinical parameters in RA patients.

Results. Patients with RA reported minimal adverse effects in response to synovial biopsy. Comparable

Supported by the NIH (grant AR-064313 to Dr. Cuda and grants AR-064546, HL-134375, AG-049665, and UH2-AR-067687), a Pfizer ASPIRE award (to Dr. Pope), the United States–Israel Binational Science Foundation (grant 2013247), the Rheumatology Research Foundation (grant Agmt 05/06/14 to Dr. Perlman), and in part by the Arthritis National Research Foundation (grant to Dr. Winter). Dr. Perlman's work was also supported by the Northwestern University Feinberg School of Medicine Mabel Greene Myers Professorship in Medicine and donations to the Rheumatology Precision Medicine Fund.

¹Arthur M. Mandelin II, MD, PhD, Philip J. Homan, PhD, Alexander M. Shaffer, BA, Carla M. Cuda, PhD, Salina T. Dominguez, BA, Emily Bacalao, BA, Mary Carns, MS, Monique Hinchcliff, MD, Jungwha Lee, PhD, Kathleen Aren, BA, Anjali Thakrar, BA, Anna B. Montgomery, PhD, Eric M. Ruderman, MD, Vince Morgan, BA, Hiam Abdala-Valencia, PhD, Alexander V. Misharin, MD, PhD, G. Scott Budinger, MD, Elizabeth T. Bartom, PhD, Richard M. Pope, MD, Harris Perlman, PhD, Deborah R. Winter, PhD: Northwestern University Feinberg School of Medicine, Chicago, Illinois; ²S. Louis Bridges Jr., MD, PhD, Laura B. Hughes, MD: University of Alabama at Birmingham; ³Joan M. Bathon, MD, Laura Geraldino-Pardilla, MD: Columbia University, New York, New York; ⁴John P. Atkinson, MD, Deborah Parks, MD: Washington University School of Medicine, St. Louis, Missouri; ⁵David A. Fox, MD, Robert Ike, MD, Kristine Phillips, MD: University of Michigan School of Medicine, Ann Arbor;

⁶Eric L. Matteson, MD, Kerry Wright, MD: Mayo Clinic College of Medicine and Science, Rochester, Minnesota; ⁷Christopher D. Buckley, MD, PhD, Andrew Filer, MD, PhD: University of Birmingham Research Laboratories, Queen Elizabeth Hospital Birmingham, Birmingham, UK; ⁸Costantino Pitzalis, MD, Stephen Kelly, MD: William Harvey Research Institute and Barts and The London School of Medicine and Dentistry, Queen Mary University of London, London, UK.

Drs. Mandelin and Homan and Mr. Shaffer contributed equally to this work.

Address correspondence to Richard M. Pope, MD, Northwestern University, Feinberg School of Medicine, Department of Medicine, Division of Rheumatology, 240 East Huron Street, Room M320, Chicago, IL 60611 (e-mail: rmp158@northwestern.edu); or to Harris Perlman, PhD, Northwestern University, Feinberg School of Medicine, Department of Medicine, Division of Rheumatology, 240 East Huron Street, Room M314, Chicago, IL 60611 (e-mail: h-perlman@northwestern.edu); or to Deborah R. Winter, PhD, Northwestern University, Feinberg School of Medicine, Department of Medicine, Division of Rheumatology, 240 East Huron Street, Room M309, Chicago, IL 60611 (e-mail: Deborah.winter@northwestern.edu).

Submitted for publication March 17, 2017; accepted in revised form February 8, 2018.

RNA quality was observed from synovial tissue and isolated macrophages between patients with RA and patients with OA. Whole tissue samples from patients with RA demonstrated a high degree of transcriptional heterogeneity. In contrast, the transcriptional profile of isolated RA synovial macrophages highlighted different subpopulations of patients and identified 6 novel transcriptional modules that were associated with disease activity and therapy.

***Conclusion.* Performance of synovial tissue biopsies by rheumatologists in the US is feasible and generates high-quality samples for research. Through the use of cutting-edge technologies to analyze synovial biopsy specimens in conjunction with corresponding clinical information, a precision medicine-based approach for patients with RA is attainable.**

Despite the many therapies available for patients with rheumatoid arthritis (RA), there is little information to guide selection of the most effective treatment for an individual patient. Forty-six percent of patients with RA respond (defined as 50% improvement based on the American College of Rheumatology criteria [ACR50]) to conventional disease-modifying antirheumatic drugs (DMARDs) (1,2) or conventional DMARDs plus anti-tumor necrosis factor (anti-TNF) therapy (3–11). However, 20–40% of patients in clinical trials never demonstrate even a minimal response (never meet the ACR20 response criteria) (7–11). Based on a population of >300 million in the US, a disease prevalence of 0.6%, and a course of 3–4 months per biologic DMARD therapy, as much as \$2.5 billion is wasted annually on inadequate therapy (12,13). There is a clear need to develop precision-based therapy for patients with RA, whereby clinical information such as novel biomarkers will enhance our ability to predict the therapeutic response and thereby limit ineffective therapy.

Previous studies have linked macrophages to the pathogenesis of RA. Synovial macrophages are highly activated, express elevated levels of Toll-like receptor 2 (TLR-2), TLR-4, and TLR-7 (14,15), and contribute directly and indirectly to synovial inflammation and the destruction of cartilage and bone through the production of degradative enzymes, cytokines, and chemokines. Further, TLR-2, TLR-3, and TLR-7 play essential roles in the development of inflammatory arthritis in mice (16–18). More importantly, macrophages are the central producers of interleukin-1 β (IL-1 β), IL-6, and TNF, which comprise the 3 essential proinflammatory cytokines that contribute to RA pathogenesis. To date, approved therapies, including anti-TNF, anti-IL-6, JAK inhibitors, CTLA-4Ig, and anti-

CD20, have all been shown to decrease synovial inflammation and bone destruction and, more importantly, reduce macrophage numbers in the synovial sublining (19–21). Despite the fact that synovial macrophages were discovered more than a half-century ago and are crucial for RA pathogenesis (22), surprisingly very little is known about them.

Biomarkers that indicate sensitivity or resistance to a particular therapy are sorely lacking in RA. For the most part, researchers have used peripheral blood, with minimal success, to identify biomarkers for predicting a response to therapy (23). Similarly, the results of genetic approaches have been disappointing (24). More recent studies suggest that the synovium, as the target organ in RA, may have greater potential in determining therapeutic response (23). Currently, the most well-known and reproducible biomarker for response to RA therapy is a reduction in the number of sublining synovial macrophages, determined by immunohistochemical analysis of synovial tissue (25). While arthroscopy has been the most commonly used method to obtain synovial tissue before and after therapy (26–32) and yields substantial amounts of synovial tissue, it is invasive, requires surgical suites, and is expensive, thus limiting its usefulness in clinical practice and clinical studies. Synovectomy and joint replacement surgery are other common mechanisms for researchers to obtain synovial tissue, but patients undergoing these procedures typically exhibit end-stage disease characteristics and samples likely do not reflect the overall pathophysiology at the time when therapeutic decisions are made, prior to progressive joint damage.

Ultrasound technology has advanced significantly and is widely used by rheumatologists as a mechanism for determining the degree of synovitis and inflammation, detecting erosions, and identifying sites for therapeutic injection (33). Over the past decade, ultrasound has been used to facilitate the collection of synovial tissue (29). Minimally invasive ultrasound-guided synovial tissue biopsies have been performed for research purposes throughout Europe, and the standardization for these procedures has been fully evaluated (23,29,34–46). However, there are currently no published studies from the US describing the use of ultrasound-guided synovial tissue biopsies for research. The potential reasons that this technique has not been commonly adopted for research in the US include a lack of training, differences in the medical system and patient populations between Europe and the US, and a lack of “buy-in” from rheumatologists who would recommend the procedure to their patients.

We assembled a consortium of established academic rheumatology groups in the US, including the University of Alabama at Birmingham, Columbia University, Mayo Clinic, Washington University, University of

Michigan, and Northwestern University, to form the Rheumatoid Arthritis SynOvial tissue Network (REASON). Our consortium was trained in minimally invasive ultrasound-guided synovial biopsy techniques in the UK and has since performed more than 41 biopsies on RA patients with active disease in the US. RNA was extracted from whole synovial tissue and from synovial macrophages isolated by fluorescence-activated cell sorting (FACS) for RNA sequencing (RNA-seq) analysis. The transcriptional profiles of isolated macrophages were used to distinguish between RA patient groups and identify modules of co-regulated genes that were associated with clinical disease and medication. We believe that these studies demonstrate the utility of isolating individual populations of cells within the synovium to understand the pathobiology of the disease and to establish a precision medicine-based approach for RA patients.

PATIENTS AND METHODS

Patients. Adult patients with RA, diagnosed according to either the ACR 1987 criteria (47) or ACR/European League Against Rheumatism 2010 criteria (48), were selected as candidates for ultrasound-guided synovial biopsy based on the presence of palpable synovitis documented by clinical examination (49,50). To increase the uniformity of the collected tissue, only wrists were sampled in this study. Candidate joints were scanned with standard 2-dimensional B-mode ultrasound with and without Doppler (SonoSite M-MSK with a 15–6 MHz linear probe; FujiFilm SonoSite), and were included in the study if they had a grayscale synovitis score of ≥ 2 on a 4-point scale (35). Exclusion criteria included uncontrolled comorbid diseases, anticoagulation therapy (low-dose aspirin and nonsteroidal antiinflammatory drugs [NSAIDs] were allowed), use of systemic steroids in excess of prednisone 10 mg daily or equivalent, administration of intramuscular steroids within the previous 4 weeks or intra-articular steroids into the target joint within the past 8 weeks, chronic or recurrent infection, intolerance to lidocaine or chlorhexidine, inability to communicate effectively in English, and membership in a vulnerable population (prisoners, pregnant women, etc.).

Training for ultrasound-guided synovial biopsy. The REASON consortium was created to adopt ultrasound-guided synovial biopsy for research purposes in the US. Rheumatologists from REASON who were experienced in ultrasonography traveled to the UK for a 2-day training session with Drs. Andrew Filer, Christopher D. Buckley, Stephen Kelly, and Costantino Pitzalis on ultrasound-guided synovial biopsy. This session included observation of ultrasound-guided synovial biopsies followed by a practice session using cadavers. Following the training session, the rheumatologists from REASON attended 2 additional practice sessions using cadavers at Northwestern University for refresher training.

Ultrasound-guided synovial biopsy procedure. Procedures were performed either in examination rooms in outpatient rheumatology clinics or in a designated research space. After the presence of synovitis was re-confirmed by sonographic criteria as described above using customary non-sterile techniques, patients

were dressed in a laboratory cover-up or examination gown, surgical mask, and surgical hair net. Rheumatologists performing the biopsy were in surgical scrubs with cap, mask, sterile surgical gown, and sterile gloves. The ultrasound probe was placed in a sterile cover. The patient's hand and arm were scrubbed with chlorhexidine from the fingertips to the mid-forearm, and the patient then placed the hand palm down onto a surgical wrist support in a prepared sterile field. The arm was draped in a sterile manner with a fenestrated sheet centered on the wrist, and sterile ultrasound gel was applied.

Ultrasound scanning over the dorsal aspect of the wrist joint in both the longitudinal and transverse planes was then used to locate the region of greatest synovitis in the wrist, usually immediately dorsal/superficial to either the proximal or the distal row of carpal bones. A wheal of lidocaine was used to anesthetize the skin at the ulnar aspect of the wrist. While monitoring the procedure under ultrasound in real time with the probe in the transverse position, an initial ultrasound-guided lidocaine pass into the target joint was made with a 25-gauge \times 1.5-inch needle. A second ultrasound-guided lidocaine pass was made into the same wound and needle track with an 18-gauge \times 1.5-inch needle to ensure anesthesia and a clear path for the biopsy device. Care was taken to avoid neurovascular structures and tendons, especially the extensor digiti minimi. An appropriately sized Quick-Core Biopsy needle (Cook Medical) was then selected based on the target wrist (usually 18 gauge \times 9 cm, with 10-mm throw) and introduced into the same needle track.

Using continuous real-time ultrasound imaging, the jaw of the device was positioned within the synovium (defined by Outcome Measures in Rheumatology [51] as intraarticular, hypoechoic, non-displaceable, poorly compressible tissue) at the point of its greatest abundance, usually between the common extensor tendon bundle and the underlying carpal row. The device was triggered and removed. The sample was removed from the device by scraping with a sterile 21-gauge needle and placed into phosphate buffered saline (PBS) (Thermo Fisher). The process was repeated to obtain a total of 12 samples. Not all biopsy passes yielded tissue; most procedures resulted in 1–3 “empty passes,” and thus most patients underwent a total of 13–15 passes to obtain 12 samples of synovium. All samples were taken through the same skin wound but with varying positions of the jaw of the device within the region of most abundant synovitis, with the intent of sampling the entire chosen region uniformly. Variations in the position of the device also included variations in the radial orientation of the jaw with respect to the axis of the device. For example, some samples were taken from 12 o'clock, closer to the extensor tendon bundle, and some from 6 o'clock, closer to the carpal row.

At the completion of the procedure the biopsy site was washed, and after confirming hemostasis, an adhesive bandage was applied to the single puncture wound. None of the patients needed a suture. Patients were instructed in routine after-care and encouraged to use over-the-counter acetaminophen for any discomfort, with permission to escalate to over-the-counter NSAIDs if needed. Patients were instructed to contact the research team by telephone to report any adverse events, including delayed healing or pain not controlled with over-the-counter agents as described above. Most procedures lasted a total of 45–60 minutes from the non-sterile scout imaging to the patient departing the procedure room. Patients did not require conscious sedation and were sent home immediately with no postprocedure observation or recovery period and no activity restrictions.

Tolerability. Tolerability of the procedure was assessed by questionnaires administered before and after the procedure as previously described (36). Patients were asked to rate pain, swelling, and stiffness on a 10-point visual analog scale (VAS). After the procedure, patients were also asked by questionnaire to rate their discomfort during the procedure (none, mild, moderate, or severe) and to rate their likelihood to agree to undergo another procedure (very likely, somewhat likely, unsure, somewhat unlikely, or very unlikely).

Tissue preparation and flow cytometric analysis. From the 12 pieces of synovial tissue obtained per patient by needle biopsies, 4 were selected at random and placed into 10% neutral buffered formalin for histologic analysis, 4 more randomly selected pieces were placed into RNeasy lysis buffer (Qiagen) for whole tissue processing, and the remaining 4 were placed into PBS for tissue digestion. Osteoarthritis (OA) synovial tissue was received from the National Disease Research Interchange and was shipped in Dulbecco's modified Eagle's medium and antibiotics overnight on wet ice. Only soft tissues containing meniscus and synovium were processed. OA synovial tissue was processed identically to tissue from patients with RA.

The length of digestion (30–60 minutes) and intensity of mechanical disaggregation before and after incubation were varied to optimize macrophage isolation. Mechanical disaggregation was performed on a gentleMACS Dissociator (Miltenyi Biotec). The pre-set gentleMACS programs *m_lung_01* and *m_brain_01* were used to test moderate and aggressive mechanical disaggregation, respectively. Sorted macrophages used for analysis were processed by infusing tissue with a digestion buffer (RPMI 1640 [Sigma], Liberase TL [0.1 mg/ml; Roche], and DNase [0.1 mg/ml; Roche]) and minced with scissors. Tissue suspensions were transferred to C-tubes (Miltenyi Biotec) and incubated for 1 hour at 37°C with aggressive disaggregation before and after incubation. The digestion reaction was quenched with magnetic-activated cell sorter (MACS) buffer (Miltenyi Biotec), and the tissue suspension was filtered over a 40-micron filter. Red blood cells were lysed (BD Pharm Lyse) and then washed twice with Hanks' balanced salt solution (Thermo Fisher). Cells were counted (Invitrogen Countess) and stained with a viability dye (0.5 µl/ml for 15 minutes at 25°C in the dark) (data are available upon request from the corresponding author). Cells were then washed twice with MACS buffer, incubated with Fc block (BD Biosciences) (6 µl/60 µl total volume; maximum of 5×10^6 cells for 15 minutes at 4°C in the dark), stained with antibody cocktail (for 30 minutes at 4°C in the dark) (data are available upon request from the corresponding author), washed twice, resuspended in MACS buffer, and kept on ice until sorted.

Synovial macrophages (CD45+, CD11b+, HLA-DR+, CD15-, CD1c-, CD206+) were sorted on a BD FACSAria Sora instrument (BD Biosciences) at the Northwestern University Robert H. Lurie Comprehensive Cancer Center Flow Cytometry Core Facility. Cells from RA synovial biopsies were sorted directly into 100 µl PicoPure RNA extraction buffer (Arcturus Bioscience). Cells (>10,000) from OA tissues were sorted into cold MACS buffer (Miltenyi Biotec) and immediately centrifuged at 4°C. Supernatant was removed, and cells were resuspended in 100 µl PicoPure RNA extraction buffer. All cells were stored at -80°C until RNA was extracted.

Histopathologic and immunohistochemical analysis. The 4 biopsy pieces fixed in 10% neutral buffered formalin for histologic analysis were stored overnight and submitted to the Pathology Core Facility at Northwestern University. Paraffin-embedded

tissue sections were stained with hematoxylin and eosin (H&E) and for CD45 or CD68. Slide images were taken at 40× and 100× magnification using an Olympus BX41 microscope and Olympus DP21 camera. Since not all samples subjected to this procedure demonstrate synovial lining, other characteristics including CD45 and CD68 staining were included to provide a semiquantitative or qualitative analysis of inflammation in the biopsied tissue. RA synovial biopsy sections stained with H&E or with antibodies to either CD45 or CD68 antigens were scored for the percent synovium of all 4 pieces of tissue. The CD45 and CD68 scores were determined using a modified scoring system of 0–4 that indicates the percent of CD45 or CD68 positivity in identified synovium (35). All scoring was performed by an experienced rheumatologist (RMP) who was blinded with regard to the origin of the samples.

Preparation of the RNA library. RNA was isolated from whole synovial tissue by homogenizing tissue with 3.0 mm of high-impact zirconium beads and a BeadBlaster 24 microtube homogenizer (Benchmark Scientific). RNA was extracted from the cell homogenate using a Qiagen Plus Mini kit. RNA from sorted macrophages was extracted using a PicoPure RNA isolation kit according to the instructions of the manufacturer (Arcturus). RNA quality and quantity were measured using a High-Sensitivity RNA ScreenTape System (Agilent Technologies). Whole synovial tissue RNA-seq libraries were prepared from 90 ng of total RNA using a NEBNext Ultra Kit with poly(A) enrichment. RNA-seq libraries from sorted macrophage populations were prepared using a SMART-Seq v4 Ultra Low Input RNA Kit (Clontech Laboratories) followed by Nextera XT protocol (Illumina). RNA-seq libraries were sequenced on a NextSeq 500 instrument (Illumina) with ~5–10 × 10⁶ aligned reads per sample. A commercially available universal human RNA reference was prepared along with the synovial RNA to represent background RNA expression.

RNA-seq analysis. RNA-seq data were de-multiplexed using *bcl2fastq*, and RNA-seq reads were aligned to the human reference genome (NCBI, hg19) using *TopHat2* (version 2.17.1.14) aligners (52). Gene coverage of samples was calculated using the *RSeQC* package (53). Sample complexity was calculated using the *samtools makeTagDirectory* command and identifying the uniquely aligned positions compared to the number of aligned reads. Normalized gene counts were calculated using *HTSeq* (54). For our analysis, we focused on genes in which at least 2 samples had \log_2 (fragments per kilobase per million [FPKM]) expression >3. For visualization, *GENE-E* software (<https://software.broadinstitute.org/GENE-E/>) was used to generate Pearson's pairwise correlation matrices and to perform K-means and hierarchical clustering. Differential gene expression between RA and OA samples in the whole tissue data set was determined using the *edgeR* Bioconductor package parameters as previously described (adjusted $P < 0.01$) (55,56). Gene Ontology (GO) associations were determined by *GOrilla* (57). To account for the increased noise of the low-input macrophage-specific RNA-seq, we focused our analysis on genes in which at least 2 samples had \log_2 (FPKM + 1) expression >5, and lower values were set to 5. We defined differentially expressed genes across patients with RA as those with an adjusted range (\log_2 fold change between the second highest and second lowest samples) >1. We removed genes driven by 1 outlier sample (defined as genes where the difference between the maximum and second highest values was greater than the difference between the second highest and second lowest values), leaving 553 genes for the analysis. Modules were identified by clustering genes using K-means clustering and calculating pairwise Pearson's correlation

between each gene. The enrichment or depletion of modules within each patient was determined by a Kolmogorov-Smirnov test comparing the expression level of genes in a given module to all 553 genes (with *P* values less than 0.05 considered significant).

Statistical analysis. Associations between RNA-seq expression patterns in patients and clinical parameters, including disease duration, swollen joint count (SJC), tender joint count (TJC), early disease (defined as a disease duration of <2 years), rheumatoid factor (RF), anti-cyclic citrullinated peptide (anti-CCP) antibodies, and history of treatment with biologic agents or methotrexate, were determined (Table 1). Disease duration, SJC, and TJC were recorded as continuous variables. Early disease, RF, anti-CCP antibodies, and patient medication history were recorded as categorical data (either positive or negative). Patients were divided into 2 groups based on global gene expression data, and associations of patient treatment and clinical data with group 1 and group 2 were determined using Fisher's exact test for categorical variables and Student's *t*-test for continuous variables. Pearson's correlation was used to determine the association between the

patient's median gene expression for each module and continuous variables. The log₂ fold change of the average median module expression between patients with a positive value and those with a negative value was used to calculate associations with categorical variables (data are available upon request from the corresponding author). Significant changes in gene expression were determined using Student's *t*-test.

RESULTS

Patient demographics. The REASON consortium was created to adopt ultrasound-guided synovial biopsy for research purposes in the US. Over 2 years, we recruited 41 patients with RA from REASON sites for ultrasound-guided synovial biopsies. Patient demographics, clinical data, and other pertinent information are presented in Table 1.

Table 1. Patient characteristics and sample data*

Patient characteristics		Histologic findings in RA synovial biopsy specimens, mean ± SEM (n = 30)‡	
Age, years (n = 41)	57.5 ± 11.4	% synovial tissue	36.0 ± 5.6
Sex, no. (%) female/male	29 (71)/12 (29)	CD45 score (range 0–4)	1.7 ± 0.2
Disease duration, years (n = 40)	9.3 ± 8.4	CD68 score (range 0–4)	1 ± 0.1
Early disease, no. (%) (n = 40)†	9 (23)	RNA sequencing data, mean ± SEM	
Rheumatoid factor positive, no. (%) (n = 40)	23 (58)	Whole tissue samples (n = 9 RA and 9 OA)	
Anti-CCP positive, no. (%) (n = 36)	19 (53)	RIN	
ESR, mm/hour (n = 14)	33.5 ± 21.7	RA	6.7 ± 0.5
DAS28 (n = 17)	4.7 ± 1.3	OA	8.0 ± 0.2
CDAI (n = 20)	21.5 ± 10.6	Number of aligned reads, million	
RAPID3 (n = 25)	11.4 ± 7.4	RA	9.2 ± 0.7
PGA (n = 24)	4.7 ± 3.1	OA	12.9 ± 1.1
HAQ (n = 18)	0.7 ± 0.5	% of total reads aligned	
TJC (n = 31)	5.8 ± 6.0	RA	81.9 ± 1.2
SJC (n = 31)	7.1 ± 4.9	OA	85.3 ± 1.2
Treatment, no. (%) (n = 31)		% complexity	
No treatment	3 (10)	RA	54.8 ± 1.7
Methotrexate		OA	56.2 ± 1.9
Current	15 (48)	Sorted macrophage samples (n = 15 RA and 9 OA)	
Past	9 (29)	Cells sorted	
TNF inhibitor		RA	1,642 ± 1,178
Current	12 (38)	OA	77,414 ± 26,413
Past	17 (55)	Number of aligned reads, million	
IL-6 inhibitor		RA	21.0 ± 4.2
Current	2 (6)	OA	21.1 ± 6.8
Past	2 (6)	% of total reads aligned	
JAK inhibitor		RA	53.9 ± 6.0
Current	3 (10)	OA	65.2 ± 1.5
Past	5 (16)	% complexity	
Other treatment		RA	37.2 ± 2.7
Current	11 (35)	OA	38.1 ± 2.2
Past	12 (39)		
Prednisone <5 mg, current	1 (3)		
Prednisone 5–10 mg, current	6 (19)		

* Except where indicated otherwise, values are the mean ± SD. Anti-CCP = anti-cyclic citrullinated peptide; ESR = erythrocyte sedimentation rate; DAS28 = Disease Activity Score in 28 joints; CDAI = Clinical Disease Activity Index; RAPID3 = Routine Assessment of Patient Index Data 3; PGA = physician's global assessment; HAQ = Health Assessment Questionnaire; TJC = tender joint count; SJC = swollen joint count; TNF = tumor necrosis factor; IL-6 = interleukin-6; RA = rheumatoid arthritis; OA = osteoarthritis; RIN = RNA integrity number.

† Disease duration of <2 years.

‡ All slides were scored by the same physician (RMP), who was blinded with regard to the origin of the samples. The amount of synovial tissue in each biopsy specimen was estimated by analysis of structure, lining, and leukocyte content.

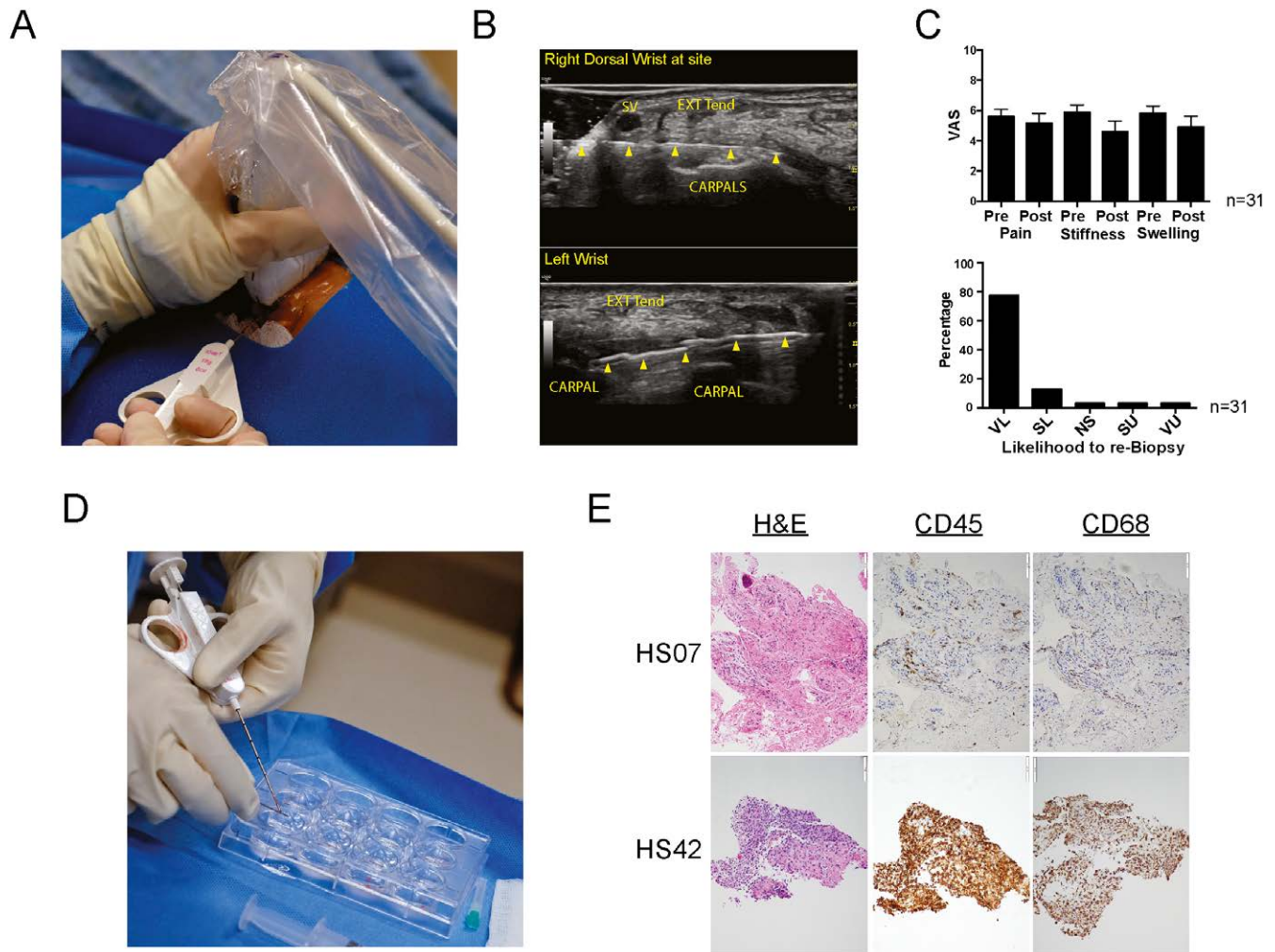


Figure 1. Acquisition and analysis of synovial tissue from patients with rheumatoid arthritis (RA). **A**, Ultrasound-guided synovial biopsy of an inflamed wrist using an 18-gauge \times 1.5-inch needle. **B**, Dorsal transverse (axial) view of a right wrist showing a needle track created with a 25-gauge \times 1.5-inch needle (**arrowheads**) and a left wrist in which an 18-gauge \times 9-cm needle biopsy device has been introduced into the needle track with a 10-mm throw opened (second and third **arrowheads** from the left). SV = superficial vein; Ext Tend = extensor tendon complex; Carpals = proximal row of carpal bones. **C**, Top, Patient-reported pain, stiffness, and swelling before and after the biopsy procedure on a visual analog scale (VAS) of 1–10. Bars show the mean \pm SEM. Bottom, Patient-reported likelihood of agreeing to a subsequent procedure. VL = very likely; SL = somewhat likely; NS = not sure; SU = somewhat unlikely; VU = very unlikely. **D**, Removal of synovial tissue from the biopsy device. Tissue was placed into phosphate buffered saline on ice until processed. **E**, Histomorphologic features of synovial biopsy specimens obtained from 2 representative RA patients. Representative photomicrographs of sections stained with hematoxylin and eosin (H&E), anti-CD45 (for hematopoietic cells), and anti-CD68 antibodies (for macrophages) are shown. HS07 = human sample 07.

Safety and tolerability of ultrasound-guided synovial biopsy. Real-time ultrasound images were used to guide placement of the needle device for biopsy within the synovium of the dorsal side of the wrist (Figures 1A and B). Thirty-one of the 41 patients responded with complete preprocedure and postprocedure VAS assessments of pain, stiffness, and swelling of the biopsied wrist. There were no differences between the preprocedure and postprocedure scores in these patients (Figure 1C). Patients were then asked to rate their likelihood of agreeing to repeat the

procedure, and 90.3% of the patients reported that they would be very likely or somewhat likely to repeat the biopsy, while only 6.5% stated that they would be somewhat or very unlikely to have a repeat biopsy (Figure 1C).

Histologic assessment of synovial tissue. The quality of the synovial biopsy specimens obtained from patients with RA was first quantified by histologic assessment of tissue structure, presence of synovial lining, and leukocytes (Table 1 and Figures 1D and E). Importantly, all but 5 samples contained synovial tissue (>10%), and

11 biopsy specimens contained $\geq 50\%$ synovial tissue. The abundance of CD45-positive and CD68-positive cells in each sample was scored on a modified scale of 0–4 (35), revealing a substantial enrichment of hematopoietic cells and, more specifically, macrophages in most biopsy samples (Table 1).

RNA-seq analysis of whole tissue synovial biopsy specimens. The fidelity of the complementary DNA library created from whole synovial tissue obtained from

RA synovial biopsy specimens or from OA patients following whole joint replacement was assessed by a variety of criteria (Table 1). The quality of the RNA-seq data for whole tissue samples was determined by plotting the number of detectable genes at varying FPKM thresholds across samples. There was no observable difference between the number of genes expressed in RA versus OA samples (Figure 2A). The read density over the length of genes revealed that all samples had comparable coverage

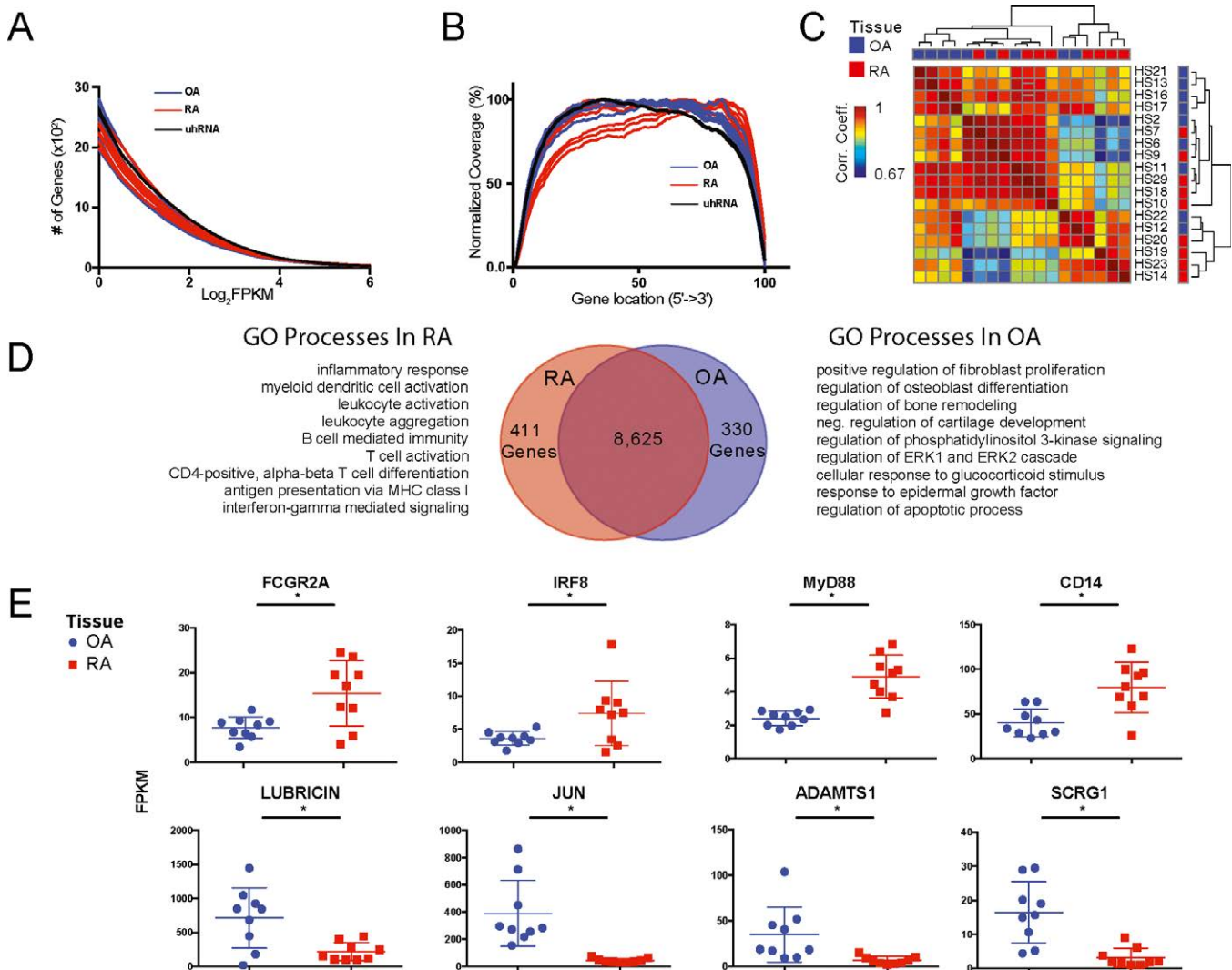


Figure 2. Analysis of whole tissue RNA sequencing libraries. **A**, Number of genes with an expression level greater than a given \log_2 (fragments per kilobase per million [FPKM]) value for each osteoarthritis (OA), rheumatoid arthritis (RA), and universal human RNA (uhrRNA) control sample. **B**, Gene coverage plot displaying the average read density across genes from 5' to 3'. **C**, Pairwise Pearson's correlations of gene expression between individual patient samples. Samples are organized by hierarchical clustering based on their Pearson's correlation coefficients (corr. coeff.) across samples. Numbers to the right of the matrix are the patient numbers for each sample. HS21 = human sample 21. **D**, Venn diagram of the genes expressed in RA and OA samples. The differential analysis (adjusted $P < 0.01$) revealed 411 and 330 genes that were preferentially expressed in RA and OA tissue, respectively. Select processes from gene ontology (GO) enrichment analysis of genes preferentially expressed in each tissue type are listed. **E**, Normalized gene expression of individual genes in RA versus OA samples. Symbols represent individual samples; horizontal lines and error bars show the median and interquartile range. * = adjusted $P < 0.01$.

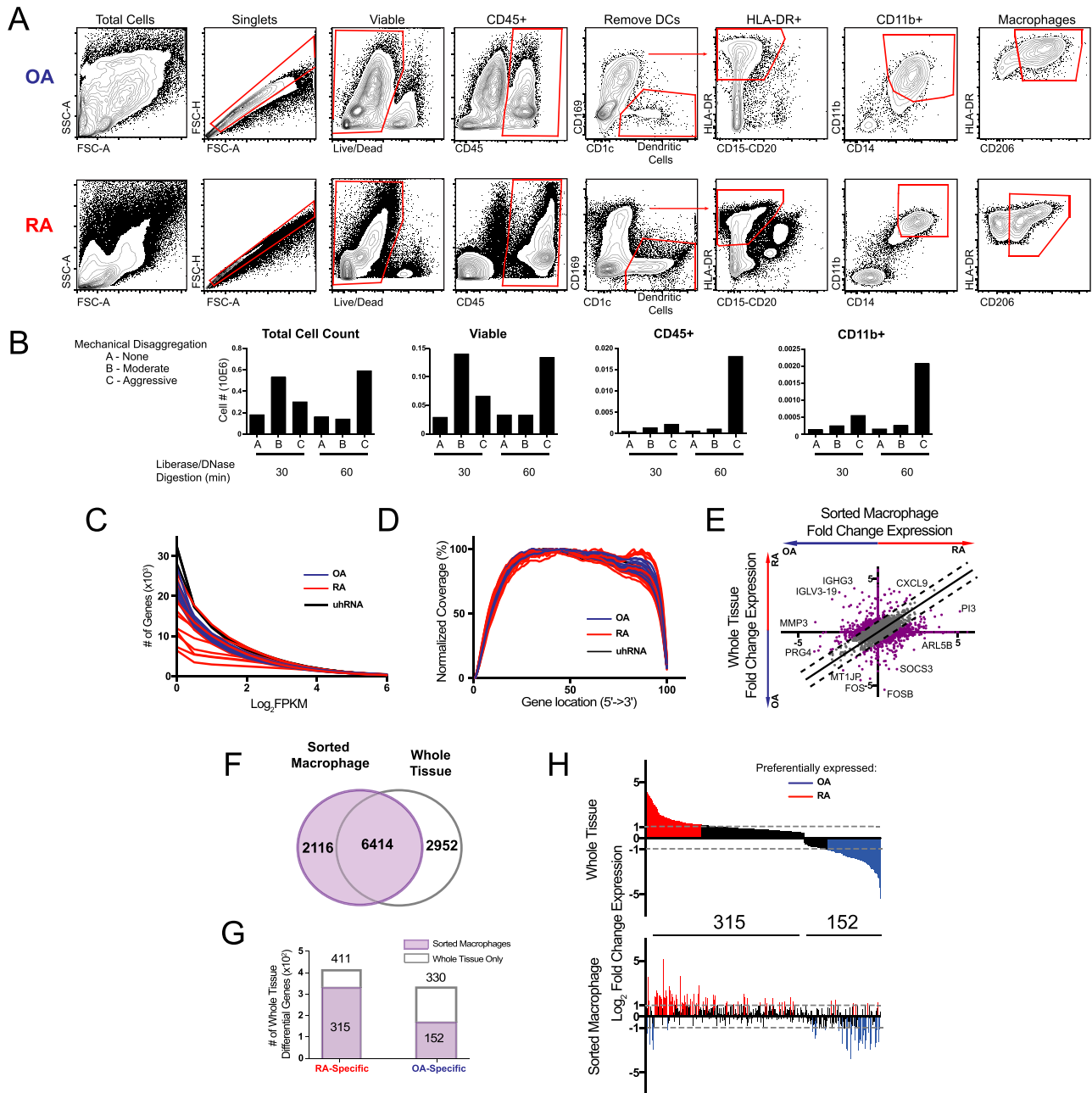


Figure 3. Isolation of synovial macrophages and macrophage-specific RNA sequencing. **A**, Gating strategy used to identify synovial macrophages in osteoarthritis (OA) and rheumatoid arthritis (RA) tissue. DC = dendritic cell. **B**, Optimization of the synovial tissue processing procedure. The success of tissue processing was evaluated by the number of viable, CD45+, and CD11b+ cells identified by flow cytometry. **C**, Number of genes with an expression level greater than a given \log_2 (fragments per kilobase per million [FPKM]) value for each OA, RA, and universal human RNA (uhRNA) control sample. **D**, Gene coverage plot displaying the average read density across genes from 5' to 3'. **E**, \log_2 fold change of gene expression between RA and OA whole tissue samples and macrophages. Broken lines indicate a difference of 1; solid line indicates no change in expression. Select genes are displayed. **F**, Venn diagram comparing numbers of genes expressed in sorted macrophages and whole tissue. **G**, Numbers of genes differentially expressed in whole tissue that were also detected in sorted macrophages from RA and OA samples. **H**, \log_2 fold change in expression of the 467 differentially expressed genes (in **G**) in whole tissue and sorted macrophages. Genes are ordered along the x-axis by decreasing fold change in whole tissue. The numbers of genes preferentially expressed in RA tissue (\log_2 fold change >1) and OA tissue (\log_2 fold change <-1) are indicated in red and blue, respectively.

across the genome (Figure 2B). Nine RA synovial biopsy samples and 9 OA tissue samples produced high-quality RNA-seq libraries and were used for further analyses, concentrating on a set of 9,366 expressed genes. The global gene expression profiles from synovial tissue samples were heterogeneous across the RA samples and did not clearly cluster apart from the OA samples (Figure 2C). The variability among patients highlights the complexity in the presentation of RA in whole tissue and points to a shift in gene expression in individual cell types that could be associated with disease activity status and therapy at the time of biopsy.

Differential expression analysis identified genes that were specific to either RA or OA synovial tissue samples. We found 411 RA-specific genes and 330 OA-specific genes (Figure 2D). GO analysis revealed that RA-specific genes were associated with a wide range of immune processes, including leukocyte activation, T cell activation, and B cell-mediated immunity, while OA-specific genes were associated with more homeostatic processes, such as osteoblast differentiation, bone remodeling, and the epidermal growth factor receptor signaling pathway. Specifically, we found several macrophage-related genes (FCGR2A, IRF8, MyD88, and CD14) that were significantly up-regulated in RA relative to OA synovial tissue (Figure 2E). Genes that

were preferentially expressed in OA, such as lubricin (58), JUN (59), ADAMTS1 (60), and SCRG1 (61), have previously been linked to differences in synovial tissue function in OA. The broad range of pathways involved in RA at the level of whole tissue highlights the need for a cell type-specific approach to better understand the role of particular cell populations.

Synovial macrophage digestion and RNA-seq analysis. Multiparameter flow cytometry was used to isolate macrophages from RA and OA synovial tissue (Figure 3A). Macrophages were gated via the inclusion of singlets, viable, CD45+, and HLA-DR+ cells. Macrophages were further isolated by excluding dendritic cells and then gating on the remaining HLA-DR+ cells followed by CD11b+ cells to identify the CD206+ macrophage populations. An optimized digestion protocol was developed to isolate viable macrophages from synovial tissue. The effectiveness of tissue digestion was assessed by maximizing the number of viable, CD45+, and CD11b+ cells within a given single-cell suspension (Figure 3B). A mean \pm SEM of $1,642 \pm 1,178$ macrophages was isolated from digested biopsy samples and prepared for RNA-seq analysis (Table 1). An identical digestion protocol was used to isolate cell populations from OA synovial tissue as

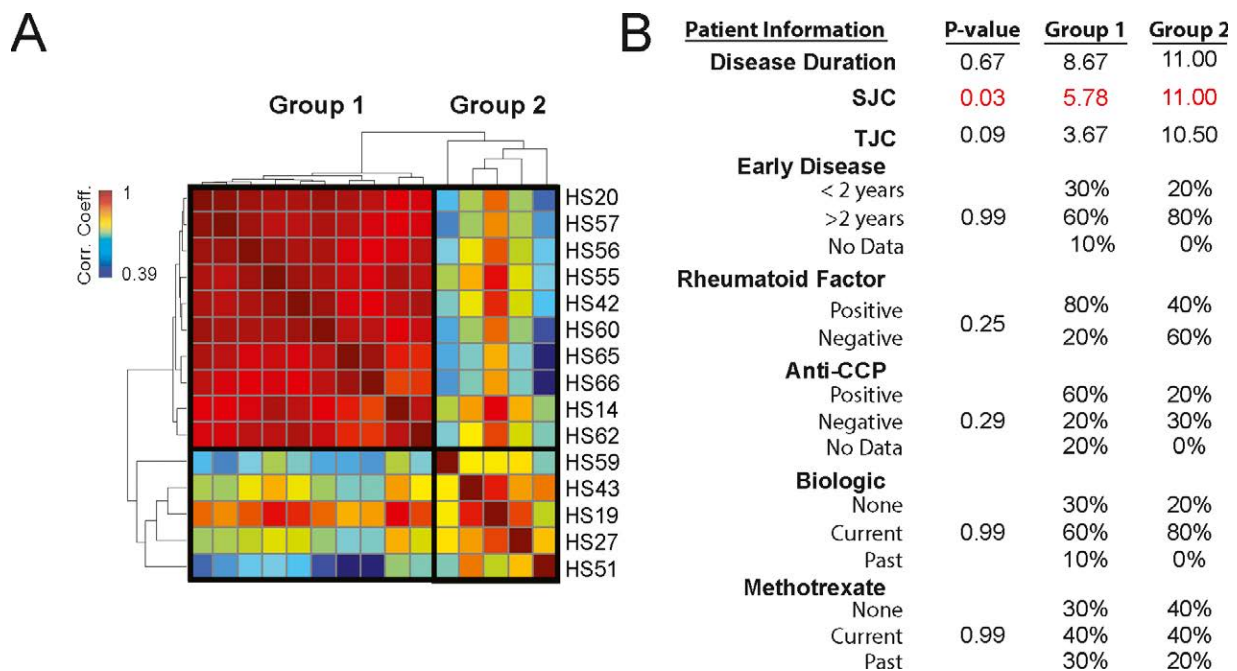


Figure 4. Analysis of global gene expression profiles in sorted macrophages from patients with rheumatoid arthritis. **A**, Pairwise Pearson's correlation of gene expression between individual patient samples. Samples are organized by hierarchical clustering based on their Pearson's correlation coefficients (corr. coeff.) across samples, forming 2 groups. HS20 = human sample 20. **B**, Table of association analysis of group 1 and group 2 (as defined in **A**) with clinical parameters. Values reflect either the group average (for continuous variables) or percent of patients (for categorical variables). *P* values for disease duration, swollen joint count (SJC), and tender joint count (TJC) were determined by Student's *t*-test, and *P* values for early disease, rheumatoid factor, anti-cyclic citrullinated peptide (anti-CCP) antibody, and treatment status were determined by Fisher's exact test. Significant values are shown in red.

described above, resulting in an average of 77,414 macrophages per sample (Table 1).

Isolated macrophages from 15 RA biopsy samples and 9 OA tissue samples were collected and passed sequencing quality control for further analysis. The percent alignment of reads (average 54%) was lower than in whole tissue (average 82%) likely due to the increased noise of low input. There was a minimal difference in the number of genes detected in RA versus OA macrophages (Figure 3C). RA macrophages demonstrated comparable complexity (Table 1) and gene coverage (Figure 3D) to OA samples even though the number of RA macrophages was 45 times less than the number of sorted OA macrophages.

To determine whether RNA-seq data from macrophages provided additional information that could not be gleaned from the whole tissue data, we investigated the “macrophage-specific” gene expression profiles. A comparison of fold change in gene expression between RA and OA revealed differentially expressed genes that were detected only by whole tissue or only by macrophage-specific RNA-seq (Figure 3E). For example, genes associated with inflammatory arthritis, such as PI3 (62) and MMP3 (63), were preferentially expressed in RA and OA macrophages, respectively, while no change in expression was observed in whole tissue RNA-seq. Further comparison revealed that 6,414 genes were expressed in both data sets, while 2,952 genes were exclusively found in whole tissue, and 2,116 genes were macrophage specific (Figure 3F). Genes exclusively expressed by whole tissue were likely associated with other cell types, while macrophage-specific genes were likely below the limit of detection of whole tissue RNA-seq. Of the 411 RA-specific and 330 OA-specific genes from whole tissue (Figure 2D), 315 and 152, respectively, were expressed in the macrophage-specific data set (Figure 3G). However, many of these 467 genes were not differentially expressed in the same direction in the macrophage-specific data set (Figure 3H).

Next, we compared the global gene expression profiles from synovial macrophages across patients. We identified 2 distinct groups of RA patients based on gene expression profiles (Figure 4A). Group 1 consisted of two-thirds of the patients (10 of 15) with highly similar gene expression profiles, while group 2 contained the remaining 5 patients with divergent gene expression. Patients in group 2 exhibited significantly higher SJC than those in group 1 ($P = 0.03$). These findings demonstrate the possibility for cell type-specific transcriptional profiles of RA patients to provide information about disease severity.

Modules of co-regulated genes may represent pathways that perform specific functions in disease. To identify gene modules within the macrophage

transcriptional profiles, we defined a subset of 553 genes as differentially expressed across 15 RA patients after accounting for noise and outliers (see Patients and Methods). These genes were clustered into 6 modules (modules 1–6) based on the similarity in their patterns of expression across patients (Figure 5A). We calculated the enrichment or depletion of each gene module within the expression profile of each patient to determine which patients were driving these modules (Figure 5B).

Despite the limited statistical power of a sample set of 15 patients, we were able to identify associations between the expression of these gene modules in patients and clinical parameters (Figures 5C and D). For example, expression levels of module 2 genes, including CCR1 and TREM2 (Figure 5E), were significantly increased (1.31 fold or 0.39 \log_2 fold change; $P = 0.05$) (Figure 5D) in patients who had stopped taking methotrexate. In addition, expression levels of genes in module 3 were negatively correlated with disease severity as measured by SJC ($P = 0.007$) and had 1.7-fold higher expression in patients recently diagnosed as having RA (\log_2 fold change = 0.78; $P = 0.04$) (Figure 5D). Module 3 genes, such as NFKB1A and TIMP1, are involved in the cellular response to IL-1 as determined by GO enrichment (data are available upon request from the corresponding author). Module 4 genes were 1.7-fold more highly expressed in patients who were not taking a biologic medication at the time of biopsy (\log_2 fold change = 0.78; $P = 0.01$). Module 4 was enriched with immune response genes such as TNF and MAFB (Figure 5E). Expression of module 5 genes, such as MIF and HMGB2, was positively associated with disease severity as measured by TJC ($P = 0.03$) (Figure 5C). Genes in module 6, such as CD83 and CXCR4, were 2.0-fold higher in patients who were negative for RF (\log_2 fold change = 1.0; $P = 0.03$). Taken together, our data demonstrate for the first time that transcriptional profiling of isolated synovial macrophages obtained using ultrasound-guided synovial biopsies may be used to characterize patients in a biologically relevant manner.

DISCUSSION

Recent advances in ultrasound technology have opened up a new opportunity for rheumatologists to perform minimally invasive ultrasound-guided synovial tissue biopsies (25). While arthroplasty allows for the collection of large pieces of synovial tissue, using it as a method of obtaining tissue from RA patients for research purposes in the US and in a longitudinal manner is challenging (23,29,41,45,64–67). Moreover, the tissue obtained from arthroplasty is usually late stage and may not reflect ongoing active disease, unlike tissue which may be obtained

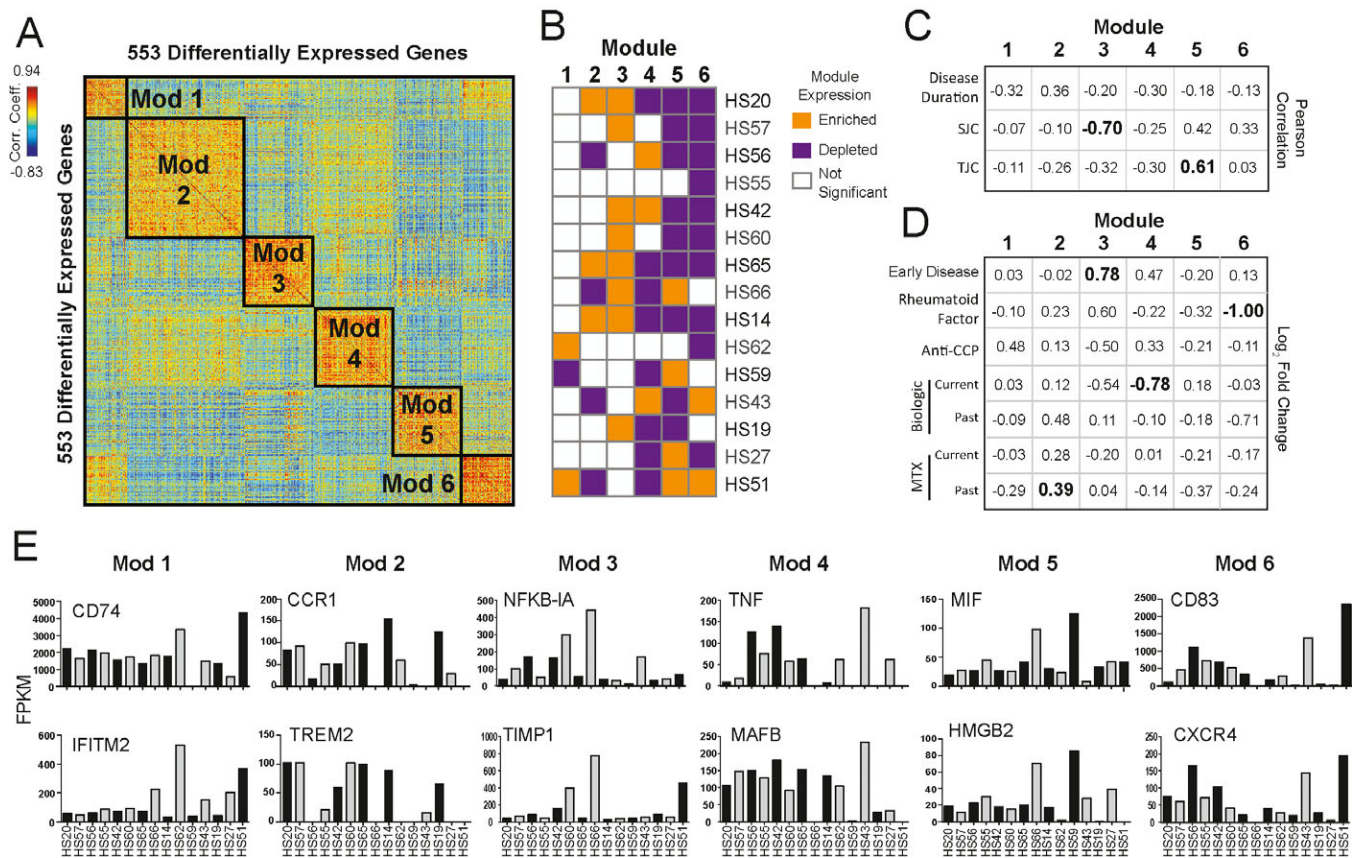


Figure 5. A, Pairwise Pearson’s correlations between 553 differentially expressed genes across sorted macrophages from rheumatoid arthritis (RA) patients. Genes were clustered using K-means clustering, and 6 modules (mod) of co-regulated genes were identified. B, Expression of genes in each module in each patient. The Kolmogorov-Smirnov test was used to determine if genes were enriched or depleted ($P < 0.05$). C, Table of association displaying Pearson’s correlations between the median expression of gene modules in patients and the given clinical parameters (continuous variables). Correlation coefficients (corr. coeff.) with a P value less than 0.05 are shown in boldface. D, Table of association displaying the average fold change (\log_2 fold change) between the median expression of gene modules in patients who were positive versus those who were negative for the indicated clinical parameters (categorical variables). Current treatment compares patients who were receiving the medication at the time of biopsy with those who were not receiving the medication at the time of biopsy. Past treatment compares patients who had stopped the medication with those who had never received the medication. Significant comparisons ($P < 0.05$, by t -test) are shown in boldface. E, Expression levels (fragments per kilobase per million [FPKM]) of individual genes selected across the 6 modules in patients with RA. HS20 = human sample 20; SJC = swollen joint count; TJC = tender joint count; anti-CCP = anti-cyclic citrullinated peptide; MTX = methotrexate.

using ultrasound-guided synovial biopsy. The fact that ultrasound-guided synovial biopsies may be performed in the clinic without a surgical suite and require minimal to no recovery time for the patient outweighs the smaller amount of tissue retrieved (23,29,41,45,64–67). In fact, in several countries in Europe, this technique is used to obtain synovial tissue for research purposes in a large number of patients without significant complications (34–36,38–40,68–73). The procedure itself is well accepted by both patients and referring rheumatologists in the US, at rates similar to those observed by our European colleagues (34,36).

Previous studies have focused on access to the joint, intrajoint synovial variation, and reproducibility of measurements using the ultrasound-guided synovial biopsy technique (34–36). Furthermore, these biopsies do

not appear to affect subsequent clinical or ultrasound disease activity assessments, which is important for patients who might subsequently enroll in clinical trials (74). European groups have also performed numerous studies to validate the needle biopsy and portal and forceps procedures and tissue sampling (34–36,38–40,68,75,76). Our data demonstrate that the ultrasound-guided synovial tissue biopsy specimens obtained from patients with RA are sufficient for RNA-seq, distinguish differences between patients with RA and those with OA, and, importantly, set the framework for the stratification of patients with RA according to the most prominent disease pathway. We also report an optimized digestion protocol for synovial tissue obtained by ultrasound-guided biopsies and demonstrate the ability to sort viable hematopoietic cells

by FACS. Further, we show that only small numbers of cells (as few as 10 cells) are sufficient for generation of libraries for quality RNA-seq analysis. With our initial cohort of 41 patients, we have been able to link the cell type-specific transcriptional signatures with patients' treatment regimen and clinical information.

Currently, the standard of care for RA is to prescribe biologic therapy through a costly and time-consuming trial-and-error process. Therefore, the utility of a biomarker to identify how a patient will respond to a particular therapy cannot be overstated. While peripheral blood is attractive for identifying a potential biomarker due to its ease of attainability, this approach has not been fruitful. Early studies by Dr. Paul Tak and colleagues demonstrated the potential of obtaining synovial tissue as a means to determine a biomarker for responsiveness to therapy (31). In his seminal studies, he showed that a reduction in the number of synovial sublining macrophages correlates with a decrease in disease activity (i.e., the Disease Activity Score in 28 joints) (31). The abundance of synovial sublining macrophages is currently a leading candidate for a viable biomarker of therapeutic response in RA (25).

We posit that transcriptional signatures in macrophages regardless of location (sublining versus synovial lining) will predict responsiveness to specific non-biologic and/or biologic therapies. Our data suggest the existence of associations between the transcriptional signature of macrophages and treatment course (or patient compliance). However, the present study is limited in its ability to predict response to therapy because of the constraint of obtaining tissue at a single time point for each patient at different stages of disease. Future studies beyond the scope of the present one will entail collection of synovial biopsy specimens from a larger cohort longitudinally, prior to and following therapy. Therefore, this study serves as proof of the principle that transcriptional analysis of synovial macrophages using ultrasound-guided synovial biopsies may function to uncover novel pathways underlying disease pathogenesis or response to therapy. Currently, studies are also underway in the Accelerating Medicines Partnership which will take advantage of synovial biopsies for identification of molecular pathways (77).

In summary, this study is the first in the US to harness the potential of ultrasound-guided synovial biopsies as a method of obtaining synovial tissue from patients with RA. Based on the recent success of REASON using minimally invasive ultrasound-guided synovial biopsies, coupled with our ability to interrogate synovial tissue at multiple levels using cutting-edge technologies, we believe that future studies have the potential to provide critical information to rheumatologists in establishing precision medicine as a reality for our patients.

ACKNOWLEDGMENTS

In loving memory of Colleen Pope Vitu. We thank the patients who underwent synovial biopsy for this study and acknowledge technical assistance at each site. We thank Stephanie Ledbetter, MS, Laticia Woodruff, RN, and Keith Wanzeck, BS at University of Alabama at Birmingham. We also thank Drs. Terrance Peabody, Ali Shilatifard, Hussain Bhikapurwala, and Danette Ko for their assistance. Flow cytometry cell sorting was performed in the Northwestern University Lurie Cancer Center Flow Cytometry Core Facility (supported by National Cancer Institute [NCI] P30-CA060553) and on a BD FACSAria SORP system (purchased through the support of National Institutes of Health 1S10OD011996-01). Histology services were provided by the Northwestern University Mouse Histology and Phenotyping Laboratory (supported by NCI P30-CA060553 awarded to the Robert H. Lurie Comprehensive Cancer Center). RNA sequencing was performed in the Northwestern University Division of Rheumatology and Pulmonary and Critical Care sequencing facility.

AUTHOR CONTRIBUTIONS

All authors were involved in drafting the article or revising it critically for important intellectual content, and all authors approved the final version to be published. Dr. Perlman had full access to all of the data in the study and takes responsibility for the integrity of the data and the accuracy of the data analysis.

Study conception and design. Mandelin, Homan, Shaffer, Cuda, Dominguez, Bacalao, Carns, Hinchcliff, Lee, Aren, Thakrar, Montgomery, Bridges, Bathon, Atkinson, Fox, Matteson, Buckley, Pitzalis, Parks, Hughes, Geraldino-Pardilla, Ike, Phillips, Wright, Filer, Kelly, Ruderman, Morgan, Abdala-Valencia, Misharin, Budinger, Bartom, Pope, Perlman, Winter.

Acquisition of data. Mandelin, Homan, Shaffer, Cuda, Dominguez, Bacalao, Carns, Hinchcliff, Lee, Aren, Thakrar, Montgomery, Bridges, Bathon, Atkinson, Fox, Matteson, Buckley, Pitzalis, Parks, Hughes, Geraldino-Pardilla, Ike, Phillips, Wright, Filer, Kelly, Ruderman, Morgan, Abdala-Valencia, Misharin, Budinger, Bartom, Pope, Perlman, Winter.

Analysis and interpretation of data. Mandelin, Homan, Shaffer, Cuda, Dominguez, Bacalao, Carns, Hinchcliff, Lee, Aren, Thakrar, Montgomery, Bridges, Bathon, Atkinson, Fox, Matteson, Buckley, Pitzalis, Parks, Hughes, Geraldino-Pardilla, Ike, Phillips, Wright, Filer, Kelly, Ruderman, Morgan, Abdala-Valencia, Misharin, Budinger, Bartom, Pope, Perlman, Winter.

REFERENCES

- O'Dell JR, Curtis JR, Mikuls TR, Cofield SS, Bridges SL Jr, Ranganath VK, et al. Validation of the methotrexate-first strategy in patients with early, poor-prognosis rheumatoid arthritis: results from a two-year randomized, double-blind trial. *Arthritis Rheum* 2013;65:1985–94.
- Saevarsdottir S, Wallin H, Seddighzadeh M, Ernestam S, Geborek P, Petersson IF, et al. Predictors of response to methotrexate in early DMARD naive rheumatoid arthritis: results from the initial open-label phase of the SWEFOT trial. *Ann Rheum Dis* 2011;70:469–75.
- Bathon JM, Martin RW, Fleischmann RM, Tesser JR, Schiff MH, Keystone EC, et al. A comparison of etanercept and methotrexate in patients with early rheumatoid arthritis. *N Engl J Med* 2000;343:1586–93.
- Breedveld FC, Weisman MH, Kavanaugh AF, Cohen SB, Pavelka K, van Vollenhoven R, et al. The PREMIER study: a multicenter, randomized, double-blind clinical trial of combination therapy with adalimumab plus methotrexate versus methotrexate

- alone or adalimumab alone in patients with early, aggressive rheumatoid arthritis who had not had previous methotrexate treatment. *Arthritis Rheum* 2006;54:26–37.
5. Emery P, Breedveld FC, Hall S, Durez P, Chang DJ, Robertson D, et al. Comparison of methotrexate monotherapy with a combination of methotrexate and etanercept in active, early, moderate to severe rheumatoid arthritis (COMET): a randomised, double-blind, parallel treatment trial. *Lancet* 2008;372:375–82.
 6. Moreland LW, O'Dell JR, Paulus HE, Curtis JR, Bathon JM, St.Clair EW, et al. A randomized comparative effectiveness study of oral triple therapy versus etanercept plus methotrexate in early aggressive rheumatoid arthritis: the treatment of Early Aggressive Rheumatoid Arthritis trial. *Arthritis Rheum* 2012;64:2824–35.
 7. Greenberg JD, Reed G, Decktor D, Harrold L, Furst D, Gibofsky A, et al. A comparative effectiveness study of adalimumab, etanercept and infliximab in biologically naive and switched rheumatoid arthritis patients: results from the US CORRONA registry. *Ann Rheum Dis* 2012;71:1134–42.
 8. Hetland ML, Christensen IJ, Tarp U, Dreyer L, Hansen A, Hansen IT, et al. Direct comparison of treatment responses, remission rates, and drug adherence in patients with rheumatoid arthritis treated with adalimumab, etanercept, or infliximab: results from eight years of surveillance of clinical practice in the nationwide Danish DANBIO registry. *Arthritis Rheum* 2010;62:22–32.
 9. Jobanputra P, Maggs F, Deeming A, Carruthers D, Rankin E, Jordan AC, et al. A randomised efficacy and discontinuation study of etanercept versus adalimumab (RED SEA) for rheumatoid arthritis: a pragmatic, unblinded, non-inferiority study of first TNF inhibitor use: outcomes over 2 years. *BMJ Open* 2012;2.
 10. Markenson JA, Gibofsky A, Palmer WR, Keystone EC, Schiff MH, Feng J, et al. Persistence with anti-tumor necrosis factor therapies in patients with rheumatoid arthritis: observations from the RADIUS registry. *J Rheumatol* 2011;38:1273–81.
 11. Rendas-Baum R, Wallenstein GV, Koncz T, Kosinski M, Yang M, Bradley J, et al. Evaluating the efficacy of sequential biologic therapies for rheumatoid arthritis patients with an inadequate response to tumor necrosis factor- α inhibitors. *Arthritis Res Ther* 2011;13:R25.
 12. Helmick CG, Felson DT, Lawrence RC, Gabriel S, Hirsch R, Kwoh CK, et al. Estimates of the prevalence of arthritis and other rheumatic conditions in the United States. Part I. *Arthritis Rheum* 2008;58:15–25.
 13. Myasoedova E, Crowson CS, Kremers HM, Therneau TM, Gabriel SE. Is the incidence of rheumatoid arthritis rising? Results from Olmsted County, Minnesota, 1955–2007. *Arthritis Rheum* 2010;62:1576–82.
 14. Chamberlain ND, Kim SJ, Vila OM, Volin MV, Volkov S, Pope RM, et al. Ligation of TLR7 by rheumatoid arthritis synovial fluid single strand RNA induces transcription of TNF α in monocytes. *Ann Rheum Dis* 2013;72:418–26.
 15. Huang Q, Pope RM. Toll-like receptor signaling: a potential link among rheumatoid arthritis, systemic lupus, and atherosclerosis. *J Leukoc Biol* 2010;88:253–62.
 16. Duffau P, Menn-Josephy H, Cuda CM, Dominguez S, Aprahamian TR, Watkins AA, et al. Promotion of inflammatory arthritis by interferon regulatory factor 5 in a mouse model. *Arthritis Rheumatol* 2015;67:3146–57.
 17. Huang QQ, Koessler RE, Birkett R, Perlman H, Xing L, Pope RM. TLR2 deletion promotes arthritis through reduction of IL-10. *J Leukoc Biol* 2013;93:751–9.
 18. Palmer G, Chobaz V, Talabot-Ayer D, Taylor S, So A, Gabay C, et al. Assessment of the efficacy of different statins in murine collagen-induced arthritis. *Arthritis Rheum* 2004;50:4051–9.
 19. Nuki G, Bresnihan B, Bear MB, McCabe D. Long-term safety and maintenance of clinical improvement following treatment with anakinra (recombinant human interleukin-1 receptor antagonist) in patients with rheumatoid arthritis: extension phase of a randomized, double-blind, placebo-controlled trial. *Arthritis Rheum* 2002;46:2838–46.
 20. Genovese MC, Bathon JM, Martin RW, Fleischmann RM, Tesser JR, Schiff MH, et al. Etanercept versus methotrexate in patients with early rheumatoid arthritis: two-year radiographic and clinical outcomes. *Arthritis Rheum* 2002;46:1443–50.
 21. De Rycke L, Baeten D, Foell D, Kruithof E, Veys EM, Roth J, et al. Differential expression and response to anti-TNF α treatment of infiltrating versus resident tissue macrophage subsets in autoimmune arthritis. *J Pathol* 2005;206:17–27.
 22. Barland P, Novikoff AB, Hamerman D. Electron microscopy of the human synovial membrane. *J Cell Biol* 1962;14:207–20.
 23. Filkova M, Cope A, Mant T, Galloway J. Is there a role of synovial biopsy in drug development? *BMC Musculoskelet Disord* 2016;17:172.
 24. Sieberts SK, Zhu F, Garcia-Garcia J, Stahl E, Pratap A, Pandey G, et al. Crowdsourced assessment of common genetic contribution to predicting anti-TNF treatment response in rheumatoid arthritis. *Nat Commun* 2016;7:12460.
 25. Udalova IA, Mantovani A, Feldmann M. Macrophage heterogeneity in the context of rheumatoid arthritis. *Nat Rev Rheumatol* 2016;12:472–85.
 26. De Hair MJ, van de Sande MG, Ramwadhoebe TH, Hansson M, Landewé R, van der Leij C, et al. Features of the synovium of individuals at risk of developing rheumatoid arthritis: implications for understanding preclinical rheumatoid arthritis. *Arthritis Rheumatol* 2014;66:513–22.
 27. Gerlag D, Tak PP. Synovial biopsy. *Best Pract Res Clin Rheumatol* 2005;19:387–400.
 28. Gerlag DM, Tak PP. How useful are synovial biopsies for the diagnosis of rheumatic diseases? *Nat Clin Pract Rheumatol* 2007;3:248–9.
 29. Gerlag DM, Tak PP. How to perform and analyse synovial biopsies. *Best Pract Res Clin Rheumatol* 2013;27:195–207.
 30. Haringman JJ, Vinkenoog M, Gerlag DM, Smeets TJ, Zwinderman AH, Tak PP. Reliability of computerized image analysis for the evaluation of serial synovial biopsies in randomized controlled trials in rheumatoid arthritis. *Arthritis Res Ther* 2005;7:R862–7.
 31. Jahangier ZN, Jacobs JW, Kraan MC, Wenting MJ, Smeets TJ, Bijlsma JW, et al. Pretreatment macrophage infiltration of the synovium predicts the clinical effect of both radiation synovectomy and intra-articular glucocorticoids. *Ann Rheum Dis* 2006;65:1286–92.
 32. Kraan MC, Reece RJ, Smeets TJ, Veale DJ, Emery P, Tak PP. Comparison of synovial tissues from the knee joints and the small joints of rheumatoid arthritis patients: implications for pathogenesis and evaluation of treatment. *Arthritis Rheum* 2002;46:2034–8.
 33. Koski JM, Hammer HB. Ultrasound-guided procedures: techniques and usefulness in controlling inflammation and disease progression. *Rheumatology (Oxford)* 2012;51 Suppl 7:vii31–5.
 34. Humby F, Kelly S, Bugatti S, Manzo A, Filer A, Mahto A, et al. Evaluation of minimally invasive, ultrasound-guided synovial biopsy techniques by the OMERACT filter: determining validation requirements. *J Rheumatol* 2016;43:208–13.
 35. Humby F, Kelly S, Hands R, Rocher V, DiCicco M, Ng N, et al. Use of ultrasound-guided small joint biopsy to evaluate the histopathologic response to rheumatoid arthritis therapy: recommendations for application to clinical trials. *Arthritis Rheumatol* 2015;67:2601–10.
 36. Kelly S, Humby F, Filer A, Ng N, Di Cicco M, Hands RE, et al. Ultrasound-guided synovial biopsy: a safe, well-tolerated and reliable technique for obtaining high-quality synovial tissue from both large and small joints in early arthritis patients. *Ann Rheum Dis* 2015;74:611–7.
 37. Koski JM, Helle M. Ultrasound guided synovial biopsy using portal and forceps. *Ann Rheum Dis* 2005;64:926–9.
 38. Lazarou I, D'Agostino MA, Naredo E, Humby F, Filer A, Kelly SG. Ultrasound-guided synovial biopsy: a systematic review according to the OMERACT filter and recommendations for

- minimal reporting standards in clinical studies. *Rheumatology (Oxford)* 2015;54:1867–75.
39. Ramírez J, Celis R, Usategui A, Ruiz-Esqueda V, Faré R, Cuervo A, et al. Immunopathologic characterization of ultrasound-defined synovitis in rheumatoid arthritis patients in clinical remission. *Arthritis Res Ther* 2015;18:74.
 40. Scirè CA, Epis O, Codullo V, Humby F, Morbini P, Manzo A, et al. Immunohistological assessment of the synovial tissue in small joints in rheumatoid arthritis: validation of a minimally invasive ultrasound-guided synovial biopsy procedure. *Arthritis Res Ther* 2007;9:R101.
 41. Sitt JC, Griffith JF, Wong P. Ultrasound-guided synovial biopsy. *Br J Radiol* 2016;89:20150363.
 42. Van Vugt RM, van Dalen A, Bijlsma JW. Ultrasound guided synovial biopsy of the wrist. *Scand J Rheumatol* 1997;26:212–4.
 43. Filer A, de Pablo P, Allen G, Nightingale P, Jordan A, Jobanputra P, et al. Utility of ultrasound joint counts in the prediction of rheumatoid arthritis in patients with very early synovitis. *Ann Rheum Dis* 2011;70:500c7.
 44. Filkova M, Aradi B, Senolt L, Ospelt C, Vettori S, Mann H, et al. Association of circulating miR-223 and miR-16 with disease activity in patients with early rheumatoid arthritis. *Ann Rheum Dis* 2014;73:1898–904.
 45. Pitzalis C, Kelly S, Humby F. New learnings on the pathophysiology of RA from synovial biopsies. *Curr Opin Rheumatol* 2013;25:334–44.
 46. Yeo L, Toellner KM, Salmon M, Filer A, Buckley CD, Raza K, et al. Cytokine mRNA profiling identifies B cells as a major source of RANKL in rheumatoid arthritis. *Ann Rheum Dis* 2011;70:2022–8.
 47. Arnett FC, Edworthy SM, Bloch DA, McShane DJ, Fries JF, Cooper NS, et al. The American Rheumatism Association 1987 revised criteria for the classification of rheumatoid arthritis. *Arthritis Rheum* 1988;31:315–24.
 48. Aletaha D, Neogi T, Silman AJ, Funovits J, Felson DT, Bingham CO III, et al. 2010 rheumatoid arthritis classification criteria: an American College of Rheumatology/European League Against Rheumatism collaborative initiative. *Arthritis Rheum* 2010;62:2569–81.
 49. Singh JA, Saag KG, Bridges SL Jr, Akl EA, Bannuru RR, Sullivan MC, et al. 2015 American College of Rheumatology guideline for the treatment of rheumatoid arthritis. *Arthritis Rheumatol* 2016;68:1–26.
 50. Singh JA, Saag KG, Bridges SL Jr, Akl EA, Bannuru RR, Sullivan MC, et al. 2015 American College of Rheumatology guideline for the treatment of rheumatoid arthritis. *Arthritis Care Res (Hoboken)* 2016;68:1–25.
 51. Wakefield RJ, Balint PV, Szkudlarek M, Filippucci E, Backhaus M, D'Agostino MA, et al. Musculoskeletal ultrasound including definitions for ultrasonographic pathology. *J Rheumatol* 2005;32:2485–7.
 52. Kim D, Perteau G, Trapnell C, Pimentel H, Kelley R, Salzberg SL. TopHat2: accurate alignment of transcriptomes in the presence of insertions, deletions and gene fusions. *Genome Biol* 2013;14:R36.
 53. Wang L, Wang S, Li W. RSeQC: quality control of RNA-seq experiments. *Bioinformatics* 2012;28:2184–5.
 54. Anders S, Pyl PT, Huber W. HTSeq: a Python framework to work with high-throughput sequencing data. *Bioinformatics* 2015;31:166–9.
 55. Robinson MD, McCarthy DJ, Smyth GK. edgeR: a Bioconductor package for differential expression analysis of digital gene expression data. *Bioinformatics* 2010;26:139–40.
 56. McCarthy DJ, Chen Y, Smyth GK. Differential expression analysis of multifactor RNA-Seq experiments with respect to biological variation. *Nucleic Acids Res* 2012;40:4288–97.
 57. Eden E, Navon R, Steinfeld I, Lipson D, Yakhini Z. GOrilla: a tool for discovery and visualization of enriched GO terms in ranked gene lists. *BMC Bioinformatics* 2009;10:48.
 58. Ruan MZ, Erez A, Guse K, Dawson B, Bertin T, Chen Y, et al. Proteoglycan 4 expression protects against the development of osteoarthritis. *Sci Transl Med* 2013;5:176ra34.
 59. Zhang X, Yuan Z, Cui S. Identifying candidate genes involved in osteoarthritis through bioinformatics analysis. *Clin Exp Rheumatol* 2016;34:282–90.
 60. Nagase H, Kashiwagi M. Aggrecanases and cartilage matrix degradation. *Arthritis Res Ther* 2003;5:94–103.
 61. Ochi K, Derfoul A, Tuan RS. A predominantly articular cartilage-associated gene, SCRG1, is induced by glucocorticoid and stimulates chondrogenesis in vitro. *Osteoarthritis Cartilage* 2006;14:30–8.
 62. Li J, Hsu HC, Mountz JD. Managing macrophages in rheumatoid arthritis by reform or removal. *Curr Rheumatol Rep* 2012;14:445–54.
 63. Han Z, Boyle DL, Manning AM, Firestein GS. AP-1 and NF- κ B regulation in rheumatoid arthritis and murine collagen-induced arthritis. *Autoimmunity* 1998;28:197–208.
 64. Humby FC, Al Balushi F, Lliso G, Cauli A, Pitzalis C. Can synovial pathobiology integrate with current clinical and imaging prediction models to achieve personalized health care in rheumatoid arthritis? *Front Med (Lausanne)* 2017;4:41.
 65. Orr C, Vieira-Sousa E, Boyle DL, Buch MH, Buckley CD, Canete JD, et al. Synovial tissue research: a state-of-the-art review. *Nat Rev Rheumatol* 2017;13:630.
 66. Van de Sande MG, Gerlag DM, Lodde BM, van Baarsen LG, Alivernini S, Codullo V, et al. Evaluating antirheumatic treatments using synovial biopsy: a recommendation for standardisation to be used in clinical trials. *Ann Rheum Dis* 2011;70:423–7.
 67. Wechalekar MD, Smith MD. Utility of arthroscopic guided synovial biopsy in understanding synovial tissue pathology in health and disease states. *World J Orthop* 2014;5:566–73.
 68. Najm A, Orr C, Heymann MF, Bart G, Veale DJ, Le Goff B. Success rate and utility of ultrasound-guided synovial biopsies in clinical practice. *J Rheumatol* 2016;43:2113–9.
 69. Sitt JC, Griffith JF, Lai FM, Hui M, Chiu KH, Lee RK, et al. Ultrasound-guided synovial Tru-cut biopsy: indications, technique, and outcome in 111 cases. *Eur Radiol* 2017;27:2002–2010.
 70. De Groof A, Ducreux J, Humby F, Nzeusseu Toukap A, Badot V, Pitzalis C, et al. Higher expression of TNF α -induced genes in the synovium of patients with early rheumatoid arthritis correlates with disease activity, and predicts absence of response to first line therapy. *Arthritis Res Ther* 2016;18:19.
 71. Kelly S, Bombardieri M, Humby F, Ng N, Marrelli A, Riahi S, et al. Angiogenic gene expression and vascular density are reflected in ultrasonographic features of synovitis in early rheumatoid arthritis: an observational study. *Arthritis Res Ther* 2015;17:58.
 72. Frank-Bertoncelj M, Trenkmann M, Klein K, Karouzakis E, Rehrauer H, Bratus A, et al. Epigenetically-driven anatomical diversity of synovial fibroblasts guides joint-specific fibroblast functions. *Nat Commun* 2017;8:14852.
 73. Luukkonen J, Pascual LM, Patlaka C, Lang P, Turunen S, Halleen J, et al. Increased amount of phosphorylated proinflammatory osteopontin in rheumatoid arthritis synovia is associated to decreased tartrate-resistant acid phosphatase 5B/5A ratio. *PLoS One* 2017;12:e0182904.
 74. Lazarou I, Kelly S, Humby F, Di Cicco M, Zou L, Rocher-Ros V, et al. Ultrasound-guided synovial biopsy of the wrist does not alter subsequent clinical or ultrasound disease activity assessments: a prospective study for incorporation of imaging in clinical trials. *Clin Exp Rheumatol* 2016;34:802–7.
 75. Choi IY, Karpus ON, Turner JD, Hardie D, Marshall JL, de Hair MJ, et al. Stromal cell markers are differentially expressed in the synovial tissue of patients with early arthritis. *PLoS One* 2017;12:e0182751.
 76. Filer A, Ward LS, Kemble S, Davies CS, Munir H, Rogers R, et al. Identification of a transitional fibroblast function in very early rheumatoid arthritis. *Ann Rheum Dis* 2017;76:2105–12.
 77. Accelerating Medicines Partnership (AMP). URL: <https://www.nih.gov/research-training/accelerating-medicines-partnership-amp>.

Augmented Th17 Differentiation Leads to Cutaneous and Synovio-Enthesal Inflammation in a Novel Model of Psoriatic Arthritis

Lu Yang, Melania H. Fanok, Aranzazu Mediero-Munoz, Laura K. Fogli, Carmen Corciulo, Shahla Abdollahi, Bruce N. Cronstein, Jose U. Scher, and Sergei B. Koralov

Objective. To introduce a novel preclinical animal model of psoriatic arthritis (PsA) in R26Stat3C^{stopfl/fl} CD4Cre mice, and to investigate the role of Th17 cytokines in the disease pathogenesis.

Methods. We characterized a novel murine model of Th17-driven cutaneous and synovio-enthesal disease directed by T cell-specific expression of a hyperactive Stat3 allele. By crossing R26Stat3C^{stopfl/fl} CD4Cre mice onto an interleukin-22 (IL-22)–knockout background or treating the mice with a neutralizing antibody against IL-17, we interrogated how these Th17 cytokines could contribute to the pathogenesis of PsA.

Results. R26Stat3C^{stopfl/fl} CD4Cre mice developed acanthosis, hyperkeratosis, and parakeratosis of the skin, as well as enthesitis/tendinitis and periarticular bone erosion in different joints, accompanied by osteopenia. T cell-specific expression of a hyperactive Stat3C allele was found to drive the augmented Th17 response in these animals. Careful characterization of the mouse bone marrow revealed an increase in osteoclast progenitor (OCP) and RANKL-producing cells, which contributed to the osteopenia phenotype observed in the mutant animals. Abrogation of the Th17 cytokines IL-17 or IL-22 improved both the skin and bone phenotype in R26Stat3C^{stopfl/fl} CD4Cre mice, revealing a central role of Th17 cells in the regulation of OCP and RANKL expression on stromal cells.

Conclusion. Perturbation of the IL-23/Th17 axis instigates Th17-mediated inflammation in R26Stat3C^{stopfl/fl} CD4Cre mice, leading to cutaneous and synovio-enthesal inflammation and bone pathologic features highly reminiscent of human PsA. Both IL-17A and IL-22 produced by Th17 cells appear to play critical roles in promoting the cutaneous and musculoskeletal inflammation that characterizes PsA.

Ms Yang's work was supported by the A*STAR National Science Scholarship of Singapore. Dr. Fanok's work was supported by the NIH (NIAMS grant F31-AR-070094 and Training grant T32-AI-100853-3). Dr. Mediero-Munoz's work was supported by Instituto de Salud Carlos III and Fondo Europeo de Desarrollo Regional (Miguel Servet program). Dr. Fogli's work was supported by the NIH (grant F31-CA-171596-02). Support was also provided through grants to Dr. Cronstein from the Arthritis Foundation, the NIH (grants R01-AR-056672 and R01-AR-068593), and the New York University Health and Hospitals Corporation Clinical and Translational Science Institute (grants UL1-TR-000038-05 and UL1-TR-000038-05S1) and grants to Dr. Scher from the NIH (National Institute of Arthritis and Musculoskeletal and Skin Diseases [NIAMS] grants R03-AR-072182 and K23-AR-064318), the Riley Family Foundation, and the Beatrice Snyder Foundation. Dr. Koralov's laboratory was supported by the Judith and Stewart Colton Center for Autoimmunity, the NIH (grant R01-HL-125816), the New York University Department of Medicine (Pilot grant), and the Drs. Martin and Dorothy Spatz Foundation.

Lu Yang, Melania H. Fanok, PhD, Aranzazu Mediero-Munoz, PhD (current address: Universidad Autónoma de Madrid, Madrid, Spain), Laura K. Fogli, PhD, Carmen Corciulo, PhD, Shahla Abdollahi, PhD, Bruce N. Cronstein, MD, Jose U. Scher, MD, Sergei B. Koralov, PhD: New York University School of Medicine, New York, New York.

Ms Yang and Drs. Fanok, Mediero-Munoz, and Fogli contributed equally to this work.

Address correspondence to Sergei B. Koralov, PhD, 550 First Avenue, MSB 531, New York, NY 10016. E-mail: sergei.koralov@med.nyu.edu.

Submitted for publication June 1, 2017; accepted in revised form February 6, 2018.

Psoriatic arthritis (PsA) is a chronic inflammatory disease characterized by the presence of psoriasis and concomitant spondyloarthritis, affecting 2.5 million people in the United States (1). In a majority of PsA patients, characteristic skin lesions precede the onset of articular inflammation (1,2). The clinical presentation is heterogeneous in nature, affecting both the peripheral and axial joints. Other frequent manifestations include enthesitis and dactylitis (2–4). The clinical course of PsA is variable, but it is estimated that ~50% of patients will develop erosive arthritis within 1 year of presentation, if left untreated (2,4). In addition, osteoporosis is prevalent in PsA patients, contributing to

a higher risk of incidental fractures in this population (5,6).

Insight into the etiology and pathogenesis of psoriasis and PsA has significantly advanced over time. Consequently, multiple signaling pathways and cell populations have been implicated in the disease pathogenesis (7). Since their initial characterization as a discrete subset of CD4⁺ T helper lymphocytes, Th17 cells have been shown to play a critical role in many autoimmune and chronic inflammatory diseases, including psoriasis and PsA (8–10). Th17 differentiation is driven by cytokines such as transforming growth factor β (TGF β), interleukin-6 (IL-6), and IL-23, resulting in the phosphorylation of Smad and STAT-3 and subsequent retinoic acid receptor-related orphan nuclear receptor γ t (ROR γ t) transcription (11). Th17 cells are enriched in the skin lesions of patients with psoriasis, where they promote an inflammatory response through their signature cytokines (i.e., IL-17 and IL-22). IL-17 induces chemokine production by epithelial cells, attracting neutrophils to the sites of inflammation, while IL-22 stimulates hyperproliferation of keratinocytes in diseased skin and hyperproliferation of synovial fibroblasts in the joints (10,12).

In patients with PsA, Th17 cells are not only enriched in cutaneous lesions, but also notably increased in the synovium (13). Consistent with these findings, genome-wide association studies have frequently linked single-nucleotide polymorphisms in genes critical to Th17 differentiation (IL23A, IL23R, and STAT3) and those that play a role in Th17 effector cell function (IL17RD, IL22, and IL21) to the pathogenesis of psoriasis and PsA (14). These observations have established the importance of the IL-23/Th17 axis in PsA (15).

In addition, biologic therapies targeting IL-23 signaling, Th17 cell differentiation, and the functional cytokines of this lineage have been successful in ameliorating the symptoms of psoriatic arthritis, providing a great alternative to treatments targeting the tumor necrosis factor (TNF) signaling pathway. In particular, monoclonal antibodies against the p40 subunit of IL-12/IL-23 (ustekinumab) or the p19 subunit of IL-23 (guselkumab), IL-17A-neutralizing antibodies (secukinumab, ixekizumab), and IL-17 receptor-blocking antibodies (brodalumab) have all been approved by the US Food and Drug Administration (FDA) and have shown great promise in the alleviation of symptoms of psoriasis and PsA (16,17), further highlighting the contribution of the IL-23/Th17 axis to disease pathogenesis (18).

In this report, we describe a novel animal model of PsA driven by an augmented Th17 response downstream of T cell-specific expression of a hyperactive Stat3C allele (19). R26Stat3C^{stopfl/fl} CD4Cre mice

develop a cutaneous and synovio-enthesal bone disease highly reminiscent of PsA. Importantly, STAT3 is one of the genes associated with PsA susceptibility, and augmentation of IL-23 signaling has been implicated in the pathogenesis of PsA (20). We carefully characterized the disease phenotype in this animal model and utilized R26Stat3C^{stopfl/fl} CD4Cre mice to gain novel insights into the contribution of Th17 cells to the etiology of PsA, with the aim of establishing R26Stat3C^{stopfl/fl} CD4Cre mice as an excellent preclinical model of PsA.

MATERIALS AND METHODS

Mice. All experimental mice were housed under specific pathogen-free conditions in the NYU Langone Medical Center Skirball animal facility or The Jackson Laboratory. All experimental procedures and protocols were approved by the Institutional Animal Care and Use Committee. More details on the generation of these mice and specific study techniques used are available in Supplementary Methods (on the *Arthritis & Rheumatology* web site at <http://onlinelibrary.wiley.com/doi/10.1002/art.40447/abstract>).

Quantification of the psoriasis phenotype in the mouse model. Weekly phenotype scoring, conducted by investigators who were blinded with regard to genotype, was performed. The skin phenotype was assessed in each mouse by assigning a skin phenotype score of 0–3, where a score of 0 indicates the skin appearance of a wild-type C57BL/6 mouse, score of 1 indicates thinning body hair, dry tail, or dry ears, score of 2 indicates hair loss on either the back or the head or dry skin, and score of 3 indicates >50% hair loss or very dry or crusty skin.

Anti-IL-17A antibody treatment. The neutralizing anti-IL-17A antibody was injected intraperitoneally into pregnant female mice and continued until the offspring had reached 10 days of age. The treatment was then performed on the offspring directly until they reached ~8 weeks of age; the mice were then euthanized for experimental analysis. A dose of 100 μ g anti-IL-17A antibody (17F3; BioCell) was given to pups between 10 days old and 21 days old, while pregnant female mice and pups older than age 21 days were given 200 μ g anti-IL-17A antibody per injection. The mice were treated twice per week. Control animals either received isotype control (MOPC-21; BioCell) or were left untreated.

Statistical analysis. Statistical analyses were performed using unpaired, nonparametric Mann-Whitney U tests or the Sign test (when comparing normalized values). More than 3 independent experiments were performed in each analysis, unless stated otherwise. Data are presented as the mean \pm SEM. *P* values less than or equal to 0.05 were considered significant.

RESULTS

Development of spontaneous psoriasisiform skin lesions in R26Stat3C^{stopfl/fl} CD4Cre mice. To examine whether STAT3 hyperactivity in T cells is sufficient to drive Th17-associated disease (e.g., psoriasis), we utilized

a mouse model in which the conditional allele of the hyperactive Stat3 gene, Stat3C, was expressed selectively in T lymphocytes (21). These mice began to display a diseased skin phenotype at ~5 weeks of age, with thinning body hair and dry skin observed on their ears and tails. As the mice aged, they developed focal hair loss with dry and flaky skin, mirroring the phenotype of cutaneous psoriatic

lesions (Figures 1A and B). Disease severity varied from mild dry skin to nearly complete loss of hair on some animals (Supplementary Figure 1, available on the *Arthritis & Rheumatology* web site at <http://onlinelibrary.wiley.com/doi/10.1002/art.40447/abstract>). Histopathologic analysis of the affected skin revealed acanthosis or thickened epidermis, hyperkeratosis, regions of parakeratosis or

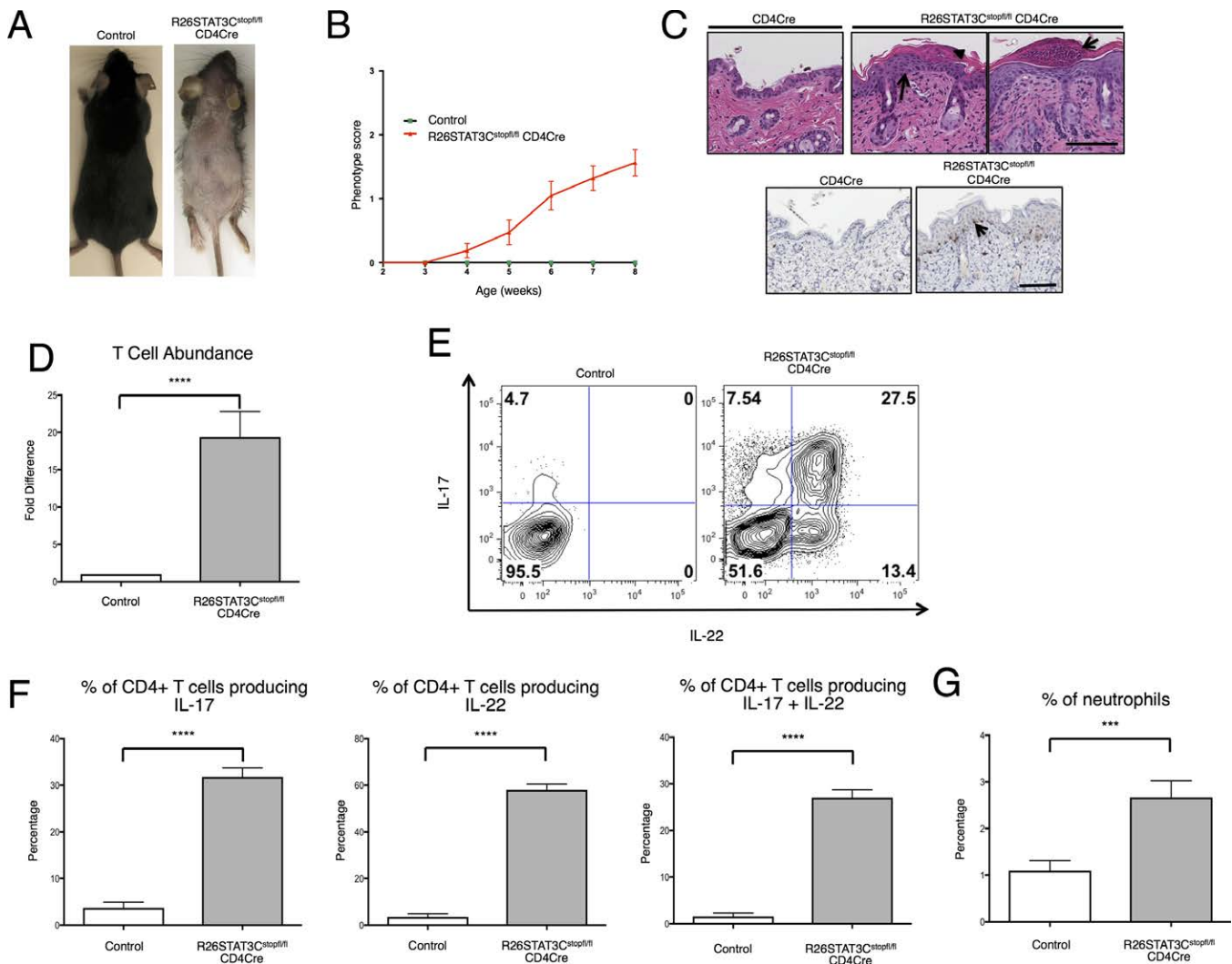


Figure 1. Development of a psoriatic-like skin phenotype in R26Stat3C^{stopfl/fl} CD4Cre mice. **A**, Representative images of an 8-week-old R26Stat3C^{stopfl/fl} CD4Cre mouse (skin phenotype score of 3) and littermate R26Stat3C^{stopfl/fl} control mouse. **B**, Skin phenotype scores in R26Stat3C^{stopfl/fl} CD4Cre mice (n = 61) and control mice (n = 20) at ages 2–8 weeks, with a score scale ranging from 0 (no phenotype) to 3 (>50% fur loss and/or visibly dry and crusty skin) (see Materials and Methods for a detailed description of the scoring system). Results are the mean ± SEM. **C**, Representative histologic skin sections from 8-week-old control and R26Stat3C^{stopfl/fl} CD4Cre mice. Top, Hematoxylin and eosin staining, revealing acanthosis (arrow in middle panel), parakeratosis in an area of hyperkeratosis (arrowhead in middle panel), and an area reminiscent of Munro's abscess (arrow in right panel). Bottom, Anti-CD3 staining, showing T cells tracking the epidermal–dermal boundary (arrow). Bars = 100 μm. **D**, Fold difference in the number of CD3+CD4+ T cells isolated from the skin of R26Stat3C^{stopfl/fl} CD4Cre mice relative to control mice. **E**, Representative results from intracellular flow cytometry analysis of CD3+CD4+ T cells isolated from the skin of 6–10-week-old R26Stat3C^{stopfl/fl} CD4Cre mice and control mice. **F**, Percentage of CD3+CD4+ skin T cells expressing interleukin-17 (IL-17), IL-22, or both. **G**, Percentage of neutrophils in the skin. In **D–G**, results are the mean ± SEM of ≥17 mice (ages 6–10 weeks) per genotype; data are representative of 15 independent experiments. *** = $P \leq 0.001$; **** = $P \leq 0.0001$, by Sign test in **D** and by Mann-Whitney U test in **F** and **G**.

retained nuclei in keratinocytes of the stratum corneum, and evidence of an increase in the number of CD3+ T cells tracking the epidermal–dermal border (Figure 1C). Flow cytometry analysis of the immune infiltrate showed an ~20-fold increase in the percentage of CD3+CD4+ T lymphocytes in the skin of R26Stat3C^{stopfl/fl} CD4Cre mice compared to control mice (Figure 1D), thus reaffirming the histologic observations.

To assess the subtype of CD4+ T cells and to evaluate their effector function, intracellular cytokine staining was performed. These experiments revealed a significantly higher percentage of IL-17, IL-22, and IL-17/IL-22 double-producing T helper cells among skin-infiltrating lymphocytes in R26Stat3C^{stopfl/fl} CD4Cre mice compared to controls (Figures 1E and F). Enrichment of Th17 cells in the skin was consistent with previous findings in patients with psoriasis (2). In addition, levels of both Th1 and Th2 cytokines were reduced in the skin of R26Stat3C^{stopfl/fl} CD4Cre mice as compared to controls (Supplementary Figures 2A and B, <http://onlinelibrary.wiley.com/doi/10.1002/art.40447/abstract>).

Finally, cell clusters with an appearance similar to that of Munro's micro-abscesses, a pathologic hallmark of inflammatory psoriasis, were observed in the skin of R26Stat3C^{stopfl/fl} CD4Cre mice (Figure 1C). Munro's micro-abscesses are characterized by a large infiltration of neutrophils. A significant increase in neutrophil abundance was indeed evident in the enzymatically digested skin of R26Stat3C^{stopfl/fl} CD4Cre mice, as revealed by flow cytometry (Figure 1G).

Evidence of tendon inflammation, joint erosion, and osteopenia in conjunction with psoriasiform skin lesions in R26Stat3C^{stopfl/fl} CD4Cre mice. Up to 30% of patients with psoriasis develop arthritis within 7 years of disease incidence (2). Although some genetic and clinical risk factors have been established, the underlying etiology of this progression remains to be elucidated. Even though gross inspection of R26Stat3C^{stopfl/fl} CD4Cre mice did not reveal obvious joint swelling, we aimed to examine the joints of these animals thoroughly, since there are similarities between the skin phenotype observed and the clinical hallmarks of psoriatic lesions. It has been proposed that articular inflammation in PsA begins in the tendons and entheses, with enthesitis being a unique feature of PsA and related spondyloarthritis (22,23).

To investigate whether R26Stat3C^{stopfl/fl} CD4Cre mice develop enthesitis or tendinitis, we collected RNA from the Achilles tendons of R26Stat3C^{stopfl/fl} CD4Cre mice and their littermate controls. Quantitative polymerase chain reaction was performed to examine the expression of messenger RNA (mRNA) for several inflammatory genes.

Compared to the controls, R26Stat3C^{stopfl/fl} CD4Cre mice exhibited a significant increase in the expression of mRNA for the pan-hematopoietic marker CD45 and the T helper cell marker CD4 (Figure 2A). This was demonstrated as an infiltration of immune cells, such as CD4+ T cells, to the tendons of R26Stat3C^{stopfl/fl} CD4Cre mice.

These findings were confirmed by flow cytometry analysis, in which it was shown that cells isolated from the tendon tissue of R26Stat3C^{stopfl/fl} CD4Cre mice contained a higher percentage of CD45+ cells than that of their littermate controls (Supplementary Figure 3A, <http://onlinelibrary.wiley.com/doi/10.1002/art.40447/abstract>). Furthermore, an up-regulation in the expression of IL23R and ROR γ t mRNA was observed in R26Stat3C^{stopfl/fl} CD4Cre mice (Supplementary Figure 3B, <http://onlinelibrary.wiley.com/doi/10.1002/art.40447/abstract>), consistent with prior observations of IL23R/ROR γ t double-positive cells at the entheses in a mouse model with features of spondyloarthritis (24) as well as in a study comparing normal and injured human entheses (25). Other inflammatory cytokines, including IL-17 and interferon- γ (IFN γ), were highly expressed in the Achilles tendons of R26Stat3C^{stopfl/fl} CD4Cre mice when compared to controls (Supplementary Figure 3B). These data suggest that a low-grade inflammation was present in the synovio-enthesal compartments of these animals.

To further inspect and characterize the ankle joints of R26Stat3C^{stopfl/fl} CD4Cre mice, we performed histopathologic analysis. Staining of the ankle joints with hematoxylin and eosin and Giemsa revealed infiltration and accumulation of cells in the Achilles tendons of R26Stat3C^{stopfl/fl} CD4Cre mice, but not in control animals (Figure 2B and Supplementary Figure 3C [<http://onlinelibrary.wiley.com/doi/10.1002/art.40447/abstract>]). We also observed clusters of cells accumulating at the enthesal tissue in some R26Stat3C^{stopfl/fl} CD4Cre mice (Supplementary Figure 3C).

We then performed immunofluorescence analysis using an anti-CD3 antibody, which revealed infiltration of T cells to the tendons in the ankle joints of R26Stat3C^{stopfl/fl} CD4Cre mice (Figure 2C). In addition to enthesitis, we observed synovitis in the footpad regions of R26Stat3C^{stopfl/fl} CD4Cre mice (Supplementary Figure 4, <http://onlinelibrary.wiley.com/doi/10.1002/art.40447/abstract>). The data from immunofluorescence analysis again validated our findings of infiltration of CD3+ T lymphocytes to these sites of inflammation (Supplementary Figure 4). In addition to the ankle joint, we observed tertiary lymphoid organ–like structures in the infrapatellar fat pad beneath the patella tendon of R26Stat3C^{stopfl/fl} CD4Cre mice (Supplementary Figure 5, <http://onlinelibrary.wiley.com/doi/10.1002/art.40447/abstract>). R26Stat3C^{stopfl/fl}

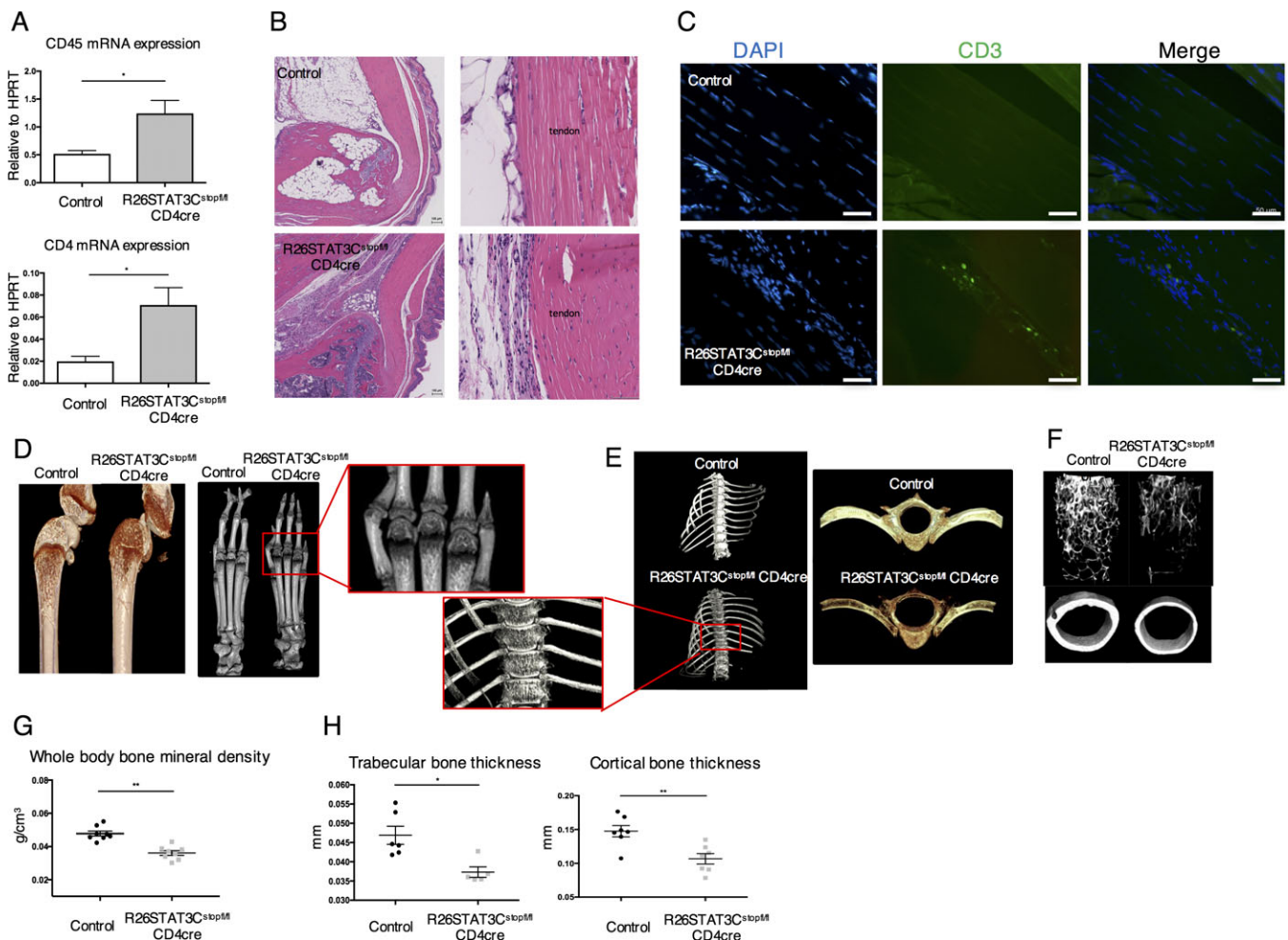


Figure 2. Presentation of tendinitis/enthesitis, periarticular bone erosion, and the osteopenia phenotype in R26Stat3^{stopfl/fl} CD4Cre mice. **A**, Quantitative polymerase chain reaction analysis of CD45 and CD4 mRNA expression in the Achilles tendon and enthesal tissue of R26Stat3C^{stopfl/fl} CD4Cre mice and their littermate controls (R26Stat3C^{stopfl/+} or R26Stat3C^{stopfl/fl} mice). Results are the mean \pm SEM of ≥ 3 independent experiments, with values normalized to the expression of hypoxanthine guanine phosphoribosyltransferase (HPRT). **B**, Representative hematoxylin and eosin staining of ankle joint sections from control mice and R26Stat3C^{stopfl/fl} CD4Cre mice. Bars = 100 μ m. **C**, Representative examples of immunofluorescence staining of the Achilles tendon from control and R26Stat3C^{stopfl/fl} CD4Cre mice. Bars = 50 μ m. **D–F**, Representative microfocal computed tomography (micro-CT) images of the knees (left) and paws (right) (**D**), vertebra (**E**), and femurs (**F**) of R26Stat3C^{stopfl/fl} CD4Cre mice and their littermate controls. **G**, Whole-body bone mineral density measurements in control and R26Stat3C^{stopfl/fl} CD4Cre mice, as measured by dual x-ray absorptiometry. **H**, Micro-CT analysis of the trabecular and cortical thickness of the femurs of control and R26Stat3C^{stopfl/fl} CD4Cre mice. Analyses were performed on 6–10-week-old mice. Symbols in **G** and **H** represent individual animals; horizontal lines with bars show the mean \pm SEM. * = $P \leq 0.05$; ** = $P \leq 0.01$, by nonparametric 2-tailed Mann-Whitney U test.

CD4Cre mice spontaneously developed tendinitis, enthesitis, and synovitis, whereas these features were absent in control animals.

To investigate whether infiltration of the joints with inflammatory cells in R26Stat3C^{stopfl/fl} CD4Cre mice was accompanied by cartilage and bone erosion or remodeling, we performed microfocal computed tomography (micro-CT) to look at periarticular bone density in these animals. Reduction in bone density was clearly seen in the knees of R26Stat3C^{stopfl/fl} CD4Cre mice, whereas we did

not observe consistent changes in the cartilage. Specifically, we observed a loss of subchondral bone in the femur and tibia (Figure 2D). Bone erosion was also observed at the metacarpophalangeal and interphalangeal joints of R26Stat3C^{stopfl/fl} CD4Cre mice (Figure 2D). In addition to peripheral arthritis, R26Stat3C^{stopfl/fl} CD4Cre mice also displayed deformity along the spine. These mice often presented a hunched posture reminiscent of kyphosis, and data from micro-CT analysis showed erosive destruction to their vertebral bodies (Figure 2E). This

suggested that inflammation occurs both in the peripheral joints and in the axial joints of R26Stat3^{stopfl/fl} CD4Cre mice.

In addition to the articular defects observed, the R26Stat3^{stopfl/fl} CD4Cre mice presented a severe osteopenia phenotype. Skeletal bones of the R26Stat3^{stopfl/fl} CD4Cre mice were notably small and more fragile than those from littermate controls. These observations were further substantiated by the bone mineral density measurements obtained with a dual x-ray absorptiometry scanner

(Figure 2G and Supplementary Figure 6A [http://onlinelibrary.wiley.com/doi/10.1002/art.40447/abstract]). Micro-CT analysis of the femurs of R26Stat3^{stopfl/fl} CD4Cre mice also showed a reduction in both trabecular and cortical bone thickness in these animals (Figures 2F and H). Overall, we found that R26Stat3^{stopfl/fl} CD4Cre mice exhibited many key features of PsA—a psoriatic skin phenotype, arthritis in multiple joints, and osteopenia—thus making these mice an excellent model for this inflammatory disease.

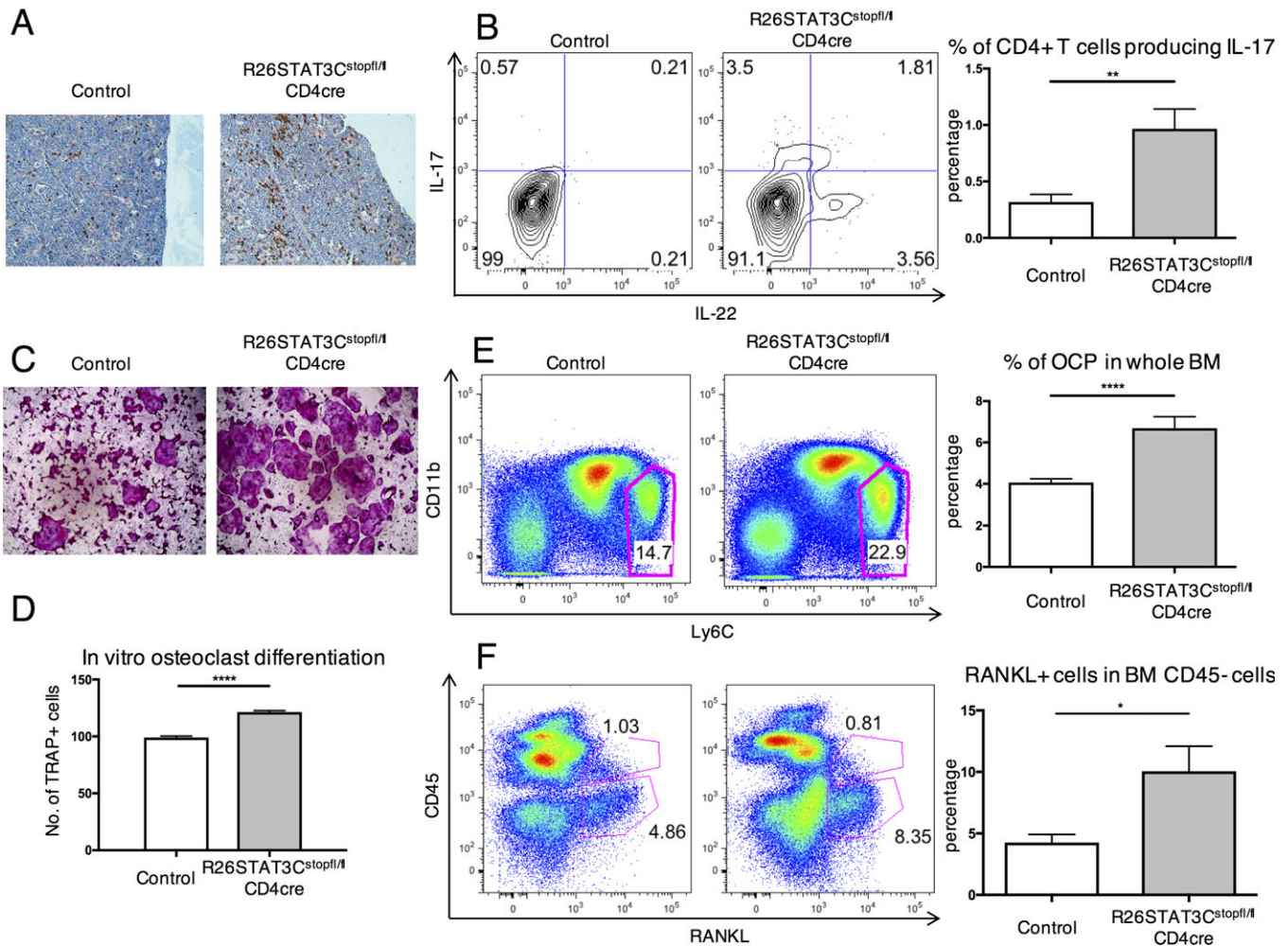


Figure 3. Correlation of the Th17-driven osteopenia phenotype in R26Stat3^{stopfl/fl} CD4Cre mice with an increase in the number of osteoclast progenitor (OCP) cells and RANKL⁺ cells in the local environment. **A**, Representative immunohistochemical staining for CD3 in the femurs of control and R26Stat3^{stopfl/fl} CD4Cre mice. Original magnification $\times 120$. **B**, Representative intracellular staining for interleukin-17 (IL-17) and IL-22 in CD3⁺CD4⁺ T cells in the bones of control and R26Stat3^{stopfl/fl} CD4Cre mice (left), and quantified percentage of IL-17 producers in CD3⁺CD4⁺ T cells (right). **C**, Representative images of tartrate-resistant acid phosphatase (TRAP)-stained osteoclasts following in vitro osteoclast differentiation of bone marrow (BM) cells from R26Stat3^{stopfl/fl} CD4Cre mice and their littermate controls. Original magnification $\times 120$. **D**, Number of TRAP⁺ cells on day 10 of an in vitro osteoclast differentiation protocol, with values normalized to the number of TRAP⁺ cells derived from control bone marrow. **E** and **F**, Flow cytometry analysis of the OCP cell population (**E**) and RANKL-producing cells (**F**) in the bone marrow of R26Stat3^{stopfl/fl} CD4Cre mice and their littermate controls. All analyses were performed on 6–10-week-old mice. Results are the mean \pm SEM of ≥ 3 independent experiments for all assays. * = $P \leq 0.05$; ** = $P \leq 0.01$; **** = $P \leq 0.0001$, by nonparametric 2-tailed Mann-Whitney U test.

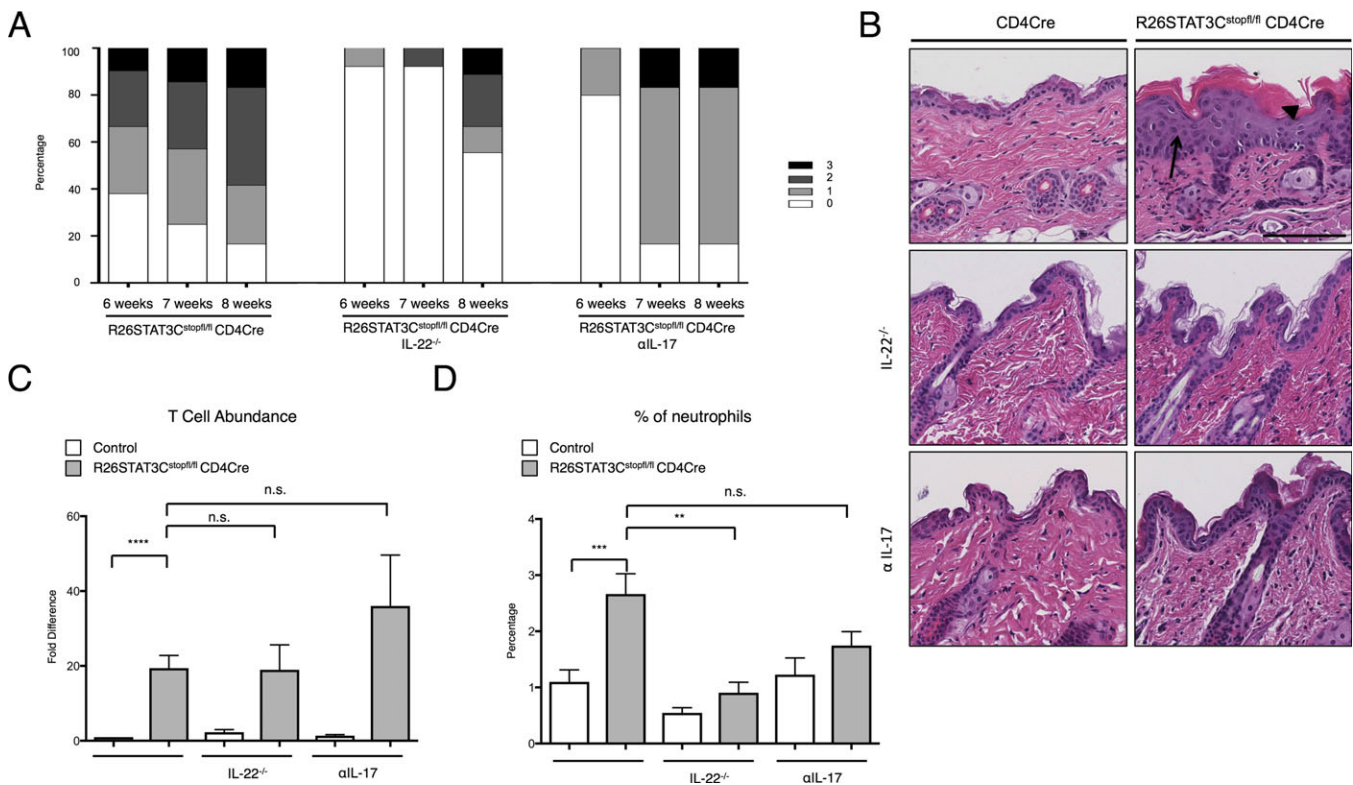


Figure 4. Amelioration of the psoriatic skin phenotype by genetic ablation of interleukin-22 (IL-22) and by anti-IL-17 antibody treatment in R26Stat3C^{stopfl/fl} CD4Cre mice. **A**, Skin phenotype score of R26Stat3C^{stopfl/fl} CD4Cre mice, R26Stat3C^{stopfl/fl} CD4Cre IL-22^{-/-} mice, and anti-IL-17-treated R26Stat3C^{stopfl/fl} CD4Cre mice at ages 6, 7, and 8 weeks. The score scale (shown on right) ranges from 0 (no phenotype) to 3 (>50% fur loss and/or visibly dry and crusty skin) (see Materials and Methods for a detailed description of the scoring system). Data represent 10–21 mice per group. **B**, Representative hematoxylin and eosin staining of skin sections from control and R26Stat3C^{stopfl/fl} CD4Cre mice at age 8 weeks. Top, Skin from untreated mice (arrow indicates acanthosis, arrowhead indicates hyperkeratosis). Middle, Skin from mice on an IL-22-knockout background. Bottom, Skin from anti-IL-17-treated mice. Bar = 100 μ m. **C**, Fold difference in the number of CD3+CD4+ T cells from the skin of R26Stat3C^{stopfl/fl} CD4Cre mice and control mice, normalized to the values in untreated controls within each experiment. **D**, Percentage of neutrophils from the skin of R26Stat3C^{stopfl/fl} CD4Cre and control mice. In **C** and **D**, results are the mean \pm SEM of ≥ 6 mice (ages 6–10 weeks) per genotype; data are representative of ≥ 3 independent experiments. ** = $P \leq 0.01$; *** = $P \leq 0.001$; **** = $P \leq 0.0001$, by Sign test in **C** and by non-parametric 2-tailed Mann-Whitney U test in **D**. NS = not significant.

Promotion of osteoclastogenesis by the augmented Th17 response in R26Stat3C^{stopfl/fl} CD4Cre mice via increased levels of osteoclast progenitor (OCP) cells and RANKL+ cells. T cell-specific hyperactivation of the STAT-3 signaling pathway in R26Stat3C^{stopfl/fl} CD4Cre mice was sufficient to promote inflammatory responses in the skin and synovio-entheses of these mice (as shown in Figures 1 and 2). Immunohistologic analysis also revealed an increase in the percentage of CD3+ T cells in the bones of R26Stat3C^{stopfl/fl} CD4Cre mice (Figure 3A). Flow cytometry analysis of leukocytes from the bone marrow of R26Stat3C^{stopfl/fl} CD4Cre mice similarly revealed an enrichment of IL-17- and/or IL-22-producing T cells in the bone marrow (Figure 3B).

Beyond their established role in the skin and musculoskeletal inflammation, Th17 cells have been

ascribed osteoclastogenic properties in PsA (26). Concurrent with the increase in the Th17 population, the percentages of other subsets of T helper cells, including Th1, Th2, and regulatory T cells, were reduced in the bone marrow of R26Stat3C^{stopfl/fl} CD4Cre mice (Supplementary Figures 7A–C, <http://onlinelibrary.wiley.com/doi/10.1002/art.40447/abstract>). These subsets of T cells were postulated to inhibit osteoclastogenesis through the effector molecules they secreted (27). We hypothesized that changes in the bone-resorbing osteoclast cell population might be a causal factor in the osteopenia phenotype observed in R26Stat3C^{stopfl/fl} CD4Cre mice.

To confirm this, we first performed a conventional 10-day in vitro osteoclast differentiation assay using the bone marrow of R26Stat3C^{stopfl/fl} CD4Cre mice and their

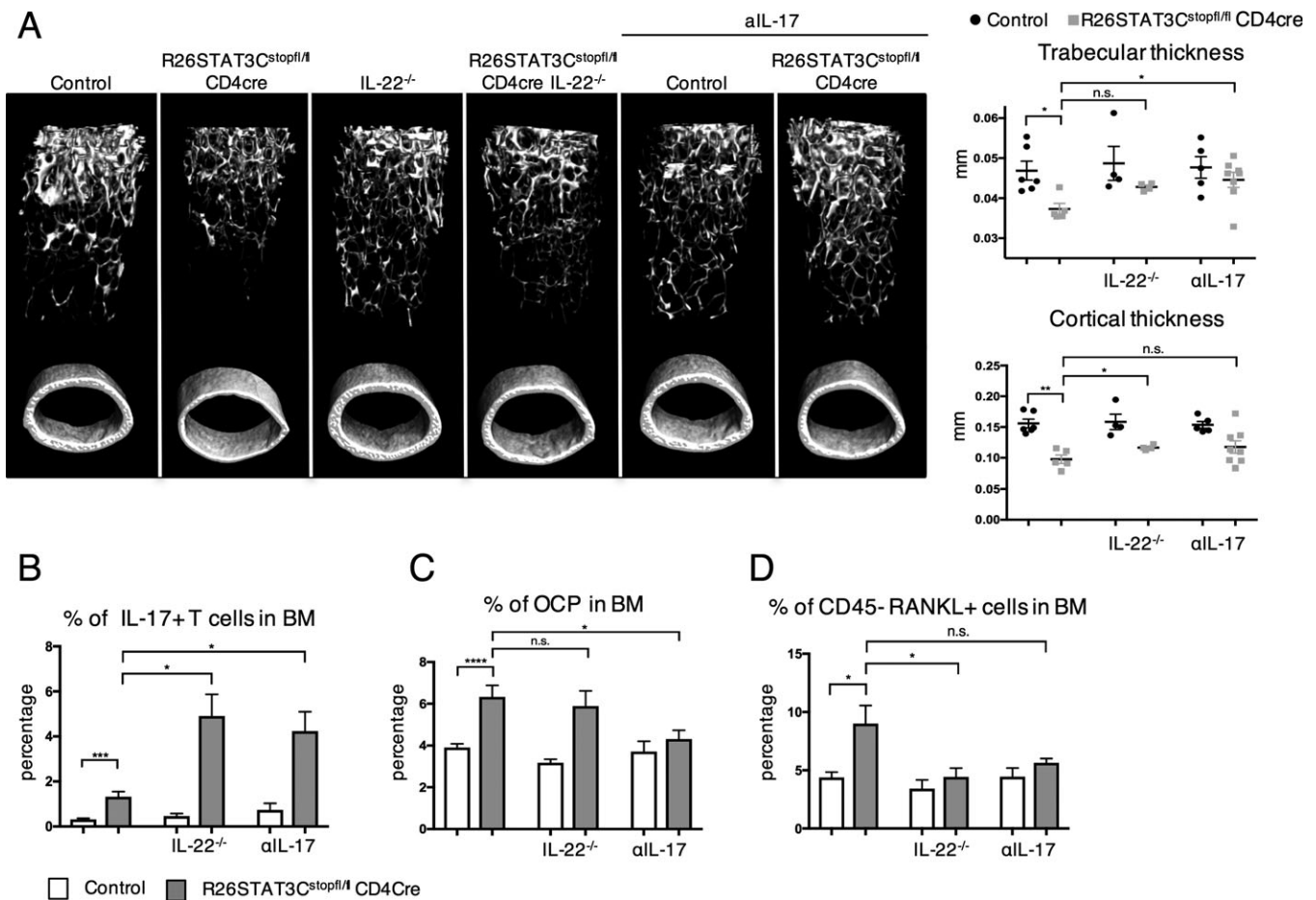


Figure 5. Partial amelioration of bone defects by interleukin-22 deficiency (IL-22^{-/-}) or anti-IL-17 antibody treatment in R26Stat3C^{stopfl/fl} CD4Cre mice. In all analyses, R26Stat3C^{stopfl/fl} CD4Cre mice and their littermate controls were assessed in comparison to R26Stat3C^{stopfl/fl} CD4Cre mice and control mice that were either crossed onto an IL-22^{-/-} background or treated with anti-IL-17. **A**, Representative results of microfocus computed tomography are shown in 3-dimensional images of the femurs (left), and trabecular and cortical thickness of the femurs was quantified (right). Symbols represent individual mice; horizontal lines with bars show the mean \pm SEM. **B**, The percentage of CD3+CD4+ cells producing IL-17 in the bone marrow (BM) was determined. **C** and **D**, The percentage of osteoclast progenitor (OCP) cells and RANKL producers in the bone marrow was determined. Results are the mean \pm SEM of ≥ 4 mice (ages 6–10 weeks) per group; data are representative of ≥ 3 independent experiments for all assays. * = $P \leq 0.05$; ** = $P \leq 0.01$; **** = $P \leq 0.0001$, by nonparametric 2-tailed Mann-Whitney U test. NS = not significant.

littermate controls. Consistently, bone marrow from the R26Stat3C^{stopfl/fl} CD4Cre mice differentiated into more osteoclasts than were observed in the bone marrow from control mice, as identified by tartrate-resistant acid phosphatase (TRAP) staining (Figures 3C and D). Moreover, a higher number of osteoclasts were observed in the bones of the R26Stat3C^{stopfl/fl} CD4Cre mice than in the bones of control animals, as revealed by immunostaining of femur sections for cathepsin K (Supplementary Figure 6B, <http://onlinelibrary.wiley.com/doi/10.1002/art.40447/abstract>).

In order to better quantify the number of osteoclasts in vivo, we performed flow cytometry analysis on mouse bone marrow. Although there are no reliable

markers of mature osteoclasts that can be utilized in fluorescence-activated cell sorting analysis, we were able to evaluate the frequency of OCP cells in the mouse bone marrow, a cell population that has previously been described as CD3⁻CD19⁻Ter119⁻(lineage-negative)CD11b^{low/-}Ly6C⁺ cells (28). The monocyte/macrophage markers used to identify this progenitor population reflect the putative myeloid lineage cell origin of osteoclasts. The bone marrow of R26Stat3C^{stopfl/fl} CD4Cre mice was found to contain a higher percentage of OCP cells, as determined by flow cytometry (Figure 3E).

To validate whether these cells were true OCPs, we sorted the OCP cells and other non-OCP cell populations

from wild-type mice and performed a 4-day in vitro osteoclast differentiation assay. In the presence of appropriate cytokines (i.e., macrophage colony-stimulating factor and RANKL), only sorted OCP cells differentiated into TRAP⁺ osteoclast cells (Supplementary Figure 8A, <http://onlinelibrary.wiley.com/doi/10.1002/art.40447/abstract>). Therefore, a higher number of OCP cells might explain the increased differentiation of osteoclasts in the 10-day in vitro assay of the bone marrow from R26Stat3^{stopfl/fl} CD4Cre mice (Figures 3C and D).

Th17 cells are known to induce osteoclastogenesis by directly expressing RANKL as well as by inducing surrounding mesenchymal cells to produce RANKL, which in turn promotes osteoclast differentiation (29). Analysis of surface RANKL expression on the T lymphocytes from the bone marrow of R26Stat3^{stopfl/fl} CD4Cre mice failed to detect an appreciable increase (Supplementary Figure 9, <http://onlinelibrary.wiley.com/doi/10.1002/art.40447/abstract>). However, a conspicuous increase in RANKL expression was evident in CD45⁺ cells (representing cells of nonhematopoietic origin) from the bone marrow of these animals (Figure 3F). These data suggest that augmented Th17 responses in R26Stat3^{stopfl/fl} CD4Cre mice may lead to an accumulation of OCPs and enhanced production of RANKL in the bones, contributing to the osteopenia phenotype observed in these animals.

Having found striking differences in osteoclasts, we also aimed to examine the differentiation of osteoblasts in the bone marrow of R26Stat3^{stopfl/fl} CD4Cre mice, since the homeostasis of bone remodeling is governed both by bone-resorbing osteoclasts and by bone-building osteoblasts. Bone marrow cells from R26Stat3^{stopfl/fl} CD4Cre mice failed to develop into proper osteoblasts in in vitro assays (Supplementary Figure 8B, <http://onlinelibrary.wiley.com/doi/10.1002/art.40447/abstract>). These data suggest that the osteopenia present in the R26Stat3^{stopfl/fl} CD4Cre mice was caused by a disturbance of the dynamic homeostasis in bone remodeling, with a concomitant loss of osteoblasts and augmented differentiation of osteoclasts.

Amelioration of the psoriasis phenotype with neutralizing antibodies against IL-17 and ablation of IL-22.

Given the large increase in the levels of IL-22 and IL-17 that we observed in the skin and bones of R26Stat3^{stopfl/fl} CD4Cre mice, we interrogated whether reduction or elimination of these cytokines would ameliorate the disease phenotype. We monitored the skin of the mice prior to euthanizing them, to determine whether treatment could alter the course of disease progression. Treatment of mice with an anti-IL-17 neutralizing antibody resulted in a delay of phenotype progression (Figure 4A), thereby

representing an important corollary to human disease in that several therapeutic agents targeting the IL-17 pathway have been approved by the FDA for the treatment of patients with psoriasis or PsA, resulting in notable clinical outcomes (30,31). The improvement in phenotype was additionally observed in histologic sections of the mouse skin, since treatment with anti-IL-17 restored epidermal thickness to control levels (Figure 4B).

Similarly, genetic ablation of IL22 also delayed the progression of psoriatic disease, arguably to a greater extent than that achieved with IL-17 blockade, as judged by the disease severity score and histologic evaluation (Figures 4A and B). Neither treatment with anti-IL-17 nor ablation of IL22 resulted in a reduction in the total number of CD4⁺ T cells in the skin. Nevertheless, genetic deletion of IL22 lowered the percentage of CD4⁺ T cells in the skin that produced IL-17, IL-22, or both cytokines (Figure 4C and Supplementary Figures 10A–C [<http://onlinelibrary.wiley.com/doi/10.1002/art.40447/abstract>]). IL22 ablation also reduced the number of neutrophils in the skin of R26Stat3^{stopfl/fl} CD4Cre mice, likely by reducing the percentage of cells producing IL-22 or IL-17, both of which act as potent recruitment factors (Figure 4D). In addition, R26Stat3^{stopfl/fl} CD4Cre mice with IL-22 knockout (IL-22^{-/-} mice) showed increased production of IFN γ in CD4⁺ T cells in the skin, as well as an increased percentage of Treg cells in the skin, whereas IL-4 production was not affected (Supplementary Figures 10D–F, <http://onlinelibrary.wiley.com/doi/10.1002/art.40447/abstract>).

Association between amelioration of the osteopenia phenotype and changes in the abundance of OCPs and RANKL⁺ cells in R26Stat3^{stopfl/fl} CD4Cre mice.

Abrogating the Th17 cytokines IL-22 and IL-17 by genetic ablation and through the use of a neutralizing antibody treatment, respectively, resulted in the amelioration of the osteopenia phenotype in R26Stat3^{stopfl/fl} CD4Cre mice. The R26Stat3^{stopfl/fl} CD4Cre IL-22^{-/-} mice showed an improved cortical and trabecular bone thickness, as visualized by micro-CT scan (Figure 5A). Similarly, R26Stat3^{stopfl/fl} CD4Cre mice treated with anti-IL-17 developed thicker trabecular bones in the femur, albeit the levels did not reach those observed in control animals (Figure 5A). Both IL-22 deficiency and anti-IL-17 treatment resulted in a higher percentage of T cells producing IL-17 in the bone marrow of R26Stat3^{stopfl/fl} CD4Cre mice (Figure 5B).

In addition, the percentages of Th1, Th2, and Treg cells in the bone marrow of R26Stat3^{stopfl/fl} CD4Cre IL-22^{-/-} mice and R26Stat3^{stopfl/fl} CD4Cre mice treated with anti-IL-17 were also increased (Supplementary Figures 11A–C, <http://onlinelibrary.wiley.com/doi/10.1002/art.40447/abstract>).

com/doi/10.1002/art.40447/abstract), which could potentially mitigate the osteoclastogenic effects of the elevated numbers of Th17 cells. R26Stat3C^{stopfl/fl} CD4Cre mice treated with anti-IL-17 showed a reduction in the percentage of OCP cells in the bones of these mice (Figure 5C). Conversely, the percentage of RANKL-producing cells in the bone marrow of R26Stat3C^{stopfl/fl} CD4Cre IL-22^{-/-} mice had decreased (Figure 5D). Thus, Th17 cells induced osteoclastogenesis, at least in part, through the promotion of an increase in the numbers of OCP cells and RANKL producers in the bones.

DISCUSSION

PsA is a debilitating disease with a molecular mechanism that has yet to be fully elucidated. In an effort to understand the etiology of this disease, several mouse models of PsA have been put forward in prior studies, but none have thoroughly recapitulated the complex and heterogeneous manifestations of disease symptoms. For example, keratinocyte-specific deletion of JunB and c-Jun genes, which are found in the psoriatic susceptibility locus PSORS6 (19p13), led to psoriatic-like skin lesions and arthritis in the extremities in a mechanism involving TNF and lymphocytes (32). However, the description of this mouse phenotype did not address the joint inflammation common to human patients with PsA, and there have not been any follow-up reports investigating articular inflammation in this model. In other models, such as in aging DBA/1 mice or mice instilled with mini-circle IL-23, the mice developed spondyloarthritis but were devoid of psoriasis (24,33). A further shortcoming of the DBA/1 mouse model was that, whereas PsA affects females and males equally in human patients, only aged male DBA/1 mice developed arthritis. In addition to genetic manipulation, application of the Toll-like receptor 7 agonist imiquimod could trigger psoriatic skin lesions in mice, and although this model was highly useful for studies of psoriasis pathogenesis, the treatment failed to induce arthritis (34).

Recently, it was shown that skin and joint inflammation could manifest following intraperitoneal injection of carbohydrate mannan from *Saccharomyces cerevisiae* (35). In that model, the contribution of conventional α/β T cells and B cells to the disease was entirely dispensable, whereas IL-17 from γ/δ T cells alone was sufficient to drive PsA-like phenotypes. The model highlighted the important role of γ/δ T cells in skin inflammation, but the phenotype was more akin to systemic shock-induced responses rather than a chronic inflammatory disease.

Herein we present R26Stat3C^{stopfl/fl} CD4Cre mice as a new model with several features of PsA, in which the mice spontaneously developed psoriatic skin lesions, accompanied by inflammatory infiltrates in multiple joints, with associated periarticular bone erosion and severe osteopenia. The R26Stat3C^{stopfl/fl} CD4Cre mice presented most of the phenotypes found in patients with PsA in a fully penetrant manner, without deliberate triggers, despite the mutant Stat3 expression being limited exclusively to the T cell lineage. Previously, Sano et al demonstrated that ectopic expression of Stat3C in keratinocytes is sufficient to drive psoriasis (36). Furthermore, expression of Stat3C in keratinocytes using K5-Stat3C, together with a global expression of F759 mutant gp130 allele, led to the development of both skin and joint inflammation, reminiscent of that in patients with PsA. Taken together, these results highlight the importance of STAT-3 signaling in the continuum of psoriasis pathogenesis.

In addition, R26Stat3C^{stopfl/fl} CD4Cre mice developed the PsA phenotype in response to perturbation in the IL-23/Th17 axis, whose role in the pathogenesis of PsA has been established (15,26). In the R26Stat3C^{stopfl/fl} CD4Cre mouse model, this signaling pathway was augmented by expression of a hyperactive Stat3 gene selectively in T lymphocytes. Stat3C dimerized in response to IL-6 receptor signaling, which is crucial for Th17 differentiation (37). Genome-wide association studies have demonstrated an association between STAT3 and susceptibility to PsA (20). Therefore, in R26Stat3C^{stopfl/fl} CD4Cre mice, several features of the phenotype, as well as the underlying disease mechanisms of PsA, were mimicked.

Of utmost importance to the field is the fact that enthesitis is present in one-third of patients with PsA, including inflammation of the Achilles tendons, plantar fascia, and lateral epicondyles (38). The presence of enthesitis is part of the classification criteria for PsA, but its clinical diagnosis remains very challenging (39,40). This leads to underappreciation of the early phases of the disease and a concomitant suboptimal treatment during the timeframe of active inflammation, whereas current therapies could potentially alter the natural history of this process. Indeed, several groups have stressed the role of the entheses as an initiating site of inflammation in a proportion of PsA patients who go on to develop synovitis and destructive arthritis (23,40–42). However, very little is known about the biology and molecular mechanisms by which proinflammatory resident cells can drive downstream systemic effects. Our finding that Stat3 hyperactivity in the T cells was sufficient to promote concomitant

inflammation in the skin and synovio-entheses of these mice adds insight into the disease pathogenesis and suggests that Th17 cells are central to this early manifestation of PsA.

PsA is a multiorgan chronic inflammatory disease that affects patients' skin, ligaments, joints, and bones. A severe and common comorbidity in patients with PsA is osteoporosis. Homeostasis in the bone is well maintained by distinct cell populations, including osteoclasts that resorb bone and osteoblasts that promote bone formation. Imbalance between these populations can reduce bone mineral density, leading to osteopenia. When we analyzed the bones of R26Stat3C^{stopfl/fl} CD4Cre mice, we observed an increase in the CD3–CD19–Ter119–CD11^{low}Ly6C^{high} cell population, a subset that has been demonstrated to represent OCP cells (28). Blood samples from patients with PsA that had started developing bone erosions exhibited an increased population of CD14+ OCP cells (43). Interestingly, CD14+ monocytes in humans were found to correspond to Ly6C+ myeloid cells in mice (44), and there was an increased proportion of OCPs in the bones of R26Stat3C^{stopfl/fl} CD4Cre mice with high expression of the Ly6C surface marker.

Our study of R26Stat3C^{stopfl/fl} CD4Cre mice allowed us to probe the cells directly from the bones and to further investigate the mechanism behind the changes locally. These OCP cells differentiated into bone-resorbing osteoclasts upon exposure to cytokines such as RANKL. Although it was proposed that Th17 cells could express RANKL, which directly activates differentiation of OCPs (27), we demonstrated that the increase in RANKL-producing cells in our mouse model was restricted to the CD45– cell population in the bones. This suggests that an indirect pathway plays a role in this process, where IL-17 from Th17 cells acts on mesenchymal cells, including osteoblasts and fibroblasts, which then up-regulate the expression of RANKL to drive osteoclast differentiation. Besides the promotion of osteoclastogenesis, defects in osteoblast differentiation, as observed in the bone marrow from R26Stat3C^{stopfl/fl} CD4Cre mice, suggested that Th17 cytokines have a suppressive role in these bone-forming cells, consistent with recent observations by Wagner and colleagues, who recently demonstrated in 2 murine models of psoriasis that IL-17 suppressed the differentiation of osteoblasts and osteocytes (45).

Although disease-modifying antirheumatic drugs are still the first-line choice when treating patients with PsA, biologic therapies have revolutionized the field, due to their high efficacy and safety profile. TNF antagonists, including monoclonal antibodies and fusion proteins, are the most commonly used biologic agents

and the first to be approved by the FDA for treating PsA. Biologics targeting the IL-23/IL-17 axis have gained interest in recent years. Ustekinumab, which targets the p40 subunit of both IL-12 and IL-23 cytokines, and a monoclonal antibody against IL-17 (secukinumab) have each shown promising therapeutic outcomes and have also been approved by the FDA for the treatment of PsA (46,47). Because of the heightened Th17 response observed in the R26Stat3C^{stopfl/fl} CD4Cre mice, we decided to mimic such treatment with the use of a neutralizing antibody against IL-17. Anti-IL-17 treatment reversed the progression of the psoriatic skin lesions in R26Stat3C^{stopfl/fl} CD4Cre mice and partially improved the osteopenia phenotype. This finding confirmed the efficacy of biologics in targeting one of the central signaling pathways contributing to PsA pathogenesis.

Furthermore, elimination of IL-22 led to amelioration of the skin and bone phenotype in R26Stat3C^{stopfl/fl} CD4Cre mice, reinforcing the potential importance of this cytokine in driving disease pathogenesis, suggesting that this cytokine may also play a central role in the pathogenesis of PsA. R26Stat3C^{stopfl/fl} CD4Cre IL-22^{-/-} mice did have a considerable reduction in RANKL-producing cells in their bones. This was noteworthy since IL-17 is known to promote RANKL expression. However, the role of IL-22 in osteoclastogenesis is less appreciated. IL-22 was previously shown to stimulate RANKL expression in synovial fibroblasts obtained from rheumatoid arthritis patients, and fibroblasts pretreated with IL-22 could stimulate the differentiation of osteoclasts from monocytes in the absence of exogenous RANKL (48). Both the results of that study and our observations of the reduction in RANKL-producing cells in R26Stat3C^{stopfl/fl} CD4Cre IL-22^{-/-} mice indicate that both IL-22 and IL-17 appear to contribute to osteoclastogenesis.

In addition to our observations of skin, synovio-enthesal, and bone inflammation in R26Stat3C^{stopfl/fl} CD4Cre mice, a heavy immune cell infiltration in the lung is also characteristically found in this model (21), with little or no inflammation at other sites. We have previously identified infiltration of neutrophils and chemokine up-regulation as characteristics that lead to lung function impairment in R26Stat3C^{stopfl/fl} CD4Cre mice (21). These lung defects likely contribute to the short lifespan of these mice (duration of 8–12 weeks, depending on the facility). This limited lifespan may also explain why we have yet to observe full-blown inflammation in the joints of these mice. The mechanisms at play that direct Th17-mediated infiltration at only these distinct sites, namely, the skin, joints, bone, and lung, remain to be elucidated.

There are still many questions unanswered in the field of PsA, and one obstacle has been the lack of an accurate animal model. The R26Stat3C^{stopfl/fl} CD4Cre animal model faithfully recapitulates many of the clinical features of PsA to a degree that other models have failed to capture. The disease manifestation was spontaneous, highly penetrant, and driven by a genetic perturbation relevant to human disease. As such, this murine model provides an excellent platform for further studies examining the role of additional genetic and environmental triggers in PsA, and is a useful addition to the repertoire of preclinical animal models of this rheumatic disease.

ACKNOWLEDGMENTS

We thank the New York University Medical Center Core Facilities (Histopathology, Immunohistochemistry, Flow Cytometry, and New York University College of Dentistry Micro-CT Core) for providing expert assistance. We also thank Drs. Leonid Korolov and Aristotelis Tsigirgos for their guidance in statistical analysis of the data. We are grateful to Dr. Wenjun Ouyang for kindly sharing with us the IL-22-knockout animals.

AUTHOR CONTRIBUTIONS

All authors were involved in drafting the article or revising it critically for important intellectual content, and all authors approved the final version to be published. Dr. Korolov had full access to all of the data in the study and takes responsibility for the integrity of the data and the accuracy of the data analysis.

Study conception and design. Yang, Fanok, Mediero-Munoz, Fogli, Abdollahi, Cronstein, Scher, Korolov.

Acquisition of data. Yang, Fanok, Mediero-Munoz, Fogli, Corciulo, Abdollahi, Korolov.

Analysis and interpretation of data. Yang, Fanok, Mediero-Munoz, Fogli, Corciulo, Abdollahi, Cronstein, Scher, Korolov.

REFERENCES

- Moll J, Wright V. Psoriatic arthritis. *Semin Arthritis Rheum* 1973;3:55–78.
- Ritchlin CT, Colbert RA, Gladman DD. Psoriatic arthritis. *N Engl J Med* 2017;376:957–70.
- Cantini F, Niccoli L, Nannini C, Kaloudi O, Bertoni M, Cassara E. Psoriatic arthritis: a systematic review. *Int J Rheum Dis* 2010;13:300–17.
- Gladman D, Antoni C, Mease P, Clegg D, Nash P. Psoriatic arthritis: epidemiology, clinical features, course, and outcome. *Ann Rheum Dis* 2005;64:ii14–ii7.
- Ogdie A, Harter L, Shin D, Baker J, Takeshita J, Choi HK, et al. The risk of fracture among patients with psoriatic arthritis and psoriasis: a population-based study. *Ann Rheum Dis* 2017;76:882–5.
- Frediani B, Allegrì A, Falsetti P, Storri L, Bisogno S, Baldi F, et al. Bone mineral density in patients with psoriatic arthritis. *J Rheumatol* 2001;28:138–43.
- Cai Y, Fleming C, Yan J. New insights of T cells in the pathogenesis of psoriasis. *Cell Mol Immunol* 2012;9:302–9.
- Maddur MS, Miossec P, Kaveri SV, Bayry J. Th17 cells: biology, pathogenesis of autoimmune and inflammatory diseases, and therapeutic strategies. *Am J Pathol* 2012;181:8–18.
- Leipe J, Grunke M, Dechant C, Reindl C, Kerzendorf U, Schulze-Koops H, et al. Role of Th17 cells in human autoimmune arthritis. *Arthritis Rheum* 2010;62:2876–85.
- Karczewski J, Dobrowolska A, Rychlewska-Hanczewska A, Adamski Z. New insights into the role of T cells in pathogenesis of psoriasis and psoriatic arthritis. *Autoimmunity* 2016;1–16.
- O’Shea JJ, Steward-Tharp SM, Laurence A, Watford WT, Wei L, Adamson AS, et al. Signal transduction and Th17 cell differentiation. *Microbes Infect* 2009;11:599–611.
- Mitra A, Raychaudhuri SK, Raychaudhuri SP. Functional role of IL-22 in psoriatic arthritis. *Arthritis Res Ther* 2012;14:R65.
- Benham H, Norris P, Goodall J, Wechalekar MD, FitzGerald O, Szentpetery A, et al. Th17 and Th22 cells in psoriatic arthritis and psoriasis. *Arthritis Res Ther* 2013;15:R136.
- O’Rielly DD, Rahman P. Genetics of psoriatic arthritis. *Best Pract Res Clin Rheumatol* 2014;28:673–85.
- Suzuki E, Mellins ED, Gershwin ME, Nestle FO, Adamopoulos IE. The IL-23/IL-17 axis in psoriatic arthritis. *Autoimmun Rev* 2014;13:496–502.
- Ritchlin CT, Krueger JG. New therapies for psoriasis and psoriatic arthritis. *Curr Opin Rheumatol* 2016;28:204–10.
- Reich K, Armstrong AW, Foley P, Song M, Wasfi Y, Randazzo B, et al. Efficacy and safety of guselkumab, an anti-interleukin-23 monoclonal antibody, compared with adalimumab for the treatment of patients with moderate to severe psoriasis with randomized withdrawal and retreatment: results from the phase III, double-blind, placebo- and active comparator-controlled VOYAGE 2 trial. *J Am Acad Dermatol* 2017;76:418–31.
- Raychaudhuri SP, Raychaudhuri SK. IL-23/IL-17 axis in spondyloarthritis—bench to bedside. *Clin Rheumatol* 2016;35:1437–41.
- Casola S, Cattoretti G, Uyttersprot N, Korolov SB, Seagal J, Hao Z, et al. Tracking germinal center B cells expressing germ-line immunoglobulin $\gamma 1$ transcripts by conditional gene targeting. *Proc Natl Acad Sci U S A* 2006;103:7396–401.
- Cénit MC, Ortego-Centeno N, Raya E, Callejas JL, García-Hernández FJ, Castillo-Palma MJ, et al. Influence of the STAT3 genetic variants in the susceptibility to psoriatic arthritis and Behcet’s disease. *Hum Immunol* 2013;74:230–3.
- Fogli LK, Sundrud MS, Goel S, Bajwa S, Jensen K, Derudder E, et al. T cell-derived IL-17 mediates epithelial changes in the airway and drives pulmonary neutrophilia. *J Immunol* 2013;191:3100–11.
- Siegel EL, Orbai AM, Ritchlin CT. Targeting extra-articular manifestations in PsA: a closer look at enthesitis and dactylitis. *Curr Opin Rheumatol* 2015;27:111–7.
- McGonagle D, Lories RJ, Tan AL, Benjamin M. The concept of a “synovio-entheseal complex” and its implications for understanding joint inflammation and damage in psoriatic arthritis and beyond. *Arthritis Rheum* 2007;56:2482–91.
- Sherlock JP, Joyce-Shaikh B, Turner SP, Chao CC, Sathe M, Grein J, et al. IL-23 induces spondyloarthropathy by acting on ROR- γ t+ CD3+CD4-CD8-entheseal resident T cells. *Nat Med* 2012;18:1069–76.
- Cuthbert RJ, Fragkakis EM, Dunsmuir R, Li Z, Coles M, Marzo-Ortega H, et al. Group 3 innate lymphoid cells in human enthesitis. *Arthritis Rheumatol* 2017;69:1816–22.
- Maeda S, Hayami Y, Naniwa T, Ueda R. The Th17/IL-23 axis and natural immunity in psoriatic arthritis. *Int J Rheumatol* 2012;2012:539683.
- Sato K, Suematsu A, Okamoto K, Yamaguchi A, Morishita Y, Kadono Y, et al. Th17 functions as an osteoclastogenic helper T cell subset that links T cell activation and bone destruction. *J Exp Med* 2006;203:2673–82.
- Charles JF, Hsu LY, Niemi EC, Weiss A, Aliprantis AO, Nakamura MC. Inflammatory arthritis increases mouse osteoclast

- precursors with myeloid suppressor function. *J Clin Invest* 2012; 122:4592–605.
29. Okamoto K, Takayanagi H. Regulation of bone by the adaptive immune system in arthritis. *Arthritis Res Ther* 2011;13:219.
 30. Campa M, Mansouri B, Warren R, Menter A. A review of biologic therapies targeting IL-23 and IL-17 for use in moderate-to-severe plaque psoriasis. *Dermatol Ther (Heidelb)* 2016;6:1–12.
 31. Wasilewska A, Winiarska M, Olszewska M, Rudnicka L. Interleukin-17 inhibitors. A new era in treatment of psoriasis and other skin diseases. *Postepy Dermatol Alergol* 2016;33:247–52.
 32. Zenz R, Eferl R, Kenner L, Florin L, Hummerich L, Mehic D, et al. Psoriasis-like skin disease and arthritis caused by inducible epidermal deletion of Jun proteins. *Nature* 2005;437:369–75.
 33. Braem K, Carter S, Lories RJ. Spontaneous arthritis and ankylosis in male DBA/1 mice: further evidence for a role of behavioral factors in “stress-induced arthritis”. *Biol Proced Online* 2012; 14:10.
 34. Van der Fits L, Mourits S, Voerman JS, Kant M, Boon L, Laman JD, et al. Imiquimod-induced psoriasis-like skin inflammation in mice is mediated via the IL-23/IL-17 axis. *J Immunol* 2009; 182:5836–45.
 35. Khmaladze I, Kelkka T, Guerard S, Wing K, Pizzolla A, Saxena A, et al. Mannan induces ROS-regulated, IL-17A-dependent psoriasis arthritis-like disease in mice. *Proc Natl Acad Sci U S A* 2014;111:E3669–E78.
 36. Sano S, Chan KS, Carbajal S, Clifford J, Peavey M, Kiguchi K, et al. Stat3 links activated keratinocytes and immunocytes required for development of psoriasis in a novel transgenic mouse model. *Nat Med* 2005;11:43–9.
 37. Li L, Shaw PE. Elevated activity of STAT3C due to higher DNA binding affinity of phosphotyrosine dimer rather than covalent dimer formation. *J Biol Chem* 2006;281:33172–81.
 38. Polachek A, Li S, Chandran V, Gladman DD. Clinical enthesitis in a prospective longitudinal psoriatic arthritis cohort: incidence, prevalence, characteristics, and outcome. *Arthritis Care Res (Hoboken)* 2017;69:1685–91.
 39. Taylor W, Gladman D, Helliwell P, Marchesoni A, Mease P, Mielants H. Classification criteria for psoriatic arthritis: development of new criteria from a large international study. *Arthritis Rheum* 2006;54:2665–73.
 40. Kehl AS, Corr M, Weisman MH. Enthesitis: new insights into pathogenesis, diagnostic modalities, and treatment [review]. *Arthritis Rheumatol* 2016;68:312–22.
 41. Polachek A, Cook R, Chandran V, Gladman DD, Eder L. The association between sonographic enthesitis and radiographic damage in psoriatic arthritis. *Arthritis Res Ther* 2017;19:189.
 42. Schett G, Lories RJ, D’Agostino MA, Elewaut D, Kirkham B, Soriano ER, et al. Enthesitis: from pathophysiology to treatment. *Nat Rev Rheumatol* 2017;13:731–41.
 43. Ritchlin CT, Haas-Smith SA, Li P, Hicks DG, Schwarz EM. Mechanisms of TNF- α -and RANKL-mediated osteoclastogenesis and bone resorption in psoriatic arthritis. *J Clin Invest* 2003; 111:821–31.
 44. Ginhoux F, Jung S. Monocytes and macrophages: developmental pathways and tissue homeostasis. *Nat Rev Immunol* 2014;14:392–404.
 45. Uluçkan Ö, Jimenez M, Karbach S, Jeschke A, Graña O, Keller J, et al. Chronic skin inflammation leads to bone loss by IL-17-mediated inhibition of Wnt signaling in osteoblasts. *Sci Transl Med* 2016;8:330ra37.
 46. Mease PJ, McInnes IB, Kirkham B, Kavanaugh A, Rahman P, van Der Heijde D, et al. Secukinumab inhibition of interleukin-17A in patients with psoriatic arthritis. *N Engl J Med* 2015; 373:1329–39.
 47. McInnes IB, Kavanaugh A, Gottlieb AB, Puig L, Rahman P, Ritchlin C, et al. Efficacy and safety of ustekinumab in patients with active psoriatic arthritis: 1 year results of the phase 3, multi-centre, double-blind, placebo-controlled PSUMMIT 1 trial. *Lancet* 2013;382:780–9.
 48. Kim KW, Kim HR, Park JY, Park JS, Oh HJ, Woo YJ, et al. Interleukin-22 promotes osteoclastogenesis in rheumatoid arthritis through induction of RANKL in human synovial fibroblasts. *Arthritis Rheum* 2012;64:1015–23.

Long-Term Safety and Efficacy of Belimumab in Patients With Systemic Lupus Erythematosus

A Continuation of a Seventy-Six–Week Phase III Parent Study in the United States

Richard A. Furie,¹ Daniel J. Wallace,² Cynthia Aranow,³ James Fettiplace,⁴ Barbara Wilson,⁵ Prafull Mistry,⁶ David A. Roth,⁷ and David Gordon⁷

Objective. We undertook this US multicenter continuation study (GlaxoSmithKline study BEL112233; ClinicalTrials.gov identifier: NCT00724867) to assess long-term safety and efficacy of belimumab in patients with systemic lupus erythematosus (SLE) who completed the Study of Belimumab in Subjects with SLE 76-week trial (ClinicalTrials.gov identifier: NCT00410384).

Methods. Patients continued to receive the same belimumab dose plus standard therapy; patients previously receiving placebo received 10 mg/kg belimumab. The primary outcome measure was long-term safety of belimumab (frequency of adverse events [AEs] and damage assessed using the Systemic Lupus International Collaborating Clinics/American College of Rheumatology Damage Index [SDI], evaluated every 48 weeks [1 study year]). Other assessments included the SLE Responder

Index (SRI), flare rates (using the modified SLE Flare Index [SFI]), prednisone use, and B cell levels.

Results. Of 268 patients, 140 completed the study and 128 withdrew. The mean \pm SD score on the Safety of Estrogens in Lupus Erythematosus National Assessment version of the SLE Disease Activity Index (SELENA–SLEDAI) at baseline was 7.8 ± 3.86 . The mean \pm SD SDI score increased by 0.4 ± 0.68 from its value at baseline (1.2 ± 1.51). The overall incidence of treatment-related and serious AEs remained stable or declined through study year 7. An SRI response was achieved by 41.9% and 75.6% of patients at the study year 1 and study year 7 midpoints, respectively. At the study year 7 midpoint, relative to baseline, 78.2% had achieved a ≥ 4 -point reduction in the SELENA–SLEDAI score, 98.4% had no new British Isles Lupus Assessment Group (BILAG) A organ domain score and no more than 1 new BILAG B organ domain score, 93.7% had no worsening in the physician's global assessment of disease activity, 20.6% had experienced ≥ 1 severe SFI flare, the mean decrease in prednisone dose was 31.4%, and the median change in CD20+ B cell numbers was -83.2% .

Conclusion. These long-term exposure results confirm the previously observed safety and efficacy profiles of belimumab in patients with SLE.

Systemic lupus erythematosus (SLE) is a chronic autoimmune disorder that affects a number of organ systems (1) and causes a marked impairment in quality of life (QoL) (2,3). Active disease (4,5) and medication toxicities contribute to the accrual of long-term organ damage (6–8). Corticosteroids and immunosuppressant drugs have demonstrated clinical benefits (9); however, concerns remain about the safety of their long-term use (6–8).

Belimumab is a human IgG1 λ monoclonal antibody licensed for the treatment of adult patients with

ClinicalTrials.gov identifier: NCT00724867.

Supported by GlaxoSmithKline.

¹Richard A. Furie, MD: Northwell Health, Great Neck, New York; ²Daniel J. Wallace, MD, FACP, FACR: Cedars-Sinai Medical Center, University of California, Los Angeles; ³Cynthia Aranow, MD: The Feinstein Institute for Medical Research, Manhasset, New York; ⁴James Fettiplace, MD (current address: Mundipharma Research, Cambridge, UK): GlaxoSmithKline, Uxbridge, UK; ⁵Barbara Wilson, MEd: GlaxoSmithKline, Research Triangle Park, North Carolina; ⁶Prafull Mistry, MSc: GlaxoSmithKline, Stevenage, UK; ⁷David A. Roth, MD, MSCE, David Gordon, MB, ChB: GlaxoSmithKline, Philadelphia, Pennsylvania.

Dr. Furie has received consulting fees from GlaxoSmithKline (more than \$10,000) and research support from that company. Dr. Wallace has received research support from GlaxoSmithKline. Dr. Aranow has received consulting fees from GlaxoSmithKline (less than \$10,000) and research support as an investigator in that company's sponsored clinical trials. Drs. Fettiplace, Roth, and Gordon and Ms Wilson and Mr. Mistry own stock or stock options in GlaxoSmithKline.

Address correspondence to Richard A. Furie, MD, Division of Rheumatology, Northwell Health, Hofstra Northwell School of Medicine, 865 Northern Boulevard, Suite 302, Great Neck, NY 11021. E-mail: furie@nshs.edu.

Submitted for publication September 22, 2016; accepted in revised form January 30, 2018.

active, autoantibody-positive SLE who are receiving standard therapy. Belimumab binds to and inhibits the activity of soluble human B lymphocyte stimulator protein (10). A placebo-controlled phase II study showed that intravenous (IV) belimumab plus standard therapy was generally well tolerated (11); a good safety profile was maintained over 7 years (12). Two phase III studies, the Study of Belimumab in Subjects with SLE 52-week (BLISS-52) and 76-week (BLISS-76) trials, demonstrated the safety and efficacy of belimumab in patients with autoantibody-positive, active SLE (13,14). The long-term safety and efficacy of belimumab were examined in 2 open-label continuation studies (GlaxoSmithKline [GSK] studies BEL112233 and BEL112234) in patients who completed the BLISS studies. A pooled interim analysis of these 2 long-term continuation studies demonstrated low rates of organ damage accrual in patients with moderate-to-severe SLE, and safety over 5 years of exposure (15). Herein, we present the clinical results of the complete BLISS-76 continuation study BEL112233 conducted in US-only patients. Due to the study design, all non-US patients in BLISS-76 and BLISS-52 entered the rest-of-world continuation study BEL112234 (ClinicalTrials.gov identifier: NCT00712933).

The objectives of this continuation study were to provide continuing treatment to patients who completed BLISS-76 and evaluate the long-term safety and tolerability, impact on QoL, and efficacy of belimumab treatment in patients with SLE. The long-term impact of belimumab on QoL in patients with SLE will be reported separately.

PATIENTS AND METHODS

Study design. This was a multicenter, continuation study (GSK study BEL112233; ClinicalTrials.gov identifier: NCT00724867) conducted in patients who completed the 76-week phase III parent study BLISS-76 (GSK study BEL110751; ClinicalTrials.gov identifier: NCT00410384) in the US (14). In BLISS-76, patients were randomized to receive 1 mg/kg belimumab IV, 10 mg/kg belimumab IV, or placebo, plus standard therapy for 76 weeks (14). Patients who previously received placebo received 10 mg/kg belimumab in the continuation study. Patients randomized to receive belimumab continued to receive the same dose as in the parent study (1 or 10 mg/kg IV every 28 days) plus standard therapy. Following a protocol amendment (March 9, 2011), patients receiving 1 mg/kg belimumab had their dose increased to 10 mg/kg. Data on all patients receiving belimumab during this study were pooled for analysis.

To be eligible for enrollment, patients had to have completed BLISS-76 through week 72 and be able to receive the first dose of belimumab within 4 weeks (minimum 2 weeks, maximum 8 weeks). Patients were excluded if in the investigator's opinion they presented with clinical evidence of uncontrolled, acute, or chronic disease not due to SLE. Other

key exclusion criteria included occurrence of an adverse event (AE) in the parent trial that would place the patient at undue risk, or laboratory abnormalities.

Since the study was designed to have 48-week study years, study years do not align with calendar years. The study was designed to end either after 5 calendar years from the date of enrollment of the last patient or when fewer than 100 patients remained in the trial, whichever occurred first. The study was conducted from August 5, 2008 to March 26, 2015, and up to 8 calendar years of data were collected (maximum exposure 2,908 days) (Figure 1).

Clinical site personnel remained blinded with regard to parent study treatment until results of the parent study were made public. The study was performed in accordance with the Declaration of Helsinki (16). All sites maintained ethics committee and institutional review board approval, and written informed consent was obtained from all patients.

Study end points. The primary objective of this study was the evaluation of the long-term safety of belimumab, as assessed by AEs, AEs of special interest, vital signs, and clinical laboratory tests (hematology, chemistry, routine urinalysis, and immunogenicity testing). Organ damage was assessed using the Systemic Lupus International Collaborating Clinics/American College of Rheumatology Damage Index (SDI) (17). Assessments were performed at week 24 (study year midpoint) and week 48 (study year end, referred to hereafter as study year). AEs were monitored throughout the study and for 8 weeks following the last dose of belimumab. Clinical laboratory assessments were performed on day 0, at weeks 4, 12, 24, 36, and 48 of study year 1, and at weeks 24 and 48 of each study year thereafter. Organ damage was assessed every 48 weeks.

Efficacy and biomarker assessments were exploratory. The primary efficacy assessment was the SLE Responder Index (SRI) (18) response rate, a validated composite end point defined as a ≥ 4 -point reduction from baseline in the Safety of Estrogens in Lupus Erythematosus National Assessment version of the SLE Disease Activity Index (SELENA-SLEDAI) score (19), no worsening in the physician's global assessment of disease activity on a 0–10-cm visual analog scale (< 0.3 points from baseline), and no new British Isles Lupus Assessment Group (BILAG) A or no more than 1 new BILAG B organ domain score (20).

Other efficacy assessments included the SELENA-SLEDAI, BILAG, physician's global assessment of disease activity, flare rates, prednisone use, and biomarkers. Flare rates were assessed by the SLE Flare Index (SFI) (19) and the BILAG. SFI flare rates (mild/moderate or severe) were defined by the modified SELENA-SLEDAI SFI (the modified SFI excludes severe flares that were triggered only by an increase in the SELENA-SLEDAI score to > 12) (21). BILAG flare was defined by at least 1 new BILAG A organ domain score or > 1 new BILAG B organ domain score compared with baseline (21). Biomarker assessments included anti-double-stranded DNA (anti-dsDNA) levels, serum complement levels, proteinuria values, serum Ig levels, and B cell subsets. Patients with a baseline SELENA-SLEDAI score of < 4 at entry into the continuation study were excluded from the SRI analysis. Efficacy and biomarker assessments were performed every 24 weeks from the first dose of belimumab, with the exception of serum Ig levels, which were tested at week 24 and week 48 during study year 1 and then every 48 weeks. Concomitant corticosteroids were converted to a prednisone equivalent average daily dose (mg/day).

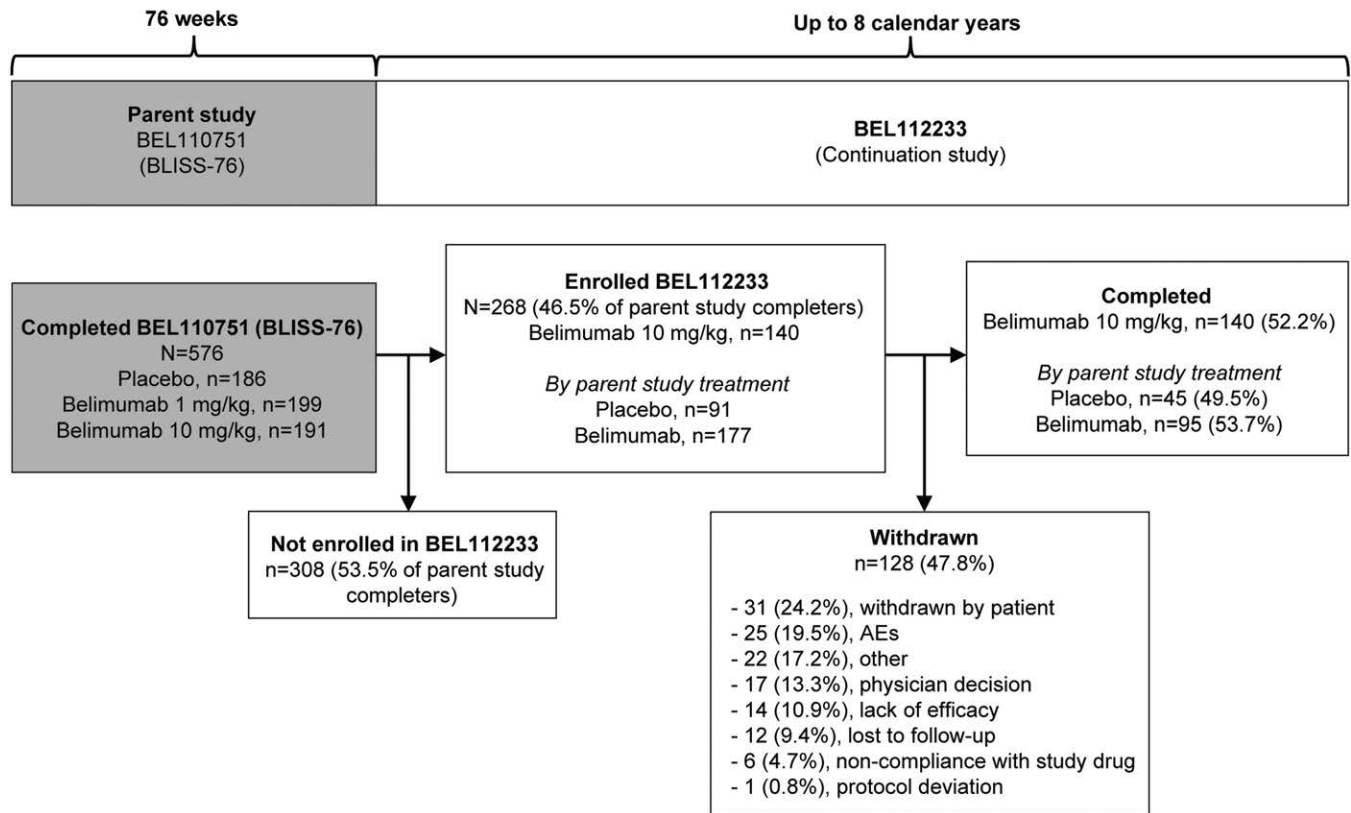


Figure 1. Disposition of the systemic lupus erythematosus (SLE) patients and enrollment by treatment in the Study of Belimumab in Subjects with SLE 76-week (BLISS-76) trial. This continuation study (GlaxoSmithKline [GSK] study BEL112233) was designed to end either after 5 calendar years from the date of enrollment of the last patient or when fewer than 100 patients remained in the trial, whichever occurred first. Patients at non-US sites were not eligible for enrollment into this study and had the opportunity to enroll in another open-label, long-term continuation study, GSK study BEL112234. For patients who received placebo in the parent study (BLISS-76; GSK study BEL110751), baseline was the last assessment prior to their first dose of belimumab, at the start of the continuation study. For patients who received belimumab in the parent study, baseline was the latest assessment prior to commencing the parent study. One patient who withdrew from the continuation study reported an adverse event (AE) leading to discontinuation, but the investigator-recorded reason for withdrawal was “physician decision.”

Post hoc analyses were carried out for several parameters of interest. Baseline disease characteristics were examined for patients who withdrew and those who completed the study, to investigate completer bias. Withdrawals among SRI responders were reported, and severe flares were examined according to which severe SFI flare criteria were met. In addition, the proportions of patients who experienced normalization of anti-dsDNA and complement levels and who discontinued prednisone during the study were examined.

Statistical analysis. No formal statistical hypothesis testing was performed, and all analyses were descriptive and exploratory. Analyses included those patients enrolled in the continuation study who received at least 1 dose of belimumab. Patients who received 1 mg/kg or 10 mg/kg belimumab in the parent study were pooled for all analyses. Baseline was defined as the last assessment prior to the first dose of belimumab (day 0). Therefore, baseline for the parent study placebo group was the last assessment prior to their first dose of belimumab, at the start of the continuation study. For patients receiving active

treatment in the parent study, baseline was the latest assessment prior to commencing the parent study, BLISS-76.

AEs from both the parent and continuation studies were coded according to the Medical Dictionary for Regulatory Activities, version 17.1. All AE data were summarized by study year according to the recorded start date of the AE. AEs that continued for >1 study year were reported in the year they first occurred; repeat AE episodes were reported in the year they reappeared. If the AE onset date was missing, it was assumed the start date was study year 1. If the AE end date was missing, it was assumed the AE continued until study end. AEs of special interest included malignant neoplasms, postinfusion systemic reactions, infections, depression, suicide, and self-injury. Continuous variables were summarized, reporting mean and SD, median and 25th and 75th percentile, and minimum and maximum. Categorical variables were summarized with frequency counts and percentages. All analyses were performed using SAS software, version 9.3.

RESULTS

Patient population. The modified intent-to-treat (ITT) population comprised 268 patients (46.5% of parent study completers; non-US patients in the parent study were not eligible for this study); 140 patients (52.2%) completed the continuation study, and 128 patients (47.8%) withdrew. The majority of patients were white (186 of 268 [69.4%]) and female (250 of 268 [93.3%]), with a mean \pm SD age of 42.8 ± 11.33 years (Table 1). The duration of SLE ranged from 0 to 36 years, with a mean \pm SD of 7.7 ± 6.77 years. The majority of patients (188 of 268 [70.1%]) entered the continuation study with a baseline SELENA-SLEDAI score of ≤ 9 and a mean \pm SD SDI of 1.2 ± 1.51 . The mean \pm SD duration of belimumab exposure was $1,962.1 \pm 746.44$ days, with a median of 2,166.5 days (range 28–2,908).

The number of patients withdrawing from the study each year remained consistent throughout the study, and the number of patients starting each yearly interval declined at similar rates among patients initially treated with belimumab in the parent study and those treated with placebo (see Supplementary Figure 1, available on the *Arthritis & Rheumatology* web site at <http://online.library.wiley.com/doi/10.1002/art.40439/abstract>). The 3 most common reasons for withdrawal were withdrawal by patient (31 of 128 [24.2%]), AE (25 of 128 [19.5%]), and other (22 of 128 [17.2%]) (Figure 1). A post hoc review of the data indicated that where a reason was provided for withdrawal by patient, the 2 requests most often cited were a desire to conceive and logistical reasons (data not shown). The majority of patients (11 of 14) who withdrew due to lack of efficacy did so in the first 4 years of the study. Disease flares were a commonly cited reason for withdrawal due to lack of efficacy (5 of 14 patients).

Baseline characteristics of patients who withdrew from the study and of those who completed were examined post hoc. The mean \pm SD SELENA-SLEDAI scores at baseline were 7.8 ± 3.85 and 7.8 ± 3.89 among those who withdrew and those who completed, respectively. Thirty-eight of 128 patients (29.7%) who withdrew had a SELENA-SLEDAI score of ≥ 10 at baseline, compared with 42 of 140 patients (30.0%) who completed the study. Of patients who withdrew, 91 of 128 (71.1%) had a score of >1 on the physician's global assessment of disease activity, compared with 98 of 140 patients (70.0%) who completed the study. Among patients who withdrew, 63 of 128 (49.2%) had active disease at baseline, defined as ≥ 1 BILAG A or ≥ 2 BILAG B organ domain scores, while 74 of 140 patients (52.9%) who completed the study had active

Table 1. Baseline characteristics of the 268 patients*

Female	250 (93.3)
Age, mean \pm SD years	42.8 ± 11.33
BMI, mean \pm SD kg/m ²	28.4 ± 7.43
Race	
White	186 (69.4)
Black or African American/African heritage	57 (21.3)
Asian	13 (4.9)
SLE disease duration, mean \pm SD years	7.7 ± 6.77
SELENA-SLEDAI score (0–105), mean \pm SD	7.8 ± 3.86
SELENA-SLEDAI score	
≤ 9	188 (70.1)
≥ 10	80 (29.9)
Complement levels	
Low C3 and/or low C4	119 (44.4)
No low C3 or C4	149 (55.6)
PGA (0–10-cm VAS), mean \pm SD	1.19 ± 0.60
SDI score (0–47), mean \pm SD	1.2 ± 1.51
SLE Flare Index	
At least 1 flare	65 (24.3)
At least 1 severe flare	2 (0.7)
BILAG organ domain involvement†	137 (51.1)
Concomitant medications	
Corticosteroids only	21 (7.8)
Immunosuppressant drugs only	11 (4.1)
Antimalarials only	41 (15.3)
Average prednisone dose	
0 mg/day	95 (35.4)
>0 to ≤ 7.5 mg/day	87 (32.5)
>7.5 to ≤ 40 mg/day	86 (32.1)

* Except where indicated otherwise, values are the number (%). BMI = body mass index; SLE = systemic lupus erythematosus; SELENA-SLEDAI = Safety of Estrogens in Lupus Erythematosus National Assessment version of the SLE Disease Activity Index; PGA = physician's global assessment of disease activity; VAS = visual analog scale; SDI = Systemic Lupus International Collaborating Clinics/American College of Rheumatology Damage Index.

† At least 1 new British Isles Lupus Assessment Group (BILAG) A organ domain score or >1 new BILAG B organ domain score compared with baseline.

disease at baseline. At baseline, ≥ 1 SFI flare had been experienced by 28 of 128 patients (21.9%) who then withdrew and by 37 of 140 patients (26.4%) who completed. Among patients who withdrew, 2 of 128 (1.6%) experienced ≥ 1 severe flare prior to baseline; no patients who completed the study had a severe flare prior to baseline. Twenty-three of 128 patients (18.0%) who withdrew from the study had proteinuria >0.5 gm/24 hours at baseline, compared with 13 of 140 (9.3%) who completed. Low C3/C4 levels (C3 <0.9 gm/liter and/or C4 <0.16 gm/liter) at baseline were reported in 52 of 128 patients (40.6%) who withdrew and 67 of 140 (47.9%) who completed. Overall, baseline disease characteristics between patients who withdrew and those who completed were similar.

Safety. AEs. At least 1 AE was experienced by 267 of 268 patients (99.6%), and 145 of 268 patients (54.1%) had an AE that was considered by the investigator to be drug-related (Table 2). Discontinuation of belimumab due to an AE occurred in 26 of 268

Table 2. Incidence of treatment-emergent AEs by study year*

	Any time postbaseline (n = 268)	Year 0–1 (n = 268)	Year 1–2 (n = 259)	Year 2–3 (n = 244)	Year 3–4 (n = 219)	Year 4–5 (n = 202)	Year 5–6 (n = 192)	Year 6–7 (n = 130)	Year 7+ (n = 65)
At least 1 AE	267 (99.6)	260 (97.0)	235 (90.7)	206 (84.4)	184 (84.0)	167 (82.7)	145 (75.5)	87 (66.9)	31 (47.7)
At least 1 treatment-related AE†	145 (54.1)	89 (33.2)	55 (21.2)	40 (16.4)	35 (16.0)	30 (14.9)	32 (16.7)	13 (10.0)	3 (4.6)
At least 1 serious AE	112 (41.8)	33 (12.3)	30 (11.6)	25 (10.2)	22 (10.0)	24 (11.9)	16 (8.3)	13 (10.0)	3 (4.6)
Serious AEs by system organ class‡									
Infections and infestations	44 (16.4)	13 (4.9)	9 (3.5)	4 (1.6)	6 (2.7)	8 (4.0)	7 (3.6)	2 (1.5)	1 (1.5)
Musculoskeletal and connective tissue	22 (8.2)	7 (2.6)	5 (1.9)	3 (1.2)	2 (0.9)	4 (2.0)	2 (1.0)	1 (0.8)	0
At least 1 severe AE	100 (37.3)	31 (11.6)	19 (7.3)	23 (9.4)	21 (9.6)	18 (8.9)	15 (7.8)	10 (7.7)	3 (4.6)
Severe AEs by system organ class‡									
Infections and infestations	28 (10.4)	7 (2.6)	2 (0.8)	4 (1.6)	7 (3.2)	6 (3.0)	3 (1.6)	0	1 (1.5)
Musculoskeletal and connective tissue	23 (8.6)	9 (3.4)	4 (1.5)	4 (1.6)	1 (0.5)	5 (2.5)	3 (1.6)	1 (0.8)	0
At least 1 AE resulting in study agent discontinuation	26 (9.7)	3 (1.1)	4 (1.5)	7 (2.9)	8 (3.7)	0	2 (1.0)	2 (1.5)	0
All infections of special interest§	43 (16.0)	14 (5.2)	13 (5.0)	8 (3.3)	6 (2.7)	7 (3.5)	11 (5.7)	6 (4.6)	0
Serious	5 (1.9)	1 (0.4)	1 (0.4)	1 (0.4)	0	1 (0.5)	1 (0.5)	0	0
Opportunistic infections of special interest¶	16 (6.0)	3 (1.1)	3 (1.2)	4 (1.6)	0	3 (1.5)	6 (3.1)	2 (1.5)	0
Serious	0	0	0	0	0	0	0	0	0
All herpes zoster	27 (10.1)	9 (3.4)	6 (2.3)	4 (1.6)	4 (1.8)	5 (2.5)	7 (3.6)	3 (2.3)	0
Opportunistic¶	9 (3.4)	1 (0.4)	2 (0.8)	2 (0.8)	0	2 (1.0)	5 (2.6)	2 (1.5)	0
Serious	1 (0.4)	0	1 (0.4)	0	0	0	0	0	0
Malignant neoplasms (excluding nonmelanoma skin cancer)	10 (3.7)	0	1 (0.4)	4 (1.6)	2 (0.9)	0	0	2 (1.5)	1 (1.5)
Postinfusion systemic reactions#	50 (18.7)	23 (8.6)	11 (4.2)	7 (2.9)	5 (2.3)	4 (2.0)	6 (3.1)	5 (3.8)	1 (1.5)
Any depression/suicide/self-injury§	73 (27.2)	25 (9.3)	22 (8.5)	17 (7.0)	6 (2.7)	8 (4.0)	3 (1.6)	4 (3.1)	1 (1.5)
Deaths	2 (0.7)	0	1 (0.4)	0	1 (0.5)	0	0	0	0

* Values are the number (%) of patients. Patients reporting multiple adverse events (AEs) within a study year are only counted once in each of the appropriate categories.

† Possibly, probably, or definitely related.

‡ Two most frequently occurring AE system organ classes presented.

§ Per custom Medical Dictionary for Regulatory Activities (MedDRA) query.

¶ Per adjudication by GlaxoSmithKline.

Per custom MedDRA query, broad search.

patients (9.7%), with the majority (n = 22) of these occurring in the first 4 years of the study. With the exception of intraductal proliferative breast lesion (n = 2), all AEs that led to study drug discontinuation were different. The most common AEs (occurring in $\geq 25\%$ of patients) were arthralgia (108 of 268 [40.3%]), nausea (88 of 268 [32.8%]), headache (86 of 268 [32.1%]), and infections, including bacterial upper respiratory tract infection (77 of 268 [28.7%]), viral upper respiratory tract infection (76 of 268 [28.4%]), and bacterial urinary tract infection (70 of 268 [26.1%]). At least 1 serious AE was reported in 112 of 268 patients (41.8%), and at least 1 severe AE (grade 3 or grade 4 events listed as life-threatening) was reported in 100 of 268 patients (37.3%). Two deaths occurred (0.7%); neither was considered study drug-related (hypertensive heart disease, polydrug toxicity [later adjudicated as suicide]). AEs of special interest are summarized in Table 2. Sixteen patients acquired an opportunistic infection (none categorized as serious), and 3 incidents

of suicidal behavior (1.1%) were reported. Overall, the incidence of AEs, treatment-related AEs, serious AEs, and severe AEs remained stable or declined from study year 1 to study year 7+.

Clinical laboratory evaluations and vital signs. Lymphocyte count was the only hematologic measure in which $\geq 10\%$ of patients had either grade 3 or grade 4 values during the study; 50 of 177 patients (28.2%) had a grade 3 value. The percentage of patients who had at least a 2-grade shift from baseline in clinical chemistry studies (liver function, electrolytes, and other chemistry studies) was generally stable or declined over time, not exceeding 12% postbaseline. The percentage of patients with grade 3 or grade 4 values at any time postbaseline did not exceed 5% for any clinical chemistry parameter or urinalysis, and no trends of clinical concern were noted. During the study, 7 of 268 patients (2.6%) had a grade 3 value for IgG, and none of these patients experienced a serious or severe infection. Two patients had a persistent positive anti-human antibody response that

occurred during at least 2 consecutive assessments or once at the final assessment, although no patient had >2 consecutive positive results. Mean diastolic and systolic blood pressures were stable over time.

Organ damage. The mean ± SD SDI score was 1.2 ± 1.51 at baseline. At study year 7 the mean ± SD SDI score had increased by 0.4 ± 0.68.

Efficacy. SRI response. An SRI response had been achieved by 96 of 229 patients (41.9%) and 90 of 119 patients (75.6%) overall at the study year 1 and study year 7 midpoints, respectively (Figure 2A). Withdrawals between these 2 time points were examined post hoc, along with the occurrence of new responses, to account for the decrease in absolute number of responders. Of the patients who withdrew (113 of 268;

modified ITT population) between these 2 time points, 34 of 113 (30.1%) were responders at the study year 1 midpoint. Of the 90 patients who were SRI responders at the study year 7 midpoint, 35 of them (38.9%) had not been responders at the study year 1 midpoint (52 patients [57.8%] were responders at the study year 1 midpoint).

SELENA–SLEDAI score. The overall percentage of patients with a ≥4-point reduction from baseline in the SELENA–SLEDAI score increased from 44.4% (104 of 234 patients) to 78.2% (93 of 119 patients) at the study year 1 and study year 7 midpoints, respectively (Figure 2B). The overall mean ± SD percentage reduction from the baseline SELENA–SLEDAI score (7.8 ± 3.86) increased from 27.1 ± 48.29% at the study

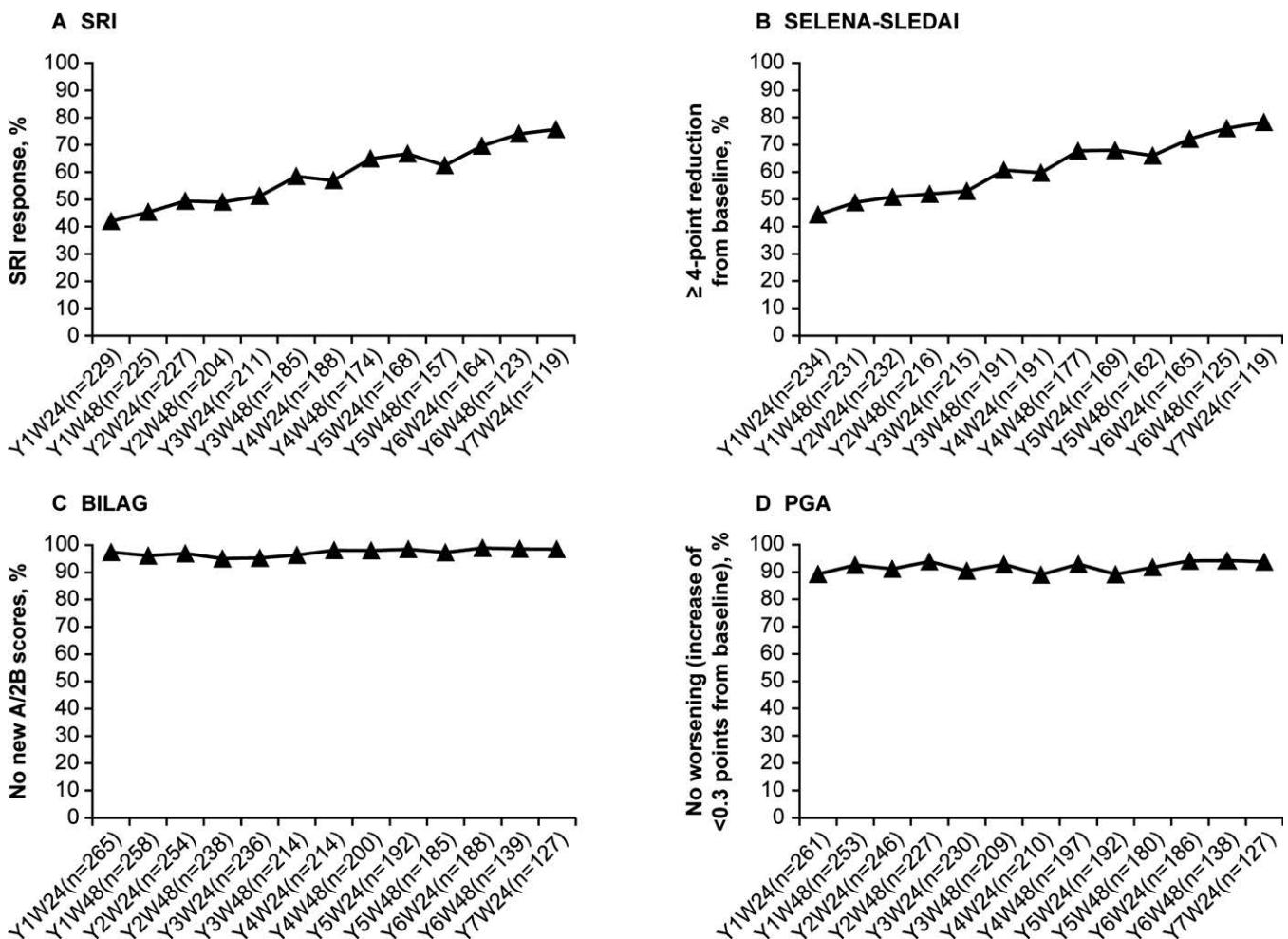


Figure 2. Efficacy end points. **A**, Systemic Lupus Erythematosus Responder Index (SRI) response. **B**, Safety of Estrogens in Lupus Erythematosus National Assessment version of the Systemic Lupus Erythematosus Disease Activity Index (SELENA–SLEDAI) score. **C**, British Isles Lupus Assessment Group (BILAG) score. In **A** and **B**, patients with baseline SELENA–SLEDAI scores of <4 were excluded from the analyses. No new A/2B scores = no new BILAG A organ domain score and no more than 1 new BILAG B organ domain score. **D**, Physician’s global assessment of disease activity (PGA) score. Y1W24 = year 1, week 24.

year 1 midpoint (n = 252) to $64.9 \pm 37.46\%$ at the study year 7 midpoint (n = 125).

BILAG worsening. At baseline, the percentage of patients with at least 1 BILAG A or 2 BILAG B organ domain scores was 51.1% (137 of 268). Overall, at each visit, $\geq 95\%$ of patients had no new BILAG A organ domain score and no more than 1 new BILAG B organ domain score. At the study year 1 midpoint, 258 of 265 patients (97.4%) had no new BILAG A organ domain score and no more than 1 new BILAG B organ domain score. This remained stable throughout the study, with 125 of 127 patients (98.4%) meeting this criterion at the study year 7 midpoint (Figure 2C). Among patients with a postbaseline flare assessment, 33 of 267 (12.4%) and 84 of 267 (31.5%) had at least 1 BILAG flare by the study year 1 and study year 7 midpoints, respectively.

Worsening in physician's global assessment of disease activity. The overall percentage of patients with no new worsening (increase of <0.30 points) from baseline in the physician's global assessment of disease activity was $\geq 89\%$ up to the study year 7 midpoint visit (119 of 127 patients [93.7%]) (Figure 2D).

SFI flare. By the study year 1 midpoint, 149 of 267 patients (55.8%) had experienced at least 1 SFI flare, and 15 of 267 (5.6%) had experienced at least 1 severe flare. Up to and including the study year 7 midpoint visit, these percentages increased to 92.5% (247 of 267) and 20.6% (55 of 267), respectively (cumulative). Of the 55 patients with a severe flare at the study year 7 midpoint, new/worse severe symptoms were experienced by 23.6% of patients (13 of 55), 63.6% of patients (35 of 55) had an increase in daily prednisone dose to >0.5 mg/kg, and 38.2% of patients (21 of 55) had 1 new medication for SLE activity. An increase to a score of ≥ 2.5 on the physician's global assessment of disease activity was recorded in 5 of 55 patients (9.1%), and 10 of 55 patients (18.2%) were hospitalized for SLE activity.

Prednisone use. Among patients receiving concomitant prednisone (n = 77), the mean decrease from baseline in prednisone dose at the study year 7 midpoint was 31.4% (Figure 3). The percentage of patients with a baseline prednisone dose of >7.5 mg/day whose dose was reduced to ≤ 7.5 mg/day was 50.0% (32 of 64) at the study year 3 midpoint, 39.5% (15 of 38) at study year 7, and 58.3% (7 of 12) at study year 8. Some patients (23 of 173 [13.3%]) discontinued prednisone permanently during the study (post hoc analyses).

Biomarkers. At baseline, 135 of 268 patients (50.4%) were anti-dsDNA positive (≥ 30 IU/ml), 86 of 268 (32.1%) had low C3 levels, and 98 of 268 (36.6%) had low C4 levels. Post hoc analyses showed that

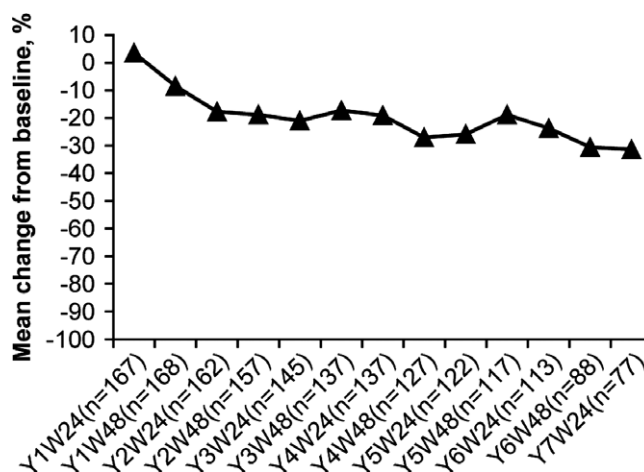


Figure 3. Mean percentage change from baseline in prednisone dose. Y1W24 = year 1, week 24.

among those who were anti-dsDNA positive at baseline, levels in 23 of 135 (17.0%) normalized during the study, while levels in 10 of 86 (11.6%) with low C3 and levels in 20 of 98 (20.4%) with low C4 normalized. Overall, mean levels of anti-dsDNA antibodies decreased by 44.1% (n = 123) from baseline to study year 7 (Table 3), and mean C3 and C4 levels increased by 18.9% (n = 123) and 50.0% (n = 123), respectively.

Among the 36 patients with elevated baseline proteinuria (>0.5 gm/24 hours), mean levels in 14 patients improved by 69.1% from baseline to the study year 7 midpoint. Normal levels were achieved by 11 of 34 of these patients (32.4%) at the study year 1 midpoint and by 9 of 14 of these patients (64.3%) at the study year 7 midpoint.

IgG levels decreased by 29.0% (n = 112) from baseline to study year 7. The median percentage change from baseline in CD20+ B cells was -83.22% (n = 107) at the study year 7 midpoint (Table 3). Reductions were also observed for CD19+, naive, activated, plasma, SLE subset, and plasmacytoid B cells. The median percentage change from baseline in memory B cells was 87.65% (n = 244) at the study year 1 midpoint and -67.18% (n = 106) at the study year 7 midpoint. Although variable over time, the median percentage change from baseline in short-lived plasma B cells was -47.50% (n = 114) at the study year 7 midpoint.

DISCUSSION

Long-term treatment with belimumab was associated with a stable or decreased incidence of AEs and sustained efficacy across 7 study years of exposure, similar to the safety and efficacy profiles of belimumab

Table 3. Biomarkers observed at baseline and change from baseline (modified intent-to-treat population)*

Biomarker	Observed value at baseline	Study year 1 midpoint (observed)	Study year 1 midpoint (% change from baseline)	Study year 7 midpoint (observed)	Study year 7 midpoint (% change from baseline)
Anti-dsDNA, IU/ml	88.10 ± 73.565/268	78.53 ± 67.774/253	-7.61 ± 19.068/253	78.50 ± 292.110/123	-44.07 ± 148.281/123
Complement level, gm/liter					
C3	1.068 ± 0.310/268	1.103 ± 0.296/253	6.74 ± 26.443/253	1.226 ± 0.311/123	18.90 ± 30.975/123
C4	0.198 ± 0.099/268	0.220 ± 0.101/253	19.82 ± 38.678/253	0.250 ± 0.101/123	49.96 ± 96.800/123
Proteinuria level, gm/24 hours					
All patients	0.31 ± 0.561/268	0.28 ± 0.666/251	10.44 ± 84.097/251	0.15 ± 0.170/120	-11.26 ± 75.237/120
Patients with >0.5 gm/24 hours at baseline	1.36 ± 1.013/36	1.17 ± 1.534/34	-17.51 ± 81.675/34	0.41 ± 0.368/14	-69.09 ± 25.846/14
IgG, gm/liter	15.16 ± 6.062/268	12.93 ± 4.704/252	-12.80 ± 14.078/252	10.09 ± 3.745/112†	-28.97 ± 16.733/112†
B cells/μl					
CD19+	114.00 (58.00, 191.00)/265	69.00 (36.00, 113.00)/253	-32.56 (-57.58, 5.88)/250	18.50 (8.00, 34.00)/122	-82.73 (-89.01, -68.73)/120
CD20+	112.50 (55.00, 189.00)/262	68.00 (35.00, 113.00)/251	-31.82 (-56.40, 9.15)/245	20.00 (10.00, 36.00)/111	-83.22 (-89.24, -69.05)/107
Naive (CD20+CD27-)	88.00 (38.00, 155.00)/262	36.00 (16.00, 64.00)/251	-55.56 (-73.74, -29.41)/245	13.00 (6.00, 24.00)/111	-87.39 (-92.77, -73.53)/107
Activated (CD20+CD69+)	190.00 (106.00, 320.00)/257	131.00 (72.00, 206.00)/247	-33.35 (-65.19, 36.11)/240	3.00 (1.00, 5.00)/122	-98.85 (-99.62, -96.45)/116
Memory (CD20+CD27+)	17.00 (8.00, 28.00)/262	30.00 (14.00, 55.00)/251	87.65 (27.43, 167.54)/244	6.00 (3.00, 12.00)/111	-67.18 (-80.00, -47.06)/106
Plasma (CD20-CD138+)	41.00 (17.00, 128.00)/261	31.00 (12.00, 69.00)/251	-37.20 (-66.75, 27.50)/244	4.50 (1.00, 11.00)/122	-92.31 (-98.05, -73.68)/118
SLE subset (CD19+CD27 ^{bright} CD38 ^{bright})	17.00 (6.00, 45.00)/262	13.00 (6.00, 34.00)/251	-16.13 (-71.43, 88.89)/243	9.00 (3.00, 25.00)/122	-50.00 (-81.44, 28.57)/117
Short-lived plasma (CD19+CD20-CD27 ^{high+})	16.00 (7.00, 46.00)/258	13.00 (5.00, 32.00)/247	-32.29 (-73.13, 61.54)/238	9.00 (4.00, 24.00)/122	-47.50 (-79.17, 41.67)/114
Plasmacytoid (CD20+CD138+)	95.00 (58.00, 182.00)/261	64.00 (31.00, 108.00)/251	-32.49 (-73.33, 32.00)/243	2.00 (1.00, 5.00)/122	-98.00 (-99.61, -94.22)/117

* Values are the mean ± SD/number of patients or median (interquartile range)/number of patients. Anti-dsDNA = anti-double-stranded DNA; SLE = systemic lupus erythematosus.

† Study year 7 end.

previously established during studies of patients with SLE (12–14,22). In the present study, three-fourths of patients were SRI responders at the study year 7 midpoint, an observation that is consistent with the phase II continuation study, in which 65% of patients had achieved an SRI response by study year 7 (73% in the completer analysis) (12).

Secondary analyses of the BLISS studies have shown that patients treated with belimumab (plus standard therapy) experienced reduced rates of severe flares when compared with those receiving placebo (plus standard therapy) (13,14). In the BLISS-52 and BLISS-76 studies, rates of severe SFI flare were 14% (40 of 290 patients) and 21% (56 of 273 patients), respectively (13,14), among patients who received 10 mg/kg belimumab. In this continuation study, the percentage of patients experiencing a new severe SFI flare between the study year 1 and study year 7 midpoints was low; the cumulative count increased from 15 of 267 patients (5.6%) to 55 of 267 patients (20.6%) during this period. In the phase II continuation study, the percentages of severe flares were also low, decreasing from 7% to 2% across each year of belimumab treatment (12).

Organ damage accrual in this continuation study was low when compared with prospective SLE inception cohorts measuring damage accrual (23–25), with a mean increase in SDI of 0.4 over 7 study years. However, while observational cohorts included the full spectrum of patients, the BLISS studies excluded patients with severe lupus nephritis and central nervous system disease (13,14), manifestations that may result in higher rates of damage accrual (26,27). These exclusions, in addition to treatment with belimumab, could account, in part, for the reported lower rates of organ damage.

One of the major goals of SLE therapy is to reduce corticosteroid exposure (28). In the current study, mean prednisone dose decreased over time, and approximately one-eighth of patients were able to discontinue prednisone.

Quantitative analysis of B cell phenotypes performed in this study represents the first evaluation of long-term changes in B cells in response to belimumab treatment. The results presented are consistent with those of a small 2-year study that investigated the effects of belimumab treatment on levels of B cell subsets (29). Over the duration of the study, there was a decrease in levels for the majority of B cell subsets, but no subsets were completely depleted. As demonstrated in that earlier study (29), memory B cells were initially found to increase in response to belimumab, while a decrease was seen after study year 1.

There are several limitations to the interpretation of these data, primarily the open-label design with no

placebo control group. In addition, selection bias could have been responsible for enriching the study population with patients more likely to respond well to treatment over time. Furthermore, approximately one-third of the study population was treated with placebo during the parent study. Since these patients continued to receive placebo (and standard therapy) for 76 weeks before entering this extension study, they may have entered this extension study with more benign disease (32% of patients in the placebo arm withdrew from the parent study). However, the post hoc analysis did not indicate an imbalance in SLE disease activity or characteristics at baseline between those who withdrew over the course of the study and those who completed. In addition, the decline in the number of patients starting each yearly interval was similar between patients initially treated with belimumab in the parent study and those treated with placebo. Withdrawals from the study were more prevalent among nonresponders, although the reasons for withdrawal among nonresponders cannot be confirmed. The impact of the withdrawals may have created responder bias by affecting the composition of the remaining study population.

Although the duration of treatment with belimumab 10 mg/kg differed (depending on initial treatment assignment), all treatment groups were pooled for analysis. In addition, low numbers of patients for some analyses, particularly at later time points, may confound interpretation. Data on AEs of special interest, particularly rates of infection, should be interpreted with caution, as fewer patients contributed to the denominator in later intervals.

This study demonstrates the long-term benefits of belimumab in addition to standard therapy in patients with active SLE. Belimumab was well tolerated, and patients benefited from an overall decrease in disease activity. Moreover, prednisone use declined, and accrual of organ damage was low.

ACKNOWLEDGMENTS

We thank Nicole Cash, MRes, PhD and Emma Hargreaves (Fishawack Indicia Ltd., UK) for medical writing assistance funded by GlaxoSmithKline.

AUTHOR CONTRIBUTIONS

All authors were involved in drafting the article or revising it critically for important intellectual content, and all authors approved the final version to be published. Dr. Furie had full access to all of the data in the study and takes responsibility for the integrity of the data and the accuracy of the data analysis.

Study conception and design. Furie, Fettiplace, Roth, Gordon.

Acquisition of data. Furie, Wallace, Aranow.

Analysis and interpretation of data. Furie, Wallace, Aranow, Fettiplace, Wilson, Mistry, Roth, Gordon.

ROLE OF THE STUDY SPONSOR

GlaxoSmithKline was involved in designing the study, contributed to the collection, analysis, and interpretation of the data, supported the authors in the development of the manuscript, and funded the medical writing assistance provided by Fishawack Indicia Ltd. All authors, including those employed by GlaxoSmithKline, approved the content of the submitted manuscript and were involved in the decision and to submit the manuscript for publication.

REFERENCES

- Kyrtaris VC. Systemic lupus erythematosus: from genes to organ damage. *Methods Mol Biol* 2010;662:265–83.
- Zhu TY, Tam LS, Lee VW, Lee KK, Li EK. Relationship between flare and health-related quality of life in patients with systemic lupus erythematosus. *J Rheumatol* 2010;37:568–73.
- Zheng Y, Ye DQ, Pan HF, Li WX, Li LH, Li J, et al. Influence of social support on health-related quality of life in patients with systemic lupus erythematosus. *Clin Rheumatol* 2009;28:265–9.
- Fernandez D, Kirou KA. What causes lupus flares? *Curr Rheumatol Rep* 2016;18:1–10.
- Stoll T, Sutcliffe N, Mach J, Klaghofer R, Isenberg DA. Analysis of the relationship between disease activity and damage in patients with systemic lupus erythematosus: a 5-yr prospective study. *Rheumatology (Oxford)* 2004;43:1039–44.
- Zonana-Nacach A, Barr SG, Magder LS, Petri M. Damage in systemic lupus erythematosus and its association with corticosteroids. *Arthritis Rheum* 2000;43:1801–8.
- Oglesby A, Shaul AJ, Pokora T, Paramore C, Cragin L, Dennis G, et al. Adverse event burden, resource use, and costs associated with immunosuppressant medications for the treatment of systemic lupus erythematosus: a systematic literature review. *Int J Rheumatol* 2013;2013:347520.
- Al Sawah S, Zhang X, Zhu B, Magder LS, Foster SA, Iikuni N, et al. Effect of corticosteroid use by dose on the risk of developing organ damage over time in systemic lupus erythematosus: the Hopkins Lupus Cohort. *Lupus Sci Med* 2015;2:e000066.
- Yildirim-Toruner C, Diamond B. Current and novel therapeutics in treatment of SLE. *J Allergy Clin Immunol* 2011;127:303–14.
- Baker KP, Edwards BM, Main SH, Choi GH, Wager RE, Halpern WG, et al. Generation and characterization of LymphoStat-B, a human monoclonal antibody that antagonizes the bioactivities of B lymphocyte stimulator. *Arthritis Rheum* 2003;48:3253–65.
- Wallace DJ, Stohl W, Furie RA, Lisse JR, McKay JD, Merrill JT, et al. A phase II, randomized, double-blind, placebo-controlled, dose-ranging study of belimumab in patients with active systemic lupus erythematosus. *Arthritis Rheum* 2009;61:1168–78.
- Ginzler EM, Wallace DJ, Merrill JT, Furie RA, Stohl W, Chatham WW, et al. Disease control and safety of belimumab plus standard therapy over 7 years in patients with systemic lupus erythematosus. *J Rheumatol* 2014;41:300–9.
- Navarra SV, Guzman RM, Gallacher AE, Hall S, Levy RA, Jimenez RE, et al. Efficacy and safety of belimumab in patients with active systemic lupus erythematosus: a randomised, placebo-controlled, phase 3 trial. *Lancet* 2011;377:721–31.
- Furie R, Petri M, Zamani O, Cervera R, Wallace DJ, Tegzová D, et al. A phase III, randomized, placebo-controlled study of belimumab, a monoclonal antibody that inhibits B lymphocyte stimulator, in patients with systemic lupus erythematosus. *Arthritis Rheum* 2011;63:3918–30.
- Bruce IN, Urowitz M, van Vollenhoven R, Aranow C, Fettiplace J, Oldham M, et al. Long-term organ damage accrual and safety in patients with SLE treated with belimumab plus standard of care. *Lupus* 2016;25:699–709.
- World Medical Journal. WMA Declaration of Helsinki: ethical principles for medical research involving human subjects. 2013. URL: <https://www.wma.net/policies-post/wma-declaration-of-helsinki-ethical-principles-for-medical-research-involving-human-subjects/>.
- Gladman DD, Goldsmith CH, Urowitz MB, Bacon P, Fortin P, Ginzler E, et al. The Systemic Lupus International Collaborating Clinics/American College of Rheumatology (SLICC/ACR) damage index for systemic lupus erythematosus international comparison. *J Rheumatol* 2000;27:373–6.
- Furie RA, Petri MA, Wallace DJ, Ginzler EM, Merrill JT, Stohl W, et al. Novel evidence-based systemic lupus erythematosus responder index. *Arthritis Care Res (Hoboken)* 2009;61:1143–51.
- Petri M, Kim MY, Kalunian KC, Grossman J, Hahn BH, Sammaritano LR, et al, for the OC-SELENA Trial. Combined oral contraceptives in women with systemic lupus erythematosus. *N Engl J Med* 2005;353:2550–8.
- Symmons DP, Coppock JS, Bacon PA, Bresnihan B, Isenberg DA, Maddison P, et al, and Members of the British Isles Lupus Assessment Group (BILAG). Development and assessment of a computerized index of clinical disease activity in systemic lupus erythematosus. *Q J Med* 1988;69:927–37.
- Petri M, Buyon J, Kim M. Classification and definition of major flares in SLE clinical trials. *Lupus* 1999;8:685–91.
- Wallace D, Navarra S, Petri M, Gallacher A, Thomas M, Furie R, et al. Safety profile of belimumab: pooled data from placebo-controlled phase 2 and 3 studies in patients with systemic lupus erythematosus. *Lupus* 2013;22:144–54.
- Bruce IN, O’Keeffe AG, Farewell V, Hanly JG, Manzi S, Su L, et al. Factors associated with damage accrual in patients with systemic lupus erythematosus: results from the Systemic Lupus International Collaborating Clinics (SLICC) Inception cohort. *Ann Rheum Dis* 2014;74:1706–13.
- Becker-Merok A, Nossent HC. Damage accumulation in systemic lupus erythematosus and its relation to disease activity and mortality. *J Rheumatol* 2006;33:1570–7.
- Alarcón GS, Roseman JM, McGwin G, Uribe A, Bastian HM, Fessler BJ, et al. Systemic lupus erythematosus in three ethnic groups. XX. Damage as a predictor of further damage. *Rheumatology (Oxford)* 2004;43:202–5.
- Yung S, Cheung KF, Zhang Q, Chan TM. Mediators of inflammation and their effect on resident renal cells: implications in lupus nephritis. *Clin Dev Immunol* 2013;2013:3176–82.
- Hanly JG, McCurdy G, Fougere L, Douglas JA, Thompson K. Neuropsychiatric events in systemic lupus erythematosus: attribution and clinical significance. *J Rheumatol* 2004;31:2156–62.
- European Medicines Association. Guideline on clinical investigation of medicinal products for the treatment of systemic lupus erythematosus, cutaneous lupus and lupus nephritis. 2013. URL: http://www.ema.europa.eu/ema/doc_index.jsp?curl=pages/includes/document/document_detail.jsp?webContentId=WC500139615&url=menus/document_library/document_library.jsp&mid=0b01ac058009a3dc.
- Jacobi AM, Huang W, Wang T, Freimuth W, Sanz I, Furie R, et al. Effect of long-term belimumab treatment on B cells in systemic lupus erythematosus: extension of a phase II, double-blind, placebo-controlled, dose-ranging study. *Arthritis Rheum* 2010;62:201–10.

Twin DNA Methylation Profiling Reveals Flare-Dependent Interferon Signature and B Cell Promoter Hypermethylation in Systemic Lupus Erythematosus

Constance J. Ulf-Møller ¹, Fazila Asmar,² Yi Liu,³ Anders J. Svendsen ⁴, Florence Busato,³ Kirsten Grønbaek,⁵ Jörg Tost ³ and Søren Jacobsen ⁵

Objective. Systemic lupus erythematosus (SLE) has limited monozygotic twin concordance, implying a role for pathogenic factors other than genetic variation, such as epigenetic changes. Using the disease-discordant twin model, we investigated genome-wide DNA methylation changes in sorted CD4⁺ T cells, monocytes, granulocytes, and B cells in twin pairs with at least 1 SLE-affected twin.

Methods. Peripheral blood obtained from 15 SLE-affected twin pairs (6 monozygotic and 9 dizygotic) was processed using density-gradient centrifugation for the granulocyte fraction. CD4⁺ T cells, monocytes, and B cells were further isolated using magnetic beads. Genome-wide DNA methylation was analyzed using Infinium HumanMethylation450K BeadChips. When comparing probes from SLE-affected twins and co-twins, differential DNA methylation was considered statistically significant when the *P* value was less than 0.01 and biologically relevant when the median DNA methylation difference was >7%. Findings were validated by

pyrosequencing and replicated in an independent case-control sample.

Results. In paired analyses of twins discordant for SLE restricted to the gene promoter and start region, we identified 55, 327, 247, and 1,628 genes with differentially methylated CpGs in CD4⁺ T cells, monocytes, granulocytes, and B cells, respectively. All cell types displayed marked hypomethylation in interferon-regulated genes, such as *IFI44L*, *PARP9*, and *IFITM1*, which was more pronounced in twins who experienced a disease flare within the past 2 years. In contrast to what was observed in the other cell types, differentially methylated CpGs in B cells were predominantly hypermethylated, and the most important upstream regulators included *TNF* and *EP300*.

Conclusion. Hypomethylation of interferon-regulated genes occurs in all major cellular compartments in SLE-affected twins. The observed B cell promoter hypermethylation is a novel finding with potential significance in SLE pathogenesis.

Supported by the Danish Rheumatism Association (grants R123-A3159 and R97-A1028) and the A. P. Møller Foundation (grant 14-447). Dr. Ulf-Møller's work was supported by the Rigshospitalets Research Foundation. Dr. Asmar's work was supported by the Independent Research Fund (Denmark). Dr. Grønbaek's work was supported by the Novo Nordic Foundation.

¹Constance J. Ulf-Møller, MD, PhD: Rigshospitalet and University of Copenhagen, Copenhagen, Denmark, and Commissariat à l'énergie atomique et aux énergies alternatives, Institut de Biologie François Jacob, Evry, France; ²Fazila Asmar, MD, PhD: Rigshospitalet, Copenhagen, Denmark; ³Yi Liu, PhD, Florence Busato, MSc, Jörg Tost, PhD: Commissariat à l'énergie atomique et aux énergies alternatives, Institut de Biologie François Jacob, Evry, France; ⁴Anders J. Svendsen, MD, PhD: University of Southern Denmark, Odense, Denmark; ⁵Kirsten Grønbaek, MD, DMSci, Søren Jacobsen, MD, DMSci: Rigshospitalet and University of Copenhagen, Copenhagen, Denmark.

Drs. Tost and Jacobsen contributed equally to this work.

Address correspondence to Constance J. Ulf-Møller, MD, PhD, Copenhagen Lupus and Vasculitis Clinic, Centre for Rheumatology and Spine Diseases, Rigshospitalet, Blegdamsvej 9, DK-2100 Copenhagen, Denmark. E-mail: CJU@dadlnet.dk.

Submitted for publication March 8, 2017; accepted in revised form January 17, 2018.

Systemic lupus erythematosus (SLE) is a multisystem autoimmune disease characterized by its protean nature, relapsing–remitting clinical course, and autoantibody production. Genetic factors account for 44–66% of the phenotypic variation (1–3), and genome-wide association studies have identified >50 susceptibility genes involved in SLE, which may explain up to 28% of the heritability (4). However, studies in SLE-affected twins show only limited twin concordance (~14%) in monozygotic (MZ) twins and 4.4% in dizygotic (DZ) twins (5). Although complete MZ concordance would indicate a dominantly inherited disease with high penetrance, lower concordance suggests the involvement of other pathogenic factors, which might explain phenotypic differences. In recent years, research has focused on the involvement of epigenetic mechanisms, such as DNA methylation, which regulate gene expression by altering the transcriptional accessibility of gene

regulatory regions (6), in the development of autoimmune diseases.

One early large-scale candidate study comparing 5 MZ twins discordant for SLE identified 49 differentially methylated genes in white blood cells and provided the first indication that interferon (IFN)-regulated genes, such as *CD9*, *IFGMR2*, and *AIM2*, are differentially methylated in SLE (7). Later case-control epigenome-wide association studies (EWAS) using 27K and 450K BeadChips showed pronounced DNA methylation changes in type I IFN-regulated genes in CD4+ T cells and naive CD4+ T cells (8–10).

Only 2 EWAS have investigated other cell types and confirmed the presence of cell type-independent DNA methylation changes in IFN-regulated genes in monocytes, B cells (8), and granulocytes (11), but these changes have not been thoroughly investigated. The comparison of discordant twins constitutes a powerful study design for investigating epigenetic alterations, because genetic differences can be ruled out in the case of identical twins, while fraternal twins share, on average, 50% of their genetic variation. This may allow for better discerning between genetic and epigenetic determinants in SLE pathogenesis (12). Selecting the cellular focus in EWAS is essential, because DNA methylation patterns may vary between cell populations (8,13). Given the complex pathogenesis of SLE (14), it is important to study DNA methylation differences between various immune cell subsets, which might help reveal complementary parts of the disease mechanisms.

In the current study, we make use of a well-defined SLE twin cohort (5) to investigate genome-wide DNA methylation changes in SLE-affected twins and their co-twins in all major cellular compartments: CD4+ T cells, monocytes, granulocytes, and B cells. We observed that promoter hypomethylation of IFN-regulated genes, which previously was observed primarily in CD4+ T cells, was pronounced in all cell types studied. There was additional promoter hypermethylation in B cells, which may be of interest for future studies.

PATIENTS AND METHODS

Twin recruitment. All living Danish twins with an SLE diagnosis in the National Patient Register (15) were identified in the Danish Twin Registry (16) using the unique identification number assigned to all Danish residents in the Civil Registration System (17), as previously described (5). The following 15 twin pairs were included: 6 MZ, 6 same-sex dizygotic (DZss), and 3 opposite-sex dizygotic (DZos) (Table 1). Seven of the twins were male (2 MZ, 2 DZss, and 3 DZos). The mean age of the twins at the time of recruitment was 41.1 years (range 23–67 years). Medical records were consulted for information on SLE or other diagnoses, clinical manifestations, medical history, and time since

last disease flare. Seventeen twin individuals fulfilled ≥ 4 American College of Rheumatology classification criteria for SLE (18), including 1 MZ and 1 DZss SLE-concordant twin pairs. Four co-twins were affected by other autoimmune diseases (Table 1). Disease activity was evaluated using the SLE Disease Activity Index 2000 (SLEDAI-2K) (19). Disease flare was defined as a SLEDAI score ≥ 4 . The project was approved by the Danish Scientific Ethics Committee (journal no. H-1-2014-079) and the Danish Data Inspection Board (journal no. 30-1245). Written informed consent was obtained from all study participants.

Blood preparation, cell isolation, and DNA/RNA extraction. On the same day as sampling, 50 ml of peripheral blood in EDTA was processed using density-gradient centrifugation (Ficoll-Paque Plus; GE Healthcare), and the granulocyte fraction was stored at -80°C . Serial cell sorting was performed on the mononuclear cell fraction, using a RoboSep device (StemCell Technologies) with CD14-positive selection, then CD4-positive selection, and finally B cell enrichment. Cell purity was assessed using the following antibodies: allophycocyanin (APC)-conjugated surface membrane CD3, phycoerythrin (PE)-conjugated CD4, fluorescein isothiocyanate-conjugated CD8, APC-H7-conjugated CD14, V450-C-conjugated CD45 (BD Biosciences), and PE-Cy7-conjugated CD19 (Beckman Coulter), and analyzed using a BD FACSCanto II flow cytometer (BD Biosciences) after overnight fixation with 1% paraformaldehyde. The purity of the granulocyte fraction was $>80\%$. The mean purity of CD14+ monocytes, CD4+ T cells, and CD19+ B cells was 90%, 91%, and 97%, respectively. DNA and RNA were extracted using an AllPrep DNA/RNA/miRNA Universal Kit (Qiagen) and quantified using a NanoDrop 2000 spectrophotometer and a Quant-iT dsDNA Broad-Range Assay Kit (Thermo Fisher Scientific) according to the instructions of the manufacturer. DNA quality control was performed by analyzing DNA size on an agarose gel and polymerase chain reaction amplification of 2 microsatellite markers for sex verification.

DNA methylation analyses using BeadChips and pyrosequencing. Genome-wide DNA methylation patterns were analyzed using an Infinium HumanMethylation450K BeadChip (Illumina), which interrogates DNA methylation on $>480,000$ CpG sites, as previously described (20). Normalized and raw data are available at GEO (GEO accession no. GSE110607). Samples were randomized on the BeadChips to avoid batch effect confounding with phenotypic parameters. Bisulfite treatment was performed on 1 μg of DNA using an EpiTect Fast DNA Bisulfite kit (Qiagen). DNA methylation changes were validated by pyrosequencing, which is a quantitative high-resolution technique yielding DNA methylation profiles at single-nucleotide resolution (21).

Statistical analysis. Raw data from the BeadChips were extracted using Genome Studio (V.2011.1; Illumina) and normalized using the subset quantile normalization pipeline stratified by cell type (22). CpG sites that did not fulfill the following criteria were excluded from further analysis: *P* value for signal detection <0.01 , detection *P* value threshold of $>90\%$, no single-nucleotide polymorphisms with a frequency of $>5\%$ (European population in the 1000 Genomes Project [23]) within 50 bp of the probe, and ≥ 3 successful beads per probe. Nonspecific probes were excluded from further analysis (24). In the primary analyses, sex chromosomes were filtered out during normalization. Beta values were calculated as the ratio between the signal intensity of methylated CpG sites and the total signal intensity on a scale of 0 to 1.

Table 1. Characteristics of the twin pairs*

Twin ID	Zygoty	Age, years	Sex	Diagnosis	No. of ACR criteria	SLEDAI score	ANA	Anti-DNA	Current medication
1a	DZss	67	F	SLE	5	0	+	-	HCO
1b	DZss	67	F	None	0	0	-	-	None
2a	DZss	62	F	SLE	5	0	+	-	None
2b	DZss	62	F	None	2	2	+	+	None
3a	MZ	58	M	None	2	2	+	+	None
3b	MZ	58	M	SLE	5	2	+	+	HCO, MTX, pred.
4a	MZ	55	F	Autoimmune thyroiditis	2	2	+	+	None
4b	MZ	55	F	SLE	8	0	+	-	HCO, pred.
5a	MZ	52	F	SSc, SS, primary biliary cirrhosis	1	0	+	-	None
5b	MZ	52	F	SLE	5	0	+	-	None
6a	DZss	49	F	Autoimmune thyroiditis	1	2	+	-	None
6b	DZss	49	F	SLE	4	2	+	+	HCO
7a	DZos	46	M	None	2	2	+	+	None
7b	DZos	46	F	SLE	8	4	+	+	Pred.
8a	DZos	45	F	SLE	6	4	+	+	MMF
8b	DZos	45	M	Multiple sclerosis	1	0	+	-	DMF
9a	MZ	40	F	SLE	6	0	+	-	HCO
9b	MZ	40	F	None	1	0	+	-	None
10a	MZ	39	F	SLE	7	2	+	-	None
10b	MZ	39	F	SLE	5	2	+	-	HCO
11a	DZss	34	F	SLE	6	4	+	-	MMF, pred.
11b	DZss	34	F	None	0	0	-	-	None
12a	DZss	31	M	None	1	0	-	-	None
12b	DZss	31	M	SLE	5	2	+	+	None
13a	DZos	27	F	SLE	4	0	+	-	AZA, HCO
13b	DZos	27	M	None	0	0	-	-	None
14a	MZ	24	F	SLE	8	5	+	+	HCO, pred.
14b	MZ	24	F	None	1	0	+	-	None
15a	DZss	23	F	SLE	6	2	+	-	HCO, MTX
15b	DZss	23	F	SLE	6	2	+	-	AZA, HCO

* ACR = American College of Rheumatology; SLEDAI = Systemic Lupus Erythematosus (SLE) Disease Activity Index; ANA = antinuclear antibody; DZss = same-sex dizygotic; HCO = hydroxychloroquine; MZ = monozygotic; MTX = methotrexate; pred. = prednisolone; SSc = systemic sclerosis; SS = Sjögren's syndrome; DZos = opposite-sex dizygotic; MMF = mycophenolate mofetil; DMF = dimethyl fumarate; AZA = azathioprine.

Paired analyses of discordant twins ($n = 13$ twin pairs) were performed using the nonparametric Wilcoxon signed rank test. P values less than 0.01 were considered significant, and median differential methylation of $>7\%$ was considered biologically relevant. Subsequently, we restricted the analyses to probes located in the gene promoter and start regions (TSS200, TSS1500, and the 5'-untranslated region [5'-UTR] according to the HumanMethylation450K BeadChip annotation file). Differential methylation of known epigenetic regulators in the promoter/start region in discordant twins was identified using a gene list derived from the EpiFactors database (25).

In paired subset analyses restricted to the promoter/start region, we further compared twins with recent disease flare (<2 years since the last flare; $n = 9$ SLE-affected twins) with twins in clinical remission (while receiving or not receiving treatment) for ≥ 2 years ($n = 8$ SLE-affected twins). Unpaired subset analyses in MZ twins were performed using a Mann-Whitney U test ($n = 6$ twin pairs). In both subset analyses, the significance level was set to $P < 0.05$ and a differential methylation level of $>7\%$, due to the low sample number. For subset analyses of female twins only, the normalization process was repeated including the sex chromosomes in order to examine DNA methylation changes on the X chromosome, using $P < 0.001$ by Mann-Whitney U test and median differential methylation levels of $>7\%$ to determine statistical significance ($n = 23$ twin individuals).

A permutation test was performed in anti-DNA-positive ($n = 6$) versus anti-DNA negative twins with SLE ($n = 11$) and

in all anti-DNA positive ($n = 10$) versus anti-DNA-negative individuals ($n = 20$), using 10,000 permutations. In an additional analysis, we used the iEVORA algorithm to test for increased epigenetic variability by identifying the most variable CpGs between SLE-affected twins and co-twins or healthy co-twins and re-ranking the most differentially variable CpG according to DNA methylation T statistics (26). A false discovery rate of <0.001 for differentially variable values and an unadjusted P value of 0.05 for the DNA methylation values were considered statistically significant.

Pyrosequencing data were analyzed using the Wilcoxon signed rank test, in which $P < 0.05$ defined statistical significance. Gene lists for differentially methylated genes in the promoter/start region with ≥ 1 differentially methylated probe in the primary paired analyses were submitted to Ingenuity Pathway Analysis (Qiagen), which was used to identify upstream regulators ($P < 0.001$ by Fisher's exact test) and enriched biologic terms and canonical pathways (statistical significance defined as a Benjamini-Hochberg-corrected P value of <0.05). The same gene lists were used to identify IFN-regulated genes in the Interferome database (interferome.org) (27). All statistical analyses were conducted using the computing environment R (V.3.3.1; r-project.org).

Validation using an independent SLE case-control sample. In order to replicate selected results observed in the twin sample, peripheral blood from 20 SLE patients (mean \pm SD SLEDAI score 13.5 ± 4.7) and 20 healthy controls was

sorted into granulocytes, CD19+ B cells, CD14+ monocytes, and CD4+ T cells and analyzed by pyrosequencing. Unpaired analyses were performed using a Mann-Whitney U test, with *P* values less than 0.05 defining statistical significance.

RESULTS

Differential methylation in SLE-discordant twins.

First, we examined genome-wide DNA methylation patterns according to cell type in 13 SLE-discordant twin pairs to determine cell type-specific differences. We then investigated DNA methylation changes within the promoter/start region of each gene, which are more likely to have a functional impact on gene expression.

In CD4+ T cells, 176 probes were differentially methylated in twins discordant for SLE, distributed across 48 probes not associated with a gene and 115 genes (Figure 1A; see also Supplementary Data, available on the *Arthritis & Rheumatology* web site at <http://onlinelibrary.wiley.com/doi/10.1002/art.40422/abstract>). These were located in the promoter/start region of 55 genes, with 39

genes showing hypomethylation (71%) and 16 showing hypermethylation (29%) (Supplementary Table 1A, available on the *Arthritis & Rheumatology* web site at <http://onlinelibrary.wiley.com/doi/10.1002/art.40422/abstract>). Only 9 genes had ≥ 2 differentially methylated probes in the promoter/start region (7 hypomethylated and 2 hypermethylated) (Table 2).

In monocytes, 510 probes distributed across 160 probes not associated with a gene and 327 genes were differentially methylated in SLE-discordant twins (Figure 1B; see also Supplementary Data). In the promoter/start region, 136 genes were differentially methylated, of which 53 were hypomethylated (39%) and 83 were hypermethylated (61%) (see Supplementary Table 1B). Six genes had ≥ 2 differentially methylated probes in the promoter/start region, 4 of which were hypomethylated and 2 of which were hypermethylated (Table 2).

In granulocytes, 393 probes distributed across 123 probes not associated with a gene and 247 genes were differentially methylated in SLE-discordant twins

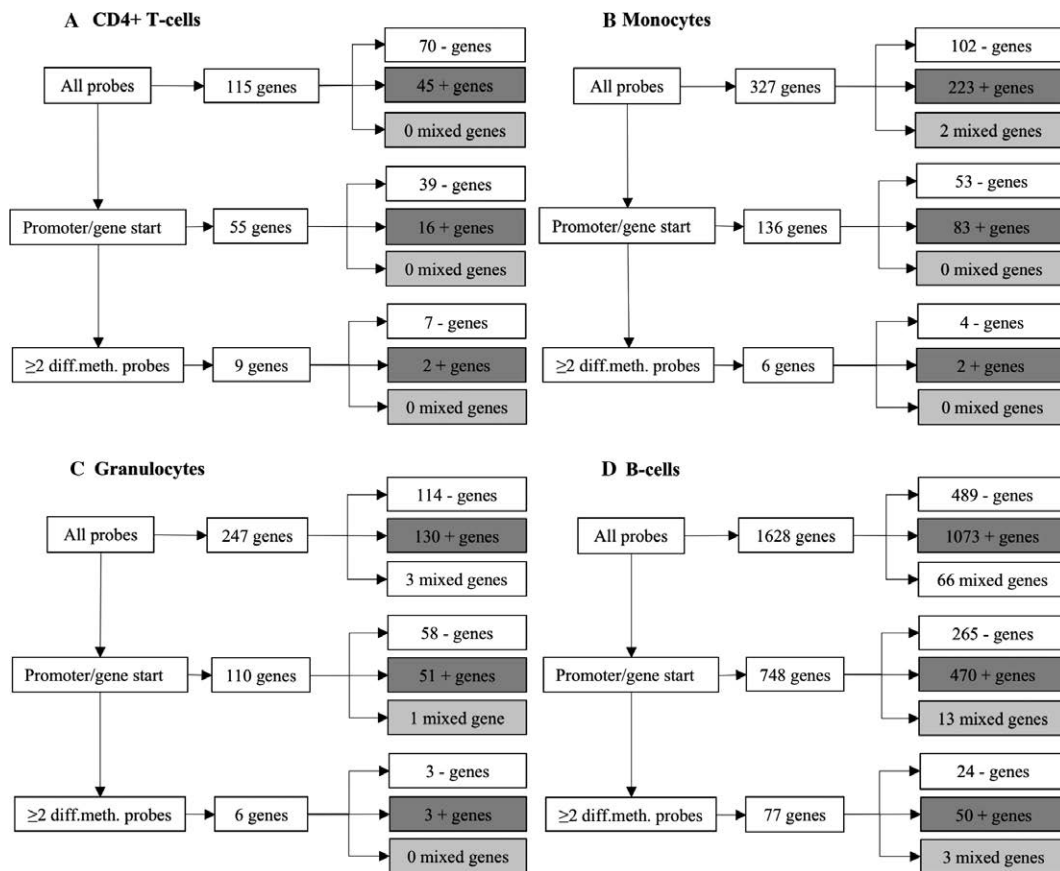


Figure 1. Numbers of differentially methylated (diff.meth.) genes in 13 twin pairs discordant for systemic lupus erythematosus, according to cell type. **A**, CD4+ T cells. **B**, Monocytes. **C**, Granulocytes. **D**, B cells. Paired analyses were performed using the nonparametric Wilcoxon signed rank test. *P* values less than 0.01 were considered significant, and median differential methylation of >7% was considered biologically relevant. Plus symbols represent hypermethylation; minus symbols represent hypomethylation.

Table 2. Top differentially methylated genes with ≥ 2 differentially methylated probes in the promoter/start region in 13 twin pairs discordant for systemic lupus erythematosus, by the indicated cell type*

Gene ID	No. of CpG sites	$\Delta\beta$	CpG sites	Gene ID	No. of CpG sites	$\Delta\beta$	CpG sites
CD4+ T cells							
Hypomethylated							
<i>IFI44L</i>	5	-0.1549	cg17980508, cg03607951, cg05696877, cg06872964, cg00855901	<i>CALDI</i>	4	-0.1091	cg16253634, cg24956866, cg14009688, cg19679250
<i>DTX3L</i>	3	-0.2135	cg00959259, cg08122652, cg22930808	<i>IFITM1</i>	3	-0.1036	cg27032101, cg01971407, cg22963452
<i>EIF2AK2</i>	3	-0.1056	cg14126601, cg17326313, cg245223650	<i>LOXL1</i>	3	-0.0831	cg07317017, cg04436755, cg00028013
<i>PARP9</i>	3	-0.2135	cg00959259, cg08122652, cg22930808	<i>RSAD2</i>	2	-0.1653	cg10549986, cg010959651
<i>LGALS3BP</i>	2	-0.1014	cg18749404, cg22713958	<i>H0XB6</i>	2	-0.1507	cg08832695, cg01324550
<i>NIN</i>	2	-0.0820	cg20033652, cg03048432	<i>LOC404266</i>	2	-0.1507	cg08832695, cg01324550
<i>TRIM2</i>	2	-0.2175	cg20027946, cg01022974	<i>CCDC144NL</i>	2	-0.1395	cg08288433, cg06809326
Hypomethylated				<i>PLSCR1</i>	2	-0.1362	cg06981309, cg27133310
<i>GTF2AIL</i>	2	0.1028	cg26162813, cg10067510	<i>IFI44L</i>	2	-0.1254	cg06872964, cg17980508
<i>STON1</i>	2	0.1028	cg26162813, cg10067510	<i>HLA-H</i>	2	-0.1139	cg24389386, cg17134700
Monocytes				<i>SPN</i>	2	-0.1124	cg26769927, cg08480068
Hypomethylated				<i>Hyper/hypomethylated</i>	2	-0.1117	cg22713958, cg25178683
<i>IFITM1</i>	5	-0.0904	cg20566897, cg09026253, cg27032101, cg01971407, cg10552523	<i>B3GALT4</i>	11	0.0881	cg03721978, cg03169472, cg23950233, cg17103217, cg21618521, cg03127244, cg06362282, cg00163549, cg19882268, cg27147350, cg13882090
<i>TACSTD2</i>	2	-0.1828	cg04863005, cg17210938	<i>DDR1</i>	7	0.1339	cg19215110, cg03270204, cg24727290, cg16707952, cg16537676, cg13329862, cg02695062
<i>LOXL1</i>	2	-0.1054	cg20652404, cg12594244	<i>TM4SF19</i>	4	0.1140	cg01883662, cg13314965, cg21845080, cg23250593
<i>ATP13A3</i>	2	-0.0989	cg15977148, cg10173291	<i>RUNX3</i>	3	0.1462	cg13461622, cg14425908, cg23916689
Hypomethylated				<i>SFTD3</i>	3	0.1267	cg20154206, cg24925163, cg14285788
<i>LIME1</i>	2	0.0771	cg12413156, cg00446123	<i>DLK1</i>	3	0.1025	cg16544010, cg09212014, cg18122767
<i>RUNX3</i>	2	0.0762	cg07801894, cg14425908	<i>CBFA2T3</i>	3	0.1005	cg04032292, cg06326865, cg26776806
Granulocytes				<i>RCAN2</i>	3	0.0944	cg06665622, cg04652496, cg00782811
Hypomethylated				<i>ABI3</i>	3	0.0940	cg26334023, cg17839611, cg25451120
<i>NW1</i>	4	-0.1003	cg19784428, cg19344626, cg20249566, cg15845821	<i>GNGT2</i>	3	0.0940	cg26334023, cg17839611, cg25451120
<i>IFITM1</i>	4	-0.0924	cg09026253, cg20566897, cg11694510, cg01971407	<i>RGSI3</i>	3	0.0873	cg24679007, cg07178206, cg18194426
<i>LOXL1</i>	3	-0.0977	cg02812767, cg12594244, cg00028013	<i>DTX1</i>	3	0.0836	cg18567954, cg01984511, cg02875120
Hypomethylated				<i>Hyper/hypomethylated</i>	1/2	0.0954/-0.1343	cg02948259/cg22764925, cg05543864
<i>CPSE4L</i>	2	0.1082	cg18772573, cg19393755	<i>FYN</i>	2/1	0.1101/-0.0749	cg05517541, cg20596647/cg05716821
<i>Clorf65</i>	2	0.0915	cg10441522, cg13684305	<i>HECW1</i>	2/1	0.14567/-0.0731	cg00514713, cg18477666/cg22007536
<i>B3GALT4</i>	2	0.0706	cg23950233, cg22878489				
B cells							
Hypomethylated							
<i>TACSTD2</i>	5	-0.1995	cg04863005, cg01821018, cg17210938, cg13443627, cg16699148				

* Purified CD4+ T cells, monocytes, granulocytes, and B cells were analyzed. *P* values were determined using the nonparametric Wilcoxon signed rank test. *P* values less than 0.01 were considered statistically significant, and a median DNA methylation difference $> 7\%$ ($\Delta\beta$) was considered biologically relevant. The full gene list is shown in Supplementary Data, available on the *Arthritis & Rheumatology* web site at <http://online.library.wiley.com/doi/10.1002/art.40422/abstract>.

(Figure 1C and Supplementary Data, available on the *Arthritis & Rheumatology* web site at <http://onlinelibrary.wiley.com/doi/10.1002/art.40422/abstract>). In the promoter/start region, 110 genes were differentially methylated: 58 were hypomethylated (53%), 51 were hypermethylated (46%), and 1 showed the concomitant presence of hypomethylated and hypermethylated probes (1%) (Supplementary Table 1C). Six genes had ≥ 2 differentially methylated probes in the promoter/start region, of which 3 were hypomethylated and 3 were hypermethylated (Table 2).

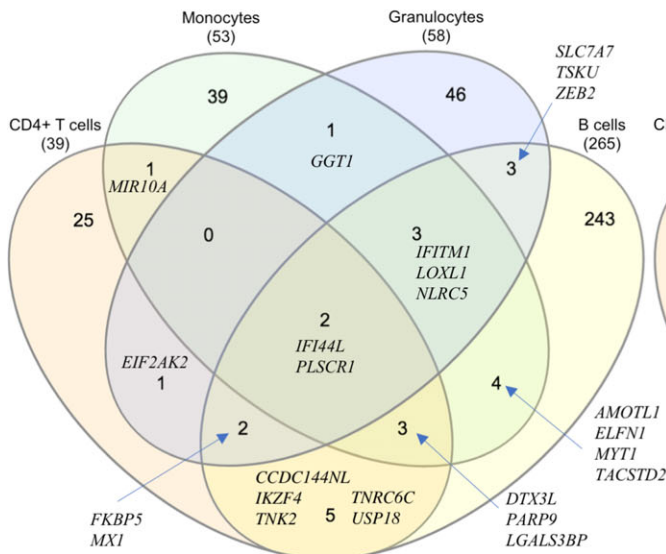
In B cells, 2,882 probes distributed across 987 probes not associated with a gene and 1,628 genes were differentially methylated in SLE-affected twins compared with co-twins (Figure 1D and Supplementary Data, available on the *Arthritis & Rheumatology* web site at <http://onlinelibrary.wiley.com/doi/10.1002/art.40422/abstract>). In the promoter/start region, 748 genes were differentially methylated, of which 265 were hypomethylated (35%), 470 were hypermethylated (63%), and 13 showed the presence of both hypomethylated and hypermethylated probes (2%) (see Supplementary Table 1D, <http://onlinelibrary.wiley.com/doi/10.1002/art.40422/abstract>). Altogether, ≥ 2 differentially methylated probes were

observed in 77 promoters, of which 24 were hypomethylated (31%), 50 were hypermethylated (65%), and 3 had both hypomethylated and hypermethylated probes (4%) (Table 2).

Next, we identified recurrent DNA methylation changes by investigating the degree of overlap between cell subsets, using gene lists from the primary analyses with ≥ 1 differentially methylated probe in the promoter/start region (see Supplementary Data, <http://onlinelibrary.wiley.com/doi/10.1002/art.40422/abstract>). *IFI44L* and *PLSCR1* were hypomethylated in all cell types. There was overlap between 3 cell types for *IFITM1*, *LOXL1*, and *NLRC5*, *DTX3L*, *PARP9*, and *LGALS3BP*, *FKBP5*, and *MX1* (Figure 2A). *B3GALT4* was hypermethylated in 3 cell types, while there was some overlap between hypermethylated genes in monocytes and B cells, e.g., *CBFA2T3* and *RUNX3* (Figure 2B).

IFN-regulated genes. To more thoroughly describe the expected IFN signature, we submitted gene lists from the primary paired analyses of probes located in the promoter/start region to the Interferome database (27). The proportions of differentially methylated IFN-regulated genes were 41.8%, 43.4%, 36.4%, and 35.8% in CD4+ T cells, monocytes, granulocytes, and B cells, respectively.

A Hypomethylated genes



B Hypermethylated genes

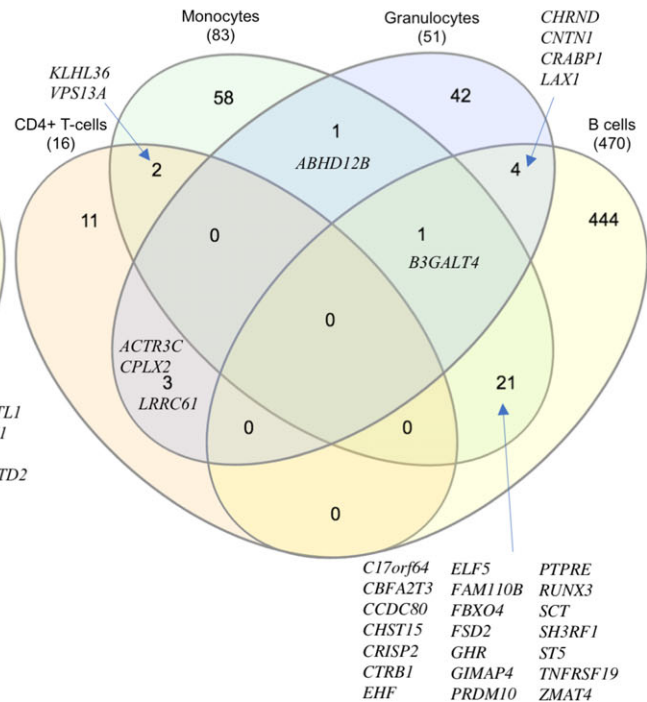


Figure 2. Overlap between CD4+ T cells, monocytes, granulocytes, and B cells for differentially methylated genes with ≥ 1 differentially methylated probe in the promoter/start region. **A**, Hypomethylated genes. **B**, Hypermethylated genes. Paired analyses were performed using the nonparametric Wilcoxon signed rank test. *P* values less than 0.01 were considered significant, and median differential methylation of $>7\%$ was considered biologically relevant.

There was some, but not complete, overlap between cell types, with 56.5%, 38.9%, 39.4%, and 12.6% of CD4+ T cells, monocytes, granulocytes, and B cells, respectively, sharing IFN-regulated genes with at least 1 other cell type.

Pyrosequencing. To validate results from the array-based analysis, 14 probes of interest were selected for

quantitative measurement of DNA methylation patterns at single-nucleotide resolution, by pyrosequencing (Table 3 and Supplementary Table 2, available at <http://onlinelibrary.wiley.com/doi/10.1002/art.40422/abstract>). We evaluated 5 IFN-regulated genes, *IFI44L*, *IFITM1*, *LGALS3BP*, *PARP9*, and *PLSCR1* (examined in all cell types), 3

Table 3. Median differential methylation by pyrosequencing (Δ Median) compared with median differential methylation by 450K array ($\Delta\beta$) in SLE-affected twins versus healthy co-twins, as well as median differential methylation by pyrosequencing in an independent sample of 20 SLE cases versus 20 healthy controls*

Gene	Cell type	Pyrosequencing		450K array†		Case-control sample	
		Δ Median, %	<i>P</i>	$\Delta\beta$	<i>P</i>	Δ Median, %	<i>P</i>
<i>CXCR5</i>	CD19B	6.57	0.017	6.82	0.0034	14.46	7.9×10^{-7}
<i>DDR1</i>	CD4T	3.24	0.142	0.74	0.0215		
<i>IFI44L amplicon 1</i>	CD19B	13.35	0.005	11.01	0.0002	16.97	1.6×10^{-5}
	CD4T	-8.50	0.002	-15.85	0.0005	-	-
	CD14M	-6.52	0.030	-5.31	0.0171	-	-
<i>IFI44L amplicon 2</i>	GR	-1.25	0.002	-4.31	0.0002	-	-
	CD19B	-12.00	0.005	-13.11	0.0017	-	-
	CD4T	-25.73	0.004	-15.07	0.0012	-47.00	2.7×10^{-5}
	CD14M	-49.27	0.025	-25.49	0.0171	-80.87	1.2×10^{-5}
<i>IFITM1</i>	GR	-42.58	0.036	-26.00	0.0398	-77.61	3.3×10^{-6}
	CD19B	-36.74	0.008	-17.22	0.0266	-61.75	2.8×10^{-4}
	CD4T	-4.67	0.003	-1.49	0.0266	-	-
	CD14M	-7.11	0.045	-8.45	0.0024	-	-
<i>LGALS3BP</i>	GR	-11.49	0.006	-8.60	0.0007	-	-
	CD19B	-10.76	0.012	-5.76	0.0046	-	-
	CD4T	-9.15	0.003	-6.15	0.0007	-	-
	CD14M	-5.31	0.036	-5.73	0.0007	-	-
<i>LOXL1</i>	GR	-6.04	0.030	-3.35	0.0024	-18.18	2.7×10^{-4}
	CD19B	-9.36	0.021	-8.16	0.0002	-	-
	CD14M	-3.01	0.045	-9.15	0.0005	-	-
<i>MIR10A</i>	GR	-2.83	0.021	-8.96	0.0061	-	-
	CD19B	-3.55	0.036	-6.37	0.0017	-	-
	CD4T	-4.22	0.006	-8.52	0.0081	-	-
<i>MIR146B</i>	CD14M	-1.79	0.030	-6.93	0.0012	-	-
	GR	-2.63	0.038	-5.31	0.0012	-	-
	CD19B	-5.46	0.108	-8.65	0.0012	-	-
<i>PARP9</i>	CD4T	-1.71	0.255	-6.65	0.0171	-	-
	CD14M	-0.42	0.196	-1.42	0.0266	-	-
	GR	-2.10	0.108	-3.87	0.0215	-	-
	CD19B	-3.51	0.013	-7.73	0.0005	-	-
<i>PLSCR1</i>	CD4T	-14.64	0.003	-21.35	0.0002	-32.46	6.9×10^{-6}
	CD14M	-44.93	0.012	-38.88	0.0046	-61.08	6.9×10^{-6}
	GR	-38.83	0.030	-30.10	0.0105	-56.62	9.5×10^{-6}
<i>RSAD2</i>	CD19B	-17.72	0.036	-11.07	0.0068	-28.93	1.2×10^{-3}
	CD4T	-11.59	0.003	-17.24	0.0007	-33.52	4.3×10^{-5}
	CD14M	-32.04	0.013	-8.12	0.0046	-16.61	2.5×10^{-2}
	GR	-17.03	0.006	-4.90	0.0002	-30.25	6.0×10^{-6}
<i>TACSTD2</i>	CD19B	-28.75	0.003	-15.89	0.0034	-31.17	2.7×10^{-2}
	CD4T	-5.40	0.003	-7.68	0.0012	-	-
	CD14M	-4.14	0.017	-7.61	0.0081	-	-
	GR	-4.26	0.008	-5.92	0.0061	-	-
<i>TRAF5</i>	CD19B	-12.81	0.006	-16.53	0.0007	-	-
	CD4T	-11.16	0.093	-16.96	0.2734	-	-
	CD14M	-6.34	0.050	-13.36	0.0012	-	-
	GR	-1.49	0.017	-5.77	0.0681	-	-
<i>TRAF5</i>	CD19B	-13.43	0.030	-20.96	0.0005	-	-
	CD4T	4.70	0.142	1.03	0.1272	-	-
	CD19B	14.41	0.002	16.02	0.0046	11.23	6.7×10^{-6}

* SLE = systemic lupus erythematosus; CD19B = CD19+ B cells; CD4T = CD4+ T cells; CD14M = CD14+ monocytes; CD19B = CD19+ B cells; GR = granulocyte.

† Represents the mean change in all CpGs in the amplicon and the lowest *P* value in the amplicon, based on primary paired analyses on the 450K array.

non-IFN-regulated genes, *MIR10A* and *TACSTD2* (all cell types), and *LOXL1* (monocytes, granulocytes, and B cells), and 5 genes that were differentially methylated only in B cells in the array-based analysis, *MIR146B*, *RSAD2* (all cell types), *DDRI*, *TRAF5* (B cells and CD4+ T cells), and *CXCR5* (B cells only).

Of the 14 selected probes, all except *TACSTD2* in monocytes were validated by pyrosequencing (Table 3 and Supplementary Table 3). However, several genes gained statistical significance in specific cell types during pyrosequencing, all of which were differentially methylated in the same direction as in the array-based analysis. For instance, *PARP9* was hypomethylated in all cells except granulocytes in the array-based analysis but was hypomethylated in all cell types by pyrosequencing, suggesting that some minor changes are, as expected, less well-detected using 450K BeadChip technology (28). The largest overall difference between discordant twins was

observed in *IFI44L* in monocytes and granulocytes, with median hypomethylation of -49.3% ($P = 0.025$) and -42.6% ($P = 0.036$), respectively (Figure 3A and Table 3). Of the 5 genes that were differentially methylated exclusively in B cells in the array-based analysis, *CXCR5*, *TRAF5*, *DDRI*, *MIR146B*, and *RSAD2* were validated (Table 3). *CXCR5*, *TRAF5*, and *DDRI* were hypermethylated (Figures 3B–D), while *RSAD2* was hypomethylated in all cell types, although to a larger extent in B cells.

In an independent sample of 20 SLE patients and 20 healthy controls, selected results were replicated by pyrosequencing for *CXCR5*, *DDRI*, *IFI44L*, *LGALS3BP*, *PARP9*, *PLSCR1*, and *TRAF5*. All genes showed statistically significant differential methylation in the same direction as in the twin analyses (Table 3). Specifically, the observed B cell hypermethylation in SLE-affected twins was validated (see Supplementary

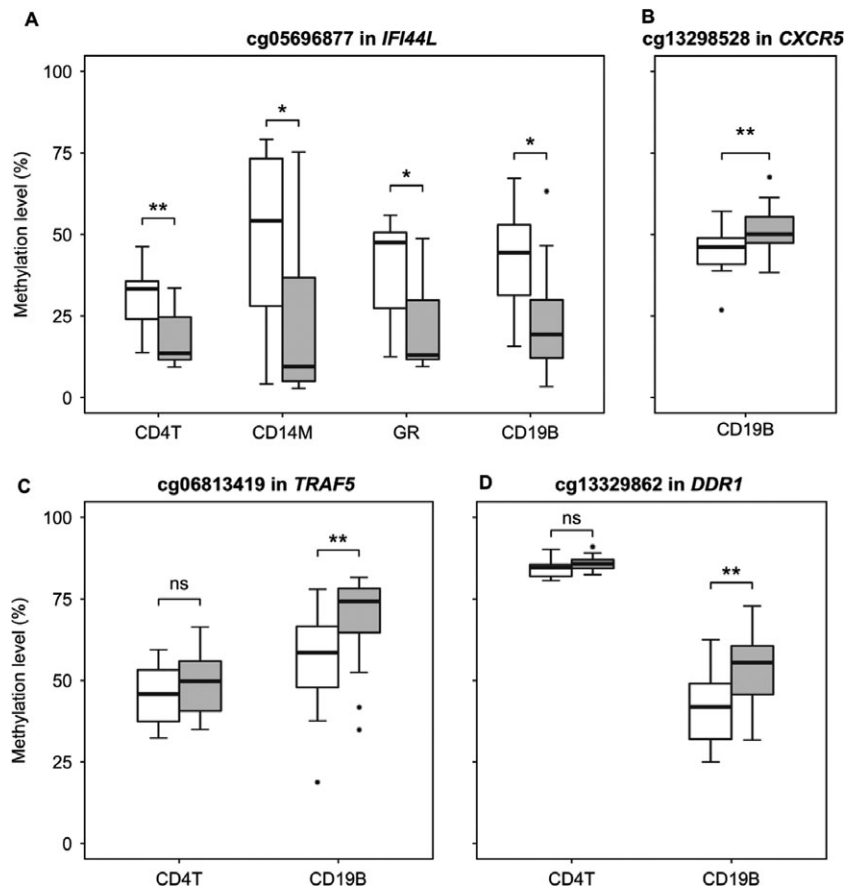


Figure 3. DNA methylation levels in CD4+ T cells (CD4T), monocytes (CD14M), granulocytes (GR), and B cells (CD19B) from healthy twins (open boxes) versus twins with systemic lupus erythematosus (shaded boxes) as determined by pyrosequencing in *IFI44L* (A), *CXCR5* (B), *TRAF5* (C), and *DDRI* (D). All cell types showed hypermethylation of *IFI44L*. Only B cells showed hypermethylation of *CXCR5*, *TRAF5*, and *DDRI*. Data are presented as box plots, where the boxes represent the 25th to 75th percentiles, the lines within the boxes represent the median, and the lines outside the boxes represent the 10th and 90th percentiles. Circles indicate outliers. * = $P < 0.05$; ** = $P < 0.01$. NS = not significant.

Figure 1, <http://onlinelibrary.wiley.com/doi/10.1002/art.40422/abstract>).

Differential methylation according to disease flare history. To investigate whether the observed DNA methylation differences might vary according to disease activity, we compared twins with SLE and a recent disease flare (within the past 2 years; mean 9 months) ($n = 9$ twins) with twins with SLE in clinical remission (mean age 11 years) ($n = 8$ twins) in paired analyses restricted to the promoter/start region. The mean SLEDAI score was 2.8 in twins discordant for SLE with a recent flare and 0.75 in the remaining twins at the time of examination. First, we examined overlapping genes between SLE-affected twins with recent flare compared with the remaining SLE-affected twins to identify common denominators between disease activity states. We then analyzed unique differentially methylated genes in twins with SLE who experienced a recent disease flare in order to identify potential flare-related changes.

In CD4⁺ T cells, 22 differentially methylated genes in the promoter/start region were shared between SLE-affected twins regardless of flare status, including *DTX3L*, *PARP9*, *IFI44L*, and *PLSCR1*, with more pronounced hypomethylation in twins with recent flare. Unique genes in twins with recent flare included *DDX60*, *EIF2AK2*, *IFIT5*, *IFITM1*, *RSAD2*, and *STAT1*, which were hypomethylated, and *DDR1* and *PRIC285*, which were hypermethylated (see Supplementary Table 4A, <http://onlinelibrary.wiley.com/doi/10.1002/art.40422/abstract>).

In monocytes, 31 genes were differentially methylated in the promoter/start region in twins regardless of flare status. *IFITM1* and *TACSTD2* showed more pronounced hypomethylation in twins with recent flare. Unique hypomethylated genes in twins with recent flare included *IFI44L*, *LGALS3BP*, *DTX3L*, *PARP9*, *GGT1*, and *MX1*, while hypermethylated genes included *B3GALT4* and *PRIC285* (Supplementary Table 4B).

In granulocytes, 34 differentially methylated genes in the promoter/start region were common to all twins regardless of flare status, including *LOXL1* and *NLRC5*. Hypomethylated genes unique to twins with recent flare included *IFITM1*, *LGALS3BP*, *IFI44L*, *DTX3L*, *PARP9*, *MX1*, and *RSAD2*, while hypermethylated genes included *B3GALT4* and *PRIC285* (see Supplementary Table 4C, <http://onlinelibrary.wiley.com/doi/10.1002/art.40422/abstract>).

In B cells, 196 genes were differentially methylated in the promoter/start region in twins regardless of flare status. *HOXB6* and *RSAD2* showed more pronounced hypomethylation in twins with recent flare, while *B3GALT4*, *DDR1*, *NFATC1*, *DTX1*, and *SGTA* displayed more pronounced hypermethylation. Unique hypomethylated genes

in twins with recent flare included *IFI44L*, *LGALS3BP*, *LOXL1*, *MIR10A*, *MIR146B*, *IFITM1*, and *PLSCR1*, while the most hypermethylated gene was *FBXO10* (see Supplementary Table 4D).

Differential methylation in MZ twins. Using unpaired analyses, we compared differentially methylated genes in the promoter/start regions in 6 MZ twin pairs (including 1 concordant twin pair and 2 co-twins affected by systemic sclerosis and autoimmune thyroid disease) with gene lists from the primary paired analyses. In CD4⁺ T cells, hypomethylated genes in MZ twins with SLE included *IFI44L*, *LOXL1*, *EIF2AK2*, *IKZF4*, *MIR10A*, *TNK2*, *TRIM2*, and *TRIM22*, while *NOS1* was hypermethylated (see Supplementary Table 5A, available at <http://onlinelibrary.wiley.com/doi/10.1002/art.40422/abstract>). In monocytes, hypomethylated genes included *NLRC5*, *CSDE1*, *DDX60*, *DTX3L*, *PARP9*, and *PRIC285*, while hypermethylated genes included *SIGLEC7* and *PTPRE* (see Supplementary Table 5B). In granulocytes, *MX1*, *DTX3L*, *PARP9*, *NLRC5*, and *GGT1* were hypomethylated in MZ twins with SLE, while the most hypermethylated gene was *ZBTB38* (Supplementary Table 5C). In B cells, hypomethylated genes included *IFI44L*, *DTX3L*, *PARP9*, *NLRC5*, *RSAD2*, and *USP18*, while the most hypermethylated genes included *ARPP-21* and *NFATC1* (Supplementary Table 5D).

X-linked methylation. In unpaired analyses of 15 female twins with SLE and 8 healthy female co-twins, the only differentially methylated gene with ≥ 2 probes on the X chromosome was *SCML2* in monocytes, which showed average hypomethylation of 8.6% at 3 probes in the promoter/start region (data not shown).

Anti-DNA antibodies. To examine whether the observed DNA methylation changes could be antibody-driven, a permutation test was performed, showing no relationship between differential methylation and the presence of anti-double-stranded DNA (anti-dsDNA) antibodies (data not shown).

Differential variability. Due to the stochastic nature of DNA methylation changes in cells at risk for pathologic change, we examined differential variability in twins with SLE ($n = 17$) compared with co-twins ($n = 13$) to identify loci with disease-specific highly variable DNA methylation patterns that would not have been detected in the main analysis. Of note, *IFI44L* was highly variable at cg13304609 in the TSS1500 region of CD4⁺ T cells and B cells, while *USP18* was highly variable at cg14293575 in the 5'-UTR in monocytes and granulocytes (see Supplementary Table 6, available at <http://onlinelibrary.wiley.com/doi/10.1002/art.40422/abstract>). The results were largely unchanged when co-twins with other autoimmune

diseases were excluded from the analyses (data not shown).

Epigenetic regulators. Differential methylation of known epigenetic regulators including DNA methyltransferases and the activation-induced deaminase pathway was examined to determine whether this might help explain the observed findings. There were no genes with multiple probes showing differential DNA methylation, apart from *DTX3L* in CD4+ T cells (hypomethylated in 3 cell types) and *CTBP2* and *PRKAG2* hypermethylation in B cells (see Supplementary Table 7, available at <http://onlinelibrary.wiley.com/doi/10.1002/art.40433/abstract>).

Pathway analysis. Upstream regulators were identified using Ingenuity Pathways Analysis software, and included IFN-regulated genes such as *IFNLI* in CD4+ T cells ($P = 1.2 \times 10^{-13}$), monocytes ($P = 5.3 \times 10^{-5}$), granulocytes ($P = 6.0 \times 10^{-7}$), and B cells ($P = 1.2 \times 10^{-5}$) (see Supplementary Table 8). The most prominent upstream regulators in B cells included *EP300* ($P = 1.8 \times 10^{-7}$), *ESRI* ($P = 8.3 \times 10^{-7}$), *CREBBP* ($P = 5.4 \times 10^{-6}$), and *TNF* ($P = 7.6 \times 10^{-6}$). Due to the observed predominance of B cell hypermethylation, we repeated the analyses stratified by methylation state, which revealed that the top upstream regulators of hypermethylated genes in B cells included *TNF* ($P = 2.0 \times 10^{-6}$) and *EP300* ($P = 5.5 \times 10^{-5}$) (data not shown).

In canonical pathway analyses, only the list of hypermethylated genes in B cells showed significant enrichment of pathways after Benjamini-Hochberg correction. The best-supported pathways included thyroid hormone receptor/retinoid X receptor activation ($P = 2 \times 10^{-3}$), role of macrophages, fibroblasts, and endothelial cells in rheumatoid arthritis (RA) ($P = 1.9 \times 10^{-2}$), and NF- κ B signaling ($P = 1.9 \times 10^{-2}$) in hypermethylated genes in B cells.

Network analysis identified antimicrobial and inflammatory response ($P = 2.1 \times 10^{-6}$), infectious disease ($P = 6.7 \times 10^{-5}$), and cancer ($P = 7.5 \times 10^{-5}$) as prominent enriched functions in CD4+ T cells; cancer ($P = 1.5 \times 10^{-5}$), hematologic disease ($P = 1.5 \times 10^{-5}$), and immunologic disease ($P = 1.5 \times 10^{-5}$) in monocytes; antimicrobial response ($P = 7.5 \times 10^{-5}$), cancer ($P = 8.4 \times 10^{-4}$), and organismal injury and abnormalities ($P = 8.4 \times 10^{-4}$) in granulocytes; and cancer ($P = 1.6 \times 10^{-22}$), organismal injury and abnormalities ($P = 1.6 \times 10^{-22}$), gastrointestinal disease ($P = 1.1 \times 10^{-19}$), and dermatologic disease and conditions ($P = 1.5 \times 10^{-17}$) in B cells. The networks best supported by the data are shown in Supplementary Figure 2, available at <http://onlinelibrary.wiley.com/doi/10.1002/art.40422/abstract>.

DISCUSSION

In the current study, we examined genome-wide DNA methylation in sorted CD4+ T cells, monocytes, granulocytes, and B cells from twins discordant for SLE. Hypomethylation of IFN-regulated genes was robust and common to all cell subsets and more pronounced in twins who had experienced a disease flare within the past 2 years. Differential methylation was more widespread in B cells with predominant hypermethylation, with *TNF* and *EP300* being the most important upstream regulators.

Previous EWAS of SLE have mostly focused on CD4+ T cells, demonstrating hypomethylation of IFN-regulated genes (8,9). Two studies suggested that the IFN signature is also present in monocytes, B cells (8), and granulocytes (11), but the current study is the first to show that the IFN signature is common to all major cellular compartments but with limited gene overlap. We further observed that CD4+ T cells actually displayed the fewest DNA methylation changes, followed by granulocytes, monocytes, and B cells.

Previous studies have shown conflicting results regarding the association between disease activity and DNA methylation changes, with some showing more pronounced hypomethylation of IFN-regulated genes in relation to higher disease activity (9,29), while others showed no association (8,10,30). In the current study, all twins had relatively quiescent disease. However, despite clear DNA methylation differences, the IFN signature was much attenuated in twins who had not had any disease flares for at least 2 years (mean age 11 years). This might suggest that the IFN signature is relatively stable but may gradually fade over years.

In the current study, *IFI44L* and *PLSCR1* promoter hypomethylation was common to all investigated cell types. A recent study suggested that *IFI44L* promoter hypomethylation in peripheral blood mononuclear cells might potentially be valid as a diagnostic biomarker for SLE, distinguishing SLE patients from healthy controls and patients with RA or Sjögren's syndrome (SS) (29). In 30 longitudinally sampled SLE patients, *IFI44L* became less hypomethylated during disease remission, in accordance with our findings. However, in a recent EWAS in patients with SS, *IFI44L* was also shown to be highly demethylated (20,31), and in a large gene expression study comparing the IFN signature between SLE, dermatomyositis, polymyositis, RA, and systemic sclerosis, the most overexpressed common genes were *IFI44L*, *IFI44*, *RSAD2*, *IFI27*, and *IFI6* (32). Thus, further studies are needed to elucidate the validity of *IFI44L* methylation and other IFN-regulated genes as diagnostic biomarkers for SLE, but they might prove to be convincing candidates

for biomarkers of disease activity in autoimmune diseases with known IFN overexpression.

The finding of predominant B cell hypermethylation in SLE has not previously been reported. Only one previous EWAS has investigated B cells in SLE alongside CD4⁺ T cells and monocytes. Absher et al identified an IFN signature with predominant hypomethylation in all cell types, which was the strongest in CD4⁺ T cells (8). Reanalysis of this publicly available data (GEO accession no. GSE59250) did not show evidence for the B cell hypermethylation observed in our study. The origin of this discrepancy is currently unclear. One explanation for the more widespread changes observed in B cells might derive from the extensive DNA methylation changes occurring during B cell differentiation, which affects 30% of CpG sites and is primarily related to DNA hypomethylation at later stages of B cell differentiation (33). Previous SLE studies showed an expansion of memory and plasma B cell compartments at the expense of naive B cells (34), in which case a more profound hypomethylation would, however, have been expected. Based on our data, it cannot be excluded that the DNA methylation changes observed in B cells represent a compositional change in the B cell population. To investigate this, further B cell subfractionation is required to identify the exact source of the observed B cell hypermethylation in SLE patients. Using 2 orthogonal technologies in the twin as well as the validation sample, we observed that B cells from SLE patients are clearly different from those from healthy controls, suggesting either early and/or defective reprogramming of B cells in SLE patients. Alternatively, the observed B cell hypermethylation may represent aberrant DNA methylation regulation in SLE. The observed B cell hypermethylation was, however, not associated with either the flare history or differential methylation in known epigenetic regulators (except *CTBP2* and *PRKAG2*).

Previous studies have suggested that the observed B cell hypermethylation may not, however, be restricted to SLE. Two independent EWAS in patients with SS showed marked DNA methylation changes in B cells rather than in CD4⁺ T cells with predominant B cell hypermethylation (20,31). The question of whether the same pathogenic pathway is shared between SS and SLE in B cells remains unanswered. However, at least *CXCR5*, *TRAF5*, and *DDR1* were hypermethylated in B cells from patients with SS and patients with SLE, which might be of pathogenic interest. *CXCR5* in particular is down-regulated in the B cells from SLE patients (35) and might play a role in B cell homing to secondary lymphoid organs (36), while TNF receptor-associated factor 5 (*TRAF5*) is a signal transducer for CD40 and activates the NF- κ B pathway (37). Discoidin domain receptor 1 is a collagen

receptor that appears to play a role in leukocyte migration (38). Similarly, DNA methylation analysis of CD19⁺ B cells from treatment-naive patients with RA showed 4 times more hypermethylated CpGs compared with hypomethylated CpGs (82.3% versus 17.7%), while similar numbers of hypermethylated and hypomethylated probes were detected in CD4⁺ T cells from the same patients, which provides further evidence for B cell-specific hypermethylation in systemic inflammatory autoimmune diseases (39). Only 1 study analyzing CD19⁺ B cells in primary SS also analyzed the gene expression patterns in this cell population, and although there was good correlation between hypomethylation and increased gene expression, hypermethylation was not correlated with expression changes (31). However, expression was analyzed in only a few hypermethylated genes, and thus further investigation is required.

One important upstream regulator of the observed hypermethylated genes in B cells is tumor necrosis factor (TNF), which is a cytokine with paradoxical effects, because it can trigger both proinflammatory and anti-inflammatory pathways (40,41). The role of TNF in SLE remains controversial (41), but in several autoimmune diseases, including RA, TNF inhibitors are a well-established treatment, which may, however, induce anti-nuclear antibody and anti-dsDNA antibody production (42). Rarely, TNF inhibitors may trigger lupus-like disease, which usually improves upon drug withdrawal. The observed B cell hypermethylation of genes downstream of TNF might suggest a novel mechanism for TNF dysregulation in SLE. Other important upstream regulators in B cells included *EP300* and *CREBBP*, which encode p300 and CREB-binding protein, respectively. These are highly homologous transcriptional coactivators with histone acetyltransferase activity, which regulate RNA polymerase II-mediated transcription (43) and are among the most commonly mutated tumor suppressor genes in B cell lymphoma (44). Interestingly, mice with acetyltransferase-deficient p300 specifically in B cells have been shown to exhibit lupus-like disease, with anti-dsDNA antibody production and glomerulonephritis (45). This might suggest a link between dysregulated DNA methylation and defective histone acetylation in the B cells of patients with SLE.

In the current study, most differentially methylated genes were found in more than 1 cellular subset. Although most cellular subsets were of high purity, the purity of the granulocyte fraction was >80% pure, which could lead to the lack of detection of some very small DNA methylation differences specific to granulocytes. Furthermore, we were not able to correct for differences in immunosuppressive treatment between SLE twins due

to the small sample size, which may potentially have influenced the results. A strength, however, was that the use of MZ twins cancels out the influence of genetic effects, which suggests that the observed DNA methylation changes in SLE were not merely present due to a specific genotype. Also, we validated some of the major findings in an independent case–control sample. Overall, our data show that there were both common denominators and major differences between immune cell subsets.

In conclusion, in this genome-wide DNA methylation study, we demonstrate that discordant SLE twins have a clear cell type–dependent IFN signature in CD4+ T cells, monocytes, granulocytes, and B cells, which was strongest in SLE twins who had experienced a disease flare within the last 2 years. B cells exhibited more widespread DNA methylation changes with predominant promoter hypermethylation, which is a novel finding that is of potential interest for further studies of SLE pathogenesis.

AUTHOR CONTRIBUTIONS

All authors were involved in drafting the article or revising it critically for important intellectual content, and all authors approved the final version to be published. Dr. Ulf-Møller had full access to all of the data in the study and takes responsibility for the integrity of the data and the accuracy of the data analysis.

Study conception and design. Ulf-Møller, Asmar, Svendsen, Grønbaek, Tost, Jacobsen.

Acquisition of data. Ulf-Møller, Liu, Busato.

Analysis and interpretation of data. Ulf-Møller, Tost, Jacobsen.

REFERENCES

- Yang J, Visscher PM, Wray NR. Sporadic cases are the norm for complex disease. *Eur J Hum Genet* 2010;18:1039–43.
- Kuo CF, Grainge MJ, Valdes AM, See LC, Luo SF, Yu KH, et al. Familial aggregation of systemic lupus erythematosus and coaggregation of autoimmune diseases in affected families. *JAMA Intern Med* 2015;175:1518–26.
- Lawrence JS, Martins CL, Drake GL. A family survey of lupus erythematosus. Part 1. Heritability. *J Rheumatol* 1987;14:913–21.
- Morris DL, Sheng Y, Zhang Y, Wang YF, Zhu Z, Tomblason P, et al. Genome-wide association meta-analysis in Chinese and European individuals identifies ten new loci associated with systemic lupus erythematosus. *Nat Genet* 2016;48:940–6.
- Ulf-Møller CJ, Svendsen AJ, Viemose LN, Jacobsen S. Concordance of autoimmune disease in a nationwide Danish systemic lupus erythematosus twin cohort. *Semin Arthritis Rheum* 2018;47:538–44.
- Ballestar E. Epigenetic alterations in autoimmune rheumatic diseases. *Nat Rev Rheumatol* 2011;7:263–71.
- Javierre BM, Fernandez AF, Richter J, Al-Shahrour F, Ignacio Martin-Subero J, Rodriguez-Ubreva J, et al. Changes in the pattern of DNA methylation associate with twin discordance in systemic lupus erythematosus. *Genome Res* 2010;20:170–9.
- Absher DM, Li X, Waite LL, Gibson A, Roberts K, Edberg J, et al. Genome-wide DNA methylation analysis of systemic lupus erythematosus reveals persistent hypomethylation of interferon genes and compositional changes to CD4+ T-cell populations. *PLoS Genet* 2013;9:e1003678.
- Jeffries M, Dozmorov M, Tang Y, Merrill JT, Wren JD, Sawalha AH. Genome-wide DNA methylation patterns in CD4+ T cells from patients with systemic lupus erythematosus. *Epigenetics* 2011;6:593–601.
- Coit P, Jeffries M, Altork N, Dozmorov MG, Koelsch KA, Wren JD, et al. Genome-wide DNA methylation study suggests epigenetic accessibility and transcriptional poisoning of interferon-regulated genes in naïve CD4+ T cells from lupus patients. *J Autoimmun* 2013;43:78–84.
- Coit P, Yalavarthi S, Ogenovski M, Zhao W, Hasni S, Wren JD, et al. Epigenome profiling reveals significant DNA demethylation of interferon signature genes in lupus neutrophils. *J Autoimmun* 2015;58:59–66.
- Ballestar E. Epigenetics lessons from twins: prospects for autoimmune disease. *Clin Rev Allergy Immunol* 2010;39:30–41.
- Reinius LE, Acevedo N, Joerink M, Pershagen G, Dahlén SE, Greco D, et al. Differential DNA methylation in purified human blood cells: implications for cell lineage and studies on disease susceptibility. *PLoS One* 2012;7:e41361.
- Liu Z, Davidson A. Taming lupus: a new understanding of pathogenesis is leading to clinical advances. *Nat Med* 2012;18:871–82.
- Lyng E, Sandegaard JL, Rebolj M. The Danish National Patient Register. *Scand J Public Health* 2011;39:30–3.
- Skytthe A, Ohm Kyvik K, Vilstrup Holm N, Christensen K. The Danish Twin Registry. *Scand J Public Health* 2011;39:75–8.
- Pedersen CB, Gotzsche H, Moller JO, Mortensen PB. The Danish Civil Registration System: a cohort of eight million persons. *Dan Med Bull* 2006;53:441–9.
- Tan EM, Cohen AS, Fries JF, Masi AT, McShane DJ, Rothfield NF, et al. The 1982 revised criteria for the classification of systemic lupus erythematosus. *Arthritis Rheum* 1982;25:1271–7.
- Gladman DD, Ibañez D, Urowitz MB. Systemic lupus erythematosus disease activity index 2000. *J Rheumatol* 2002;29:288–91.
- Miceli-Richard C, Wang-Renault SF, Boudaoud S, Busato F, Lallemand C, Bethune K, et al. Overlap between differentially methylated DNA regions in blood B lymphocytes and genetic at-risk loci in primary Sjögren's syndrome. *Ann Rheum Dis* 2016;75:933–40.
- Tost J, Gut IG. DNA methylation analysis by pyrosequencing. *Nat Protoc* 2007;2:2265–75.
- Touleimat N, Tost J. Complete pipeline for Infinium® Human Methylation 450K BeadChip data processing using subset quantile normalization for accurate DNA methylation estimation. *Epigenomics* 2012;4:325–41.
- The 1000 Genomes Project Consortium, McVean GA, Altshuler DM, Durbin RM, Abecasis GR, Bentley DR, et al. An integrated map of genetic variation from 1,092 human genomes. *Nature* 2012;491:56–65.
- Chen Y, Lemire M, Choufani S, Butcher DT, Grafodatskaya D, Zanke BW, et al. Discovery of cross-reactive probes and polymorphic CpGs in the Illumina Infinium HumanMethylation450 microarray. *Epigenetics* 2013;8:203–9.
- Medvedeva YA, Lennartsson A, Ehsani R, Kulakovskiy IV, Vorontsov IE, Panahandeh P, et al. EpiFactors: a comprehensive database of human epigenetic factors and complexes. *Database (Oxford)* 2015;2015:bav067.
- Teschendorff AE, Gao Y, Jones A, Ruebner M, Beckmann MW, Wächter DL, et al. DNA methylation outliers in normal breast tissue identify field defects that are enriched in cancer. *Nat Commun* 2016;7:10478.
- Rusinova I, Forster S, Yu S, Kannan A, Masse M, Cumming H, et al. Interferome v2.0: an updated database of annotated interferon-regulated genes. *Nucleic Acids Res* 2013;41:D1040–6.
- Bock C, Halbritter F, Carmona FJ, Tierling S, Datlinger P, Assenov Y, et al. Quantitative comparison of DNA methylation assays for biomarker development and clinical applications. *Nat Biotechnol* 2016;34:726–37.
- Zhao M, Zhou Y, Zhu B, Wan M, Jiang T, Tan Q, et al. IFI44L promoter methylation as a blood biomarker for systemic lupus erythematosus. *Ann Rheum Dis* 2016;75:1998–2006.

30. Coit P, Renauer P, Jeffries MA, Merrill JT, McCune WJ, Maksimowicz-McKinnon K, et al. Renal involvement in lupus is characterized by unique DNA methylation changes in naïve CD4⁺ T cells. *J Autoimmun* 2015;61:29–35.
31. Imgenberg-Kreuz J, Sandling JK, Almlöf JC, Nordlund J, Signér L, Norheim KB, et al. Genome-wide DNA methylation analysis in multiple tissues in primary Sjögren's syndrome reveals regulatory effects at interferon-induced genes. *Ann Rheum Dis* 2016; 75:2029–36.
32. Higgs BW, Liu Z, White B, Zhu W, White WI, Morehouse C, et al. Patients with systemic lupus erythematosus, myositis, rheumatoid arthritis and scleroderma share activation of a common type I interferon pathway. *Ann Rheum Dis* 2011;70:2029–36.
33. Kulis M, Merkel A, Heath S, Queirós AC, Schuyler RP, Castellano G, et al. Whole-genome fingerprint of the DNA methylome during human B cell differentiation. *Nat Genet* 2015;47:746.
34. Salazar-Camarena DC, Ortiz-Lazareno PC, Cruz A, Oregon-Romero E, Machado-Contreras JR, Muñoz-Valle JF, et al. Association of BAFF, APRIL serum levels, BAFF-R, TACI and BCMA expression on peripheral B-cell subsets with clinical manifestations in systemic lupus erythematosus. *Lupus* 2016;25:582–92.
35. Becker AM, Dao KH, Han BK, Kornu R, Lakhanpal S, Mobley AB, et al. SLE peripheral blood B cell, T cell and myeloid cell transcriptomes display unique profiles and each subset contributes to the interferon signature. *PLoS One* 2013;8:e67003.
36. Müller G, Höpken UE, Lipp M. The impact of CCR7 and CXCR5 on lymphoid organ development and systemic immunity. *Immunol Rev* 2003;195:117–35.
37. Hildebrand JM, Yi Z, Buchta CM, Poovassery J, Stunz LL, Bishop GA. Roles of tumor necrosis factor receptor associated factor 3 (TRAF3) and TRAF5 in immune cell functions. *Immunol Rev* 2011;244:55–74.
38. Yoshimura T, Matsuyama W, Kamohara H. Discoidin domain receptor 1: a new class of receptor regulating leukocyte-collagen interaction. *Immunol Res* 2005;31:219–30.
39. Glossop JR, Emes RD, Nixon NB, Packham JC, Fryer AA, Matthey DL, et al. Genome-wide profiling in treatment-naïve early rheumatoid arthritis reveals DNA methylome changes in T and B lymphocytes. *Epigenomics* 2016;8:209–24.
40. Mageed R, Isenberg D. Tumour necrosis factor α in systemic lupus erythematosus and anti-DNA autoantibody production. *Lupus* 2002;11:850–5.
41. Jacob N, Stohl W. Cytokine disturbances in systemic lupus erythematosus. *Arthritis Res Ther* 2011;13:228.
42. Moulis G, Sommet A, Lapeyre-Mestre M, Montastruc JL. Is the risk of tumour necrosis factor inhibitor-induced lupus or lupus-like syndrome the same with monoclonal antibodies and soluble receptor? A case/non-case study in a nationwide pharmacovigilance database. *Rheumatology (Oxford)* 2014;53:1864–71.
43. Kalkhoven E. CBP and p300: HATs for different occasions. *Biochem Pharmacol* 2004;68:1145–55.
44. Pasqualucci L, Dominguez-Sola D, Chiarenza A, Fabbri G, Grunn A, Trifonov V, et al. Inactivating mutations of acetyltransferase genes in B-cell lymphoma. *Nature* 2011;471:189–95.
45. Forster N, Gallinat S, Jablonska J, Weiss S, Elsässer HP, Lutz W. Mice erythematosus-like autoimmune disease in suppresses systemic lupus p300 protein acetyltransferase activity p300 protein acetyltransferase activity suppresses systemic lupus erythematosus-like autoimmune disease in mice 1. *J Immunol* 2007;178:6941–8.

Antiphospholipid Antibodies Inhibit Trophoblast Toll-Like Receptor and Inflammasome Negative Regulators

Melissa J. Mulla,¹ Ingrid C. Weel,² Julie A. Potter,¹ Stefan M. Gysler,¹ Jane E. Salmon,³ Maria T. S. Peraçoli,⁴ Carla V. Rothlin,¹ Lawrence W. Chamley,⁵ and Vikki M. Abrahams¹

Objective. Women with antiphospholipid antibodies (aPL) are at risk for pregnancy complications associated with poor placentation and placental inflammation. Although these antibodies are heterogeneous, some anti- β_2 -glycoprotein I (anti- β_2 GPI) antibodies can activate Toll-like receptor 4 (TLR-4) and NLRP3 in human first-trimester trophoblasts. The objective of this study was to determine the role of negative regulators of TLR and inflammasome function in aPL-induced trophoblast inflammation.

Methods. Human trophoblasts were not treated or were treated with anti- β_2 GPI aPL or control IgG in the presence or absence of the common TAM (TYRO3, AXL, and Mer tyrosine kinase [MERTK]) receptor ligand growth arrest-specific protein 6 (GAS6) or the autophagy-inducer rapamycin. The expression and function of the TAM receptor pathway and autophagy were measured by quantitative reverse transcription-polymerase chain reaction (qRT-PCR), Western blotting, and enzyme-linked immunosorbent assay (ELISA). Antiphospholipid

antibody-induced trophoblast inflammation was measured by qRT-PCR, activity assays, and ELISA.

Results. Anti- β_2 GPI aPL inhibited trophoblast TAM receptor function by reducing cellular expression of the receptor tyrosine kinases AXL and MERTK and the ligand GAS6. The addition of GAS6 blocked the effects of aPL on the TLR-4-mediated interleukin-8 (IL-8) response. However, the NLRP3 inflammasome-mediated IL-1 β response was not affected by GAS6, suggesting that another regulatory pathway was involved. Indeed, anti- β_2 GPI aPL inhibited basal trophoblast autophagy, and reversing this with rapamycin inhibited aPL-induced inflammasome function and IL-1 β secretion.

Conclusion. Basal TAM receptor function and autophagy may serve to inhibit trophoblast TLR and inflammasome function, respectively. Impairment of TAM receptor signaling and autophagy by anti- β_2 GPI aPL may allow subsequent TLR and inflammasome activity, leading to a robust inflammatory response.

Dr. Abraham's work was supported in part by the March of Dimes Foundation (Gene Discovery and Translational Research grant 6-FY12-255), the American Heart Association (grant 15GRNT2448 0140), and the Lupus Research Institute (Novel Research grant). Dr. Weel's work was supported by an International Scholarship from the São Paulo Research Foundation. Dr. Gysler's work was supported by a Yale University School of Medicine Medical Student Fellowship. Dr. Salmon's work was supported by the NIH (National Institute of Arthritis and Musculoskeletal and Skin Diseases grant AR-49772).

¹Melissa J. Mulla, MS, Julie A. Potter, MS, Stefan M. Gysler, MD, Carla V. Rothlin, PhD, Vikki M. Abrahams, PhD: Yale University, New Haven, Connecticut; ²Ingrid C. Weel, PhD: Yale University, New Haven, Connecticut, and São Paulo State University, São Paulo, Brazil; ³Jane E. Salmon, MD: Hospital for Special Surgery, New York, New York; ⁴Maria T. S. Peraçoli, PhD: São Paulo State University, São Paulo, Brazil; ⁵Lawrence W. Chamley, PhD: University of Auckland, Auckland, New Zealand.

Address correspondence to Vikki M. Abrahams, PhD, Department of Obstetrics, Gynecology & Reproductive Sciences, Yale School of Medicine, 310 Cedar Street, LSOG 305C, New Haven, CT 06510. E-mail: vikki.abrahams@yale.edu.

Submitted for publication August 11, 2017; accepted in revised form January 9, 2018.

Women with antiphospholipid antibodies (aPL) are at high risk for recurrent pregnancy loss and late gestational pregnancy complications, such as preeclampsia (1). Placental inflammation is a hallmark of adverse pregnancy outcomes such as preeclampsia, including those complicated by aPL (2,3). Antiphospholipid antibodies recognizing β_2 -glycoprotein I (β_2 GPI) preferentially bind the placental trophoblast and subsequently alter trophoblast function (4,5). Our group previously demonstrated that aPL recognizing β_2 GPI trigger human first-trimester trophoblasts to produce elevated levels of proinflammatory cytokines/chemokines via activation of Toll-like receptor 4 (TLR-4) (6) and independently of TLR-4, inhibit spontaneous trophoblast migration and modulate trophoblast angiogenic factor secretion (7,8). Further investigation of this TLR-4-mediated inflammatory response revealed that anti-

β_2 GPI aPL increased induction of endogenous uric acid in the trophoblast, which in turn activated the NLRP3 inflammasome to induce interleukin-1 β (IL-1 β) processing and secretion (9). In parallel, anti- β_2 GPI aPL induced trophoblast expression of microRNA-146a-3p (miR-146a-3p) through activation of TLR-4, which in turn activated the RNA sensor TLR-8 to drive IL-8 secretion (10).

Despite the ability of some aPL to induce a robust TLR-4 and NLRP3 inflammasome-mediated inflammatory response, human first-trimester trophoblast cells do not generate a classic inflammatory response to physiologic doses of the natural TLR-4 ligand, bacterial lipopolysaccharide (LPS) (11–14). Thus, in human first-trimester trophoblasts, TLR-4 function and subsequent inflammasome activation may be tightly regulated, and aPL might override this braking mechanism.

One way in which TLR function can be inhibited is via activation of TAM receptor tyrosine kinases, a novel family of negative regulators (15,16). Three TAM receptors, TYRO3, AXL, and Mer tyrosine kinase (MERTK), are activated by 2 endogenous ligands: growth arrest-specific protein 6 (GAS6) and protein S1 (PROS1). GAS6 binds and activates all 3 TAM receptors, while PROS1 activates TYRO3 and MERTK (15,16). Upon ligand binding, TAM receptors trigger STAT-1 phosphorylation, inducing expression of suppressor of cytokine signaling 1 (SOCS-1) and SOCS-3, which inhibits TLR signaling (15,16). While autophagy is a regulatory process that facilitates the degradation and recycling of cytoplasmic components via lysosomes (17), autophagy is also a negative regulator of inflammasome activity and subsequent IL-1 β production (18,19). Furthermore, in normal pregnancy, extravillous trophoblasts express high levels of basal autophagy, which is necessary for their invasion and vascular remodeling (20). The aim of this study was to determine the role of negative regulators of TLR and inflammasome function in anti- β_2 GPI aPL-induced trophoblast inflammation, by investigating the TAM receptor pathway and autophagy.

MATERIALS AND METHODS

Reagents. Recombinant GAS6 was purchased from R&D Systems. The autophagy inducer rapamycin and the autophagy inhibitor bafilomycin were obtained from InvivoGen. The ADAM-17 inhibitor tumor necrosis factor α processing inhibitor 0 (TAPI-0) was purchased from Sigma-Aldrich.

Trophoblast cell lines. The human first-trimester extravillous trophoblast telomerase-transformed cell line Sw.71 (21) was used in these studies. The human first-trimester extravillous trophoblast cell line HTR-8 was also used and was a kind gift from Dr. Charles Graham (Queens University, Kingston, Ontario, Canada) (22).

Isolation of primary trophoblasts from first-trimester placentas. Placentas from first-trimester pregnancies (7–12 weeks' gestation) were obtained from elective terminations of normal pregnancies performed at Yale New Haven Hospital. The use of patient samples was approved by the Yale University Human Research Protection Program. Trophoblast isolation was performed as previously described (10).

Antiphospholipid antibodies. Unless specified otherwise, we used the aPL IIC5, which is a mouse IgG1 anti-human β_2 GPI monoclonal antibody (mAb). For some experiments, the aPL ID2, which also is an IgG mouse anti-human β_2 GPI mAb, was used. These aPL have been previously characterized. Similar to patient-derived polyclonal aPL, IIC5 and ID2 bind β_2 GPI when immobilized on a negatively charged surface such as phospholipids, cardiolipin, phosphatidylserine, or irradiated polystyrene and thus behave as both anticardiolipin and anti- β_2 GPI antibodies (23). IIC5 and ID2 react specifically with an epitope within domain V of β_2 GPI (24). Furthermore, both IIC5 and ID2 have pronounced lupus anticoagulant activity, and thus both antibodies are “triple positive” aPL (25). IIC5 and ID2 are appropriate models for human aPL, because they share similar epitopes; IIC5 and ID2 can block human polyclonal aPL binding to β_2 GPI (26). Moreover, IIC5 and ID2 bind to human first-trimester extravillous trophoblast cells (6,27,28) and alter their function in a manner similar to patient-derived polyclonal IgG aPL (9) and polyclonal IgG aPL recognizing β_2 GPI (6,8). In particular, for this study, both anti-human β_2 GPI mAb and patient-derived aPL up-regulated trophoblast secretion of inflammatory IL-8 and IL-1 β (6,9). Mouse IgG1 clone 107.3 (BD Biosciences) was used as an isotype control. Trophoblast cells were treated with aPL or the IgG isotype control at 20 μ g/ml, as previously described (6–10).

RNA isolation and quantitative reverse transcription-polymerase chain reaction (qRT-PCR). Trophoblast cell RNA was extracted using TRIzol, as previously described (29). Expression of miR-146a-3p was measured by qRT-PCR using a TaqMan MicroRNA Assay (Life Technologies) and normalized to the housekeeping gene U6, as previously described (10). For expression of *TYRO3*, *AXL*, *MERTK*, *GAS6*, *PROS1*, *SOCS1*, *SOCS3*, *IFNA*, *IFNB*, and *GAPDH* messenger RNA (mRNA), qRT-PCR was performed using a KAPA SYBR FAST qPCR kit (Kapa Biosystems), and PCR amplification was performed using a Bio-Rad CFX Connect Real-time PCR Detection System. Data were analyzed using the $\Delta\Delta C_t$ method and plotted as the fold change in microRNA or mRNA expression normalized to the endogenous control/internal reference.

Western blotting. Western blot analysis was performed as previously described (9). Hsp90 was used as an internal control to validate the amount of protein loaded onto the gels. Images were recorded, and semiquantitative densitometry was performed using a Kodak Gel Logic 100 system and Kodak Molecular Imaging software (Eastman Kodak) and normalized to signals for Hsp90. The following primary antibodies to human proteins were used: TYRO3 (catalog no. MAB859; R&D Systems); AXL (catalog no. AF154; R&D Systems); MERTK (catalog no. AF891; R&D Systems), phosphorylated AXL (catalog no. 9271; Cell Signaling Technology), phosphorylated MERTK (catalog no. ab192649; Abcam), total STAT-1 (catalog no. 9172; Cell Signaling Technology), phosphorylated STAT-1 (catalog no. 7649; Cell

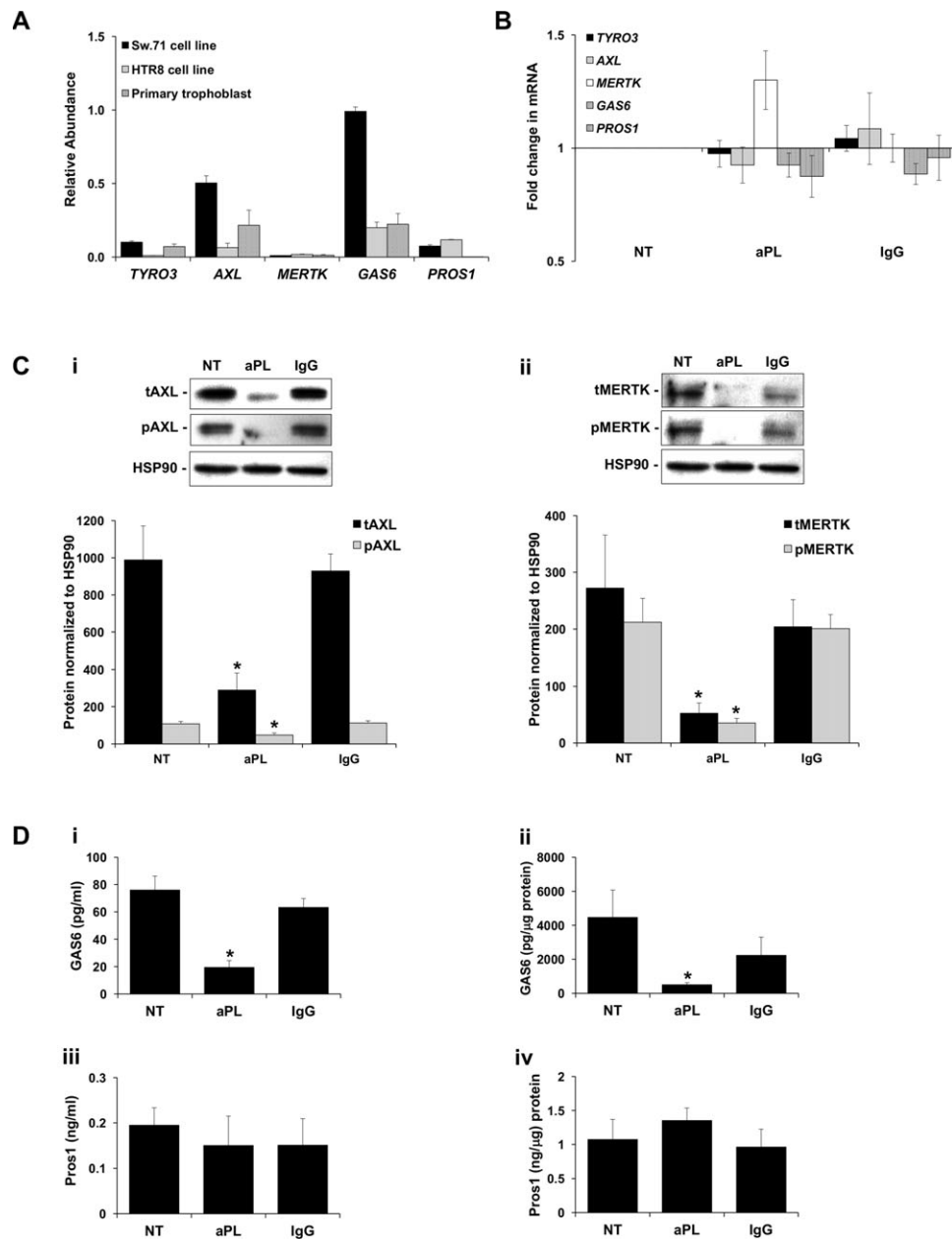


Figure 1. Antiphospholipid antibodies (aPL) inhibit trophoblast TAM (TYRO3, AXL, Mer tyrosine kinase [MERTK]) receptor and ligand expression. **A**, Quantitative reverse transcription–polymerase chain reaction was used to measure basal *TYRO3*, *AXL*, *MERTK*, *GAS6*, and *PROS1* mRNA levels in the Sw.71 cell line ($n = 6$), the HTR-8 cell line ($n = 3$), and primary first-trimester trophoblasts ($n = 3$). **B**, After 48 hours of no treatment (NT) or exposure to aPL or control IgG, *TYRO3*, *AXL*, *MERTK*, *GAS6*, and *PROS1* mRNA levels were measured in Sw.71 cells ($n = 8$). **C** and **D**, Sw.71 cells were not treated or were treated with aPL or control IgG. After 72 hours, cell-free supernatants and cellular protein were collected. **C**, Total AXL (tAXL) and phosphorylated AXL (pAXL) (part **i**) and total MERTK (tMERTK) and phosphorylated MERTK (pMERTK) (part **ii**) were measured by Western blotting. Hsp90 served as a loading control. **D**, Enzyme-linked immunosorbent assays were performed to measure secreted growth arrest–specific protein 6 (GAS6) and cellular GAS6 (parts **i** and **ii**, respectively) and secreted protein S1 (PROS1) and cellular PROS1 ($n = 4$ –8) (parts **iii** and **iv**). Total AXL and phosphorylated AXL and total MERTK and phosphorylated MERTK levels were determined by densitometry, after normalization to Hsp90 ($n = 4$ –6). Blots are from 1 representative experiment. Bars show the mean \pm SEM of pooled independent experiments. * = $P < 0.05$ versus NT.

Signaling Technology), SOCS-1 (catalog no. 3950; Cell Signaling Technology), SOCS-3 (catalog no. 2923; Cell Signaling Technology), light chain 3B-I (LC3B-I/II) (catalog no. 2775; Cell Signaling Technology), SQSTM1/p62 (catalog no. 5114; Cell Signaling Technology), and Hsp90 (catalog no. H-114; Santa Cruz Biotechnology).

Measurement of cytokines, uric acid, caspase 1, and TAM receptor ligands, and trophoblast migration. Trophoblast culture supernatants and (for some factors) lysates, were analyzed for IL-1 β , vascular endothelial growth factor (VEGF), placenta growth factor (PlGF), soluble endoglin, and GAS6 using enzyme-linked immunosorbent assay (ELISA) kits from R&D Systems; for IL-8 using an ELISA kit from Enzo Life Sciences; and for total PROS1 using an ELISA kit from Innovative Research. For the measurement of uric acid, supernatants were analyzed using a QuantiChrom Assay Kit from Bioassay Systems. Caspase 1 activity was measured using a Caspase-Glo 1 Inflammasome Assay (Promega). Trophoblast cell migration was measured using a 2-chamber colorimetric assay (EMD Millipore), as previously described (7,10).

Measurement of soluble AXL, soluble MERTK, and GAS6 in patient samples. Plasma was collected as part of the Predictors of Pregnancy Outcome: Biomarkers in Antiphospholipid Antibody Syndrome and Systemic Lupus Erythematosus (PROMISSE) study, a multicenter National Institutes of Health-funded prospective observational study of pregnancy in women with aPL, systemic lupus erythematosus (SLE), or both, as well as healthy pregnant controls. Details about this cohort of women, as well as inclusion and exclusion criteria, have been previously reported (9,10,30–33). The current study involves a subset of aPL-positive pregnant women with SLE or without SLE ($n = 38$) and healthy pregnant controls ($n = 16$). We also studied SLE patients without aPL ($n = 29$). Adverse pregnancy outcomes were defined as the occurrence of ≥ 1 of the following: 1) otherwise unexplained fetal death, 2) neonatal death prior to hospital discharge and due to complications of prematurity, 3) indicated preterm delivery prior to 37 weeks' gestation because of gestational hypertension, preeclampsia, or placental insufficiency, 4) birth weight less than the fifth percentile and/or delivery before 37 weeks because of intrauterine growth retardation and confirmed by a birth weight less than the 10th percentile. The frequency of adverse pregnancy outcomes in the entire cohort was previously reported (10). Among individuals who did or did not have SLE and were aPL-positive, 20 had an adverse pregnancy outcome; among patients with SLE who were aPL-negative, 11 had an adverse pregnancy outcome. Plasma collected during the second trimester (18–27 weeks' gestation) was analyzed for soluble AXL, soluble MERTK, and GAS6 using ELISA (R&D Systems).

Statistical analysis. Each treatment experiment was performed at least 3 times. All analyses were performed in duplicate or triplicate. All data are presented as the mean \pm SEM of pooled independent experiments. For normally distributed data, significance was determined by either one-way analysis of variance for multiple comparisons or a *t*-test. For non-normally distributed data, significance was determined using a nonparametric multiple comparison test or Wilcoxon's matched pairs signed rank test. Statistical analyses were performed using GraphPad Prism software. *P* values less than 0.05 were considered significant.

RESULTS

Inhibition of trophoblast TAM receptor and ligand expression by aPL. As shown in Figure 1A, first-trimester trophoblast cell lines (Sw.71 and HTR-8) as well as primary human first-trimester trophoblasts expressed basal mRNA levels of the TAM receptors *TYRO3*, *AXL*, and *MERTK* and their ligands, *GAS6* and *PROS1*. After treatment with aPL or an IgG isotype control, trophoblast *TYRO3*, *AXL*, *MERTK*, *GAS6*, and *PROS1* mRNA levels were not significantly different from those in the no treatment (NT) control group (Figure 1B). However, as shown in Figures 1C and D, aPL treatment did change their protein expression. Under NT and IgG control conditions, trophoblasts expressed high levels of total and phosphorylated AXL and MERTK (Figure 1C, parts i and ii, respectively). After exposure to aPL, the levels of total and phosphorylated AXL were significantly reduced (mean \pm SEM 75.9 \pm 9.1% and 49.9 \pm 11.7%, respectively), as were the levels of total and phosphorylated MERTK (84.1 \pm 4.7% and 76.0 \pm 6.2%, respectively) compared to the NT control (Figure 1C, parts i and ii, respectively). *TYRO3* protein expression was undetectable under all conditions (data not shown). As shown in Figure 1D, under NT and IgG control conditions, trophoblasts expressed high levels of secreted and cellular *GAS6* and *PROS1*. After exposure to aPL, secreted (part i) and cellular (part ii) *GAS6* levels were significantly reduced (78.6 \pm 5.3% and 81.4 \pm 3.4%, respectively) compared to the NT control. In contrast, aPL had no significant effect on either secreted or cellular levels of *PROS1* compared to controls (Figure 1D, parts iii and iv, respectively).

Inhibition of trophoblast TAM receptor signaling by aPL. Having demonstrated reduced expression of AXL, MERTK, and GAS6 protein and reduced AXL and MERTK activation in trophoblasts exposed to aPL, we investigated the functional impact of this inhibition by examining the downstream signaling pathway. Under NT and IgG control conditions, trophoblasts expressed high levels of phosphorylated and total STAT-1 and high levels of SOCS-1 and SOCS-3 (Figure 2A). After treatment with aPL, the phosphorylated STAT-1:total STAT-1 ratio was significantly inhibited (mean \pm SEM 62.4 \pm 11.6%) compared to the NT control (Figures 2A and B). After treatment with aPL, the expression of SOCS-1 and SOCS-3 protein was also significantly inhibited (mean \pm SEM 76.4 \pm 6.0% and 30.1 \pm 5.2%, respectively) compared to the NT control (Figures 2A and C). This was reflected at the mRNA level. Treatment of trophoblasts with aPL significantly reduced *SOCS1* and *SOCS3* mRNA levels (mean \pm SEM 58.9 \pm 11.3% and 30.1 \pm

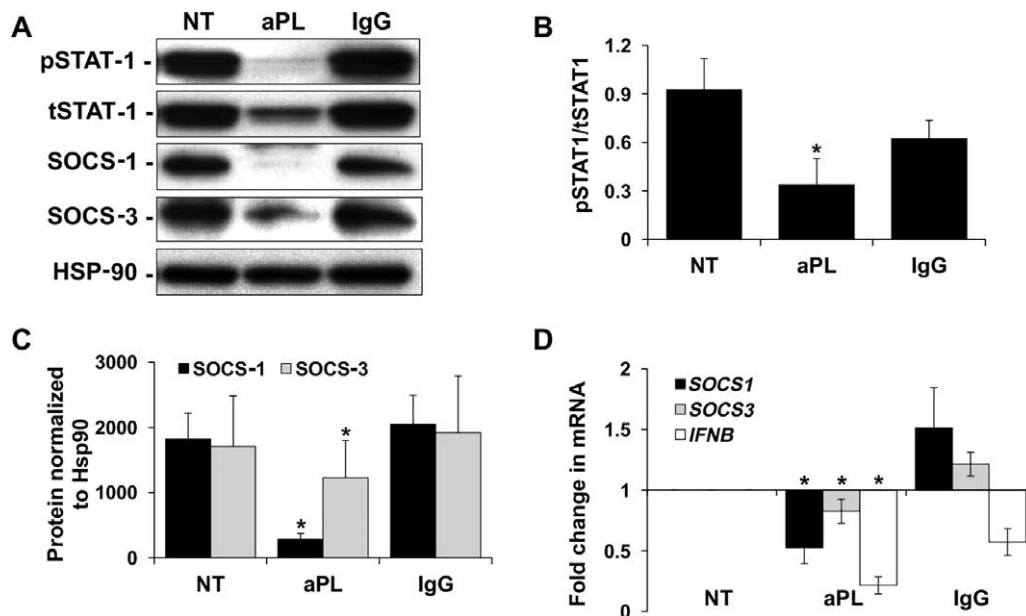


Figure 2. Antiphospholipid antibodies inhibit trophoblast TAM receptor signaling. Sw.71 cells were not treated (NT) or were treated with aPL or control IgG. Cellular RNA was collected after 48 hours, and cellular protein was collected after 72 hours. **A**, Western blotting was performed to detect phosphorylated STAT-1 (pSTAT-1) and total STAT-1 (tSTAT-1) as well as SOCS-1 and SOCS-3 levels. Hsp90 served as a loading control. Blots are from 1 representative experiment. **B** and **C**, The pSTAT-1:tSTAT-1 ratio ($n = 5$) (**B**) and SOCS-1 and SOCS-3 levels (**C**) were determined by densitometry, after normalization to Hsp90. **D**, The levels of *SOCS1*, *SOCS3*, and *IFNB* mRNA after normalization to GAPDH are shown. Bars show the mean \pm SEM of 3–5 samples (**C**) and 7–8 independent experiments (**D**). * = $P < 0.05$ versus NT. See Figure 1 for other definitions.

8.3%, respectively) when compared to the NT control (Figure 2D). Because type I interferons (IFNs) can also induce SOCS-1/SOCS-3 expression through activation of the IFN- α/β receptor (IFNAR) (34), the effects of aPL on these factors were examined. As shown in Figure 2D, treatment of trophoblasts with aPL significantly reduced *IFNB* mRNA levels ($78.6 \pm 7.0\%$) compared to the NT control, while control IgG had no significant effect. *IFNA* mRNA levels were not altered under all conditions (data not shown).

GAS6 reverses aPL-induced miR-146a-3p expression and IL-8 secretion, but not uric acid or IL-1 β production. To determine whether attenuation of the TAM receptor signaling pathway by aPL plays a role in regulating the trophoblast TLR-4-mediated inflammatory response (6,9,10), recombinant GAS6 was introduced into the culture. As shown in Figure 3A, TLR-4-mediated aPL-induced IL-8 secretion (part i) and miR-146a-3p expression (part ii) were both inhibited by the presence of recombinant GAS6. Recombinant GAS6 significantly inhibited aPL-induced IL-8 secretion ($29.7 \pm 9.8\%$) and miR-146a-3p expression ($37.8 \pm 9.0\%$). In contrast, the TLR-4-mediated induction of IL-1 β secretion (part iii), uric acid production (part iv), and caspase 1 activation (part v) by aPL was not altered by recombinant GAS6

(Figure 3A). As shown in Figure 3B, the aPL-mediated TLR-4-independent regulation of trophoblast VEGF, PlGF, soluble endoglin, and cell migration (7,8) was not reversed by the presence of recombinant GAS6. However, there were some minimal, yet statistically significant, effects of recombinant GAS6 on trophoblast angiogenic factor production. As shown in Figure 3B, recombinant GAS6 significantly increased aPL-induced VEGF (mean \pm SEM 1.1 ± 0.1 -fold) (part i), reduced basal PlGF ($16.8 \pm 10.1\%$) (part ii), and increased basal and aPL-induced expression of soluble endoglin (1.1 ± 0.1 and 1.2 ± 0.1 -fold, respectively) (part iii).

Antiphospholipid antibodies promote trophoblast soluble MERTK release through ADAM-17. We next investigated the mechanism by which aPL inhibit the TAM receptor signaling pathway, allowing for subsequent TLR-4-mediated miR-146a-3p expression and IL-8 secretion. The ectodomain of MERTK is proteolytically cleaved by the metalloproteinase ADAM-17 to generate soluble MERTK (35,36), while soluble AXL is released through activation of ADAM-10 (37). To investigate whether aPL treatment promoted the release of soluble AXL and soluble MERTK, which may account for the reduced cellular expression, trophoblasts were treated with or without aPL, and the cell-free culture supernatants

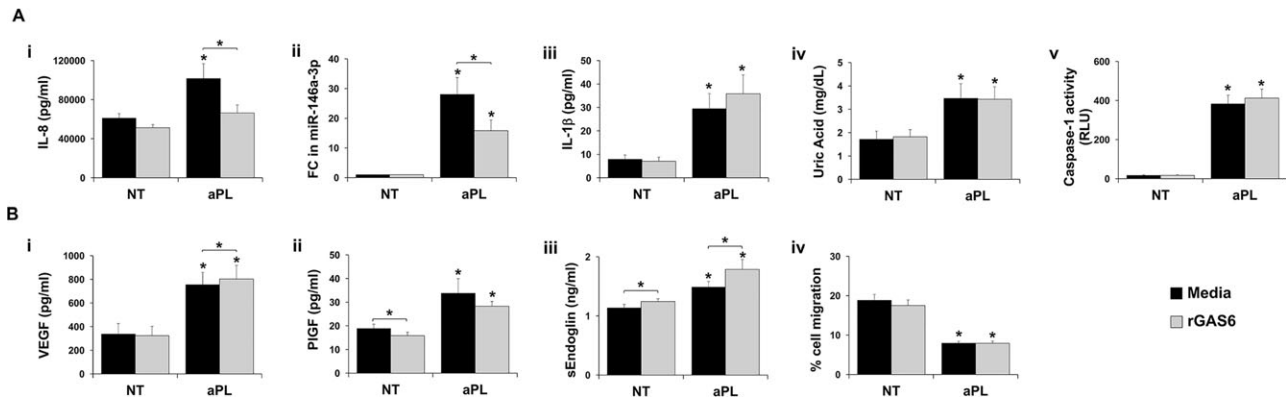


Figure 3. Recombinant growth arrest-specific protein 6 (rGAS6) reverses aPL-induced microRNA-146a-3p (miR-146a-3p) expression and interleukin-8 (IL-8) secretion. Sw.71 or HTR8 cells were not treated or were treated with aPL in the presence of media or rGAS6 (100 ng/ml). Cellular RNA was collected or cell migration was measured after 48 hours ($n = 5$), and cell-free supernatants were collected after 72 hours ($n = 5$). **A**, Toll-like receptor 4 (TLR-4)-mediated IL-8 secretion (part i), fold change (FC) in miR-146a-3p expression (part ii), IL-1 β secretion (part iii), uric acid secretion (part iv), and caspase 1 activity (part v) were measured. **B**, TLR-4-independent regulation of vascular endothelial growth factor (VEGF) secretion (part i) and placenta growth factor (PlGF) secretion (part ii), soluble endoglin (sEndoglin) secretion (part iii), and cell migration (part iv) were measured. Bars show the mean \pm SEM. * = $P < 0.05$ versus NT (media or rGAS6) unless otherwise indicated. RLU = relative luminescence units (see Figure 1 for other definitions).

were evaluated for the soluble receptors. As shown in Figure 4A, under both NT and IgG control conditions, soluble MERTK was undetectable by Western blotting. However, after exposure to aPL, there was a significant (mean \pm SEM 32.8 ± 3.1 -fold) increase in soluble MERTK expression. Surprisingly, under NT and IgG control conditions, there was a high amount of detectable soluble AXL, and treatment with aPL significantly reduced this ($57.7 \pm 13.9\%$) (Figure 4A). To examine the mechanism by which aPL promote trophoblast

soluble MERTK release, trophoblasts were treated with aPL in the presence or absence of an ADAM-17 inhibitor. As shown in Figure 4B, treatment of trophoblasts with the ADAM-17 inhibitor TAPI-0 completely and significantly reversed the ability of aPL to reduce cellular MERTK expression.

Elevated levels of circulating soluble AXL in pregnant women with aPL and adverse pregnancy outcomes. We next sought to determine whether our in vitro findings, which model what occurs in the placental

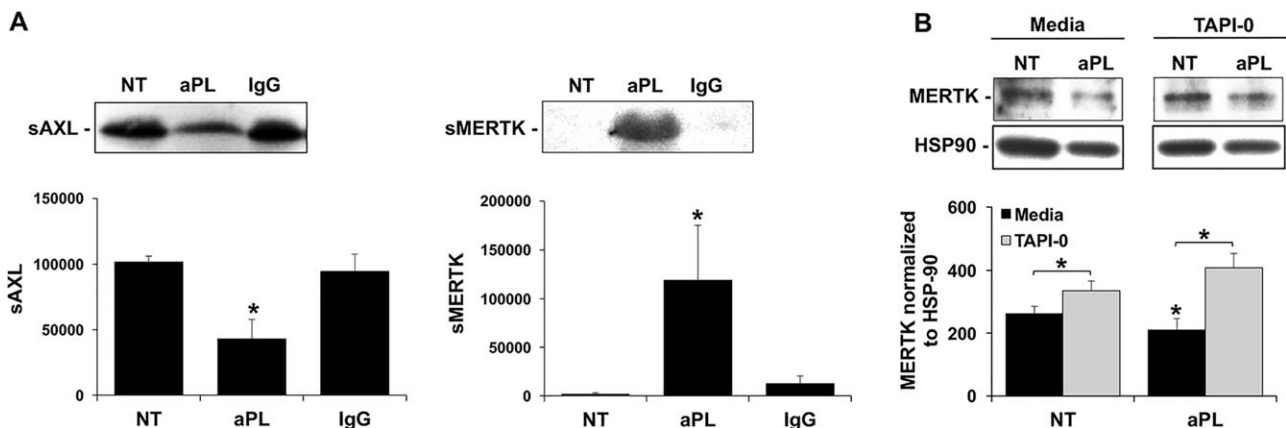


Figure 4. Antiphospholipid antibodies promote trophoblast soluble Mer tyrosine kinase (sMERTK) release through ADAM-17. **A**, Sw.71 cells were not treated or were treated with aPL or control IgG for 72 hours, after which cell-free supernatants were analyzed for soluble AXL (sAXL) and sMERTK by Western blotting. **B**, Sw.71 cells were not treated or were treated with aPL in the presence of media or the ADAM-17 inhibitor tumor necrosis factor α processing inhibitor 0 (TAPI-0) ($2.5 \mu\text{M}$). After 72 hours, cell lysates were collected. Soluble MERTK expression was measured by Western blotting. Hsp90 served as a loading control. The levels of sAXL and sMERTK were determined by densitometry ($n = 4$) after normalization to Hsp90. Blots are from 1 representative experiment. Bars show the mean \pm SEM. * = $P < 0.05$ versus NT under each condition (media or TAPI-0) unless otherwise indicated. See Figure 1 for other definitions.

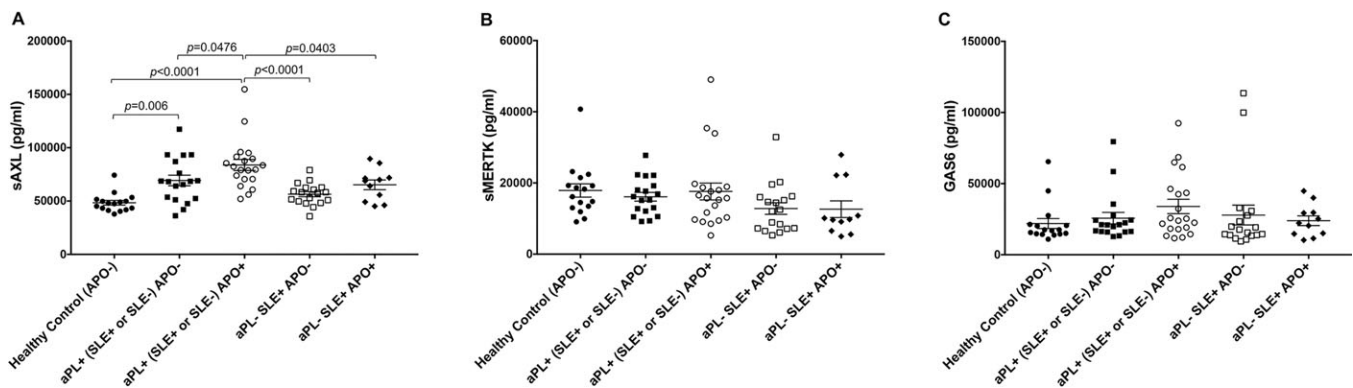


Figure 5. Circulating soluble AXL (sAXL) levels are elevated in pregnant women with antiphospholipid antibodies (aPL) and adverse pregnancy outcomes. The levels of soluble AXL (A), soluble Mer tyrosine kinase (sMERTK) (B), and growth arrest-specific protein 6 (GAS6) (C) were measured in plasma from healthy controls who did not have an adverse pregnancy outcome (APO-) ($n = 16$), aPL-positive women with or without systemic lupus erythematosus (SLE) who did not have an adverse pregnancy outcome ($n = 18$), aPL-positive women with or without SLE who had an adverse pregnancy outcome ($n = 20$), aPL-negative women with SLE who did not have an adverse pregnancy outcome ($n = 19$), and aPL-negative women with SLE who had an adverse pregnancy outcome ($n = 11$). Symbols represent individual subjects; horizontal lines with bars indicate the mean \pm SEM.

trophoblast at the maternal–fetal interface, were detectable at the systemic level. We analyzed plasma samples that were collected at 18–27 weeks’ gestation from aPL-positive pregnant women (with or without SLE) for soluble AXL, soluble MERTK, and GAS6 levels, and compared them to women with or without an adverse pregnancy outcome. As shown in Figure 5A, plasma levels of soluble AXL in aPL-positive women (with or without SLE) who did or did not have an adverse pregnancy outcome were significantly higher compared to the levels in plasma from healthy controls. Moreover, aPL-positive women (with or without SLE) who had an adverse pregnancy outcome had significantly higher levels of soluble AXL compared to aPL-positive women (with or without SLE) without an adverse pregnancy outcome (Figure 5A). To determine whether adverse pregnancy outcomes in women with autoimmune disease but without detectable aPL have aberrant expression of soluble AXL, we analyzed plasma from aPL-negative SLE patients with or without adverse pregnancy outcomes. Plasma levels of soluble AXL in aPL-negative SLE patients, either with an adverse pregnancy outcome or without an adverse pregnancy outcome, were not significantly different from those in healthy controls and were significantly lower than the levels in aPL-positive women (with or without SLE) with an adverse pregnancy outcome (Figure 5A). There were no significant differences in the plasma levels of soluble MERTK (Figure 5B) or GAS6 (Figure 5C) between any of the patient groups or controls.

Antiphospholipid antibodies inhibit trophoblast autophagy, leading to inflammasome activation. Despite inhibiting TAM receptor function, recombinant GAS6

did not reverse the effects of aPL on TLR-4-mediated uric acid production, caspase 1 activation, and subsequent IL-1 β secretion (9). Therefore, we examined other regulatory pathways that might be involved in the modulation of this aPL inflammasome-mediated response (9). Because autophagy is a negative regulator of inflammasome activity (18,19) and is active under normal conditions in extravillous trophoblasts (20), we investigated this process. As shown in Figure 6A, under NT and IgG control conditions, trophoblasts expressed the autophagy markers LC3B-I and LC3B-II and sequestosome 1 (p62), a specific autophagy substrate (38). After treatment with 2 different aPL (IIC5 and ID2), the trophoblast LC3B-II:LC3B-I ratio was significantly reduced compared to NT control (mean \pm SEM $43.3 \pm 20.1\%$ and $60.3 \pm 16.1\%$, respectively), while levels of p62 were unchanged under all treatment conditions (Figure 6A).

The levels of p62 are known to stabilize or accumulate when LC3B-II/LC3B-I-associated autophagy is impaired in the trophoblast and other model systems (20,38,39). To determine whether the observed reduction in autophagy might allow for aPL-mediated inflammasome function, trophoblast cells were treated with aPL in the presence of the autophagy inducer rapamycin. As shown in Figure 6B, although aPL-induced uric acid production was not affected by the presence of rapamycin (part i), aPL-induced caspase 1 activity (part i) and IL-1 β secretion (part ii) were significantly inhibited ($52.0 \pm 2.6\%$ and $77.1 \pm 3.6\%$, respectively). Figure 6C shows that in the absence of aPL, treatment of trophoblasts with the autophagy

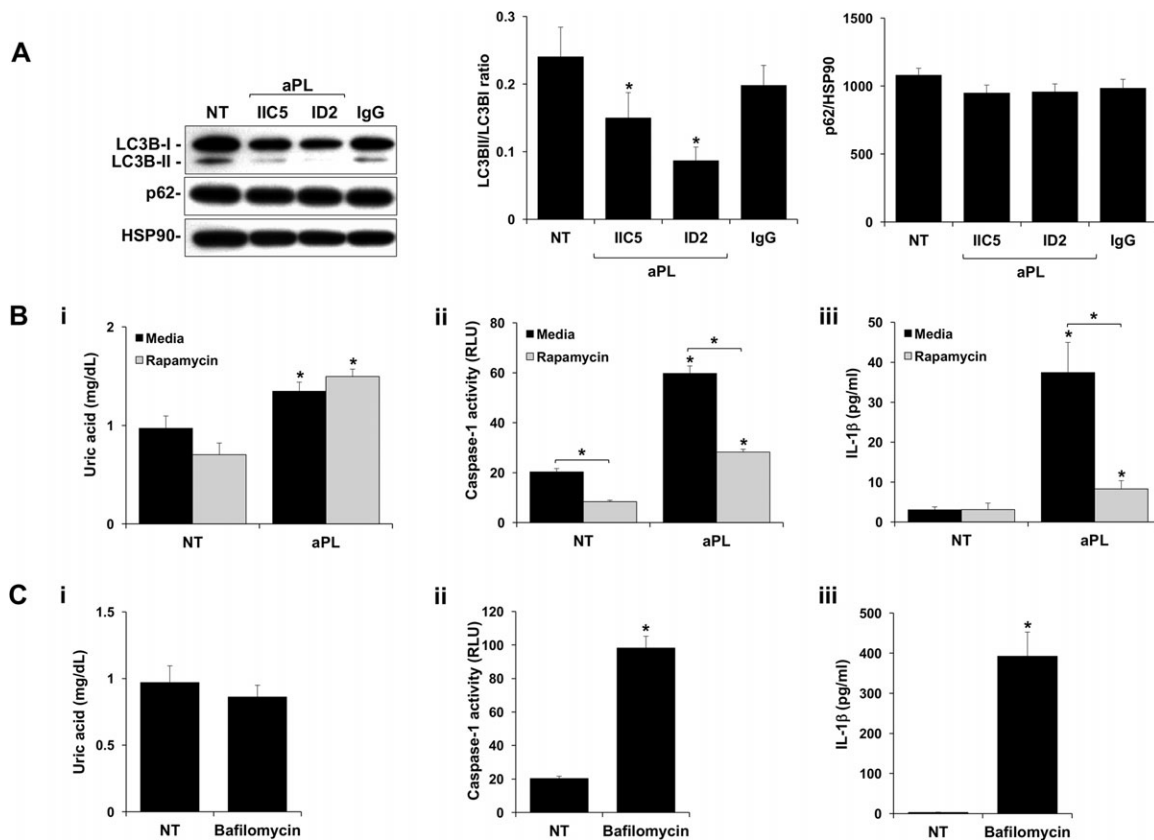


Figure 6. Antiphospholipid antibodies (aPL) inhibit trophoblast autophagy, leading to inflammasome activation. **A**, Sw.71 cells were not treated (NT) or were treated with aPL or control IgG. After 8 hours, cellular protein was collected. Western blotting was performed to detect light chain 3B-I (LC3B-I), LC3B-II, and p62. Hsp90 served as a loading control. Blots are from 1 representative experiment. The LC3B-II:LC3B-I ratio and levels of p62 were determined by densitometry after normalization to Hsp90 ($n = 4$). **B**, Sw.71 cells were not treated or were treated with aPL in the presence of media or rapamycin (500 nM). After 72 hours, supernatants were measured for uric acid (part i), caspase 1 activity (part ii), or interleukin-1 β (IL-1 β) (part iii) ($n = 6-7$). **C**, Sw.71 cells were not treated or were treated with bafilomycin (0.5 μ M). After 72 hours, supernatants were measured for uric acid (part i), caspase 1 activity (part ii), or IL-1 β (part iii) ($n = 6-7$). Bars show the mean \pm SEM. * = $P < 0.05$ versus NT control, unless otherwise indicated. RLU = relative luminescence units.

inhibitor bafilomycin had no effect on uric acid production (part i). However, when compared to the NT control, bafilomycin significantly increased trophoblast caspase 1 activity (4.8 ± 0.2 -fold) (part ii) and IL-1 β secretion (181.9 ± 50.8 -fold) (part iii).

DISCUSSION

Placental inflammation is a hallmark of pregnancy complications such as preeclampsia and preterm birth (40), but in many cases the trigger and mechanisms involved are unknown. In obstetric antiphospholipid syndrome, it is well established that pathogenic aPL recognizing β_2 GPI target the placenta, causing pathology that results in pregnancy loss and late gestational complications (5). Although pregnancies complicated by aPL show evidence of inflammation at the maternal-fetal interface

(2,3), our understanding of the mechanisms involved is incomplete. In the current study, we report for the first time that aPL override negative regulators of placental trophoblast TLR and inflammasome signaling to induce a robust inflammatory response.

Through the expression of a wide range of innate immune TLRs, nucleotide-binding oligomerization domain-like receptors (NLRs), and inflammasome family members, the trophoblast can generate diverse inflammatory, specialized, and regulatory responses to infectious stimuli (11,41). These pathways can also be activated by noninfectious triggers (42-44), including aPL (6,9,10). Specifically, aPL recognizing β_2 GPI, upon binding to human first-trimester extravillous trophoblasts, activate the TLR-4 pathway to induce endogenous secondary signals that in turn activate other innate immune pathways within the cell (6). TLR-4-mediated uric acid production in response

to anti- β_2 GPI antibodies activates the NLRP3 inflammasome, promoting an IL-1 β response (9). At the same time, TLR-4-mediated expression of miR-146a-3p leads to activation of TLR-8, promoting an IL-8 response (10). Recent studies of endothelial cells have also demonstrated that aPL activation of TLR-4 can lead to the induction of secondary mediators of pathology (45). It is important to note that both human polyclonal aPL and the well-characterized anti- β_2 GPI mAb used in the current study induced similar trophoblast inflammatory responses, specifically elevated IL-8 and uric acid-mediated IL-1 β processing and secretion (6,9). However, aPL are highly heterogeneous, and thus our findings may not apply to all aPL.

Despite being able to sense and respond to a number of different TLR and NLR ligands (41,46), physiologic doses of the natural TLR-4 agonist, LPS, are not sufficient to induce human first-trimester trophoblasts to generate a classic inflammatory cytokine response (11–14). A recent study showed that the type I interferon IFN β serves as a key immunomodulator of LPS-driven TLR-4 activation in the trophoblast (14), indicating that in these cells, TLR-4 signaling is indeed tightly regulated. Thus, in contrast to immune system cells, the trophoblast innate immune properties may be constitutively limited by negative regulatory mechanisms (16). The aim of the current study was to investigate how aPL recognizing β_2 GPI, which can directly interact with TLR-4 (45,47,48) and activate the TLR-4 pathway (6,9), might overcome such braking mechanisms.

Herein, we report that under basal conditions, human first-trimester trophoblasts constitutively express high levels of the TAM receptors AXL and MERTK and the TAM receptor ligands GAS6 and PROS1, indicating that TLR function in these cells is constitutively suppressed (16). Indeed, the TAM receptor signaling pathway is highly active in these cells under resting conditions, as evidenced by AXL, MERTK, and STAT-1 phosphorylation and high expression of SOCS-1 and SOCS-3. Although AXL has a greater affinity for GAS6 than does MERTK (49), unlike AXL, MERTK can bind both GAS6 and PROS1 (16). Thus, because trophoblasts produce both ligands, MERTK might be the dominant functional TAM receptor in resting human first-trimester trophoblasts. After exposure to anti- β_2 GPI aPL, trophoblast expression of total and phosphorylated AXL and MERTK as well as GAS6 was inhibited, resulting in inactivation of the TAM receptor signaling pathway. This allowed for the TLR-4-mediated miR-146a-3p-TLR-8 arm of the aPL-driven inflammatory pathway (10) to occur, since this could be blocked by recombinant GAS6. In addition to acting as a TAM receptor ligand, GAS6 can modulate AXL and MERTK expression (50,51).

Thus, the addition of recombinant GAS6 may serve as both an agonist and receptor modulator in order to reestablish TAM receptor function. As expected, the TLR-4-independent effects of aPL on trophoblast function were not reversed by recombinant GAS6.

One way in which TAM receptor expression and activation can be regulated is through the generation of proteolytically cleaved soluble proteins. Soluble AXL and soluble MERTK are released through activation of the metalloproteinases ADAM-10 and ADAM-17, respectively (35–37). In the current study, we show that under basal conditions, trophoblasts constitutively released soluble AXL, but not soluble MERTK. This further supports the notion that MERTK might be the dominant functional TAM receptor in human first-trimester trophoblasts under basal conditions. Treatment of trophoblasts with aPL induced the release of soluble MERTK, while soluble AXL release was reduced. Furthermore, under aPL conditions, ADAM-17 inhibition reversed the reduced cellular expression of MERTK. This suggests that aPL promotes the release of soluble MERTK from the trophoblast cell surface, which may account for the reduced cellular expression. Indeed, in other cell types, LPS can promote soluble MERTK release, resulting in reduced cellular expression (35,36). In contrast, the aPL-induced inhibition of cellular AXL expression may account for reduced soluble AXL release. How aPL are able to inhibit AXL protein expression in the trophoblast remains unclear but may involve AXL protein degradation. Soluble AXL and soluble MERTK act as decoy receptors for GAS6 to further prevent cell surface receptor activation. Thus, under aPL conditions, binding of GAS6 by the remaining soluble AXL and the increased level of soluble MERTK may also sequester it from detection and may be responsible, in part, for the aPL-mediated reduction in trophoblast GAS6.

Having demonstrated that aPL differentially regulated trophoblast release of soluble AXL and soluble MERTK, we sought to determine whether this might also be seen clinically at the systemic level. To investigate this, soluble AXL, soluble MERTK, and GAS6 levels were measured in plasma from aPL-negative and aPL-positive women enrolled in the PROMISSE study (9,10,30–33). Soluble MERTK and GAS6 levels in plasma were not different between the patient groups and controls. However, aPL-positive pregnant women (with or without SLE) had higher levels of circulating soluble AXL compared to controls. Moreover, aPL-positive women with an adverse pregnancy outcome had higher circulating levels of soluble AXL compared to aPL-positive women without an adverse pregnancy outcome. This finding was specific for aPL positivity, because soluble AXL levels in the aPL-negative groups with SLE were not different from those

in healthy controls. Although these findings did not reflect our *in vitro* findings, and thus what might occur locally at the maternal–fetal interface, these clinical data suggest that soluble AXL levels in plasma measured during the second trimester (18–27 weeks' gestation) might correlate with pregnancy outcome, although further investigation is warranted. Prior to this study, circulating soluble AXL, soluble MERTK, and GAS6 levels had been studied in nonpregnant patients with SLE, soluble AXL and soluble MERTK levels have been reported as being higher in SLE patients (52–54), while data for GAS6 levels vary (53,55). One study also showed that in SLE patients, elevated levels of soluble AXL and soluble MERTK were correlated with aPL positivity (56). However, our findings constitute the first report of soluble AXL, soluble MERTK, and GAS6 levels in pregnant women with aPL and/or SLE.

Another potential contributor to the disabled TAM receptor pathway in the trophoblast was the observed alterations in IFN β , because type I IFNs (through IFNAR), either alone or in cooperation with TAM receptors, can induce SOCS-1/SOCS-3 (34). Thus, inhibition of trophoblast IFN β expression by anti- β_2 GPI antibodies might contribute to inactivation of the TAM receptor signaling pathway. The ability of aPL to render IFN β signaling inactive is similar to findings in which trophoblasts were infected with a virus (14).

Although restoration of TAM receptor signaling by recombinant GAS6 prevented an aPL-mediated IL-8 response in the trophoblast, the TLR-4-mediated uric acid response, and subsequent NLRP3 inflammasome-mediated IL-1 β response (9) were not affected. This suggested that additional inhibitory pathways may be involved in regulating the aPL-induced trophoblast inflammatory response. Autophagy is a regulatory process that facilitates the degradation and recycling of cytoplasmic components via lysosomes (17). Although autophagy is important for cellular homeostasis and cell survival in response to a number of stresses (57), it can also act as a negative regulator of inflammasome activity and subsequent IL-1 β production (18,19).

In normal pregnancy, basal autophagy is essential for extravillous trophoblast invasion and vascular remodeling (20). Moreover, in the setting of preeclampsia, extravillous trophoblast autophagy is impaired, as evidenced by reduced LC3B expression and stabilization or accumulation of p62 (20), as has been observed in other systems (38,39). Consistent with this observation, we observed expression of the autophagy marker LC3B-II under resting conditions, but in the presence of aPL, LC3B-II expression was inhibited, and p62 levels were stabilized, indicating that autophagy was impaired.

Furthermore, inhibition of autophagy by bafilomycin induced a similar response to aPL, while maintenance of autophagy by rapamycin prevented aPL-induced inflammasome activity and subsequent IL-1 β secretion. Mechanisms by which autophagy may prevent inflammasome activation include inhibiting production of reactive oxygen species (58), promoting inflammasome degradation (18), or sequestering pro-IL-1 β and targeting it for lysosomal degradation (58). This latter mechanism is unlikely, because pro-IL-1 β is highly expressed in untreated trophoblasts (9). How the TLR-4-mediated uric acid response is regulated remains unclear, because it is modulated by neither the TAM receptor pathway nor autophagy.

In summary, our data showed that human extravillous trophoblast TLR and inflammasome function are tightly regulated by immunomodulatory pathways: TAM receptor activity and autophagy. Disabling of the TAM receptor signaling pathway by an anti- β_2 GPI antibody results in TLR-4 activation, leading to subsequent TLR-8-mediated IL-8 release. Impaired autophagy by this anti- β_2 GPI aPL allows inflammasome activity leading to IL-1 β production. These advancements in our understanding of the mechanisms by which anti- β_2 GPI aPL might mediate placental inflammation may further the potential for new predictive markers and therapeutic targets for preventing obstetric antiphospholipid syndrome.

ACKNOWLEDGMENTS

We thank Dr. Nancy Stanwood and Dr. Aileen Garpey for their assistance collecting patient tissue samples.

AUTHOR CONTRIBUTIONS

All authors were involved in drafting the article or revising it critically for important intellectual content, and all authors approved the final version to be published. Dr. Abrahams had full access to all of the data in the study and takes responsibility for the integrity of the data and the accuracy of the data analysis.

Study conception and design. Weel, Salmon, Peraçoli, Rothlin, Chamley, Abrahams.

Acquisition of data. Mulla, Weel, Potter, Gysler.

Analysis and interpretation of data. Mulla, Weel, Abrahams.

REFERENCES

1. D'Cruz DP, Khamashta MA, Hughes GR. Systemic lupus erythematosus. *Lancet* 2007;369:587–96.
2. Salmon JE, Girardi G, Lockshin MD. The antiphospholipid syndrome as a disorder initiated by inflammation: implications for the therapy of pregnant patients. *Nat Clin Pract Rheumatol* 2007;3:140–7.
3. Viall CA, Chamley LW. Histopathology in the placenta of women with antiphospholipid antibodies: a systematic review of the literature. *Autoimmun Rev* 2015;14:446–71.

4. Tong M, Viall CA, Chamley LW. Antiphospholipid antibodies and the placenta: a systematic review of their in vitro effects and modulation by treatment. *Hum Reprod Update* 2015;21:97–118.
5. Pantham P, Abrahams VM, Chamley LW. The role of anti-phospholipid antibodies in autoimmune reproductive failure. *Reproduction* 2016;151:R79–90.
6. Mulla MJ, Brosens JJ, Chamley LW, Giles I, Pericleous C, Rahman A, et al. Antiphospholipid antibodies induce a pro-inflammatory response in first trimester trophoblast via the TLR4/MyD88 pathway. *Am J Reprod Immunol* 2009;62:96–111.
7. Mulla MJ, Myrtolli K, Brosens JJ, Chamley LW, Kwak-Kim JY, Paidas MJ, et al. Antiphospholipid antibodies limit trophoblast migration by reducing IL-6 production and STAT3 activity. *Am J Reprod Immunol* 2010;63:339–48.
8. Carroll TY, Mulla MJ, Han CS, Brosens JJ, Chamley LW, Giles I, et al. Modulation of trophoblast angiogenic factor secretion by antiphospholipid antibodies is not reversed by heparin. *Am J Reprod Immunol* 2011;66:286–96.
9. Mulla MJ, Salmon JE, Chamley LW, Brosens JJ, Boeras CM, Kavathas PB, et al. A role for uric acid and the Nalp3 inflammasome in antiphospholipid antibody-induced IL-1 β production by human first trimester trophoblast. *PLoS One* 2013;8:e65237.
10. Gysler SM, Mulla MJ, Guerra M, Brosens JJ, Salmon JE, Chamley LW, et al. Antiphospholipid antibody-induced miR-146a-3p drives trophoblast interleukin-8 secretion through activation of Toll-like receptor 8. *Mol Hum Reprod* 2016;22:465–74.
11. Abrahams VM, Visintin I, Aldo PB, Guller S, Romero R, Mor G. A role for TLRs in the regulation of immune cell migration by first trimester trophoblast cells. *J Immunol* 2005;175:8096–104.
12. Abrahams VM, Bole-Aldo P, Kim YM, Straszewski-Chavez SL, Chaiworapongsa T, Romero R, et al. Divergent trophoblast responses to bacterial products mediated by TLRs. *J Immunol* 2004;173:4286–96.
13. Cardenas I, Mor G, Aldo P, Lang SM, Stabach P, Sharp A, et al. Placental viral infection sensitizes to endotoxin-induced pre-term labor: a double hit hypothesis. *Am J Reprod Immunol* 2011;65:110–7.
14. Racicot K, Kwon JY, Aldo P, Abrahams V, El-Guindy A, Romero R, et al. Type I interferon regulates the placental inflammatory response to bacteria and is targeted by virus: mechanism of polymicrobial infection-induced preterm birth. *Am J Reprod Immunol* 2016;75:451–60.
15. Lemke G, Rothlin CV. Immunobiology of the TAM receptors. *Nat Rev Immunol* 2008;8:327–36.
16. Rothlin CV, Carrera-Silva EA, Bosurgi L, Ghosh S. TAM receptor signaling in immune homeostasis. *Annu Rev Immunol* 2015;33:355–91.
17. Klionsky DJ, Emr SD. Autophagy as a regulated pathway of cellular degradation. *Science* 2000;290:1717–21.
18. Yuk JM, Jo EK. Crosstalk between autophagy and inflammasomes. *Mol Cells* 2013;36:393–9.
19. Latz E, Xiao TS, Stutz A. Activation and regulation of the inflammasomes. *Nat Rev Immunol* 2013;13:397–411.
20. Nakashima A, Yamanaka-Tatematsu M, Fujita N, Koizumi K, Shima T, Yoshida T, et al. Impaired autophagy by soluble endoglin, under physiological hypoxia in early pregnant period, is involved in poor placentation in preeclampsia. *Autophagy* 2013;9:303–16.
21. Straszewski-Chavez SL, Abrahams VM, Alvero AB, Aldo PB, Ma Y, Guller S, et al. Isolation and characterization of a novel telomerase immortalized first trimester trophoblast cell line, Swan 71. *Placenta* 2009;30:939–48.
22. Graham CH, Hawley TS, Hawley RG, MacDougall JR, Kerbel RS, Khoo N, et al. Establishment and characterization of first trimester human trophoblast cells with extended lifespan. *Exp Cell Res* 1993;206:204–11.
23. Chamley LW, Konarkowska B, Duncalf AM, Mitchell MD, Johnson PM. Is interleukin-3 important in antiphospholipid antibody-mediated pregnancy failure? *Fertil Steril* 2001;76:700–6.
24. Albert CR, Schlesinger WJ, Viall CA, Mulla MJ, Brosens JJ, Chamley LW, et al. Effect of hydroxychloroquine on antiphospholipid antibody-induced changes in first trimester trophoblast function. *Am J Reprod Immunol* 2014;71:154–64.
25. Viall CA, Chen Q, Stone PR, Chamley LW. Human extravillous trophoblasts bind but do not internalize antiphospholipid antibodies. *Placenta* 2016;42:9–16.
26. Viall CA, Chen Q, Liu B, Hickey A, Snowise S, Salmon JE, et al. Antiphospholipid antibodies internalised by human syncytiotrophoblast cause aberrant cell death and the release of necrotic trophoblast debris. *J Autoimmun* 2013;47:45–57.
27. Chamley LW, Allen JL, Johnson PM. Synthesis of β 2 glycoprotein 1 by the human placenta. *Placenta* 1997;18:403–10.
28. Quenby S, Mountfield S, Cartwright JE, Whitley GS, Chamley L, Vince G. Antiphospholipid antibodies prevent extravillous trophoblast differentiation. *Fertil Steril* 2005;83:691–8.
29. Potter JA, Garg M, Girard S, Abrahams VM. Viral single stranded RNA induces a trophoblast pro-inflammatory and antiviral response in a TLR8-dependent and -independent manner. *Biol Reprod* 2015;92:17.
30. Lockshin MD, Kim M, Laskin CA, Guerra M, Branch DW, Merrill J, et al. Prediction of adverse pregnancy outcome by the presence of lupus anticoagulant, but not anticardiolipin antibody, in patients with antiphospholipid antibodies. *Arthritis Rheum* 2012;64:2311–8.
31. Salmon JE, Heuser C, Triebwasser M, Liszewski MK, Kavanagh D, Roumenina L, et al. Mutations in complement regulatory proteins predispose to preeclampsia: a genetic analysis of the PROMISSE cohort. *PLoS Med* 2011;8:e1001013.
32. Buyon JP, Kim MY, Guerra MM, Laskin CA, Petri M, Lockshin MD, et al. Predictors of pregnancy outcomes in patients with lupus: a cohort study. *Ann Intern Med* 2015;163:153–63.
33. Andrade D, Kim M, Blanco LP, Karumanchi SA, Koo GC, Redecha P, et al. Interferon- α and angiogenic dysregulation in pregnant lupus patients who develop preeclampsia. *Arthritis Rheumatol* 2015;67:977–87.
34. Rothlin CV, Ghosh S, Zuniga EI, Oldstone MB, Lemke G. TAM receptors are pleiotropic inhibitors of the innate immune response. *Cell* 2007;131:1124–36.
35. Sather S, Kenyon KD, Lefkowitz JB, Liang X, Varnum BC, Henson PM, et al. A soluble form of the Mer receptor tyrosine kinase inhibits macrophage clearance of apoptotic cells and platelet aggregation. *Blood* 2007;109:1026–33.
36. Thorp E, Vaisar T, Subramanian M, Mautner L, Blobel C, Tabas I. Shedding of the Mer tyrosine kinase receptor is mediated by ADAM17 protein through a pathway involving reactive oxygen species, protein kinase C δ , and p38 mitogen-activated protein kinase (MAPK). *J Biol Chem* 2011;286:3335–44.
37. Weinger JG, Omari KM, Marsden K, Raine CS, Shafit-Zagardo B. Up-regulation of soluble Axl and Mer receptor tyrosine kinases negatively correlates with Gas6 in established multiple sclerosis lesions. *Am J Pathol* 2009;175:283–93.
38. Tanaka S, Hikita H, Tatsumi T, Sakamori R, Nozaki Y, Sakane S, et al. Rubicon inhibits autophagy and accelerates hepatocyte apoptosis and lipid accumulation in nonalcoholic fatty liver disease in mice. *Hepatology* 2016;64:1994–2014.
39. Wu YT, Tan HL, Shui G, Bauvy C, Huang Q, Wenk MR, et al. Dual role of 3-methyladenine in modulation of autophagy via different temporal patterns of inhibition on class I and III phosphoinositide 3-kinase. *J Biol Chem* 2010;285:10850–61.
40. Kim CJ, Romero R, Chaemsaitong P, Kim JS. Chronic inflammation of the placenta: definition, classification, pathogenesis, and clinical significance. *Am J Obstet Gynecol* 2015;213 Suppl:S53–69.
41. Abrahams VM. The role of the Nod-like receptor family in trophoblast innate immune responses. *J Reprod Immunol* 2011;88:112–7.
42. Han CS, Herrin MA, Pitruzzello MC, Mulla MJ, Werner EF, Pettker CM, et al. Glucose and metformin modulate human first trimester trophoblast function: a model and potential therapy for

- diabetes-associated uteroplacental insufficiency. *Am J Reprod Immunol* 2015;73:362–71.
43. Mulla MJ, Myrtolli K, Potter J, Boeras C, Kavathas PB, Sfakianaki AK, et al. Uric acid induces trophoblast IL-1 β production via the inflammasome: implications for the pathogenesis of preeclampsia. *Am J Reprod Immunol* 2011;65:542–8.
 44. Shirasuna K, Seno K, Ohtsu A, Shiratsuki S, Ohkuchi A, Suzuki H, et al. AGEs and HMGB1 increase inflammatory cytokine production from human placental cells, resulting in an enhancement of monocyte migration. *Am J Reprod Immunol* 2016;75:557–68.
 45. Laplante P, Fuentes R, Salem D, Subang R, Gillis MA, Hachem A, et al. Antiphospholipid antibody-mediated effects in an arterial model of thrombosis are dependent on Toll-like receptor 4. *Lupus* 2016;25:162–76.
 46. Abrahams VM. Pattern recognition at the maternal-fetal interface. *Immunol Invest* 2008;37:427–47.
 47. Sorice M, Longo A, Capozzi A, Garofalo T, Misasi R, Alessandri C, et al. Anti- β 2-glycoprotein I antibodies induce monocyte release of tumor necrosis factor α and tissue factor by signal transduction pathways involving lipid rafts. *Arthritis Rheum* 2007;56:2687–97.
 48. Raschi E, Chighizola CB, Grossi C, Ronda N, Gatti R, Meroni PL, et al. β 2-glycoprotein I, lipopolysaccharide and endothelial TLR4: three players in the two hit theory for anti-phospholipid-mediated thrombosis. *J Autoimmun* 2014;55:42–50.
 49. Schoumacher M, Burbridge M. Key roles of AXL and MER receptor tyrosine kinases in resistance to multiple anticancer therapies. *Curr Oncol Rep* 2017;19:19.
 50. Sun B, Qi N, Shang T, Wu H, Deng T, Han D. Sertoli cell-initiated testicular innate immune response through Toll-like receptor-3 activation is negatively regulated by Tyro3, Axl, and Mer receptors. *Endocrinology* 2010;151:2886–97.
 51. Cross SN, Potter JA, Aldo P, Kwon JY, Pitruzzello M, Tong M, et al. Viral infection sensitizes human fetal membranes to bacterial lipopolysaccharide by MERTK inhibition and inflammasome activation. *J Immunol* 2017;199:2885–95.
 52. Ekman C, Jonsen A, Sturfelt G, Bengtsson AA, Dahlback B. Plasma concentrations of Gas6 and sAxl correlate with disease activity in systemic lupus erythematosus. *Rheumatology (Oxford)* 2011;50:1064–9.
 53. Zhu H, Sun X, Zhu L, Hu F, Shi L, Fan C, et al. Different expression patterns and clinical significance of mAxl and sAxl in systemic lupus erythematosus. *Lupus* 2014;23:624–34.
 54. Wu J, Ekman C, Jonsen A, Sturfelt G, Bengtsson AA, Gottsater A, et al. Increased plasma levels of the soluble Mer tyrosine kinase receptor in systemic lupus erythematosus relate to disease activity and nephritis. *Arthritis Res Ther* 2011;13:R62.
 55. Kim HA, Nam JY, Jeon JY, An JM, Jung JY, Bae CB, et al. Serum growth arrest-specific protein 6 levels are a reliable biomarker of disease activity in systemic lupus erythematosus. *J Clin Immunol* 2013;33:143–50.
 56. Zizzo G, Guerrieri J, Dittman LM, Merrill JT, Cohen PL. Circulating levels of soluble MER in lupus reflect M2c activation of monocytes/macrophages, autoantibody specificities and disease activity. *Arthritis Res Ther* 2013;15:R212.
 57. Saito S, Nakashima A. The role of autophagy in extravillous trophoblast function under hypoxia [review]. *Placenta* 2013;34 Suppl:S79–84.
 58. Chen S, Sun B. Negative regulation of NLRP3 inflammasome signaling. *Protein Cell* 2013;4:251–8.
-

**The American College of Rheumatology is Launching an Open Access Journal
and Seeking an Editor-in-Chief**

DOI 10.1002/art.40553

The American College of Rheumatology is excited to announce that a third official journal of the College, *ACR Open Rheumatology*, is scheduled to be launched in January 2019. This journal will be entirely open access. The application for the position of Editor-in-Chief (2019–2021) is now available on the ACR web site. The deadline for applying is June 21, 2018. ACR/ARHP members who have current or past experience on the editorial board of *Arthritis & Rheumatology* or *Arthritis Care & Research* (Associate Editor level or higher) are invited to apply.

- diabetes-associated uteroplacental insufficiency. *Am J Reprod Immunol* 2015;73:362–71.
43. Mulla MJ, Myrtolli K, Potter J, Boeras C, Kavathas PB, Sfakianaki AK, et al. Uric acid induces trophoblast IL-1 β production via the inflammasome: implications for the pathogenesis of preeclampsia. *Am J Reprod Immunol* 2011;65:542–8.
 44. Shirasuna K, Seno K, Ohtsu A, Shiratsuki S, Ohkuchi A, Suzuki H, et al. AGEs and HMGB1 increase inflammatory cytokine production from human placental cells, resulting in an enhancement of monocyte migration. *Am J Reprod Immunol* 2016;75:557–68.
 45. Laplante P, Fuentes R, Salem D, Subang R, Gillis MA, Hachem A, et al. Antiphospholipid antibody-mediated effects in an arterial model of thrombosis are dependent on Toll-like receptor 4. *Lupus* 2016;25:162–76.
 46. Abrahams VM. Pattern recognition at the maternal-fetal interface. *Immunol Invest* 2008;37:427–47.
 47. Sorice M, Longo A, Capozzi A, Garofalo T, Misasi R, Alessandri C, et al. Anti- β 2-glycoprotein I antibodies induce monocyte release of tumor necrosis factor α and tissue factor by signal transduction pathways involving lipid rafts. *Arthritis Rheum* 2007;56:2687–97.
 48. Raschi E, Chighizola CB, Grossi C, Ronda N, Gatti R, Meroni PL, et al. β 2-glycoprotein I, lipopolysaccharide and endothelial TLR4: three players in the two hit theory for anti-phospholipid-mediated thrombosis. *J Autoimmun* 2014;55:42–50.
 49. Schoumacher M, Burbridge M. Key roles of AXL and MER receptor tyrosine kinases in resistance to multiple anticancer therapies. *Curr Oncol Rep* 2017;19:19.
 50. Sun B, Qi N, Shang T, Wu H, Deng T, Han D. Sertoli cell-initiated testicular innate immune response through Toll-like receptor-3 activation is negatively regulated by Tyro3, Axl, and Mer receptors. *Endocrinology* 2010;151:2886–97.
 51. Cross SN, Potter JA, Aldo P, Kwon JY, Pitruzzello M, Tong M, et al. Viral infection sensitizes human fetal membranes to bacterial lipopolysaccharide by MERTK inhibition and inflammasome activation. *J Immunol* 2017;199:2885–95.
 52. Ekman C, Jonsen A, Sturfelt G, Bengtsson AA, Dahlback B. Plasma concentrations of Gas6 and sAxl correlate with disease activity in systemic lupus erythematosus. *Rheumatology (Oxford)* 2011;50:1064–9.
 53. Zhu H, Sun X, Zhu L, Hu F, Shi L, Fan C, et al. Different expression patterns and clinical significance of mAxl and sAxl in systemic lupus erythematosus. *Lupus* 2014;23:624–34.
 54. Wu J, Ekman C, Jonsen A, Sturfelt G, Bengtsson AA, Gottsater A, et al. Increased plasma levels of the soluble Mer tyrosine kinase receptor in systemic lupus erythematosus relate to disease activity and nephritis. *Arthritis Res Ther* 2011;13:R62.
 55. Kim HA, Nam JY, Jeon JY, An JM, Jung JY, Bae CB, et al. Serum growth arrest-specific protein 6 levels are a reliable biomarker of disease activity in systemic lupus erythematosus. *J Clin Immunol* 2013;33:143–50.
 56. Zizzo G, Guerrieri J, Dittman LM, Merrill JT, Cohen PL. Circulating levels of soluble MER in lupus reflect M2c activation of monocytes/macrophages, autoantibody specificities and disease activity. *Arthritis Res Ther* 2013;15:R212.
 57. Saito S, Nakashima A. The role of autophagy in extravillous trophoblast function under hypoxia [review]. *Placenta* 2013;34 Suppl:S79–84.
 58. Chen S, Sun B. Negative regulation of NLRP3 inflammasome signaling. *Protein Cell* 2013;4:251–8.
-

**The American College of Rheumatology is Launching an Open Access Journal
and Seeking an Editor-in-Chief**

DOI 10.1002/art.40553

The American College of Rheumatology is excited to announce that a third official journal of the College, *ACR Open Rheumatology*, is scheduled to be launched in January 2019. This journal will be entirely open access. The application for the position of Editor-in-Chief (2019–2021) is now available on the ACR web site. The deadline for applying is June 21, 2018. ACR/ARHP members who have current or past experience on the editorial board of *Arthritis & Rheumatology* or *Arthritis Care & Research* (Associate Editor level or higher) are invited to apply.

A Multicenter Study of the Validity and Reliability of Responses to Hand Cold Challenge as Measured by Laser Speckle Contrast Imaging and Thermography

Outcome Measures for Systemic Sclerosis–Related Raynaud’s Phenomenon

Jack D. Wilkinson,¹ Sarah A. Leggett², Elizabeth J. Marjanovic², Tonia L. Moore², John Allen³, Marina E. Anderson⁴, Jason Britton⁵, Maya H. Buch,⁶ Francesco Del Galdo⁶, Christopher P. Denton⁷, Graham Dinsdale², Bridgett Griffiths,⁸ Frances Hall,⁹ Kevin Howell⁷, Audrey MacDonald,³ Neil J. McHugh,¹⁰ Joanne B. Manning², John D. Pauling¹¹, Christopher Roberts,¹ Jacqueline A. Shipley,¹⁰ Ariane L. Herrick¹² and Andrea K. Murray²

Objective. Reliable and objective outcome measures to facilitate clinical trials of novel treatments for systemic sclerosis (SSc)–related Raynaud’s phenomenon (RP) are badly needed. Laser speckle contrast imaging (LSCI) and thermography are noninvasive measures of perfusion that have shown excellent potential. This multicenter study was undertaken to determine the reliability and validity of a hand cold challenge protocol using LSCI, standard thermography, and low-cost cell phone/mobile

phone thermography (henceforth referred to as mobile thermography) in patients with SSc-related RP.

Methods. Patients with RP secondary to SSc were recruited from 6 UK tertiary care centers. The patients underwent cold challenge on 2 consecutive days. Changes in cutaneous blood flow/skin temperature at each visit were imaged simultaneously using LSCI, standard thermography, and mobile thermography. Measurements included area under the curve (AUC) for reperfusion/rewarming and maximum blood flow rate/skin temperature after

Supported by Arthritis Research UK (Clinical Studies grant 20656 and Centre for Epidemiology grant 20380), Actelion Pharmaceuticals (unrestricted educational grant), and the Manchester Academic Health Sciences Centre.

¹Jack D. Wilkinson, BSc, MSc, PhD, Christopher Roberts, BSc, PhD: University of Manchester, Manchester Academic Health Science Centre, Manchester, UK; ²Sarah A. Leggett, BSc, Elizabeth J. Marjanovic, BSc, PhD, Tonia L. Moore, BSc, Graham Dinsdale, MPhys, PhD, Joanne B. Manning, HNC, Andrea K. Murray, MPhys, PhD: University of Manchester, Manchester, UK, and Salford Royal Foundation, NHS Trust, Manchester Academic Health Science Centre, Salford, UK; ³John Allen, BEng, MSc, PhD, ASIS, FRPS, Audrey MacDonald, BSc, MSc: Freeman Hospital and Newcastle University, Newcastle upon Tyne, UK; ⁴Marina E. Anderson, FRCP, PhD: University of Liverpool, Liverpool, UK; ⁵Jason Britton, BSc, MSc, CSci: Leeds Teaching Hospitals NHS Trust, Leeds, UK; ⁶Maya H. Buch, MB ChB, FRCP, PhD, Francesco Del Galdo, MD, PhD: NIHR Leeds Musculoskeletal Biomedical Research Unit and Leeds Institute of Rheumatic and Musculoskeletal Medicine, Chapel Allerton Hospital, Leeds, UK; ⁷Christopher P. Denton, PhD, FRCP, Kevin Howell, BSc, MSc, PhD: University College London Medical School, London, UK; ⁸Bridgett Griffiths, MB ChB, MD, FRCP: Freeman Hospital, Newcastle upon Tyne Hospitals NHS Foundation Trust, Newcastle upon Tyne, UK; ⁹Frances Hall, MAxon, FRCP, DPhil: Cambridge University Hospitals NHS Foundation Trust, Cambridge, UK; ¹⁰Neil J. McHugh, MB ChB, MD, Jacqueline A. Shipley, BSc, MSc, PhD: Royal National Hospital for Rheumatic Diseases, Royal United Hospitals NHS

Foundation Trust, Bath, UK; ¹¹John D. Pauling, BMedSci, PhD, FRCP: Royal National Hospital for Rheumatic Diseases, Royal United Hospitals NHS Foundation Trust and University of Bath, Bath, UK; ¹²Ariane L. Herrick, MD, FRCP: University of Manchester and NIHR Manchester Musculoskeletal Biomedical Research Centre, Central Manchester NHS Foundation Trust, Manchester Academic Health Science Centre, Manchester, UK, and Salford Royal Foundation, NHS Trust, Manchester Academic Health Science Centre, Salford, UK.

Prof. Denton has received consulting fees, speaking fees, and/or honoraria from GlaxoSmithKline, Celgene, Actelion, Bayer, Sanofi, Roche-Genentech, Inventiva, and CSL Behring and Actelion (less than \$10,000 each). Dr. Pauling has received consulting fees, speaking fees, and/or honoraria (less than \$10,000) and research support from Actelion. Prof. Herrick has received consulting fees, speaking fees, and/or honoraria from Actelion, Apicrus, and GlaxoSmithKline (less than \$10,000 each) and research support from Actelion. Dr. Murray has received consulting fees, speaking fees, and/or honoraria from GlaxoSmithKline and Actelion (less than \$10,000) and research support from Actelion.

Address correspondence to Andrea K. Murray, MPhys, PhD, Room C214, Clinical Sciences Building, Centre for Musculoskeletal Research, School of Biological Sciences, Faculty of Biology, Medicine and Health, Division of Musculoskeletal and Dermatological Sciences, University of Manchester, Manchester Academic Health Science Centre, Salford Royal NHS Foundation, Manchester M13 9PT, UK. E-mail: Andrea.murray@manchester.ac.uk.

Submitted for publication August 4, 2017; accepted in revised form February 13, 2018.

rewarming (MAX). Test–retest reliability was assessed using intraclass correlation coefficients (ICCs). Estimated latent correlations (estimated from multilevel models, taking values between -1 and 1 ; denoted as rho values) were used to assess the convergent validity of LSCI and thermography.

Results. In total, 159 patients (77% with limited cutaneous SSc) were recruited (84% female, median age 63.3 years). LSCI and standard thermography both had substantial reliability, with ICCs for the reperfusion/rewarming AUC of 0.67 (95% confidence interval [95% CI] 0.54, 0.76) and 0.68 (95% CI 0.58, 0.80), respectively, and ICCs for the MAX of 0.64 (95% CI 0.52, 0.75) and 0.72 (95% CI 0.64, 0.81), respectively. Very high latent correlations were present for the AUCs of LSCI and thermography ($\rho = 0.94$; 95% CI 0.87, 1.00) and for the AUCs of standard and mobile thermography ($\rho = 0.98$; 95% CI 0.94, 1.00).

Conclusion. This is the first multicenter study to examine the reliability and validity of cold challenge using LSCI and thermography in patients with SSc-related RP. LSCI and thermography both demonstrated good potential as outcome measures. LSCI, standard thermography, and mobile thermography had very high convergent validity.

Systemic sclerosis (SSc)–related digital vasculopathy is painful and disabling, and has significant impact on quality of life. Raynaud’s phenomenon (RP) occurs in most patients with SSc (96%) and is consistently the highest ranked symptom of SSc in terms of frequency and impact on daily function (1,2). In patients with SSc, RP often progresses to severe digital vasculopathy, with up to 50% of patients developing painful digital ulceration (3–11).

Treatments are far from ideal, and Cochrane reviews (<http://www.cochranelibrary.com>) as well as other reviews have highlighted the lack of evidence base for the treatment of both primary and SSc-related RP (12–15). One of the reasons for this shortcoming is the lack of reliable outcome measures, which are necessary to deliver successful clinical trials. Technological advances in laboratory measurements of blood flow (laser speckle contrast imaging [LSCI] and thermography [skin temperature, a pseudo measure of perfusion]) hold promise as objective outcome measures (16,17). The Outcome Measures in Rheumatology 6 (OMERACT 6) report, describing the current status of outcome measure development for clinical trials in SSc, concluded that whether imaging techniques made the transition from research pathophysiologic measurement techniques to outcome measures for RP was dependent on whether “data are published or available to show their validity” (18). The requirement for reliable outcome measures to facilitate

highly powered clinical trials in SSc-related RP is now especially pertinent due to ongoing novel drug developments (19–23). Whereas patient-reported outcome measures such as the Raynaud’s condition score (RCS; a measure of RP disease activity with a possible score range of 0–10, with higher scores indicating more active disease) (24) are well suited for later (i.e., phase III) studies, objective, noninvasive imaging techniques would provide confirmatory testing to inform stop–go decision-making in earlier (i.e., phase II) studies.

Our main aim in the present study was to determine whether LSCI and thermography, performed subsequent to application of a cold challenge to the hands, are sufficiently reliable and valid to allow their use as outcome measures in multicenter clinical trials. Our primary objectives were to evaluate test–retest reliability and construct validity (25), which we defined as the ability of LSCI and thermography to measure important features of SSc-related digital vasculopathy. Our secondary objectives were to assess the interobserver reliability, as well as feasibility, of the techniques. Just prior to commencement of our study, cell phone/mobile phone thermography (henceforth referred to as mobile thermography) came on the market as an imaging method, potentially offering a more cost-effective and portable alternative to LSCI and “standard” thermography. Thus, an additional secondary objective was to assess the utility of mobile thermography in comparison to standard thermography.

PATIENTS AND METHODS

Patients. Six UK tertiary care centers that provide clinical care to patients with SSc took part in the study. Individuals responsible for imaging and analysis attended a central training session prior to the start of recruitment. At least one person from each center attended the training.

The study aimed to recruit 180 patients with SSc (for the inclusion and exclusion criteria used, including current digital ulceration, see Supplementary Table 1, available on the Arthritis & Rheumatology web site at <http://onlinelibrary.wiley.com/doi/10.1002/art.40457/abstract>). The study was approved by the Cambridgeshire and Hertfordshire National Research Ethics Service Committee (approval number 15/EE/0083), and all patients gave written consent to participate.

All patients were recruited between October 1, 2015 and February 28, 2016, to minimize interindividual variation related to season. Each visit took ~1 hour.

Imaging equipment. An LSCI thermal camera (FLPI-2; Moor Instruments) (16,17) was leased to each center (Figures 1A and 2B). Five of the 6 centers used their own thermal cameras (referred to as “standard thermography”) (Figures 1A, B, and D) (26), and the sixth center leased a camera. A mobile phone/device–connectable thermography camera (FLIR One) (Figures 1A and C) and an Apple iPhone 5 were purchased for each center, along with all other cold challenge equipment, to minimize variation between centers. Furthermore, to minimize differences between centers, equipment at each site was set up

according to strict guidelines for positioning to ensure images were obtained in as similar a manner as possible (in terms of angles and distances), and a calibration protocol was applied to the equipment at the start and end of the study (carried out by a single person from the central site [EJM]). LSCI settings were adjusted for distance, frequency, duration, focus, intensity overlay, processing mode (high resolution), and color image acquisition. Thermal camera settings were adjusted for room temperature, distance to hands, and skin emissivity. Mobile thermography settings were limited but the “matte” emissivity setting was chosen.

Cold challenge. Patients were requested to wear light clothing and refrain from vigorous exercise, caffeine, and alcohol for 4 hours prior to the assessment. Upon arrival, patients were seated comfortably for 20 minutes and acclimatized, and clinical research forms were completed. Immediately prior to the cold challenge, a baseline image of both hands (dorsal aspect) was obtained with LSCI and both thermal cameras. As required for LSCI imaging, all images were acquired in low-lit rooms.

The patient’s hands were placed on a black, thermally insulated surface (1 meter away from the thermal cameras and 70 cm [± 5 cm] from the LSCI). Small sticky dots were used to mark the location of each finger at baseline. Both hands were placed in nitrile gloves and immersed to the metacarpophalangeal joints for 1 minute into cooled water (temperature of 15°C [$\pm 1^{\circ}\text{C}$], measured by calibrated thermometer) in 2 standard containers, one on either side of the patient. After the cold challenge, the gloves were removed and the hands were returned to their original position on the insulating surface, secured by double-sided sticky tape to avoid movement between images.

Reperfusion/rewarming after application of the cold challenge was imaged simultaneously by LSCI at 15 frames per minute, and thermography at 4 frames per minute, for 15 minutes

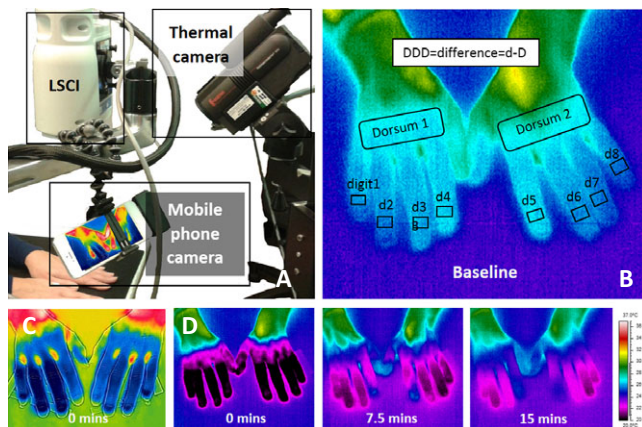


Figure 1. A, Photograph of the imaging equipment set up to allow simultaneous imaging, showing laser speckle contrast imaging (LSCI), standard thermography, and mobile thermography. B, Baseline image of the hands obtained with standard thermography, showing distal dorsal difference (DDD) regions of interest, with fingers being cooler than dorsum. C, An example of hands imaged by mobile thermography at 0 minutes post-cold challenge, with fingers being cooler than dorsum (scale unavailable for image due to the software used). D, An example of hands undergoing rewarming (same subject as in B) imaged by the standard thermal camera at 0 minutes, 7.5 minutes, and 15 minutes after cooling. Scale on the right refers to the temperature range ($20\text{--}37^{\circ}\text{C}$) shown in B and D.

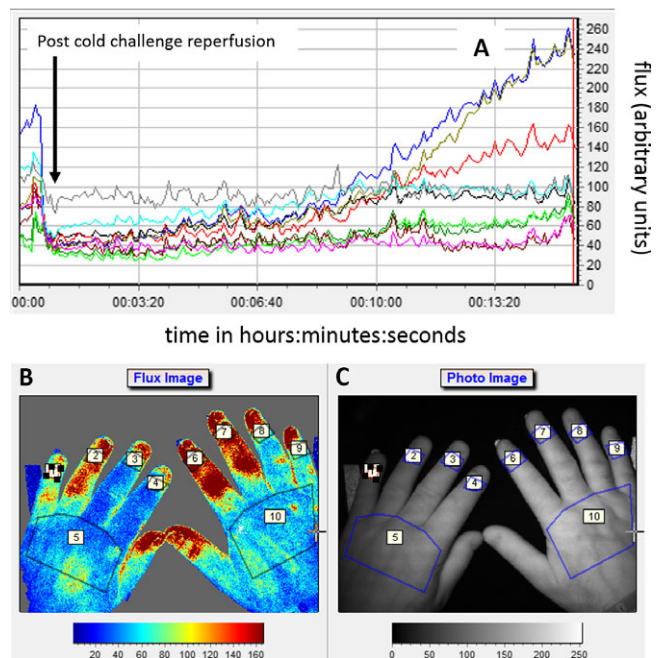


Figure 2. A, Laser speckle contrast imaging (LSCI) reperfusion graphs for 8 digits (regions of interest [ROIs] 1–4 and 6–9, as shown in B) and 2 dorsa (ROIs 5 and 10). Graphs show reperfusion post-cold challenge (i.e., flux, which was proportional to the product of the average speed of the blood cells and their concentration, expressed in arbitrary perfusion units) versus time. B, Example of a flux image (i.e., perfusion map) showing ROIs marked (as described in Figure 1). C, Photograph of the hands showing the ROIs assessed by LSCI.

(i.e., contemporaneous measurement for 15 minutes postcooling). Mobile thermography did not allow for continuous video images to be obtained, and thus single images from which data could be extracted were acquired at set time points: baseline, 0 minutes after cold challenge, and 15 minutes after cold challenge. At the end of the 15 minutes, 1 extra image was obtained for LSCI and standard thermography, to allow the reperfusion/rewarming gradient from the last data point to be calculated; thus, a total of 225 images/scans were obtained for LSCI, 61 for thermography, and 3 for mobile thermography during the 15 minutes of measurement.

Analysis of the images was performed using Moor Instruments Laser Perfusion Imager software (version 4.0) for LSCI, and Research IR Max (version 4.2; FLIR) for standard and mobile thermography. Patients completed the RCS (possible score range 0–10) at each visit (a measure referred to as “RCS on the day”), measuring the severity and impact of their RP for that day (24).

The cold challenge was repeated 1 day later (on day 2), as close as possible to the same time of day in order to minimize variation due to circadian rhythms (27). The repetition over 2 consecutive days (i.e., ~ 24 hours) minimized any variations within individuals over time (e.g., menstrual cycle effects) and seasonal variation in weather (28). Five centers had 1 observer, while 1 center had 2 observers. Each examiner re-examined the same subject on days 1 and 2; for example, at the central site, 1 observer imaged 60 patients, twice, on consecutive days. Figure 3 shows the study design.

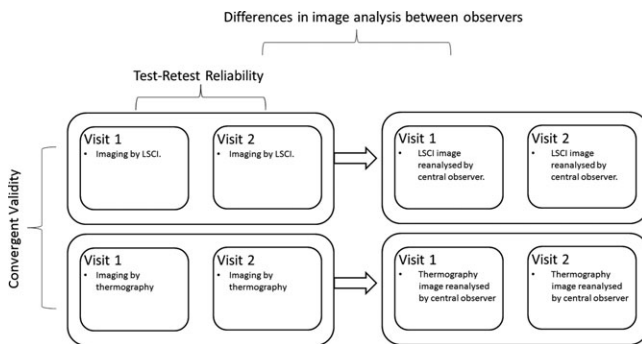


Figure 3. Study design. The images obtained were assessed for convergent validity, test–retest reliability, and interobserver differences. LSCI = laser speckle contrast imaging.

Image analysis for summary measures of response.

Image analysis was carried out locally by an internal, nonblinded observer at each center. These were the same observers who had obtained the images. Regions of interest (ROIs) (Figures 1B and 2B and C) were highlighted in the baseline (pre–cold challenge) image and in sequential images for 15 minutes postcooling. The distal dorsal difference (DDD) (defined as the difference in measurements between the dorsum and the finger, with DDD_L , DDD_T , and DDD_M representing the values based on LSCI, standard thermography, and mobile thermography, respectively) (29,30) was calculated for each finger at baseline. In the sequential images, the ROIs were confined to the 8 distal phalanges. The area under the curve (AUC) for reperfusion/rewarming in each finger (with AUC_L , AUC_T , and AUC_M representing the values based on LSCI, standard thermography, and mobile thermography, respectively) was calculated manually, not by automation (Figure 4) (standard thermography), from 61 postchallenge images. In addition, the maximum blood flow rate/skin temperature after rewarming (MAX; with MAX_L , MAX_T , and MAX_M representing the values based on LSCI, standard thermography, and mobile thermography, respectively) and the gradient of reperfusion/rewarming in the first 2 minutes post–cold challenge (GRAD; with $GRAD_L$, $GRAD_T$, and $GRAD_M$ representing the values based on LSCI, standard thermography, and mobile thermography, respectively) were determined. Data were averaged for all fingers, as was done in previous studies (16). For mobile thermography, the DDD was obtained from the first of 3 images, and the AUC was approximated by averaging the data over the latter 2 images. Analysis took <1 hour per participant, per visit.

Saved images and ROI local analysis data were also analyzed by the blinded central observer (TLM). Mobile thermography image analysis was carried out only at the central site.

Assessment of feasibility. The feasibility of each technique was assessed at the end of the study based on the individual opinion of the clinical scientist or technician. Feasibility was measured as the ease of use and the ease of analysis (score scale for each 0–10, where 0 = difficult, 10 = easy), and preference of LSCI over thermography (standard or mobile thermography) for acquiring and analyzing images.

Measurement of room temperature. A prerequisite of the cold challenge, and thus a criterion for center participation, was a temperature-controlled room at each center. All measurements were obtained in a temperature-controlled room (aimed at a room temperature of $23^\circ\text{C} \pm 2^\circ\text{C}$). Room temperatures

were recorded with data monitors (TinyTag; Gemini Data Loggers) to assess the impact of temperature on measurements, with an interest in examining whether reliability could be improved by achieving greater temperature control.

Identification of edge effects from LSCI. It became apparent when the study began that the blood flow appeared to be lower at the edges of the LSCI images than in the center. This implied that the distribution of the laser light across the hands was not equal, with less light incident toward the edges than at the center of the image. If true, then the consequence of this would be an artificially lower value for perfusion in the little fingers (edge of image) (Figure 2B) compared to index fingers (center of image) in the LSCI images. Thus, this was investigated further, as detailed below.

Statistical analysis. Sample size calculation. Analyses of the data were performed using R version 3.2.3 (31). Based on observations in a previous thermography study (16), a sample size of 180 patients would allow us to estimate the test–retest reliability to within 0.05. A full discussion of the sample size calculation and other aspects of the statistical analyses (extended statistical analysis) are available from the corresponding author upon request.

Determination of test–retest reliability. To determine the test–retest reliability of each technique, intraclass correlation coefficients (ICCs) were obtained using linear mixed effects models. Each summary measure was included as a dependent variable, with center included as a fixed effect.

Determination of between-observer reliability. The data over both visits for each patient were averaged, and the resulting average values were compared between the central observer and the center-specific observers by calculating the difference (with 95% confidence interval [95% CI]) in the paired mean values (details available from the corresponding author upon request). It is not possible to calculate a valid interobserver ICC from these data, since it would require at least some of the participants to have traveled to all sites for imaging and a large subset of images to be analyzed by all observers (32).

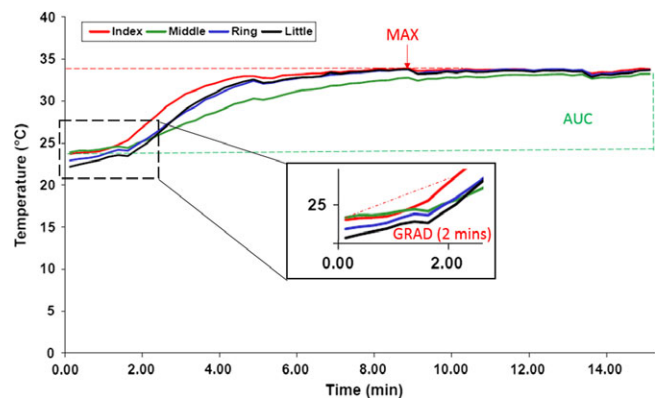


Figure 4. Example of a reperfusion/rewarming area under the curve (AUC), maximum blood flow rate/skin temperature after rewarming (MAX), and gradient of reperfusion/rewarming in the first 2 minutes post–cold challenge (GRAD) for 1 hand, measured with standard thermography. The data for the index, middle, ring, and little finger are shown as 4 solid lines, one for each finger (regions of interest were confined to the 8 distal phalanges, as indicated in Figure 2B). Color figure can be viewed in the online issue, which is available at <http://onlinelibrary.wiley.com/doi/10.1002/art.40457/abstract>.

Determination of validity of the techniques. Convergent validity (one aspect of construct validity) was assessed using bivariate linear mixed models, which included fixed center terms and separate random patient intercepts for 1) LSCI and standard thermography, and 2) standard and mobile thermography. We estimated the latent correlation coefficients (if the techniques measured the same construct, the latent correlation would be a rho value of 1). For clarity, the statistical analysis protocol for this joint model is available from the corresponding author upon request.

A post hoc analysis was conducted in which the responses to the RCS corresponding to the study day were assessed for correlation with all measurements, using linear mixed models.

Feasibility data. Descriptive statistics were used to summarize the feasibility data.

Mixed effects models accounting for room temperature. The mean room temperature at each patient visit was added to the mixed effects models for each summary measure. ICCs were recalculated, and these values were compared to the previously calculated estimates.

Analysis of edge effects. Edge effects were investigated in a post hoc analysis by calculating the trend across fingers for LSCI measurements, and then comparing these measurements to those from thermography. Linear mixed models were used to assess any linear trends in the measurements from the index finger to the little finger. Fingers were numbered. Finger-level summary measures of response were then regressed on finger number for both LSCI and thermography; this linear approximation was crude, but sufficient. Random intercept and slope terms were included to account for the fact that there was variation from patient to patient in these trends, not attributable to the imaging techniques. Measurements were standardized prior to analysis, thereby allowing for comparisons to be made between LSCI and thermography.

RESULTS

Characteristics of the patients. In total, 159 patients were recruited (60 from the central center, 16–20

from each of the other centers). Among the patients, 157 (99%) fulfilled the American College of Rheumatology/European League Against Rheumatism 2013 classification criteria for SSc (33). The median age of the patients was 63.3 years (interquartile range [IQR] 53.8–69.5 years) and 123 (77%) had limited cutaneous SSc (34). The median disease duration since first non-Raynaud's symptom was 9.6 years (IQR 4.5–17.4 years). Of the 159 patients with SSc, 142 (89%) were receiving treatment with vasodilators (61 with calcium channel blockers, 27 with angiotensin-converting enzyme inhibitors, 27 with angiotensin II receptor antagonist, 22 with phosphodiesterase 5 inhibitor, 4 with endothelin receptor antagonist, and 1 with nitrates), of whom 35 were receiving ≥ 1 vasodilator. Moreover, 4 patients (3%) had previously undergone finger surgical debridements, 5 (3%) had previously had amputations, and 30 (19%) had experienced ulcers in the preceding year.

Test-retest reliability of the techniques. There was at least moderate to substantial reliability in the DDD_L , DDD_M , and DDD_T , the AUC_L , AUC_T , and AUC_M , and the MAX_L and MAX_T . The $GRAD_L$ and $GRAD_T$ had fair to substantial test-retest reliability (Table 1). The strength of reliability was assessed according to previously defined score classifications (see ref. 35), as follows: ICC 0.00–0.20 = slight, ICC 0.21–0.40 = fair, ICC 0.41–0.60 = moderate, ICC 0.61–0.80 = substantial, and ICC 0.81–1.00 = almost perfect. However, these classifications are, to some extent, arbitrary and should be treated as a rough guide.

Reliability between observers. When the data from each visit, observer, and center, and additionally at the patient level, were analyzed for reliability (see Supplementary Table 2 and Supplementary Figure 1, available

Table 1. Reliability and validity of LSCI and thermography (standard and mobile phone-based) in patients with systemic sclerosis-related Raynaud's phenomenon*

Summary measure	Test-retest reliability			Difference in reliability, LSCI versus standard thermography	Validity	
	LSCI (n = 159)	Standard thermography (n = 159)	Mobile phone thermography (n = 141)†		LSCI and standard thermography	Standard and mobile phone thermography
Distal dorsal difference	0.67 (0.56, 0.77)	0.58 (0.43, 0.71)	0.61 (0.51, 0.73)	0.08 (–0.05, 0.25)	0.65 (0.50, 0.79)	0.90 (0.79, 0.97)
Reperfusion/rewarming AUC_{log}	0.67 (0.54, 0.76)	0.68 (0.58, 0.80)	0.61 (0.51, 0.72)‡	–0.01 (–0.17, 0.11)	0.94 (0.87, 1.00)	0.98 (0.94, 1.00)
MAX_{log}	0.64 (0.52, 0.75)	0.72 (0.64, 0.81)	NA	–0.09 (–0.21, 0.03)	0.87 (0.77, 0.95)	NA
Gradient over first 2 minutes	0.46 (0.40, 0.69)	0.56 (0.40, 0.74)	NA	–0.09 (–0.24, 0.18)	0.52 (0.33, 0.70)	NA

* Data for the summary measures of distal dorsal difference, reperfusion/rewarming area under the curve (AUC_{log}), maximum blood flow rate/skin temperature after rewarming (MAX_{log}), and gradient of reperfusion/rewarming over the first 2 minutes have been averaged over 8 digits. Values are the intraclass correlation coefficients (ICCs) (with 95% confidence intervals [95% CIs]) for the test-retest reliability of laser speckle contrast imaging (LSCI), standard thermography, and mobile phone-based thermography, the difference (with 95% CIs) in ICC point estimates between LSCI and standard thermography, and the estimated validity, expressed as latent correlation coefficients (with 95% CIs), between LSCI and standard thermography and between standard and mobile phone thermography. NA = not applicable.

† For mobile phone thermography, 141 data sets were available (n = 18 missing due to technical fault at 2 of the centers).

‡ The AUC_{log} for mobile phone thermography was approximated from the mean values of 2 frames, post-cold challenge of the hand.

on the Arthritis & Rheumatology web site at <http://online.library.wiley.com/doi/10.1002/art.40457/abstract>), we considered that if the measures were perfectly reliable, the subplot for each center would look like 2 identical ladder plots (but it is not expected that the plots would be identical between centers). Our data suggest that there were systematic differences between the central observer and one of the centers (center 2, and possibly center 3 [details available from the corresponding author upon request]) in extracting data from LSCI images. For thermography, agreement between the central and local observer was generally high for all centers, albeit with a large discrepancy in the data from several patients at one of their visits (results available from the corresponding author upon request).

Validity of the techniques. The latent correlation between LSCI and standard thermography (i.e., evidence that LSCI and standard thermography measure the same construct, which, in this case, was blood flow returning to the finger after cold challenge) was as follows: for the DDD, $\rho = 0.65$ (95% CI 0.50, 0.79); for the reperfusion/re-warming AUC, $\rho = 0.94$ (95% CI 0.87, 1.00); and for the MAX, $\rho = 0.87$ (95% CI 0.77, 0.95). In contrast, for the GRAD, the latent correlation between LSCI and standard thermography was only 0.52 (95% CI 0.33, 0.70) (Table 1). High latent correlation is indicative of convergent validity. Therefore, a value of 0.7 could be considered high, such that both the MAX and the AUC displayed strong convergent validity.

Correlation between mobile thermography and standard thermography was also very high. The latent correlation was 0.98 (95% CI 0.94, 1.00) for the AUC, and 0.90 (95% CI 0.79, 0.97) for the DDD (Table 1). Latent correlation between LSCI and mobile thermography was 0.86 (95% CI 0.74, 0.97) for the AUC, and 0.49 (95% CI 0.29, 0.66) for the DDD.

With the exception of some weak evidence of a decreasing DDD as measured on thermography with increasing RCS score (mean \pm SEM change in the DDD_T of -0.15 ± 0.07 for a 1-point increase in the RCS), we found no evidence of correlation between the summary measures and the RCS.

Feasibility. Standard thermography was deemed to be more feasible than LSCI (see Discussion). The proportion of raters giving a score of ≥ 7 for ease of use was 50% for LSCI, 75% for standard thermography, and 38% for mobile thermography. Ease of analysis was rated as ≥ 7 by 25% of raters for LSCI and by 50% of raters for standard thermography. One center preferred LSCI to thermography for acquiring images, and 1 center preferred LSCI to thermography for analyzing images. Conversely, the number of centers preferring standard thermography over LSCI was 3 for acquiring

images, and 4 for analyzing images. The remaining centers showed no preference.

Models including room temperature. When included as a covariate, room temperature was not associated with any of the summary measures, as measured by either LSCI or thermography. Additionally, the ICCs were not affected by the inclusion of room temperature in the analysis. This does not mean that a regulated room temperature is not important, but that small changes in temperature are acceptable (see Supplementary Table 3, available on the Arthritis & Rheumatology web site at <http://onlinelibrary.wiley.com/doi/10.1002/art.40457/abstract>).

Edge effects. When moving from the thumb to the little finger on imaging, all of the trends in the AUC, MAX, and GRAD were in the opposite direction for the 2 modalities, with a decrease in these values when assessed by LSCI and an increase in these values when assessed by thermography (see Supplementary Table 4, available on the Arthritis & Rheumatology web site at <http://onlinelibrary.wiley.com/doi/10.1002/art.40457/abstract>) Estimates of the DDD were positive with both techniques, but this was attenuated on images obtained by LSCI. This is consistent with the notion of an edge effect artificially producing lower values for the little fingers when LSCI is used for imaging. The cause of the edge effect was attributed to the distribution of light over the imaging area, due to LSCI being used at the upper limit of the suggested imaging distance in order to fit both hands into the imaging area. These data indicate that care must be taken to understand the variations over the field of view, so that these can be accounted for; decreasing the field of view would minimize this effect in future studies.

DISCUSSION

To date, LSCI techniques and thermography have been insufficiently studied as outcome measures in clinical trials. Those studies in which they have been included show very little consistency in terms of protocol design (36–38), choice of dynamic challenge, and extracted outcome measures, making it difficult to compare results between studies or establish a standard protocol. The main finding of our study is that the reliability of both LSCI and thermography (the AUC and MAX) were sufficiently high for use as study outcome measures. The reliability of the MAX_T was slightly superior to the MAX_L. Other than this, there were no substantive differences in reliability between the 2 techniques.

The AUC_M and DDD_M showed adequate reliability for use as outcome measures. Moreover, there was strong correlation between mobile thermography and

standard thermography data. The technique of mobile thermography was added at a late stage in this project (since it had only just come on the market). Our reason for including it was primarily for feasibility assessment. While it is clear that further work is required to validate mobile thermography, the performance in the present study is highly encouraging, because, as a low-cost tool, it could potentially be readily available for widespread use among rheumatologists.

Although it was not our primary objective, we examined differences between observers. Systematic differences between observers at different centers would not be particularly problematic for a multicenter randomized controlled trial (RCT), provided that the randomization would be stratified by center. We note that this should be the default for any multicenter trial, since differences between centers may otherwise bias the estimated treatment effect. This is particularly true in small populations, since simple randomization is less likely to produce balance within centers. Standardized training would reduce measurement variation across centers, and centralized extraction and analysis of LSCI data, conducted in a blinded manner, might also minimize variation by removing multiobserver differences in an RCT setting. Given the small sample size at each center, we are unable to determine whether truly systematic differences were observed. Ideally, a study to assess interobserver reliability would involve participants having images analyzed by all observers.

Convergence between the techniques was shown to be very high for the AUC and MAX (particularly for the AUC). This finding provides evidence that the same underlying construct is being measured when using these summaries of response. Convergence appeared to be weaker (although still moderate) for the DDD. Convergence was weakest for the GRAD, which may be a reflection of the lag between reperfusion and rewarming, whereby tissue reperfusion (measured using LSCI) is translated into skin rewarming (measured using thermography), during the 2 minutes immediately following cold challenge.

Since there is no gold standard to which we may compare either imaging technique, and we are comparing 2 techniques that measure perfusion by very different methods (skin temperature and a measure of red blood cell concentration and speed by light), it is possible to measure convergence between these techniques for validity (25). It would be unlikely for these 2 techniques to converge if both of them were poor outcome measures, since they would both have to be deficient in distinct but very specific ways, so as to bring the erroneous observations into alignment. Therefore, we can conclude in this instance that their convergence implies validity.

The OMERACT review of 2003 (18) assessed the validity of several noninvasive techniques as possible objective outcome measures, but none was deemed ready for use in clinical trials. These techniques included nail-fold capillaroscopy, which is a well-established diagnostic technique now included in the diagnostic criteria to differentiate primary and secondary RP (34). The microscopy technique allows visualization of cutaneous capillaries at the nailbed and identification of the structural changes characteristic of SSc. However, this is not a substitute for functional measures of flow (although functional flow and oxygenation have recently been reported). Plethysmography allows the change in vascular volume to be measured (i.e., detection of a pulse) in combination with cold challenge. The technique can measure full fields in the same way as LSCI, but remains unvalidated. There was no relationship between the summary measures and the RCS on the day of the study visits, for either LSCI or thermography.

Patient-centered outcome measures are crucial for evaluating the effectiveness (rather than just the efficacy) of treatments. However, patient-centered outcomes often comprise more “noise” compared to more objective measures of response, and therefore necessitate larger sample sizes to ensure adequate power in clinical trials. For small populations, there is therefore a tension between direct relevance to patients and feasibility of conducting a trial. One solution may be to power studies on the basis of objective measures, such as those considered herein, and to additionally (and consistently) report patient-centered outcomes to facilitate an eventual meta-analysis. Another solution might be to seek confirmatory evidence for the vasodilatory potential of candidate interventions, using objective measures, before proceeding to larger, phase III clinical trials.

The relationship between 2 measures is limited by the reliability of each (39). Although the relative stability of the RCS between baseline and follow-up has been observed in clinical trials/studies (38,40), there has been little work formally assessing its intraindividual reliability.

With regard to feasibility of the techniques, it has been noted that LSCI is sensitive to movement, vibrations, and lighting, indicating the importance of environmental conditions during the imaging. For mobile thermography, present limitations in feasibility include the battery life (LSCI is mainly operated but standard thermography is powered by long-life batteries), a fixed focusing distance, and lack of analysis for video images, as well as mounting difficulties; however, if the correlation between mobile and standard thermography can be replicated in future studies, these limitations may be acceptable in light of the lower cost and ambulatory (convenient) nature of the technique.

When comparing the feasibility of LSCI to the feasibility of thermography, it should be noted that most centers were familiar with thermography but not with LSCI, and therefore this may have influenced the assessment of feasibility.

One limitation of the study was that we did not recruit the planned number of participants, due to a seventh center not participating as planned. However, the study was designed to be robust to under-recruitment. Although the 95% CIs for our estimates were wider than they would have been had the target been met, we were still able to demonstrate sufficient reliability and convergent validity of the AUC and MAX to observe differences that would indicate that the performance of DDD was weaker, and to show that the performance of GRAD was relatively poor.

In conclusion, our design was relatively pragmatic, with the aim of establishing the performance of the different techniques as they would be employed in a multicenter clinical trial. Our study successfully established a working group of tertiary care centers for SSc, and together, the group developed a consensus calibration and cold challenge protocol. The summary measures of AUC and MAX both displayed good reliability and strong convergent validity. There was a possible advantage of thermography in relation to the reliability of MAX, although this was not definitive. We found evidence of edge effects when using LSCI, although our summary measures appeared to be quite robust to these in relation to reliability, perhaps suggesting that these effects were fairly consistent (details available upon request from the corresponding author).

The results of this study also confirm that small variations in room temperature are acceptable during the imaging, and that, subject to further validation, mobile phone cameras may be a suitable, affordable, and highly portable alternative to more expensive standard imaging equipment (although mobile phones are battery operated and with less functionality [at present] than larger thermal cameras). The mobile phone data obtained in this study will facilitate the design of future validation studies assessing mobile thermography-derived outcome measures. Although the design precluded formal assessment of interobserver reliability, there was a suggestion of systematic differences between the central observer and observers at some of the centers, highlighting the importance of image analysis training and potentially a role for centralized or automated image analysis. For multicenter RCTs, we would also recommend that, where possible or appropriate, randomization be stratified by center to balance any center-specific effects and prevent bias.

In summary, LSCI and thermography should now be incorporated as secondary outcome measures in upcoming treatment efficacy trials. This will allow

an assessment of responsiveness to treatment as well as longitudinal validity. The present study leads us to recommend the summary measures of AUC and MAX, measured using either thermography or LSCI (but especially using thermography), as suitable outcome measures for RCTs in patients with SSc-related RP.

ACKNOWLEDGMENTS

We are grateful to the trial steering and data monitoring committee members (Dr. Mohammed Akil, Prof. David D'Cruz, and the late Prof. Peter Wells). We also thank Dipa Ghedia at the London site and Sookhoe Eng at the Leeds site for patient recruitment, Darren Hart at the Bath site for imaging and analysis, and Anita Furlong and Tracey Drayton at the Cambridge site for imaging. We wish to thank the UK Scleroderma Study Group for their advice and support in the development and running of this study, and Moor Instruments and Thermal Vision Research for their advice and training. We would also like to acknowledge the assistance given by IT Services and the use of the Computational Shared Facility at The University of Manchester.

AUTHOR CONTRIBUTIONS

All authors were involved in drafting the article or revising it critically for important intellectual content, and all authors approved the final version to be published. Dr. Murray had full access to all of the data in the study and takes responsibility for the integrity of the data and the accuracy of the data analysis.

Study conception and design. Wilkinson, Leggett, Marjanovic, Moore, Allen, Anderson, Britton, Buch, Del Galdo, Denton, Dinsdale, Griffiths, Hall, Howell, MacDonald, McHugh, Manning, Pauling, Roberts, Shipley, Herrick, Murray.

Acquisition of data. Wilkinson, Leggett, Marjanovic, Moore, Allen, Anderson, Britton, Buch, Del Galdo, Denton, Dinsdale, Griffiths, Hall, Howell, MacDonald, McHugh, Manning, Pauling, Roberts, Shipley, Herrick, Murray.

Analysis and interpretation of data. Wilkinson, Moore, Allen, Anderson, Britton, Buch, Del Galdo, Denton, Dinsdale, Griffiths, Hall, Howell, MacDonald, McHugh, Manning, Pauling, Roberts, Shipley, Herrick, Murray.

REFERENCES

1. Walker UA, Tyndall A, Czirják L, Denton C, Farge-Bancel D, Kowal-Bielecka O, et al. Clinical risk assessment of organ manifestations in systemic sclerosis: a report from the EULAR Scleroderma Trials and Research Group database. *Ann Rheum Dis* 2007;66:754–63.
2. Willems LM, Kwakkenbos L, Leite CC, Thombs BD, van den Hoogen FH, Maia AC, et al. Frequency and impact of disease symptoms experienced by patients with systemic sclerosis from five European countries. *Clin Exp Rheumatol* 2014;32:S88–93.
3. Rodnan GP, Myerowitz RL, Justh GO. Morphological changes in the digital arteries of patients with progressive systemic sclerosis (scleroderma) and Raynaud's phenomenon. *Medicine* 1980;59:393–408.
4. Herrick A. Diagnosis and management of scleroderma peripheral vascular disease. *Rheum Dis Clin North Am* 2008;34:89–114.
5. Steen VD, Powell DL, Medsger TA Jr. Clinical correlations and prognosis based on serum autoantibodies in patients with systemic sclerosis. *Arthritis Rheum* 1988;31:196–203.

6. Della Rossa A, Valentini G, Bombardieri S, Bencivelli W, Silman AJ, D'Angelo S, et al. European multicentre study to define disease activity criteria for systemic sclerosis: clinical and epidemiological features of 290 patients from 19 centres. *Ann Rheum Dis* 2001;60:585–91.
7. Ferri C, Valentini G, Cozzi F, Sebastiani M, Michelassi C, La Montagna G, et al. Systemic sclerosis: demographic, clinical and serologic features and survival in 1,012 Italian patients. *Rheumatology (Oxford)* 2002;81:139–53.
8. Mawdsley AH. Patient perception of UK scleroderma services: results of an anonymous questionnaire. *Rheumatology (Oxford)* 2006;45:1573.
9. Tiev KP, Diot E, Clerson P, Dupuis-Siméon F, Hachulla E, Hatron PY, et al. Clinical features of scleroderma patients with or without prior or current ischemic digital ulcers: post-hoc analysis of a nationwide multicenter cohort (ItinérAIR-Sclérodermie). *J Rheumatol* 2009;36:1470–6.
10. Khimdas S, Harding S, Bonner A, Zummer B, Baron M, Pope J, et al. Associations with digital ulcers in a large cohort of systemic sclerosis: results from the Canadian Scleroderma Research Group Registry. *Arthritis Care Res (Hoboken)* 2011;63:142–9.
11. Ennis H, Vail A, Wragg E, Taylor A, Moore T, Murray A, et al. A prospective study of systemic sclerosis-related digital ulcers: prevalence, location, and functional impact. *Scand J Rheumatol* 2013;42:483–6.
12. Ennis H, Hughes M, Anderson ME, Wilkinson J, Herrick AL. Calcium channel blockers for primary Raynaud's phenomenon. *Cochrane Database Syst Rev* 2016;2:CD002069.
13. Herrick AL. Raynaud's phenomenon (secondary). *BMJ Clin Evid* 2008;1125.
14. Stewart M, Morling JR. Oral vasodilators for primary Raynaud's phenomenon. *Cochrane Database Syst Rev* 2012:CD006687.
15. García de la Peña Lefebvre P, Nishishinya MB, Pereda CA, Loza E, Sifuentes Giraldo WA, Román Ivorra JA, et al. Efficacy of Raynaud's phenomenon and digital ulcer pharmacological treatment in systemic sclerosis patients: a systematic literature review. *Rheumatol Int* 2015;35:1447–59.
16. Murray AK, Moore TL, Manning JB, Taylor C, Griffiths CE, Herrick AL. Noninvasive imaging techniques in the assessment of scleroderma spectrum disorders. *Arthritis Rheum* 2009;61:1103–11.
17. Pauling JD, Shipley JA, Raper S, Watson ML, Ward SG, Harris ND, et al. Comparison of infrared thermography and laser speckle contrast imaging for the dynamic assessment of digital microvascular function. *Microvasc Res* 2012;83:162–7.
18. Merkel PA, Clements PJ, Reveille JD, Suarez-Almazor ME, Valentini G, Furst DE, et al. Current status of outcome measure development for clinical trials in systemic sclerosis: report from OMERACT 6. *J Rheumatol* 2003;30:1630–47.
19. Herrick AL. Secondary Raynaud's phenomenon. *BMJ Clin Evid* 2008:1125.
20. Cerinic M, Denton CP, Furst DE, Mayes MD, Hsu VM, Carpentier P, et al. Bosentan treatment of digital ulcers related to systemic sclerosis: results from the RAPIDS-2 randomised, double-blind, placebo-controlled trial. *Ann Rheum Dis* 2011;70:32–8.
21. Fava A, Wung PK, Wigley FM, Hummers LK, Daya NR, Ghazarian SR, et al. Efficacy of Rho kinase inhibitor fasudil in secondary Raynaud's phenomenon. *Arthritis Care Res (Hoboken)* 2012;64:925–9.
22. Khanna D, Denton CP, Merkel PA, Krieg T, Le Brun FO, Marr A, et al. Effect of macitentan on the development of new ischemic digital ulcers in patients with systemic sclerosis: DUAL-1 and DUAL-2 randomized clinical trials. *JAMA* 2016;315:1975–88.
23. Seibold JR, Wigley FM, Schiopu E, Denton CP, Silver RM, Steen VD, et al. Digital ulcers in SSc treated with oral treprostinil: a randomized, double-blind, placebo-controlled study with open-label follow-up. *J Scleroderma Relat Disord* 2017;2:42–9.
24. Merkel PA, Herlyn K, Martin RW, Anderson JJ, Mayes MD, Bell P, et al. Measuring disease activity and functional status in patients with scleroderma and Raynaud's phenomenon. *Arthritis Rheum* 2002;46:2410–20.
25. Streiner DL, Norman GR, Cairney J. Health measurement scales: a practical guide to their development and use. New York: Oxford University Press; 2014.
26. Clark S, Dunn G, Moore T, Jayson M IV, King TA, Herrick AL. Comparison of thermography and laser Doppler imaging in the assessment of Raynaud's phenomenon. *Microvasc Res* 2003;66:73–6.
27. Houben AJ, Slaaf DW, Huvers FC, de Leeuw PW, Nieuwenhuijzen Kruseman AC, Schaper NC. Diurnal variations in total forearm and skin microcirculatory blood flow in man. *Scand J Clin Lab Invest* 1994;54:161–8.
28. Bartelink ML, Wollersheim H, Theeuwes A, van Duren D, Thien T. Changes in skin blood flow during the menstrual cycle: the influence of the menstrual cycle on the peripheral circulation in healthy female volunteers. *Clin Sci (Lond)* 1990;78:527–32.
29. Clark S, Hollis S, Campbell F, Moore T, Jayson M, Herrick A. The "distal-dorsal difference" as a possible predictor of secondary Raynaud's phenomenon. *J Rheumatol* 1999;26:1125–8.
30. Anderson M, Moore T, Lunt M, Herrick AL. The 'distal-dorsal difference': a thermographic parameter by which to differentiate between primary and secondary Raynaud's phenomenon. *Rheumatology (Oxford)* 2007;46:533–8.
31. R Core Team (2015). The R project for statistical computing web site. URL: <https://www.R-project.org/>.
32. Eliasziw M, Young SL, Woodbury MG, Fryday-Field K. Statistical methodology for the concurrent assessment of interrater and intrarater reliability: using goniometric measurements as an example. *Phys Ther* 1994;74:777–88.
33. Van den Hoogen F, Khanna D, Fransen J, Johnson SR, Baron M, Tyndall A, et al. 2013 classification criteria for systemic sclerosis: an American College of Rheumatology/European League Against Rheumatism collaborative initiative. *Arthritis Rheum* 2013;65:2737–47.
34. LeRoy EC, Black C, Fleischmajer R, Jablonska S, Krieg T, Medsger TA Jr, et al. Scleroderma (systemic sclerosis): classification, subsets and pathogenesis. *J Rheumatol* 1988;15:202–5.
35. Landis JR, Koch GG. The measurement of observer agreement for categorical data. *Biometrics* 1977;33:159–74.
36. Pauling J, Shipley J, Harris N, McHugh NJ. Use of infrared thermography as an endpoint in therapeutic trials of Raynaud's phenomenon and systemic sclerosis. *Clin Exp Rheumatol* 2012;30:S103–15.
37. Allen J, Howell K. Microvascular imaging: techniques and opportunities for clinical physiological measurements. *Physiol Meas* 2014;35:R91–141.
38. Pauling JD, Shipley JA, Hart DJ, McGrogan A, McHugh NJ. Use of laser speckle contrast imaging to assess digital microvascular function in primary Raynaud phenomenon and systemic sclerosis: a comparison using the Raynaud Condition Score Diary. *J Rheumatol* 2015;42:1163–8.
39. Fleiss JL. Reliability of measurement. In: *The design and analysis of clinical experiments*. Hoboken: John Wiley & Sons; 2011. p. 1–32.
40. Gladue H, Maranian P, Paulus HE, Khanna D. Evaluation of test characteristics for outcome measures used in Raynaud's phenomenon clinical trials. *Arthritis Care Res (Hoboken)* 2013;65:630–6.

Skin Gene Expression Is Prognostic for the Trajectory of Skin Disease in Patients With Diffuse Cutaneous Systemic Sclerosis

Giuseppina Stifano,¹ Thierry Sornasse,² Lisa M. Rice,¹ Leo Na,¹ Haiyin Chen-Harris,² Dinesh Khanna,³ Angelika Jahreis,² Yuqing Zhang,¹ Jeff Siegel,² and Robert Lafyatis⁴

Objective. At present, there are no clinical or laboratory measures that accurately forecast the progression of skin fibrosis and organ involvement in patients with systemic sclerosis (SSc). The goal of this study was to identify skin biomarkers that could be prognostic for the progression of skin fibrosis in patients with early diffuse cutaneous SSc (dcSSc).

Methods. We analyzed clinical data and gene expression in skin biopsy samples from 38 placebo-treated patients, part of the Roche Safety and Efficacy of Subcutaneous Tocilizumab in Adults with Systemic Sclerosis (FASSCINATE) phase II study of tocilizumab in SSc. RNA samples were analyzed using nCounter. A trajectory model based on a modified Rodnan skin thickness score was used to describe 3 skin disease trajectories over time. We examined the association of skin gene expression with skin score trajectory groups, by

chi-square test. Logistic regression was used to examine the prognostic power of each gene identified.

Results. We found that placebo-treated patients with high expression of messenger RNA for CD14, SERPINE1, IL13RA1, CTGF, and OSMR at baseline were more likely to have progressive skin score trajectories. We also found that those genes were prognostic for the risk of skin progression and that IL13RA1, OSMR, and SERPINE1 performed the best.

Conclusion. Skin gene expression of biomarkers associated with macrophages (CD14, IL13RA1) and transforming growth factor β activation (SERPINE1, CTGF, OSMR) are prognostic for progressive skin disease in patients with dcSSc. These biomarkers may provide guidance in decision-making about which patients should be considered for aggressive therapies and/or for clinical trials.

Currently there are no clinical or laboratory measures that accurately predict the progression of skin fibrosis and organ involvement in patients with systemic sclerosis (SSc). Several studies, including retrospective cohort analyses and randomized clinical trials, have shown that the severity of skin fibrosis, as assessed by the modified Rodnan skin thickness score (MRSS) (1), is predictive of disease mortality (2,3). In particular, Shand et al defined 3 distinct skin score trajectory subgroups, using latent variable modeling, and showed that patients with the worst skin score trajectories had significantly increased mortality (4).

Several clinical and serologic measures have been associated with progressive skin disease. It is generally accepted that the fastest rates of skin disease progression are recorded early in the disease (5). A recent observational study from the European League Against Rheumatism (EUSTAR) has shown that joint synovitis, short disease duration (<15 months), and low MRSS at baseline predict more progressive skin fibrosis (6). Anti-RNA polymerase III is associated with scleroderma renal crisis and more severe skin disease, though less associated with

ClinicalTrials.gov identifier: NCT01532869.

Supported by Boston University Medical Center (NIH Clinical and Translational Science Institute grant UL1-TR-000157) and the NIH (Research Project Grant Program grant 2R01-AR-051089). Dr. Lafyatis' work was supported by grant 5P30-AR-061271 from the National Institute of Arthritis and Musculoskeletal and Skin Diseases Scleroderma Core Centers, and grants 1P50-AR-060780 and 2R01-AR-051089 from the Scleroderma Center of Research Translation.

¹Giuseppina Stifano, MD, PhD, Lisa M. Rice, PhD, Leo Na, MPH, Yuqing Zhang, DSc: Boston University School of Medicine, Boston, Massachusetts; ²Thierry Sornasse, PhD, Haiyin Chen-Harris, PhD, Angelika Jahreis, MD, Jeff Siegel, MD: Genentech, San Francisco, California; ³Dinesh Khanna, MD, MS: University of Michigan Scleroderma Program, Ann Arbor; ⁴Robert Lafyatis, MD: University of Pittsburgh Medical Center, Pittsburgh, Pennsylvania.

Drs. Sornasse, Chen-Harris, and Siegel own stock or stock options in Hoffmann-La Roche. Dr. Khanna has received consulting fees from Actelion, Bayer, Covis, Cytori, EMD Serono, Genentech/Roche, Gilead, GlaxoSmithKline, and Sanofi-Aventis (less than \$10,000 each) and research support from Bayer, Bristol-Myers Squibb, Genentech/Roche, and Sanofi-Aventis. Dr. Jahreis owns stock or stock options in Hoffmann-La Roche and holds a patent for tocilizumab.

Address correspondence to Giuseppina Stifano, MD, PhD, Boston University School of Medicine, 72 East Concord Street, E5 Arthritis Center, Boston, MA 02118. E-mail: stifanog@bu.edu.

Submitted for publication January 24, 2017; accepted in revised form February 8, 2018.

interstitial lung disease (5,7). Despite these findings, there remains no broadly accepted methodology for assessing the likelihood of progressive skin disease and no validated prognostic biomarkers of skin disease evolution, limiting patient risk-stratification and consequently the ability to select patients with progressive disease to receive innovative therapies.

We recently reported that CD14 expression correlates strongly with progressive skin disease (8). In this report, using data collected from the Safety and Efficacy of Subcutaneous Tocilizumab in Adults with Systemic Sclerosis (FASSCINATE) study, an international trial of tocilizumab (TCZ) in SSc (9), we describe trajectory patterns of skin score change over time, as determined using a group-based modeling approach in placebo-treated patients. We assessed several potential prognostic biomarkers associated with these changes. In addition, we examined the relationship of each biomarker to the change in skin score over time.

PATIENTS AND METHODS

Study design and participants. Samples and clinical data for the discovery cohort used in this study were from the FASSCINATE phase II study (10). Briefly, the FASSCINATE study was a randomized, double-blind, placebo-controlled, phase II study of TCZ (162 mg/week, administered subcutaneously) in early diffuse cutaneous SSc (dcSSc) patients age ≥ 18 years, with progressive disease of < 5 years' duration since the first non-Raynaud's phenomenon sign or symptom. Investigators who enrolled at least one patient in the FASSCINATE study are listed in Appendix A. In the current analysis, we focused on the FASSCINATE patients treated with placebo. Of these patients ($n = 44$), we excluded 6 subjects. Two patients did not have a biopsy at baseline. One patient had only 2 MRSS values recorded (at baseline and at 8 weeks) and discontinued the study at week 16. The other 3 excluded patients had a decrease in MRSS of > 12 units in 2 sequential assessments, suggesting that the measurement of the MRSS trajectory in these patients would be unreliable.

Skin biopsy gene expression analysis. RNA samples, used for assessment of gene expression, were analyzed using nCounter (NanoString Technologies). Expression of the genes was normalized to expression of 12 housekeeping genes. Of the 83 genes selected for confirmation and expression analysis, 62 transcripts were significantly overexpressed and 2 were significantly underexpressed in SSc patients compared with healthy controls (significance assessed by *t*-test with Bonferroni correction for multiple comparisons). Microarray data from the FASSCINATE trial, used for selecting prognostic genes, has been deposited at the GEO (accession no. GSE106358) at the NCBI.

Statistical analysis. We have described patterns of skin score change over time using a semiparametric mixture model (11). Specifically, the distinctive skin score trajectories were derived by modeling skin score as a function of time, i.e., the number of days in the study, using a SAS macro (more specifically, TRAJ, a procedure created by Jones et al [12] for estimating developmental trajectories). We assumed each skin score

trajectory had a linear pattern of decline, and tested this assumption by including a quadratic term (i.e., testing for the possibility that change in skin score has a curved shape) and evaluated statistical significance of these terms for each trajectory group. Linear model terms were statistically significant ($P < 0.05$), but quadratic model terms were not; thus, we included only a linear term in our final models. The probability of each trajectory membership for a particular subject was estimated using the group-based model. Each subject was assigned to a specific trajectory group that had the highest estimated probability (i.e., posterior probability) compared with those of other trajectory groups. We used Bayesian information criterion (BIC) and entropy (i.e., amount of classification error indexed by average posterior probability) to assess the model fit. In general, models with lower BIC values provided a better fit to the data, and entropy statistics close to 1 (> 0.8) convey a model with well-separated trajectories (11).

We divided expression of each gene into tertiles. The association of each gene with skin score trajectory groups was examined by chi-square test. Additionally, we examined the association between expression of each gene at baseline and change in skin score over time from baseline, using generalized estimating equations in SAS with the "exchange" option for the working correlation matrix. In the regression model, the lowest tertile of each gene expression measure was used as the referent group to test the difference in change in MRSS. Finally, we collapsed regressive and stable trajectories into one group and modeled the predictive ability of each gene by logistic regression. Using SAS, we then assessed the predictive ability of the model according to discrimination and calibration. Discrimination was evaluated using the area under the curve; the guidelines suggested that values of ≥ 0.70 are needed for adequate prediction. Calibration was determined using the Hosmer-Lemeshow test (13), with a significant result being indicative of poor calibration. Pearson's correlation coefficients were calculated using GraphPad Prism software. *P* values less than 0.05 were considered significant.

RESULTS

Study patients. All patients enrolled in the FASSCINATE study met the 1980 American College of

Table 1. Characteristics of placebo-treated patients from the FASSCINATE study*

Characteristic	Placebo-treated patients (n = 38)
Age	
Mean \pm SD years	47.2 \pm 13.0
Median (range)	49.5 (19–69)
Sex, no. (%)	
Female	30 (78.9)
Male	8 (21.1)
MRSS	
Mean \pm SD	25.1 \pm 5.2
Median (range)	25 (15–37)
Disease duration, mean \pm SD months	19.8 \pm 16.8

* Patients met the 1980 American College of Rheumatology criteria for systemic sclerosis. Disease duration was defined by the time since the first non-Raynaud's phenomenon symptom. FASSCINATE = Safety and Efficacy of Subcutaneous Tocilizumab in Adults with Systemic Sclerosis; MRSS = modified Rodnan skin thickness score.

Rheumatology criteria for SSc (14), had active disease of ≤ 5 years' duration since the first non-Raynaud's phenomenon symptom, and had an MRSS between 15 and 40. Additionally, at screening, active progressive disease of < 1 year's duration was required for study inclusion, which was signified by any of the following: an increase in MRSS of ≥ 3 units, involvement of 1 new body area with an increase in MRSS of ≥ 2 units or involvement of > 2 new body areas with an increase in MRSS of ≥ 1 unit, other documentation of worsening skin thickening in the previous 6 months, or ≥ 1 tendon friction rub accompanied by ≥ 1 laboratory criterion (C-reactive protein ≥ 10.0 mg/liter, erythrocyte sedimentation rate ≥ 28 mm/hour, or platelet count $\geq 330 \times 1,000/\mu\text{l}$) (9).

The discovery cohort, which was used to identify prognostic biomarkers, consisted of 38 patients from the placebo-treated patient group (Table 1). For validation, we studied microarray gene expression data from a

second cohort of patients with dcSSc (20 patients total). The clinical features of the patients in this group were similar to those of the discovery cohort. All of the patients had early dcSSc (≤ 5 years from the first non-Raynaud's phenomenon symptom). However, patients in the validation group had some significant differences compared with those in the discovery group. First, patients in the validation group were treated with immunosuppressants, whereas the patients in the discovery group received only placebo during the study. Second, only 2 measurements of MRSS were obtained for patients in the validation group—1 at baseline and another at 24 weeks. Third, patients in the discovery cohort met certain additional criteria to define disease activity (15).

Gene expression and correlation with MRSS. Microarray data (from mid-forearm skin biopsies) that were generated as part of the clinical trial were analyzed for genes that were the most highly correlated with the

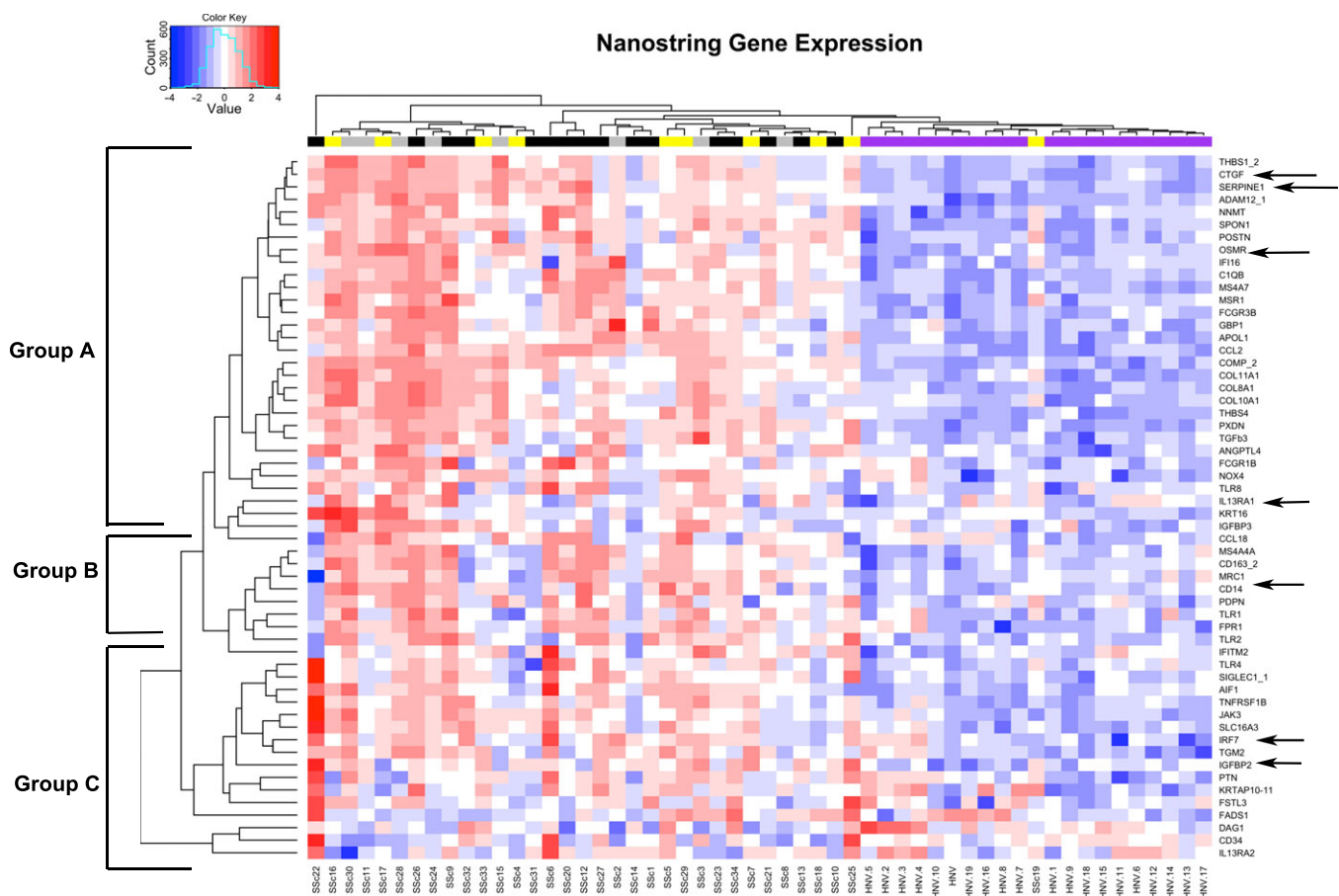


Figure 1. NanoString heatmap depicting gene expression in the skin of patients with diffuse cutaneous systemic sclerosis (dcSSc) compared to healthy controls, showing unsupervised hierarchical clustering in 20 healthy controls (violet bar) and 34 dcSSc patients (divided into regressive [yellow], stable [black], and progressive [gray] trajectories). Genes were grouped into 3 different clusters of transforming growth factor β /profibrotic genes (group A), macrophage-associated genes (group B), or genes without an evident biologic relationship (group C). Color code corresponds to Z scores of intensities. Red indicates higher expression and blue indicates lower expression. **Arrows** show genes selected for trajectory and tertiles analysis.

change in skin score from baseline to 6 months after treatment with placebo. From a microarray that was generated as part of the FASSCINATE study, we selected 83 genes that correlated highly with the changes in skin scores at 6 months (see Supplementary Figure 1, available on the *Arthritis & Rheumatology* web site at <http://onlinelibrary.wiley.com/doi/10.1002/art.40455/abstract>). Sixty-two of these genes were overexpressed in dcSSc patients compared with healthy controls. Most of the genes that correlated most highly with the changes in MRSS were in gene clusters identifiable as part of transforming growth factor β (TGF β)/profibrotic, interleukin-6 (IL-6)/STAT-3, or interferon pathways, or were associated with macrophages. Other genes of interest were also included in the nCounter panel, and gene expression from each of the patients was tested using nCounter technology, as described previously (9).

Using these gene expression data, we calculated the correlation coefficient (r) in 34 of the 38 placebo-treated patients between gene expression at baseline and the change in MRSS at week 16 (4 patients were not included because of missing values at 16 weeks and/or at baseline). Based on this correlation, we clustered all of the genes with an r value of >0.2 (Figure 1). By inspection, these genes were grouped into 3 different clusters. Two of the clusters (groups A and B) contained many recognizable genes based on known biologic relevance: TGF β /profibrotic genes (group A) and macrophage-associated genes (group B). The third cluster contained genes without evident biologic relationships (group C).

We compared the correlation between baseline gene expression and the change in MRSS in this cohort of patients (the discovery cohort) with microarray data from a second group of dcSSc patients (the validation cohort). We found that the correlation coefficients had the same trend for many of the genes in both cohorts (see Supplementary Table 1, available on the *Arthritis & Rheumatology* web site at <http://onlinelibrary.wiley.com/doi/10.1002/art.40455/abstract>), even though the r values were different between the 2 groups. This might be due to differences in clinical features between the 2 groups, as well as the 2 different methods used for gene expression analyses (NanoString versus microarray).

From the group of the genes that we identified (see Supplementary Table 1), we chose 7 genes for further analysis based on the strength of correlation between baseline gene expression and the change in MRSS in both the discovery and validation cohorts ($r > 0.2$). Since expression levels of many of the genes correlated highly with each other, we limited our analysis of co-regulated genes to the genes showing the largest correlation coefficients. Notably, expression levels of the genes for CD14,

Table 2. Comparison of correlations (r) between gene expression and changes in skin score in the discovery and validation groups

Gene	r	
	Discovery group	Validation group
IL13RA1	0.6	0.25
SERPINE1	0.54	0.31
OSMR	0.52	0.27
CTGF	0.45	0.23
CD14	0.59	0.36
IRF7	-0.2	-0.24
IGFBP2	-0.44	-0.32

CCL2, CD163, macrophage scavenger receptor 1 (MSR1), and membrane-spanning 4 domains, subfamily A, member 4A (MS4A4A) were highly correlated and therefore we chose to focus only on CD14. The following genes were analyzed further: CD14, IL13RA1, SERPINE1, OSMR, CTGF, IGFBP2, and IRF7 (Table 2). All of these genes were overexpressed in dcSSc patient skin compared with that of healthy controls (Figure 1).

Descriptive trajectory data. As shown in Figure 2, we identified 3 trajectory patterns of skin score change (y) over 48 weeks: 12 patients (30%) showed a regressive trajectory ($y = 17.69773 - [0.12504 \times \text{weeks}]$), 18 (45%) showed a stable trajectory ($y = 25.02055 - [0.8435 \times \text{weeks}]$), and 10 (25%) exhibited a progressive trajectory ($y = 31.12353 + [0.11507 \times \text{weeks}]$). The progressive trajectory group started with a higher average MRSS (30.65) than the other 2 trajectory groups, and the average skin score had increased by 17.7% at the end of 48 weeks. The regressive trajectory group started with a lower average MRSS (19.93), which had decreased by 33.9% at the end of the follow-up period. The stable trajectory group

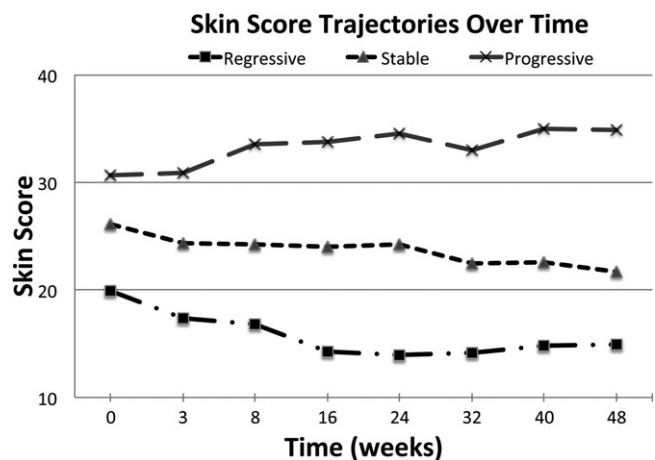


Figure 2. Skin score trajectory changes over time. Trajectories were defined according to baseline modified Rodnan skin score value and pattern. Symbols show the mean at each time point.

started with an intermediate average MRSS (26.12) that decreased slightly (16.2%) over the same time period. The average posterior probability of allocating study participants into trajectories (i.e., entropy) was ≥ 0.97 , indicating an excellent precision that individuals were assigned to their most likely trajectories.

Association of gene expression and pattern of skin score progression. We examined the 7 genes selected from the cluster groups (CD14, IL13RA1, SERPINE1, OSMR, CTGF, IGFBP2, and IRF7) in relation to the skin score trajectory over time. Subjects expressing high levels of CD14, IL13RA1, SERPINE1, OSMR, and CTGF at baseline were more likely to exhibit a progressive skin score trajectory (Table 3). No association was found between levels of either IRF7 or IGFBP2 gene expression and skin score trajectories. We further examined the performance of each of these genes as prognostic biomarkers of progressive versus stable/regressive skin disease. Expression of 5 genes (CD14, IL13RA1, SERPINE1, OSMR, and CTGF) was prognostic for the risk of skin progression (see Supplementary Table 2, available on the *Arthritis & Rheumatology* web site at <http://onlinelibrary.wiley.com/doi/10.1002/art.40455/abstract>). IL13RA1 performed the best, followed by OSMR and SERPINE1.

Table 3. Association of gene expression and skin score trajectory over the follow-up period

Gene expression	Skin score trajectory			P
	Regressive	Stable	Progressive	
CD14				0.013
Low	5	6	1	
Medium	4	7	2	
High	0	5	8	
IL13RA1				0.026
Low	4	7	1	
Medium	5	6	2	
High	1	4	8	
SERPINE1				0.049
Low	5	6	1	
Medium	4	6	3	
High	1	4	8	
OSMR				0.058
Low	6	6	0	
Medium	2	6	5	
High	2	5	6	
CTGF				0.020
Low	5	5	2	
Medium	4	8	1	
High	1	4	8	
IRF7				0.345
Low	5	6	1	
Medium	2	6	5	
High	3	5	5	
IGFBP2				0.566
Low	3	4	5	
Medium	3	8	2	
High	4	5	4	

Table 4. Association of gene expression and skin score change over time

Gene expression tertile groups	Mean skin score change (95% confidence interval)	P
CD14		0.0793
Middle vs. lowest	-0.28 (-3.46, 2.90)	0.86
Highest vs. lowest	3.48 (0.31, 6.66)	0.03
IL13RA1		0.0532
Middle vs. lowest	1.63 (-1.51, 4.77)	0.31
Highest vs. lowest	4.08 (1.36, 6.80)	0.003
SERPINE1		0.0696
Middle vs. lowest	-0.74 (-3.99, 2.51)	0.65
Highest vs. lowest	3.16 (0.59, 5.72)	0.016
OSMR		0.0184
Middle vs. lowest	1.07 (-1.93, 4.07)	0.48
Highest vs. lowest	4.08 (1.87, 6.29)	0.0003
CTGF		0.0491
Middle vs. lowest	-0.71 (-3.86, 2.44)	0.66
Highest vs. lowest	3.32 (0.87, 5.76)	0.008
IRF7		0.4539
Middle vs. lowest	0.90 (-1.53, 3.32)	0.44
Highest vs. lowest	-1.23 (-4.39, 1.93)	0.47
IGFBP2		0.1241
Middle vs. lowest	0.37 (-1.94, 2.69)	0.75
Highest vs. lowest	-3.10 (-6.29, 0.10)	0.058

Association of gene expression and skin score change. Expression of several genes, i.e., CD14, IL13RA1, SERPINE1, OSMR, and CTGF, was also associated with skin score change over time from baseline. Compared with those in the lowest tertile, patients in the highest tertile of CD14, IL13RA1, SERPINE1, OSMR, and CTGF expression showed an increased MRSS. In contrast, those in the highest tertile of IGFBP2 expression appeared to show an improvement of MRSS over time (Table 4). Similar results were also observed in the validation group.

DISCUSSION

At present, it is difficult to predict the trajectory of skin disease in dcSSc patients on the basis of clinical criteria (16). After analyzing skin gene expression, our findings revealed that messenger RNA for CD14, SERPINE1, IL13RA1, CTGF, and OSMR expression is prognostic for the trajectory of skin disease in patients with active dcSSc for 1 year following skin biopsy. Thus, increased expression of these genes may serve as better markers for selecting patients with progressive skin disease for therapies/clinical trials than currently available methods.

In this study, we utilized skin biopsy samples from patients treated with placebo in the Roche FASSCINATE phase II study of TCZ in SSc (9). These samples provided a rare opportunity to examine prognostic biomarkers in a group of patients with active dcSSc who were not treated with any immunosuppressive drugs. However, the inclusion criteria for this study may have impacted the results.

All patients had active dcSSc of ≤ 5 years' duration since the first non-Raynaud's phenomenon symptom and, at screening, an MRSS between 15 and 40. Additionally at screening, active progressive disease of < 1 year's duration was required, and was defined by an increase in MRSS of ≥ 3 units, involvement of 1 new body area with an increase in MRSS of ≥ 2 units or 2 new body areas with an increase in MRSS of ≥ 1 unit, other documentation of worsening skin thickening in the previous 6 months, or ≥ 1 tendon friction rub accompanied by ≥ 1 laboratory criterion (C-reactive protein ≥ 10.0 mg/liter, erythrocyte sedimentation rate ≥ 28 mm/hour, or platelet count $\geq 330 \times 1,000/\mu\text{l}$). Using these eligibility criteria to enrich the patient population for early active disease may have led to enrollment of patients with more progressive disease.

We found that the prognostic biomarkers identified using placebo-treated patients enrolled in the FASSCINATE study also showed trends in r values that were prognostic in a cohort of patients from Boston University Medical Center. The center's patients had received treatment with a variety of immunosuppressive medications (15). Thus, these prognostic biomarkers may have broader predictive value in other patients with early dcSSc. However, it is also possible that these biomarkers may act as predictors only in the preselected FASSCINATE cohort.

Defining progressive skin disease (by worsening MRSS) is important to enhance the patient population for clinical trials in which separation between the control and active treatment groups over a relatively short period of time (i.e., ≤ 1 year) is desirable. The 3 trajectory groups indicated that the patients whose disease symptoms were most likely to progress showed high baseline MRSS values. We found that only 25% of placebo-treated patients showed a progressive trajectory, despite an effort to enrich the patient population for active disease. Similar results were found previously in a larger study in which 192 patients with dcSSc were grouped using latent linear trajectory (4). In contrast, the trajectories we identified appear, at least on the surface, to be discrepant with the findings in a recent study of patients from the EUSTAR database (17). The most apparent possible reason for this difference would be a difference in patient selection between the 2 studies. The EUSTAR database is an observational study that recruits dcSSc patients with a broad range of disease durations, whereas FASSCINATE is a clinical trial in patients with early dcSSc and elevated acute-phase reactant levels.

In this study, we demonstrated that levels of the macrophage markers CD14, IL13RA1, MSR1, CD163, and MS4A4A correlate with progressive skin disease trajectories. Our current findings are in accordance with the results of previous studies, showing that levels of the

macrophage markers SIGLEC1 and MRC1 are increased in lesional SSc skin (18,19). In addition, we recently showed that changes in skin gene expression of MS4A4A correlate highly with changes in the MRSS, helping define a 2-gene pharmacodynamic biomarker (20). Further, in peripheral blood mononuclear cells, IL13RA1 gene expression correlates highly with pulmonary arterial hypertension in patients with limited cutaneous SSc (21). Finally, we recently reported that treatment with TCZ results in the down-regulation of skin CD14 expression in SSc patients (9). Taken together, these observations indicate an important function of macrophages in dcSSc tissue inflammation and fibrosis. As these cells are found surrounding blood vessels, these data suggest that macrophages bridge the fibrotic and vascular features with the pathology seen in the skin of SSc patients.

Two of the prognostic biomarkers identified here, SERPINE1 and CTGF, are strongly induced by TGF β (22,23). TGF β has long been suspected to be an important mediator of fibrosis in SSc as well as a variety of other fibrotic diseases, including renal, pulmonary, cardiac, and liver fibrosis (24–26). These 2 genes were significantly decreased in patients treated with fresolimumab (anti-TGF β antibody) (20), further supporting the notion that TGF β has a role in the pathogenesis of this disease.

Finally, we identified OSMR, which forms the oncostatin M (OSM) receptor with the common signaling partner gp130, as a prognostic biomarker. OSM, an IL-6 family cytokine, is produced by a variety of immune cells, including macrophages, neutrophils, and activated T cells (27). It has been implicated in a number of biologic processes, including the induction of inflammation and the modulation of extracellular matrix. OSM is up-regulated in the bronchoalveolar lavage fluid of patients with idiopathic pulmonary fibrosis and SSc (27) and is increased in the serum of dcSSc patients (28).

In conclusion, the present results indicate that dcSSc patients with elevated expression of CD14, CTGF, IL13RA1, OSMR, and SERPINE1 at baseline are more likely to have progressive skin score trajectories. The use of these biomarkers might help to guide decisions about which patients should be considered for therapies and/or for clinical trials. This observation will be further explored in the ongoing phase III study of TCZ in SSc patients (29).

AUTHOR CONTRIBUTIONS

All authors were involved in drafting the article or revising it critically for important intellectual content, and all authors approved the final version to be published. Dr. Stifano had full access to all of the data in the study and takes responsibility for the integrity of the data and the accuracy of the data analysis.

Study conception and design. Stifano, Rice, Na, Jahreis, Zhang, Lafyatis.
Acquisition of data. Stifano, Sornasse, Chen-Harris, Khanna, Jahreis.
Analysis and interpretation of data. Stifano, Sornasse, Rice, Na, Chen-Harris, Zhang, Siegel, Lafyatis.

ADDITIONAL DISCLOSURES

Drs. Sornasse, Chen-Harris, Jahreis, and Siegel are employees of Genentech.

REFERENCES

- Clements PJ, Lachenbruch PA, Seibold JR, Zee B, Steen VD, Brennan P, et al. Skin thickness score in systemic sclerosis: an assessment of interobserver variability in 3 independent studies. *J Rheumatol* 1993;20:1892–6.
- DeMarco PJ, Weisman MH, Seibold JR, Furst DE, Wong WK, Hurwitz EL, et al. Predictors and outcomes of scleroderma renal crisis: the high-dose versus low-dose D-penicillamine in early diffuse systemic sclerosis trial. *Arthritis Rheum* 2002;46:2983–9.
- Steen VD, Medsger TA Jr. Severe organ involvement in systemic sclerosis with diffuse scleroderma. *Arthritis Rheum* 2000;43:2437–44.
- Shand L, Lunt M, Nihtyanova S, Hoseini M, Silman A, Black CM, et al. Relationship between change in skin score and disease outcome in diffuse cutaneous systemic sclerosis: application of a latent linear trajectory model. *Arthritis Rheum* 2007;56:2422–31.
- Domsic RT. Scleroderma: the role of serum autoantibodies in defining specific clinical phenotypes and organ system involvement. *Curr Opin Rheumatol* 2014;26:646–52.
- Maurer B, Graf N, Michel BA, Müller-Ladner U, Czirják L, Denton CP, et al. Prediction of worsening of skin fibrosis in patients with diffuse cutaneous systemic sclerosis using the EUSTAR database. *Ann Rheum Dis* 2015;74:1124–31.
- Okano Y, Steen VD, Medsger TA Jr. Autoantibody reactive with RNA polymerase III in systemic sclerosis. *Ann Intern Med* 1993;119:1005–13.
- Stifano G, Affandi AJ, Mathes AL, Rice LM, Nakerakanti S, Nazari B, et al. Chronic Toll-like receptor 4 stimulation in skin induces inflammation, macrophage activation, transforming growth factor β signature gene expression, and fibrosis. *Arthritis Res Ther* 2014;16:R136.
- Khanna D, Denton CP, Jahreis A, van Laar JM, Frech TM, Anderson ME, et al. Safety and efficacy of subcutaneous tocilizumab in adults with systemic sclerosis (faSScinate): a phase 2, randomised, controlled trial. *Lancet* 2016;387:2630–40.
- Hoffmann-La Roche, sponsor. A phase II/III multicenter, randomized, double-blind, placebo-controlled study to assess the efficacy and safety of tocilizumab versus placebo in patients with systemic sclerosis. ClinicalTrials.gov identifier: NCT01532869; 2012.
- Nagin DS, Odgers CL. Group-based trajectory modeling in clinical research. *Annu Rev Clin Psychol* 2010;6:109–38.
- Jones B, Nagin D, Roeder K. A SAS procedure based on mixture models for estimating developmental trajectories. *Soc Meth Res* 2001;29:374–93.
- David W, Hosmer J, Lemeshow S, Sturdivant RX. Applied logistic regression. 3rd ed. New York: John Wiley & Sons; 2013. p. 528.
- Subcommittee for Scleroderma Criteria of the American Rheumatism Association Diagnostic and Therapeutic Criteria Committee. Preliminary criteria for the classification of systemic sclerosis (scleroderma). *Arthritis Rheum* 1980;23:581–90.
- Rice LM, Ziemek J, Stratton EA, McLaughlin SR, Padilla CM, Mathes AL, et al. A longitudinal biomarker for the extent of skin disease in patients with diffuse cutaneous systemic sclerosis. *Arthritis Rheumatol* 2015;67:3004–15.
- Merkel PA, Silliman NP, Clements PJ, Denton CP, Furst DE, Mayes MD, et al. Patterns and predictors of change in outcome measures in clinical trials in scleroderma: an individual patient meta-analysis of 629 subjects with diffuse cutaneous systemic sclerosis. *Arthritis Rheum* 2012;64:3420–9.
- Maurer B, Graf N, Michel BA, Müller-Ladner U, Czirják L, Denton CP, et al. Prediction of worsening of skin fibrosis in patients with diffuse cutaneous systemic sclerosis using the EUSTAR database. *Ann Rheum Dis* 2015;74:1124–31.
- York MR, Nagai T, Mangini AJ, Lemaire R, van Seventer JM, Lafyatis R. A macrophage marker, Siglec-1, is increased on circulating monocytes in patients with systemic sclerosis and induced by type I interferons and Toll-like receptor agonists. *Arthritis Rheum* 2007;56:1010–20.
- Christmann RB, Hayes E, Pendergrass S, Padilla C, Farina G, Affandi AJ, et al. Interferon and alternative activation of monocyte/macrophages in systemic sclerosis-associated pulmonary arterial hypertension. *Arthritis Rheum* 2011;63:1718–28.
- Rice LM, Padilla CM, McLaughlin SR, Mathes A, Ziemek J, Goummih S, et al. Fresolimumab treatment decreases biomarkers and improves clinical symptoms in systemic sclerosis patients. *J Clin Invest* 2015;125:2795–807.
- Pendergrass SA, Hayes E, Farina G, Lemaire R, Farber HW, Whitfield ML, et al. Limited systemic sclerosis patients with pulmonary arterial hypertension show biomarkers of inflammation and vascular injury. *PloS One* 2010;5:e12106.
- Wahl SM, Hunt DA, Wakefield LM, McCartney-Francis N, Wahl LM, Roberts AB, et al. Transforming growth factor type β induces monocyte chemotaxis and growth factor production. *Proc Natl Acad Sci U S A* 1987;84:5788–92.
- Lund LR, Riccio A, Andreasen PA, Nielsen LS, Kristensen P, Laiho M, et al. Transforming growth factor- β is a strong and fast acting positive regulator of the level of type-1 plasminogen activator inhibitor mRNA in WI-38 human lung fibroblasts. *EMBO J* 1987;6:1281–6.
- Gewin L, Zent R. How does TGF- β mediate tubulointerstitial fibrosis? *Semin Nephrol* 2012;32:228–35.
- Inagaki Y, Higashiyama R, Higashi K. Novel anti-fibrotic modalities for liver fibrosis: molecular targeting and regenerative medicine in fibrosis therapy. *J Gastroenterol Hepatol* 2012;27 Suppl 2: 85–8.
- Maher TM. Idiopathic pulmonary fibrosis: pathobiology of novel approaches to treatment. *Clin Chest Med* 2012;33:69–83.
- Mozaffarian A, Brewer AW, Trueblood ES, Luzina IG, Todd NW, Atamas SP, et al. Mechanisms of oncostatin M-induced pulmonary inflammation and fibrosis. *J Immunol* 2008;181:7243–53.
- Feeny M, Syed F, Khan K, Shiwen X, Sully K, Trinder S, et al. Oncostatin M as a potential molecular target in systemic sclerosis [abstract]. *Arthritis Rheumatol* 2015;67 Suppl 10. URL: <http://acrabstracts.org/abstract/oncostatin-m-as-a-potential-molecular-target-in-systemic-sclerosis/>.
- Hoffman-La Roche, sponsor. A phase III, multicenter, randomized, double-blind, placebo-controlled, parallel-group study to assess the efficacy and safety of tocilizumab versus placebo in patients with systemic sclerosis. ClinicalTrials.gov identifier: NCT02453256; 2015.

APPENDIX A: FASSCINATE STUDY INVESTIGATORS

The study investigators who enrolled at least one patient in the FASSCINATE study are as follows: in Canada, Murray Baron (McGill University and Sir Mortimer B. Davis Jewish General Hospital, Montreal, Quebec), Janet E. Pope (Saint Joseph's Health Care, London, Ontario); in France, Yannick Allanore (Hôpital Cochin, Paris), Joel Constans (Hôpital Saint André, Bordeaux), Thierry Martin (Hôpital Civil, Strasbourg), Carle Paul (Hôpital Larrey Université Paul Sabatier, Toulouse); in Germany, Frank Behrens (Centrum für innovative Diagnostik und Therapie Rheumatologie/Immunologie GmbH, Frankfurt am

Main), Christoph Fiehn (Rheumazentrum Baden-Baden GmbH, Baden-Baden), Gerhard Fierlbeck (Universitätsklinikum Tübingen, Tübingen), Nicolas T. Hunzelmann (Universitätsklinikum Köln, Köln), Nina S. Lahner (Ruhr-Universität Bochum, Bochum), Ulf Müller-Ladner (Kerckhoff-Klinik GmbH, Bad Nauheim), Christiane Pfeiffer (Universitätsklinikum Ulm, Ulm), Gabriela Riemekasten (Charité-Universitätsmedizin Berlin, Berlin), Leonore Unger (Krankenhaus Dresden-Friedrichstadt, Städtisches Klinikum, Dresden); in the UK, Marina E. Anderson (Aintree University Hospitals NHS Foundation Trust, Liverpool), Maya Buch (Chapel Allerton Hospital, Leeds), Christopher P. Denton (Royal Free Hospital, London), Bridget Griffiths (Freeman Hospital, Newcastle Upon Tyne), Neil McKay (Western General Hospital, Edinburgh), Sanjay Pathare (The James Cook University Hospital, Middlesbrough); in the US, Soumya Chatterjee (Cleveland Clinic, Cleveland, OH), Lorinda S. Chung (Stanford

University, Redwood City, CA), Philip J. Clements (University of California, Los Angeles), Christine Coddling (Health Research of Oklahoma, Oklahoma City), Dinesh Khanna (University of Michigan, Ann Arbor), David Fox (University of Michigan, Ann Arbor), Tracy M. Frech (University of Utah, Salt Lake City), Richard A. Furie (North Shore-Long Island Jewish Health System, Great Neck, NY), Vivien M. Hsu (University of Medicine and Dentistry, New Brunswick, NJ), Oscar H. Irigoyen (Thomas Jefferson University, Philadelphia, PA), Dan Furst (University of California, Los Angeles), Suzanne Kafaja (University of California, Los Angeles), Arthur F. Kavanaugh (University of California, San Diego, La Jolla), Santhanam Lakshminarayanan (University of Connecticut Health Center, Farmington), Richard Silver (Medical University of South Carolina, Charleston), Virginia D. Steen (Georgetown University Hospital, Washington, DC), John Varga (Northwestern University, Chicago, IL).

Molecular Basis for Dysregulated Activation of NKX2-5 in the Vascular Remodeling of Systemic Sclerosis

Athina Dritsoula,¹ Ioannis Papaioannou,¹ Sandra G. Guerra,¹ Carmen Fonseca,¹ Javier Martin,² Ariane L. Herrick,³ David J. Abraham,¹ Christopher P. Denton,¹ and Markella Ponticos¹ 

Objective. NKX2-5 is a homeobox transcription factor that is required for the formation of the heart and vessels during development, with significant postnatal down-regulation and reactivation in disease states, characterized by vascular remodeling. The purpose of this study was to investigate mechanisms that activate NKX2-5 expression in diseased vessels, such as systemic sclerosis (scleroderma; SSc)-associated pulmonary hypertension (PH), and to identify genetic variability that potentially underlies susceptibility to specific vascular complications.

Methods. We explored NKX2-5 expression in biopsy samples from patients with SSc-associated PH and in pulmonary artery smooth muscle cells (PASMCs) from patients with scleroderma. Disease-associated putative functional single-nucleotide polymorphisms (SNPs) at the NKX2-5 locus were cloned and studied in reporter gene assays. SNP function was further examined through protein–DNA binding assays, chromatin immunoprecipitation assays, and RNA silencing analyses.

Results. Increased NKX2-5 expression in biopsy samples from patients with SSc-associated PH was localized to remodeled vessels and PASMCs. Meta-analysis of 2 independent scleroderma cohorts revealed an association

of rs3131917 with scleroderma ($P = 0.029$). We demonstrated that disease-associated SNPs are located in a novel functional enhancer, which increases NKX2-5 transcriptional activity through the binding of GATA-6, c-Jun, and myocyte-specific enhancer factor 2C. We also characterized an activator/coactivator transcription-enhancer factor domain 1 (TEAD1)/Yes-associated protein 1 (YAP1) complex, which was bound at rs3095870, another functional SNP, with TEAD1 binding the risk allele and activating the transcription of NKX2-5.

Conclusion. NKX2-5 is genetically associated with scleroderma, pulmonary hypertension, and fibrosis. Functional evidence revealed a regulatory mechanism that results in NKX2-5 transcriptional activation in PASMCs through the interaction of an upstream promoter and a novel downstream enhancer. This mechanism can act as a model for NKX2-5 activation in cardiovascular disease characterized by vascular remodeling.

NKX2-5 is a transcription factor that belongs to the family of NK2-homeobox DNA binding transcription activators. One of the earliest known markers of cardiac development in vertebrates (1,2), NKX2-5 is crucial for blood vessel development during embryogenesis (3,4). In humans, NKX2-5 is not expressed in normal vasculature postnatally. However, we have accumulating evidence that NKX2-5 drives phenotypic dedifferentiation of vascular smooth muscle cells (VSMCs) in blood vessels undergoing vascular remodeling (5,6). Vascular remodeling is the term used to describe the structural rearrangement of the vessel wall in response to inflammation, repair, or other stimuli (7). It is the hallmark of many vascular diseases, including atherosclerosis, pulmonary arterial hypertension (PAH), and scleroderma (SSc)-associated pulmonary hypertension (PH).

SSc is a multisystem disease characterized by increased dysregulation of the immune system, inflammation, extensive fibrosis of the skin and internal organs, and prominent vasculopathy (8). As in other rare heterogeneous

Supported by the British Heart Foundation (grant FS 12/70/30009), Arthritis Research UK, Royal Free Hospital Charity, and Scleroderma Research UK.

¹Athina Dritsoula, PhD, Ioannis Papaioannou, PhD, Sandra G. Guerra, PhD, Carmen Fonseca, MD, PhD, David J. Abraham, PhD, Christopher P. Denton, MD, PhD, Markella Ponticos, PhD: University College London, London, UK; ²Javier Martin, MD, PhD: Instituto de Parasitología y Biomédicina López-Neyra, Granada, Spain; ³Ariane L. Herrick, MD, PhD: University of Manchester, Salford Royal NHS Foundation Trust and Central Manchester NHS Foundation Trust, Manchester Academic Health Science Centre, Manchester, UK.

Address correspondence to Markella Ponticos, PhD, Centre for Rheumatology and Connective Tissue Diseases, Division of Medicine, University College London, Royal Free Hospital Campus, Rowland Hill Street, London NW3 2PF, UK. E-mail: m.ponticos@ucl.ac.uk.

Submitted for publication September 14, 2017; accepted in revised form January 11, 2018.

diseases, it is likely that a combination of both genetic and environmental factors interact to cause SSc (9). The unmet need in the medical management of SSc is high, including the high rates of death from cardiorespiratory complications. SSc-associated PH is a leading cause of death among SSc patients (8), and PH develops in 18–24% of SSc cases (10).

SSc-associated PH occurs through several mechanisms, including World Health Organization (WHO) group I PAH, as well as WHO group II (postcapillary) and group III (lung fibrosis associated) forms. Collectively, these are termed SSc-associated PH. PH can develop throughout the course of the disease, and recent studies suggest that 1–2% of SSc patients develop PH each year in a screened population (10), suggesting that SSc confers substantial susceptibility. All forms of PH are associated with vascular remodeling, and it is likely that overlapping molecular pathways are involved in the development of this, and possibly other, SSc-associated vascular manifestations.

Transcriptional regulation of the murine *Nkx2-5* gene has proven to be very complex, with a number of *cis*- and *trans*-acting elements over a large 23-kb genomic region regulating expression in a temporospatial-specific manner (11). BMP signaling is necessary for *Nkx2-5* activation through the binding of Smad and GATA transcription factors at an upstream enhancer (12,13). Other signaling pathways, epigenetic modifications, and autoregulatory mechanisms also govern *Nkx2-5* regulation (14,15). Despite our knowledge of the structure of the murine *Nkx2-5* gene and the high homology (87%) between the mouse and human genes, little is known about the regulation of human *NKX2-5*. Most studies focus on *NKX2-5* genetic variations, with 56 mutations and 250 single-nucleotide polymorphisms (SNPs) having been identified, many of which are associated with types of congenital heart disease (16,17).

Postnatal activation of developmental regulatory pathways may explain the molecular pathology of the adult disease, and genetic association of functional polymorphisms can explain the susceptibility and phenotypic variability. In this study, we investigated the regulatory mechanisms of human *NKX2-5* resulting in increased expression in adult vasculature. We delineated a transcriptional mechanism through which *NKX2-5* is activated. We also identified and validated a downstream enhancer, which results in enhanced transcriptional activation in human pulmonary artery smooth muscle cells (PASMCs).

PATIENTS AND METHODS

Patient cohorts. A genetic study was conducted in 2 independent cohorts of Caucasian origin: UK and Spanish SSc patients. The UK cohort consisted of 1,334 SSc patients

presenting to the Centre for Rheumatology at the Royal Free Hospital and the Centre for Musculoskeletal Research at the University of Manchester, as well as 901 control DNA samples matched to the patients for age, sex, and ethnicity. The Spanish cohort consisted of 1,736 SSc patients and 1,753 control DNA samples collected at the Institute of Parasitology and Biomedicine Lopez-Neyra in Granada, Spain. The study was approved by the local ethics committees, in compliance with the Helsinki Declaration, and all participants gave written informed consent to participate in the study.

All patients had a definite diagnosis of SSc, and the majority fulfilled the American College of Rheumatology/European League Against Rheumatism 2013 criteria for the classification of SSc (18). Patients were categorized according to disease subsets (limited/diffuse) or the presence of the following autoantibodies: anticentromere, antitopoisomerase, and anti-RNA polymerase III. The presence of pulmonary fibrosis was assessed by high-resolution computed tomography and a restrictive pattern on lung function testing. Patients with estimated systolic pulmonary arterial pressure (PAP) of ≥ 45 mm Hg on echocardiogram or a mean PAP of ≥ 25 mm Hg at the time of right-sided heart catheterization were classified as having PH. Those without clinically significant lung fibrosis but with a confirmed pulmonary arterial wedge pressure of ≤ 15 mm Hg at right-sided heart catheterization were defined as having WHO group I PAH (19). Renal crisis was diagnosed according to the acute onset of severe hypertension and acute kidney injury (20). Medical management of the study cohorts was consistent with current practice, with regular review and annual assessment for new organ-based complications.

Extended protocols and information regarding the experimental procedures are provided in the Supplementary Methods (available on the *Arthritis & Rheumatology* web site at <http://onlinelibrary.wiley.com/doi/10.1002/art.40419/abstract>).

Selection of tagging SNPs. Tagging SNPs around the *NKX2-5* genomic region (chromosome 5: 173,272,104–173,240,312; GenBank GRCh38.p7 assembly) were selected with Tagger software (21) using SNP genotype data from the northern European population (Utah Residents [CEPH] of North and Western European ancestry [CEU]) available from the International HapMap Project, Release 28 (22). All SNPs had a minor allele frequency of >0.01 and were in Hardy-Weinberg equilibrium (cutoff value 0.001).

In silico analyses were performed using annotations from the following open-access curated databases: Encyclopedia of DNA Elements (ENCODE) (23), TRANSFAC (24), JASPAR (25), and HaploReg (26).

DNA extraction and genotyping. DNA was extracted from whole blood as described elsewhere (27). SNPs rs703752, rs3131917, rs3132139, rs12514371, and rs2277923 were genotyped using TaqMan SNP genotyping assays. For rs3095870, a high-resolution melting analysis was performed using a Type-it high-resolution melting polymerase chain reaction (PCR) kit (Qiagen).

Genetic association study. The case-control association analysis and the subphenotype analysis were performed in Plink (28). Successful call rates per SNP and per individual ($\geq 90\%$) were applied. Permutation analysis was used to correct for multiple comparisons. Haplotype analysis was performed in Haploview (29).

Cell culture, cloning, and luciferase assays. Primary human PASMCs (catalog no. C-12521; PromoCell) and immortalized human PASMCs (catalog no. T0558; ABM Good) were used for the in vitro experiments. *NKX2-5* gene expression in patients

with SSc-associated PH and in matched controls was assessed in primary PASMCs isolated from human tissue as described previously (30). All SMCs were cultured in media supplemented with 5% serum at 70–80% confluency. Primary cells were used between passages 3 and 9. Human PASMCs were immortalized via a lentiviral vector containing SV40.

Disease-associated SNPs were cloned into reporter vectors and transfected into primary human PASMCs. Luciferase assays were then performed.

RNA silencing, binding assays, and Western blotting. Immortalized human PASMCs were transfected for 48–72 hours with small interfering RNA (siRNA) oligonucleotides specific for transcription-enhancer factor domain 1 (TEAD1), TEAD3, and Yes-associated protein 1 (YAP1) (On-Target Plus SMART-pool siRNA; Dharmacon). RNA and protein were extracted and subjected to quantitative PCR (qPCR), sodium dodecyl sulfate–polyacrylamide gel electrophoresis (SDS-PAGE), and Western blotting.

Electrophoretic mobility shift assay (EMSA), DNA–protein pull-down assays, and chromatin immunoprecipitation (ChIP) assays were performed to identify protein complexes that bind the associated SNPs.

Nuclear (NE-PER kit; Pierce) and total cell (radioimmunoprecipitation assay) protein extracts were prepared. Cell lysates were subjected to SDS-PAGE and Western blotting. Specific antibodies against NKX2-5, TEAD1, TEAD3, phospho-YAP1, and YAP1 were used. GAPDH served as a housekeeping gene. Densitometry analysis was performed using ImageJ software (31).

RNA extraction and qPCR. Total RNA was extracted according to standard protocols using an RNeasy kit (Qiagen) and was then subjected to qPCR analysis using a QuantiFast SYBR Green PCR kit (Qiagen). NKX2-5 gene expression was normalized against the expression of the β -actin gene or the TATA box binding protein, as indicated below.

Immunohistochemistry. Immunohistochemistry was performed on formalin-fixed paraffin-embedded tissue. After antigen retrieval with citric buffer, pH 6.0, sections were immunodecorated with optimally diluted (2 μ g/ml in Tris buffered saline [TBS]) antibody NKX2-5 (catalog no. sc-14033; Santa Cruz Biotechnology). Biotinylated goat anti-rabbit secondary antibody (catalog no. BA-1000; Vector) diluted 2 μ g/ml in TBS was used prior to developing with 3,3'-diaminobenzidine reagent (catalog no. SK-4100; Vector). Specificity of staining was confirmed using isotype-matched IgG control antibodies (2 μ g/ml).

Statistical analysis. Results are reported as the mean \pm SEM of data from at least 3 independent experiments. Statistical analyses (Student's unpaired *t*-test) and graphs were performed using GraphPad Prism 6 software. *P* values less than 0.05 were considered significant.

RESULTS

Up-regulation of NKX2-5 and expression in vascular diseases such as SSc-associated PH. Initially, NKX2-5 expression was determined in the pulmonary vasculature of patients with SSc-associated PH. Immunohistochemical staining revealed that NKX2-5 was highly expressed in all muscularized arteries in the patients' lungs, but absent from the vasculature of the healthy subjects' lungs

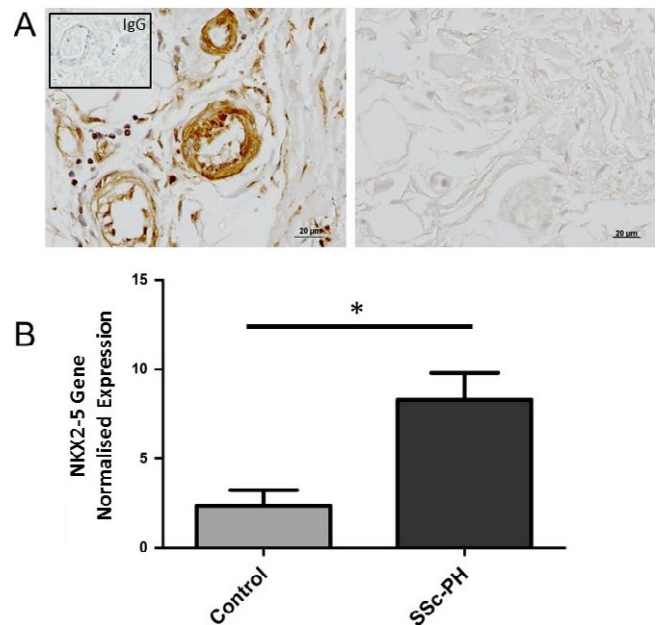


Figure 1. Expression of NKX2-5 in systemic sclerosis (SSc)-related pulmonary hypertension (PH). **A**, Representative sections of lung tissue from a patient with SSc-associated PH (of 4 examined) (left) and a healthy control subject (right). Sections were immunodecorated with NKX2-5 antibody (brown). **Inset**, IgG isotype control. **B**, Normalized expression of the NKX2-5 gene in pulmonary artery smooth muscle cells isolated from the lung vessels of patients with SSc-associated PH ($n = 5$) and healthy control subjects ($n = 3$). Values are the mean \pm SEM. * = $P < 0.05$ by Student's *t*-test.

(Figure 1A). We also used PASMCs isolated from SSc-associated PH patients and healthy subjects to determine NKX2-5 messenger RNA (mRNA) expression and found a significant increase ($P = 0.02$) in NKX2-5 gene expression in the patients (Figure 1B). Our data suggest that NKX2-5 plays an important role in the vasculature of patients with SSc-associated PH and that it is regulated at both the gene and protein levels.

Since NKX2-5 regulation in blood vessels is largely unknown, we investigated the mechanisms at the genetic and transcriptional levels by carrying out a genetic association analysis of the NKX2-5 locus in SSc patients followed by a functional analysis of the disease-associated polymorphisms.

Identification of disease-associated SNPs in the NKX2-5 locus. Six tagging SNPs were selected along the NKX2-5 locus (Figure 2A) and genotyped in 2 independent cohorts of SSc patients (described in detail in Supplementary Tables 1 and 2; available at <http://onlinelibrary.wiley.com/doi/10.1002/art.40419/abstract>). Meta-analysis of the 2 cohorts showed association of rs3131917 with SSc (corrected $P = 0.029$, odds ratio [OR] 0.91) (Table 1). Subphenotype association analysis showed that the same

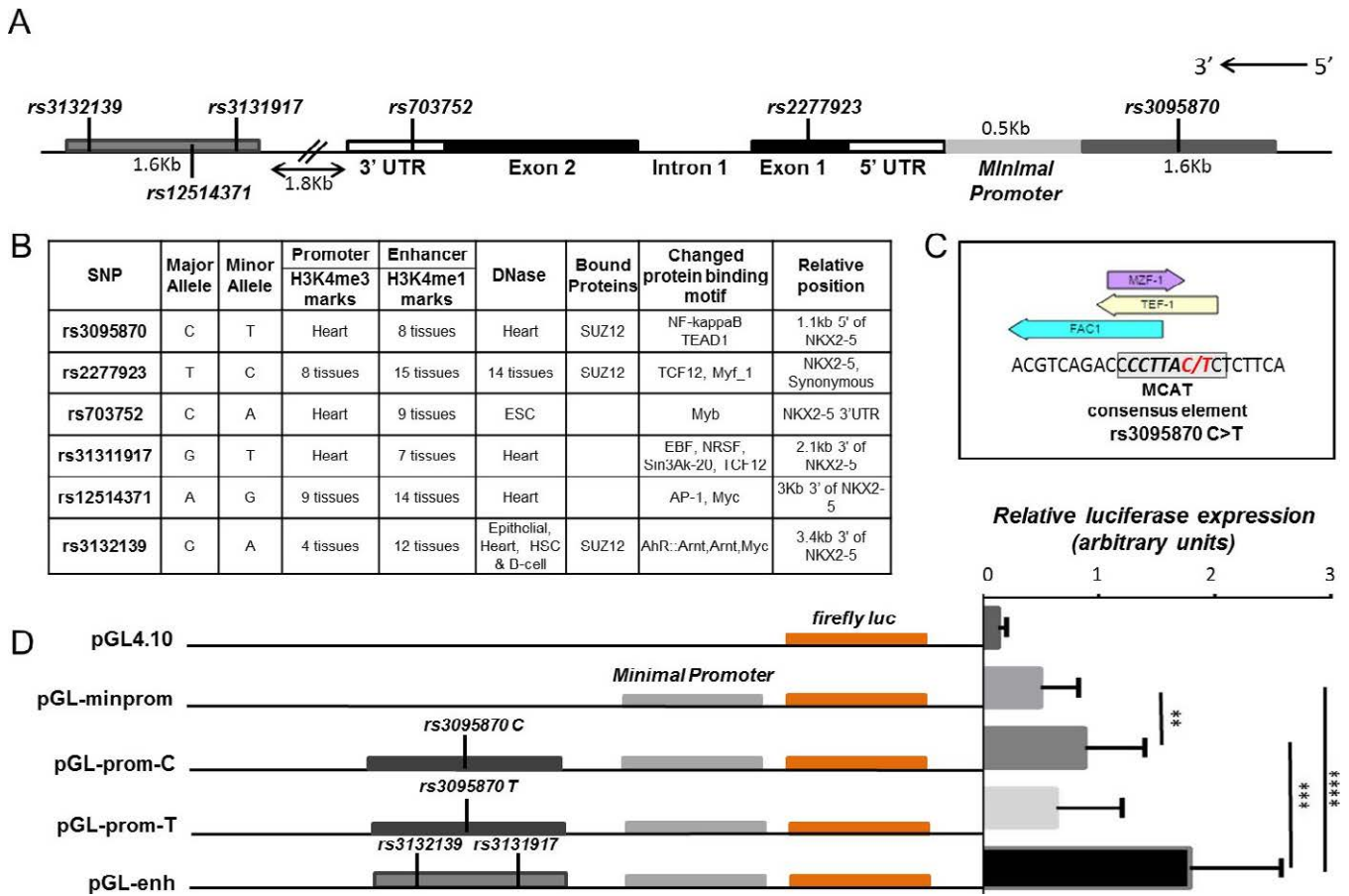


Figure 2. Disease-associated single-nucleotide polymorphisms (SNPs) in functional regulatory regions. **A**, Schematic representation of the *NKX2-5* gene with its introns, exons, and untranslated regions (3'-UTR and 5'-UTR). The location of the tagging SNPs is shown in the schematic map of the *NKX2-5* genomic locus. **B**, Findings of in silico analysis of the tagging SNPs using HaploReg and Encyclopedia of DNA Elements (ENCODE) data. **C**, Transcription factor binding sites around rs3095870, as determined using the TRANSFAC and JASPAR databases. Boxed area shows the consensus-binding element for transcription-enhancer factor domain 1 (TEAD1) on the MCAT site; the alleles of rs3095870 are shown in red. **D**, Transcriptional activity in primary human pulmonary artery smooth muscle cells transfected with reporter gene constructs containing the minimal promoter (pGL-minprom), upstream promoter with either the rs3095870 C allele (pGL-prom-C) or the rs3095870 T allele (pGL-prom-T), or the downstream enhancer (pGL-enh) are shown at the left. The pGL4.10 vector, which contains the firefly luciferase (*luc*) gene, was used as the cloning vector. The relative luciferase expression for each of the 5 constructs is shown at the right. Values are the mean \pm SEM of 3 independent experiments. ** = $P < 0.01$; *** = $P < 0.001$; **** = $P < 0.0001$ by Student's *t*-test. TCF-12 = T cell factor 12; ESC = embryonic stem cell; EBF = early B cell factor; NRSF = neuron-restrictive silencer factor; AP-1 = activator protein 1; HSC = hematopoietic stem cell; AhR = aryl hydrocarbon receptor; ARNT = aryl hydrocarbon nuclear translocator; MZF-1 = myeloid zinc finger 1; TEF-1 = transcriptional enhancer factor 1. Color figure can be viewed in the online issue, which is available at <http://onlinelibrary.wiley.com/doi/10.1002/art.40419/abstract>.

SNP was also significantly associated with PH and pulmonary fibrosis in a Spanish cohort (corrected $P = 0.005$ and corrected $P = 0.04$, respectively, OR 0.72 and OR 0.84, respectively) (Table 1), as well as with the anti-RNA polymerase III antibody-positive subgroup in the UK cohort (corrected $P = 0.023$, OR 1.34) (Table 1). Aside from rs3131917, other SNPs within *NKX2-5* were genetically associated with disease subphenotypes. SNP rs3132139 showed a significant association with PH (corrected $P = 0.002$, OR 1.396) and rs3095870 showed a marginal association with pulmonary fibrosis (corrected $P = 0.04$) in the

Spanish cohort (Supplementary Table 3, available at <http://onlinelibrary.wiley.com/doi/10.1002/art.40419/abstract>).

We further examined the structure of *NKX2-5* using genotype data on the CEU population. The data showed an extended linkage disequilibrium pattern across the region (Supplementary Figure 1A, available at <http://onlinelibrary.wiley.com/doi/10.1002/art.40419/abstract>), with similar patterns observed in the SSc cohorts (Supplementary Figures 1B and C). The 6 tagging SNPs were merged into 1 haplotype, and an association analysis was performed, which showed a significant association with

Table 1. Genetic association analyses of rs3931917 in a UK and a Spanish cohort of SSc patients via allelic testing*

rs3131917	Minor allele	Minor allele frequency		Chi-square	$P_{\text{corr}}\dagger$	OR (95% CI)
		Cases	Controls			
Overall association analysis						
UK, SSc+ vs. SSc-	T	0.48	0.46	1.16	0.28	1.06 (0.94–1.2)
Spanish, SSc+ vs. SSc-	G	0.48	0.51	3.6	0.05	0.9 (0.82–1)
Meta-analysis					0.029	0.91
Subphenotype analysis						
UK, anti-RNAP III+ vs. control	T	0.54	0.46	6.25	0.023	1.34 (1.06–1.7)
Spanish, PH+ vs. control	G	0.42	0.51	7.8	0.005	0.72 (0.57–0.9)
Spanish, PF+ vs. control	G	0.46	0.51	3.97	0.04	0.84 (0.72–0.99)

* Shown are chi-square test values, corrected P (P_{corr}) values, and odds ratios (ORs) with 95% confidence intervals (95% CIs) for the genetic association of the rs3131917 single-nucleotide polymorphism with systemic sclerosis (SSc) in a meta-analysis of 2 independent cohorts (UK and Spanish), as well as for a subphenotype analysis of the association of rs3131917 with the anti-RNA polymerase III (anti-RNAP III) autoantibody, pulmonary hypertension (PH), and pulmonary fibrosis (PF). The minor allele and its frequencies in cases and controls are also shown. Genetic analyses were performed using Plink.

† P_{corr} values for multiple comparisons were determined by permutation analysis.

SSc ($P \leq 0.01$) (Supplementary Table 4, available at <http://onlinelibrary.wiley.com/doi/10.1002/art.40419/abstract>). These findings suggest that there is a synergistic, rather than a single-locus, effect of the SNPs and emphasize the importance of *NKX2-5* in SSc and vascular pathologies as a whole.

Presence of disease-associated SNPs in potential regulatory regions. The genetic association study revealed that rs3131917 and rs3132139 were strongly associated with SSc-associated PH. Since our aim was to determine how *NKX2-5* is activated in diseased vessels, we further explored the potential functional role of the SNPs. Due to the extensive linkage disequilibrium (Supplementary Figure 1), strong associations may mask other functional polymorphisms. Although significantly high P values suggest genetic association with disease, they do not necessarily indicate functionality of the associated SNPs. Therefore, using our genetic association data as a guide, we performed in silico studies using HaploReg (26) and ENCODE (23) data to evaluate any potential functional effect of all 6 tagging SNPs (Figure 2B).

SNPs rs3132139, rs3131917, and rs3095870 are located in potential regulatory regions, such as an upstream promoter and a downstream enhancer, based on accumulated evidence from functional annotations, including histone marks specific for promoter and enhancer regions, DNase hypersensitivity sites, and scores for transcription factor binding sites. SNP rs3095870 is located 1.1 kb upstream of the *NKX2-5* transcriptional start site, while rs3131917 and rs3132139 are located 5 kb and 6.4 kb, respectively, downstream of *NKX2-5*, in a region that was previously identified as a putative *NKX2-5* enhancer (32).

First, we looked for transcription factor binding sites that might be affected by the various SNP alleles. Interestingly, we found that rs3095870 is located within a

TEAD1 (transcriptional enhancer factor 1 [TEF-1]) binding site. TEAD1 is a member of the TEA/ATTS domain family transcription regulators with distinct and important roles in VSMC differentiation and in cardiovascular disease (33–35). All 4 members of the family recognize and bind specifically at the MCAT consensus element: 5'-TCATTCCT-3' (Figure 2C). The minor T allele of rs3095870 disrupts the consensus sequence and could obliterate the TEAD1 binding site (Figure 2C). This suggests that TEAD1 might regulate *NKX2-5* expression, depending on the presence of the rs3095870 C allele. The rs3095870 C allele showed a marginal association with pulmonary fibrosis (corrected $P = 0.04$) in the Spanish cohort (Supplementary Table 3).

We investigated the effect of the C/T alleles of rs3095870 and the other associated SNPs on *NKX2-5* transcriptional activity using luciferase reporter assays. A 1.6-kb genomic region containing the rs3095870 C allele was cloned into a pGL4.10 reporter vector (pGL-prom-C) driven by the *NKX2-5* minimal promoter (pGL-minprom). The alternative T allele was introduced by site-directed mutagenesis (pGL-prom-T), and the constructs were transfected into primary human PSMCs. Addition of the 1.6-kb upstream region increased the relative expression of luciferase as compared to the minimal promoter, but only in the presence of the rs3095870 C allele ($P < 0.01$) (Figure 2D). These data suggest that rs3095870 is a functional SNP that requires further investigation.

When a 1.6-kb genomic region downstream of *NKX2-5*-containing SNPs rs3132139 and rs3131917 was cloned next to the minimal promoter (pGL-enh), luciferase expression was increased significantly compared to both pGL-prom-C and pGL-prom-T ($P < 0.0001$) (Figure 2D). The data demonstrate that the 3 associated SNPs are indeed present within functional regulatory elements that directly influence *NKX2-5* transcriptional

activity, and they confirm that the region containing rs3132139 and rs3131917 is an active enhancer.

TEAD1 regulation of *NKX2-5* transcription through binding on rs3095870. To corroborate the reporter gene data and the effect of TEAD1 binding on *NKX2-5* gene expression, we conducted DNA–protein binding and ChIP assays. TEAD1 specifically binds DNA on MCAT elements, but it also requires cofactors to exert its activity. YAP1 has been identified as the best candidate for TEAD-dependent transcription (36,37). Using EMSA,

we found that different bands were formed for each allele, suggesting that nuclear protein binding was different for the C and T alleles of rs3095870 (Supplementary Figure 2, available at <http://onlinelibrary.wiley.com/doi/10.1002/art.40419/abstract>). Supershift assays confirmed that TEAD1 and YAP1 are both components of the rs3095870 C-binding complex (Figure 3A).

To provide further evidence, we performed protein pull-down assays using biotinylated DNA probes containing either the C or the T allele of rs3095870. The assays

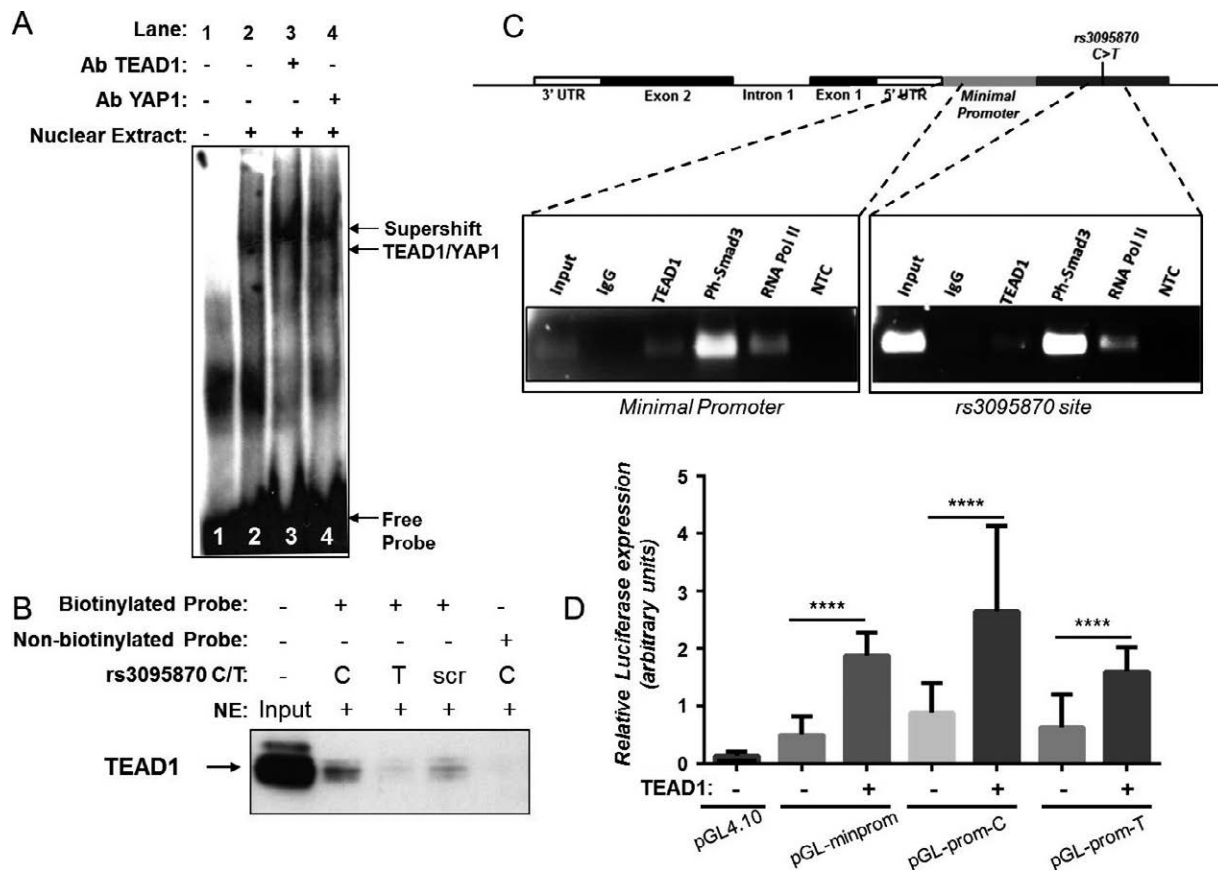


Figure 3. Binding of transcription-enhancer factor domain 1 (TEAD1) at the rs3095870 site and increased *NKX2-5* transcriptional activity. Binding assays were performed using nuclear extracts (NE) from transforming growth factor β -treated immortalized human pulmonary artery smooth muscle cells (PASCs) and biotinylated DNA probes containing the rs3095870 C/T alleles (A–C). **A**, Electrophoretic mobility shift assay with rs3095870 C allele biotinylated probe (lane 2), and supershifts with TEAD1 and Yes-associated protein 1 (YAP1) antibodies (Ab) (lanes 3 and 4), as well as without nuclear extract (lane 1). **B**, Pull-down assay using streptavidin beads and biotinylated DNA probes specific to rs3095870 C/T alleles. Complexes were analyzed by sodium dodecyl sulfate–polyacrylamide gel electrophoresis and Western blotting and immunodecorated with TEAD1 antibody. Nonbiotinylated and scrambled (scr) biotinylated probes were used as controls. Input was 5% of total nuclear extract. **C**, Chromatin immunoprecipitation assays using antibodies specific for TEAD1, phosphorylated Smad3 (Ph-Smad3), and RNA polymerase II (RNA Pol II). Specific polymerase chain reaction primers were designed and used to detect enrichment. Immunoprecipitation with IgG was used as a control. No template control (NTC) was also used. Input was 10% of the initial chromatin used per immunoprecipitation assay. A schematic representation of the *NKX2-5* gene, showing intron 1, exons 1 and 2, and untranslated regions (3'-UTR and 5'-UTR), as well as the locations of the minimal promoter and rs3095870 C>T site, is shown at the top. **D**, Luciferase reporter gene assays of primary human PASCs. TEAD1 expression vector was cotransfected with DNA constructs containing either the minimal promoter (pGL-minprom) or the upstream promoter with the rs3095870-C/T alleles (pGL-prom-C/T). The pGL4.10 vector, which contains the firefly luciferase gene, was used as the control. Values are the mean \pm SEM of 3 independent experiments. **** = $P \leq 0.0001$ by Student's *t*-test.

demonstrated that TEAD1 specifically binds the C allele of the SNP (Figure 3B). In addition, ChIP assays confirmed TEAD1 binding in the region upstream of the *NKX2-5* transcriptional start site in transforming growth factor β (TGF β)-treated immortalized human PSMCs (Figure 3C). Interestingly, ChIP assay analysis revealed strong enrichment for phosphorylated Smad3 protein on the *NKX2-5* upstream region (Figure 3C), verifying the involvement of TGF β in *NKX2-5* regulation, which has previously been reported (12). Although enriched binding for both TEAD1 and phosphorylated Smad3 antibodies was observed on the minimal *NKX2-5* promoter, the upstream rs3095870 region was also immunoprecipitated despite the strong input signal. The finding that RNA polymerase II also precipitated the same region (Figure 3C) suggests that

TEAD1 and phosphorylated Smad3 are engaged in the transcriptional machinery bound to the minimal promoter.

We investigated a potential mechanism of *NKX2-5* transcriptional activation by TEAD1. As expected, when TEAD1 expression vector was cotransfected into human PSMCs together with the pGL-prom-C/T constructs, the transcriptional activity was strongly increased ($P < 0.0001$) (Figure 3D). Taken together, these data indicate a mechanism of transcriptional regulation through the specific binding of TEAD1 on the C allele of rs3095870 in the upstream promoter region of *NKX2-5*.

We next investigated whether knockdown of TEAD1 using siRNA affects *NKX2-5* expression in immortalized human PSMCs. Indeed, we found that *NKX2-5* protein levels were decreased when TEAD1 was knocked

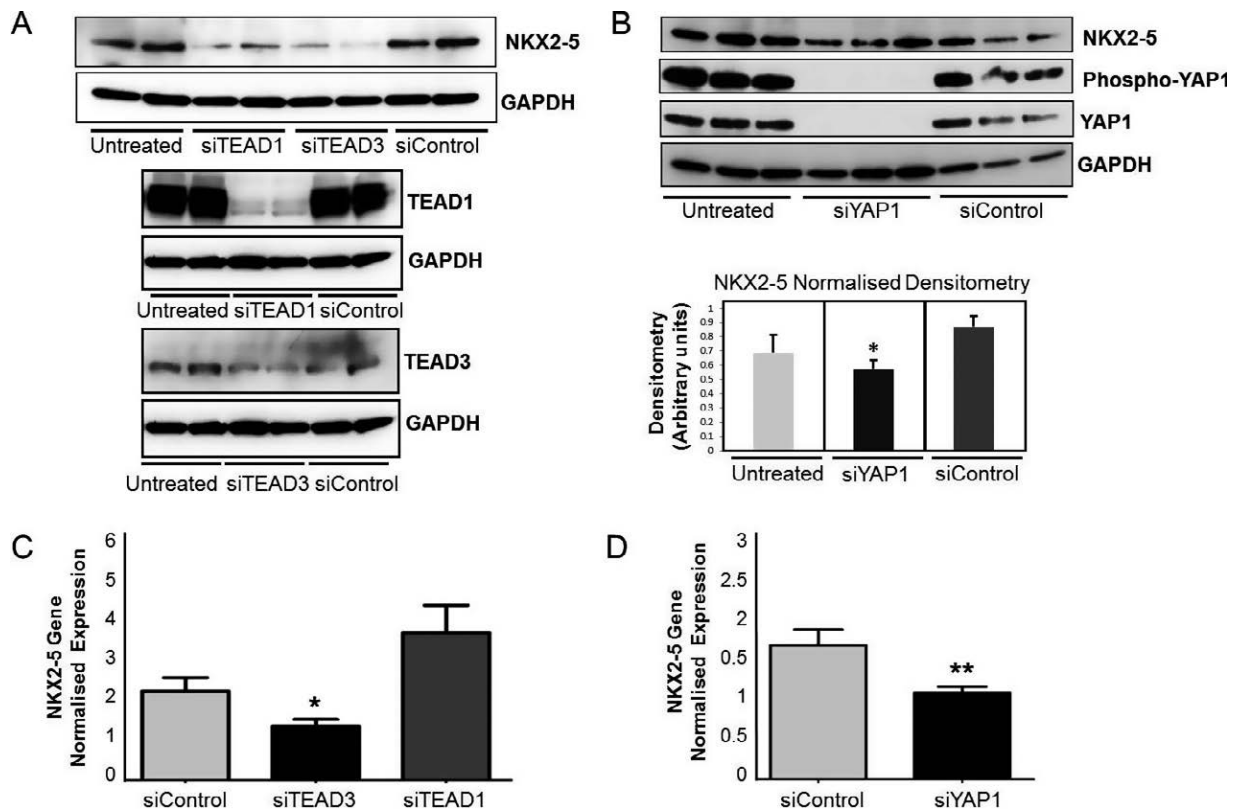


Figure 4. *NKX2-5* transcriptional regulation through transcription-enhancer factor domain 1 (TEAD1)/Yes-associated protein 1 (YAP1) complexes. **A**, *NKX2-5* expression in immortalized human pulmonary artery smooth muscle cells (PSMCs), as determined by sodium dodecyl sulfate–polyacrylamide gel electrophoresis (SDS-PAGE) and Western blotting after TEAD1 and TEAD3 protein knockdown using small interfering RNA (siRNA)-specific oligonucleotides (siTEAD1 and siTEAD3). To evaluate the efficiency of silencing, TEAD1 and TEAD3 protein levels were also determined by SDS-PAGE and Western blotting. Scrambled nontargeting siRNA molecules were used as a control (siControl), and GAPDH was used as a housekeeping gene. **B**, Protein levels of *NKX2-5*, phosphorylated YAP1, and YAP1 in immortalized human PSMCs, as determined by SDS-PAGE and Western blotting after YAP1 knockdown using specific siRNA (siYAP1) (top). Protein levels of *NKX2-5* were then analyzed by densitometry, and the normalized levels are shown at the bottom. Values are the mean \pm SEM of 3 independent experiments. **C** and **D**, *NKX2-5* gene expression in total RNA isolated from immortalized human PSMCs after treatment with siTEAD1 or siTEAD3 (**C**) or with siYAP1 (**D**), as determined by quantitative polymerase chain reaction analysis. Scrambled siControl was used for comparison, and *NKX2-5* gene expression was normalized against levels of TATA-binding protein (housekeeping gene). Values are the mean \pm SEM of 3 independent experiments. * = $P \leq 0.05$; ** = $P \leq 0.01$ by Student's *t*-test.

down (Figure 4A), but there was no statistically significant change in the mRNA levels (Figure 4C). Since all the TEAD family members recognize and bind the same DNA consensus element, we wanted to determine whether another member of the family may also be implicated in the regulatory mechanism. A recent study showed that TEAD3 is expressed in human aortic SMCs and is required for the TGFβ signaling cascade (38), and we therefore

investigated whether TEAD3 can also regulate *NKX2-5*. When TEAD3 was knocked down by siRNA, the gene and protein levels of *NKX2-5* were significantly decreased (Figures 4A and C). However, when immortalized human PASMCs were cotransfected with TEAD3 expression vector together with the pGL-prom-C/T constructs, the luciferase activity was not altered (Supplementary Figure 3, available at <http://onlinelibrary.wiley.com/doi/10.1002/art>.

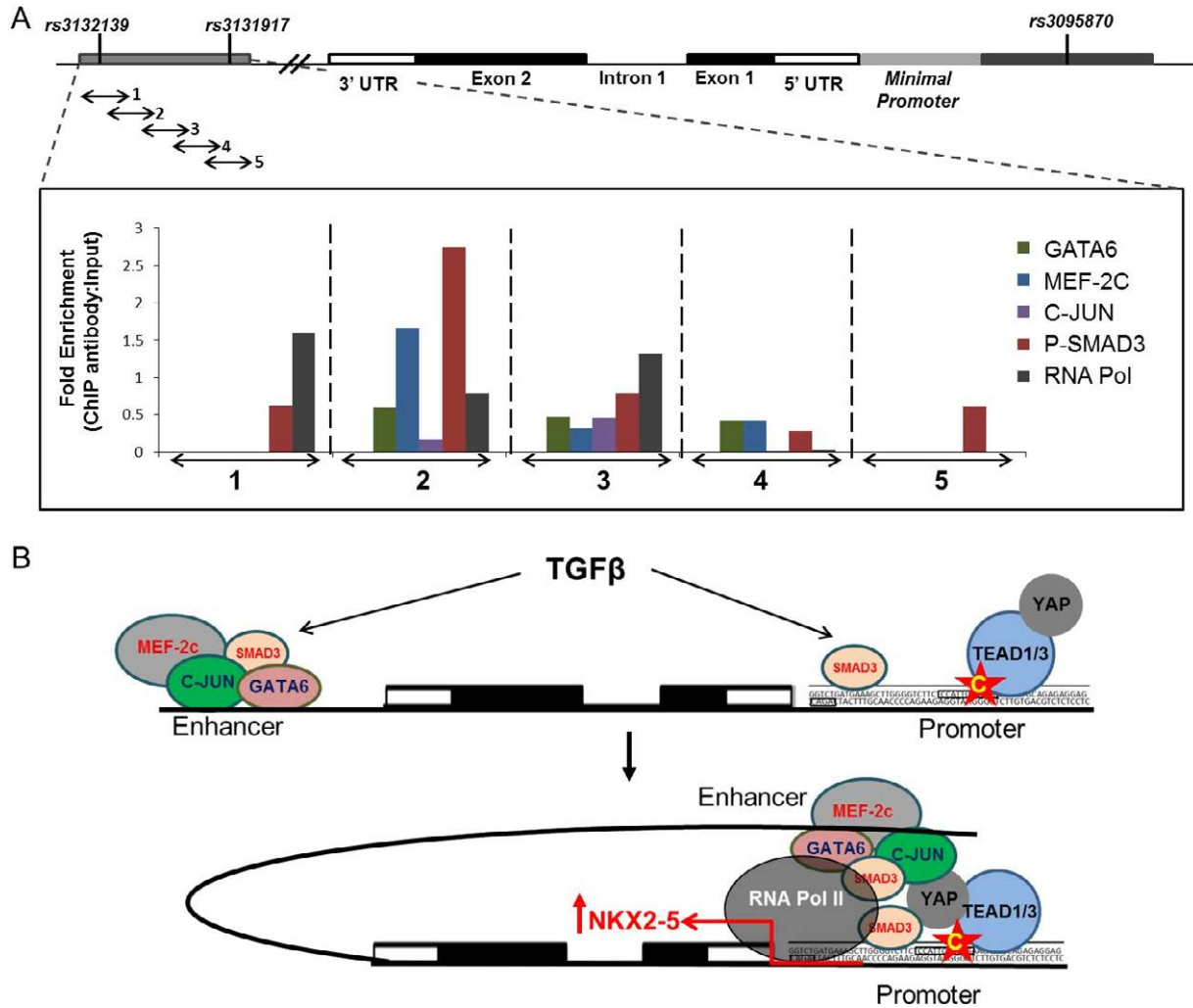


Figure 5. An upstream promoter and a downstream enhancer involved in *NKX2-5* transcription. **A**, Analysis of the enrichment of GATA-6, myocyte-specific enhancer factor 2C (MEF-2C), c-Jun, phosphorylated Smad3, and RNA polymerase II (RNA Pol) as determined by chromatin immunoprecipitation (ChIP) assays of transforming growth factor β (TGFβ)-treated immortalized human pulmonary artery smooth muscle cells. Chromatin was immunoprecipitated using specific antibodies. Five primer pairs (1–5) were designed to cover the 1.6-kb genomic region of the downstream enhancer. Results are shown as the fold enrichment of each protein in every genomic segment. The data were normalized against the intensity of the input (10% of initial chromatin used per immunoprecipitation assay). A schematic representation of the *NKX2-5* gene, showing intron 1, exons 1 and 2, and untranslated regions (3'-UTR and 5'-UTR), as well as the locations of rs3132139, rs3131917, rs3095870, and the minimal promoter sites, is shown at the top. **B**, Proposed model of the transcriptional regulation of *NKX2-5*. Functional studies revealed an upstream promoter region and a novel downstream functional enhancer that are engaged in the transcriptional initiation machinery of *NKX2-5* through the binding of TEAD1/TEAD3/YAP1 complex and other transcription activators, such as MEF-2C, c-Jun, phosphorylated Smad3, and GATA-6. **Red arrow** to the right of *NKX2-5* is the transcription start site. Star with the letter C indicates the C allele of rs3095870. Color figure can be viewed in the online issue, which is available at <http://onlinelibrary.wiley.com/doi/10.1002/art.40419/abstract>.

40419/abstract). We next verified that YAP1 is a cofactor for TEAD1/3 proteins by showing that NKX2-5 gene and protein levels were significantly decreased when YAP1 was knocked down using siRNA (Figures 4B and D).

Taken together, these data suggest a complex regulatory role of TEAD1 and TEAD3. The data are consistent with a transcriptional mechanism whereby TEAD3 is responsible for basal levels of expression and TEAD1 is required for higher activation. At the same time, it is possible that they both control factors that regulate NKX2-5 at the posttranscriptional and posttranslational levels. Regardless, the data confirm that the TEAD site at rs3095870 is functional and that binding of TEAD/YAP1 regulates NKX2-5 expression in human PSMCs.

Transcriptional regulation of *NKX2-5* through the downstream enhancer. The rest of the disease-associated SNPs (rs3132139, rs3131917) are located downstream of *NKX2-5*. This region was previously described as a candidate cardiac enhancer sequence due to its proximity to the *NKX2-5* gene, although it has not yet been verified experimentally (32). In this study, we used luciferase reporter gene assays to confirm that the region is indeed a *NKX2-5* enhancer in human PSMCs (Figure 2D).

To obtain more information on the transcription factors that can potentially interact with this enhancer and the 2 SNPs in particular, we conducted another in silico analysis. It revealed several binding sites for a number of DNA binding proteins known to regulate transcription through enhancer regions during heart development and SMC differentiation, such as GATA-6, myocyte-specific enhancer factor 2C (MEF-2C), and c-Jun. Since enhancer effects are usually cell type-specific, we performed ChIP assays in immortalized human PSMCs.

Surprisingly, we found significant enrichment for MEF-2C, GATA-6, and c-Jun at the 5' end of the enhancer region (Figure 5A). Phosphorylated Smad3 protein showed significant binding across the entire region, suggesting that TGF β could also activate the enhancer to positively regulate *NKX2-5* expression (Figure 5A). In addition, an interesting finding was the RNA polymerase II enrichment toward the 5' end of the region, suggesting that the enhancer is engaged with the transcriptional machinery through an enhancer-promoter interaction (Figure 5A). These data confirm that the downstream genomic locus, which contains the disease-associated SNPs, is a functional enhancer that activates *NKX2-5* transcription in human PSMCs through the binding of GATA-6, MEF-2C, and c-Jun.

DISCUSSION

In this study, we demonstrated the molecular mechanisms that underlie the overexpression of NKX2-5

in SSc. We also identified potential genetic associations with functional polymorphisms that may contribute to SSc susceptibility and specifically to the important vascular complication of SSc-associated PH.

Recent published work proposes that modulated NKX2-5 expression is implicated in vascular homeostasis and vascular disease-associated phenotypes (39–41). In our previous studies, we demonstrated a critical role of NKX2-5 in vascular remodeling and atherosclerosis, with expression being detected in atherosclerotic lesions, in the fibrous cap, and in the cells within the media (5,6). However, the mechanisms that lead to up-regulation of NKX2-5 expression in vessels remain unknown. In the present study, we performed candidate gene association analysis to explore our evidence-based hypothesis that *NKX2-5* is genetically associated with vascular disease characterized by vascular remodeling as well as to investigate the functional effect of any associated loci. Despite the numerous reports of genomic data either published or stored in repositories, limited information is available on *NKX2-5*, presumably due to the perception that the role of the gene is important exclusively in embryonic development (1–4).

Autoimmunity and dysregulation of immune responses are well-established components of SSc, and the major histocompatibility complex has been predominantly associated with SSc by the majority of genetic studies and genome-wide association studies (42,43). However, outside autoimmunity, only a few genes have been associated with SSc, with *CTGF* (*CCN2*) being the most studied (44,45). We performed a genetic association study in 2 independent cohorts of SSc patients as a model of vascular and pulmonary pathology. Interestingly, in the meta-analysis, we found rs3131917 to be associated with SSc ($P = 0.029$). This is a de novo finding of an association between SSc and a gene unrelated to immunity in a meta-analysis across 2 independent cohorts of similar origin.

The groups of SSc patients with pulmonary complications such as PH and pulmonary fibrosis have the highest mortality rates (46). We found that rs3132139 and rs3131917 are genetically associated with PH (Table 1 and Supplementary Table 3). These data support our hypothesis that the *NKX2-5* genomic locus is important in pulmonary/vascular pathology. In fact, rs3132139 showed a significant association ($P = 0.006$) in a meta-analysis of 46 genome-wide association studies in patients with coronary artery disease (CAD) (47). CAD is an arterial disease characterized by plaque formation and constrictive vascular remodeling in the carotid artery, as well as endothelial dysfunction and inflammation (48). This finding further supports our hypothesis for the functional involvement of NKX2-5 in vascular remodeling.

Surprisingly, both rs3131917 and rs3132139 reside in a region that was identified as a putative enhancer (chromosome 5: 173,228,601–173,230,244) for *NKX2-5* in heart tissue by ChIP-Seq analysis (32). This enhancer should be activated when *NKX2-5* exerts its unique and nonredundant role during heart development. We hypothesized that the same mechanism that activates *NKX2-5* in embryogenesis could also activate the gene in diseased vessels in adulthood. In this study, we validated the region as a functional downstream *NKX2-5* enhancer. In reporter gene assays, luciferase activity was significantly increased in the presence of this enhancer compared to the proximal minimal promoter. We have shown that there is enriched binding of the transcription factors MEF-2C, GATA-6, and c-Jun on this enhancer. This result supports early studies showing that MEF-2C/*NKX2-5*/GATA form a positive regulatory network (12,49,50). Further studies are being carried out on this enhancer in order to characterize its precise function.

We also identified TEAD1 as a transcription regulator for *NKX2-5* activation in human PSMCs. TEAD1 can only bind the *NKX2-5* upstream promoter at –1.1 kb in the presence of the rs3095870 C allele. TEADs are expressed in VSMCs, where they are known to control phenotype modulation from the contractile to the synthetic state, as well as cell proliferation and the cell cycle (33,34). We demonstrated that TEAD1 bound strongly on the upstream promoter at the rs3095870 C allele; however, it did not significantly affect *NKX2-5* mRNA in siRNA knockdown experiments. On the contrary, specific siRNA for TEAD3 significantly decreased both the protein and RNA levels of *NKX2-5*. TEAD3 cotransfection in human PSMCs, however, did not increase luciferase expression.

These data indicate a complex transcriptional mechanism that involves both TEAD1 and TEAD3. One explanation could be that TEAD3 is directly required for basal levels of *NKX2-5* transcription through binding on another MCAT element located outside the 1.6-kb upstream region containing rs3095870 (chromosome 5: 173,235,792–173,237,444). In the presence of TEAD1, however, the transcription is significantly enhanced (Figure 3D), as TEAD1 is required for the overexpression of *NKX2-5* by binding to the promoter containing rs3095870 in response to injury or disease-associated stimuli.

A recent study showed that TEAD3 is required for TGF β signaling through association with Smad3 in human aortic SMCs in a risk locus for atherosclerosis (38). Our data add to the accumulating evidence of the emerging roles of TEADs and TGF β signaling in VSMCs in cardiovascular disease. The four members of the TEAD family recognize the same MCAT binding

element, and they require cofactors in order to regulate the expression of downstream targets. YAP1 is the most common associating partner of TEADs, especially in VSMCs (36,37). Indeed, we were able to confirm that YAP1 is important for *NKX2-5* activity, corroborating the role of TEAD/YAP1 in *NKX2-5* transcriptional regulation.

We propose a new mechanism for the regulation of the *NKX2-5* gene in human PSMCs, which is described in detail in Figure 5B. The mechanism involves an upstream promoter activated through the binding of the TEAD/YAP1 complex. This promoter is engaged with the RNA polymerase II complex, and a downstream enhancer that binds GATA-6, MEF-2C, and c-Jun. Enrichment of phosphorylated Smad3 binding confirmed that TGF β , which is known to activate *NKX2-5* expression, exerts its effect on *NKX2-5* through Smad3 binding at multiple CAGA sites on both the upstream promoter and the downstream enhancer. Evidence from the ChIP assays clearly shows that both regions interact with the RNA polymerase II complex and the transcriptional machinery. Detailed studies will be necessary to further investigate a potential combined synergistic effect of the upstream promoter and the downstream enhancer on the transcriptional activity of *NKX2-5* in human PSMCs. Transcriptional activation, and therefore *NKX2-5* expression, in VSMCs results in the up-regulation of *NKX2-5* downstream targets associated with inflammation, proliferation, migration, extracellular matrix production, and deposition within the vascular wall, all of which are key features of vascular remodeling and ultimately lead to disease-associated pathogenic phenotypes (5,6).

In summary, we have shown that *NKX2-5* is genetically associated with SSc and PH, and we propose for the first time a regulatory mechanism for the transcriptional activation of the human *NKX2-5* gene in diseased vessels. The mechanism involves an upstream promoter that binds the TEAD/YAP1 complex and a novel enhancer activated through the binding of GATA-6, MEF-2C, and c-Jun. We believe that this is a key mechanism that is common in conditions characterized by different types of vascular remodeling, including but not limited to PAH, CAD, peripheral artery disease, and stroke.

ACKNOWLEDGMENTS

We thank Drs. Lara Bossini-Castillo and Elena Lopez-Isac for their scientific contribution during the data collection and analysis and Dr. Joanne B. Manning for her contribution to the data and information transfer of the Manchester clinical cohort. *NKX2-5* expression data in PSMCs from patients with SSc-associated PH were kindly provided by Dr. K. R. Stenmark (University of Colorado, Denver, CO).

AUTHOR CONTRIBUTIONS

All authors were involved in drafting the article or revising it critically for important intellectual content, and all authors approved the final version to be published. Dr. Ponticos had full access to all of the data in the study and takes responsibility for the integrity of the data and the accuracy of the data analysis.

Study conception and design. Dritsoula, Martin, Herrick, Abraham, Denton, Ponticos.

Acquisition of data. Dritsoula, Ponticos.

Analysis and interpretation of data. Dritsoula, Papaioannou, Guerra, Fonseca, Ponticos.

REFERENCES

1. Tanaka M, Chen Z, Bartunkova S, Yamasaki N, Izumo S. The cardiac homeobox gene *Csx/Nkx2.5* lies genetically upstream of multiple genes essential for heart development. *Development* 1999;126:1269–80.
2. Lyons I, Parsons LM, Hartley L, Li R, Andrews JE, Robb L, et al. Myogenic and morphogenetic defects in the heart tubes of murine embryos lacking the homeo box gene *Nkx2-5*. *Genes Dev* 1995;9:1654–66.
3. Paffett-Lugassy N, Singh R, Nevis KR, Guner-Ataman B, O'Loughlin E, Jahangiri L, et al. Heart field origin of great vessel precursors relies on *nkx2.5*-mediated vasculogenesis. *Nat Cell Biol* 2013;15:1362–9.
4. Nagelberg D, Wang J, Su R, Torres-Vazquez J, Targoff KL, Poss KD, et al. Origin, specification, and plasticity of the great vessels of the heart. *Curr Biol* 2015;25:2099–110.
5. Ponticos M, Partridge T, Black CM, Abraham DJ, Bou-Gharios G. Regulation of collagen type I in vascular smooth muscle cells by competition between *Nkx2.5* and δ EF1/ZEB1. *Mol Cell Biol* 2004;24:6151–61.
6. Ponticos M, Jackson C, Bou-Gharios G, Abraham D. The role of the homeobox transcription factor *NKX2.5* in the regulation of collagen in vessels and in the atherosclerotic lesion. *Vascul Pharmacol* 2006;45:e45–e6.
7. Renna NF, Garcia R, Ramirez J, Miatello RM. Vascular repair and remodeling: a review. In: Simionescu D, Simionescu A, editors. *Physiologic and pathologic angiogenesis - signaling mechanisms and targeted therapy*. Rijeka (Croatia): InTech; 2017. p. 195–212.
8. Denton CP. Advances in pathogenesis and treatment of systemic sclerosis. *Clin Med (London)* 2016;16:55–60.
9. Stern EP, Denton CP. The pathogenesis of systemic sclerosis. *Rheum Dis Clin North Am* 2015;41:367–82.
10. Nihtyanova SI, Schreiber BE, Ong VH, Rosenberg D, Moynzadeh P, Coghlan JG, et al. Prediction of pulmonary complications and long-term survival in systemic sclerosis. *Arthritis Rheumatol* 2014;66:1625–35.
11. Reecy JM, Li X, Yamada M, DeMayo FJ, Newman CS, Harvey RP, et al. Identification of upstream regulatory regions in the heart-expressed homeobox gene *Nkx2-5*. *Development* 1999;126:839–49.
12. Brown CO III, Chi X, Garcia-Gras E, Shirai M, Feng XH, Schwartz RJ. The cardiac determination factor, *Nkx2-5*, is activated by mutual cofactors *GATA-4* and *Smad1/4* via a novel upstream enhancer. *J Biol Chem* 2004;279:10659–69.
13. Schwartz RJ, Olson EN. Building the heart piece by piece: modularity of cis-elements regulating *Nkx2-5* transcription. *Development* 1999;126:4187–92.
14. Wang J, Zhang H, Iyer D, Feng XH, Schwartz RJ. Regulation of cardiac specific *nkx2.5* gene activity by small ubiquitin-like modifier. *J Biol Chem* 2008;283:23235–43.
15. Clark CD, Zhang B, Lee B, Evans SI, Lassar AB, Lee KH. Evolutionary conservation of *Nkx2.5* autoregulation in the second heart field. *Dev Biol* 2013;374:198–209.
16. Su W, Zhu P, Wang R, Wu Q, Wang M, Zhang X, et al. Congenital heart diseases and their association with the variant distribution features on susceptibility genes. *Clin Genet* 2017;91:349–54.
17. Abdul Samad F, Suliman BA, Basha SH, Manivasagam T, Essa MM. A comprehensive In Silico analysis on the structural and functional impact of SNPs in the congenital heart defects associated with *NKX2-5* gene—a molecular dynamic simulation approach. *PLoS One* 2016;11:e0153999.
18. Van den Hoogen F, Khanna D, Franssen J, Johnson SR, Baron M, Tyndall A, et al. 2013 classification criteria for systemic sclerosis: an American College of Rheumatology/European League Against Rheumatism collaborative initiative. *Arthritis Rheum* 2013;65:2737–47.
19. Coghlan JG, Denton CP, Grünig E, Bonderman D, Distler O, Khanna D, et al. Evidence-based detection of pulmonary arterial hypertension in systemic sclerosis: the DETECT study. *Ann Rheum Dis* 2014;73:1340–9.
20. Lynch BM, Stern EP, Ong V, Harber M, Burns A, Denton CP. UK Scleroderma Study Group (UKSSG) guidelines on the diagnosis and management of scleroderma renal crisis. *Clin Exp Rheumatol* 2016;34 Suppl 100:106–9.
21. De Bakker PI, Yelensky R, Pe'er I, Gabriel SB, Daly MJ, Altshuler D. Efficiency and power in genetic association studies. *Nat Genet* 2005;37:1217–23.
22. International HapMap Consortium. The International HapMap Project. *Nature* 2003;426:789–96.
23. ENCODE Project Consortium. An integrated encyclopedia of DNA elements in the human genome. *Nature* 2012;489:57–74.
24. Matys V, Kel-Margoulis OV, Fricke E, Liebich I, Land S, Barre-Dirrie A, et al. TRANSFAC and its module TRANSCOMP: transcriptional gene regulation in eukaryotes. *Nucleic Acids Res* 2006;34:D108–10.
25. Mathelier A, Fornes O, Arenillas DJ, Chen CY, Denay G, Lee J, et al. JASPAR 2016: a major expansion and update of the open-access database of transcription factor binding profiles. *Nucleic Acids Res* 2016;44:D110–5.
26. Ward LD, Kellis M. HaploReg: a resource for exploring chromatin states, conservation, and regulatory motif alterations within sets of genetically linked variants. *Nucleic Acids Res* 2012;40:D930–4.
27. Miller SA, Dykes DD, Polesky HF. A simple salting out procedure for extracting DNA from human nucleated cells. *Nucleic Acids Res* 1988;16:1215.
28. Purcell S, Neale B, Todd-Brown K, Thomas L, Ferreira MA, Bender D, et al. PLINK: a tool set for whole-genome association and population-based linkage analyses. *Am J Hum Genet* 2007;81:559–75.
29. Barrett JC, Fry B, Maller J, Daly MJ. Haploview: analysis and visualization of LD and haplotype maps. *Bioinformatics* 2005;21:263–5.
30. Frid MG, Aldashev AA, Dempsey EC, Stenmark KR. Smooth muscle cells isolated from discrete compartments of the mature vascular media exhibit unique phenotypes and distinct growth capabilities. *Circ Res* 1997;81:940–52.
31. Rasband WS, National Institutes of Health. ImageJ: Image processing and analysis in Java. URL: <http://imagej.nih.gov/ij/>.
32. May D, Blow MJ, Kaplan T, McCulley DJ, Jensen BC, Akiyama JA, et al. Large-scale discovery of enhancers from human heart tissue. *Nat Genet* 2012;44:89–93.
33. Liu F, Wang X, Hu G, Wang Y, Zhou J. The transcription factor *TEAD1* represses smooth muscle-specific gene expression by abolishing myocardin function. *J Biol Chem* 2014;289:3308–16.
34. Gan Q, Yoshida T, Li J, Owens GK. Smooth muscle cells and myofibroblasts use distinct transcriptional mechanisms for smooth muscle α -actin expression. *Circ Res* 2007;101:883–92.
35. Yoshida T, Sinha S, Dandre F, Wamhoff BR, Hoofnagle MH, Kremer BE, et al. Myocardin is a key regulator of CArG-dependent transcription of multiple smooth muscle marker genes. *Circ Res* 2003;92:856–64.

36. Zhao B, Ye X, Yu J, Li L, Li W, Li S, et al. TEAD mediates YAP-dependent gene induction and growth control. *Genes Dev* 2008;22:1962–71.
37. Xie C, Guo Y, Zhu T, Zhang J, Ma PX, Chen YE. Yap1 protein regulates vascular smooth muscle cell phenotypic switch by interaction with myocardin. *J Biol Chem* 2012;287:14598–605.
38. Almontashiri NA, Antoine D, Zhou X, Vilmundarson RO, Zhang SX, Hao KN, et al. 9p21.3 coronary artery disease risk variants disrupt TEAD transcription factor-dependent transforming growth factor β regulation of p16 expression in human aortic smooth muscle cells. *Circulation* 2015;132:1969–78.
39. Du M, Wang X, Tan X, Li X, Huang D, Huang K, et al. Nkx2-5 is expressed in atherosclerotic plaques and attenuates development of atherosclerosis in apolipoprotein E-deficient mice. *J Am Heart Assoc* 2016;5:e004440.
40. Hautefort A, Chesne J, Preussner J, Pullamsetti SS, Tost J, Looso M, et al. Pulmonary endothelial cell DNA methylation signature in pulmonary arterial hypertension. *Oncotarget* 2017;8:52995–3016.
41. Wang L, Qiu P, Jiao J, Hirai H, Xiong W, Zhang J, et al. Yes-associated protein inhibits transcription of myocardin and attenuates differentiation of vascular smooth muscle cell from cardiovascular progenitor cell lineage. *Stem Cells* 2017;35:351–61.
42. Martin JE, Assassi S, Diaz-Gallo LM, Broen JC, Simeon CP, Castellvi I, et al. A systemic sclerosis and systemic lupus erythematosus pan-meta-GWAS reveals new shared susceptibility loci. *Hum Mol Genet* 2013;22:4021–9.
43. Mayes MD, Bossini-Castillo L, Gorlova O, Martin JE, Zhou X, Chen WV, et al. Immunochip analysis identifies multiple susceptibility loci for systemic sclerosis. *Am J Hum Genet* 2014;94:47–61.
44. Fonseca C, Lindahl GE, Ponticos M, Sestini P, Renzoni EA, Holmes AM, et al. A polymorphism in the CTGF promoter region associated with systemic sclerosis. *N Engl J Med* 2007;357:1210–20.
45. Zhang X, Nie S, Si X, Luo Y, Tang W. Association between the CTGF –945C/G polymorphism and systemic sclerosis: a meta-analysis. *Gene* 2012;509:1–6.
46. Steen V, Medsger TA Jr. Predictors of isolated pulmonary hypertension in patients with systemic sclerosis and limited cutaneous involvement. *Arthritis Rheum* 2003;48:516–22.
47. Nikpay M, Goel A, Won HH, Hall LM, Willenborg C, Kanoni S, et al. A comprehensive 1,000 Genomes-based genome-wide association meta-analysis of coronary artery disease. *Nat Genet* 2015;47:1121–30.
48. Heusch G, Libby P, Gersh B, Yellon D, Bohm M, Lopaschuk G, et al. Cardiovascular remodeling in coronary artery disease and heart failure. *Lancet* 2014;383:1933–43.
49. Skerjanc IS, Petropoulos H, Ridgeway AG, Wilton S. Myocyte enhancer factor 2C and Nkx2-5 up-regulate each other's expression and initiate cardiomyogenesis in P19 cells. *J Biol Chem* 1998;273:34904–10.
50. Lien CL, Wu C, Mercer B, Webb R, Richardson JA, Olson EN. Control of early cardiac-specific transcription of Nkx2-5 by a GATA-dependent enhancer. *Development* 1999;126:75–84.

Transforming Growth Factor β Activation Primes Canonical Wnt Signaling Through Down-Regulation of Axin-2

Justin Gillespie,¹ Rebecca L. Ross,² Clarissa Corinaldesi,² Filomena Esteves,²
Emma Derrett-Smith,³ Michael F. McDermott,² Gina M. Doody,² Christopher P. Denton,³
Paul Emery,¹ and Francesco Del Galdo ¹

Objective. Aberrant activation of Wnt signaling has been observed in tissues from patients with systemic sclerosis (SSc). This study aimed to determine the role of transforming growth factor β (TGF β) in driving the increased Wnt signaling, through modulation of axis inhibition protein 2 (Axin-2), a critical regulator of the Wnt canonical pathway.

Methods. Canonical Wnt signaling activation was analyzed by TOPflash T cell factor/lymphoid enhancer factor promoter assays. Axin-2 was evaluated in vitro by analysis of Axin-2 primary/mature transcript expression and decay, TGF β receptor type I (TGF β RI) blockade, small interfering RNA-mediated depletion of tristetrapirolin 1, and XAV-939-mediated Axin-2 stabilization. In vivo, Axin-2 messenger RNA (mRNA) and protein expression was determined in skin and lung biopsy samples from mice that express a kinase-deficient TGF β RII specifically on fibroblasts (T β RII Δ k-fib-transgenic mice) and from littermate controls.

Results. SSc fibroblasts displayed an increased response to canonical Wnt ligands despite basal levels of Wnt signaling that were comparable to those in healthy control fibroblasts in vitro. Notably, we showed that SSc fibroblasts had reduced basal expression of Axin-2, which was caused by an endogenous TGF β -dependent increase in Axin-2 mRNA decay. Accordingly, we observed that TGF β decreased Axin-2 expression both in vitro in healthy control fibroblasts and in vivo in T β RII Δ k-fib-transgenic

mice. Additionally, using Axin-2 gain- and loss-of-function experiments, we demonstrated that the TGF β -induced increased response to Wnt activation characteristic of SSc fibroblasts depended on reduced bioavailability of Axin-2.

Conclusion. This study highlights the importance of reduced bioavailability of Axin-2 in mediating the increased canonical Wnt response observed in SSc fibroblasts. This novel mechanism extends our understanding of the processes involved in Wnt/ β -catenin-driven pathology and supports the rationale for targeting the TGF β pathway to regulate the aberrant Wnt signaling observed during fibrosis.

Tissue fibroblasts are the key cellular elements of fibrosis, and are primarily involved in regulating extracellular matrix (ECM) homeostasis. Dysregulated fibroblast activation can result in the excessive synthesis and deposition of collagens and other ECM proteins within tissues, leading to organ dysfunction and failure (1,2). Sustained transforming growth factor β (TGF β) activity has been shown to be a central mediator of fibroblast activation and can reproduce many of the hallmarks associated with fibrosis both in vitro and in vivo (3–6). Indeed, TGF β -treated fibroblasts display a gene expression profile similar to that of dermal fibroblasts from patients with diffuse cutaneous systemic sclerosis (dcSSc) (7).

The T β RII Δ k-fib-transgenic mouse model, characterized by constitutive TGF β signaling through *Colla2*-mediated fibroblast-specific expression of a kinase-deficient TGF β receptor type II (TGF β RII), replicates key constitutive features of SSc, including dermal fibrosis as well as susceptibility to other organ-based complications, such as lung fibrosis and pulmonary hypertension (8). This model has proven to be valuable for the delineation of profibrotic pathways and especially for investigating cross-talk between TGF β and other relevant mediators (9).

Recently, several studies have shown that canonical Wnt signaling is activated during fibrosis in SSc

Supported by the European League Against Rheumatism Orphan Disease Programme.

¹Justin Gillespie, PhD, Paul Emery, MD, FRCP, Francesco Del Galdo, MD, PhD: University of Leeds and Leeds Teaching Hospitals NHS Trust, Leeds, UK; ²Rebecca L. Ross, PhD, Clarissa Corinaldesi, PhD, Filomena Esteves, PhD, Michael F. McDermott, DMed, MRCPI, Gina M. Doody, PhD: University of Leeds, Leeds, UK; ³Emma Derrett-Smith, PhD, MRCP, Christopher P. Denton, PhD, FRCP: University College London, London, UK.

Address correspondence to Francesco Del Galdo, MD, PhD, Leeds Institute of Rheumatic and Musculoskeletal Medicine, University of Leeds, Leeds LS9 7TF, UK. E-mail: f.delgaldo@leeds.ac.uk.

Submitted for publication September 19, 2016; accepted in revised form January 30, 2018.

and in other fibrotic conditions (10–14). Indeed, this activation may have an important role in the initiation/maintenance of fibrosis; however, the biochemical and biophysical mechanisms of this activation are yet to be identified, and the relative contribution of cross-talk to TGF β pathway activation is unclear.

Canonical Wnt signaling is dependent on β -catenin bioavailability, which is regulated by the β -catenin destruction complex. This complex is primarily composed of axis inhibition protein (Axin), adenomatous polyposis coli, casein kinase 1, and glycogen synthase kinase 3 β (GSK-3 β), which together facilitate the phosphorylation and subsequent ubiquitin-mediated degradation of β -catenin (15). Canonical Wnt agonist activation of this pathway recruits the destruction complex to the plasma membrane, thereby lowering its capacity to induce β -catenin proteasomal degradation (16). As a result, increased levels of free cytosolic β -catenin can undergo nuclear translocation, leading to the up-regulation of canonical Wnt target genes through β -catenin-mediated activation of the T cell factor (TCF)/lymphoid enhancer factor (LEF) transcription factors.

Specifically, Axin-2 and Axin-1 are essential scaffold proteins for the formation of the β -catenin destruction complex and therefore act as negative regulators of Wnt signaling (17–19). While the gene for Axin-1 is constitutively expressed, the gene for Axin-2 is a direct transcriptional target of canonical Wnt signaling, acting as part of a negative feedback system to control Wnt signaling activation (20,21).

Axin-2^{-/-} mice are viable, and delivery of Axin-2 complementary DNA (cDNA) can rescue the lethal Axin-1^{-/-} phenotype (22,23). Uniquely, heterozygous Axin-2 germline mutations in humans can lead to familial tooth agenesis (24). Interestingly, in the chondrocyte lineage, TGF β promotes β -catenin accumulation while inhibiting the expression of Axin-1 and Axin-2, thus providing a context-specific example of the interplay between these pathways (25). Recently, the endogenous Wnt antagonist, Dkk-1, has been described to be TGF β responsive with transgenic expression attenuating experimental fibrosis (26). Our study aimed to determine whether increased TGF β signaling could play a role in the observed canonical Wnt signaling hyperactivation of tissue fibroblasts during SSc.

PATIENTS AND METHODS

Reagents. Adult human dermal fibroblasts were obtained from 5 patients with early dcSSc and 5 healthy controls and cultured (PromoCell) (see Supplementary Table 1, available on the *Arthritis & Rheumatology* web site at <http://onlinelibrary.wiley.com/doi/10.1002/art.40437/abstract>). Primary cells were immortalized using human telomerase reverse transcriptase (hTERT) to make healthy control hTERT and SSc hTERT. Briefly, hTERT

pBABE (Neo) (a kind gift from Prof. M. A. Knowles, University of Leeds, Leeds, UK) was transfected into Phoenix amphotropic retroviral packaging cells using *TransIT-293* (Mirus Bio), and virus supernatant containing 8 μ g/ml Polybrene was added to primary cells and selected with 1,000 μ g/ml G418 48 hours after transduction. Cells were cultured in Dulbecco's modified Eagle's medium (DMEM; Sigma-Aldrich) containing 10% fetal calf serum (FCS; Biosera) and incubated at 37°C under 5% CO₂. All experiments conducted with hTERT fibroblasts were validated with primary (not immortalized) fibroblasts. Primary fibroblasts were used between passages 2 and 5. Starvation was performed with 0.5% serum DMEM, and stimulations were performed with recombinant human TGF β (5 ng/ml; Sigma-Aldrich) or recombinant human Wnt-3a (100 ng/ml; R&D Systems). The messenger RNA (mRNA) decay rate was investigated using actinomycin D (5 μ g/ml; Sigma-Aldrich). Axin stabilization was achieved using XAV-939 Tankyrase 1/2 Inhibitor (1 μ M; Calbiochem), and TGF β signaling was inhibited using SD-208 T β RI Kinase Inhibitor (1 μ M; Sigma-Aldrich).

Study approval. Informed consent was obtained from all patients, and studies were granted approval by the Leeds Teaching Hospitals NHS Trust Medical Ethics Committee (Leeds Teaching Hospital Research Ethics Committee approval no. 10/H1306/88). All scleroderma patients fulfilled the American College of Rheumatology/European League Against Rheumatism 2013 classification criteria for SSc (27) and were classified as having dcSSc according to the LeRoy and Medsger criteria (28).

T β RIIAk-fib-transgenic mice. The generation of T β RIIAk-fib-transgenic mice has been described previously (8). Constitutive TGF β signaling is mediated by fibroblast-specific expression of kinase-deficient TGF β RII. Dermal and lung tissues were obtained from 6–8-week-old age-matched transgenic and wild-type (WT) littermates, and each experiment was performed on at least 5 mice for each condition. Animals were housed in a clean conventional colony, with access to food and water ad libitum. Strict adherence to institutional guidelines was practiced, and full local ethics committee and Home Office approvals were obtained.

Histology studies. Formalin-fixed skin specimens were embedded in paraffin and sections were cut at 5 μ m. Skin fibrosis was evaluated by measuring the thickness between the dermal-epidermal boundary and the dermal-subcutaneous fat boundary and further evaluated using Masson's trichrome blue staining. Antigen retrieval was performed using 10 mM sodium citrate (pH 6.0), and sections were stained with anti-Axin-2 antibody (Sigma-Aldrich) followed by staining with StreptAB-Complex/HRP (DakoCytomation) and visualized with 3,3'-diaminobenzidine tetrahydrochloride (Vector). Microscopic analysis was performed using an Olympus BX50 with MicroFire (Optronics), and images were captured at 20 \times magnification using Stereo Investigator software (MBF Bioscience).

Cell lysate preparation. Cells were lysed in radioimmunoprecipitation assay buffer (Sigma-Aldrich) supplemented with complete protease and phosphatase inhibitor cocktails (Roche). Whole cell lysate protein concentration was then quantified using a bicinchoninic acid (BCA) colorimetric protein assay kit in accordance with the protocol of the manufacturer (Thermo Fisher).

Western blotting. Cell lysates were electrophoresed on a 4–12% Bis-Tris gradient gel using a NuPAGE gel system and transferred onto an Immobilon-P PVDF membrane (EMD Millipore). The membranes were blocked with 5% milk in Tris buffered saline–0.1% Tween 20 and incubated with anti-Axin-2 (New England Biolabs), anti-Axin-1 (New England Biolabs), and

anti- α -smooth muscle actin (anti- α -SMA; Abcam). Incubation with the appropriate horseradish peroxidase-conjugated secondary antibody allowed for chemiluminescence detection using enhanced chemiluminescence reagent (GE Healthcare). Equal loading of proteins was achieved using a BCA protein assay kit and confirmed by visualization of GAPDH (Abcam).

Quantitative reverse transcriptase-polymerase chain reaction (qRT-PCR). Total cellular RNA extraction and purification were performed using an RNeasy kit (Qiagen), and cDNA was prepared using a SuperScript II first-strand cDNA synthesis kit (Life Technologies) in accordance with manufacturer protocols. Gene expression was quantified by SYBR Green RT-PCR on an ABI Prism 7700 Sequence Detection System (Life Technologies).

The following primers were designed: for Axin-2, 5'-CGGGAGC-CACACCCTTC-3' (forward) and 5'-TGGACACCTGCCAGTT-TCTTT-3' (reverse); for 18S ribosomal RNA (rRNA), 5'-GTAA-CCCCTTGAACCCCAT-3' (forward) and 5'-CCAATAATCGG-TAGTAGCG-3' (reverse); for α -SMA, 5'-TGTATGTGGCTATC-CAGGCG-3' (forward) and 5'-AGAGTCCAGCAGATGC-CAG-3' (reverse); for Dkk-1, 5'-GACTGTGCCTCAGGATT-GTGT-3' (forward) and 5'-CAGATCTTGGACCAGAAGTGT-CT-3' (reverse). Analysis of the Axin-2 primary transcript used primers spanning intron-exon junctions specifically limiting amplification to unprocessed RNA primary transcript-Axin-2 (5'-TGATGCGCTGACGGATGATT-3' [forward] and 5'-ATCCA-CTCCCAAGCAAGCC-3' [reverse]). For mouse Axin-2 expression,

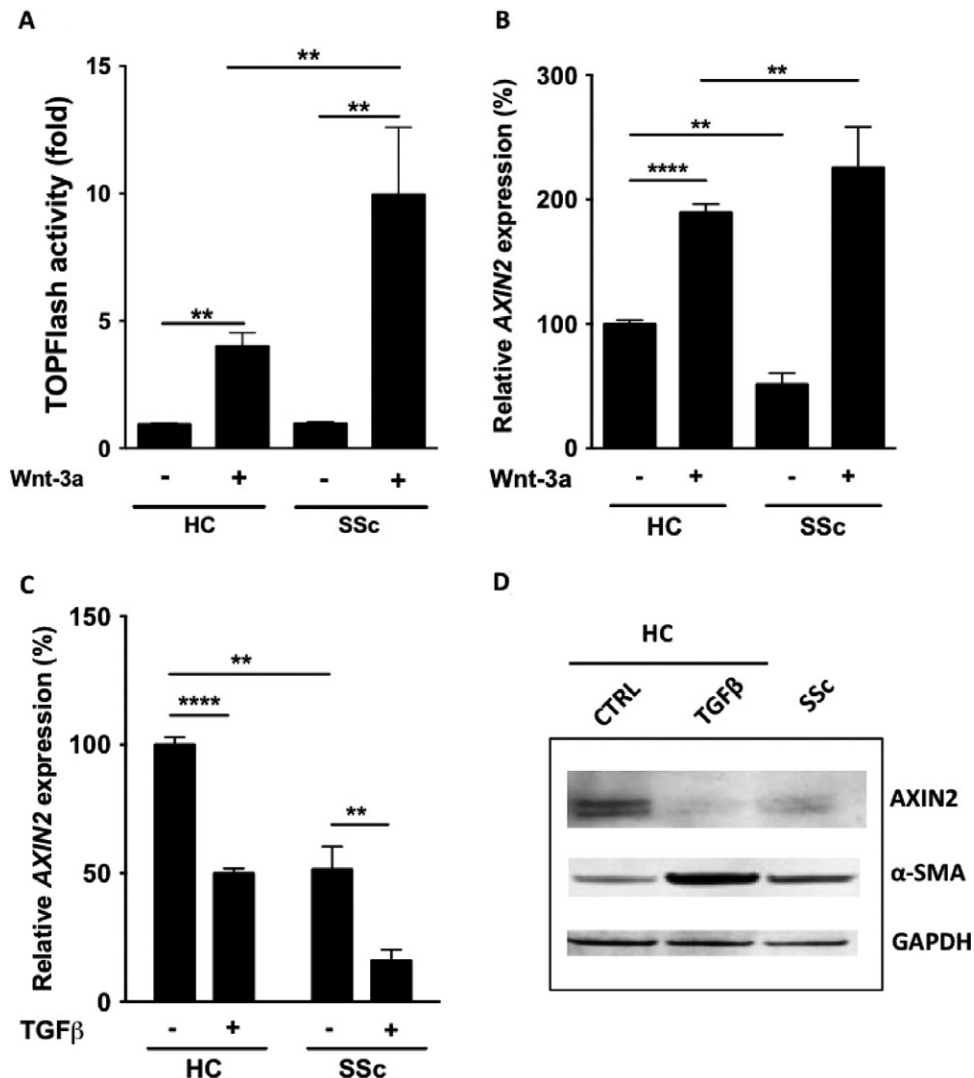


Figure 1. Increased response to canonical Wnt signaling and decreased expression of axis inhibition protein 2 (Axin-2) in fibroblasts from patients with systemic sclerosis (SSc). **A**, β -catenin-dependent TOPflash (T cell factor/lymphoid enhancer factor) reporter activity in healthy control (HC) and SSc dermal fibroblasts 24 hours after treatment with 100 ng/ml recombinant human Wnt-3a. **B** and **C**, Expression of mRNA for the canonical Wnt target Axin-2 in healthy control and SSc dermal fibroblasts 24 hours after treatment with 100 ng/ml recombinant human Wnt-3a (**B**) or 5 ng/ml transforming growth factor β (TGF β) (**C**), quantified by quantitative reverse transcriptase-polymerase chain reaction. Data were normalized to 18S ribosomal RNA, and values displayed are relative to those in untreated healthy controls. **D**, Axin-2 protein expression determined by Western blot analysis under the same conditions as in **C**. Values are the mean \pm SEM ($n = 5$ experiments). ** = $P < 0.01$; **** = $P < 0.001$ by Mann-Whitney U test. α -SMA = α -smooth muscle actin.

we used 5'-AGCCTAAAGGTCTTATGTGG-3' (forward), 5'-ATGGAATCGTCGGTCAGT-3' (reverse), and the 18S rRNA primers shown above. Amplifications were analyzed with SDS software, version 2.3 (Life Technologies) and normalized to 18S rRNA using the $\Delta\Delta C_t$ method.

TOPflash reporter assay. The TOPflash/FOPflash luciferase reporter system (a kind gift from Prof. Randall Moon, University of Washington, Seattle) measured β -catenin-driven TCF/LEF transcriptional activation. Fibroblasts were transfected with the TOPflash construct at a concentration of 1 μ g/ml per well in a 12-well plate using Lipofectamine 2000 transfection reagent (Life Technologies). For transfection efficiency normalization, cells were cotransfected with a pCMV-*Renilla* luciferase vector at a concentration of 100 ng/ml. Transfection complexes were removed after 2 hours, and cells were stimulated with Wnt-3a in DMEM/0.5% FCS for 24 hours. Cell lysates were prepared, and luciferase activity was evaluated using a dual luciferase reporter system in accordance with the protocol of the manufacturer (Promega). Firefly luciferase activity was normalized to *Renilla* luciferase activity and expressed as the relative fold change.

Small interfering RNA (siRNA)-mediated gene silencing. Cells were seeded to reach a confluence of 70% on the day of transfection in DMEM/10% FCS. On the day of transfection, cell medium was changed to DMEM/5% FCS. Silencer Select, predesigned, nontargeting (scrambled) siRNA (AM4611), Axin-2 siRNA (S15818), and tristetraprolin 1 (TTP-1) siRNA (s14978) (Life Technologies) were transfected using N-TER transfection reagent (Sigma-Aldrich). Transfection complexes were added to fibroblasts at a final siRNA concentration of 10 nM and removed after 24 hours. Gene silencing was monitored for 24–96 hours posttransfection at the mRNA and protein levels.

Statistical analysis. Statistical analyses were performed using the nonparametric Mann-Whitney U test for unpaired samples. Experimental data are presented as the mean \pm SEM. *P* values less than or equal to 0.05 were considered significant. Statistical analysis was performed using GraphPad Prism software, version 5.0.

RESULTS

Increased canonical Wnt signaling responsiveness displayed by SSc fibroblasts. To measure the activation of the canonical Wnt signaling pathway in explanted dermal fibroblasts from SSc patients and healthy controls, β -catenin-mediated TCF/LEF transcription was quantified by TOPflash reporter activity. Compared to healthy control fibroblasts, no increase in basal level TOPflash activity was observed in SSc fibroblasts. However, following 24 hours of treatment with canonical Wnt-3a ligand, SSc fibroblasts displayed a 9.9-fold increase in reporter activity compared to a 4.8-fold increase observed in healthy control fibroblasts ($P < 0.01$) (Figure 1A). Consistent with these findings, Wnt-3a induced expression of mRNA for Axin-2 5.0-fold in SSc fibroblasts relative to basal levels, compared to a 1.8-fold increase in healthy control fibroblasts ($P < 0.001$) (Figure 1B).

Interestingly, we found that basal expression of mRNA for Axin-2 was reduced by 52% in SSc fibroblasts

(Figure 1B). Since Axin-2 plays an essential role in regulating the activity of the Wnt signaling pathway, we set out to evaluate the regulatory effects of TGF β on expression of mRNA for Axin-2. Stimulation of healthy control fibroblasts with TGF β for 24 hours reduced expression of mRNA for Axin-2 to 49% at 24 hours ($P < 0.001$), which was analogous to the basal levels of expression observed in SSc fibroblasts (i.e., 52% of basal levels in healthy control fibroblasts) (Figure 1C). Additionally, TGF β treatment of SSc fibroblasts further reduced expression of mRNA for Axin-2 to 20% of basal levels in healthy control fibroblasts ($P < 0.01$) (Figure 1C). Consistently, Axin-2 protein expression in healthy control fibroblasts treated with TGF β was comparable to the level observed in SSc fibroblasts (Figure 1D).

Constitutive TGF β activation leads to tissue fibrosis and reduced Axin-2 expression in T β RII Δ k-fib-transgenic mice. The T β RII Δ k-fib-transgenic mouse model of SSc was used to validate the effects of TGF β signaling on Axin-2 expression in vivo. Consistent with reported data, T β RII Δ k-fib-transgenic mice developed a significant dermal fibrosis characterized by increased dermal thickness, collagen deposition, and loss of subcutaneous fat compared to WT controls (8,29) (Figure 2A). Immunohistochemistry studies determined that dermal tissue from these mice had an overall reduction in Axin-2 expression (Figures 2B and C), which was evident in both the epidermal and dermal compartments. Accordingly, in transgenic mouse skin, expression of mRNA for Axin-2 was reduced by 65% compared to that in WT control mouse skin ($P < 0.05$) (see Supplementary Figure 1A, <http://onlinelibrary.wiley.com/doi/10.1002/art.40437/abstract>). Furthermore, Axin-2 protein expression was also reduced in lung tissue from transgenic mice, particularly in areas where the normal architecture was lost (Figure 2D).

TGF β priming of fibroblasts reproduces the increased canonical Wnt signaling amplitude observed in SSc fibroblasts through Axin-2 down-regulation. To determine whether the TGF β -mediated decrease in Axin-2 expression could be responsible for the increased sensitivity of fibroblasts to canonical Wnt ligands, we performed 24-hour sequential stimulation experiments. TGF β -primed healthy control fibroblasts showed a 9.8-fold increase in TOPflash activation in response to Wnt-3a, compared to the 4.8-fold increase in cells not previously treated with TGF β ($P < 0.001$) (Figure 3A). The increased response to Wnt was observable as early as 2 hours following TGF β stimulation and persisted for up to 72 hours (see Supplementary Figure 1B, <http://onlinelibrary.wiley.com/doi/10.1002/art.40437/abstract>). Importantly, fibroblasts treated with TGF β alone did not show any increase of TOPflash activity (Figure 3A).

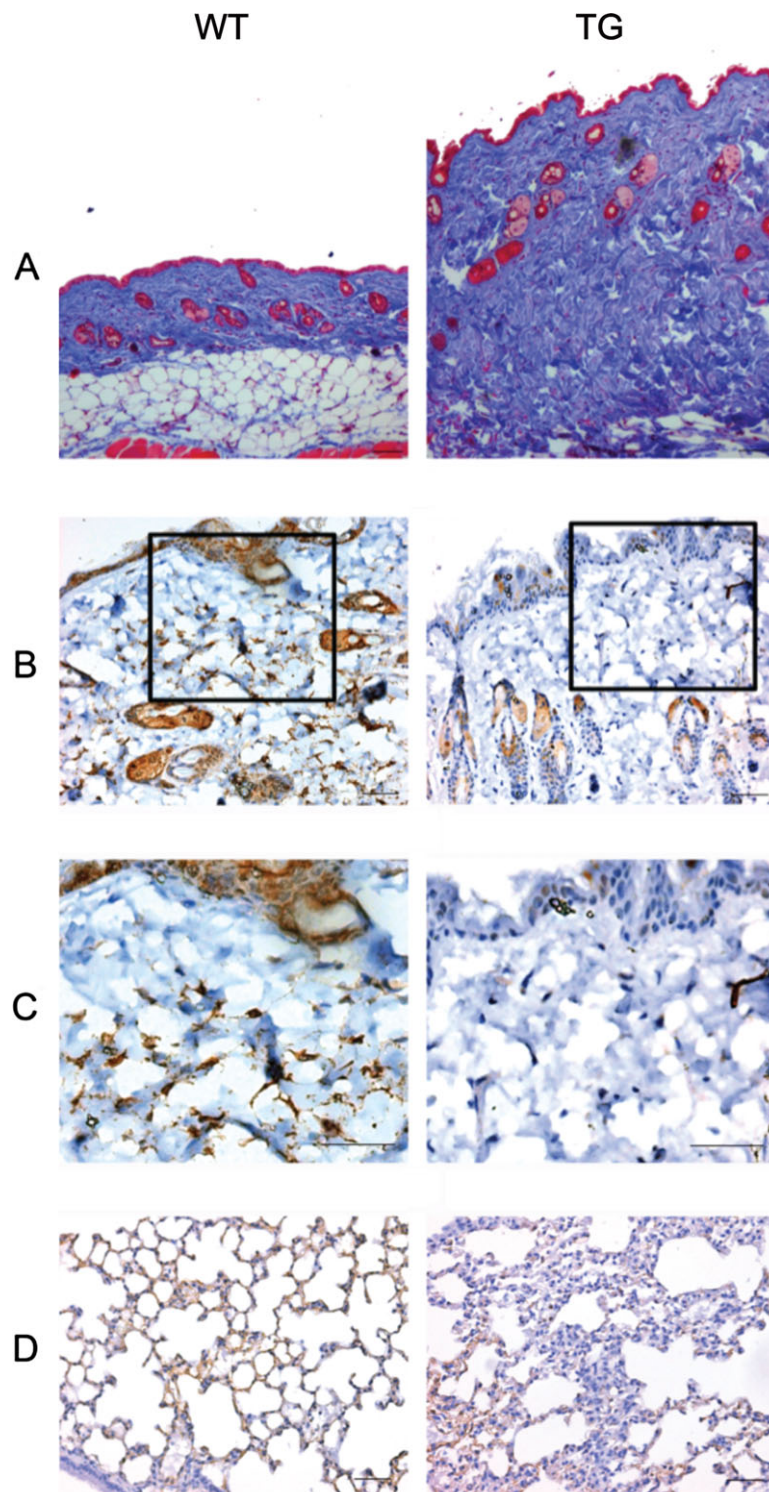


Figure 2. Constitutive TGF β activation leads to tissue fibrosis and reduced Axin-2 expression in mice that express a kinase-deficient TGF β receptor type II specifically on fibroblasts (T β RII Δ k-fib-transgenic [TG] mice; a model of SSc). **A**, Evaluation of dermal fibrosis in age-matched wild-type (WT) and T β RII Δ k-fib-transgenic mice by Masson's trichrome staining (blue). **B–D**, Immunohistochemistry analysis for Axin-2 expression (brown) in skin sections (**B** and **C**) and lung sections (**D**). Boxed areas in **B** are shown at higher magnification in **C**. Sections stained in **B–D** are matched to those from mice in **A**. No staining was detected with an isotype control antibody (results not shown). Bars = 100 μ m. Images are representative of 5 independent experiments. See Figure 1 for other definitions.

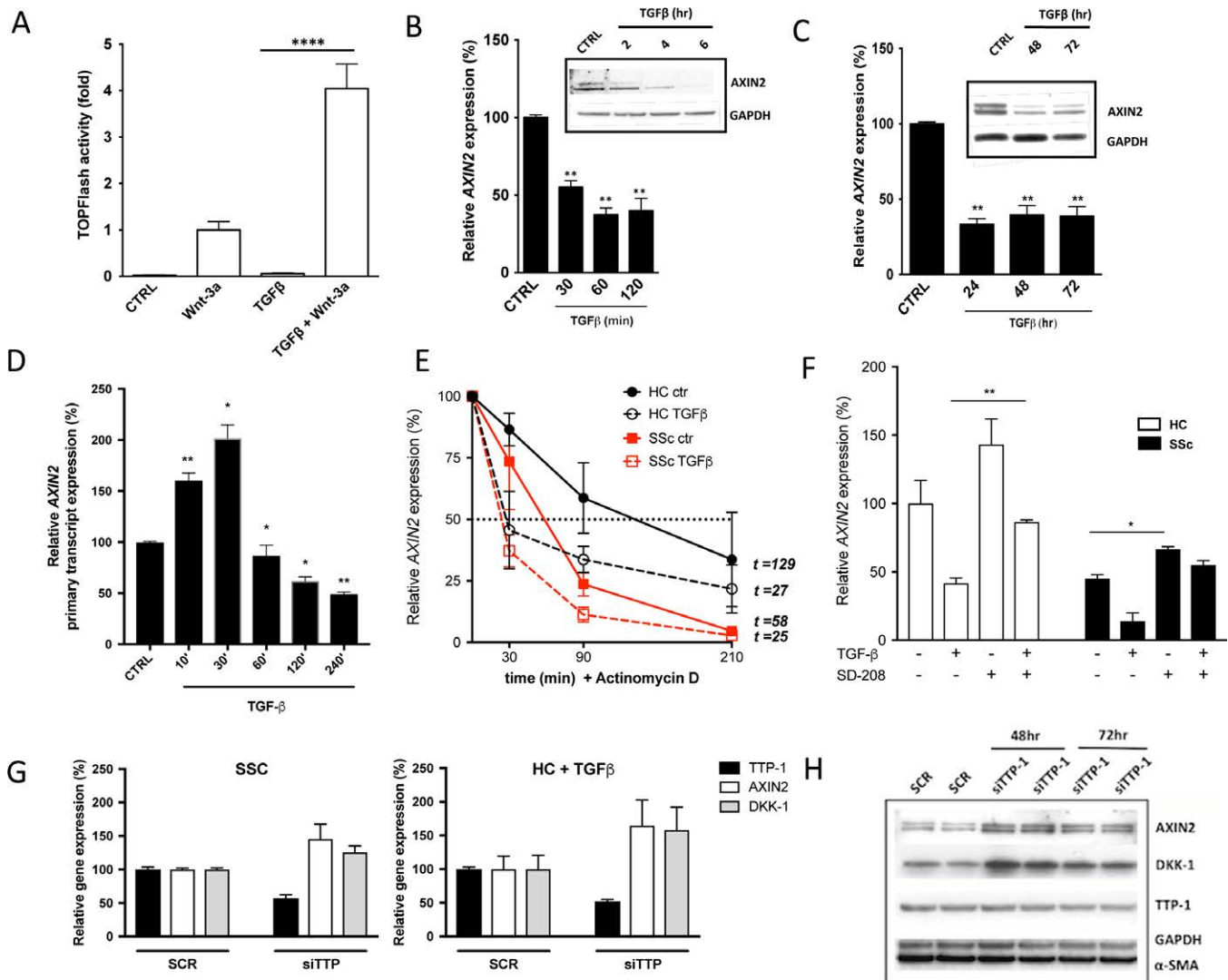


Figure 3. TGFβ priming of fibroblasts reproduces the increased canonical Wnt signaling amplitude observed in SSc fibroblasts through posttranscriptional regulation of Axin-2 expression. **A**, Results of assay for TOPflash activity in healthy control fibroblasts incubated in media alone or primed for 24 hours with 5 ng/ml TGFβ prior to sequential Wnt-3a treatment. **B** and **C**, Kinetic analysis of the effect of TGFβ treatment on expression of mRNA for Axin-2 or Axin-2 protein, for shorter time periods (**B**) and longer time periods (**C**), determined by quantitative reverse transcriptase–polymerase chain reaction (qRT-PCR) and Western blot analysis. **D**, Axin-2 primary transcript expression, using primers spanning an intron–exon boundary, determined by qRT-PCR. **E**, Analysis of Axin-2 mRNA stability in healthy control and SSc fibroblasts following treatment with TGFβ and 5 μg/ml of the transcriptional inhibitor actinomycin D, quantified by qRT-PCR and compared to control. Time points indicate half-life of mRNA for Axin-2. **F**, Effect of 48-hour 1 μM SD-208-mediated blockade of TGFβ receptor type I on expression of mRNA for Axin-2 in healthy control and SSc fibroblasts, determined by qRT-PCR. All data are shown relative to healthy control fibroblasts with no stimulation (100%). **G**, Effect of knockdown of tristetrin-1 (TTP-1) by small interfering RNA (siRNA) specific for TTP-1 (siTTP) on TGFβ-mediated expression of mRNA for Axin-2 and Dkk-1 in healthy control fibroblasts (with TGFβ) and SSc fibroblasts, determined by qRT-PCR. **H**, Effect of TTP-1 knockdown by TTP-1-specific siRNA (siTTP-1) on TGFβ-mediated expression of Axin-2, Dkk-1, and α-SMA protein in healthy control fibroblasts (with TGFβ), quantified by Western blot analysis. Values are the mean ± SEM (n = 3–8 experiments). * = $P < 0.05$; ** = $P < 0.01$; **** = $P < 0.001$ by Mann-Whitney U test. SCR = scrambled (see Figure 1 for other definitions). Color figure can be viewed in the online issue, which is available at <http://onlinelibrary.wiley.com/doi/10.1002/art.40437/abstract>.

Next, we set out to determine the mechanism by which TGFβ regulates Axin-2 expression in fibroblasts. TGFβ induced a significant and time-dependent reduction in expression of mRNA for Axin-2 that was

observable within 30 minutes, and this persisted for up to 72 hours ($P < 0.01$) (Figures 3B and C). Similarly, Axin-2 protein expression was decreased within 2 hours, and the decrease continued up to 72 hours (Figures 3B and C). In

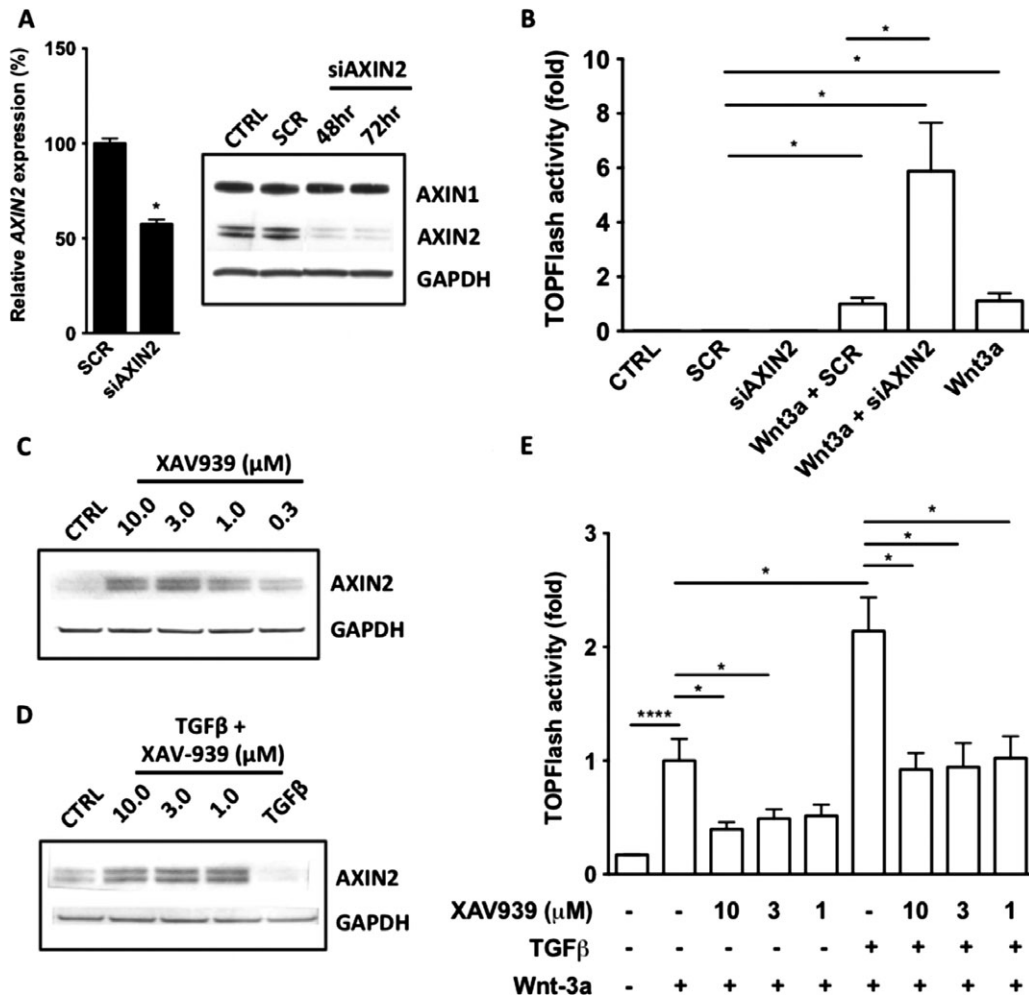


Figure 4. Silencing of Axin-2 expression is sufficient to reproduce the canonical Wnt signaling amplitude observed in Ssc and TGF β -primed fibroblasts. **A**, Healthy control fibroblasts were transfected with scrambled (SCR) small interfering RNA (siRNA) or Axin-2-specific siRNA (siAXIN2). Expression of Axin-2 mRNA at 24 hours and expression of Axin-2 protein at 48 and 72 hours were quantified by quantitative reverse transcriptase-polymerase chain reaction and Western blot analysis, respectively. **B**, Healthy control fibroblasts were transfected with the TOPflash reporter 24 hours prior to transfection with scrambled siRNA or Axin-2-specific siRNA for 48 hours. Subsequently, cells were either left untreated or were treated with Wnt-3a for a further 24 hours prior to determination of reporter activity. TOPflash activity of Wnt-3a-stimulated scrambled siRNA-transfected cells was set to 1. **C**, Healthy control fibroblasts were treated with 1 μ M of Axin-stabilizing XAV-939 for 24 hours, and expression of Axin-2 was determined by Western blot analysis. **D**, One hour after XAV-939 treatment, XAV-939-mediated Axin-2 stability in the presence of TGF β for 24 hours was validated by Western blot analysis. **E**, Fibroblasts were transfected with the TOPflash reporter for 24 hours, and XAV-939 was added 1 hour prior to either no treatment or treatment with TGF β for 24 hours. Fibroblasts were then treated for a further 24 hours with Wnt-3a, and luciferase reporter activity was assayed. Values are the mean \pm SEM ($n = 4-5$ experiments). * = $P < 0.05$; **** = $P < 0.001$ by Mann-Whitney U test. See Figure 1 for other definitions.

contrast, TGF β treatment had a modest effect on expression of mRNA for Axin-1 and, unlike the case with Axin-2, protein expression remained unchanged (see Supplementary Figure 1C, <http://onlinelibrary.wiley.com/doi/10.1002/art.40437/abstract>).

To determine whether TGF β could regulate Axin-2 at the transcriptional level, expression of the Axin-2 primary transcript was evaluated. TGF β induced an increase in primary transcript expression at 10 minutes and 30 minutes by 166.9% ($P < 0.01$) and 199.6% ($P < 0.05$),

respectively (Figure 3D). At time points ≥ 60 minutes, TGF β reduced the expression of the primary transcript to a maximum of 49.4% ($P < 0.05$) (Figure 3D). As reduction of primary transcript expression occurred at ≥ 60 minutes, actinomycin D was used to determine the posttranscriptional effects of TGF β on the mature Axin-2 transcript. In the presence of TGF β , the half-life of mRNA for Axin-2 in healthy control fibroblasts decreased from 129 minutes to 27 minutes over a time period of 30–210 minutes, which is equal to a 4.7-fold ($P < 0.01$)

increase in the rate of mRNA decay (Figure 3E). Under the same experimental conditions, the basal half-life of mRNA for Axin-2 in SSc fibroblasts was 58 minutes compared to 129 minutes in healthy control fibroblasts (2.2-fold faster decay; $P < 0.05$), which was further reduced to 25 minutes by TGF β stimulation (Figure 3E).

To determine whether these effects were a direct consequence of TGF β R activation, SD-208 T β RI Kinase Inhibitor was used to selectively antagonize TGF β signaling. In healthy control fibroblasts, TGF β -mediated reduction of mRNA for Axin-2 by 64% ($P < 0.01$) was prevented in the presence of SD-208, as expected (Figure 3F). The same effects were observed at the protein level (see Supplementary Figure 2A, <http://onlinelibrary.wiley.com/doi/10.1002/art.40437/abstract>) and on down-regulation of mRNA for Dkk-1 and up-regulation of mRNA for α -SMA, as expected (see Supplementary Figure 2B). More interestingly, a similar pattern was also seen in SSc fibroblasts (Figure 3F). Although levels of mRNA for Axin-2 in SD-208-treated SSc fibroblasts were not fully restored to levels in untreated healthy control fibroblasts, we observed a 50% increase in basal levels of mRNA for Axin-2 ($P < 0.05$) (Figure 3F), which confirms that endogenous activation of TGF β RI kinase is at least in part responsible for the decreased basal levels of mRNA for Axin-2 in SSc fibroblasts.

Bioinformatic analysis revealed the presence of several AU-rich elements (AREs) located in the 3'-untranslated region (3'-UTR) of the Axin-2 transcript (see Supplementary Figure 2C, <http://onlinelibrary.wiley.com/doi/10.1002/art.40437/abstract>). Recruitment of TTP-1 to ARE-containing transcripts leads to destabilization and degradation (30–34). Concordantly, siRNA-mediated silencing of mRNA for TTP-1 in SSc fibroblasts increased expression of mRNA for Axin-2 and Dkk-1 relative to non-targeting (scrambled) siRNA by 151% ($P < 0.05$) and 142% ($P < 0.05$), respectively, and in healthy control fibroblasts treated with TGF β by 162.1% ($P < 0.01$) and 161.5% ($P < 0.01$), respectively (Figure 3G). Consistent with these data, Axin-2 and Dkk-1 protein expression was substantially up-regulated by TTP-1 knockdown in healthy control fibroblasts treated with TGF β at 48 and 72 hours (Figure 3H).

Axin-2 expression critically regulates canonical Wnt signaling hyperactivation in TGF β -primed fibroblasts. TGF β priming reproduced the increased canonical Wnt signaling response in healthy control fibroblasts at levels equivalent to those in SSc fibroblasts. Since SSc fibroblasts had a reduction in Axin-2, we sought to determine whether the TGF β -mediated down-regulation of Axin-2 was sufficient to explain this increased activation.

Small interfering RNA-mediated silencing of mRNA for Axin-2 reduced its expression to 50%, and similar results were observed at the protein level, at 48

and 72 hours, compared to expression in fibroblasts transfected with scrambled siRNA (Figure 4A). Wnt-3a stimulation of healthy control fibroblasts transfected with Axin-2 siRNA showed an increase in TOPflash activity, which was 5.8-fold higher than TOPflash activity in Wnt-3a-stimulated cells transfected with scrambled siRNA ($P < 0.05$) (Figure 4B).

Following a reciprocal approach, Axin-2 bioavailability was increased by treating fibroblasts with XAV-939, a small-molecule inhibitor known to stabilize Axin by inhibiting its proteasomal degradation (35). As expected, TGF β -treated fibroblasts treated with XAV-939 stabilized Axin-2 in a dose-dependent manner and also prevented TGF β -induced down-regulation of Axin-2 following 48-hour stimulation (Figures 4C and D). Subsequently, we determined the effects of Axin stabilization on canonical signaling activity. Healthy control fibroblasts treated with Wnt-3a for 24 hours were used as positive controls of TOPflash activity (Figure 4E). Cotreatment with incremental concentrations of XAV-939 led to a dose-dependent suppression of Wnt-3a-induced TOPflash activation (Figure 4E). Similarly, in TGF β -primed fibroblasts, the Wnt-3a-induced 2.1-fold hyperactivation of TOPflash activity was completely suppressed in the presence of XAV-939 (Figure 4E).

DISCUSSION

TGF β has an established role in the fibroblast-mediated pathogenesis of tissue fibrosis. Recently, several studies have shown significantly increased Wnt signaling activation in fibroblasts resident in fibrotic tissues, suggesting that the Wnt pathway could be as important as that of TGF β in the pathogenic process (10,11). The current study has identified a new mechanism by which TGF β cross-talk mediates hyperactivation of the canonical Wnt/ β -catenin signaling response in fibroblasts without inducing a direct stimulatory effect.

Although explanted SSc fibroblasts do not display an autonomous increase in canonical Wnt signaling activation, a significant increase in response to canonical agonist treatment is observed when compared to healthy control fibroblasts. This suggests that canonical signaling hyperactivation in vivo is likely to be influenced by the secretion of Wnt agonists from other cell types present in the local microenvironment. Several in vivo studies support the role of differential Wnt ligand expression in the increased activation of the canonical Wnt signaling pathway in SSc and models of experimental fibrosis (10,11,36). The current study extends these previous observations and indicates the importance of TGF β -responsive Axin-2 expression in the regulation of canonical Wnt signaling pathway hyperactivation.

Consistently, SSc fibroblasts also display a decrease in the basal expression of Axin-2, a critical scaffold protein important in the formation and function of the β -catenin destruction complex (18,19). In support of the relationship between TGF β signaling and Axin-2 expression, T β RII Δ k-fib-transgenic mice, which have constitutively active and fibroblast-specific TGF β signaling, showed reduced Axin-2 expression in both fibrotic skin and lung tissue. Indeed, suboptimal assembly of the β -catenin destruction complex, through down-regulation of the Axin-2 scaffold protein, could explain the increased nuclear β -catenin staining observed in tissue expression studies as well as the amplitude of canonical Wnt signaling evident in SSc fibroblasts (10,11). Complementary to this hypothesis, TGF β induced a quantitatively similar reduction in Axin-2 expression in healthy control fibroblasts and conferred the enhanced canonical Wnt signaling amplitude observed in SSc fibroblasts. Gene profiling of TGF β -responsive genes in dcSSc dermal fibroblasts, which are limited to an intrinsic SSc gene signature described by Milano et al, showed a significant down-regulation of Axin-2 and Dkk-1, 2 important negative regulators of Wnt signaling, despite the overall absence of a distinct Wnt signaling profile (7,36,37).

Taken together, these data suggest that a TGF β -primed microenvironment can lead to the increased canonical Wnt/ β -catenin signaling in dermal fibroblasts observed during fibrosis, through its associated repression of key mediators regulating the Wnt signaling pathway. Interestingly, TGF β did not directly induce canonical Wnt activation in dermal fibroblasts, and therefore the increased canonical Wnt signaling response in vivo is likely to be through secretion of Wnt agonists by other cell types present in the local microenvironment rather than through an autocrine mechanism. These data offer a mechanistic explanation for both our observations on Axin-2 and the data already reported by Akhmetshina et al, which show a decrease in Dkk-1 expression following stimulation with TGF β (26). In this sense, TGF β -induced degradation of mRNA for Axin-2 and Dkk-1 can work synergistically in priming and potentiating Wnt signaling acting at the extracellular level by reduction of a Wnt antagonist (reduction in Dkk-1) and at the intracellular level by decreased activity of GSK complex inhibition.

In this context, our observation of decreased expression of Axin-2 in T β RII Δ k-fib-transgenic mice is rather indicative of a lack of direct Wnt activation in this model, and it suggests that the observed increase in Wnt signaling in scleroderma remains dependent on the presence of Wnt ligands. This is also supported by our in vitro data showing a lack of TOPflash activity in cells treated only with TGF β .

Indeed, Wei et al have observed an increase in Wnt-10a ligand in SSc skin and a TGF β -independent profibrotic signature in skin from transgenic mice with overexpression of Wnt-10a (38). Further studies dissecting the functional effects of physiologic or aberrant Wnt signaling in this model are warranted to elucidate this cross-talk further.

Mechanistically, the TGF β -induced down-regulation of Axin-2 in dermal fibroblasts was mediated by an increase in the rate of decay of mRNA for Axin-2, while analysis of the primary transcript indicated involvement in transcriptional repression at later time points. Interestingly, TGF β -mediated repression of Axin-2 in chondrocytes was not similarly affected until 24 hours posttreatment; thus, the regulation of Axin-2 by TGF β appears to be context dependent (25).

The degradation of the majority of eukaryotic mRNAs occurs through poly(A) tail shortening and is mediated by the recruitment of the RNA-degrading exosome complex (30). TTP-1, a TGF β -responsive ARE-binding protein, can facilitate the recruitment of the exosome complex and enhance mRNA decay in transcripts containing 3'-UTR ARE motifs, including *TNF*, *c-myc*, and *CCND1* (30–34). Consistent with the presence of ARE motifs located within the 3'-UTR of the Axin-2 gene, silencing of TTP-1 expression led to a significant up-regulation of both Axin-2 mRNA and protein expression. Likewise, expression of the gene for Dkk-1, which also harbors 3'-UTR ARE motifs, was similarly increased. These data extend findings from a previous study linking canonical signaling activation to a reduction in a secreted Wnt signaling regulator, Dkk-1, driven by TGF β signaling in lung fibroblasts and the Ad-T β RI model of experimental fibrosis (39). Taken together, these data suggest that ARE-mediated decay of mRNA for Axin-2 and Dkk-1, 2 regulators of canonical Wnt signaling, might be a common mechanism by which TGF β positively regulates the amplitude of canonical Wnt signaling and contributes to the pathogenic fibrotic response of fibroblasts.

We confirmed our hypothesis with gain- and loss-of-function experiments, in which depletion of Axin-2 in healthy control fibroblasts increased canonical Wnt signaling and reproduced the SSc fibroblast phenotype. Reciprocally, inhibition of Axin protein degradation by XAV-939 treatment completely ablated the canonical Wnt signaling hyperactivation conferred by TGF β priming. In vivo, this has proved effective in protecting against experimental fibrosis (39).

Overall, our study highlights the importance of TGF β cross-talk in regulating mediators of the canonical Wnt signaling pathway and shows that it is possible to reproduce the hyperresponsiveness to Wnt stimulation characteristic of SSc fibroblasts through depletion of Axin-2. This suggests that the increased canonical Wnt/

β -catenin signaling in fibroblasts, observed during fibrosis, is a consequence of a TGF β -primed microenvironment. This novel mechanism extends our understanding of the processes involved in Wnt/ β -catenin-driven pathology and extends the rationale for developing TGF β -targeted treatment to the possibility of regulating the aberrant Wnt activation observed during fibrosis.

AUTHOR CONTRIBUTIONS

All authors were involved in drafting the article or revising it critically for important intellectual content, and all authors approved the final version to be published. Dr. Del Galdo had full access to all of the data in the study and takes responsibility for the integrity of the data and the accuracy of the data analysis.

Study conception and design. Gillespie, Ross, Corinaldesi, Esteves.

Acquisition of data. Gillespie, Ross, Corinaldesi, Del Galdo.

Analysis and interpretation of data. Gillespie, Ross, Corinaldesi, Derrett-Smith, McDermott, Doody, Denton, Emery, Del Galdo.

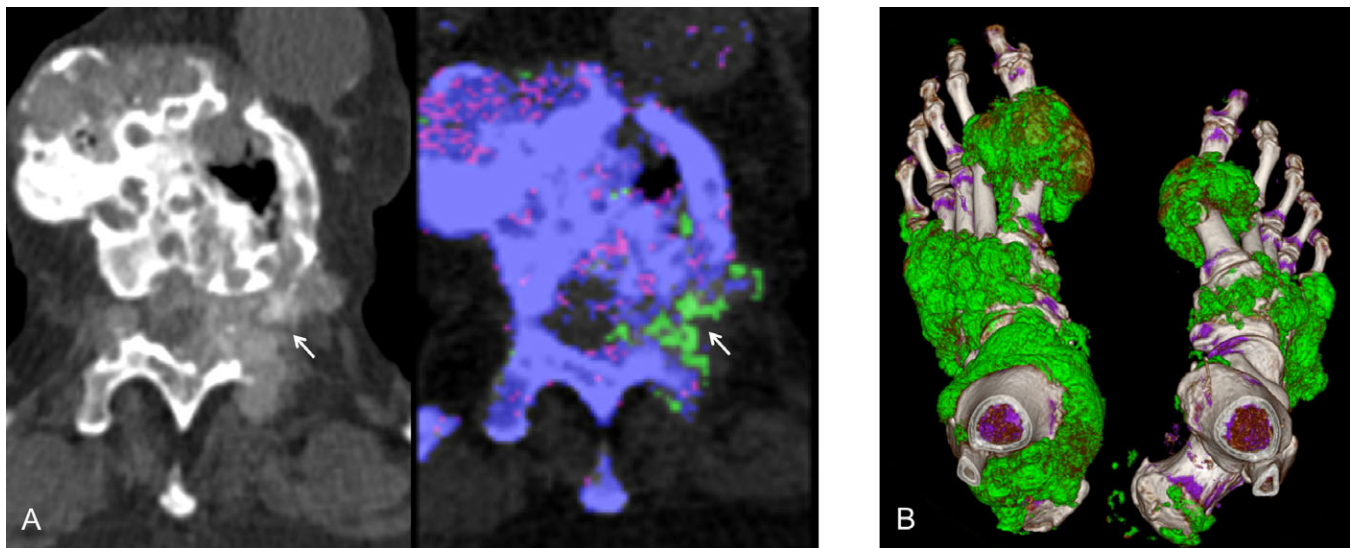
REFERENCES

- Lu P, Takai K, Weaver VM, Werb Z. Extracellular matrix degradation and remodeling in development and disease. *Cold Spring Harb Perspect Biol* 2011;3:a005058.
- Cox TR, Ertler JT. Remodeling and homeostasis of the extracellular matrix: implications for fibrotic diseases and cancer. *Dis Model Mech* 2011;4:165–78.
- Smith EA, LeRoy EC. A possible role for transforming growth factor- β in systemic sclerosis. *J Invest Dermatol* 1990;95:125S–7S.
- Leask A, Abraham DJ. TGF- β signalling and the fibrotic response. *FASEB J* 2004;18:816–27.
- Varga J, Pasche B. Transforming growth factor- β as a therapeutic target in systemic sclerosis. *Nat Rev Rheumatol* 2009;5:200–6.
- Sonnlyal S, Denton CP, Zheng B, Keene DR, He R, Adams HP, et al. Postnatal induction of transforming growth factor β signaling in fibroblasts of mice recapitulates clinical, histologic, and biochemical features of scleroderma. *Arthritis Rheum* 2007;56:334–44.
- Sargent JL, Milano A, Bhattacharyya S, Varga J, Connolly MK, Chang HY, et al. A TGF β -responsive gene signature is associated with a subset of diffuse scleroderma with increased disease severity. *J Invest Dermatol* 2009;130:694–705.
- Denton CP, Zheng B, Evans LA, Shi-wen X, Ong VH, Fisher I, et al. Fibroblast-specific expression of a kinase-deficient type II transforming growth factor β (TGF β) receptor leads to paradoxical activation of TGF β signalling pathways with fibrosis in transgenic mice. *J Biol Chem* 2003;278:25109–19.
- Hoyles RK, Khan K, Shiwen X, Howat SL, Lindahl GE, Leoni P, et al. Fibroblast-specific perturbation of transforming growth factor β signaling provides insight into potential pathogenic mechanisms of scleroderma-associated lung fibrosis: exaggerated response to alveolar epithelial injury in a novel mouse model [published erratum appears in *Arthritis Rheumatol* 2015;67:2741]. *Arthritis Rheum* 2008;58:1175–88.
- Wei J, Fang F, Lam AP, Sargent JL, Hamburg E, Hinchcliff ME, et al. Wnt/ β -catenin signaling is hyperactivated in systemic sclerosis and induces Smad-dependent fibrotic responses in mesenchymal cells. *Arthritis Rheum* 2012;64:2734–45.
- Beyer C, Schramm A, Akhmetshina A, Dees C, Kireva T, Gelse K, et al. β -catenin is a central mediator of pro-fibrotic Wnt signalling in systemic sclerosis. *Ann Rheum Dis* 2012;71:761–7.
- Chilosi M, Poletti V, Zamò A, Lestani M, Montagna L, Piccoli P, et al. Aberrant Wnt/ β -catenin pathway activation in idiopathic pulmonary fibrosis. *Am J Pathol* 2003;162:1495–502.
- Borok Z. Role for $\alpha 3$ integrin in EMT and pulmonary fibrosis. *J Clin Invest* 2009;119:7–10.
- Königshoff M, Kramer M, Balsara N, Wilhelm J, Amarie OV, Jahn A, et al. WNT1-inducible signalling protein-1 mediates pulmonary fibrosis in mice and is upregulated in humans with idiopathic pulmonary fibrosis. *J Clin Invest* 2009;119:772–87.
- Stamos JL, Weis WI. The β -catenin destruction complex. *Cold Spring Harb Perspect Biol* 2013;5:a007898.
- Moon RT, Kohn AD, De Ferrari GV, Kaykas A. WNT and β -catenin signalling: diseases and therapies. *Nat Rev Genet* 2004;5:691–701.
- Hart MJ, de los Santos R, Albert IN, Rubinfeld B, Polakis P. Downregulation of β -catenin by human Axin and its association with the APC tumor suppressor, β -catenin and GSK3 β . *Curr Biol* 1998;8:573–81.
- Liu C, Li Y, Semenov M, Han C, Baeg GH, Tan Y, et al. Control of β -catenin phosphorylation/degradation by a dual-kinase mechanism. *Cell* 2002;108:837–47.
- Chia IV, Costantini F. Mouse Axin and Axin2/conductin proteins are functionally equivalent in vivo. *Mol Cell Biol* 2005;25:4371–6.
- Jho E, Zhang T, Domon C, Joo CK, Freund JN, Costantini F. Wnt/ β -catenin/Tcf signalling induces the transcription of Axin2, a negative regulator of the signalling pathway. *Mol Cell Biol* 2002;22:1172–83.
- Leung JY, Kolligs FT, Wu R, Zhai Y, Kuick R, Hanash S, et al. Activation of AXIN2 expression by β -catenin-T cell factor: a feedback repressor pathway regulating Wnt signalling. *J Biol Chem* 2002;277:21657–65.
- Perry WL III, Vasicek TJ, Lee JJ, Rossi JM, Zeng L, Zhang T, et al. Phenotypic and molecular analysis of a transgenic insertional allele of the mouse fused locus. *Genetics* 1995;141:321–32.
- Behrens J, Jerchow BA, Würtele M, Grimm J, Asbrand C, Wirtz R, et al. Functional interaction of an axin homolog, conductin, with β -catenin, APC, and GSK3 β . *Science* 1998;280:596–9.
- Lammi L, Arte S, Somer M, Jarvinen H, Lahermo P, Thesleff I, et al. Mutations in AXIN2 cause familial tooth agenesis and predispose to colorectal cancer. *Am J Hum Genet* 2004;74:1043–50.
- Dao DY, Yang X, Chen D, Zuscik M, O'Keefe RJ. Axin1 and Axin2 are regulated by TGF- β and mediate cross-talk between TGF- β and Wnt signalling pathways. *Ann N Y Acad Sci* 2007;1116:82–99.
- Akhmetshina A, Palumbo K, Dees C, Bergmann C, Venalis P, Zerr P, et al. Activation of canonical Wnt signalling is required for TGF- β -mediated fibrosis. *Nat Commun* 2012;3:735.
- Van den Hoogen F, Khanna D, Fransen J, Johnson SR, Baron M, Tyndall A, et al. 2013 classification criteria for systemic sclerosis: an American College of Rheumatology/European League Against Rheumatism collaborative initiative. *Arthritis Rheum* 2013;65:2737–47.
- LeRoy EC, Medsger TA. Criteria for the classification of early systemic sclerosis. *J Rheumatol* 2001;28:1573–6.
- Derrett-Smith EC, Dooley A, Khan K, Shi-wen X, Abraham D, Denton CP. Systemic vasculopathy with altered vasoreactivity in a transgenic mouse model of scleroderma. *Arthritis Res Ther* 2010;12:R69.
- Houseley J, Tollervey D. The many pathways of RNA degradation. *Cell* 2009;136:763–76.
- Ogawa K, Chen F, Kim YJ, Chen Y. Transcriptional regulation of tristetrarolin by transforming growth factor- β in human T cells. *J Biol Chem* 2003;278:30373–81.
- Marderosian M, Sharma A, Funk AP, Vartanian R, Masri J, Jo OD, et al. Tristetraprolin regulates cyclin D1 and c-Myc mRNA stability in response to rapamycin in an Akt-dependent manner via p38 MAPK signalling. *Oncogene* 2006;25:6277–90.
- Kang S, Min A, Im SA, Song SH, Kim SG, Kim HA, et al. TGF- β suppresses COX-2 expression by tristetrarolin-mediated RNA destabilization in A549 human lung cancer cells. *Cancer Res Treat* 2014;47:101–9.
- Blanco FF, Sanduja S, Deane NG, Blackshear PJ, Dixon DA. Transforming growth factor regulates P-body formation through induction of the mRNA decay factor tristetrarolin. *Mol Cell Biol* 2014;34:180–95.

35. Huang SM, Mishina YM, Liu S, Cheung A, Stegmeier F, Michaud GA, et al. Tankyrase inhibition stabilizes axin and antagonizes Wnt signalling. *Nature* 2009;461:614–20.
36. Bayle J, Fitch J, Jacobsen K, Kumar R, Lafyatis R, Lemaire R. Increased expression of Wnt2 and SFRP4 in Tsk mouse skin: role of Wnt signalling in altered dermal fibrillin deposition and systemic sclerosis. *J Invest Dermatol* 2008;128:871–81.
37. Milano A, Pendergrass SA, Sargent JL, George LK, McCalmont TH, Connolly MK, et al. Molecular subsets in the gene expression signatures of scleroderma skin. *PLoS One* 2008;3:e2696.
38. Wei J, Melichian D, Komura K, Hinchcliff M, Lam AP, Lafyatis R, et al. Canonical Wnt signaling induces skin fibrosis and subcutaneous lipodystrophy: a novel mouse model for scleroderma? *Arthritis Rheum* 2011;63:1707–17.
39. Beyer C, Reichert H, Akan H, Mallano T, Schramm A, Dees C, et al. Blockade of canonical Wnt signalling ameliorates experimental dermal fibrosis. *Ann Rheum Dis* 2013;72:1255–8.

DOI: 10.1002/art.40434

Clinical Images: Paraparesis revealing tophaceous gout



The patient, a 77-year-old man with a history of intermittent inflammatory arthritis of the feet, was hospitalized for a paraparesis that had progressed for 6 months, resulting in severe gait impairment. Magnetic resonance imaging revealed a 4-cm extradural mass lesion at T10 compressing the spinal cord, with heterogeneous peripheral enhancement after gadolinium administration. Since examination of the foot showed a large soft-tissue mass compatible with giant gouty tophi, dual-energy computed tomography (DECT) was performed on both feet and the dorsal spine. The basis material decomposition feature of DECT allows effective differentiation of tophi from other types of masses (1). In our patient, DECT scanning revealed evidence of spontaneous dense urate deposition in both masses, which appeared green with application of dedicated post-processing software. DECT thus confirmed severe tophaceous gout with spinal cord compression (A) (arrows). Such involvement has been reported previously, and its prevalence may be underappreciated (2), as gout usually affects the peripheral joints such as those of the feet (B) (tophaceous gout). Spinal decompression surgery was declined by the patient, and urate-lowering therapy with febuxostat was initiated, leading to progressive neurologic recovery at 6 months.

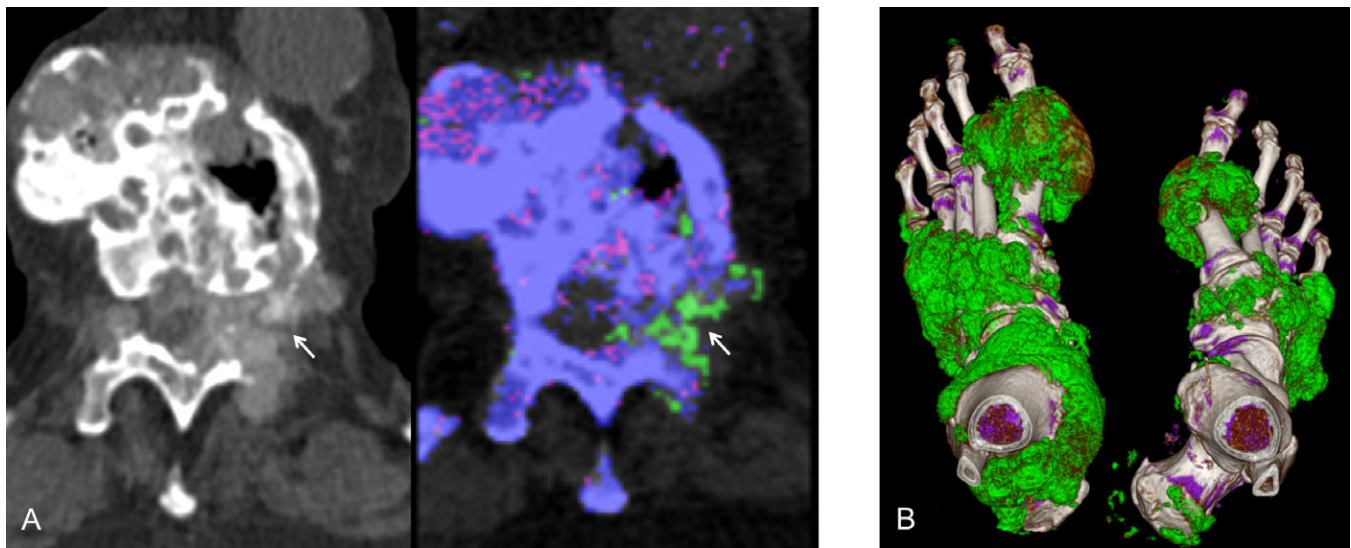
1. Komlasi P, Wintermark M. Dual energy computed tomography applications for the evaluation of the spine. *Neuroimaging Clin N Am* 2017;27:483–7.
2. Toprover M, Krasnokutsky S, Pillinger MH. Gout in the spine: imaging, diagnosis, and outcomes. *Curr Rheumatol Rep* 2015; 17:70.

Pierre Pottecher, MD
 Department of Radiology, LE2I UMR CNRS 6306
 François-Mitterrand Teaching Hospital
 Pierre Martz, MD
 Department of Orthopaedic Surgery
 François-Mitterrand Teaching Hospital
 and INSERM UMR1093-CAPS
 Université Bourgogne Franche-Comté
 Paul Ornetti, MD, PhD 
 INSERM UMR1093-CAPS
 Université Bourgogne Franche-Comté
 and Department of Rheumatology
 François-Mitterrand Teaching Hospital
 Dijon, France

35. Huang SM, Mishina YM, Liu S, Cheung A, Stegmeier F, Michaud GA, et al. Tankyrase inhibition stabilizes axin and antagonizes Wnt signalling. *Nature* 2009;461:614–20.
36. Bayle J, Fitch J, Jacobsen K, Kumar R, Lafyatis R, Lemaire R. Increased expression of Wnt2 and SFRP4 in Tsk mouse skin: role of Wnt signalling in altered dermal fibrillin deposition and systemic sclerosis. *J Invest Dermatol* 2008;128:871–81.
37. Milano A, Pendergrass SA, Sargent JL, George LK, McCalmont TH, Connolly MK, et al. Molecular subsets in the gene expression signatures of scleroderma skin. *PLoS One* 2008;3:e2696.
38. Wei J, Melichian D, Komura K, Hinchcliff M, Lam AP, Lafyatis R, et al. Canonical Wnt signaling induces skin fibrosis and subcutaneous lipodystrophy: a novel mouse model for scleroderma? *Arthritis Rheum* 2011;63:1707–17.
39. Beyer C, Reichert H, Akan H, Mallano T, Schramm A, Dees C, et al. Blockade of canonical Wnt signalling ameliorates experimental dermal fibrosis. *Ann Rheum Dis* 2013;72:1255–8.

DOI: 10.1002/art.40434

Clinical Images: Paraparesis revealing tophaceous gout



The patient, a 77-year-old man with a history of intermittent inflammatory arthritis of the feet, was hospitalized for a paraparesis that had progressed for 6 months, resulting in severe gait impairment. Magnetic resonance imaging revealed a 4-cm extradural mass lesion at T10 compressing the spinal cord, with heterogeneous peripheral enhancement after gadolinium administration. Since examination of the foot showed a large soft-tissue mass compatible with giant gouty tophi, dual-energy computed tomography (DECT) was performed on both feet and the dorsal spine. The basis material decomposition feature of DECT allows effective differentiation of tophi from other types of masses (1). In our patient, DECT scanning revealed evidence of spontaneous dense urate deposition in both masses, which appeared green with application of dedicated post-processing software. DECT thus confirmed severe tophaceous gout with spinal cord compression (A) (arrows). Such involvement has been reported previously, and its prevalence may be underappreciated (2), as gout usually affects the peripheral joints such as those of the feet (B) (tophaceous gout). Spinal decompression surgery was declined by the patient, and urate-lowering therapy with febuxostat was initiated, leading to progressive neurologic recovery at 6 months.

1. Komlasi P, Wintermark M. Dual energy computed tomography applications for the evaluation of the spine. *Neuroimaging Clin N Am* 2017;27:483–7.
2. Toprover M, Krasnokutsky S, Pillinger MH. Gout in the spine: imaging, diagnosis, and outcomes. *Curr Rheumatol Rep* 2015; 17:70.

Pierre Pottecher, MD
 Department of Radiology, LE2I UMR CNRS 6306
 François-Mitterrand Teaching Hospital
 Pierre Martz, MD
 Department of Orthopaedic Surgery
 François-Mitterrand Teaching Hospital
 and INSERM UMR1093-CAPS
 Université Bourgogne Franche-Comté
 Paul Ornetti, MD, PhD 
 INSERM UMR1093-CAPS
 Université Bourgogne Franche-Comté
 and Department of Rheumatology
 François-Mitterrand Teaching Hospital
 Dijon, France

Reversal of Sepsis-Like Features of Neutrophils by Interleukin-1 Blockade in Patients With Systemic-Onset Juvenile Idiopathic Arthritis

Nienke M. ter Haar,¹ Tamar Tak,² Michal Mokry,¹ Rianne C. Scholman,² Jenny M. Meerding,² Wilco de Jager,¹ Anouk Verwoerd,² Dirk Foell,³ Thomas Vogl,³ Johannes Roth,³ Pieter H. C. Leliefeld,² Jorg van Loosdregt,¹ Leo Koenderman,² Sebastiaan J. Vastert,¹ and Sytze de Roock¹

Objective. Neutrophils are the most abundant innate immune cells in the blood, but little is known about their role in (acquired) chronic autoinflammatory diseases. This study was undertaken to investigate the role of neutrophils in systemic-onset juvenile idiopathic arthritis (JIA), a prototypical multifactorial autoinflammatory disease that is characterized by arthritis and severe systemic inflammation.

Methods. Fifty patients with systemic-onset JIA who were receiving treatment with recombinant interleukin-1 receptor antagonist (rIL-1Ra; anakinra) were analyzed at disease onset and during remission. RNA sequencing was performed on fluorescence-activated cell–sorted neutrophils from 3 patients with active systemic-onset JIA and 3 healthy controls. Expression of activation markers, apoptosis,

production of reactive oxygen species (ROS), and degranulation of secretory vesicles from neutrophils were assessed by flow cytometry in serum samples from 17 patients with systemic-onset JIA and 15 healthy controls.

Results. Neutrophil counts were markedly increased at disease onset, and this correlated with the levels of inflammatory mediators. The neutrophil counts normalized within days after the initiation of rIL-1Ra therapy. RNA-sequencing analysis revealed a substantial up-regulation of inflammatory processes in neutrophils from patients with active systemic-onset JIA, significantly overlapping with the transcriptome of sepsis. Correspondingly, neutrophils from patients with active systemic-onset JIA displayed a primed phenotype that was characterized by increased ROS production, CD62L shedding, and secretory vesicle degranulation, which was reversed by rIL-1Ra treatment in patients who had achieved clinical remission. Patients with a short disease duration had high neutrophil counts, more immature neutrophils, and a complete response to rIL-1Ra, whereas patients with symptoms for >1 month had normal neutrophil counts and an unsatisfactory response to rIL-1Ra. *In vitro*, rIL-1Ra antagonized the priming effect of IL-1 β on neutrophils from healthy subjects.

Conclusion. These results strongly support the notion that neutrophils play an important role in systemic-onset JIA, especially in the early inflammatory phase of the disease. The findings also demonstrate that neutrophil numbers and the inflammatory activity of systemic-onset JIA are both susceptible to IL-1 blockade.

Systemic-onset juvenile idiopathic arthritis (JIA) is a multifactorial disease with a clear autoinflammatory signature. The disease is characterized by arthritis, quotidian spiking fever, skin rash, lymphadenopathy,

Supported by the European Union Seventh Framework Programme (project MIAMI; EC-GA 305266), the Interdisciplinary Center of Clinical Research at the University of Muenster (grant Vo2/004/14 to Dr. Vogl and grant Ro2/003/15 to Dr. Roth), the German Research Foundation (grants CRC 1009 B8 and B9 to Drs. Vogl and Roth), the Federal Ministry of Education and Research (project AID-NET grant to Dr. Roth), and the Wilhelmina Children's Hospital Research Fund (institutional grant to Drs. Vastert and de Roock).

¹Nienke M. ter Haar, MD, Michal Mokry, PhD, Wilco de Jager, PhD, Jorg van Loosdregt, PhD, Sebastiaan J. Vastert, MD, PhD, Sytze de Roock, PhD: University Medical Center Utrecht, Wilhelmina Children's Hospital and Utrecht University, Utrecht, The Netherlands; ²Tamar Tak, PhD, Rianne C. Scholman, Jenny M. Meerding, Anouk Verwoerd, MD, Pieter H. C. Leliefeld, MD, Leo Koenderman, PhD: University Medical Center Utrecht and Utrecht University, Utrecht, The Netherlands; ³Dirk Foell, MD, PhD, Thomas Vogl, PhD, Johannes Roth, PhD: University of Muenster, Muenster, Germany.

Drs. Vastert and de Roock contributed equally to this work.

Address correspondence to Sebastiaan J. Vastert, MD, PhD, University Medical Center Utrecht, Laboratory for Translational Immunology, Lundlaan 6, PO Box 85090 Utrecht, Utrecht 3508 AB, The Netherlands. E-mail: b.vastert@umcutrecht.nl.

Submitted for publication September 11, 2017; accepted in revised form February 1, 2018.

hepatosplenomegaly, and/or serositis (1). The systemic inflammation is reflected by elevations in the parameters of inflammation, including an increased erythrocyte sedimentation rate (ESR), C-reactive protein (CRP) level, and ferritin level. Moreover, patients with systemic-onset JIA have shown a good response to therapeutic blockade of either interleukin-1 (IL-1) or IL-6 (2). However, some patients fail to respond to IL-1 or IL-6 blocking therapy.

It is hypothesized that autoinflammatory features, including an IL-1 signature, are most prominent in the early phase of the disease, while later in the disease course, more adaptive immune mechanisms come into play, which might explain why higher response rates have been observed in studies using IL-1 blockade as first-line therapy as compared to studies in which IL-1 blockade was initiated later in the disease course (1–4). However, this is still under debate, as the pathogenesis of systemic-onset JIA remains largely unresolved.

A prominent feature of systemic-onset JIA is the marked neutrophilia that develops during active disease (5). Besides phagocytosis, neutrophils can perform a variety of functions, including release of (bactericidal) granular proteins and reactive oxygen species (ROS) (6). Furthermore, neutrophils are a major source of S100A8/A9 and S100A12 proteins, which are found at extremely high levels in patients with active systemic-onset JIA (7–9). Because of their increased numbers and their release of inflammatory mediators, neutrophils could be a major contributor to the inflammatory cascade of systemic-onset JIA. However, studies on the role of neutrophils in the pathogenesis of systemic-onset JIA are lacking. We therefore investigated the phenotype and function of neutrophils from patients with systemic-onset JIA, using a combination of clinical data and primary patient material from a prospective systemic-onset JIA cohort (4).

PATIENTS AND METHODS

Patients. All patients with systemic-onset JIA were treated at the University Medical Center Utrecht (UMCU) in The Netherlands as part of a prospective cohort study on the efficacy of recombinant IL-1 receptor antagonist (rIL-1Ra; anakinra) as first-line treatment (4). In short, patients with systemic-onset JIA were started on rIL-1Ra treatment at a dosage of 2 mg/kg per day subcutaneously after prior treatment with nonsteroidal antiinflammatory drugs had been unsuccessful. When the disease became clinically inactive, the dosage of rIL-1Ra was tapered off over a period of 3 months. In patients with persistent symptoms, corticosteroids were added to the rIL-1Ra treatment regimen; if that failed, patient treatments were switched to an alternative biologic agent.

Clinical and laboratory data were obtained from all patients (results shown in Figures 1A–D). Protein concentrations were measured in patients for whom serum samples were available at the time of disease onset or during remission (results shown in Figures 1E and F). Supplementary Table 1 (available on the *Arthritis & Rheumatology* web site at <http://onlinelibrary.wiley.com/doi/10.1002/art.40442/abstract>) shows the baseline characteristics of the total cohort. Analyses of the phenotype and function of neutrophils (results in Figures 2–6) were performed in a subset of 9 patients with active systemic-onset JIA and 8 patients who were in remission. Supplementary Table 2 (available on the *Arthritis & Rheumatology* web site at <http://onlinelibrary.wiley.com/doi/10.1002/art.40442/abstract>) shows detailed information on the baseline characteristics of these 17 patients. As a control, blood was obtained from adult volunteers who were participating in the local donor service of UMCU; the median age of the healthy control subjects was 39 years (interquartile range 29–50 years).

The study was approved by the institutional ethics review board of UMCU. All patients and volunteers provided written informed consent.

Determination of serum compounds. Serum samples from patients with systemic-onset JIA were assessed for circulating levels of neutrophil-related proteins using a multiplex immunoassay, as described previously (10). Levels of S100A12 and S100A8/A9 in the serum and supernatant of stimulated neutrophils were measured by sandwich enzyme-linked immunosorbent assay.

Cell isolation and neutrophil selection. Blood was collected in sodium heparin tubes and processed <1 hour after withdrawal. Erythrocytes were lysed in a solution of cold isotonic ammonium chloride (155 mM)–potassium carbonate (10 mM)–EDTA (0.1 mM) for 15 minutes, followed by centrifugation at 4°C and washing steps with isolation buffer (phosphate buffered saline supplemented with 10% pasteurized plasma solution and 0.4% trisodium citrate).

For RNA-sequencing analyses and reverse transcription–quantitative polymerase chain reaction (RT-qPCR), neutrophils were sorted using a FACSARIA III fluorescence-activated cell sorter (FACS) (BD Biosciences) based on their forward/side light-scatter patterns, positive expression of CD16, and negative expression of CD14 and CD41 (see Supplementary Figure 1A for a depiction of the gating strategy, available on the *Arthritis & Rheumatology* web site at <http://onlinelibrary.wiley.com/doi/10.1002/art.40442/abstract>). For all other experiments, whole blood leukocytes were used; gating of neutrophils was performed during flow cytometry analysis (see Supplementary Figure 2A, <http://onlinelibrary.wiley.com/doi/10.1002/art.40442/abstract>).

Analysis of ROS production and degranulation. Cells (10^6 /ml) were distributed in U-shaped 96-well plates in neutrophil culture medium (20 mM HEPES, 132 mM NaCl, 6 mM KCl, 1 mM MgSO₄, and 1.2 mM KH₂PO₄, supplemented with 5 mM glucose, 1 mM CaCl₂, and 0.5% human albumin). The plates were placed in an incubator with an atmosphere of 5% CO₂ at 37°C, unless otherwise specified.

For ROS assays, whole blood leukocytes were incubated with 0.1 μM of the ROS-responsive dye dihydrorhodamine (DHR) (Sigma-Aldrich) for 5 minutes, and subsequently stimulated with 10 μM fMLP (Sigma-Aldrich) for 15 minutes. For CD62L and degranulation assays, 100 μl whole blood was stimulated with 10 μM fMLP for 15 minutes, and subsequently, lysing

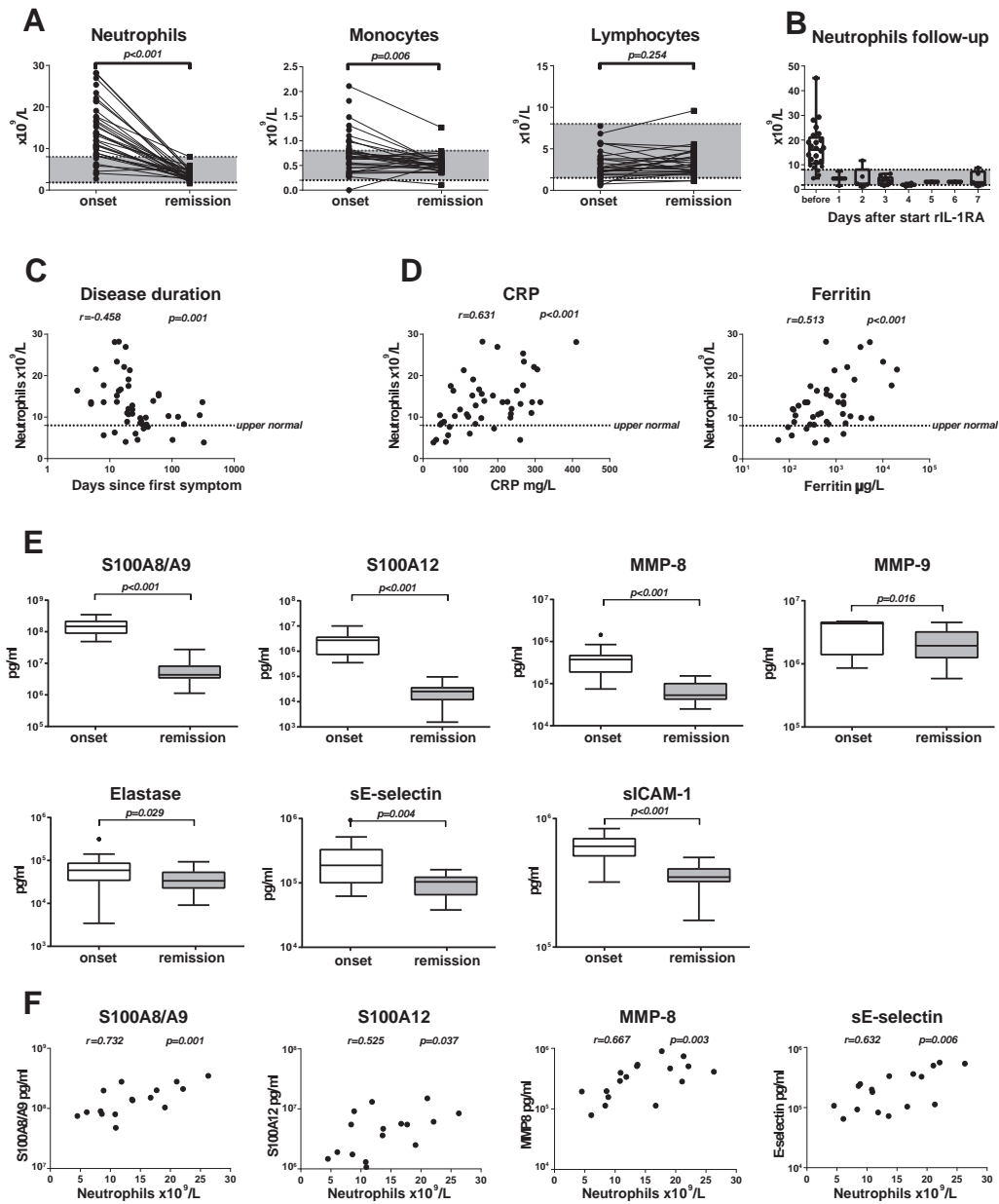


Figure 1. Elevations in the levels of neutrophils and neutrophil-associated markers in patients with systemic-onset juvenile idiopathic arthritis. **A**, Neutrophil, monocyte, and lymphocyte counts obtained by routine clinical laboratory measurements in the serum of patients at disease onset ($n = 50$) and during clinical remission after 3 months of receiving recombinant interleukin-1 receptor antagonist (rIL-1Ra) ($n = 31$). Shaded areas indicate the boundaries of a normal cell count for healthy children (pediatric reference values). **B**, Neutrophil counts before and during the first week of rIL-1Ra therapy. **C**, Correlation between the number of days since the first disease manifestation and neutrophil counts at disease onset ($n = 48$). **D**, Correlation between the levels of the acute-phase proteins C-reactive protein (CRP) ($n = 47$) and ferritin ($n = 44$) and neutrophil counts at disease onset. **E**, Serum levels of the neutrophil-related proteins S100A8/A9, S100A12, matrix metalloproteinase 8 (MMP-8), MMP-9, elastase, soluble E-selectin (sE-selectin), and soluble intercellular adhesion molecule 1 (sICAM-1) at disease onset ($n = 17$ –18) and during clinical remission after 3 months of receiving rIL-1Ra ($n = 21$). **F**, Correlation between neutrophil counts and serum levels of S100A8/A9, S100A12, MMP-8, and soluble E-selectin at disease onset ($n = 16$ –17). Data were analyzed using Wilcoxon’s signed rank test (**A**), Spearman’s rho correlation coefficients (**C**, **D**, and **F**), or Mann-Whitney U test (**E**). Data in **B** and **E** are shown as box plots. Each box represents the upper and lower interquartile range (IQR). Lines inside the boxes represent the median. Whiskers represent 1.5 times the upper and lower IQRs.

and antibody staining of erythrocytes was carried out. For RT-qPCR and analysis of cell apoptosis, sorted neutrophils were cultured for 2 hours and for 20 hours, respectively. For IL-1 assays, cells were preincubated for 5 minutes with 5 $\mu\text{g/ml}$ rIL-1Ra (Sobi) and stimulated with 20 ng/ml rIL-1 β (R&D Systems) for 10 minutes prior to the addition of DHR and/or fMLP.

Flow cytometry. For flow cytometry analyses, the following monoclonal antibodies were used: fluorescein isothiocyanate (FITC)-conjugated CD11b (clone ICRF44, concentration 1/100; BD Biosciences), Pacific Blue-conjugated CD14 (clone M5E2, concentration 1/200; BioLegend), phycoerythrin (PE)-conjugated CD16 (clone 3G8, concentration 1/1,600; BioLegend), allophycocyanin (APC)-conjugated CD35 (clone 594708, concentration 1/100; R&D Systems), FITC-conjugated CD41 (clone HIP8, concentration 1/200; BioLegend), PE-Cy7-conjugated CD62L (clone DREG56, concentration 1/800; BioLegend), FITC-conjugated CD64 (clone 10.1, concentration 1/200; BioLegend), and V450-conjugated CD66b (clone G10F5, concentration 1/200; BD Biosciences). Cells were incubated with the antibodies in isolation buffer for 30 minutes at 4°C and either measured on a FACSCanto flow cytometer or sorted on a FACSAria III (both from BD Biosciences).

For assays of cell apoptosis, neutrophils were stained with annexin V-APC (550474, concentration 1/100) and 7-aminoactinomycin D (7-AAD) (559925, concentration 1/100) in annexin binding buffer for 15 minutes at room temperature, as indicated by the manufacturer (BD Biosciences). Live cells were defined as those that stained negative for annexin V and 7-AAD.

RNA sequencing and RT-qPCR. Neutrophils were lysed in TRIzol LS reagent (Thermo Fisher) directly after sorting. RNA was isolated according to the manufacturer's protocol. The concentration of RNA was quantified using a Qubit RNA HS assay and Qubit fluorometer (Thermo Fisher). Polyadenylated messenger RNA was isolated using Poly(A) beads (NEXTflex), and sequencing libraries were made using the Rapid Directional RNA-seq kit (NEXTflex). Libraries were sequenced at the Utrecht Sequencing Facility using the Nextseq500 platform (Illumina), which produced single end reads of 75 bp. Reads were aligned to the human reference genome GRCh37 using STAR version 2.4.2a. Picard's AddOrReplaceReadGroups (version 1.98) was used to add read groups to the binary sequence alignment files, which were sorted using Sambamba (version 0.4.5), and transcript abundances were quantified with HTSeq-count (version 0.6.1p1) using the union mode. Subsequently, reads per kilobase per million reads sequenced (RPKM) were calculated with the edgeR RPKM function.

Differentially expressed genes were identified using the DESeq2 package with standard settings. Genes with an absolute \log_2 fold change larger than 0.6 and adjusted *P* values of less than 0.1 were considered to be differentially expressed genes. RNA-sequencing data have been deposited in the NCBI GEO data repository (11) (accessible through GEO Series accession no. GSE103170) (12). Differentially expressed genes were entered in ToppGene (13). Differentially expressed genes from publicly available microarray data sets were derived using GEO2R with default settings (11,14), and these gene sets were entered in the gene set enrichment analysis (15).

For RT-qPCR, isolated RNA was processed using a Script complementary DNA synthesis kit (Bio-Rad) and SYBR Select

Master Mix (Applied Biosystems). RT-qPCR was performed on a QuantStudio 12K (Thermo Fisher) using the following primers: for B2M, forward TGCTGTCTCCATGTTTGATGATCT and reverse TCTCTGCTCCCCACCTCTAAGT; for NFkB1, forward CAGATGGCCCATACCTTCAAAAT and reverse CGGAAAC GAAATCCTCTCTGTT; and for IL1B, forward GCTGAGGAA GATGCTGGTTC and reverse TCCATATCCTGTCCCTGGAG.

Statistical analysis. Statistical analyses were performed using the IBM SPSS Statistics program (version 21). Comparisons of distributions between 2 groups or between 3 groups were made by Mann-Whitney U test or Kruskal-Wallis test (including Dunn-Bonferroni post hoc correction [16]), respectively, and pairwise comparisons were performed using Wilcoxon's signed rank test. Correlations between 2 variables were tested with Spearman's rho correlation coefficients. Graphs were prepared in Graphpad Prism (version 7.02).

RESULTS

Rapid normalization of neutrophil counts following IL-1 blockade in patients with systemic-onset JIA, and correlation of neutrophil counts with parameters of inflammation. Using data from routine clinical laboratory measurements, we confirmed earlier findings of neutrophilia (5) in our cohort of 50 patients with systemic-onset JIA at the time of disease onset. Neutrophil counts were markedly elevated in 40 of 50 patients (median 11.9×10^9 /liter, interquartile range $8.4\text{--}16.5 \times 10^9$ /liter) (Figure 1A). In contrast, monocyte counts were elevated in only 14 of 50 patients, and no patient had increased lymphocyte counts when compared to pediatric reference values (Figure 1A). During inactive disease, at 3 months after the start of therapy with human rIL-1Ra (anakinra), all patients had normal neutrophil counts (Figure 1A). Strikingly, consistent with the rapid clinical improvement observed, neutrophil counts normalized in all patients within 1 day after initiation of rIL-1Ra therapy (Figure 1B).

Since we observed a substantial variability in the neutrophil counts in patients at the time of disease onset, we assessed correlations of the neutrophil counts with the available clinical information from each patient at the first visit. Disease duration correlated significantly with neutrophil counts, e.g., patients with a short interval between the onset of symptoms and first visit to the hospital had higher neutrophil counts than did patients who had symptoms for more than 1 month (Figure 1C). Furthermore, levels of acute-phase proteins (CRP and ferritin) correlated significantly with the neutrophil counts (Figure 1D). Monocyte and lymphocyte counts did not correlate with these variables (see Supplementary Figures 3A and B, available on the *Arthritis & Rheumatology* web site at <http://onlinelibrary.wiley.com/doi/10.1002/art.40442/abstract>). No relationship between neutrophil

counts and the age of the patients, other leukocyte counts, or ESR was found (data not shown). Collectively, these data confirm that there was an abundance of neutrophils in patients with systemic-onset JIA, especially in the early inflammatory phase of the disease, with a rapid normalization of neutrophil counts following therapy with rIL-1Ra.

Increased levels of neutrophil-related proteins at disease onset in patients with systemic-onset JIA. To further address the role of neutrophils in systemic-onset JIA, we analyzed the serum levels of several neutrophil-

related proteins. As previously reported (7–9), we confirmed that the levels of S100A8/A9 and S100A12 were significantly elevated in patients with systemic-onset JIA at the time of disease onset as compared to the time of remission at 3 months after the initiation of rIL-1Ra therapy (Figure 1E).

Moreover, other components of neutrophil granules (17,18), such as matrix metalloproteinase 8 (MMP-8), MMP-9, and elastase, and proteins involved in adhesion and chemotaxis of neutrophils, such as soluble E-selectin and soluble intercellular adhesion molecule 1, had

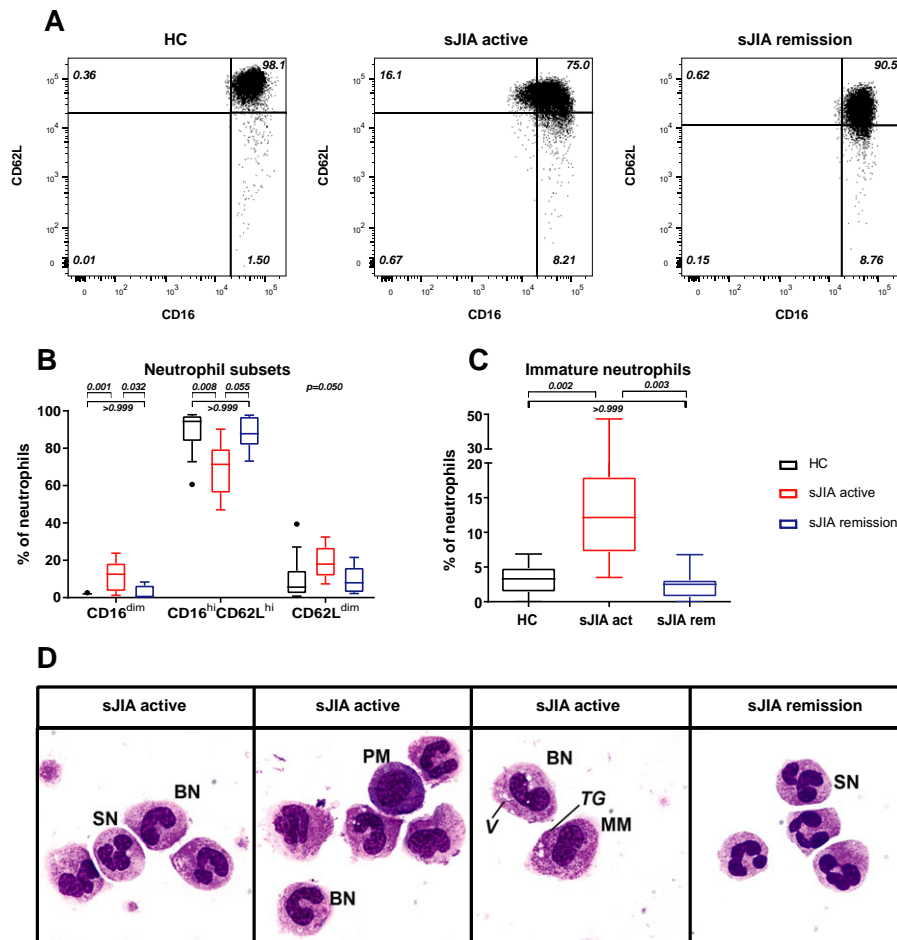


Figure 2. Phenotype of immature neutrophils in patients with active systemic-onset juvenile idiopathic arthritis (sJIA). **A**, Representative plots showing staining of neutrophils for the expression of CD62L in whole blood leukocytes from healthy controls (HC), patients with active systemic-onset JIA, and patients in clinical remission. Neutrophils were gated on their forward/side light-scatter patterns and on CD16⁺ cells. **B**, Percentages of CD16^{dim}, CD16^{high}CD62L^{high}, and CD62L^{dim} neutrophils in healthy controls (n = 14), patients with active systemic-onset JIA (n = 8), and patients in clinical remission (n = 8). **C**, Percentages of immature neutrophils (identified as banded neutrophils [BN] and granulocyte precursors, based on cell morphology) within the total neutrophil population (n = 17 healthy controls, n = 9 patients with active systemic-onset JIA [sJIA act], n = 7 patients in clinical remission [sJIA rem]). Data in **B** and **C** are shown as box plots. Each box represents the upper and lower interquartile range (IQR). Lines inside the boxes represent the median. Whiskers represent 1.5 times the upper and lower IQRs. Circles represent outliers. Differences between the groups were analyzed by Kruskal-Wallis test, with Dunn-Bonferroni correction for multiple comparisons if the distribution between the groups was significantly different. **D**, Representative images of cytopspins of whole blood leukocytes from 3 patients with active systemic-onset JIA compared to 1 patient with systemic-onset JIA in clinical remission. Cells were stained with May-Grünwald and Giemsa dye. SN = segmented neutrophil; PM = promyelocyte; MM = metamyelocyte; TG = toxic granule; V = vacuolization.

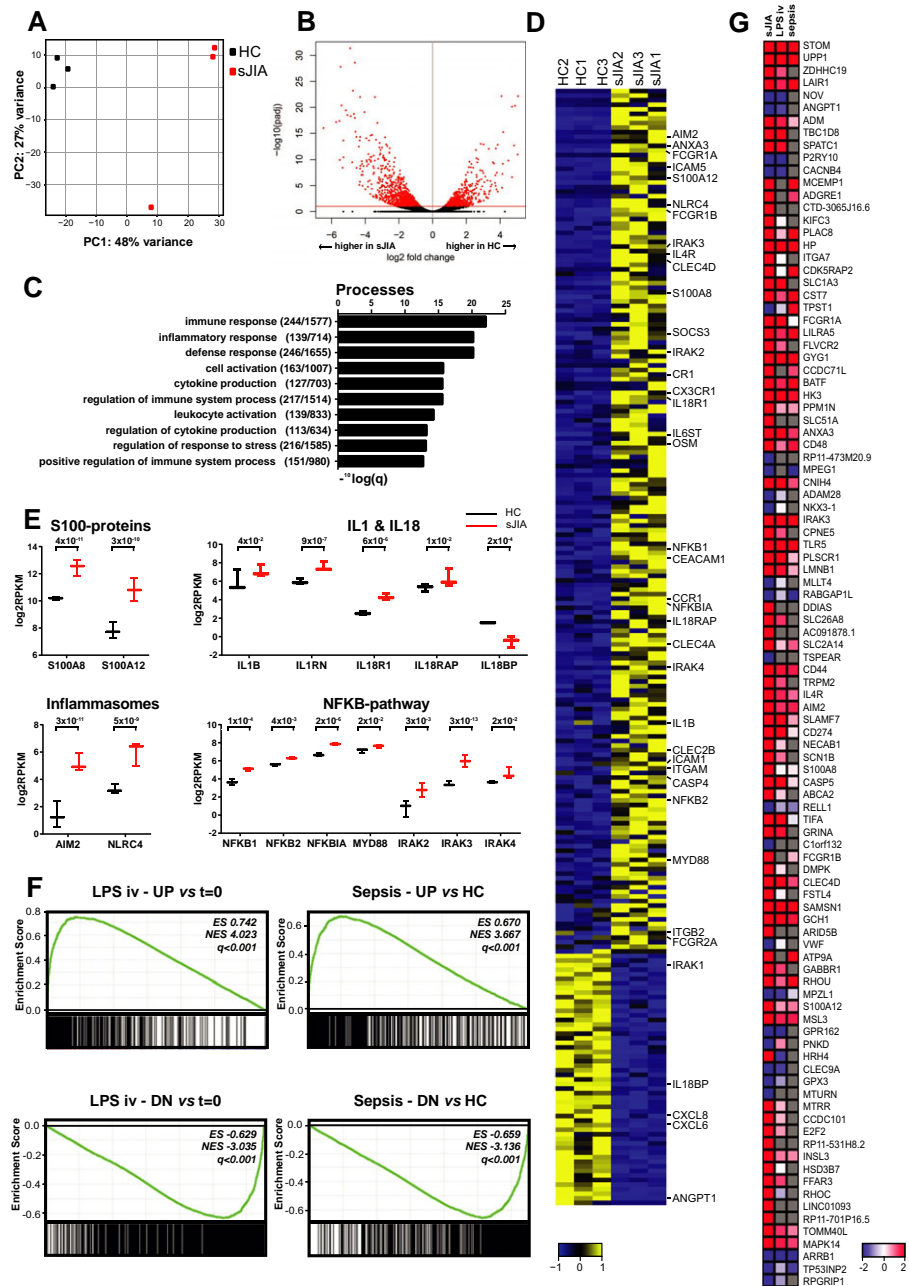


Figure 3. Up-regulation of inflammatory genes in neutrophils from patients with systemic-onset juvenile idiopathic arthritis (sJIA). RNA-sequencing analysis was performed following fluorescence-activated cell sorting of CD16+CD14−CD41− neutrophils from 3 patients with active systemic-onset JIA and 3 adult healthy controls (HCs) (further details on the gating strategy are given in Supplementary Figure 1A, <http://onlinelibrary.wiley.com/doi/10.1002/art.40442/abstract>). **A**, Principal components (PC) analysis of neutrophil gene expression using the top 1,000 most variable genes. **B**, Volcano plot of neutrophil gene expression. Differentially expressed genes (adjusted $P < 0.1$ and \log_2 fold change > 0.6) are depicted in red. **C**, Top 10 most significant biologic processes derived from the differentially expressed genes, as identified by gene ontology (GO) analysis. Values in parentheses are the number of differentially expressed genes/total number of genes in the annotated process. **D**, Heatmap of the differentially expressed genes associated with the GO biologic process "immune response," with key genes highlighted. Colors indicate normalized gene expression (yellow = high expression, blue = low expression). **E**, Expression levels of selected differentially expressed genes in the peripheral blood of 3 patients with active systemic-onset JIA and 3 healthy controls. Adjusted P values were derived from RNA-sequencing analysis. Bars show the median with interquartile range. **F**, Gene set enrichment analysis of gene sets from patients with experimental endotoxemia (LPS iv) (GEO accession no. GSE35590) and patients with sepsis (GEO accession no. GSE64456), analyzing up-regulated (UP) or down-regulated (DN) genes in comparison to time 0 (left) or to healthy controls (right). **G**, Heatmap of \log_2 fold changes in gene expression relative to healthy controls, in neutrophils from patients with active systemic-onset JIA, patients with endotoxemia, and patients with sepsis. Red indicates up-regulation versus controls, while blue indicates down-regulation; missing data are depicted in gray. The selection of genes was based on the top 100 most differentially expressed genes in patients with systemic-onset JIA, according to adjusted P values. ES = enrichment score; NES = normalized enrichment score; q = false discovery rate-corrected P value.

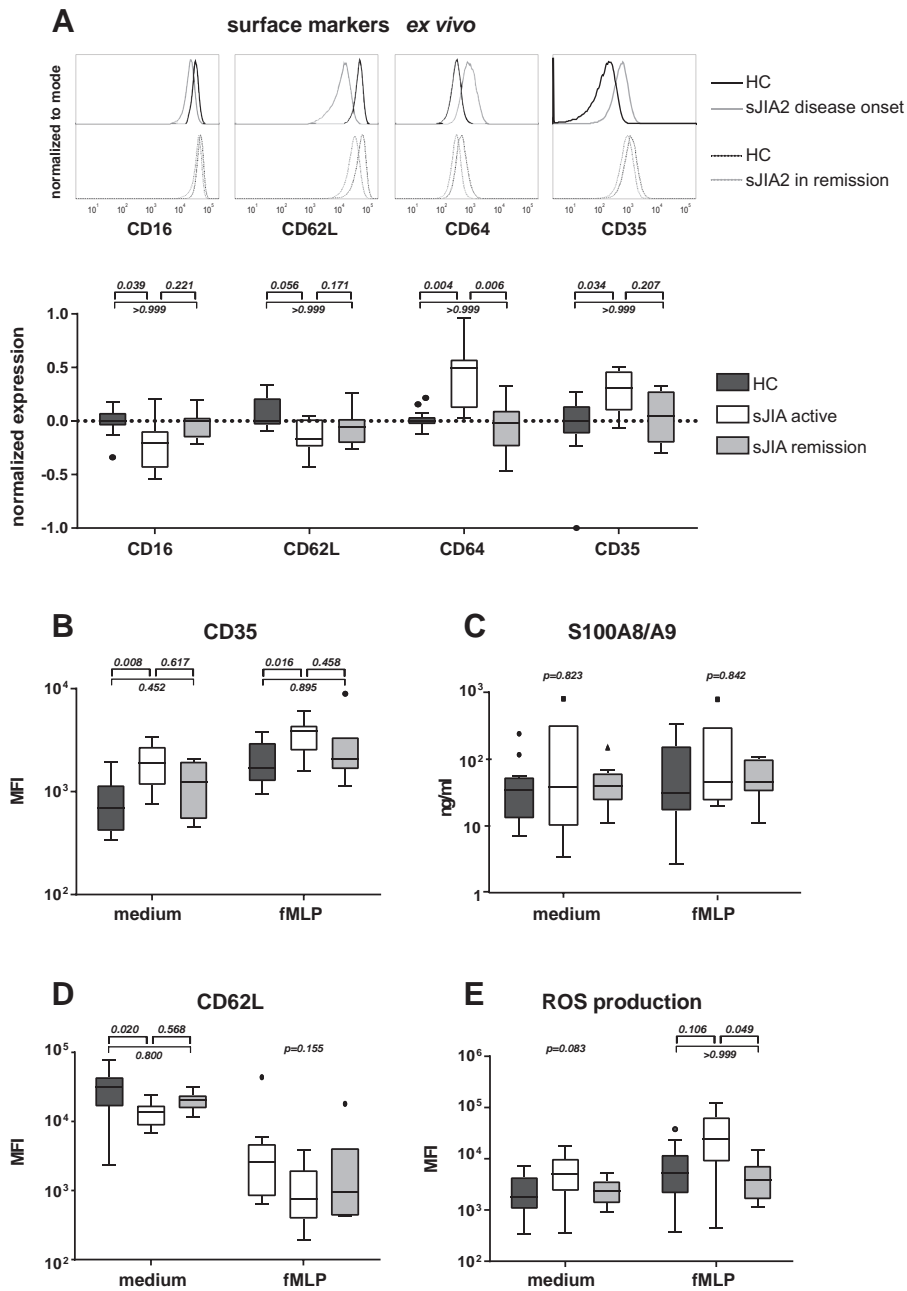


Figure 4. Neutrophils from patients with systemic-onset juvenile idiopathic arthritis (sJIA) display a primed phenotype. **A**, Flow cytometry analysis of surface marker expression was performed directly ex vivo in neutrophils from 14 healthy controls (HCs), 8 patients with active systemic-onset JIA, and 8 patients in clinical remission. Marker expression levels were normalized to the median fluorescence intensity (MFI) values in healthy controls. Representative plots (top) and quantification of marker expression (bottom) are shown. **B–E**, Whole blood leukocytes from 15 healthy controls, 8 patients with active systemic-onset JIA, and 7 patients in clinical remission were cultured for 30 minutes, with or without the addition of fMLP in the last 15 minutes, and thereafter the cells were checked for secretory vesicle degranulation (CD35 expression) (**B**), S100A8/A9 production (**C**), shedding of CD62L (**D**), and intracellular reactive oxygen species (ROS) production (**E**). Results are presented as the MFI of dihydrorhodamine staining. In all flow cytometry analyses, neutrophils from whole blood leukocytes were gated based on their forward/side light-scatter patterns and high CD16 expression (further details on the gating strategy are given in Supplementary Figure 2A, <http://onlinelibrary.wiley.com/doi/10.1002/art.40442/abstract>). Differences between groups were analyzed by Kruskal-Wallis test, with Dunn-Bonferroni correction for multiple comparisons if the distribution between the groups was significantly different. Data are presented as box plots. Each box represents the upper and lower interquartile range (IQR). Lines inside the boxes represent the median. Whiskers represent 1.5 times the upper and lower IQRs.

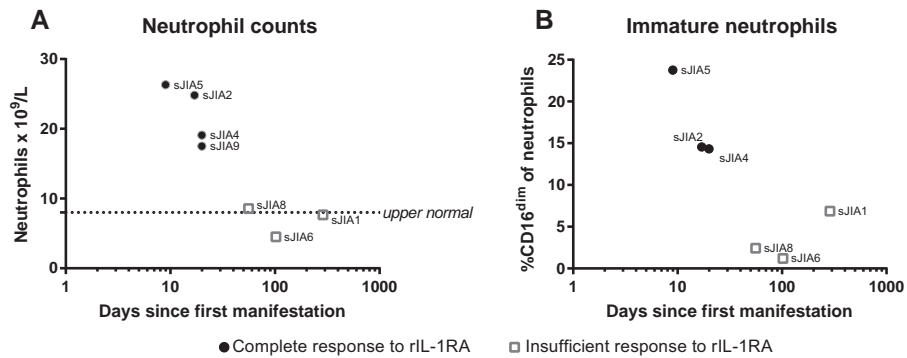


Figure 5. Better response to treatment with recombinant interleukin-1 receptor antagonist (rIL-1Ra) in patients with systemic-onset juvenile idiopathic arthritis (sJIA) who had a short interval between the onset of symptoms and first visit to the hospital and who displayed high neutrophil counts. The relationship between disease duration at first presentation and the neutrophil counts from routine clinical laboratory measurements at disease onset (**A**) or between disease duration at first presentation and the percentage of immature, CD16^{dim} neutrophils among the total neutrophil population at disease onset (**B**) was determined in a subset of 7 patients with systemic-onset JIA. Due to the limited number of patients, statistical tests were not performed.

significantly increased levels at disease onset compared to their levels at the time of remission with rIL-1Ra treatment (Figure 1E). Notably, neutrophil counts significantly correlated with the levels of S100A8/A9, S100A12, MMP-8, and soluble E-selectin (Figure 1F), whereas monocyte counts were not correlated with the levels of MMP-8 and soluble E-selectin. Monocyte counts were even negatively correlated with the levels of S100A8/A9 and S100A12 (see Supplementary Figure 3C, <http://onlinelibrary.wiley.com/doi/10.1002/art.40442/abstract>). The increased levels of neutrophil-related proteins and the correlation with neutrophil counts may serve to support the notion that neutrophils play an important role in the inflammatory response of systemic-onset JIA.

More immature and primed neutrophils in the peripheral blood of patients with systemic-onset JIA. As we observed a marked neutrophilia at disease onset in patients with systemic-onset JIA, we aimed to characterize the neutrophils in these patients. In the peripheral blood of patients with other causes of systemic inflammation, namely sepsis and experimental endotoxemia, a profound shift in neutrophil subsets has been described (19,20). In noninflammatory conditions, nearly all circulating neutrophils express high levels of CD16 (Fc γ receptor type III) and CD62L (L-selectin) and have a normal segmented nucleus (so-called “mature neutrophils”). In contrast, in systemic inflammation, 20–25% of the neutrophils are CD16^{dim} with a banded nucleus (i.e., “immature neutrophils”), and 10–15% are CD62L^{dim} with an increased number of nuclear lobes.

These subsets were found to be present in patients with systemic-onset JIA during the time of active disease. The total neutrophil population in these patients comprised 10–15% immature, CD16^{dim} neutrophils

(Figures 2A and B). The finding of significantly increased percentages of immature neutrophils (banded neutrophils and granulocyte precursors) was confirmed by cell morphology (Figures 2C and D). There was a tendency toward increased percentages of CD62L^{dim} neutrophils in patients with active systemic-onset JIA (Figure 2B), but these neutrophils did not have an increased number of nuclear lobes (Figure 2D).

Since CD62L can be shed upon stimulation, the decreased production of CD62L in neutrophils could be a reflection of the “primed” state of the neutrophils (21–23). Neutrophil priming is defined as the transition toward enhanced responsiveness, and the primed phenotype includes altered receptor expression, enhanced respiratory burst, and increased degranulation, especially after a second stimulus (23). These phenotypic changes occur after *in vitro* stimulation (e.g., by cytokines or microbial products) or *in vivo* in inflammatory conditions, such as infections and rheumatic diseases, and generally result in an amplification of the inflammatory response (23). Next to increased CD62L shedding, other signs of neutrophil priming, such as toxic granules and vacuoles (24), were identified in the majority of patients with active systemic-onset JIA (Figure 2D). Neutrophils of patients in disease remission had a normal mature phenotype, similar to that in healthy controls (Figures 2A–D). Taken together, these findings indicate that more immature neutrophils and neutrophils with a primed phenotype are characteristics detected in patients with active systemic-onset JIA.

Up-regulation of inflammatory genes with a sepsis-like signature by neutrophils from patients with systemic-onset JIA. To investigate the transcriptome of neutrophils, we performed RNA-sequencing analysis of

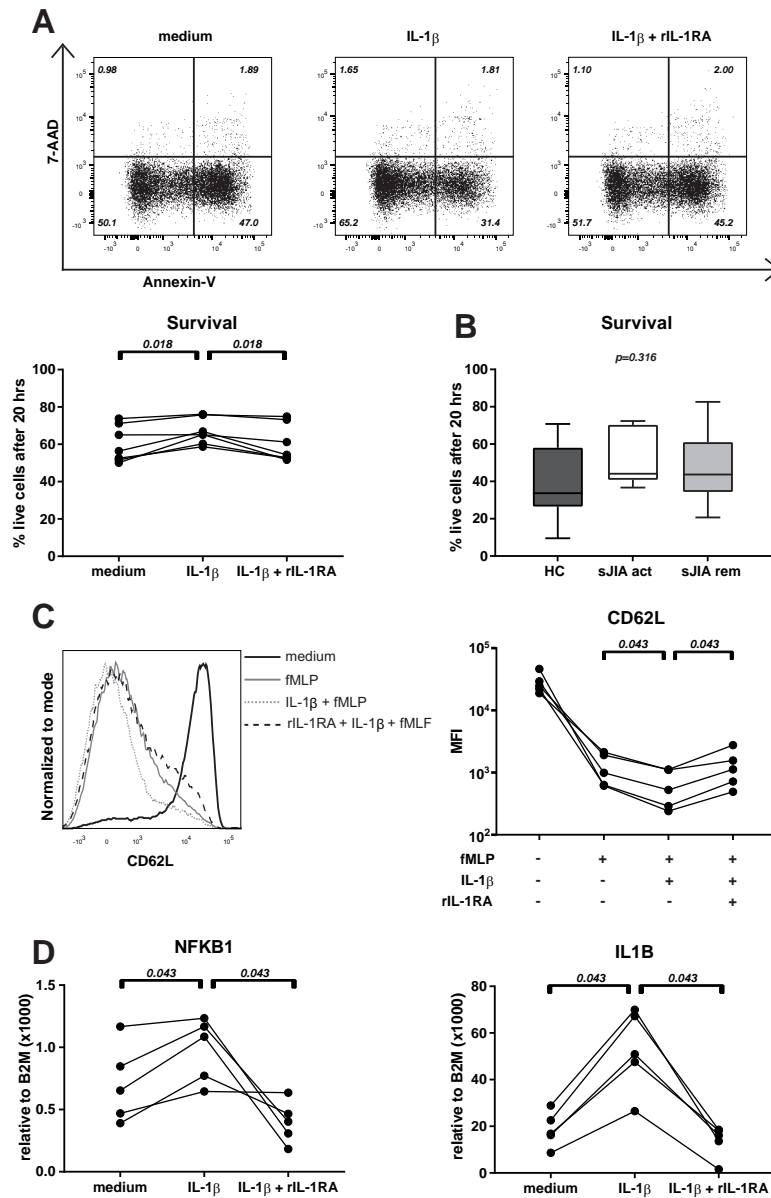


Figure 6. Susceptibility of neutrophils to interleukin-1 β (IL-1 β) and recombinant interleukin-1 receptor antagonist (rIL-1Ra). **A**, Apoptosis of neutrophils from healthy control (HC) subjects (n = 7) was analyzed after 20 hours in culture with medium, IL-1 β alone, or IL-1 β plus rIL-1Ra. Representative plots (top) and the percentage of live neutrophils (defined as those negative for annexin V and 7-aminoactinomycin D [7-AAD]) in samples from individual donors are shown. **B**, The percentage of live neutrophils in serum samples from healthy controls (n = 13), patients with active systemic-onset juvenile idiopathic arthritis (sJIA act) (n = 6), and patients with systemic-onset JIA in clinical remission (sJIA rem) (n = 6) was analyzed after 20 hours in culture medium. Data are presented as box plots. Each box represents the upper and lower interquartile range (IQR). Lines inside the boxes represent the median. Whiskers represent 1.5 times the upper and lower IQRs. **C**, Surface expression of CD62L on neutrophils from healthy controls (n = 5) was analyzed after 30 minutes in culture, with fMLP added in the last 15 minutes. Representative flow cytometry plots (left) and quantification of the results as the median fluorescence intensity (MFI) (right) are shown. **D**, Expression levels of the NFKB1 and IL1B genes, relative to the values for B2M, were determined in neutrophils from healthy controls (n = 5) after 2 hours in culture with medium, IL-1 β alone, or IL-1 β plus rIL-1Ra. Paired measurements within 1 donor (**A**, **C**, and **D**) were analyzed by Wilcoxon's signed rank test. Differences between groups (**B**) were analyzed by Kruskal-Wallis test.

neutrophils directly ex vivo (see Supplementary Figure 1A for the gating strategy, <http://onlinelibrary.wiley.com/doi/10.1002/art.40442/abstract>). Neutrophils isolated

from 3 patients with systemic-onset JIA whose disease was active before the start of therapy (2 from patients at the time of disease onset, and 1 from a patient during

a disease flare; see Supplementary Table 2 for details on these patients [<http://onlinelibrary.wiley.com/doi/10.1002/art.40442/abstract>] and neutrophils isolated from 3 adult healthy control subjects (ages 28–37 years) were compared. The transcriptome of neutrophils from patients with active systemic-onset JIA was clearly distinct from that of healthy controls (Figure 3A; see also Supplementary Figures 1B and D [<http://onlinelibrary.wiley.com/doi/10.1002/art.40442/abstract>]). In total, 1,068 genes were significantly up-regulated and 625 genes were down-regulated in patients with active systemic-onset JIA compared to healthy controls (Figure 3B; see also Supplementary Figures 1C and D [<http://onlinelibrary.wiley.com/doi/10.1002/art.40442/abstract>]). A complete list of the differentially expressed genes is shown Supplementary Table 3 (<http://onlinelibrary.wiley.com/doi/10.1002/art.40442/abstract>).

Gene ontology (GO) analysis of the biologic processes associated with the differentially expressed genes observed in patients with systemic-onset JIA indicated a very strong enrichment of immune responses in their neutrophils (Figure 3C). The majority of these immune-related genes were expressed at higher levels in patients with systemic-onset JIA compared to healthy controls (Figure 3D). Separate GO analyses revealed that only the up-regulated genes in patients with systemic-onset JIA contributed to the enrichment of immune-related processes (see Supplementary Figures 1E and F, <http://onlinelibrary.wiley.com/doi/10.1002/art.40442/abstract>). Up-regulated genes in systemic-onset JIA included S100 proteins, IL-1 family members, components of inflammasomes, and genes belonging to the NF- κ B pathway (Figure 3E).

To identify potential factors that could activate the transcription of immune-related genes, we performed an analysis of upstream regulators. This analysis revealed lipopolysaccharide (LPS) to be the most significant regulator of the gene changes observed in the neutrophils from patients with systemic-onset JIA (see Supplementary Figure 1G, <http://onlinelibrary.wiley.com/doi/10.1002/art.40442/abstract>). LPS is a component of the outer membrane of gram-negative bacteria and elicits strong immune responses via Toll-like receptor 4 (TLR-4), as is commonly seen in patients with sepsis. Because systemic-onset JIA is characterized by high levels of circulating TLR-4-binding S100A8/A9 and S100A12 proteins, we hypothesized that the immune activation of neutrophils observed in systemic-onset JIA might be similar to the neutrophil response seen in (LPS-mediated) sepsis. Indeed, in our study we found a significant enrichment of differentially expressed genes in neutrophils during bacterial sepsis (GEO accession no.

GSE64457 [22]) and in neutrophils from patients with experimental endotoxemia (GEO accession no. GSE35590 [25]) (Figure 3F). Correspondingly, the majority of the top 100 differentially expressed genes identified in patients with systemic-onset JIA were also differentially expressed in patients with sepsis or experimental endotoxemia (Figure 3G). Thus, our data indicate a strong similarity of neutrophil phenotype and activation during systemic inflammation between systemic-onset JIA and sepsis.

Evidence of a primed phenotype in neutrophils from patients with systemic-onset JIA. Since we observed signs of neutrophil priming based on the morphologic features of the cells and on gene expression data, we explored the phenotype of neutrophils in patients with systemic-onset JIA in more detail. Data from ex vivo flow cytometry analysis confirmed a decreased surface expression of CD16 and CD62L and showed an increased expression of CD64 (Fc γ receptor type I) and CD35 (a marker of secretory vesicle degranulation [26]) in neutrophils from patients with systemic-onset JIA whose disease was active as compared to healthy controls, whereas patients in remission had expression levels similar to those in healthy controls (Figure 4A) (for details on the gating strategy, see Supplementary Figure 2A, <http://onlinelibrary.wiley.com/doi/10.1002/art.40442/abstract>). The increased surface marker expression of CD35 and CD64 was not explained by the presence of CD16^{dim} or CD62L^{dim} neutrophil subsets in active systemic-onset JIA (see Supplementary Figures 2B and C, <http://onlinelibrary.wiley.com/doi/10.1002/art.40442/abstract>).

We further investigated the degranulation of secretory vesicles after in vitro stimulation with fMLP, a chemotactic peptide that induces a rapid and almost complete degranulation of secretory vesicles (26). Compared to neutrophils in a steady state, primed neutrophils show an enhanced degranulation and increased ROS production upon activation with fMLP (23). Consistent with the ex vivo data, higher surface expression of CD35 was also observed in vitro in patients with active systemic-onset JIA compared to healthy controls. Stimulation with fMLP led to even higher expression of CD35 (Figure 4B). Degranulation of gelatinase granules (as judged by surface expression of CD11b) and specific granules (CD66b) was not significantly increased in patients with systemic-onset JIA (see Supplementary Figures 2D and E, <http://onlinelibrary.wiley.com/doi/10.1002/art.40442/abstract>).

Secretory vesicles are known to contain high levels of S100 proteins (17), suggesting that an increased degranulation of these vesicles could contribute to the

high serum levels of S100 proteins found in these patients. However, when the S100A8/A9 protein concentrations were analyzed in the supernatant of stimulated neutrophils, no differences were found between patients with systemic-onset JIA and healthy controls, nor were there any differences in the protein concentrations between supernatants with fMLP stimulation and supernatants with medium control (Figure 4C). Thus, we found no evidence to indicate that the secretion of S100 proteins per neutrophil was increased. However, as the neutrophil counts were highly elevated in patients with systemic-onset JIA and correlated with the levels of S100A8/A9 and S100A12 (Figure 1F), neutrophils may still be the major source of the observed high serum levels of S100A8/A9 and S100A12 in these patients.

Consistent with the primed phenotype of neutrophils observed *ex vivo*, the expression of CD62L on neutrophils after a short *in vitro* culture was significantly lower in patients with active systemic-onset JIA compared to healthy controls (Figure 4D). Furthermore, ROS production after fMLP stimulation was increased in patients with active systemic-onset JIA compared to patients in remission or compared to healthy controls (Figure 4E). Therefore, these results indicate that neutrophils from patients with active systemic-onset JIA are primed by inflammatory mediators *in vivo*.

More immature neutrophils and better response to rIL-1Ra treatment in patients with a short disease duration. For the characterization of neutrophils in active systemic-onset JIA, we studied blood from 7 patients with systemic-onset JIA at the time of disease onset. Three of these patients had already been experiencing symptoms for more than 1 month when they first visited our hospital (1 patient [patient sJIA1 in Figure 5] had skin rash for 9 months, and fever and arthritis for 1–2 weeks; 1 patient [patient sJIA6 in Figure 5] had skin rash for 3 months, arthritis for 2 months, and fever for 2 weeks; 1 patient [patient sJIA8 in Figure 5] had skin rash and fever for 2 months, and arthritis for 6 weeks). In the other 4 patients (patients sJIA2, sJIA4, sJIA5, and sJIA9 in Figure 5), symptoms (including fever) started <1 month before the first visit to our clinic (see Supplementary Table 2, <http://onlinelibrary.wiley.com/doi/10.1002/art.40442/abstract>). Consistent with the findings shown in Figure 1C, patients with a short disease duration had high neutrophil counts, whereas patients with a disease duration of >1 month had normal or only minimally elevated neutrophil counts (Figure 5A). Moreover, the percentage of immature neutrophils within the total neutrophil population was substantially higher in patients with a short disease duration (Figure 5B).

Strikingly, the 4 patients with a disease duration of <1 month and high neutrophil counts had a complete response to first-line therapy with rIL-1Ra and were able to achieve clinical remission while off medication, within 1 year after the initiation of therapy. In contrast, the 3 patients with a disease duration of >1 month and normal neutrophil counts did not achieve inactive disease following rIL-1Ra monotherapy (Figures 5A and B; see also Supplementary Table 2), and ultimately these patients were switched to an alternative biologic agent. Albeit in a small number of patients, these observations support the hypothesis that neutrophils play a role in the early acute phase of the disease and are susceptible to IL-1 blockade.

Priming of neutrophils by IL-1 β , and reversion of the primed phenotype by rIL-1Ra. To further investigate the effects of IL-1 β and rIL-1Ra on neutrophils, we cultured healthy control neutrophils in the presence of IL-1 β , with or without preincubation with rIL-1Ra. Consistent with previous findings (27), IL-1 β increased the percentage of live cells after 20 hours in culture, which was abrogated by preincubation with rIL-1Ra (Figure 6A).

Delayed apoptosis of neutrophils is also described in patients with systemic inflammation (28,29). However, we found no significant difference in the number of apoptotic cells between patients with active systemic-onset JIA and patients in remission or healthy controls (Figure 6B).

After *in vitro* incubation with IL-1 β , neutrophils showed enhanced shedding of CD62L following stimulation with fMLP, which was reversed by preincubation with rIL-1Ra (Figure 6C). Interestingly, stimulation of neutrophils with IL-1 β increased the expression of both NFKB1 and IL1B itself, thus suggesting an autocrine loop, and this was revoked by rIL-1Ra (Figure 6D). These data, taken together with observations of the increased expression of NFKB1 and IL1B in neutrophils from patients with systemic-onset JIA (Figure 3E), indicate that neutrophils are responsive to IL-1 β and suggest that the therapeutic efficacy of rIL-1Ra in systemic-onset JIA could be at least partially attributed to its effect on neutrophils.

DISCUSSION

This study is the first to describe the phenotype, function, and transcriptome of neutrophils during the systemic inflammatory response of systemic-onset JIA. We showed that the high neutrophil counts at disease onset decreased dramatically after initiation of rIL-1Ra treatment, and found that neutrophils from patients

with active systemic-onset JIA up-regulated several immune-related processes and displayed a primed phenotype, which was reversed by IL-1 blockade.

Data on the role of neutrophils in systemic-onset JIA are limited. So far, only 2 studies have described the phenotype of neutrophils in systemic-onset JIA or its adult counterpart, adult-onset Still's disease (30,31). Unfortunately, those studies focused on one aspect of neutrophils and/or comprised patients with longstanding disease treated with several immunomodulatory drugs. Since we selected patients at the time of disease onset or a recent flare prior to initiation of therapy, it is more likely that the results of our study are a true reflection of the pathogenesis of the early inflammatory phase of systemic-onset JIA.

Unfortunately, due to the rarity of systemic-onset JIA and the practical limitations that come with neutrophil experiments (e.g., the impossibility of freezing), we were not able to replicate our findings in a separate cohort. Furthermore, small patient numbers and experimental variability made statistical testing sensitive to outliers. Ideally, sequencing experiments are performed in neutrophils of healthy children and patients with systemic-onset JIA during a period of inactive disease. As the phenotype and function of neutrophils from healthy controls and patients with systemic-onset JIA with inactive disease did not show clear differences, we focused our RNA-sequencing analyses on the comparison between active systemic-onset JIA and healthy controls. The large differences in transcriptome between neutrophils from patients with active systemic-onset JIA and neutrophils from healthy controls, in combination with the overlap with the transcriptome of other systemic inflammatory conditions, point toward the notion that there is a similar primed phenotype of neutrophils that cannot be attributed to differences in age or other confounding factors. This is supported by other studies that have shown no differences in neutrophil function between healthy children and adults (32,33).

The activated phenotype of neutrophils is in striking contrast to what we and others have observed in natural killer (NK) cells and monocytes from patients with systemic-onset JIA with active disease. Both NK cells and monocytes seem to have switched to a more counteractive or dampened activation state, suggesting that "immune-tolerizing" mechanisms are in place (5,34–36). As neutrophils did not show dampened responses, but rather had increased effector functions, we conclude that neutrophils may be a key player in the early phase of systemic-onset JIA.

The discovery of the TLR-4 ligand LPS as a major regulator of the transcriptome changes in systemic-onset

JIA neutrophils, as well as the observed strong overlap in the transcriptome of neutrophils between systemic-onset JIA and sepsis or experimental endotoxemia, suggest that *in vivo* exposure to high levels of TLR-4-stimulatory S100 proteins could explain the inflammatory gene expression in the neutrophils from patients with active systemic-onset JIA. Indeed, several studies have demonstrated the priming of neutrophils after stimulation with S100 proteins (37–42). However, other inflammatory proteins, such as IL-1 β , might also be responsible for the primed phenotype of neutrophils in systemic-onset JIA.

Neutrophils from patients with active systemic-onset JIA showed increased gene expression of IL-1 β , inflammasome components, and genes involved in the NF- κ B pathway, indicating that there was an increased production of IL-1 β . Recent studies highlighted the importance of neutrophils as a source of IL-1 β in several models of inflammatory and infectious diseases, and demonstrated the capability of neutrophils to secrete IL-1 β in either an inflammasome-dependent or inflammasome-independent manner (43–49). Those investigators concluded that, despite the relatively low production of IL-1 β by neutrophils compared to monocytes, neutrophils can still be a major source of IL-1 β , due to their abundance in the peripheral blood and at the site of inflammation. Furthermore, we found that IL-1 β itself can also prime neutrophils, a feature that can be reversed by rIL-1Ra. The dramatic decrease in neutrophil counts in patients with systemic-onset JIA upon initiation of rIL-1Ra therapy suggests that IL-1 and rIL-1Ra can also affect neutrophils *in vivo*. Taken together, these data extend the IL-1 signature in systemic-onset JIA by describing a novel role for neutrophils. This is supported by a recently published microarray analysis of adult-onset Still's disease, which showed that up-regulation of canakinumab-responsive genes was particularly pronounced in patients with strongly elevated neutrophil numbers (50).

Importantly, we found that patients whose disease duration at first visit to our clinic was relatively short had higher neutrophil counts and more immature neutrophils compared to patients who had already been experiencing symptoms for months. Moreover, albeit in only a limited number of patients, we found that patients with a shorter disease duration and high neutrophil counts had a complete response to rIL-1Ra, whereas patients with a longer time since onset of symptoms and normal neutrophil counts did not achieve inactive disease with rIL-1Ra. Consistent with previous observations (5), these data indicate that neutrophil counts could be a biomarker for the prediction of response to IL-1 blockade and therefore, in

conjunction with other biomarkers, might guide personalized treatment. This requires validation in a different and preferably larger cohort. Furthermore, our observations also fit the hypothesis that the initial phase of systemic-onset JIA is characterized by innate immune activation with an important role for neutrophils. This early auto-inflammatory phase could represent a “window of opportunity” for the early initiation of IL-1 blocking therapy before the appearance of more autoimmune-related features (2,3).

In summary, the results of this study indicate that neutrophils play an important role in the early inflammatory phase of systemic-onset JIA. Importantly, the findings confirm that neutrophil numbers and the inflammatory activity of systemic-onset JIA are strongly susceptible to IL-1 blockade.

ACKNOWLEDGMENTS

We would like to thank staff members at the Utrecht Sequence Facility, UMCU Luminex Core Facility, and UMCU Flow Core Facility for performing the RNA-sequencing and Luminex assays and for helping with the cell sorting.

AUTHOR CONTRIBUTIONS

All authors were involved in drafting the article or revising it critically for important intellectual content, and all authors approved the final version to be published. Dr. ter Haar had full access to all of the data in the study and takes responsibility for the integrity of the data and the accuracy of the data analysis.

Study conception and design. ter Haar, Tak, Leliefeld, van Loosdregt, Koenderman, Vastert, de Roock.

Acquisition of data. ter Haar, Mokry, Scholman, Meerding, de Jager, Verwoerd, Foell, Vogl, Roth, de Roock.

Analysis and interpretation of data. ter Haar, Mokry, van Loosdregt, Koenderman, Vastert, de Roock.

REFERENCES

- Mellins ED, Macaubas C, Grom AA. Pathogenesis of systemic juvenile idiopathic arthritis: some answers, more questions. *Nat Rev Rheumatol* 2011;7:416–26.
- Nigrovic PA. Is there a window of opportunity for treatment of systemic juvenile idiopathic arthritis? [review]. *Arthritis Rheumatol* 2014;66:1405–13.
- Giancane G, Minoia F, Davi S, Bracciolini G, Consolaro A, Ravelli A. IL-1 inhibition in systemic juvenile idiopathic arthritis. *Front Pharmacol* 2016;7:467.
- Vastert SJ, de Jager W, Noordman BJ, Holzinger D, Kuis W, Prakken BJ, et al. Effectiveness of first-line treatment with recombinant interleukin-1 receptor antagonist in steroid-naïve patients with new-onset systemic juvenile idiopathic arthritis: results of a prospective cohort study. *Arthritis Rheumatol* 2014;66:1034–43.
- Gattorno M, Piccini A, Lasigliè D, Tassi S, Brisca G, Carta S, et al. The pattern of response to anti-interleukin-1 treatment distinguishes two subsets of patients with systemic-onset juvenile idiopathic arthritis. *Arthritis Rheum* 2008;58:1505–15.
- Nauseef WM, Borregaard N. Neutrophils at work. *Nat Immunol* 2014;15:602–11.
- Wittkowski H, Frosch M, Wulffraat N, Goldbach-Mansky R, Kallinich T, Kuemmerle-Deschner J, et al. S100A12 is a novel molecular marker differentiating systemic-onset juvenile idiopathic arthritis from other causes of fever of unknown origin. *Arthritis Rheum* 2008;58:3924–31.
- Frosch M, Vogl T, Seeliger S, Wulffraat N, Kuis W, Viemann D, et al. Expression of myeloid-related proteins 8 and 14 in systemic-onset juvenile rheumatoid arthritis. *Arthritis Rheum* 2003;48:2622–6.
- Frosch M, Ahlmann M, Vogl T, Wittkowski H, Wulffraat N, Foell D, et al. The myeloid-related proteins 8 and 14 complex, a novel ligand of Toll-like receptor 4, and interleukin-1 β form a positive feedback mechanism in systemic-onset juvenile idiopathic arthritis. *Arthritis Rheum* 2009;60:883–91.
- De Jager W, Prakken B, Rijkers GT. Cytokine multiplex immunoassay: methodology and (clinical) applications. *Methods Mol Biol* 2009;514:119–33.
- Edgar R, Domrachev M, Lash AE. Gene expression omnibus: NCBI gene expression and hybridization array data repository. *Nucleic Acids Res* 2002;30:207–10.
- NCBI. Gene expression omnibus. URL: www.ncbi.nlm.nih.gov/geo/query/acc.cgi?acc=GSE103170.
- Chen J, Aronow BJ, Jegga AG. Disease candidate gene identification and prioritization using protein interaction networks. *BMC Bioinformatics* 2009;10:406.
- Barrett T, Wilhite SE, Ledoux P, Evangelista C, Kim IF, Tomaszewski M, et al. NCBI GEO: archive for functional genomics data sets: update. *Nucleic Acids Res* 2013;41(Database issue):D991–5.
- Subramanian A, Tamayo P, Mootha VK, Mukherjee S, Ebert BL, Gillette MA, et al. Gene set enrichment analysis: a knowledge-based approach for interpreting genome-wide expression profiles. *Proc Natl Acad Sci U S A* 2005;102:15545–50.
- Dunn OJ. Multiple comparisons using rank sums. *Technometrics* 1964;6:241–52.
- Rorvig S, Ostergaard O, Heegaard NH, Borregaard N. Proteome profiling of human neutrophil granule subsets, secretory vesicles, and cell membrane: correlation with transcriptome profiling of neutrophil precursors. *J Leukoc Biol* 2013;94:711–21.
- Rorvig S, Honore C, Larsson LI, Ohlsson S, Pedersen CC, Jacobsen LC, et al. Ficolin-1 is present in a highly mobilizable subset of human neutrophil granules and associates with the cell surface after stimulation with fMLP. *J Leukoc Biol* 2009;86:1439–49.
- Pillay J, Ramakers BP, Kamp VM, Loi AL, Lam SW, Hietbrink F, et al. Functional heterogeneity and differential priming of circulating neutrophils in human experimental endotoxemia. *J Leukoc Biol* 2010;88:211–20.
- Pillay J, Kamp VM, van Hoffen E, Visser T, Tak T, Lammers JW, et al. A subset of neutrophils in human systemic inflammation inhibits T cell responses through Mac-1. *J Clin Invest* 2012;122:327–36.
- Jung TM, Dailey MO. Rapid modulation of homing receptors (gp90MEL-14) induced by activators of protein kinase C: receptor shedding due to accelerated proteolytic cleavage at the cell surface. *J Immunol* 1990;144:3130–6.
- Demaret J, Venet F, Friggeri A, Cazalis MA, Plassais J, Jallades L, et al. Marked alterations of neutrophil functions during sepsis-induced immunosuppression. *J Leukoc Biol* 2015;98:1081–90.
- Miralda I, Uriarte SM, McLeish KR. Multiple phenotypic changes define neutrophil priming. *Front Cell Infect Microbiol* 2017;7:217.
- Sheppard O, Moore EE, Ryder J, Harken AH, Rezende-Neto JB, Banerjee A, et al. “Primed” human neutrophils on a standard peripheral blood smear. *J Am Coll Surg* 2002;195:731.
- De Kleijn S, Kox M, Sama IE, Pillay J, van Diepen A, Huijnen MA, et al. Transcriptome kinetics of circulating neutrophils during human experimental endotoxemia. *PLoS One* 2012;7:e38255.

26. Sengelov H, Follin P, Kjeldsen L, Lollike K, Dahlgren C, Borregaard N. Mobilization of granules and secretory vesicles during in vivo exudation of human neutrophils. *J Immunol* 1995;154:4157–65.
27. Watson RW, Rotstein OD, Parodo J, Bitar R, Marshall JC. The IL-1 β -converting enzyme (caspase-1) inhibits apoptosis of inflammatory neutrophils through activation of IL-1 β . *J Immunol* 1998;161:957–62.
28. Jimenez MF, Watson RW, Parodo J, Evans D, Foster D, Steinberg M, et al. Dysregulated expression of neutrophil apoptosis in the systemic inflammatory response syndrome. *Arch Surg* 1997;132:1263,9; discussion 1269–70.
29. Fanning NF, Kell MR, Shorten GD, Kirwan WO, Bouchier-Hayes D, Cotter TG, et al. Circulating granulocyte macrophage colony-stimulating factor in plasma of patients with the systemic inflammatory response syndrome delays neutrophil apoptosis through inhibition of spontaneous reactive oxygen species generation. *Shock* 1999;11:167–74.
30. Komiya A, Matsui T, Nogi S, Iwata K, Futami H, Takaoka H, et al. Neutrophil CD64 is upregulated in patients with active adult-onset Still's disease. *Scand J Rheumatol* 2012;41:156–8.
31. Omoyinmi E, Hamaoui R, Bryant A, Jiang MC, Athigapanich T, Eleftheriou D, et al. Mitochondrial and oxidative stress genes are differentially expressed in neutrophils of systemic-onset JIA patients treated with tocilizumab: a pilot microarray study. *Pediatr Rheumatol Online J* 2016;14:7.
32. Witko-Sarsat V, Halbwachs-Mecarelli L, Sermet-Gaudelus I, Bessou G, Lenoir G, Allen RC, et al. Priming of blood neutrophils in children with cystic fibrosis: correlation between functional and phenotypic expression of opsonin receptors before and after platelet-activating factor priming. *J Infect Dis* 1999;179:151–62.
33. Tsuji S, Iharada A, Kimata T, Shimo T, Hirabayashi M, Kaneko K. Production of nitric oxide is lower in Shiga toxin-stimulated neutrophils of infants compared to those of children or adults. *Tohoku J Exp Med* 2012;228:247–52.
34. De Jager W, Vastert SJ, Beekman JM, Wulffraat NM, Kuis W, Coffey PJ, et al. Defective phosphorylation of interleukin-18 receptor β causes impaired natural killer cell function in systemic-onset juvenile idiopathic arthritis. *Arthritis Rheum* 2009;60:2782–93.
35. Put K, Vandenhoute J, Avau A, van Nieuwenhuijze A, Brisse E, Dierckx T, et al. Inflammatory gene expression profile and defective interferon- γ and granzyme K in natural killer cells from systemic juvenile idiopathic arthritis patients. *Arthritis Rheumatol* 2017;69:213–24.
36. Ter Haar N, de Jager W, Scholman RS, Meerding J, Tak T, Liefeld P, et al. A1.06 phagocyte involvement in systemic onset juvenile idiopathic arthritis. *Ann Rheum Dis* 2016;75:A3.
37. Simard JC, Girard D, Tessier PA. Induction of neutrophil degranulation by S100A9 via a MAPK-dependent mechanism. *J Leukoc Biol* 2010;87:905–14.
38. Simard JC, Simon MM, Tessier PA, Girard D. Damage-associated molecular pattern S100A9 increases bactericidal activity of human neutrophils by enhancing phagocytosis. *J Immunol* 2011;186:3622–31.
39. Simard JC, Noel C, Tessier PA, Girard D. Human S100A9 potentiates IL-8 production in response to GM-CSF or fMLP via activation of a different set of transcription factors in neutrophils. *FEBS Lett* 2014;588:2141–6.
40. Rousseau LS, Pare G, Lachhab A, Naccache PH, Marceau F, Tessier P, et al. S100A9 potentiates the activation of neutrophils by the etiological agent of gout, monosodium urate crystals. *J Leukoc Biol* 2017;102:805–13.
41. Rouleau P, Vandal K, Ryckman C, Poubelle PE, Boivin A, Talbot M, et al. The calcium-binding protein S100A12 induces neutrophil adhesion, migration, and release from bone marrow in mouse at concentrations similar to those found in human inflammatory arthritis. *Clin Immunol* 2003;107:46–54.
42. Pruenster M, Kurz AR, Chung KJ, Cao-Ehlker X, Bieber S, Nussbaum CF, et al. Extracellular MRP8/14 is a regulator of β 2 integrin-dependent neutrophil slow rolling and adhesion. *Nat Commun* 2015;6:6915.
43. Guma M, Ronacher L, Liu-Bryan R, Takai S, Karin M, Corr M. Caspase 1-independent activation of interleukin-1 β in neutrophil-predominant inflammation. *Arthritis Rheum* 2009;60:3642–50.
44. Mankan AK, Dau T, Jenne D, Hornung V. The NLRP3/ASC/caspase-1 axis regulates IL-1 β processing in neutrophils. *Eur J Immunol* 2012;42:710–5.
45. Karmakar M, Sun Y, Hise AG, Rietsch A, Pearlman E. Cutting edge: IL-1 β processing during *Pseudomonas aeruginosa* infection is mediated by neutrophil serine proteases and is independent of NLRC4 and caspase-1. *J Immunol* 2012;189:4231–5.
46. Chen KW, Gross CJ, Sotomayor FV, Stacey KJ, Tschopp J, Sweet MJ, et al. The neutrophil NLRC4 inflammasome selectively promotes IL-1 β maturation without pyroptosis during acute *Salmonella* challenge. *Cell Rep* 2014;8:570–82.
47. Karmakar M, Katsnelson M, Malak HA, Greene NG, Howell SJ, Hise AG, et al. Neutrophil IL-1 β processing induced by pneumolysin is mediated by the NLRP3/ASC inflammasome and caspase-1 activation and is dependent on K⁺ efflux. *J Immunol* 2015;194:1763–75.
48. Perez-Figueroa E, Torres J, Sanchez-Zauco N, Contreras-Ramos A, Alvarez-Arellano L, Maldonado-Bernal C. Activation of NLRP3 inflammasome in human neutrophils by *Helicobacter pylori* infection. *Innate Immun* 2016;22:103–12.
49. Mohammadi N, Midiri A, Mancuso G, Patane F, Venza M, Venza I, et al. Neutrophils directly recognize group B *Streptococci* and contribute to interleukin-1 β production during infection. *PLoS One* 2016;11:e0160249.
50. Nirmala N, Brachat A, Feist E, Blank N, Specker C, Witt M, et al. Gene-expression analysis of adult-onset Still's disease and systemic juvenile idiopathic arthritis is consistent with a continuum of a single disease entity. *Pediatr Rheumatol Online J* 2015;13:50.

BRIEF REPORT

The Genetic Profile of Rheumatoid Factor–Positive Polyarticular Juvenile Idiopathic Arthritis Resembles That of Adult Rheumatoid Arthritis

Anne Hinks ¹, Miranda C. Marion,² Joanna Cobb,³ Mary E. Comeau,² Marc Sudman,⁴ Hannah C. Ainsworth,² John Bowes,¹ Juvenile Idiopathic Arthritis Consortium for ImmunoChip, Mara L. Becker,⁵ John F. Bohnsack,⁶ Johannes-Peter Haas,⁷ Daniel J. Lovell,⁴ Elizabeth D. Mellins,⁸ J. Lee Nelson,⁹ Ellen Nordal,¹⁰ Marilyn Punaro,¹¹ Ann M. Reed,¹² Carlos D. Rose,¹³ Alan M. Rosenberg,¹⁴ Marite Rygg,¹⁵ Samantha L. Smith,¹ Anne M. Stevens,¹⁶ Vibeke Videm,¹⁵ Carol A. Wallace,¹⁷ Lucy R. Wedderburn,¹⁸ Annie Yarwood,¹ Rae S. M. Yeung,¹⁹ Carl D. Langefeld,² Susan D. Thompson,⁴ Wendy Thomson,³ and Sampath Prahalad²⁰

Objective. Juvenile idiopathic arthritis (JIA) comprises 7 heterogeneous categories of chronic childhood arthritides. Approximately 5% of children with JIA have rheumatoid factor (RF)–positive arthritis, which phenotypically resembles adult rheumatoid arthritis (RA). Our objective was to compare and contrast the genetics of RF-positive polyarticular JIA with those of RA and selected other JIA categories, to more fully understand the pathophysiologic relationships of inflammatory arthropathies.

Methods. Patients with RF-positive polyarticular JIA (n = 340) and controls (n = 14,412) were genotyped using the ImmunoChip array. Single-nucleotide polymorphisms were tested for association using a logistic regression model adjusting for admixture proportions. We calculated weighted genetic risk scores (wGRS) of reported RA and JIA risk loci, and we compared the ability of these wGRS to predict RF-positive polyarticular JIA.

Results. As expected, the HLA region was strongly associated with RF-positive polyarticular JIA ($P = 5.51 \times 10^{-31}$). Nineteen of 44 RA risk loci and 6 of 27

The contents herein are solely the responsibility of the authors and do not necessarily represent the official views of the National Institutes of Health, other funders, the National Health Service, the National Institute for Health Research, or the Department of Health.

Genotyping of the US juvenile idiopathic arthritis (JIA), German JIA, and respective control collections was supported by the NIH (Center for Scientific Review [CSR] grants RC1-AR-058587 and U01-AI-067150S1). Patient recruitment and DNA preparation in the US were largely funded by the NIH (CSR grants N01-AR-42272, P01-AR-048929, P30-AR-473639, K23-AR-50177, and R01-AR-060893), with contributions from the Rheumatology Research Foundation, the Arthritis Foundation, the Val A. Browning Charitable Foundation (Salt Lake City, UT), and the Marcus Foundation, Inc. (Atlanta, GA). The Federal Ministry of Education and Research, Germany supported patient recruitment and sample preparation in Germany (BMBF grants 01GM0907 and 01 ZZ 0403). Support for computing resources and data analysis was provided by the Wake Forest School of Medicine Center for Public Health Genomics and the NIH (CSR grant R01-AR-057106). Genotyping of the UK JIA case samples was supported by Arthritis Research UK (grant 20385). Collection of some of the samples used in this study was supported by the NIHR Biomedical Research Centre. The Arthritis Research UK Centre for Genetics and Genomics laboratory is supported by the Manchester Academic Health Sciences Centre. The Childhood Arthritis Prospective Study was funded by Arthritis Research UK (grant 20542). The Childhood Arthritis Response to Medication Study was funded by Sparks UK (grant 08ICH09), Arthritis Research UK (grant 20164), and the Medical Research Council (grant MR/M004600/1) and supported by the NIHR Biomedical Research Centres at Great Ormond Street Hospital for Children NHS Foundation Trust, University College London Hospitals Trust, and the NIHR Clinical Research Network. Patient recruitment and DNA preparation in Canada was supported by the Canadian

Institutes of Health Research (grant FRN-82517), the Canadian Arthritis Society, and the Canadian Arthritis Network. The Nord-Trøndelag Health (HUNT) Study, which contributed control samples, is a collaboration between the HUNT Research Centre (Faculty of Medicine and Health Sciences, Norwegian University of Science and Technology), Nord-Trøndelag County Council, Central Norway Health Authority, and the Norwegian Institute of Public Health and was funded by the Liaison Committee between the Central Norway Regional Health Authority and the Norwegian University of Science and Technology. Sample recruitment was supported in part by the NIH (National Institute of Arthritis and Musculoskeletal and Skin Diseases grants N01-AR-62277 and AR-053483, National Institute of General Medical Sciences grant GM-103510, and National Institute of Allergy and Infectious Diseases grant AI-082714) and by the Texas Scottish Rite Hospital for Children (grant 1296353). Genotyping of control samples was supported, in part, by the Juvenile Diabetes Research Foundation International and the NIH (CSR grant U01-DK-062418).

¹Anne Hinks, PhD, John Bowes, PhD, Samantha L. Smith, PhD, Annie Yarwood, PhD: University of Manchester, Manchester, UK; ²Miranda C. Marion, MA, Mary E. Comeau, MA, Hannah C. Ainsworth, BS, Carl D. Langefeld, PhD: Wake Forest University School of Medicine, Winston-Salem, North Carolina; ³Joanna Cobb, PhD, Wendy Thomson, PhD: University of Manchester and Central Manchester University Hospitals NHS Foundation Trust, Manchester, UK; ⁴Marc Sudman, BA, Daniel J. Lovell, MD, MPH, Susan D. Thompson, PhD: Cincinnati Children's Hospital Medical Center, Cincinnati, Ohio; ⁵Mara L. Becker, MD: Children's Mercy Kansas City, Kansas City, Missouri; ⁶John F. Bohnsack, MD: University of Utah, Salt Lake City; ⁷Johannes-Peter Haas, MD: German Centre for Pediatric and Adolescent Rheumatology, Garmisch-Partenkirchen, Germany; ⁸Elizabeth D. Mellins, MD: Stanford University, Stanford, California; ⁹J. Lee Nelson,

oligoarticular/RF-negative polyarticular JIA risk loci were associated with RF-positive polyarticular JIA ($P < 0.05$). The RA wGRS predicted RF-positive polyarticular JIA (area under the curve [AUC] 0.71) better than did the oligoarticular/RF-negative polyarticular JIA wGRS (AUC 0.59). The genetic profile of patients with RF-positive polyarticular JIA was more similar to that of RA patients with age at onset 16–29 years than to that of RA patients with age at onset ≥ 70 years.

Conclusion. RF-positive polyarticular JIA is genetically more similar to adult RA than to the most common JIA categories and thus appears to be a childhood-onset presentation of autoantibody-positive RA. These findings suggest common disease mechanisms, which could lead to novel therapeutic targets and shared treatment strategies.

Juvenile idiopathic arthritis (JIA) is a heterogeneous collection of chronic arthropathies with distinct clinical and laboratory features, but all manifest with arthritis in one or more joints and present before the 16th birthday. The International League of Associations for Rheumatology (ILAR) criteria for JIA recognize 7 JIA categories (1). There is robust evidence for genetic factors conferring susceptibility to all forms of JIA (2). Without a clearer understanding of the genetic similarities and distinctions, the clinically different categories must be studied separately. Unfortunately, this stratification results in smaller sample sizes and reduced power to detect association. Thus, the JIA Consortium for Immunochip was formed with the intent to bring together the large sample sizes required for investigation of the rarer JIA categories. A full list of affiliations for consortia appears in Supplementary Information, available on the *Arthritis & Rheumatology* web site at <http://onlinelibrary.wiley.com/doi/10.1002/art.40443/abstract>. The Immunochip is a custom microarray designed by the Immunochip Consortium to fine-map autoimmune disease-associated loci from 11 autoimmune phenotypes including adult

rheumatoid arthritis (RA) (3). The Immunochip assays 196,524 variants representing ~186 loci, including dense coverage of the major histocompatibility complex region. Investigation of children with the most common categories of JIA, oligoarticular and rheumatoid factor (RF)-negative polyarticular JIA, which comprise ~70% of all cases in children of European descent, resulted in the identification of 17 loci associated with JIA at genome-wide levels of significance. In addition, 11 loci showed suggestive evidence of association (4).

Approximately 5% of children with JIA demonstrate the presence of RF and antibodies directed against citrullinated peptides, such as anti-cyclic citrullinated peptide (anti-CCP) antibodies, which are characteristic biomarkers observed in adults with seropositive RA. These children and young people tend to present at a later age at onset than those with oligoarticular or RF-negative polyarticular JIA, and often tend to have erosive disease with worse long-term outcomes. Thus, children with RF-positive polyarticular JIA phenotypically resemble adults with RA and could be considered to have childhood-onset RA. In contrast to the robust genetic studies that include large cohorts of patients with RA and oligoarticular/RF-negative polyarticular JIA, studies of children with RF-positive polyarticular JIA have been limited to small-scale candidate gene studies. These include investigations of association with the shared epitope encoding HLA-DRB1 alleles as well as several candidate loci associated with RA (5,6). To date, a systematic analysis of genetic risk for RF-positive polyarticular JIA has not been completed, largely due to the lack of sufficiently sized cohorts.

To progress beyond this limitation in cohort size and also advance the understanding of RF-positive polyarticular JIA, we have used the Immunochip to compare and contrast the genetics of RF-positive polyarticular JIA to other categories of JIA and RA. This may provide a greater understanding of the genetic architecture of RF-positive polyarticular JIA.

MD: Fred Hutchinson Cancer Research Center and University of Washington, Seattle; ¹⁰Ellen Nordal, MD, PhD: University Hospital of North Norway and UIT The Arctic University of Norway, Tromsø, Norway; ¹¹Marilynn Punaro, MD: Arthritis Clinic Texas Scottish Rite Hospital for Children and University of Texas Southwestern Medical Center, Dallas; ¹²Ann M. Reed, MD: Duke University School of Medicine, Durham, North Carolina; ¹³Carlos D. Rose, MD: DuPont Children's Hospital, Wilmington, Delaware; ¹⁴Alan M. Rosenberg, MD: University of Saskatchewan, Saskatoon, Saskatchewan, Canada; ¹⁵Marite Rygg, MD, PhD, Vibeke Videm, MD, PhD: Norwegian University of Science and Technology and St. Olav's University Hospital, Trondheim, Norway; ¹⁶Anne M. Stevens, MD: Seattle Children's Research Institute and University of Washington, Seattle; ¹⁷Carol A. Wallace, MD: Seattle Children's Hospital and Research Institute, Seattle, Washington; ¹⁸Lucy R. Wedderburn, MD, PhD: University College London and NIHR Great Ormond Street Hospital Biomedical Research Centre, London, UK; ¹⁹Rae S. M. Yeung, MD: The Hospital

for Sick Children and University of Toronto, Toronto, Ontario, Canada; ²⁰Sampath Prahalad, MD, MSc: Emory University School of Medicine and Children's Healthcare of Atlanta, Atlanta, Georgia.

Dr. Hinks and Ms Marion contributed equally to this work. Drs. Langefeld, Thompson, Thomson, and Prahalad contributed equally to this work.

Dr. Mellins has received consulting fees from Novartis (less than \$10,000). Dr. Stevens owns stock or stock options in Amgen. Dr. Prahalad has received consulting fees from Novartis (less than \$10,000).

Address correspondence to Sampath Prahalad, MD, MSc, Department of Pediatrics, Emory University School of Medicine, Division of Pediatric Rheumatology, 2015 Uppergate Drive NE, Atlanta, GA 30322. E-mail: sprahal@emory.edu.

Submitted for publication August 1, 2017; accepted in revised form February 1, 2018.

PATIENTS AND METHODS

All JIA patients had a diagnosis of polyarticular JIA according to the ILAR classification criteria (1) and were positive for RF and/or anti-CCP antibodies. The ILAR criteria do not include any recommendation for anti-CCP testing; therefore, anti-CCP is not routinely tested for in pediatric rheumatology cohorts. We do have anti-CCP data on 73 subjects (~20%). Of those tested, the prevalence of anti-CCP positivity is 79%. Among patients who were RF positive, 78% were also positive for anti-CCP, which is comparable to the value of ~59% reported in the literature for patients with RF-positive polyarticular JIA (7). Cases were ascertained at institutions in the US, UK, Germany, Canada, and Norway. Genotyping was performed using the Illumina ImmunoChip genotyping array. There were 421 patients with RF-positive polyarticular JIA and 16,403 controls before quality control. Standard single-nucleotide polymorphism (SNP) genotyping and sample quality control were performed as previously described in the ImmunoChip studies of other JIA categories (4,8). Details of cohorts can be found in Supplementary Information, <http://onlinelibrary.wiley.com/doi/10.1002/art.40443/abstract>.

For comparison with groups of RA patients with different ages at onset, RA patients in the UK who had been genotyped on the ImmunoChip array were available from a cohort described previously (9). RA patients were selected if they fell into 2 categories of age at onset, those with early-onset RA (ages 16–29 years; $n = 370$) and those with later-onset RA (ages ≥ 70 years; $n = 259$). In total, 8,675 controls from the RA cohort overlapped with the UK controls used for the JIA cohorts. To preserve independence, these controls were randomly split into 2 groups (see Supplementary Table 1, <http://onlinelibrary.wiley.com/doi/10.1002/art.40443/abstract>).

To test for SNP association with RF-positive polyarticular JIA, a logistic regression model was computed using Caucasian admixture proportions calculated by the program ADMIXTURE (10) as covariates. The additive genetic model was used for the primary analysis unless there was significant departure from additivity, whereupon the most associated genetic model was used. For markers on the X-chromosome, the logistic model was stratified by sex and inference was based on the resulting weighted inverse normal meta-analysis. Imputation of SNP genotypes was completed using IMPUTE2 with the 1000 Genomes Phase 1 integrated reference panel (11). To test for association with the imputed data, a logistic regression model with admixture adjustment was computed on the imputed allele dosage. Only SNPs that passed standard imputation quality control and had information score >0.5 and confidence score >0.9 were considered for association analysis. For each region we reported the strongest associated genotyped SNP. If there was an imputed SNP that showed stronger association than the genotyped SNP, then both SNPs were reported; imputed SNPs required at least 2 SNPs in strong linkage disequilibrium (LD) to also exhibit association. Regional plots of association were computed using LocusZoom (12).

The 45 non-HLA risk loci associated with RA using the ImmunoChip (9) and the 27 oligoarticular/RF-negative polyarticular JIA non-HLA risk loci (4) were assessed to determine if they were also associated with RF-positive polyarticular JIA in our cohort. Two weighted genetic risk scores (wGRS) were calculated. The first used the RA risk loci (9) and the second used the oligoarticular/RF-negative polyarticular JIA risk loci (4). The RA

wGRS analysis started with the 46 SNPs (including HLA) ($P < 5 \times 10^{-8}$) associated with RA as reported by Eyre et al (9). However, no proxies ($r^2 > 0.8$) were available for rs13397 at *IRAK1*, rs2240336 at *PADI4*, rs39984 at *GIN1*, or rs10683701 at *KIF5A*; therefore, there were 42 SNPs in the wGRS. The HLA region was captured through the HLA-DRB1 tag SNP rs660895 (13).

The JIA wGRS analysis started with the 28 SNPs (including HLA) ($P < 1 \times 10^{-6}$) associated with oligoarticular/RF-negative polyarticular JIA as reported by Hinks et al (4). However, no proxies were available for rs7909519 at *IL2RA*, rs2266959 at *UBE2L3*, and rs7069750 at *FAS*, so the final number of SNPs in the wGRS was 25. The HLA association was captured using the top SNP (rs7775055) in the region.

To calculate the wGRS for an individual, the natural log of the reported odds ratio was multiplied by the number of risk alleles for each SNP and summed. Individuals with missing genotypes were assigned (imputed) a score based on the expectation from the allele frequency and assuming Hardy-Weinberg equilibrium. Logistic regression was used to compare each wGRS between patients and controls. In addition, receiver operating characteristic (ROC) curves defined by the sensitivity and specificity of each wGRS were generated, and the area under the curve (AUC) was calculated. The GRS analysis did not include the imputed genotype data. Analysis was performed using Stata software, version 13.1 (StataCorp). We tested whether there was a difference between the areas under the 2 ROC curves using DeLong's method as implemented in SAS software (SAS Institute).

RESULTS

After quality control there were 340 patients with RF-positive polyarticular JIA (mean \pm SD age at onset 10.2 ± 4.2 years) and 14,412 controls (Table 1). For the X-chromosome analysis, there were 292 female patients, 8,002 female controls, 48 male patients, and 6,410 male controls.

Despite the modest sample size, association with the HLA region was identified, with the most significant association at rs3129769, near HLA-DRB1 ($P = 5.51 \times 10^{-31}$), a SNP in strong LD ($r^2 = 0.88$) with the HLA-DRB1 SNP reported in RA (rs660895; $P = 2.14 \times 10^{-29}$). These SNPs are tagging the HLA-DRB1*0401 classic allele (14). There was no significant association of the most associated SNP in the HLA region reported in the oligoarticular/RF-negative polyarticular JIA ImmunoChip study, rs7775055 ($P = 0.08$).

Table 1. Study populations of patients with rheumatoid factor-positive polyarticular juvenile idiopathic arthritis and controls before and after quality control

Population	Before quality control		After quality control	
	Patients	Controls	Patients	Controls
US	272	5,985	222	4,408
UK	104	8,940	94	8,579
Germany	15	489	1	480
Norway	14	989	13	945
Canada	16	–	10	–
Total	421	16,403	340	14,412

The most significantly associated loci identified in the oligoarticular/RF-negative polyarticular JIA and RA Immunochip study were assessed for association with RF-positive polyarticular JIA. Of the 27 non-HLA SNPs most strongly associated with oligoarticular/RF-negative polyarticular JIA (4), 6 showed evidence for association with RF-positive polyarticular JIA ($P < 0.05$) (see Supplementary Table 2, <http://onlinelibrary.wiley.com/doi/10.1002/art.40443/abstract>). Of the 44 SNPs (not including HLA and *KIF5A* regions, the latter being a deletion polymorphism and not analyzed in this study) most strongly associated with RA (9), 19 showed evidence for association with RF-positive polyarticular JIA ($P < 0.05$) (see Supplementary Table 3, <http://onlinelibrary.wiley.com/doi/10.1002/art.40443/abstract>).

The wGRS generated using the top RA loci was compared with the wGRS generated using the top oligoarticular/RF-negative polyarticular JIA loci to see which best predicted cases of RF-positive polyarticular JIA compared to controls. The wGRS generated using the top RA loci from Eyre et al (9) significantly improved prediction of cases of RF-positive polyarticular JIA compared to the wGRS generated using the top oligoarticular/RF-negative polyarticular JIA loci (AUC 0.71 versus AUC 0.59, respectively; $P = 8.26 \times 10^{-33}$) (Figure 1). The RA wGRS showed comparable prediction of cases of RF-positive polyarticular JIA and cases of early-onset RA (AUC 0.71 versus AUC 0.75, respectively; $P = 0.25$) (Figure 2A) but was less effective at predicting later-onset RA compared to predicting RF-positive polyarticular JIA (AUC 0.62 versus AUC 0.71, respectively; $P = 1.65 \times 10^{-5}$) (Figure 2B). This

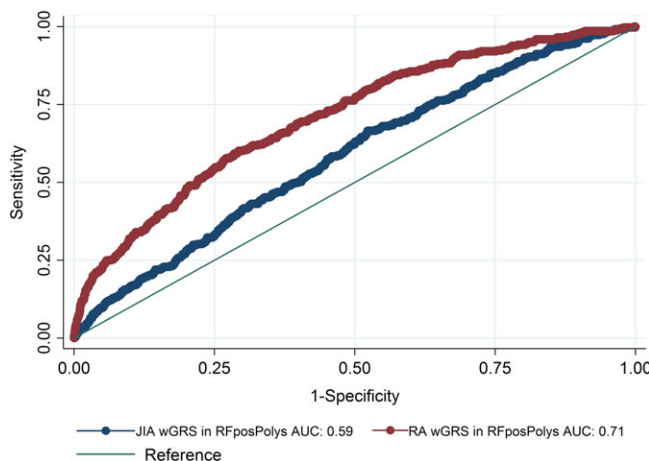


Figure 1. Comparison of the weighted genetic risk score (wGRS) generated using loci associated with the highest risk of rheumatoid arthritis (RA) with the wGRS generated using loci associated with the highest risk of oligoarticular/rheumatoid factor (RF)-negative polyarticular juvenile idiopathic arthritis (JIA) for the purpose of predicting cases of RF-positive polyarticular JIA (RFposPolys). AUC = area under the curve.

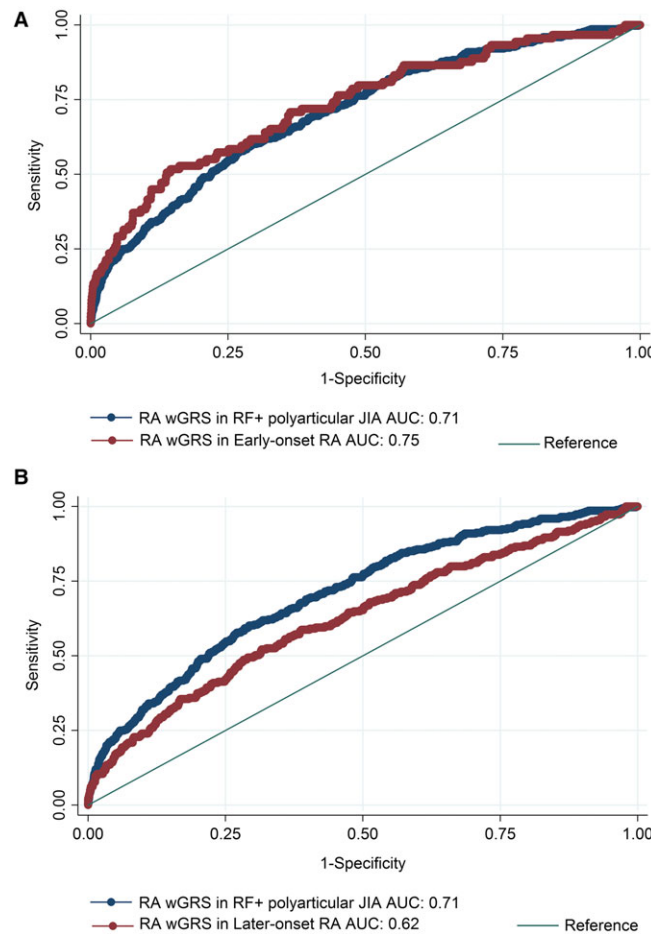


Figure 2. A, Comparison of the ability of the wGRS generated using loci associated with the highest risk of RA to predict cases of RF-positive polyarticular JIA with the ability of the same wGRS to predict cases of early-onset RA (ages 16–29 years). B, Comparison of the ability of the wGRS generated using loci associated with the highest risk of RA to predict cases of RF-positive polyarticular JIA with the ability of the same wGRS to predict cases of later-onset RA (age ≥ 70 years). See Figure 1 for definitions.

suggests that the genetic profile of patients with RF-positive polyarticular JIA is more similar to that of younger RA patients than to that of older RA patients.

No region outside the HLA region reached genome-wide significance; however, 13 regions had suggestive association ($P < 1 \times 10^{-4}$). Imputed SNP results were included when the imputed SNP had a better imputed P value than the most significant directly genotyped SNP in the region (see Supplementary Table 4 and Supplementary Figures 1 and 2, <http://onlinelibrary.wiley.com/doi/10.1002/art.40443/abstract>). Supplementary Table 4 denotes imputed SNPs with a “b” superscript. Of the 13 regions most strongly associated with RF-positive polyarticular JIA, 5 contained SNPs (or SNPs in LD, $r^2 > 0.8$) with some previous evidence for association with RA (9).

DISCUSSION

This represents the largest genetic study of RF-positive polyarticular JIA to date. We provide evidence that this uncommon category of JIA, which is phenotypically similar to adult seropositive RA, is also genetically more similar to adult RA than to the most common JIA categories, which lack the characteristic biomarkers (RF and anti-CCP). The results of the wGRS analysis generated from the top RA-associated loci predicted RF-positive polyarticular JIA case-control status better than did the wGRS generated from the oligoarticular/RF-negative polyarticular JIA top hits.

We investigated whether any of the previously associated RA loci (9) or oligoarticular/RF-negative polyarticular JIA loci (4) showed evidence for association with RF-positive polyarticular JIA. Nineteen of the 44 SNPs reaching genome-wide significance thresholds with RA show evidence for association with RF-positive polyarticular JIA ($P < 0.05$). There appears to be less overlap with the oligoarticular/RF-negative polyarticular JIA loci since only 6 of the 27 oligoarticular/RF-negative polyarticular JIA SNPs show evidence for association with RF-positive polyarticular JIA. Formal testing for a difference in the 2 proportions using the likelihood ratio test yielded suggestive but not statistically significant results ($P = 0.0676$).

As might be expected, the most significant association was within the HLA region, and the SNP is in strong LD ($r^2 = 0.88$) with the most associated HLA SNP in RA. We have previously reported the HLA associations for all the categories of JIA (8) and found that RF-positive polyarticular JIA has distinct HLA associations compared to the other categories of JIA. The HLA-DRB1 amino acid position 13 is most strongly associated with RF-positive polyarticular JIA, with a histidine residue driving the association. This is the same HLA association as found in RA (8,13). A glycine residue at this same amino acid position drives the association in oligoarticular/RF-negative polyarticular JIA. This supports separation of RF-positive polyarticular JIA from the other JIA categories and confirms that RF-positive polyarticular JIA is more similar to RA than to other JIA categories (8).

Other than the HLA region, we were unable to identify novel loci meeting genome-wide levels of significance. This may be expected, as despite being the largest genetic study to date for RF-positive polyarticular JIA, our study is still relatively underpowered to detect odds ratios of ~1.1–1.2, as are often observed in autoimmune diseases. We have identified 13 regions showing association at a significance level of $P < 1 \times 10^{-4}$, which will need validation in an independent cohort to confirm. The strongest non-HLA association for RF-positive

polyarticular JIA was rs9610687, which lies upstream of the *RAC2* gene. Mutations within *RAC2* are associated with neutrophil immunodeficiency syndrome. Polymorphisms within the *IL2RB* gene, close to *RAC2*, have previously been associated with oligoarticular/RF-negative polyarticular JIA (4) and with RA (9). However, the oligoarticular/RF-negative polyarticular JIA-associated SNP (rs2284033) is ~500 kb from the RF-positive polyarticular JIA-associated SNP. The oligoarticular/RF-negative polyarticular JIA-associated SNP in *IL2RB* was not significantly associated with RF-positive polyarticular JIA ($P = 0.70$). In RA the most associated SNP (rs3218251) in this region again lies in the *IL2RB* gene, and this SNP is not in LD with the oligoarticular/RF-negative polyarticular JIA-associated SNP.

Although this study has numerous important findings, there are some important limitations. First, the RA patients included in the wGRS analysis had a mixture of both seronegative and seropositive disease (although the largest proportion were seropositive [68% anti-CCP positive]), potentially diluting or masking effect sizes. Second, the UK RA patients and controls included in these analyses are part of the RA Immunochip study by Eyre et al (9), and this lack of independence could artificially inflate the predictive ability of the wGRS. A more recent genetic study in RA reported by Okada et al (15) identified 101 genetic regions associated with RA. Many of these regions were not covered on the Immunochip array and so it was not possible to use these in the wGRS analysis (9).

The current ILAR classification criteria (1) are based on clinical features and family history, and it is not always straightforward to assign children to a category. In addition, there still remains heterogeneity, especially in terms of prognosis, between and within the categories of JIA. In time, clear delineation of the genetics of JIA categories may contribute to a more refined classification system. While it has been recognized for many years that RF-positive polyarticular JIA is clinically and serologically similar to adult RA, there have been no systematic investigations of possible genetic overlap between these phenotypes of inflammatory arthritis. One reason for this is that several JIA categories are rare, and large-scale international collaborations such as this, and the one established for systemic-onset JIA, another rare category (16), are necessary to build up sample sizes for genetic studies of these phenotypes.

We have now shown that RF-positive polyarticular JIA is genetically more similar to adult RA than to the oligoarticular/RF-negative polyarticular JIA categories. Demonstrating that RF-positive polyarticular JIA genetically appears to be a childhood-onset presentation of RA supports further investigation of this phenotype along with the factors influencing an early-onset presentation. Broadly,

our results suggest that genetic profiling might enhance our ability to classify and understand the different phenotypes of inflammatory arthritis. Our results also provide a rationale for studying both diseases together and for translating therapeutic trials of successful pharmacologic agents from adult RA to RF-positive polyarticular JIA and vice versa.

ACKNOWLEDGMENTS

We thank Paul Gilbert for preparing UK JIA case samples for genotyping and Mary Ryan for preparing US JIA and the Cincinnati local control samples. We would like to thank the Wellcome Trust Sanger Institute Genotyping Facility and in particular Emma Gray, Sue Bumpstead, Doug Simpkin, and Hannah Blackburn for typing some of the UK samples. We gratefully acknowledge contributions from physicians at Cincinnati Children's Hospital Medical Center and collaborating clinics. We also acknowledge the assistance of Bronte Clifford and Lori Ponder for patient recruitment and coordination of clinical information at the University of Utah and Emory University, respectively. The Cincinnati normal control DNA collection was supported and made available by Cincinnati Children's Hospital Medical Center. We would like to acknowledge the assistance given by IT Services and the use of the Computational Shared Facility at The University of Manchester. We acknowledge Nils Thomas Songstad and Nina Moe for patient recruitment in the Norwegian subcohort of the Nordic JIA study, Kristin Rian for technical support, and Helse Nord Research Grants for funding collection of samples used in this study from Tromsø, Norway. Johanna Hadler, Katie Cremin, Karena Pryce, and Jessica Harris are acknowledged for excellent technical assistance. We acknowledge use of DNA from the UK Blood Services collection of common controls, which is funded by the Wellcome Trust (grant 076113/C/04/Z) and by UK NIHR program grant RP-PG-0310-1002 to the NHS Blood and Transplant. We acknowledge the use of DNA from the British 1958 Birth Cohort collection, which is funded by the UK Medical Research Council (grant G0000934) and the Wellcome Trust (grant 068545/Z/01). We thank Peter K. Gregersen at the Feinstein Institute for providing US control genotyping from the Genotype and Phenotype registry (www.gapregistry.org), supported by the NIH (grant RC2-AR-059092). We thank the National Institute of Diabetes and Digestive and Kidney Diseases Inflammatory Bowel Disease Genetics Consortium for providing North American control genotyping supported by the NIH (CSR grants DK-062431, DK-062422, DK-062420, DK-062432, DK-062423, DK-062413, and DK-062429).

AUTHOR CONTRIBUTIONS

All authors were involved in drafting the article or revising it critically for important intellectual content, and all authors approved the final version to be published. Dr. Prahalad had full access to all of the data in the study and takes responsibility for the integrity of the data and the accuracy of the data analysis.

Study conception and design. Hinks, Marion, Cobb, Langefeld, Thompson, Thomson, Prahalad.

Acquisition of data. Hinks, Marion, Cobb, Comeau, Sudman, Ainsworth, Bowes, Becker, Bohnsack, Haas, Lovell, Mellins, Nelson, Nordal, Punaro, Reed, Rose, Rosenberg, Rygg, Smith, Stevens, Videm, Wallace, Wedderburn, Yarwood, Yeung, Langefeld, Thompson, Thomson, Prahalad.

Analysis and interpretation of data. Hinks, Marion, Cobb, Comeau, Sudman, Ainsworth, Bowes, Langefeld, Thompson, Thomson, Prahalad.

REFERENCES

- Petty RE, Southwood TR, Manners P, Baum J, Glass DN, Goldenberg J, et al. International League of Associations for Rheumatology classification of juvenile idiopathic arthritis: second revision, Edmonton, 2001. *J Rheumatol* 2004;31:390-2.
- Prahalad S, Zeff AS, Pimentel R, Clifford B, McNally B, Mineau GP, et al. Quantification of the familial contribution to juvenile idiopathic arthritis. *Arthritis Rheum* 2010;62:2525-9.
- Cortes A, Brown MA. Promise and pitfalls of the ImmunoChip. *Arthritis Res Ther* 2011;13:101.
- Hinks A, Cobb J, Marion MC, Prahalad S, Sudman M, Bowes J, et al. Dense genotyping of immune-related disease regions identifies 14 new susceptibility loci for juvenile idiopathic arthritis. *Nat Genet* 2013;45:664-9.
- Prahalad S, Conneely KN, Jiang Y, Sudman M, Wallace CA, Brown MR, et al. Susceptibility to childhood-onset rheumatoid arthritis: investigation of a weighted genetic risk score that integrates cumulative effects of variants at five genetic loci. *Arthritis Rheum* 2013;65:1663-7.
- Prahalad S, Thompson SD, Conneely KN, Jiang Y, Leong T, Proznick J, et al. Hierarchy of risk of childhood-onset rheumatoid arthritis conferred by HLA-DRB1 alleles encoding the shared epitope. *Arthritis Rheum* 2012;64:925-30.
- Tebo AE, Jaskowski T, Davis KW, Whiting A, Clifford B, Zeff A, et al. Profiling anti-cyclic citrullinated peptide antibodies in patients with juvenile idiopathic arthritis. *Pediatr Rheumatol Online J* 2012;10:29.
- Hinks A, Bowes J, Cobb J, Ainsworth HC, Marion MC, Comeau ME, et al. Fine-mapping the MHC locus in juvenile idiopathic arthritis (JIA) reveals genetic heterogeneity corresponding to distinct adult inflammatory arthritic diseases. *Ann Rheum Dis* 2017;76:765-72.
- Eyre S, Bowes J, Diogo D, Lee A, Barton A, Martin P, et al. High-density genetic mapping identifies new susceptibility loci for rheumatoid arthritis. *Nat Genet* 2012;44:1336-40.
- Alexander DH, Novembre J, Lange K. Fast model-based estimation of ancestry in unrelated individuals. *Genome Res* 2009;19:1655-64.
- Howie BN, Donnelly P, Marchini J. A flexible and accurate genotype imputation method for the next generation of genome-wide association studies. *PLoS Genet* 2009;5:e1000529.
- Pruim RJ, Welch RP, Sanna S, Teslovich TM, Chines PS, Gliedt TP, et al. LocusZoom: regional visualization of genome-wide association scan results. *Bioinformatics* 2010;26:2336-7.
- Raychaudhuri S, Sandor C, Stahl EA, Freudenberg J, Lee HS, Jia X, et al. Five amino acids in three HLA proteins explain most of the association between MHC and seropositive rheumatoid arthritis. *Nat Genet* 2012;44:291-6.
- De Bakker PI, McVean G, Sabeti PC, Miretti MM, Green T, Marchini J, et al. A high-resolution HLA and SNP haplotype map for disease association studies in the extended human MHC. *Nat Genet* 2006;38:1166-72.
- Okada Y, Wu D, Trynka G, Raj T, Terao C, Ikari K, et al. Genetics of rheumatoid arthritis contributes to biology and drug discovery. *Nature* 2014;506:376-81.
- Ombrello MJ, Arthur VL, Remmers EF, Hinks A, Tachmazidou I, Grom AA, et al. Genetic architecture distinguishes systemic juvenile idiopathic arthritis from other forms of juvenile idiopathic arthritis: clinical and therapeutic implications. *Ann Rheum Dis* 2017;76:906-13.

BRIEF REPORT

Novel *UNC13D* Intronic Variant Disrupting an NF- κ B Enhancer in a Patient With Recurrent Macrophage Activation Syndrome and Systemic Juvenile Idiopathic Arthritis

Grant S. Schulert,¹ Mingce Zhang,² Ammar Husami,¹ Ndate Fall,¹ Hermine Brunner,¹ Kejian Zhang,¹ Randy Q. Cron,² and Alexei A. Grom¹

Objective. Macrophage activation syndrome (MAS) is a life-threatening complication of systemic juvenile idiopathic arthritis (JIA) and has pathologic similarity to hemophagocytic lymphohistiocytosis (HLH). Intronic variants in *UNC13D* are found in patients with familial HLH type 3 (FHLH3), but the role of noncoding variants in MAS is unknown. The objective of this study was to identify deep intronic *UNC13D* variants in patients with MAS.

Methods. A custom enrichment library was constructed to sequence a genomic region of ~1 Mb flanking *UNC13D* in 24 patients with systemic JIA, recurrent MAS, and negative results of prior genetic (exon/coding) testing. The functional consequences of intronic variants were assessed using quantitative polymerase chain reaction in patient-derived peripheral blood mononuclear cells (PBMCs), electromobility shift assay, in vitro

transcriptional enhancer assays, and natural killer (NK) cell degranulation assays.

Results. We evaluated a patient with systemic JIA and recurrent MAS in whom a novel functional intronic variant in *UNC13D*, c.117+143A>G, was observed. This variant occurred in a proposed regulatory region that drives lymphocyte-specific *UNC13D* expression and is associated with reduced transcript levels in patient PBMCs. This variant also disrupted NF- κ B binding to a functional transcriptional enhancer, leading to reduced enhancer activity in vitro. Partial knockdown of *UNC13D* expression also led to impaired NK cell degranulation. An additional patient was identified with a previously described *UNC13D* intronic variant, for a total noncoding variant hit rate of 8.3% (2 of 24).

Conclusion. These findings highlight the notion that intronic variants in key regulatory regions may be associated with MAS in patients with systemic JIA and support deep sequencing approaches when causative coding variants are not identified.

Supported by the NIH (grant R01-AR-059049 to Dr. Grom). Dr. Schulert's work was supported by the Rheumatology Research Foundation (Scientist Development award) and the Cincinnati Children's Research Foundation (Procter Scholar award). Dr. M. Zhang's work was supported by the Histiocytosis Association, the UAB Center for Genomic Medicine, and HudsonAlpha.

¹Grant S. Schulert, MD, PhD, Ammar Husami, BS, Ndate Fall, MS, Hermine Brunner, MD, MSc, Kejian Zhang, PhD, Alexei A. Grom, MD: Cincinnati Children's Hospital Medical Center and University of Cincinnati College of Medicine, Cincinnati, Ohio; ²Mingce Zhang, MD, PhD, Randy Q. Cron, MD, PhD: Children's Hospital of Alabama, University of Alabama at Birmingham.

Drs. Schulert and M. Zhang contributed equally to this work.

Dr. Schulert has received consulting fees from Novartis (less than \$10,000). Dr. Cron has received consulting fees from Medac Pharma, UCB, and Sobi (less than \$10,000 each) and research support from Sobi. Dr. Grom has received consulting fees from Novartis and NovImmune (less than \$10,000 each) and research support from those companies.

Address correspondence to Randy Q. Cron, MD, PhD, Division of Pediatric Rheumatology, Children's Hospital of Alabama, University of Alabama at Birmingham, Children's Park Place, Suite G10, 1601 4th Avenue South, Birmingham, AL 35233 (e-mail: rcron@peds.uab.edu); or to Alexei A. Grom, MD, Division of Rheumatology, ML 4010, Children's Hospital Medical Center, 3333 Burnet Avenue, Cincinnati, OH 45229 (e-mail: Alexi.grom@cchmc.org).

Submitted for publication August 11, 2017; accepted in revised form January 30, 2018.

Macrophage activation syndrome (MAS) is a life-threatening episode of hyperinflammation that is characterized clinically by cytopenia, liver dysfunction, coagulopathy, and a systemic "cytokine storm." Although MAS has been reported to occur in numerous rheumatic diseases, in pediatric rheumatic diseases it is most often a complication of systemic juvenile idiopathic arthritis (JIA), a severe and distinct subtype of childhood-onset chronic arthritis (1). MAS bears striking similarity to the rare histiocytic disorder hemophagocytic lymphohistiocytosis (HLH), in which genetic defects in the perforin exocytosis pathway lead to profoundly depressed cytolytic activity of natural killer (NK) cells and CD8 T cells (2). Increasingly, hypomorphic protein-altering variants in these genes have been reported in patients with MAS, including MUNC13-4 (encoded by *UNC13D*), which mediates fusion of perforin-containing lytic granules with the plasma membrane, and a deficiency

of which causes familial HLH type 3 (FHLH3) (2–4). Deep intronic variants in *UNC13D* have also been identified in HLH patients from Europe and North America (5–7). These variants frequently involve the first intron of *UNC13D*, which appears to serve as a key regulatory region, and 1 variant, c.118-308C>T, has been shown to disrupt transcription factor binding to a cytotoxic lymphocyte-specific alternative promoter, thereby selectively diminishing *UNC13D* expression in cytolytic cells (8). However, the presence of intronic or noncoding variants in MAS has been largely unexplored.

Herein, we describe a previously healthy 13-month-old white male with systemic JIA who later developed recurrent episodes of MAS despite receiving traditionally effective treatment. Although testing for coding variants in HLH-associated genes was not revealing, the patient was found to have a novel *UNC13D* variant in the lymphocyte-specific intronic promoter. In support of a causative role for this variant, reduced levels of the alternative, lymphocyte-specific transcript were observed in the patient's peripheral blood mononuclear cells (PBMCs). Finally, we further show that this variant disrupts an NF- κ B site that functions as a transcriptional enhancer in vitro, potentially resulting in decreased *UNC13D* expression and compromised natural killer (NK) cell degranulation.

PATIENTS AND METHODS

Patient data and study approval. This study was approved by the Cincinnati Children's Hospital Institutional Review Board (no. 2011-1517), and informed consent was obtained from all patients and/or their legal guardians. Data pertaining to our patient's clinical course, laboratory values, and treatment were collected from the electronic medical records. Whole blood was obtained using sodium heparin as an anticoagulant. PBMCs were separated by Ficoll density-gradient centrifugation, and RNA was extracted using TRIzol, as previously described (9). When indicated, PBMCs were treated with recombinant human tumor necrosis factor (TNF) (Thermo Fisher) for 6 hours prior to RNA extraction.

***UNC13D* sequencing.** In order to examine possible intronic variants, a custom enrichment library was constructed using a SeqCap EZ system (NimbleGen) to sequence a genomic region of ~1 Mb on chromosome 17 (Human Genome hg19 start site 73,448,832 and stop site 74,504,525) that flanks *UNC13D*. The design specification showed that 98% of the targeted region overlapped with specific probes. Patient DNA was enriched for the target genomic region using a solution-based SeqCap EZ library with 2 million probes for the custom target. A cohort of 24 patients with recurrent systemic JIA-associated MAS or secondary HLH who had prior negative results of genetic exonic testing were sequenced in 2 runs, using Illumina HiSeq 2000 (paired-end design) and a large library (average size 600 bp) to ensure coverage of Alu sequence regions. Sequence reads were filtered first by quality measurement and then matched to the reference sequence of human genome (hg 19). Next, variants were annotated using NextGENe software version 2.3.4 (SoftGenetics LLC). Variants

were filtered based on the frequency in dbSNP and the ExAC database and then examined with respect to phyloP scores for nucleotide conservation and overlap with transcription factor binding motifs from ChIP-Seq data. Additionally, variants were assessed based on manually curating the motif score to remove lower similarity sites, and visual inspection of the quality sequence was used to remove common artifacts known in repetitive regions. Transcription factors for specific reference and mutant nucleotide sequences were matched via the TransFac database.

Real-time reverse transcription–polymerase chain reaction (RT-PCR). RNA extraction and complementary DNA (cDNA) synthesis were performed as previously described (9). Real-time PCR was performed using a ViiA 7 Real-Time PCR system with gene-specific primers and SYBR Green Supermix (Thermo Fisher). Message copy numbers were normalized against the copy number of the housekeeping gene, GAPDH. The primers for GAPDH (9) and the conventional and intron 1 transcripts of *UNC13D* (8) were described previously.

Electrophoretic mobility shift assay (EMSA). An EMSA was performed using a mixture of nuclear extracts from activated NK-92 cells and IRDye 700-labeled NF- κ B consensus oligonucleotides, as previously described (10). The wild-type (WT) oligonucleotide probe sequence for the NF- κ B-like enhancer (143A) located within *UNC13D* intron 1 was ACCCTGGGGA-GAGCCCCCTGGG. The mutant-type oligonucleotide probe sequence for the NF- κ B-like enhancer (143G) included in *UNC13D* intron 1 was ACCCTGGGGAGGGCCCCCTGGG.

Enhancer assay. The WT or mutant NF- κ B-like enhancer (143 A/G; 3xTGGGGAG[A/G]GCCCCCT) was inserted into the enhancer site of the immediate early cytomegalovirus (CMV) promoter or HIV-1 long terminal repeat (LTR)-driven green fluorescent protein (GFP) reporter plasmid previously generated (10) to create the CMV-143A/G-GRP or the HIV-143A/G-GFP constructs. These reporter plasmids were transfected into NK-92 cells by nucleofection, as previously described (10). The cells were rested for 24 hours and then stimulated with irradiated K562 cells (dead) for 1 hour (NK-92 cell-to-K562 cell ratio 2:1) prior to measuring GFP expression levels by flow cytometry, as previously described (11). To further exclude the potential influence of artificially repeated core sequences, a short genomic DNA sequence (111 nt) as shown below, including the NF- κ B-like WT or mutant sequence enhancer core DNA, was synthesized and inserted into the HIV-1 LTR-driven GFP reporter plasmid in either forward or reverse orientation to generate HIV-143A/G111nt-F/R-GFP plasmids. NK-92 cells were transfected with the GFP reporter plasmids and activated, and GFP was measured by flow cytometry as described above (short genomic DNA sequence of 111 nucleotides in length [5'-CGAAGGCTGGGACTGGGGACCAGCGACCC-TCCCCTGCCTACTCCACCCTGGGGAG(A/G)GCCCCCTGGCCAGCAGAGCAGGGGCTGCCAGATGGACTCTGGGCCACTGTGGGC-3']).

***UNC13D* knockdown and degranulation assays.** A Tri-FECTa RNAi kit was purchased from IDT Inc. Transfection of NK-92 cells was performed using a 4D-Nucleofector system (Amaxa). Specifically, 4×10^6 cells mixed with small interfering RNA (siRNA) were suspended with 100 μ l of nucleofector solution, and transfection was performed immediately using an optimally preset program. Transfected cells were cultured for 24 hours. For the degranulation assay, transfected cells were stimulated with K562 target cells (effector-to-target ratio 1:1) for 1–2 hours in the presence of phycoerythrin-conjugated anti-CD107a antibody (Bio-Legend). This was quickly followed by flow cytometric analysis, as

described above. To detect *UNC13D* messenger RNA (mRNA) expression levels, total RNA was extracted from transfected NK-92 cells and reverse transcribed into cDNA using a SuperScript III First Strand Kit from Invitrogen. Real-time PCR was performed with a Bio-Rad CFX system. The housekeeping gene *B2M* mRNA was used for normalization, and scrambled siRNA was used for the control of *UNC13D*-specific siRNA. All oligonucleotides used in these experiments are shown in Supplementary Table 1 (available on the *Arthritis & Rheumatology* web site at <http://onlinelibrary.wiley.com/doi/10.1002/art.40438/abstract>).

RESULTS

We evaluated a previously healthy 13-month-old white male with daily fever for 1 month, intermittent rash, and difficulties with crawling. His parents reported that he would be very irritable for ~1–2 hours upon awakening and then would improve over the course of the day. He was born at term and had no perinatal complications and no significant family medical history or environmental exposure history. His initial examination revealed mild hepatomegaly but no splenomegaly, diffuse salmon-colored rash, and polyarthritis involving the right wrist, bilateral elbows and knees, and left ankle. His initial laboratory evaluation was notable for an elevated white blood cell count of $32.1 \times 10^3/\mu\text{l}$, a hemoglobin concentration of 11.0 gm/dl, an erythrocyte sedimentation rate of 56 mm/hour, a C-reactive protein level of 11.0 mg/dl, and the absence of autoantibodies. Systemic JIA was diagnosed, and the patient was treated with prednisone, with the addition of methotrexate and then intermittent pulse doses of methylprednisolone for refractory polyarthritis.

Approximately 4 months after diagnosis, the patient deteriorated dramatically after developing an Epstein-Barr virus infection, with persistent fevers, rash, active arthritis, and liver and spleen enlargement. His laboratory findings included white blood cell count $17.5 \times 10^3/\mu\text{l}$, hemoglobin concentration 7.0 gm/dl, platelet count $62 \times 10^3/\mu\text{l}$, ferritin level 1,904 ng/ml, decreasing erythrocyte sedimentation rate (to 6 mm/hour), aspartate transaminase concentration 140 units/liter, fibrinogen level 246 mg/dl, and D-dimer concentration 10.87 gm/ml. In addition, the level of soluble interleukin-1 receptor α (IL-2R α ; CD25) was elevated to 30,152 pg/ml, and the level of soluble CD163 was elevated to 80,182 ng/ml. No functional testing of cytolytic or NK cells was performed at this time. He also underwent a bone marrow biopsy, which showed hemophagocytosis. He was given a clinical diagnosis of MAS, having met 5 of 8 HLH-2004 diagnostic criteria (12) and would have satisfied the 2016 classification criteria for MAS complicating systemic JIA (13). He was treated with intravenous methylprednisolone and cyclosporin A as well as the recombinant human IL-1R antagonist anakinra (1), which led to a full

recovery. However, while the patient was being weaned from steroids, he experienced a flare of MAS, with elevated transaminase levels and markedly elevated soluble CD25 levels. This was again controlled with methylprednisolone and increased dosing of cyclosporin A.

Because the patient had experienced recurrent episodes of MAS at an early age, he underwent genetic testing for possible HLH gene mutations, including *PRF1*, *UNC13D*, *STX11*, and *STXBP2*, but no variants were found in all coding exons and exon–intron boundaries. Because mutations in *UNC13D* are relatively common in patients with systemic JIA and MAS in North America (3), a more in-depth exploration of *UNC13D* was undertaken. In order to examine possible intronic variants, a custom enrichment library was constructed to sequence a genomic region of ~1 Mb on chromosome 17 that flanked *UNC13D*. This array was used to sequence DNA from our patient in a batch of samples from 24 patients with recurrent systemic JIA-associated MAS or secondary HLH who had prior negative results of exonic genetic testing. For our patient, 33 million reads were generated, of which 90% passed sequence quality filtering, and 67% of quality reads were matched to the target region. The average coverage depth was 2,122, and the target region coverage depths at 10 \times , 30 \times , and 100 \times were 95%, 94%, and 92%, respectively (complete coverage statistics for all 24 patients are shown in Supplementary Table 2, available on the *Arthritis & Rheumatology* web site at <http://onlinelibrary.wiley.com/doi/10.1002/art.40438/abstract>).

Using this approach, a heterozygous variant was identified in the first intron of *UNC13D*, c.117+143A>G (chromosome 17 [CRCh37]:g.73840159T>C; accession number NM_199242.2) (Figure 1A). Unfortunately, DNA samples from parents were not available for analysis to determine whether this variant was de novo or inherited. This variant was not present in 1000 Genomes, was present in only 1 of >30,000 alleles sequenced through gnomAD, and was not identified in any of the 23 additional sequenced patients with systemic JIA and MAS, although one of these patients did have the previously reported c.118-308C>T intronic variant, as described below and shown in Figure 1A.

Notably, there is substantial evidence that this intronic region has key roles in regulating *UNC13D* expression. First, there are reported H3K27Ac marks typical of transcriptional promoters on 7 unique cell lines, DNase I hypersensitivity clusters suggesting transcriptional activity in 125 cell types, and at least 15 transcription factor-binding motif overlaps in ChIP-Seq (Figure 1A). Second, the identified novel c.117+143A>G variant specifically overlaps with and alters a predicted consensus NF- κ B transcription factor binding site (Figure 1A; see also Supplementary Figure 1,

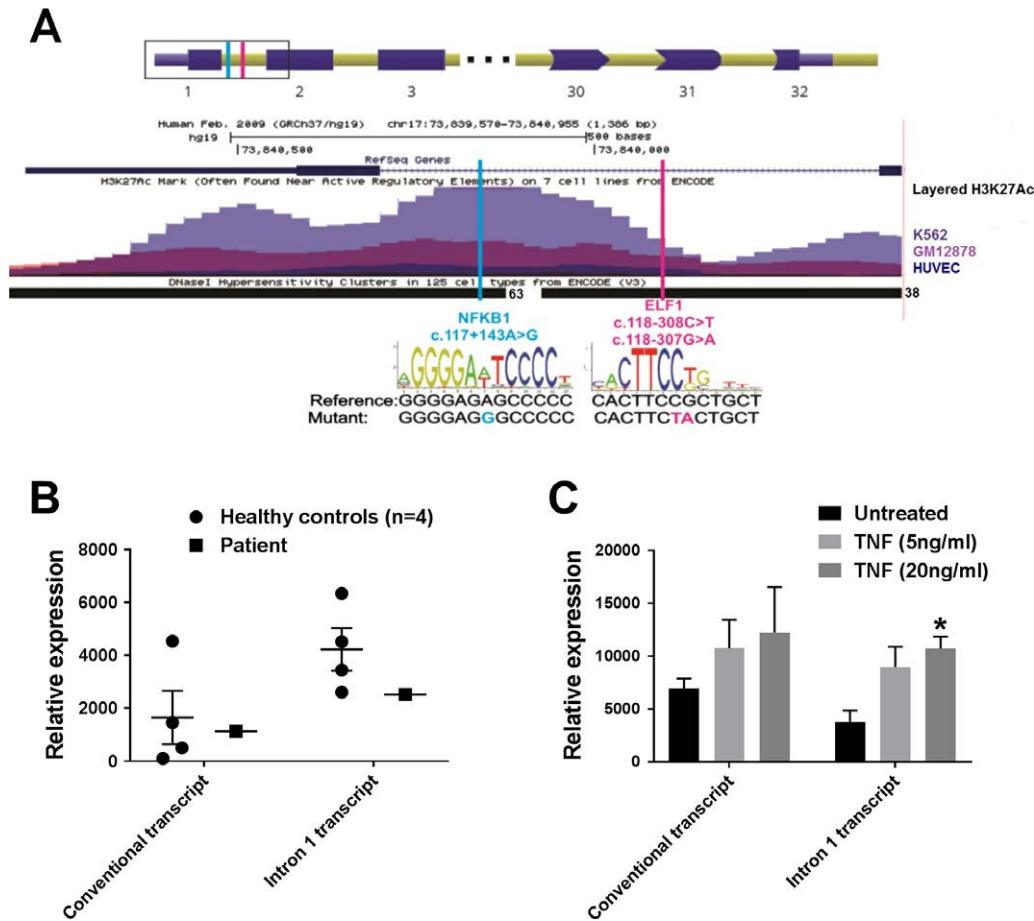


Figure 1. Novel *UNC13D* intronic variant is located in a key regulatory region. **A**, Schematic representation of the novel genomic variant c.117+143A>G (vertical blue lines) detected in our 13-month-patient with systemic juvenile idiopathic arthritis and macrophage activation syndrome and the reference variants c.118-308C>T and c.118-307G>A (vertical red lines), showing relative increased histone markers of the sequence of intron 1 of *UNC13D*. Boxed area shows consensus transcription factor binding sites that are disrupted by these changes. **B**, Levels of conventional and lymphocyte-specific alternative *UNC13D* transcripts in the patient compared with the levels in 4 healthy control subjects, as determined by quantitative reverse transcription–polymerase chain reaction. Total RNA was extracted from unstimulated peripheral blood mononuclear cells (PBMCs) obtained from the patient during a period of inactive disease. Each data point represents an individual subject. Bars show the mean \pm SEM. **C**, Levels of conventional and lymphocyte-specific alternative *UNC13D* transcripts in control PBMCs after treatment with tumor necrosis factor (TNF), as determined by quantitative reverse transcription–polymerase chain reaction. Bars show the mean \pm SEM. Data in **B** and **C** were normalized to GAPDH to obtain the relative expression. Chr. = chromosome; RefSeq = reference sequence; HUVEC = human umbilical vein endothelial cell. * = $P < 0.05$ vs. untreated samples.

available on the *Arthritis & Rheumatology* web site at <http://onlinelibrary.wiley.com/doi/10.1002/art.40438/abstract>). This variant is not predicted to disrupt additional consensus binding sites. Finally, 2 other variants from this intronic region, c.118-308C>T and c.118-307G>A, have been previously reported in patients with HLH (6,7). Indeed, the c.118-308C>T variant was also found in the heterozygous state in one of the 24 patients sequenced (patient 10). In addition, patient 10 was also found to have a previously reported 253-kb inversion that straddles the last 2 exons of *UNC13D* and has been shown to be linked to *FHL3* in both northern European and North American patients (5,6). No other rare coding or noncoding variants (minor allele

frequency <1%) were identified in *UNC13D* in any of the 24 patients.

Interestingly, the previously identified c.118-308C>T variant has been shown to markedly reduce *UNC13D* expression selectively in lymphocytes, including CD8 T cells, by disrupting transcription factor binding to an alternative promoter specifically active in cytotoxic cells (6,8). This promoter leads to production of a second, distinct *UNC13D* transcript that is preferentially expressed in cytotoxic T lymphocytes and NK cells. PBMCs from our patient were not available to permit cell type-specific transcript analysis. However, total RNA previously isolated from PBMCs during a period of inactive disease was used to determine

UNC13D mRNA levels using real-time RT-PCR analysis, as previously described (8). This demonstrated reduced levels of the alternative, lymphocyte-specific intron 1 UNC13D transcript compared with PBMCs from healthy age-matched controls, despite normal levels of the conventional UNC13D transcript (Figure 1B), suggesting that the novel c.117+143A>G variant may impair expression of lymphocyte-specific UNC13D transcript.

Of note, the sample from our patient was obtained during a period of inactive disease; because the alternative promotor contains a putative NF-κB binding site, it is reasonable to speculate that transcript expression may increase during periods of active systemic inflammation. To examine this, PBMCs from healthy control subjects were stimulated with TNF for 6 hours, and expression of UNC13D transcripts was quantified. Treatment with TNF led to a significant and dose-dependent increase in the expression of the alternative intron 1 transcript, without significant change in the expression of the conventional transcript (Figure 1C).

To further characterize the functional role of this intronic region, we examined the predicted NF-κB binding site that is altered by the c.117+143A>G variant. EMSAs were performed using a consensus NF-κB oligonucleotide probe and nuclear extracts from the human NK cell line, NK-92. Two delayed bands were identified, the upper of which could be supershifted by anti-NF-κB p65 antibody (Figure 2). The lower band migrates consistent with NF-κB p50 (10). Binding of nuclear extracts to the consensus NF-κB oligonucleotide (both p50 and p65 bands) was largely disrupted by either unlabeled self competitor or by a 22-mer probe corresponding to the WT UNC13D intron 1 region containing the predicted NF-κB motif binding (Figure 2). Notably, a competitor oligonucleotide containing the c.117+143A>G variant was less efficient at blocking formation of the NF-κB bands, thus confirming the notion that this variant is less efficient at disrupting NF-κB binding.

The deep intronic location of this NF-κB motif suggested that this genomic region could function as a transcriptional enhancer that can regulate gene expression from a distance independent of position and orientation. To determine whether this intronic region can serve as a transcriptional enhancer, a trimerized 15-mer sequence containing either the WT intronic sequence or the c.117+143A>G variant was cloned into the enhancer site of the immediate early CMV promoter or the HIV-1 LTR-driven GFP reporter plasmid and transfected into NK-92 cells (Figure 3A). Cloning of the WT (143A) trimerized 15-mer sequence into either vector enhanced GFP expression in activated NK-92 cells (Figures 3B and C). In contrast, the patient variant (143G) showed significantly reduced effect compared with the WT sequence for enhancing GFP

expression driven by promoters of either CMV or HIV-1 (Figures 3B and C).

To confirm this further and eliminate the potential influence of artificially repeating the core sequence, a 111-nt genomic DNA region including either the WT or mutant core NF-κB enhancer was inserted into the HIV-1 vector. As shown in Figures 3D and E, the short genomic DNA containing the WT enhancer significantly increased HIV-1 LTR-driven GFP expression in activated NK-92 cells, and the mutant enhancer significantly attenuated this activity. Notably, cloning of the short genomic sequence, in either the forward or reverse orientation, significantly increased GFP expression driven by the HIV-1 LTR, further demonstrating that this region can serve as a transcriptional enhancer in vitro (Figures 3D and E). Collectively, these results suggest that the c.117+143A>G variant alters the ability of NF-κB to bind to a transcriptional enhancer element and supports the finding of reduced alternative transcript levels in PBMCs from our patient.

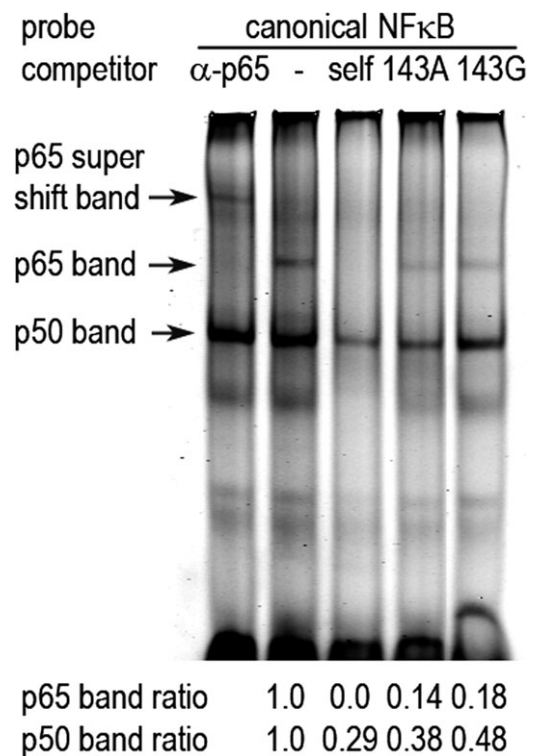


Figure 2. The mutant NF-κB-like enhancer located within the UNC13D intron partially disrupts protein binding to a consensus NF-κB probe. Electrophoretic mobility shift assay was performed using a mixture of nuclear extracts from activated NK-92 cells and IRDye-700-labeled NF-κB consensus oligonucleotide probe. The binding band was either supershifted by anti-p65 antibody or blocked by self, wild-type (143A), or mutant (143G) oligonucleotide competitors. The band intensities were analyzed using ImageJ (v1.50I). Values shown below the third through fifth lanes are relative to the respective non-competed bands (second lane) (set at 1.0).

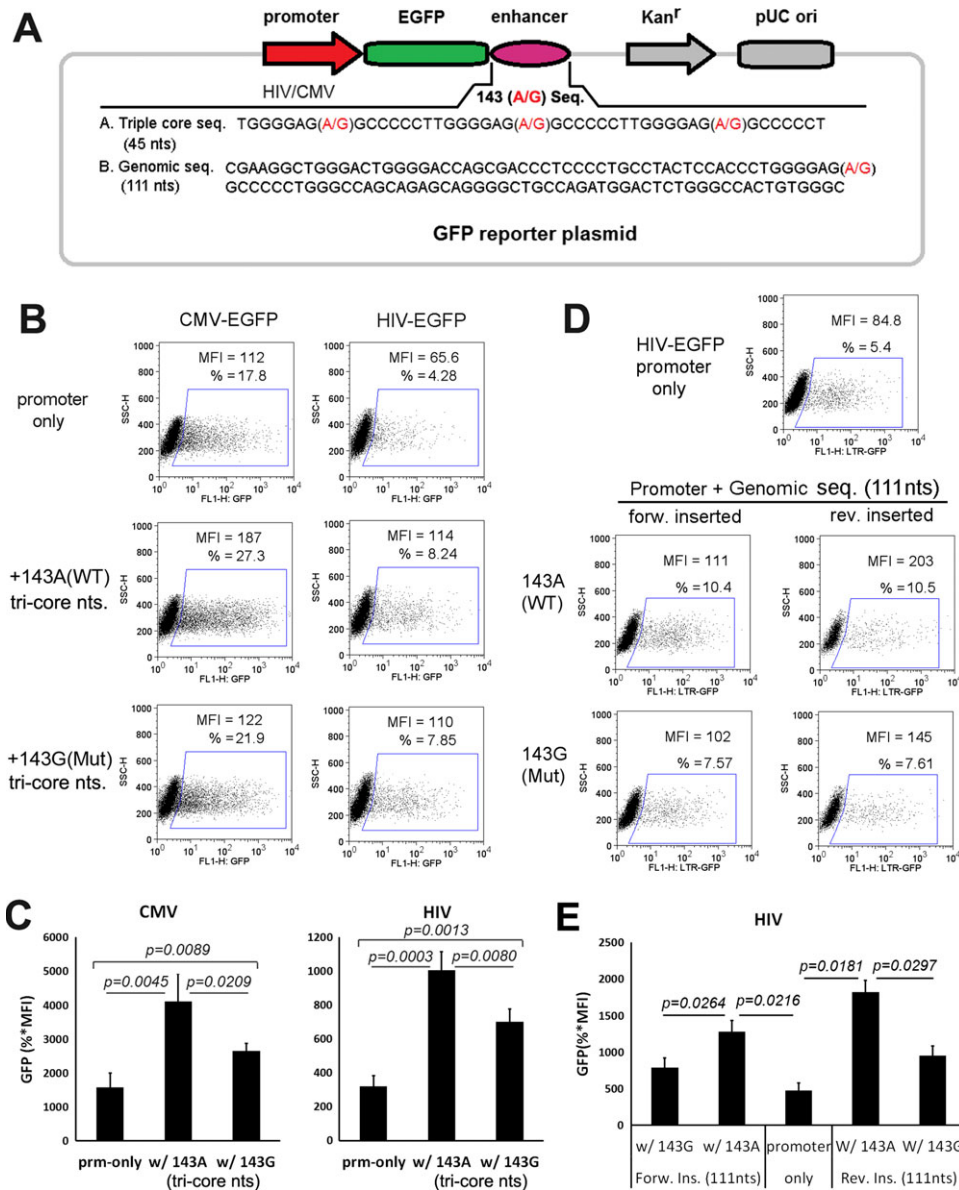


Figure 3. The NF- κ B-like enhancer is located within *UNC13D* intron 1. **A**, Schematic representation of HIV-1- and cytomegalovirus (CMV)-driven green fluorescent protein (GFP) reporter plasmids inserted with either the triple-core sequence (seq.) (45 nucleotides [nts]) or short genomic sequence (111 nts) of the enhancer. **B**, Comparison of the enhancer activity of triple-core DNA of the wild-type (WT; 143A) or mutant (Mut; 143G) enhancer sequences in augmenting GFP expression driven by either CMV or HIV-1 promoters (prm) within NK-92 cells postactivation by irradiated K562 cells. **C**, Quantification of the data shown in **B**. **D**, Comparison of the enhancer activity of short genomic DNA of the wild-type or mutant enhancer sequences, inserted in either forward or reverse orientation, in augmenting GFP expression driven by HIV-1 promoter within NK-92 cells postactivation by irradiated K562 cells. **E**, Quantification of the data shown in **D**. Bars in **C** and **E** show the mean \pm SD ($n = 3$ independent experiments). Kan^r = kanamycin resistance gene; EGFP = enhanced GFP; MFI = mean fluorescence intensity; SSC-H = side scatter height; LTR = long terminal repeat; Forw. Ins. = forward inserted; Rev. Ins. = reverse inserted. Color figure can be viewed in the online issue, which is available at <http://onlinelibrary.wiley.com/doi/10.1002/art.40438/abstract>.

Taken together, these results support a model in which the c.117+143A>G variant leads to reduced lymphocyte *UNC13D* expression, causing diminished target cell killing. In order to examine whether a partial reduction in *UNC13D* expression could compromise NK cell function,

UNC13D transcript was knocked down using siRNA in the human NK-92 cell line. NK-92 cells transfected with scrambled sequence or specific *UNC13D* siRNA were incubated with K562 target cells for 1–2 hours, and NK cell degranulation was determined by CD107a cell surface staining.

Compared with cells transfected with scrambled siRNA, NK-92 cells transfected with low (5 nM) or high (10 nM) NF- κ B concentrations of specific *UNC13D* siRNA showed significantly reduced, but not absent, CD107a surface expression (see Supplementary Figure 2, available on the *Arthritis & Rheumatology* web site at <http://onlinelibrary.wiley.com/doi/10.1002/art.40438/abstract>). Indeed, the degree of impaired NK cell degranulation correlated with residual *UNC13D* expression in a dose-dependent manner (see Supplementary Figure 2). These findings demonstrate that even partial reductions in *UNC13D* expression can compromise cytolytic cell function and further support roles for hypomorphic noncoding mutations such as c.117+143A>G in the pathogenesis of MAS.

DISCUSSION

The genetic basis of MAS in patients with systemic JIA remains unclear. However, contemporary studies have shown that as many as one-third of patients with MAS associated with systemic JIA have rare, protein-altering variants in genes associated with HLH (3,14). Recent work by our group and other investigators has shown that these variants can impair lymphocyte function and may explain in part the increased risk for MAS in these patients (11,15). In addition, whole-exome sequencing in patients with systemic JIA and MAS has identified novel candidate genes that could be implicated in this process, including several that interact with known components of the cytolytic pathway (3).

Taken together, these findings suggest that hypomorphic variants in HLH-associated genes involved in the perforin cytolytic pathway may serve as risk factors for MAS, although this remains to be formally tested in a prospective manner. However, many patients, even those with recurrent MAS, lack any protein-altering variants in known or putative genes linked to cytolytic dysfunction. Noncoding regulatory genomic regions often are not examined, in either targeted gene sequencing or whole-exome sequencing. However, there is increasing evidence that intronic variants are significant contributors to human disease. Variants in the first intron of *UNC13D*, for example, are frequently identified in patients with FHLH3. The first of these to be described was c.118-308C>T, which causes a lymphocyte-specific loss of *UNC13D* expression due to disrupted transcription factor binding (6,8). In addition, the neighboring c.118-307G>A variant is associated with diminished *UNC13D* expression and impaired cytolytic cell degranulation (7). Thus, in our large North American cohort of >1,700 HLH patients, 79 were found to have FHLH3 (biallelic *UNC13D*), and more than 31% carried at least 1 noncoding mutation (5).

Here, we describe a patient with systemic JIA and recurrent MAS who was found to have a novel *UNC13D*

intronic variant c.117+143A>G that alters an NF- κ B engagement and transcription enhancer element. Several lines of evidence support the notion that this variant impacts *UNC13D* expression in cytolytic cells. First, this intronic region includes H3K27Ac marks, DNase I hypersensitivity clusters, and at least 15 transcription factor binding motif overlaps from ChIP-seq data (Figure 1A). Second, PBMCs from this patient showed a 40% reduction in levels of the alternative, lymphocyte-specific intron 1 *UNC13D* transcript compared with control samples (Figure 1B). Of note, transcript levels were quantified in samples obtained from patients during a period of inactive disease; more profound reductions in message levels could occur during periods of hyperinflammation. Indeed, we observed that TNF stimulation of control PBMCs led to a significant increase in expression of the alternative intron 1 transcript (Figure 1C).

These findings are consistent with previously reported data on other intron 1 variants, most notably c.118-308C>T, which was shown to disrupt binding of the Ets family transcription factor Elf-1 (5–7) leading to lymphocyte-specific loss of *UNC13D* expression and defective cytolytic cell degranulation. We cannot discount the possibility that the c.117+143A>G variant may also impact transcript splicing, thereby also impacting conventional *UNC13D* transcript expression. Third, this variant disrupts the consensus sequence of an NF- κ B binding site (Figure 1A), and indeed we show that the variant sequence is less efficient at blocking NF- κ B bands in EMSA (Figure 2). Finally, this sequence serves as a transcriptional enhancer in vitro, and the c.117+143A>G variant showed significantly reduced transcriptional enhancement (Figure 3). Taken together, these findings strongly support the notion that the novel c.117+143A>G mutation is a functional intronic variant that diminishes lymphocyte-specific *UNC13D* expression.

Substantial evidence supports the notion that even partially reduced lymphocyte *UNC13D* expression would have functional consequences. Patients with previously described intron 1 variants displayed both reduced lymphocyte-specific *UNC13D* expression and impaired cytolytic function (6–8), and *UNC13D* expression strongly correlated with degranulation and cytotoxicity (8). Consistent with this, previous work by our group has shown that even partial defects in the interaction of MUNC13-4 with the effector Rab27a (~50% diminished) resulted in decreased cytolytic activity, delayed granule polarization, and increased interferon- γ production resulting from prolonged engagement with target cells (11). Finally, and most importantly, in the current study we show that partial knockdown of *UNC13D* message levels with targeted siRNA leads to corresponding partial defects in NK cell degranulation (see Supplementary Figure 2, available on the *Arthritis & Rheumatology* web site at <http://onlinelibrary.wiley.com/doi/10.1002/art.40438/abstract>).

1002/art.40438/abstract). This supports a model in which variants such as c.117+143A>G reduce *UNC13D* transcript levels, causing partial defects in cytolytic function and lowering the threshold for MAS development, particularly in patients with underlying inflammation, such as those with systemic JIA (4,16).

To the best of our knowledge, this is the first report of functional intronic variants associated with MAS in children with systemic JIA. Of note, we also identified the known variant c.118-308C>T in heterozygous form in an additional patient with secondary HLH/MAS (patient 10). This rare variant is present in <0.02% of the genomes listed in gnomAD but is reported in up to 9% of alleles in patients with FHLH3 (5). Extensive functional study of this variant has demonstrated that it disrupts binding of the Ets family transcription factor Elf-1, impairing recruitment of STAT-4 and diminishing chromatin remodeling (8). Interestingly, Elf-1 can cooperate with NF- κ B to activate transcription (17), which could suggest that the biologic consequences of these 2 intronic variants are linked. Thus, together with the novel c.117+143A>G variant identified herein, the total hit rate for potentially deleterious *UNC13D* intronic variants in the current study was 8.3% (2 of 24).

Taken together, the findings in these patients suggest that intronic variants in key conserved regulatory regions should be examined in children with systemic JIA and MAS, and that genetic screening for variants in *UNC13D* should be expanded to include intron 1. Along with hypomorphic coding variants in HLH-associated genes, these intronic variants may serve as further risk factors for MAS in patients with systemic JIA and could have implications for genetic counseling. The current study further supports the utility of targeted sequencing approaches or even whole-genome sequencing in cases in which causative protein-altering mutations are not identified and provides evidence for cell-specific effects of intronic variants on transcript expression.

AUTHOR CONTRIBUTIONS

All authors were involved in drafting the article or revising it critically for important intellectual content, and all authors approved the final version to be published. Dr. Grom had full access to all of the data in the study and takes responsibility for the integrity of the data and the accuracy of the data analysis.

Study conception and design. Schulert, M. Zhang, K. Zhang, Cron, Grom.

Acquisition of data. Schulert, M. Zhang, Husami, Fall, Brunner.

Analysis and interpretation of data. Schulert, M. Zhang, Husami, Fall, K. Zhang, Cron, Grom.

REFERENCES

- Ravelli A, Grom AA, Behrens EM, Cron RQ. Macrophage activation syndrome as part of systemic juvenile idiopathic arthritis: diagnosis, genetics, pathophysiology and treatment. *Genes Immun* 2012;13:289–98.
- Zhang K, Biroschak J, Glass DN, Thompson SD, Finkel T, Passo MH, et al. Macrophage activation syndrome in patients with systemic juvenile idiopathic arthritis is associated with MUNC13-4 polymorphisms. *Arthritis Rheum* 2008;58:2892–6.
- Kaufman KM, Linghu B, Szustakowski JD, Husami A, Yang F, Zhang K, et al. Whole-exome sequencing reveals overlap between macrophage activation syndrome in systemic juvenile idiopathic arthritis and familial hemophagocytic lymphohistiocytosis. *Arthritis Rheumatol* 2014;66:3486–95.
- Zhang M, Behrens EM, Atkinson TP, Shakoory B, Grom AA, Cron RQ. Genetic defects in cytotoxicity in macrophage activation syndrome. *Curr Rheumatol Rep* 2014;16:439.
- Qian Y, Johnson JA, Connor JA, Valencia CA, Barasa N, Schubert J, et al. The 253-kb inversion and deep intronic mutations in *UNC13D* are present in North American patients with familial hemophagocytic lymphohistiocytosis 3. *Pediatr Blood Cancer* 2014;61:1034–40.
- Meeths M, Chiang SC, Wood SM, Entesarian M, Schlums H, Bang B, et al. Familial hemophagocytic lymphohistiocytosis type 3 (FHL3) caused by deep intronic mutation and inversion in *UNC13D*. *Blood* 2011;118:5783–93.
- Entesarian M, Chiang SC, Schlums H, Meeths M, Chan MY, Mya SN, et al. Novel deep intronic and missense *UNC13D* mutations in familial haemophagocytic lymphohistiocytosis type 3. *Br J Haematol* 2013;162:415–8.
- Cichocki F, Schlums H, Li H, Stache V, Holmes T, Lenvik TR, et al. Transcriptional regulation of *Munc13-4* expression in cytotoxic lymphocytes is disrupted by an intronic mutation associated with a primary immunodeficiency. *J Exp Med* 2014;211:1079–91.
- Sikora KA, Fall N, Thornton S, Grom AA. The limited role of interferon- γ in systemic juvenile idiopathic arthritis cannot be explained by cellular hyporesponsiveness. *Arthritis Rheum* 2012;64:3799–808.
- Zhang M, Clausell A, Robinson T, Yin J, Chen E, Johnson L, et al. Host factor transcriptional regulation contributes to preferential expression of HIV type 1 in IL-4-producing CD4 T cells. *J Immunol* 2012;189:2746–57.
- Zhang M, Bracaglia C, Prencipe G, Bemrich-Stolz CJ, Beukelman T, Dimmitt RA, et al. A heterozygous *RAB27A* mutation associated with delayed cytolytic granule polarization and hemophagocytic lymphohistiocytosis. *J Immunol* 2016;196:2492–503.
- Henter JI, Horne A, Arico M, Egeler RM, Filipovich AH, Imashuku S, et al. HLH-2004: diagnostic and therapeutic guidelines for hemophagocytic lymphohistiocytosis. *Pediatr Blood Cancer* 2007;48:124–31.
- Ravelli A, Minoia F, Davì S, Horne A, Bovis F, Pistorio A, et al. 2016 classification criteria for macrophage activation syndrome complicating systemic juvenile idiopathic arthritis: a European League Against Rheumatism/American College of Rheumatology/Paediatric Rheumatology International Trials Organisation collaborative initiative. *Arthritis Rheumatol* 2016;68:566–76.
- Vastert SJ, van Wijk R, D'Urbano LE, de Vooght KM, de Jager W, Ravelli A, et al. Mutations in the perforin gene can be linked to macrophage activation syndrome in patients with systemic onset juvenile idiopathic arthritis. *Rheumatology (Oxford)* 2010;49:441–9.
- Schulert GS, Zhang M, Fall N, Husami A, Kissell D, Hanosh A, et al. Whole-exome sequencing reveals mutations in genes linked to hemophagocytic lymphohistiocytosis and macrophage activation syndrome in fatal cases of H1N1 influenza. *J Infect Dis* 2016;213:1180–8.
- Strippoli R, Caiello I, De Benedetti F. Reaching the threshold: a multilayer pathogenesis of macrophage activation syndrome. *J Rheumatol* 2013;40:761–7.
- John S, Reeves RB, Lin JX, Child R, Leiden JM, Thompson CB, et al. Regulation of cell-type-specific interleukin-2 receptor α -chain gene expression: potential role of physical interactions between Elf-1, HMG-I(Y), and NF- κ B family proteins. *Mol Cell Biol* 1995;15:1786–96.

CONCISE COMMUNICATION

DOI 10.1002/art.40441

Screening high-resolution computed tomography of the chest to detect interstitial lung disease in systemic sclerosis: a global survey of rheumatologists

Interstitial lung disease (ILD) affects ~40–60% of adults with systemic sclerosis (SSc) and is the leading cause of death and hospitalization in this population (1–4). Despite the life-threatening nature of ILD and the availability of therapies (5,6), there are no clinical practice guidelines that recommend screening for ILD in SSc. Although pulmonary function tests are widely used by rheumatologists to screen for SSc-related ILD, studies have shown that they are neither

sensitive nor specific for detection of ILD in this population (3). High-resolution computed tomography (HRCT) of the chest is the gold standard for detection of ILD (7), but data on rheumatologists’ practices with regard to ordering HRCTs for their SSc patients have not been reported. We undertook a study to determine rheumatologists’ use of HRCT as a screening tool in their patients with newly diagnosed SSc.

We e-mailed a REDCap survey (8) to all 676 American College of Rheumatology member rheumatologists in New York, New Jersey, Pennsylvania, and Connecticut and to 356 SSc experts worldwide (defined as rheumatologist members of the Scleroderma Clinical Trials Consortium and/or the European League Against Rheumatism Scleroderma Trials and Research Group with at least 1 publication on SSc) to

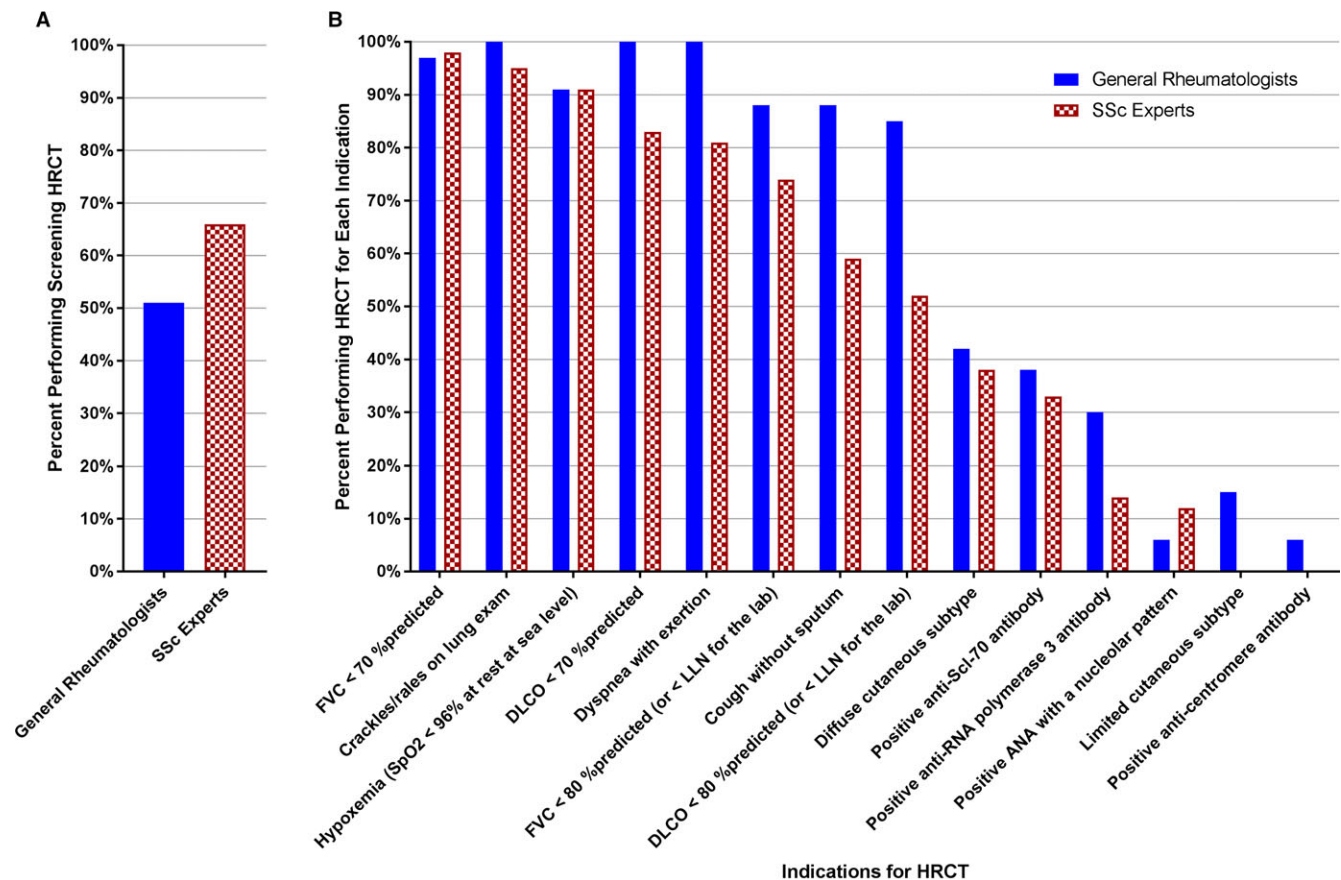


Figure 1. A, Percent of responding general rheumatologists (n = 76) and systemic sclerosis (SSc) experts (n = 135) who routinely order screening high-resolution computed tomography (HRCT) of the chest in newly diagnosed SSc patients. B, Indications for chest HRCT among general rheumatologists (n = 34) and SSc experts (n = 43) who do not routinely order screening HRCT in all newly diagnosed SSc patients. The denominator ranges from 32 to 34 for general rheumatologists and 41 to 43 for SSc experts, due to variable response rates for individual questions. FVC = forced vital capacity; SpO₂ = peripheral arterial oxygen saturation; DLCO = diffusing capacity for carbon monoxide; LLN = lower limit of normal; ANA = antinuclear antibody.

identify current HRCT screening practices for SSc-related ILD. Seventy-six (11%) of the general rheumatologists responded (of whom 73 see at least 1 new SSc patient per year), as did 135 (38%) of the SSc experts.

Overall, 51% of the general rheumatologist respondents and 66% of the SSc expert respondents reported routinely ordering HRCTs in all newly diagnosed SSc patients (Figure 1A). We identified significant global practice variation in HRCT screening practices among SSc experts. Screening HRCTs were routinely ordered by 0% of the respondents in Australia (0 of 5), 33% in Canada (2 of 6), 60% in the US (28 of 47), 79% in Europe (45 of 57), 80% in Asia (4 of 5), and 100% in Latin America (7 of 7). Moreover, among rheumatologists who do not routinely order screening HRCTs in their SSc patients, there was very little consensus regarding indications for HRCT in SSc (Figure 1B). For example, only 81% of SSc experts would order an HRCT for dyspnea on exertion, 74% for abnormal forced vital capacity (<80% of predicted), and 52% for abnormal diffusing capacity for carbon monoxide (<80% of predicted). The reason SSc specialists were less likely than general rheumatologists to order HRCT for certain indications was not explained by this study. Of the 95 SSc experts who answered a question about circumstances in which they would repeat an HRCT, 9 (9.5%) responded that they order a repeat HRCT in their SSc patients annually.

A limitation of this study is the low response rate. Given the wide practice variation in HRCT screening practices by both SSc experts and general rheumatologists, further research into the clinical impact of HRCT screening for ILD in SSc is needed. Such research will ultimately help inform the development of a clinical practice guideline for ILD screening in SSc, which would help harmonize rheumatologists' approach to identifying the leading cause of mortality in SSc.

Dr. Bernstein's work was supported by the Rheumatology Research Foundation (Scientist Development Award). Dr. Khanna's work was supported by the NIH (National Institute of Arthritis and Musculoskeletal and Skin Diseases grants K24-AR-063120 and R01-AR-070470). Dr. Lederer's work was supported by the NIH (National Heart, Lung, and Blood Institute grant K24-HL-131937). Dr. Khanna has received consulting fees from Actelion, Bayer, Bristol-Myers Squibb, Boehringer-Ingelheim, ChemomAb, Corbus, Covis, Cytos, Eicos, EMD Serono, Genentech/Roche, Gilead, GlaxoSmithKline, Pfizer, Sanofi-Aventis, and UCB (less than \$10,000 each) and has ownership interest in Eicos. Dr. Lederer has received consulting fees from Roche, Veracyte, Galapagos, Global Blood Therapeutics, Fibrogen, and Sanofi Genzyme (less than \$10,000 each).

Elana J. Bernstein, MD, MSc 
Columbia University Medical Center
New York, NY

Dinesh Khanna, MD, MS
University of Michigan
Ann Arbor, MI

David J. Lederer, MD, MS 
Columbia University Medical Center
New York, NY

AUTHOR CONTRIBUTIONS

All authors were involved in drafting the article or revising it critically for important intellectual content, and all authors approved the final version to be published. Dr. Bernstein had full access to all of the data in the study and takes responsibility for the integrity of the data and the accuracy of the data analysis.

Study conception and design. Bernstein, Khanna, Lederer.

Acquisition of data. Bernstein.

Analysis and interpretation of data. Bernstein, Lederer.

1. Steen VD, Medsger TA. Changes in causes of death in systemic sclerosis, 1972–2002. *Ann Rheum Dis* 2007;66:940–4.
2. Tyndall AJ, Bannert B, Vonk M, Airo P, Cozzi F, Carreira PE, et al. Causes and risk factors for death in systemic sclerosis: a study from the EULAR Scleroderma Trials and Research (EUSTAR) database. *Ann Rheum Dis* 2010;69:1809–15.
3. Suliman YA, Dobrota R, Huscher D, Nguyen-Kim TD, Maurer B, Jordan S, et al. Pulmonary function tests: high rate of false-negative results in the early detection and screening of scleroderma-related interstitial lung disease. *Arthritis Rheumatol* 2015;67:3256–61.
4. Steen VD, Conte C, Owens GR, Medsger TA Jr. Severe restrictive lung disease in systemic sclerosis. *Arthritis Rheum* 1994;37:1283–9.
5. Tashkin DP, Elashoff R, Clements PJ, Goldin J, Roth MD, Furst DE, et al. Cyclophosphamide versus placebo in scleroderma lung disease. *N Engl J Med* 2006;354:2655–66.
6. Tashkin DP, Roth MD, Clements PJ, Furst DE, Khanna D, Kleerup EC, et al. Mycophenolate mofetil versus oral cyclophosphamide in scleroderma-related interstitial lung disease (SLS II): a randomised controlled, double-blind, parallel group trial. *Lancet Respir Med* 2016;4:708–19.
7. Raghu G, Collard HR, Egan JJ, Martinez FJ, Behr J, Brown KK, et al. An official ATS/ERS/JRS/ALAT statement: idiopathic pulmonary fibrosis: evidence-based guidelines for diagnosis and management. *Am J Respir Crit Care Med* 2011;183:788–824.
8. Harris PA, Taylor R, Thielke R, Payne J, Gonzalez N, Conde JG. Research electronic data capture (REDCap): a metadata-driven methodology and workflow process for providing translational research informatics support. *J Biomed Inform* 2009;42:377–81.